FACILITY FORM 602
X 68 16032
(ACCESSION NUMBER) (THRU)
(PAGES) (CODE)
NASA CR 94641
(NASA CR OR TMX OR AD NUMBER) (CATE
(NSG 496) NGL-22-0 019

CASE FILE COPY

ABSOLUTE AND CONVECTIVE MICROINSTABILITIES OF A MAGNETIZED PLASMA

by

James D. Callen

CSR T-68-3 April, 1968

CENTER FOR SPACE RESEARCH
MASSACHUSETTS INSTITUTE OF TECHNOLOGY

X 68 16092

ABSOLUTE AND CONVECTIVE MICROINSTABILITIES OF A MAGNETIZED PLASMA

by

James D. Callen

CSR T-68-3 April, 1968

FOREWORD

This document was prepared by Mr. J. D. Callen of the Department of Nuclear Engineering, Massachusetts Institute of Technology, in partial fulfillment of the requirements for the degree of Doctor of Philosophy. Mr. Callen's main emphasis in the text is on the application of his results to laboratory experiments concerning magnetically confined plasmas and to fusion-oriented plasma devices. It is important to note, however, that many of his results have direct application to certain situations in space plasmas. Moreover, the knowledge gained through Mr. Callen's thorough study of plasma instabilities make possible the extension of his work to more complex situations likely to occur in the Earth's magnetosphere, the solar wind, etc.

It has been a real pleasure to be associated with Mr. Callen during the period of his doctoral research and to have him as a member of our Laboratory.

J. E. McCune
Laboratory for Plasma Physics and Space Science
Department of Aeronautics & Astronautics and
Center for Space Research

ABSOLUTE AND CONVECTIVE MICROINSTABILITIES OF A MAGNETIZED PLASMA

by

James D. Callen

Submitted to the Department of Nuclear Engineering
on April 30, 1968 in partial fulfillment of
the requirements for the degree of
Doctor of Philosophy

ABSTRACT

The electrostatic instabilities of a low β, weakly inhomogeneous, hot, fully-ionized, collisionless plasma in a magnetic field are considered. Some discussion of the values of β for which only electrostatic modes need be considered, of the restrictions which are imposed by equilibrium considerations on any magnetic field curvature which may be present and of the "local" approximation to the integro-differential dispersion equation is given. Rigorous necessary and sufficient conditions for instability of the plasma are derived. These conditions extend those previously available for homogeneous plasmas to weakly inhomogeneous plasmas, and in general justify and elucidate the commonly used marginal stability analysis. The problem of distinguishing between convective and absolute instabilities is reviewed. A new and very efficient method for determining the density at which an absolute instability of the plasma has any given temporal growth rate, including zero, is developed.

With the general instability conditions as a guide, the velocity-space anisotropy and to a lesser extent the "universal" instabilities are reviewed. The general techniques developed in this work are then employed to carry out extensive studies of the loss-cone and drift-cyclotron instabilities, which include a consideration of the absolute versus convective nature along the magnetic field of the unstable modes. The effects of variations in the electron temperature, sharpness of the $v_\perp$ distribution and density gradient on the loss-cone and drift-cyclotron instabilities are considered for all relevant wave numbers and frequencies. For pertinent plasma parameters it is found that these instabilities always become absolute (nonconvective) for sufficiently high plasma

densities. It is also found that the maximum spatial growth rate of the convective instabilities before an absolute instability appears is bounded. The magnitude of this bound is such that if it is assumed that an absolute instability mode can "fit" into any plasma which is a half-wavelength long, the convective instabilities will be a serious detriment to plasma containment only if the reflection coefficient at the axial ends of the plasma exceeds about one-quarter and even then only for electron temperatures much less than the ion temperature. Since such a large reflection coefficient seems unlikely or at least avoidable, it is concluded that only the absolute loss-cone and drift-cyclotron instabilities will be important in limiting containment of an experimental plasma.

It is found that neither increasing the electron temperature (up to the ion temperature) nor increasing the thermal spread in the $v_\perp$ distribution (up to a thermal spread roughly equal to the mean displacement) has any substantial stabilizing effect on the absolute instabilities. The transition density for the onset of the absolute drift-cyclotron instabilities is found to increase roughly with the square of the scale length of the density gradient transverse to the magnetic field. In general the absolute loss-cone and drift-cyclotron instabilities are found to occur only if the plasma density is at least high enough so that the ion plasma frequency exceeds the ion cyclotron frequency. The absolute instabilities have rather long wavelengths along the magnetic field. The implications which the results obtained for the loss-cone instabilities have on the applicability of the Rosenbluth-Post "continuum" limit is also discussed. Finally, some aspects of the instabilities which occur in a plasma that admits both loss-cone and drift-cyclotron instabilities are discussed. In general the combination modes resemble simply the more unstable of the loss-cone or drift-cyclotron modes depending on the particular plasma parameters. However, there are important exceptions, for example the threshold density for flute-like combination modes can be much lower than that for either of the separate modes.

Thesis Supervisor: James E. McCune

Title: Associate Professor of Aeronautics and Astronautics

Thesis Supervisor: Thomas H. Dupree

Title: Associate Professor of Nuclear Engineering

TABLE OF CONTENTS

1. INTRODUCTION

1.1	Introductory Remarks	11
1.2	General Approximations	19
1.3	Plasma Model	35
1.4	Thesis Guide	41

2. EQUILIBRIUM STATE

2.1	Constants of the Motion	46
2.2	Equilibrium Distribution	50
2.3	Parametric Constraints	56
2.4	On Representation of Curvature Effects by the Gravity Force	59

3. DISPERSION RELATION DERIVATION

3.1	Integro-Differential Dispersion Equation	66
3.2	Unperturbed Orbit Equations	75
3.3	Dispersion Relation: General $\langle f \rangle$	81
3.4	Dispersion Relation: Special $\langle f \rangle$	106

4. REAL-k INSTABILITY ANALYSIS

4.1	Marginal Stability Analysis	114
4.2	General Instability Criterion	128
4.3	Temporal Growth Rates	145
4.4	A Simple Example	154

5. CONVECTIVE VERSUS ABSOLUTE INSTABILITY

5.1	Distinguishing Between Convective and Absolute Instabilities	162
5.2	Determining the Transition Density	187
5.3	Absolute Instability Temporal Growth Rates	207
5.4	Realistic Stability Criteria for Finite Plasmas	213

6. VELOCITY-SPACE ANISOTROPY INSTABILITIES

6.1	Introduction; Temperature-Anisotropy Instabilities	222
6.2	Loss-Cone Instabilities	257
6.3	The Rosenbluth-Post "Continuum" Limit	300

7. "UNIVERSAL" INSTABILITIES

7.1 Introduction; Low Frequency Drift Instabilities 323
7.2 Drift-Cyclotron Instabilities 340
7.3 Combination Loss-Cone and Drift-Cyclotron Instability 378

8. CONCLUSION

8.1 Summary 391
8.2 Suggestions for Further Study 399

ACKNOWLEDGMENT 402

VITA 404

REFERENCES 406

APPENDICES

Appendix A: The Functions C and D 420

Appendix B: Plasma Dispersion Function Moments 426

Appendix C: Description of Computer Programs 430

LIST OF ILLUSTRATIONS

1.1	Plasma Model	35
4.1	Mapping Contour for Nyquist Diagram Technique ($R\to\infty$).	118
4.2	Nyquist and $F'(\omega/k)$ Plots for Various Types of Stable and Unstable Plasmas.	120
4.3	Behavior of the Functions $-2\ Z_0(w)$ and $-2\ Z_1(w)$ for Real w.	139
4.4	Nyquist and $P(\omega/\Omega_i)$ Plots for Temperature-Anisotropy Instability Case ($T_{Z_i}/T_{\perp_i}=10^{-3}$, $T_{Ze}/T_{Z_i}=1/20$, $\ell=1$, $k_y a_i=2.0$, $k_Z a_i=0.75$).	142
4.5	Typical Temporal Growth Rates for Temperature-Anisotropy Instabilities ($T_{Z_i}/T_{\perp_i}=10^{-3}$, $T_{Z_e}/T_{Z_i}=1/20$, $\ell=1$, $k_y a_i=2.0$).	151
4.6	Nyquist and $P(\omega/\Omega_i)$ Plots for Loss-Cone Instability Case ($T_{Z_i}/T_{\perp_i}=1.0$, $T_e/T_i=10^{-2}$, $\ell=1$, $k_y a_i=5.0$, $k_Z a_i=0.13$).	155
4.7	Typical Temporal Growth Rates for Loss-Cone Instabilities ($T_{Z_i}/T_{\perp_i}=1.0$, $T_e/T_i=10^{-2}$, $\ell=1$, $k_y a_i=5.0$).	157
4.8	Stability Map for Loss-Cone Instabilities with $k_y a_i=5.0$ ($T_{Z_i}/T_{\perp_i}=1.0$, $T_e/T_i=10^{-2}$, $\ell=1$).	159
5.1	Envelopes of Time Development of Convective and Absolute Instabilities.	163
5.2	Laplace and Fourier Inverse Transform Integration Contours.	169
5.3	Movement of Singularities in the k-plane as the Laplace Contour is Analytically Continued Down to the Real ω-axis (② and ⑤ are Convectively Unstable Modes).	171
5.4	Movement of Singularities in the k-plane as the Laplace Contour is Analytically Continued Down to the Real ω-axis (Coalescence of ① and ② at ω_B Indicates an Absolutely Unstable Mode).	173

5.5	Complex ω and k Solutions of the Dispersion Relation for a Set of Unstable Modes.	179
5.6	Appearance of an Absolute Instability as the Density Increases (λ decreases).	192
5.7	Typical Plot of $K(\omega)$, $H[\omega,K(\omega)]$ for Real Frequencies ($T_{Z_i}/T_{\perp_i}=1.0, T_e/T_i=10^{-2}, \ell=1, k_y a_i=5.0$).	195
5.8	Impossibility of Merging of Two Unstable Modes from a Given Isolated Set.	200
5.9	Simple Loss-Cone Instability Case.	204
5.10	B-R Contours for Simple Loss-Cone Instability Case ($T_e/T_i=10^{-2}, \ell=1, k_y a_i=5.0$). Crosses Indicate Absolute Instability Mode.	209
5.11	B-R Contours for a Loss-Cone Instability Case ($T_e/T_i=10^{-2}, \ell=1, k_y a_i=5.0$). Crosses Indicate Absolute Instability Mode. k_I Denotes $Im(k_Z)$.	210
6.1	Stability Map for Varying $T_{Z_i}/T_{\perp_i}$ with $T_e/T_{Z_i}=0.05, \ell=1$ (Taken from Beasley and Cordey (6.38) by permission of authors).	252
6.2	Effective Velocity Distribution in a Given Direction Perpendicular to the Magnetic Field Direction (Homogeneous Plasma, $\ell=1$).	261
6.3	Unstable Frequency Range with Varying $k_\perp a_i$ for Standard Loss-Cone Instability Case.	264
6.4	Effect of Varying $k_\perp a_i$ on Loss-Cone Instabilities.	269
6.5	Maximum Spatial Growth Rates of Convective Instabilities.	272
6.6	Variation of $Re(k_Z a_i)$ Along Curves in Fig. 6.4.	274
6.7	Variation of ω/Ω_i Along Curves in Fig. 6.4.	276
6.8	Effect of Varying T_e/T_i on Loss-Cone Instabilities ($\ell=1$).	279
6.9	Changes in Implicit Parameters for Varying T_e/T_i ($\ell=1$).	280

6.10 Effect of Varying T_e/T_i on $k_\perp a_i=5$ Loss-Cone Instability Modes ($\ell=1$). 284

6.11 Effect of Varying the Thermal Spread in $v_\perp$ Distribution on Loss-Cone Instabilities ($T_e/T_i=10^{-2}$). 286

6.12 Changes in Implicit Parameters for Varying ℓ ($T_e/T_i=10^{-2}$). 288

6.13 Effect of Varying the Thermal Spread in $v_\perp$ Distribution on $k_\perp \langle v_\perp \rangle / \Omega_i=5$ Loss-Cone Instabilities ($T_e/T_i=10^{-2}$). 293

6.14 Stability Map for $k_\perp a_i=25$ Loss-Cone Instability Case ($T_e/T_i=10^{-2}$, $\ell=1$). 313

6.15 Spatial Growth Rates of Convective Loss-Cone Instabilities for $k_\perp a_i=25$ ($T_e/T_i=10^{-2}, \ell=1$). 316

6.16 Real-k_Z Temporal Growth Rates of $k_\perp a_i=25$ Loss-Cone Instabilities ($T_e/T_i=10^{-2}, \ell=1$). 318

7.1 Nyquist and $P(\omega/\Omega_i)$ Plots for a Typical Low Frequency Drift Instability Case ($T_e=T_i=T_\perp=T_Z$, $\varepsilon' a_i=0.1, k_y a_i=5.0, k_Z a_i=0.0125$). 331

7.2 Effective Velocity Distribution in the y Direction (Inhomogeneous Plasma, $\frac{a_i}{n_i}\frac{dn_i}{dx} = -\varepsilon' a_i = 0.2$). 350

7.3 Unstable Frequency Range with Varying $k_y a_i$ for Standard Drift-Cyclotron Instability Case. 352

7.4 Nyquist and $P(\omega/\Omega_i)$ Plots for Drift-Cyclotron Instability Case ($T_e/T_i=10^{-2}$, $\varepsilon' a_i=-0.2$, $k_y a_i=25.0$, $k_Z a_i=0.085$). 355

7.5 Effect of Varying $k_y a_i$ on Drift-Cyclotron Instabilities. 358

7.6 Variations of $\mathrm{Re}(k_Z a_i)$ and ω/Ω_i Along Curves in Fig. 7.5 ($T_e/T_i=10^{-2}$, $\varepsilon' a_i=-0.2$). 362

7.7 Effect of Varying T_e/T_i on Drift-Cyclotron Instabilities ($\varepsilon' a_i=-0.2$). 365

7.8 Changes in Implicit Parameters for Varying T_e/T_i ($\varepsilon' a_i = -0.2$). 366

7.9 Effect of Varying $\frac{a_i}{n_i}\frac{dn_i}{dx} = -\varepsilon' a_i$ on Drift-Cyclotron Instabilities ($T_e/T_i = 10^{-2}$). 369

7.10 Changes in Implicit Parameters for Varying $\frac{a_i}{n_i}\frac{dn_i}{dx} = -\varepsilon' a_i$ ($T_e/T_i = 10^{-2}$). 370

7.11 Effect of Varying $k_y a_i$ on Drift-Cone Instabilities. 384

LIST OF TABLES

5.1 Properties of the Unstable Modes for the Simple Loss-Cone Instability Case ($T_e/T_i=10^{-2}$, $\ell=1$. $k_y a_i = 5.0$). 205

6.1 Properties of the "Marginally Stable" Absolute Instability Modes for $k_\perp a_i = 25$ Loss-Cone Instability Case ($T_e/T_i = 10^{-2}$, $\ell = 1$). 312

7.1 Sample Properties of Drift-Cone Instabilities for $k_y a_i < 10$ ($T_e/T_i=10^{-2}, \ell=1, \varepsilon' a_i=-0.2$). 386

7.2 Sample Properties of Drift-Cone Instabilities for $k_y a_i \geq 10$ ($T_e/T_i=10^{-2}, \ell=1, \varepsilon' a_i=-0.2$). 387

7.3 Sample Properties of Loss-Cone Instabilities for Comparison with Table 7.2 ($T_e/T_i=10^{-2}$, $\ell = 1$, $\varepsilon' a_i = 0.0$). 388

C-1 Imput Data Specifying Case to be Considered (Read in by INPUT or SINPUT). 433

1. INTRODUCTION

1.1 Introductory Remarks

It is generally agreed that a hot plasma confined to a specified region of space is necessary for the attainment of controlled thermonuclear fusion. Such a plasma is also of interest in astrophysical and space physics research. Since the only plasma distribution in thermodynamic equilibrium is a spatially uniform-Maxwellian velocity distribution, a confined plasma is necessarily not in equilibrium. Therefore the success of confinement is determined by the rate at which the confined plasma approaches thermodynamic equilibrium. The most obvious mechanism relaxing a plasma toward equilibrium is that of collisions, which, however, for a high enough temperature are so infrequent that this relaxation process would be very slow. At these high temperatures, if collisions were the only mechanism by which the plasma could relax itself toward equilibrium, confinement would be a simple problem. However in this regime of very infrequent collisions, the so-called "collisionless" regime, the plasma may relax itself toward equilibrium through various types of plasma instabilities which may lead either to turbulent diffusion or complete destruction of confinement. Plasma instabilities (1.1) are customarily divided into two classes: macroinstabilities and microinstabilities.

Generally speaking macroinstabilities are analogous to hydrodynamic instabilities and are derivable from the fluid equations of a plasma. Implicit in such a derivation are the assumptions that disturbances in the plasma have frequencies which are small compared to both the ion cyclotron frequency and the electron plasma frequency and have wavelengths which are long compared to the ion Larmor radius. These disturbances are large scale and when they are unstable, experiments with pinches, mirrors etc. have shown that they are violent and lead to rapid destruction of confinement. Fortunately however, as has been demonstrated both theoretically (1.2) and experimentally (1.3), most of these macroinstabilities can be stabilized by placing the plasma in a "magnetic well" which has an increasing magnetic field energy density in all directions normal to the confinement region, or by surrounding the confinement region by a heavily sheared magnetic field (1.4,1.5). Physically the "magnetic well" and the sheared magnetic field stabilize the plasma against macroinstabilities by impeding the flow of plasma out of the confinement region through magnetic pressure and by destruction of the large-scale coherence of the disturbances respectively. In addition to these magnetic field shaping techniques "line typing", that is, shorting out the transverse (to the magnetic field) electric fields driving the macroinstability through conducting end plates situated perpendicular to the magnetic

field, has been shown to be helpful in stabilizing some of the flute-like macroinstability modes encountered in magnetic mirror machines (1.6). In this work we will assume that the macroinstabilities can be stabilized by a suitable choice of the confinement scheme, and we are thus led to a consideration of the microinstabilities of a plasma.

In contrast to the fluid description of macroinstabilities, microinstabilities (1.7) are derived from a kinetic or microscopic description in which the details of the velocity distribution of the plasma are taken into account. Thus the microscopic treatment includes particle resonance effects which cannot be found in the fluid treatment. From the definitions of these two treatments, we see that all macroinstabilities are included in the microscopic treatment, albeit perhaps in an unrecognizable form. Therefore in general we define the microinstabilities to be those instabilities which can be derived only from a microscopic treatment of the plasma. In contrast to the macroinstabilities, we do not know at present how to stabilize all microinstabilities; in fact, we suspect that not all of them can be stabilizied. However, owing to their generally short wavelengths (less than or comparable to the ion Larmor radius), high frequencies (comparable to the ion cyclotron frequency) and small amounts of energy driving them, the microinstabilities

generally are expected to grow rapidly into the nonlinear regime where their growth is limited. They are therefore not expected to be as large scale and chaotic in their destruction of plasma confinement as the macroinstabilities. They may, nevertheless, cause rapid, small-scale, but relatively ordered diffusion of the plasma out of the confinement region and thus be very detrimental to plasma confinement.

The different types of microinstabilities can be conveniently classified according to the sources of "free energy" which are available to drive them. The free energy of a plasma (1.8) is defined to be that amount of energy which the plasma has in excess of the amount of energy in a uniform density plasma with the same number of particles in the same volume with a velocity distribution which is known to be stable against microinstabilities. For a strictly collisionless plasma with no magnetic field present, any equilibrium velocity distribution which is only a function of the kinetic energy has been shown to be stable against microinstabilities (1.9).

When a magnetic field is present, it is necessary to impose the further restriction that the distribution functions of each plasma particle species be monotonically decreasing functions of the single particle energy (1.10). Two important consequences of these proofs of stability for particular distribution functions are:

1) Microinstabilities cannot relax nonequilibrium plasmas toward a Maxwellian distribution.

2) Microinstabilities cannot exchange energy between different plasma particle species if all species have distribution functions which are monotonically decreasing functions of the kinetic energy.

With these observations in mind we see that the principal sources of free energy in a hot confined plasma are:

1) Expansion energy due to the lack of spatial homogeneity of the plasma,

2) Anisotropies in the velocity distribution, including the kinetic energy of drifts in the plasma and inequality of the mean velocities along and transverse to the magnetic field,

3) Diamagnetic field energy.

In this work we will neglect the diamagnetic field energy, since for a sufficiently low value of β (i.e., small ratio of plasma kinetic to magnetic field energy density) this contribution to the free energy is small and can only feed transverse (electromagnetic) waves (1.8) which we will neglect (see following section). We also note that very little of the expansion energy is available to drive the microinstabilities since we know that this is the main source of free energy driving the macroinstabilities which we are assuming to be stabilized.

The general procedure we follow in considering the effects of microinstabilities begins with the hypothesis that for reference purposes we have available a "perfect" plasma which has no free energy reservoirs and is consequently microscopically stable. Then we introduce a single particular source of free energy and determine whether or not the plasma is stable. If it is unstable we consider the potential danger of the induced microinstability. Doing this for a wide variety of particular free energy sources, we can ascertain which sources of free energy lead to microinstabilities that are the most detrimental to plasma confinement. With this information we are then able to make critical judgements as to the most prospective methods of plasma buildup and confinement. While we probably cannot avoid all of the microinstabilities inherent in a real plasma, through a judicious choice of plasma confinement procedures we may be able to overcome the mild destruction of confinement due to the remaining instabilities by continuously injecting enough plasma to make up for these losses.

Most microinstabilities exist in a plasma only if the plasma is sufficiently dense. Therefore the first measure of the potential danger of a particular type of instability is the density at which it appears. We will call this density the "threshold density." The usual method of determining the threshold density is through a marginal

stability analysis for which a general criterion for the stability of electrostatic waves in a homogeneous magnetized plasma is already known (1.11). In this work the general criterion is extended to weakly inhomogeneous magnetized plasmas and put into a form in which the threshold density is easily determined.

For densities exceeding the threshold density, it has been known for some time that we must distinguish between two types of instabilities: convective and absolute (**non**convective) instabilities (1.12). The difference between these two types of instabilities is that for a disturbance which is initially localized in both space and time the absolute instability grows temporally at all points in space while the convective does not; the convective instability wave packet also grows temporally, but it is "convected" away from the point of the initial disturbance. Thus, in determining the potential danger of various microinstabilities we will be interested in the spatial growth rates of those micro-instabilities which are convective and in the temporal growth rates of those which are absolute. Most micro-instabilities are convective for densities only slightly exceeding the threshold density, but become absolute for higher densities. Since the spatial growth rates of the convective instabilities are usually small, for bounded media with relatively little wave reflection from the edges,

the density at which the instability becomes absolute (nonconvective) is an important indication of the inherent danger of the microinstability. We will call this density the "transition density." While the spatial growth rates of the convective instabilities are relatively easy to determine, the properties of the absolute instabilities are generally much more difficult to obtain. A major contribution of this thesis (1.13) is the development of a relatively simple method for determining the transition density and the temporal growth rates of absolute instabilities in plasmas. Another important contribution of this thesis (1.14) is the understanding of absolute and convective loss-cone and drift-cyclotron instabilities which has been gained through the application of this new method.

1.2 General Approximations

In this work we will consider a hot, fully ionized, collisionless plasma. By this we mean that the plasma is sufficiently hot (but still nonrelativistic) and sparse so that the collisionless Boltzmann or Vlasov equation governs the time development of the plasma. This will be true if the collision frequency is much less than the natural oscillation frequency of the plasma, the plasma frequency. In this case the electric field fluctuations due to the collective oscillations of the plasma are much more rapid than the time required for large-angle Coulomb scattering of particles to occur by either a single collision or the accumulation of many small-angle collisions.

In order to estimate the plasma conditions necessary for the satisfaction of this intuitive criterion, we will compute the collision frequency by the usual formula $n_o \sigma v$ where here for the cross section σ we take the square of the distance of maximum particle separation for which appreciable (90°) Coulomb deflections can occur, and for v we take the electron thermal velocity. Using these estimates we can show that our intuitive criterion that the collision frequency be small compared to the plasma frequency reduces to the requirement that there be many particles within a sphere whose radius is the Debye length $\lambda_D = \left(\frac{KT}{4\pi n_o q^2}\right)^{\frac{1}{2}}$, i.e.,

$$n_o \lambda_D^3 >> 1 \qquad (1.2.1)$$

where n_o is the plasma density. Rigorous analyses (1.15) confirm that this condition is indeed appropriate to justify the use of the Vlasov equation. Condition (1.2.1) is satisfied for a wide range of plasmas of interest, including thermonuclear plasmas.

Assuming that we can neglect the effects of collisions, the electrons and each ion species in the plasma obey the Vlasov equation:

$$\frac{\partial f_j}{\partial t} + \underline{v} \cdot \frac{\partial f_j}{\partial \underline{x}} + \frac{\underline{F}_j}{m_j} \cdot \frac{\partial f_j}{\partial \underline{v}} = 0 \qquad (1.2.2)$$

where

f_j = $f_j(\underline{x},\underline{v},t)$ is the plasma distribution function at the spatial position $\underline{x}$ and velocity $\underline{v}$ at time t for the j^{th} type of particle,

m_j = mass of the j^{th} type of particle,

$\underline{F}_j$ = $q_j(\underline{E} + \frac{1}{c}\,\underline{v} \times \underline{B}) + \underline{F}_j^{ext}$, the force (Lorentz force plus an external force) on the j^{th} type of particle,

q_j = charge on the j^{th} type of particle.

In addition to these equations we need the full set of Maxwell's equations to describe how the electric field $\underline{E}$

and the magnetic field $\underline{B}$ vary in space and time. From Maxwell's equations we see that the electric and magnetic fields depend linearly on the distribution functions $f_j(\underline{x},\underline{v},t)$ and thus that the Vlasov equation is nonlinear in the distribution function. We will linearize the Vlasov equation since here we are only looking for the possible parametric ranges of instability and the initial growth rates of the instabilities, both of which can be determined from a linear analysis. The nonlinear terms which are neglected may lead to time asymptotic stabilization of potentially unstable oscillations, but such questions are beyond the scope of this work.

In order to linearize we assume that the distribution function and the electric and magnetic fields are equal to their equilibrium or average values plus very small perturbations:

$$f_j = \langle f_j(\underline{x},\underline{v}) \rangle + \delta f_j(\underline{x},\underline{v},t)$$

$$\underline{E}(\underline{x},t) = \delta\underline{E}(\underline{x},t)$$

$$\underline{B}(\underline{x},t) = \underline{B}(\underline{x}) + \delta\underline{B}(\underline{x},t)$$

where here we have assumed that any nonzero average electric field is included in the external force term. As an initial condition (at $t = -\infty$), we presume that the plasma is in its equilibrium or average state except for

a very small group of particles which deviates from this state only by an incremental amount due to their random thermal motion. At time t the perturbed quantities listed above represent the perturbations which have evolved from the originally minuscule perturbations. In order to justify the linearization of the Vlasov equation, we must also presume that at time t the perturbations are still "small." Substituting the proposed forms listed above into the Vlasov equation and ignoring the second order (nonlinear) terms in the perturbed quantities, we obtain for the zero- and first-order Vlasov equations

$$\left[\underline{v}\cdot\frac{\partial}{\partial \underline{x}} + \frac{1}{m_j}\left(\frac{q_j}{c}\,\underline{v}\times\underline{B} + \underline{F}_j^{ext}\right)\cdot\frac{\partial}{\partial \underline{v}}\right]\left\langle f_j(\underline{x},\underline{v})\right\rangle = 0 \tag{1.2.3}$$

$$\left[\frac{\partial}{\partial t} + \underline{v}\cdot\frac{\partial}{\partial \underline{x}} + \frac{1}{m_j}\left(\frac{q_j}{c}\,\underline{v}\times\underline{B} + \underline{F}_j^{ext}\right)\cdot\frac{\partial}{\partial \underline{v}}\right]\delta f_j(\underline{x},\underline{v},t)$$

$$+ \frac{q_j}{m_j}\left(\delta\underline{E} + \frac{1}{c}\,\underline{v}\times\delta\underline{B}\right)\cdot\frac{\partial\left\langle f_j(\underline{x},\underline{v})\right\rangle}{\partial \underline{v}} = 0. \tag{1.2.4}$$

The zero-order or equilibrium Vlasov equation (1.2.3) determines the functional form of the equilibrium distribution function $\langle f_j \rangle$. The first-order or perturbed Vlasov equation (1.2.4) prescribes the time evolution of the plasma perturbation δf_j for the particular equilibrium distribution under consideration.

Next we consider the question of under what conditions we may neglect transverse waves.* Normally the statement is made that "for sufficiently rarefied plasmas (low β) only electrostatic waves need be considered" and the problem is thereby ignored. In the following we will explore the background of this statement through a very approximate analysis of the problem. The analysis consists of two parts. First, it is demonstrated that for the waves of interest if we can show that the transverse parts of the electric field components are much smaller than the corresponding longitudinal parts, then the transverse waves are decoupled from the longitudinal waves and are unimportant in this work. Next we consider the limitations imposed on the β of the plasma so that we can meet this condition.

Before proceeding to this analysis, we specify the types of waves which are of interest. Since microinstabilities derive from strong particle-wave resonance effects, we obviously need not consider those waves whose phase velocities lie in regions of velocity space where there

---

* In this section "transverse" waves will always mean transverse electromagnetic waves, that is, waves whose propagation vectors are orthogonal to their electric field vectors, irrespective of their orientation with respect to the static magnetic field.

are few particles. As we are considering only non-relativistic plasmas, this means that we need only consider waves whose phase velocities are small compared to the velocity of light. Next we note that while we are excluding very low frequency waves by assuming the macro-instabilities to be stabilized, we still want to consider those waves with the next lowest frequencies of interest. These will often be waves with frequencies near the ion cyclotron frequency, a consequence of which is that the magnetic moment is no longer an invariant and "minimum-B" confinement cannot be expected to stabilize such waves. We are interested in waves having the lowest possible frequencies because for noise-initiated plasma instabilities the higher the frequency the more rapid the fluctuations and generally the smaller their scale of spatial influence (to maintain phase velocities small compared to the velocity of light). We also note that many of the high frequency microinstabilities have relatively large growth rates and consequently would be expected to rapidly grow into the nonlinear regime where their growth rates and confinement destruction capacity are presumably limited due to the small amount of energy available to drive them (1.7). Thus we will only consider frequencies which are small compared to the ion cyclotron frequency and/or of the order of or slightly larger than the ion cyclotron frequency, but always small compared to the electron cyclotron frequency.

For the purposes of the analysis in this section, we will assume that a static magnetic field is present and that the plasma is sufficiently uniform in all directions to allow us to apply normal Fourier transform techniques. We also assume that we have solved (1.2.4) in some appropriate fashion to yield the tensorial conductivity $\underline{\underline{\sigma}}$ of the plasma. Under such assumptions, for a superposition of plane waves of the form $e^{i(\underline{k}\cdot\underline{x}-\omega t)}$ the perturbed electric field wave equation deduced from Maxwell's equations is

$$\frac{\underline{k} \times (\underline{k} \times \delta\underline{E})}{k^2} = \frac{4\pi\omega}{ic^2k^2}\,\underline{\underline{\sigma}} \cdot \delta\underline{E} - \frac{\omega^2}{c^2k^2}\,\delta\underline{E} \qquad (1.2.5)$$

where $k = |\underline{k}|$ and the implicit subscript $\underline{k},\omega$ on $\delta\underline{E}$ has been omitted for simplicity in notation. For convenience we define

$$\underline{\underline{\alpha}} = -\frac{4\pi\omega}{ic^2k^2}\,\underline{\underline{\sigma}} \qquad (1.2.6)$$

and then choosing a coordinate system in which the third component of the electric field vector $\delta\underline{E}$ is aligned along the propagation vector $\underline{k}$, we can write the vector wave equation as

$$\begin{bmatrix} \frac{\omega^2}{c^2k^2} - 1 + \alpha_{11} & \alpha_{12} & \alpha_{13} \\ \alpha_{21} & \frac{\omega^2}{c^2k^2} - 1 + \alpha_{22} & \alpha_{23} \\ \alpha_{31} & \alpha_{32} & \frac{\omega^2}{c^2k^2} + \alpha_{33} \end{bmatrix} \begin{bmatrix} \delta E_{T_1} \\ \delta E_{T_2} \\ \delta E_{\ell} \end{bmatrix} = \begin{bmatrix} 0 \\ 0 \\ 0 \end{bmatrix} \qquad (1.2.7)$$

where δE_{T_1}, δE_{T_2} and δE are respectively the two transverse components and the longitudinal component of the electric field $\delta\underline{E}$. From the theory of linear algebra (1.16) we know that the perturbed electric field $\delta\underline{E}$ can have a nontrivial solution only if the determinant of its coefficient matrix (tensor) vanishes. The resultant equation prescribes the relations between the frequency ω and wave vector $\underline{k}$ of the allowed waves and is called the dispersion relation:

$$\begin{vmatrix} \frac{\omega^2}{c^2k^2} - 1 + \alpha_{11} & \alpha_{12} & \alpha_{13} \\ \alpha_{21} & \frac{\omega^2}{c^2k^2} - 1 + \alpha_{22} & \alpha_{23} \\ \alpha_{31} & \alpha_{32} & \frac{\omega^2}{c^2k^2} + \alpha_{33} \end{vmatrix} = 0. \qquad (1.2.8)$$

The terms α_{ij} which arise from the perturbed currents in the plasma are typically small and all of comparable magnitudes except for some particular choices of wave propagation directions (1.17). For the moment we will assume that they are all nearly equal. Our previous statement that we need only consider waves whose phase

velocities are small compared to the velocity of light is represented here by the condition

$$\frac{\omega^2}{c^2k^2} \ll 1 \quad . \tag{1.2.9}$$

Now, by our choice of the electric field vector coordinate system, the 3-3 component of the dispersion relation (1.2.8) when set equal to zero yields the dispersion relation for electrostatic (longitudinal) waves:

$$\frac{\omega^2}{c^2k^2} + \alpha_{33} = 0 \quad . \tag{1.2.10}$$

Having assumed that all of the α_{ij}'s are of comparable magnitudes, we conclude from this last equation [together with condition (1.2.9)] that the α_{ij}'s are small compared to unity. Considering the general dispersion relation (1.2.8), we see that under these conditions only an electrostatic wave whose dispersion relation is given by (1.2.10) and two transverse waves with dispersion relations given by

$$\omega \approx ck \tag{1.2.11}$$

exist in the plasma. Furthermore the longitudinal and transverse waves are nearly decoupled from each other. The transverse wave dispersion relation (1.2.11) is characteristic of nearly undamped plane electromagnetic waves which

propagate almost unaffected by the presence of the plasma and hence are of no concern to us in our consideration of microinstabilities.

When the α_{ij}'s are not all necessarily of comparable magnitudes, the situation becomes a bit more difficult, for then we cannot make such concrete statements about the decoupling and irrelevance of transverse waves simply by examining the general dispersion relation (1.2.8). Instead we will consider the general wave equation (1.2.7). Using the results of the preceding paragraph as a guide, we want to consider the implications of considering only those waves whose phase velocities are much smaller than the velocity of light. Excluding the possibility of fortuitous cancellations, an examination of (1.2.7) reveals that if by some independent means we could show that for the waves of interest

$$\left|\delta E_{T_{1,2}}\right| << \left|\delta E_{\ell}\right| \qquad (1.2.12)$$

then we would know that the α_{ij}'s are all small compared to unity, and our previous conclusions about transverse waves would remain correct. Therefore as long as for those waves whose phase velocities are small compared to the velocity of light we can show that condition (1.2.12) holds, the transverse waves are nearly decoupled from the longitudinal waves and unimportant in this work.

We will now consider the conditions under which we can satisfy condition (1.2.12). Here we will use the plasma dielectric constant $\underline{\underline{\epsilon}}$ which is defined by

$$\underline{\underline{\epsilon}} = \underline{\underline{I}} + \frac{4\pi i}{\omega} \underline{\underline{\sigma}} \qquad (1.2.13)$$

where $\underline{\underline{I}}$ is the identity matrix (tensor) and as before $\underline{\underline{\sigma}}$ is the plasma conductivity tensor. We will also revert to a normal rectangular coordinate system with the magnetic field parallel to the z axis and decompose the electric field vector into its transverse and longitudinal parts in this coordinate system. The longitudinal or electrostatic part is representable by a potential, i.e.,

$$\delta\underline{E} = -i\underline{k}\,\phi$$

and therefore we can write the perturbed electric field as

$$\delta\underline{E} = \delta\underline{E}_{\ell} + \delta\underline{E}_{T} = -i\underline{k}\,\phi - \frac{\underline{k} \times (\underline{k} \times \delta\underline{E})}{k^2} . \qquad (1.2.15)$$

Using (1.2.5) to define the transverse part of the electric field and the definition of the dielectric constant (1.2.13), we can write this last equation as

$$\delta\underline{E} = -i\underline{k}\,\phi + \frac{\omega^2}{c^2k^2} \underline{\underline{\epsilon}} \cdot \delta\underline{E} . \qquad (1.2.16)$$

The first term in the expression on the right is the longitudinal electric field $\delta\underline{E}_\ell$ and the second is the transverse electric field $\delta\underline{E}_T$. In order to compare the two parts of the electric field, we will assume that $\delta\underline{E}$ is approximately given by the longitudinal part $\delta\underline{E}_\ell$ and see under what conditions this assumption holds. Using the definition of the longitudinal part in terms of a potential (1.2.14) for the perturbed electric field in the second term of (1.2.16), we see that

$$\delta\underline{E} \approx - i\phi \left[\underline{k} + \frac{\omega^2}{c^2k^2} \underline{\underline{\epsilon}} \cdot \underline{k}\right] . \quad (1.2.17)$$

Thus the condition that the transverse part of the electric field be small compared to the longitudinal part reduces to a condition that $\underline{k}$ be large compared to $\frac{\omega^2}{c^2k^2} \underline{\underline{\epsilon}} \cdot \underline{k}$ for all directions $\underline{k}$. In the directions perpendicular to the magnetic field, we assume that the plasma is sufficiently isotropic so that it is unnecessary to distinguish particular directions in this plane. With this assumption, for waves propagating perpendicular to the magnetic field direction, condition (1.2.12) reduces approximately to

$$1 >> \frac{\omega^2}{c^2k^2} \left|\epsilon_\perp\right| \quad (1.2.18)$$

where $\epsilon_\perp$ is the perpendicular component of the dielectric constant of the plasma. Desiring to use only this one part

of the dielectric constant, we note that the displacement vector $\delta\underline{D}$ is defined in terms of the electric field $\delta\underline{E}$ by

$$\delta\underline{D} = \underline{\underline{\epsilon}} \cdot \delta\underline{E} \ . \qquad (1.2.19)$$

Then, remembering that we have lumped all of the effects of the plasma particle motions into the dielectric constant and thus have no "free" charges, we see from Gauss' law that

$$\underline{k} \cdot \delta\underline{D} = 0$$

or that

$$k_\perp \, \delta D_\perp = k_z \, \delta D_z \ . \qquad (1.2.20)$$

Using this last relation to define δD_z and thus $(\underline{\underline{\epsilon}} \cdot \underline{k})_z$, we see that for propagation along the magnetic field direction condition (1.2.12) reduces to

$$1 >> \frac{\omega^2}{c^2 k_z^2} \left|\epsilon_\perp\right| \left(\frac{k^2}{k^2}\right) \ . \qquad (1.2.21)$$

Next we consider the implications of conditions (1.2.18) and (1.2.21) on the β of the plasma. As a first step in this direction, we must specify the perpendicular dielectric constant $\epsilon_\perp$. In doing so it will be sufficient for this crude analysis to use the "cold plasma" dielectric constant which for our case is given roughly by (1.18)

$$\epsilon_\perp \approx \begin{cases} 1 + \dfrac{\omega_{p_i}^2}{\Omega_i^2} + \dfrac{\omega_{p_e}^2}{\Omega_e^2}, & \omega << \Omega_i \\ 1 + \dfrac{\omega_{p_e}^2}{\Omega_e^2}, & \Omega_i \lesssim \omega << \Omega_e \end{cases} \qquad (1.2.22)$$

where $\omega_{p_j} = (4\pi n_j q_j^2/m_j)^{1/2}$ (the plasma frequency) and $\Omega_j = q_j|\underline{B}|/m_j c$ (the cyclotron frequency). These expressions are the so-called "static" perpendicular dielectric constants in the presence of a magnetic field. For frequencies small compared to the ion cyclotron frequency, $\epsilon_\perp$ reflects the fact that both the ions and electrons are constrained from moving large distances in the perpendicular plane by the magnetic field. For frequencies of the order of or slightly greater than the ion cyclotron frequency, the ions can interact with the waves in such a way that they can move large distances in the perpendicular plane and hence do not contribute to the "static" dielectric constant. Assuming that the unity terms in (1.2.22) are negligible (the case of greatest interest here), we can write conditions (1.2.18) and (1.2.21) as

$$1 >> \frac{\omega^2}{c_{A_i}^2 k^2} \;, \quad 1 >> \frac{\omega^2}{c_{A_i}^2 k_z^2}\left(\frac{k_\perp^2}{k^2}\right) \;, \quad \omega << \Omega_i$$

$$1 >> \frac{\omega^2}{c_{A_e}^2 k^2} \;, \quad 1 >> \frac{\omega^2}{c_{A_e}^2 k^2}\left(\frac{k_\perp^2}{k^2}\right) \;, \quad \Omega_i \lesssim \omega << \Omega_e \qquad (1.2.23)$$

where $C_{A_j} = \dfrac{|\underline{B}|}{\sqrt{4\pi n_j m_j}}$ is the Alfvén speed. (Strictly speaking C_{A_e} is not really an Alfvén speed, but we will label it so here for convenience.) Now, since the wave phase speed in any given direction must resonant with a reasonable number of particles to produce a microinstability, we will set the phase speeds in these relations equal to the largest mean velocity in the plasma--the electron thermal velocity. Under this assumption we can write conditions (1.2.23) simply as

$$\beta << \frac{m_e}{2m_i} \;, \quad \omega << \Omega_i \qquad (1.2.24)$$

$$\beta << \frac{1}{2} \;, \quad \Omega_i \lesssim \omega << \Omega_e \qquad (1.2.25)$$

where here

$$\beta \equiv \frac{n_e k T_e}{B^2/8\pi} \approx \frac{1}{2} \frac{\text{plasma kinetic energy density}}{\text{magnetic field energy density}} \;. \qquad (1.2.26)$$

Thus, as long as the plasma pressure is sufficiently small compared to the magnetic field pressure, we may neglect the

transverse waves. Conditions (1.2.24) and (1.2.25) have also been derived by other authors ((1.19,1.20 and 1.21) respectively).

We can understand the physical significance of these conditions by referring back to (1.2.23). There we see that to neglect transverse waves we are requiring that the waves of interest (those with phase velocities near the thermal velocity) have much smaller phase velocities than the appropriate Alfvén speed and hence do not couple to or drive the transverse Alfvén waves. The appropriate Alfvén speed will be larger than the thermal velocities, providing the mass of the plasma particles "tied" to each magnetic field line is small enough. Conditions (1.2.24) and (1.2.25) prescribe the appropriate values of β, and hence plasma density for which the mass "tied" to the magnetic field lines is small enough. For larger values of β not satisfying these conditions, the mass "tied" to the magnetic field lines can move due to the transverse waves and thus "bends," but does not compress, the magnetic field lines. Many times in considering the effects of transverse waves it is only necessary to consider this "bending" of the magnetic field lines (1.22), however such considerations are beyond the scope of the present work.

1.3 Plasma Model

The exact determination of all of the microinstabilities which arise in a real plasma is an extremely difficult if not impossible task. We therefore consider here only an idealized plasma model which exhibits some of the most important features of a real plasma. The spatial part of the plasma model chosen is illustrated in Figure 1.1.

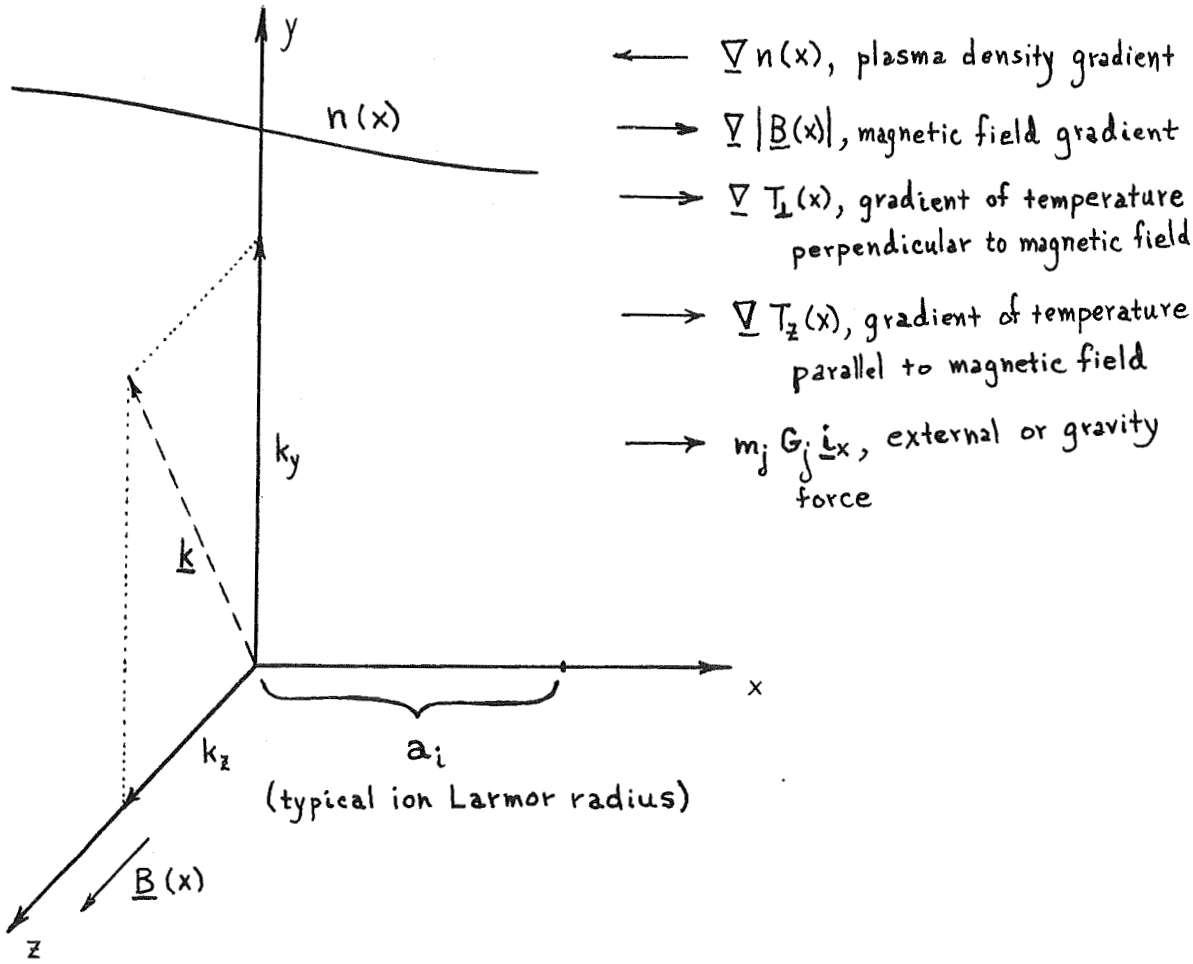

Figure 1.1. Plasma Model.

An important feature of this plasma model is that it is uniform in the y and z directions, but not in the x

direction. The maximum nonuniformity (locally) in the x direction is assumed to occur at the point x = 0 where the plasma has small (in terms of the ion Larmor radius) gradients of the magnetic field ($\nabla|B|$) and of the plasma density (∇n) and temperatures perpendicular ($\nabla T_\perp$) and parallel (∇T_z) to the magnetic field, i.e., a very general pressure gradient. Since there is free energy associated with the spatial distribution of a plasma unless it is homogeneous, each of these plasma inhomogeneities constitute sources of free energy. As noted in Fig. 1.1, we allow for an external or gravity force in the x direction which is also a source of free energy since in conjunction with the magnetic field it induces particle drifts in the y direction (see Section 3.2). This gravity force can be used to represent magnetic field curvature effects to a limited degree (see Section 2.4).

For large values of x (compared to the ion Larmor radius) the plasma is assumed to be uniform in the x direction. We will, however, only consider perturbed electric fields which can be localized (i.e., not involve plane waves extending to plus and minus infinity) in the x direction so that we need consider the characteristics of the plasma only around x = 0 (see Section 3.3). The magnetic field in this plasma model is in the z direction, and electrostatic waves are allowed to propagate in the y,z plane. Finally, we note that a small diamagnetic

current in the y direction is necessarily associated with the presence of a density (really pressure) gradient in the x direction.

Although our plasma model can represent many real plasmas, we will choose to visualize it in terms of its application to a magnetic mirror machine. The plasma model corresponds physically to that section of the plasma in a magnetic mirror machine which is off of the mirror axis and near the midplane between the magnetic mirrors. The x,y,z axes of the model correspond locally to the radial, azimuthal and axial directions respectively. We are justified in our use of a local rectangular coordinate system to describe the magnetic mirror machine only if we are far off of the magnetic mirror axis (in terms of the ion Larmor radius).

It will be noted that our plasma model does not have any provision for magnetic shear. Since one of the principal effects of shear is to change the orientation of the wave vector with respect to the magnetic field (1.20,1.23) and thus cause "uncertainty" in the wave vector, one might think that we could crudely take magnetic shear into account by examining the effects of these uncertainties in the wave vector for a particular instability. However, recent calculations (1.24) have shown that when magnetic shear is present the "local" theory and normal mode analysis such as that employed in this work are insufficient to

describe the convective nature and nonlocalization of the instabilities in the x direction. Rather, it is necessary to consider the growth and decay of wave packets of normal modes, the components of which may all be stable (1.24). Therefore we see that within the framework of the present work, very little if anything can be said about the effects of magnetic shear.

Next we specify the velocity distribution of our plasma model. In the z direction (along the magnetic field), we choose it to be a Maxwell-Boltzmann ("Maxwellian") distribution. We allow for the possibility of a current in the z direction by centering the Maxwellian around a given drift velocity, which may of course be zero.

In the plane perpendicular to the magnetic field, at least for homogeneous plasma cases (see Section 2.2), we use one of the set of velocity distributions first introduced by Dory et al. (1.25):

$$F_\perp^\ell(v_\perp) = \frac{1}{\pi\alpha_\perp^2\,\ell!}\left(\frac{v_\perp^2}{\alpha_\perp^2}\right)^\ell e^{-v_\perp^2/\alpha_\perp^2}, \quad \ell = 0,1,\ldots \tag{1.3.1}$$

For $\ell=0$ this distribution function is simply a Maxwellian. For $\ell>0$ the distribution function is zero at $v_\perp=0$ and peaked about $\langle v_\perp\rangle \equiv \alpha_\perp\sqrt{\ell}$ with a half-width at half-maximum of roughly $\alpha_\perp/2$. Thus for $\ell>0$ the total velocity distribution is cylindrically "cut-out" along the v_z axis

and therefore fairly representative of the v_z axis double-conical "cut-out" distribution which is characteristic of a magnetic mirror machine (1.26). While we do sacrifice some generality, this representation of the so-called "loss-cone" distribution of magnetic mirror machines is much easier to manipulate mathematically and results in greatly simplified dispersion relations. Finally, we note that as ℓ approaches infinity the velocity distribution given by (1.3.1) becomes a Dirac delta function (1.27) centered about $\alpha_\perp$. For further discussion of these distribution functions, see Section 6.2.

From our previous remarks on free energy, we see that our choice of the velocity distribution function includes three distinct velocity space anisotropy free energy sources. First there is the energy associated with drifts along the magnetic field. Next for $\ell > 0$ there is the free energy reservoir arising from the effective "drift" in any given direction transverse to the magnetic field direction due to the "loss-cone" nature of the $v_\perp$ distribution (see Section 6.2). Finally the average thermal velocities perpendicular and parallel to the magnetic field may be unequal, in which case the energy associated with the equilibration of the temperatures perpendicular and parallel to the magnetic field is a source of free energy.

The plasma model we have delineated in the preceding paragraphs will not be considered in its entirety in each

particular microinstability calculation. Rather, for each particular case we treat we will eliminate all but one or two of the free energy sources and explore the resultant microinstability. However, in order to demonstrate the generality of the procedures developed here, we will use the complete plasma model throughout our discussion of the marginal stability analysis and our development of techniques for determining the convective or absolute nature of the instabilities.

1.4 Thesis Guide

In this section we give a synopsis of the problems considered and particular points of interest in each of the chapters and appendices of the thesis.

The first three chapters are concerned with a statement of the problem and a derivation of the dispersion relation for the waves of interest. In this first chapter we have been concerned with giving an introduction to the thesis problem. In this regard we have discussed the general aspects of the problem of microinstabilities and the general approximations which are employed therein, either explicitly or implicitly. The question of how small the β of the plasma must be so that we can safely neglect transverse waves is considered in more detail than usual and in a unified way for all waves with frequencies less than the electron cyclotron frequency. Finally, in this first chapter we have delineated the plasma model which will be used in the following chapters. In the next chapter the equilibrium distribution of the plasma is considered in detail. In doing so, first the general form of the equilibrium distribution is found. Next, its particular form and the parametric restrictions imposed upon it by the requirements of equilibrium are specified. Finally, some comments are made on the generally unrecognized restrictions imposed by equilibrium considerations on the magnitude of the gravity force when it represents magnetic field curvature

effects. In the third chapter we derive the dispersion relation for our plasma model. In this derivation particular emphasis is placed on understanding the physical significance of the terms in the dispersion relation. The first step in this chapter is the derivation of an integro-differential dispersion equation which includes the possibility of potential fluctuations in the x direction. Next, the unperturbed orbits of the particles are calculated. Using these orbits and the integro-differential dispersion equation, we derive a general dispersion relation by using a "local" approximation for the potential fluctuations in the x direction. This derivation includes some effects (mainly for frequencies large compared to the ion cyclotron frequency) which have not previously been considered and results in further usually unrecognized constraints on the allowed magnitude of the gravity force. Finally, we find the dispersion relation for the general equilibrium distribution function which is specified in Chapter 2.

The next two chapters are concerned with a stability analysis and the development of simplified methods for determining the transition density and the growth rates of convective and absolute instabilities. In the fourth chapter we consider the question of stability for the plasma we are considering. First, we discuss the marginal stability analysis and its justification for a spatially uniform

plasma without a magnetic field. Next we extend this work to the case of a weakly inhomogeneous plasma in a magnetic field characterized by the dispersion relation of Chapter 3 and obtain a general instability criterion in a form suitable for direct computation of the threshold density for a given mode. Then we discuss methods of determining the temporal growth rates for real wave vector modes and the merits and limitations of such results. Finally, we consider a simple example of a "loss-cone" driven instability to demonstrate the methods developed. In the fifth chapter we address ourselves to the problem of distinguishing between convective and absolute instabilities. First we discuss the need for such information and review the absolute-convective instability criteria presently available. Next we develop a simplified method for locating the density at which the transition from convective to absolute instability occurs. Then we go on to develop and contrast various methods of determining the growth rates (spatial for convective instabilities and temporal for absolute instabilities) for the unstable modes. In addition, considering the very dissimilar effects of convective and absolute instabilities, we make a few remarks about realistic stability criteria for finite plasmas based upon the study of an infinite plasma model. Throughout this chapter we use the simple "loss-cone"

instability example discussed in the preceding chapter to illustrate the procedures developed.

In Chapters 6 and 7 we consider two very general types of microinstabilities in more detail. In Chapter 6 we discuss microinstabilities driven by velocity-space anisotropies. First, we thoroughly review the literature concerning these homogeneous plasma instabilities. Then, eliminating all but the "loss-cone" source of free energy, we carry out extensive numerical computations employing the techniques developed in Chapters 4 and 5 to determine the parametric regions of convective and absolute instability. The effects of varying k_z, $k_\perp$, T_e/T_i and ℓ (sharpness of the $v_\perp$ distribution) are considered. We also review the work which has been carried out using the short transverse wavelength limit of the dispersion relation (1.7,1.28). Then, to see how applicable this limit of the dispersion relation is, we consider a particular very short wavelength case ($k_\perp a_i = 25$) using the exact dispersion relation. In the seventh chapter we consider the so-called "universal" instabilities, that is those driven by a density and/or temperature gradient source of free energy. We begin by briefly reviewing the work on low frequency drift instabilities (1.7,1.19,1.20,1.22,1.23). Then, we consider the drift-cyclotron instabilities (1.29) in more detail. The latter work includes extensive numerical computations of the parametric regions of convective and absolute instability

for varying k_z, $k_\perp$, T_e/T_i and $\epsilon' a_i$ (density gradient scale length). Finally, we briefly consider the instabilities that occur in a plasma which has both density gradient and loss-cone sources of free energy.

In Chapter 8 we give a general summary of the important results found in this work and suggestions for further study. The C and D functions which arise in the derivation of the dispersion relation are discussed in Appendix A. In the next appendix we discuss the singular integrals which arise in the derivation of the dispersion relation and how they can be related to the plasma dispersion function and its derivatives. The formulas developed therein may be of general usefulness in deriving dispersion relations for plasmas with Maxwellian velocity distributions. Finally, in Appendix C we describe the general computer programs which were developed in this work and used to obtain the results displayed in Chapters 4,5,6 and 7. In this appendix we also derive a form of the dispersion relation which is more suitable for numerical computations than that given in Chapter 3 in that it requires fewer time-consuming evaluations of the plasma dispersion function and its derivatives. Since the particular cases considered in this work by no means exhaust the possible uses of the computer programs developed, these programs could be advantageously used in studying many other micro-instabilities of interest.

2. EQUILIBRIUM STATE

2.1 Constants of the Motion

In this chapter we will consider the equilibrium distribution function solutions of the zero-order or equilibrium Vlasov equation (1.2.3). The term "equilibrium distribution" as used in this and all subsequent chapters refers to the fact that a plasma having such a distribution has no net forces acting on it. Since the equilibrium Vlasov equation is simply a statement of the fact that the total time derivative of the equilibrium distribution must vanish, it is easy to see that any equilibrium distribution function which is only a function of the constants of the motion of particles moving in the plasma is a solution of this equation. Hence our task of finding an appropriate equilibrium distribution function begins with the determination of the constants of the motion.

The constants of the motion are the conserved quantities which are derived from the principles of conservation of momentum and energy. From the Hamiltonian formulation of classical mechanics (2.1), we know that a given canonical momentum component will be a conserved quantity only if the Hamiltonian is independent of the canonically conjugate spatial component. In order to determine which components of the canonical momentum are constants of the motion, we

must specify the magnetic vector potential. For the geometry shown in Figure 1.1, we will choose the magnetic vector potential to be

$$A_y(x) = B_o\, x(1 + \frac{\epsilon x}{2}),\ A_x = 0,\ A_z = 0 \ . \quad (2.1.1)$$

The curl of this magnetic vector potential gives the magnetic field

$$\underline{B}(x) = B_o(1 + \epsilon x)\underline{i}_z \quad (2.1.2)$$

where $\underline{i}_z$ is a unit vector in the z direction. This magnetic field has the desired properties of being a nearly uniform magnetic field in the z direction up to distances of the order of $1/\epsilon$ away from the point x=0. Note also that ϵ is really just a shorthand notation for the x derivative of the logarithm of the magnetic field at x=0, <u>i.e.</u>,

$$\epsilon = \frac{1}{B_o}\,\frac{d\,\underline{B}(x)}{dx} \ . \quad (2.1.3)$$

In the rectangular coordinate system we are using since the magnetic vector potential depends only on the x coordinate, the canonical momenta in the y and z directions are constants of the motion:

$$p_y = m_j v_y + \frac{q_j}{c} A_y(x) = \text{a constant of the motion} \quad (2.1.4)$$

$$p_z = m_j v_z = \text{a constant of the motion} . \qquad (2.1.5)$$

Substituting $A_y(x)$ from (2.1.1) into (2.1.4) and dividing equations (2.1.4) and (2.1.5) by $m_j \Omega_j$ (x=0) and m_j respectively, we find the constants of the motion to be

$$x + v_y/\Omega_j + \epsilon x^2/2 = \text{a constant of the motion} \qquad (2.1.6)$$

$$v_z = \text{a constant of the motion} . \qquad (2.1.7)$$

In addition to these two constants of the motion derived from the conservation of momentum, we also know that the total energy of a particle is a conserved quantity. For our geometry this statement can be written mathematically as

$$E = \frac{1}{2} m_j (v_\perp^2 + v_z^2) - m_j G_j x = \text{a constant of the motion.}$$

Or, dividing through by $m_j/2$ and remembering that v_z itself is a conserved quantity, this last constant of the motion may be simplified to

$$v_\perp^2 - 2G_j x = \text{a constant of the motion.} \qquad (2.1.8)$$

The constants of the motion have simple physical interpretations. First, since there are no equilibrium force fields acting in the z or magnetic field direction,

the velocity in the z direction should be a conserved quantity. This fact is given by (2.1.7). Second, since the velocity and hence the energy in the magnetic field direction is constant and separately the total energy is a constant, the energy perpendicular to the magnetic field must be a conserved quantity. This fact is expressed in (2.1.8). In addition we note that when $G_j = 0$, since the magnetic field is nearly uniform here, the conserved quantity in (2.1.8) is approximately equal to the first adiabatic invariant--the magnetic moment of the particle. Finally we note that in our inhomogeneous magnetic field, a particle whose instantaneous x coordinate and velocity in the y direction are x and v_y respectively has the x component of its guiding center located at $x + v_y/\Omega_j + \epsilon x^2/2$. Usually both the x and y components of the guiding center position are constants of the motion. However, in our plasma model the gravity force in the x direction together with the magnetic field in the z direction causes a uniform drift of the guiding centers in the y direction. Therefore we expect that here only the x component of the guiding center position will be a constant of the motion, and in (2.1.4) we see that this is indeed the case.

2.2 Equilibrium Distribution Function

As we have stated in Section 2.1, any distribution function will automatically satisfy the equilibrium Vlasov equation as long as it is only a function of the constants of the motion. For our plasma model the relevant conserved quantities are those given by (2.1.6), (2.1.7) and (2.1.8). In addition to this specification of its functional form, the velocity space integral of the equilibrium distribution function must be finite at all spatial positions in the vicinity of x=0 to ensure a finite plasma density in the region of interest.

In order to specify an equilibrium distribution function which represents an inhomogeneous plasma, we will follow the conventional procedure (2.2) of separating the distribution function into predominantly velocity space and coordinate space dependent parts. Since we expect the spatial coordinate dependence to come in through the guiding center position, we achieve this separation by writing the equilibrium distribution function as

$$\left\langle f_j(x,\underline{v})\right\rangle = F_j\left[v_\perp^2 - 2G_j x, (v_z - v_{o_j})^2\right] g_j\left[x + v_y/\Omega_j + \epsilon x^2/2 ,\right.$$

$$\left. v_\perp^2 - 2G_j x, (v_z - v_{o_j})^2\right] \qquad (2.2.1)$$

where we have explicitly included the possibility of a current or drift along the magnetic field with v_{o_j}. The

function g_j represents the spatial distribution of the plasma and includes the possibility of density and temperature gradients in the plasma. The function g_j will be chosen so that at $x = 0$ the integral of the entire equilibrium distribution function over all velocities is unity.

Combining a Maxwell-Boltzmann distribution along the magnetic field with that given by (1.3.1) for the velocities perpendicular to the magnetic field, we will take the velocity space or nearly homogeneous part of the distribution function to be

$$F_j\left[v_\perp^2-2G_jx,(v_z-v_{o_j})^2\right] = \frac{1}{\sqrt{\pi}\,\alpha_{z_j}} e^{-(v_z-v_{o_j})^2/\alpha_{z_j}^2} F_{\perp_j}^{\ell}\left(\sqrt{v_\perp^2-2G_jx}\right)$$

$$= \frac{1}{\pi^{3/2}\,\alpha_{\perp_j}^2\,\alpha_{z_j}\,\ell!}\sqrt{\left(\frac{v_\perp^2-2G_jx}{\alpha_{\perp_j}^2}\right)^{2\ell}} \exp\left\{-\frac{v_\perp^2-2G_jx}{\alpha_{\perp_j}^2}-\frac{(v_z-v_{o_j})^2}{\alpha_{z_j}^2}\right\}. \tag{2.2.2}$$

While this distribution function does have many desirable properties, we should note that it would not seem to be appropriate for describing mirror machine plasmas (i.e., those having loss-cone type $v_\perp$ distributions-- $\ell>0$) in which there is a significant gravity force representing magnetic field curvature drifts (see Section 2.4). This

is because in such cases the distribution given by (2.2.2) would imply that for certain values of x (whose origin is arbitrary) there would be particles having zero perpendicular kinetic energy $\frac{1}{2} m_j v_\perp^2$. In open-ended confinement devices there should be no such particles. A more reasonable way of choosing an equilibrium distribution in such cases would be to form (2.2.2) not by replacing $v_\perp^2$ in (1.3.1) by $v_\perp^2 - 2G_j x$, but rather by the constant of the motion derived as follows. First, subtracting (2.1.6) from (2.1.8), we obtain

$$v_\perp^2 - 2G_j x - 2G_j(x + v_y/\Omega_j + \epsilon x^2/2)$$

$$= v_\perp^2 - 2G_j v_y/\Omega_j - 2G_j \epsilon x^2/2$$

$$= \text{a constant of the motion.}$$

If we further add to this constant of motion the constant G_j^2/Ω_j^2, we obtain a constant of the motion which is readily recognized as being proportional to the perpendicular energy measured in the drifting frame of reference when $G_j \neq 0$. The resultant more complicated equilibrium distribution function would have the desired property that for $\ell > 0$ there are no particles with zero perpendicular kinetic energy, at least in the vicinity of $x = 0$ (G_j and ϵ are "small" parameters). In cognizance of the preceding remarks, in this work we will confine our attention to equilibria specified by (2.2.2) which have $G_j = 0$, unless $\ell = 0$.

The normalization of the distribution function given by (2.2.2) is such that

$$\int d^3v \left\langle f_j \right\rangle_{x=0} = \int d^3v \, F_j \Big|_{x=0} = 1 . \qquad (2.2.3)$$

At x = 0, the temperatures perpendicular and parallel to the magnetic field are given by

$$\frac{KT_{\perp_j}}{m_j} = \frac{\alpha_{\perp_j}^2}{2} = \int d^3v \left(v_x^2 - \frac{\langle v_\perp \rangle^2}{2} \right) \left\langle f_j \right\rangle_{x=0}$$

$$\frac{KT_{z_j}}{m_j} = \frac{\alpha_{z_j}^2}{2} = \int d^3v (v_z - v_{o_j})^2 \left\langle f_j \right\rangle_{x=0}$$

where K is the Boltzmann constant and, in the definition of the temperature perpendicular to the magnetic field, we have taken account of the effective "drift" velocity given by $\frac{\langle v_\perp \rangle}{\sqrt{2}} = \sqrt{\frac{\ell}{2}}\, \alpha_\perp$ (see Section 6.2).

For the spatially dependent part of the distribution function, we expand g_j in a form suggested by a Taylor series expansion (or, more precisely, the mean value theorem) in the x component of the guiding center position:

$$g_j = 1 + (x + v_y/\Omega_j + \epsilon x^2/2) \frac{\partial g_j}{\partial (x + v_y/\Omega_j + \epsilon x^2/2)} + \ldots \; . \qquad (2.2.4)$$

(While the normalization of the series on the right is in general arbitrary, to the order of expansion used here (see below), equation (2.2.3) requires that it be chosen as indicated in (2.2.4).) In general, around $x = 0$, $x + v_y/\Omega_j + \epsilon x^2/2$ is of the order of the Larmor radius of the j^{th} species of particles as long as $v_y \sim \alpha_\perp$. In this work we will assume that the characteristic density and temperature gradient lengths represented by the terms $\dfrac{\partial g_j}{\partial (x+v_y/\Omega_j + \epsilon x^2/2)}$ etc. are long compared to the relevant Larmor radius, and hence to first order in the ratio of these lengths we may neglect the derivatives of higher than first order in (2.2.4). In doing so we are implicitly assuming that each successive derivative term is smaller than the preceding one. Later (see Section 3.3) we will further assume that each successive derivative term is smaller than the preceding one by at least the ratio of the ion Larmor radius to the characteristic inhomogeneity length. Under these assumptions we need only concern ourselves with the first derivative term in (2.2.4). The explicit form for $\dfrac{\partial g_j}{\partial (x+v_y/\Omega_j + \epsilon x^2/2)}$ which we will use is

$$\frac{\partial g_j}{\partial (x+v_y/\Omega_j + \epsilon x^2/2)} = -\epsilon_j' + \delta_{\perp_j}\alpha_{\perp_j}^{-2}(v_\perp^2 - 2G_j x) + \delta_{z_j}\alpha_{z_j}^{-2}(v_z - v_{o_j})^2 \qquad (2.2.5)$$

where ϵ' represents a density gradient, and $\delta_\perp$ and δ_z represent gradients of the temperature perpendicular and parallel respectively to the magnetic field. Working out the density gradient explicitly from the proposed distribution function, we find that

$$\frac{1}{n_j}\left.\frac{dn_j}{dx}\right|_{x=0} = \left.\int d^2v \frac{d\langle f_j\rangle}{dx}\right|_{x=0} = -\epsilon_j' + (\ell+1)\delta_{\perp j} + \frac{1}{2}\delta_{z_j} + \frac{2G_j\,\delta_{\ell 0}}{\alpha_{\perp j}^2} \qquad (2.2.6)$$

where $\delta_{\ell 0}$ is the Kronecker delta, i.e.,

$$\delta_{\ell m} = \begin{cases} 0, & \ell \neq m \\ 1, & \ell = m \end{cases} . \qquad (2.2.7)$$

In addition we note that the temperature gradients are given by

$$\frac{1}{T_{\perp j}}\left.\frac{dT_{\perp j}}{dx}\right|_{x=0} = \left.\frac{\int d^3v \left(v_x^2 - \frac{\langle v_\perp\rangle^2}{2}\right)\frac{d\langle f_j\rangle}{dx}}{\int d^3v \left(v_x^2 - \frac{\langle v_\perp\rangle^2}{2}\right)\langle f_j\rangle}\right|_{x=0} - \frac{1}{n_j}\frac{dn_j}{dx} = (\ell+1)\delta_{\perp j} + \frac{2G_j}{\alpha_{\perp j}^2}(1-\delta_{\ell 0})$$

$$\frac{1}{T_{z_j}}\left.\frac{dT_{z_j}}{dx}\right|_{x=0} = \left.\frac{\int d^3v \,(v_z - v_{0j})^2 \frac{d\langle f_j\rangle}{dx}}{\int d^3v \,(v_z - v_{0j})^2 \langle f_j\rangle}\right|_{x=0} - \frac{1}{n_j}\frac{dn_j}{dx} = \delta_{z_j} .$$

The density gradients $\frac{1}{n_j}\frac{dn_j}{dx}$ have been subtracted here since the integrals we evaluate are really of the form $d[\ln n(x)T(x)]/dx$.

2.3 Parametric Constraints

Having chosen a particular form for the equilibrium distribution function, we will now proceed to specify the required relationships between the parameters of the distribution function for true plasma equilibrium. The first requirement which leads to such relationships is the necessity of charge neutrality in the equilibrium state (there is no static electric field present) which requires that

$$\sum_j n_j q_j \int d^3v \langle f_j \rangle = 0 . \qquad (2.3.1)$$

Using the normalization condition given in (2.2.3), at x=0 we can reduce the charge neutrality condition to

$$\sum_j n_j q_j = 0 . \qquad (2.3.2)$$

Around x=0 to first order in the ratio of the Larmor radius to the inhomogeneity lengths, the charge neutrality condition becomes

$$\sum_j n_j q_j \int d^3v \frac{d\langle f_j \rangle}{dx} = \sum_j n_j q_j \left[-\epsilon'_j + (\ell+1)\delta_{\perp_j} + \frac{1}{2}\delta_{z_j} + \frac{2G_j \delta_{\ell 0}}{\alpha_{1_j}^2} \right] = 0 . \qquad (2.3.3)$$

Or, noting from (2.2.6) that the expression in square brackets is just $\frac{1}{n_j}\frac{dn_j}{dx}$, we see that this relation is simply

$$\sum_j q_j \frac{dn_j}{dx} = 0 \quad . \tag{2.3.4}$$

Thus this part of the charge neutrality condition is just a mathematical statement of the fact that the density gradients of ions and electrons be equal in order to maintain charge neutrality.

A second condition which must be imposed on the equilibrium is that the diamagnetic current caused by the density gradient balance the curl of the external magnetic field. This condition is simply Ampere's law:

$$\frac{\partial}{\partial \underline{x}} \times \underline{B} = \frac{4\pi}{c} \underline{J} \quad . \tag{2.3.5}$$

In our physical model (2.3.5) reduces to

$$-\epsilon B_o = \frac{4\pi}{c} \sum_j n_j q_j \int d^3v \; v_y \langle f_j \rangle \quad .$$

Substituting in the general equilibrium distribution function and carrying out the indicated integrations, we can reduce this relation to

$$\epsilon = \sum_j \frac{n_j \, KT_{\perp_j}}{(B_o^2/8\pi)} \frac{1}{2}\left[\epsilon_j' - (\ell+2)\delta_{\perp_j} - \frac{1}{2}\delta_{z_j} \right] \tag{2.3.6}$$

or

$$\frac{1}{B_o}\frac{d|\underline{B}(x)|}{dx} = -\frac{1}{2}\sum_j \beta_{\perp_j}\left[\frac{1}{n_j}\frac{dn_j}{dx} - \frac{1}{(\ell+1)}\frac{1}{T_{\perp_j}}\frac{dT_{\perp_j}}{dx} - \frac{1}{(\ell+1)}\frac{2G_j}{\alpha_{\perp_j}^2}\right] \qquad (2.3.7)$$

where we have defined

$$\beta_{\perp_j} = \frac{n_j KT_{\perp_j}}{B_o^2/8\pi} = \frac{\text{perpendicular kinetic energy density of the } j^{th} \text{ species}}{\text{magnetic field energy density}} .$$

Since in Section 1.2 we have seen that our neglect of the transverse waves is reasonable only if $\beta << \left\{\begin{matrix}1\\ m_e/m_i\end{matrix}\right\}$, we see that in general the magnetic field gradient effects can be neglected in comparison to the density gradient effects. Hence in this work the only effect of the magnetic field gradient which we will retain will be its effect in balancing the diamagnetic current due to the density gradient in equilibrium. We will therefore set

$$\epsilon = \frac{1}{B_o}\frac{d|\underline{B}(x)|}{dx}$$

to zero in all further calculations, except those in the following section in which we are trying to satisfy Ampere's law in equilibrium.

2.4 On Representation of Curvature Effects by the Gravity Force

In a "magnetic well" the magnetic field energy density must increase in all directions normal to the plasma confinement region. This means that, in order to faithfully simulate a magnetic mirror machine with our plasma model, we should have magnetic field gradients along the direction of the magnetic field to confine the plasma in this direction. Such gradients lead to curvature of the magnetic field lines and hence to so-called "curvature effects." Often the curvature effects can be simulated by a gravity force (2.3). We therefore propose to use the gravity force which we introduced in the preceding analysis to simulate the effect of magnetic field curvature. In the following paragraphs we will consider the restrictions imposed on this artificial gravity force by plasma equilibrium considerations.

The analysis in this section will be the same as that of the previous work in this chapter except that a small magnetic field curvature will be explicitly introduced and only Maxwellian velocity distributions of equal temperatures parallel and perpendicular to the magnetic field will be considered. For simplicity temperature gradients and external force fields will be ignored. We begin the analysis by proposing a magnetic field of the form

$$\underline{B}(x,z) = B_o(1 + \epsilon x)\underline{i}_z + B_o\eta z\underline{i}_x \quad . \qquad (2.4.1)$$

The z component of this magnetic field is the same as before. The additional term proportional to η represents the magnetic field curvature. For this magnetic field we note that a suitable choice for the magnetic vector potential is

$$A_y(x,z) = B_o(x + \frac{\epsilon x^2}{2} - \frac{\eta z^2}{2}) \quad . \qquad (2.4.2)$$

Since this vector potential is independent of the y coordinate, the canonical momentum in the y direction is a constant of the motion, i.e.,

$$p_y = m_j v_y + \frac{q_j}{c} A_y(x,z) = \text{a constant of the motion} \quad .$$

Dividing through by $m_j \Omega_j$ we can write this as

$$x + v_y/\Omega_j + \epsilon x^2/2 - \eta z^2/2 = \text{a constant of the motion} \quad . \qquad (2.4.3)$$

In addition, the total energy of a particle is still a conserved quantity:

$$\frac{1}{2} m_j(v_\perp^2 + v_z^2) = \text{a constant of the motion}$$

or, dividing through by $m_j/2$, we obtain

$$v_\perp^2 + v_z^2 = \text{a constant of the motion} . \qquad (2.4.4)$$

Now, as before, we will choose the equilibrium distribution function to be a function of the constants of the motion so that it automatically satisfies the zero-order Vlasov equation (1.2.3). For our present purposes we choose it to be

$$\langle f_j \rangle = \frac{1}{(\pi\alpha_j^2)^{3/2}} e^{-(v_\perp^2+v_z^2)/\alpha_j^2} \left[1 - \epsilon_j'(x+v_y/\Omega_j + \epsilon x^2/2 - \eta z^2/2)\right] . \qquad (2.4.5)$$

We note that this distribution function is the same as the one developed earlier in this chapter except for the inclusion of curvature effects as represented by the term proportional to η. The velocity dependence here is simply the specialized case of equal temperature Maxwellian distributions parallel and perpendicular to the magnetic field direction.

In the vicinity of the point x=0, z=0, the conditions for charge neutrality are the same as before. However, the balancing of the density-gradient-induced diamagnetic current by the curl of the magnetic field as required by Ampere's law now reduces to

$$(\epsilon - \eta)B_o = \frac{4\pi}{c} \sum_j n_j q_j \frac{\epsilon_j'}{2\Omega_j} \alpha_j^2 . \qquad (2.4.6)$$

Ignoring temperature gradients and setting $\ell = 0$, $\alpha_{\perp_j} = \alpha_{z_j}$, $G_j = 0$ we see from (2.2.6) that

$$\epsilon_j' = -\frac{1}{n_j}\frac{dn_j}{dx} \quad . \tag{2.4.7}$$

Therefore (2.4.6) may be written as

$$\frac{1}{B_o}\frac{d|\underline{B}|}{dx} - \frac{1}{B_o}\frac{d|\underline{B}|}{dz} = \epsilon - \eta = -\sum_j \frac{n_j KT_j}{(B_o^2/8\pi)}\frac{1}{2}\left[\frac{1}{n_j}\frac{dn_j}{dx}\right]_{x=0} . \tag{2.4.8}$$

Or, defining

$$\beta_j = \frac{n_j KT_j}{(B_o^2/8\pi)}$$

we can write this last equation as

$$\frac{1}{B_o}\frac{d|\underline{B}|}{dx} - \frac{1}{B_o}\frac{d|\underline{B}|}{dz} = -\frac{1}{2}\sum_j \beta_j\left[\frac{1}{n_j}\frac{dn_j}{dx}\right]_{x=0} . \tag{2.4.9}$$

We are now ready to consider the consequences of choosing a gravity force to represent the effect of magnetic field curvature. In Section 1.2 we found that in order to neglect transverse (electromagnetic) waves it was necessary for β to be very small compared to unity. Therefore, except for special cases in which the difference of the terms on the left of (2.4.9) nearly vanishes, we see that in general the characteristic curvature length

$$R \equiv \left[\frac{1}{B_o} \frac{d|\underline{B}|}{dz}\right]^{-1}$$

must be much larger than the characteristic density gradient length

$$\left[\frac{1}{n_j} \frac{dn_j}{dx}\right]^{-1} ,$$

<u>i.e.</u>,

$$\left|\frac{1}{n_j} \frac{dn_j}{dx}\right| >> \left|\frac{1}{B_o} \frac{d|\underline{B}|}{dz}\right| . \qquad (2.4.10)$$

For the geometry under consideration, the curvature of the magnetic field is represented by a gravity in the x direction of (<u>2.3</u>)

$$G_j = - \frac{1}{R} (v_z^2 + \frac{1}{2} v_\perp^2) .$$

Assuming that the velocities in this expression can be represented by the relevant thermal velocity, we can reduce the expression to

$$G_j = - \frac{2\alpha_j^2}{R} = - \alpha_j^2 \frac{2}{B_o} \frac{d|\underline{B}|}{dz} . \qquad (2.4.11)$$

Combining this definition with condition (2.4.10), we see that for our electrostatic wave analysis to be valid we must require that

$$\left|\frac{1}{n_j}\ \frac{dn_j}{dx}\right| >> \left|\frac{G_j}{2\alpha_j^2}\right| \quad . \qquad (2.4.12)$$

We have thus shown that, strictly speaking, in order to satisfy the requirements of equilibrium when we wish to represent magnetic field curvature effects by the gravity term in our analysis, the gravity term is limited in magnitude according to condition (2.4.12).

Physically what is being required is that the density-gradient-induced diamagnetic current in the y direction balance both the x and z components of the curl of the magnetic field in a low β plasma (consider the momentum balance equation of magnetohydrodynamics). In truth, we should also allow for a density gradient in the z direction which, in turn, would induce more diamagnetic current in the y direction, thus helping to balance the total curl of the magnetic field. However, in general what we see out of this analysis is that for a low β plasma in equilibrium the density gradients are of the order of $1/\beta$ steeper than the magnetic field gradients. For larger magnetic field curvatures than those satisfying condition (2.4.10) we must explicitly take into account the induced density gradient along the magnetic field, i.e., insure that an equilibrium exists along the magnetic field lines.

As a qualification on this conclusion, we note that the lack of the existence of equilibrium along the magnetic

field lines is probably not very serious. This is because in this direction the particles and especially the electrons are free to move in such a way as to quickly establish a self-consistent equilibrium. This is in contrast to the situation in the plane perpendicular to the magnetic field where the lack of an equilibrium results in gross plasma motions due to the fact that the particles are constrained in their motions by the magnetic field. Therefore, while the lack of an equilibrium along the magnetic field lines would not appear to be catastrophic, when gravity forces representing magnetic field curvature do not satisfy condition (2.4.12) it seems necessary to at least consider the problem of the establishment of an equilibrium. In this regard it appears to us that the stabilizing effects due to magnetic field curvature, found by Krall and Rosenbluth (2.2) under conditions which violate condition (2.4.12), remain inconclusive until it can be shown that an equilibrium which does not significantly alter those effects is established.

3. DISPERSION RELATION DERIVATION

3.1 Integro-Differential Dispersion Equation

In this chapter we derive the dispersion relation for waves propagating in plasmas which conform to the requirements of the plasma model specified in Chapter 1. The first step in this derivation is to obtain a formal solution of the linearized Vlasov equation. Omitting the magnetic field perturbation term $\delta\underline{B}$ (since we are considering sufficiently low β plasmas so that only the electrostatic modes are important--see Section 1.2), we can write the linearized Vlasov equation (1.2.4) as

$$\left[\frac{\partial}{\partial t} + \underline{v} \cdot \frac{\partial}{\partial \underline{x}} + \frac{1}{m_j} \left(\frac{q_j}{c} \underline{v} \times \underline{B} + \underline{F}_j^{ext} \right) \cdot \frac{\partial}{\partial \underline{v}} \right] \delta f_j(\underline{x}, \underline{v}, t)$$

$$= - \frac{q_j}{m_j} \delta \underline{E}(\underline{x}, t) \cdot \frac{\partial \langle f_j(x, \underline{v}) \rangle}{\partial \underline{v}} . \qquad (3.1.1)$$

This equation is a first-order partial differential equation and can be solved by the method of characteristics (3.1). A convenient way to apply the method of characteristics here is to define a new coordinate system with the properties

$$m_j \frac{d\underline{v}'}{dt'} = \underline{F}_j^{ext} + \frac{q_j}{c} \underline{v}' \times \underline{B} \; ; \quad \frac{d\underline{x}'}{dt'} = \underline{v}' \qquad (3.1.2)$$

subject to the initial conditions

$$\underline{x}'(t' = t) = \underline{x} \; ; \quad \underline{v}'(t' = t) = \underline{v} \qquad (3.1.3)$$

where the prime denotes the new coordinate system. The solutions to the differential equations (3.1.2) are the characteristics of equation (3.1.1). Physically these solutions give the trajectories of the individual particles moving under the influence of the static magnetic field and external force fields. These trajectories are called the unperturbed particle orbits or simply the unperturbed orbits. Introducing the new coordinate system, we may write (3.1.1) as

$$\frac{d}{dt'} \delta f_j(\underline{x}', \underline{v}', t') = - \frac{q_j}{m_j} \delta \underline{E}(\underline{x}', t') \cdot \frac{\partial \langle f_j(x', \underline{v}') \rangle}{\partial \underline{v}'} \; .$$

Integrating this equation over time from $t' = -\infty$ up to $t' = t$, we obtain

$$\delta f_j(\underline{x}, \underline{v}, t) = - \frac{q_j}{m_j} \int_{-\infty}^{t} dt' \, \delta \underline{E}(\underline{x}', t') \cdot \frac{\partial \langle f_j(x', \underline{v}') \rangle}{\partial \underline{v}'} + \delta f_j(x', \underline{v}', t' = -\infty). \qquad (3.1.4)$$

As we have noted in Section 1.2, the perturbation δf_j is assumed to be vanishingly small at $t' = -\infty$, so for the purposes of our instability analysis the last term in this equation may be neglected. For convenience we will change the dummy variable of integration in (3.1.4) from t' to $\tau + t$, and then we may write the equation as

$$\delta f_j(\underline{x},\underline{v},t) = -\frac{q_j}{m_j}\int_{-\infty}^{0} d\tau\, \delta\underline{E}(\underline{x}',t+\tau)\cdot\frac{\partial\langle f_j(x',\underline{v}')\rangle}{\partial\underline{v}'} \quad . \tag{3.1.5}$$

We will now work out this equation in more detail for the plasma model specified in Chapter 1. For future purposes it is convenient to write the velocity space derivative of the equilibrium distribution function in terms of derivatives with respect to the constants of the motion. Writing the derivative in this manner, we have

$$\frac{\partial\langle f_j(x,\underline{v})\rangle}{\partial\underline{v}} = \frac{\partial\langle f_j\rangle}{\partial v_z}\underline{i}_z + 2\underline{v}_\perp\frac{\partial\langle f_j\rangle}{\partial(v_\perp^2-2G_jx)} + \frac{F_j}{\Omega_j}\frac{\partial g_j}{\partial(x+v_y/\Omega_j)}\underline{i}_y \, . \tag{3.1.6}$$

where we have employed definition (2.2.1) in writing the last term and $\underline{i}_y, \underline{i}_z$ are unit vectors in the y,z directions respectively.

In the following we wish to examine the physical significance of the terms which arise when (3.1.6) is substituted into (3.1.5). In order to do so simply, for the moment we will neglect any perturbed electric fields in the x direction. This is equivalent to using the "local approximation" (see Section 3.3). Setting $\delta E_x = 0$ and substituting (3.1.6) into (3.1.5), we obtain

$$\delta f_j(\underline{x},\underline{v},t) = -\frac{q_j}{m_j}\int_{-\infty}^{0} d\tau\left[\delta E_z\frac{\partial\langle f_j\rangle}{\partial v_z} + 2v_y\,\delta E_y\frac{\partial\langle f_j\rangle}{\partial(v_\perp^2-2G_jx)} + \frac{\delta E_y}{\Omega_j}F_j\frac{\partial g_j}{\partial(x+v_y/\Omega_j)}\right]. \tag{3.1.7}$$

In this equation the three terms enclosed in brackets have the form of the time derivative of an equilibrium constant of the motion multiplied by the derivative of the equilibrium distribution function with respect to the same conserved quantity. To see this we note that

$$\frac{dv_z}{dt} = \frac{q_j}{m_j}\,\delta E_z$$

$$\frac{d(v_\perp^2 - 2G_j x)}{dt} = 2v_y\,\frac{q_j}{m_j}\,\delta E_y \qquad (3.1.8)$$

$$\frac{d(x+v_y/\Omega_j)}{dt} = \frac{1}{\Omega_j}\,\frac{q_j}{m_j}\,\delta E_y$$

where we recall that we are assuming here that there are no fluctuations in the x direction so that $\delta E_x = 0$. These equations give the amount of destruction per unit time of the constancy of the equilibrium constants of the motion due to the fluctuating electric fields in the y,z directions. In the first equation of (3.1.8), we see that the acceleration of the particles along the magnetic field by the z component of the fluctuating electric field is what destroys the constancy of v_z. Similarly, in the directions perpendicular to the magnetic field it is the component of the fluctuating electric field transverse to

the magnetic field which causes $v_\perp^2 - 2G_j x$ to no longer be a conserved quantity. Finally, we note that the x component of the guiding center position is destroyed as a constant of the motion by the fluctuating electric field in the y direction. Noting that x always occurs with v_y/Ω_j, we see that it is convenient to introduce a drift velocity v_x such that

$$v_x = \frac{dx}{dt} = \frac{\delta \underline{E} \times \underline{B}}{B^2} c = \frac{1}{\Omega_j} \frac{q_j}{m_j} \delta E_y$$

and think of the last term in (3.1.7) as $\frac{dx}{dt} \frac{\partial \langle f \rangle}{\partial x}$. In this case we see that the $\delta \underline{E} \times \underline{B}$ drift in the x direction due to the y component of the fluctuating electric field is what causes the x component of the guiding center to be destroyed as a constant of the motion. With this explanation of each of the terms, we see that the physical content of (3.1.7) is that the perturbation δf_j at time t is given by the amount of destruction of each constant of the motion per unit time multiplied by the corresponding velocity space "slope" of the equilibrium distribution function, summed over all the constants of the motion and "averaged" over the particle trajectories from $\tau = -\infty$ up to time t. We therefore see that the way in which we take free energy out of the equilibrium plasma and put it into the perturbations is through electric field

fluctuations which are rapid enough and of sufficiently short wavelength to destroy the constancy of the various equilibrium conserved quantities.

Having discussed the physical content of (3.1.7), we now return to the task of finding the dispersion equation for a fluctuating electric field with components in all directions. In order to ensure that the particle number fluctuations δf_j and the electric field fluctuations $\delta \underline{E}$ are self-consistent, we must apply Gauss' law. Since we are neglecting magnetic field fluctuations, the electric field is describable by a potential, i.e.,

$$\delta \underline{E}(\underline{x},t) = - \frac{\partial}{\partial \underline{x}} \phi(\underline{x},t) \quad . \qquad (3.1.9)$$

With the perturbed electric field so defined, going back to the general expression for δf_j of (3.1.5) and employing Gauss' law, we obtain for the self-consistency equation

$$\nabla^2 \phi(\underline{x},t) = -\sum_j \omega_{p_j}^2 \int d^3v \int_{-\infty}^{0} d\tau \, \frac{\partial}{\partial \underline{x}'} \phi(\underline{x}',t+\tau) \cdot \frac{\partial \langle f_j(\underline{x}',\underline{v}') \rangle}{\partial \underline{v}'} \, . \qquad (3.1.10)$$

This integro-differential dispersion equation prescribes the time development of the perturbed potential $\phi(\underline{x},t)$ for the particular equilibrium distribution functions $\langle f_j(x,\underline{v}) \rangle$. In allowing for the x dependence of the potential, which we will not neglect here, we find it

convenient to remove the x derivative under the integral in (3.1.10) through an integration by parts. To do this we observe that

$$\frac{d\phi(\underline{x},t)}{dt} = \frac{\partial \phi(\underline{x},t)}{\partial t} + \underline{v} \cdot \frac{\partial \phi(\underline{x},t)}{\partial \underline{x}}$$

or that

$$\underline{v} \cdot \frac{\partial \phi(\underline{x},t)}{\partial \underline{x}} = \frac{d\phi(\underline{x},t)}{dt} - \frac{\partial \phi(\underline{x},t)}{\partial t} \quad . \tag{3.1.11}$$

Next we note that the velocity space derivative of the equilibrium distribution function may be written as

$$\frac{\partial \langle f_j(x,\underline{v}) \rangle}{\partial \underline{v}} = 2\underline{v} \frac{\partial \langle f_j \rangle}{\partial (v_\perp^2 - 2G_j x)} + \frac{F_j}{\Omega_j} \frac{\partial g_j}{\partial (x + v_y/\Omega_j)} \underline{i}_y + \left[\frac{\partial \langle f_j \rangle}{\partial v_z} - 2 v_z \frac{\partial \langle f_j \rangle}{\partial (v_\perp^2 - 2G_j x)} \right] \underline{i}_z \, . \tag{3.1.12}$$

Now, since the term of $\partial \langle f_j \rangle / \partial \underline{v}$ which is proportional to the velocity $\underline{v}$ is only a function of the constants of the motion, we can integrate that part of (3.1.10) schematically as

$$\int_{-\infty}^{0} d\tau \; \underline{v}' \cdot \frac{\partial \phi(\underline{x}', t+\tau)}{\partial \underline{x}'} = \phi(\underline{x}, t) - \int_{-\infty}^{0} d\tau \; \frac{\partial \phi(\underline{x}', t+\tau)}{\partial \tau} \tag{3.1.13}$$

where as with $\delta f(\tau = -\infty)$ we have neglected $\phi(\tau = -\infty)$ since we assume that the perturbation was vanishingly small

at $t = -\infty$. Before we utilize these results we go one step further by noting that, since the equilibrium distribution function is independent of y,z, we may easily Fourier analyze these components of the perturbation. The equilibrium distribution function is, however, dependent on x, and hence Fourier analysis in the x direction would result in a convolution integral. We will choose not to Fourier analyze in the x direction, but rather to consider separately the x dependence of the potential. In order to facilitate this, we Fourier analyze in the y,z directions and in time according to the following definition:

$$\phi(\underline{x},t) = \sum_{k_y,k_z\omega} \phi(x) \exp\left[i(k_y y + k_z z - \omega t) \right] \qquad (3.1.14)$$

where we have omitted the subscript k_y,k_z,ω on $\phi(x)$ for convenience. The frequency ω of the waves will, in general, be complex with unstable or temporally growing waves being characterized by Im $\omega > 0$. The wave vector component k_y will always be taken to be real in this work. The component k_z will be real, except when we are considering the convective and absolute nature of instabilities in which case k_z will, in general, be complex (see Chapters 5,6,7). Using the Ansatz of (3.1.14) and the form given by (3.1.12) in our self-consistency equation, we can reduce it to

$$\left[\frac{d^2}{dx^2} - k^2\right]\phi(x) = -2\phi(x)\sum_j \omega_{Pj}^2 \int d^3v \frac{\partial\langle f_j\rangle}{\partial(v_\perp^2 - 2G_j x)}$$

$$- i\sum_j \omega_{Pj}^2 \int d^3v \int_{-\infty}^{0} d\tau\, \phi(x')\, \exp\left\{i\left[k_y(y'-y) + k_z(z'-z) - \omega\tau\right]\right\}$$

$$\times\left\{k_z \frac{\partial\langle f_j\rangle}{\partial v_z} - 2(k_z v_z - \omega)\frac{\partial\langle f_j\rangle}{\partial(v_\perp^2 - 2G_j x)} + \frac{k_y F_j}{\Omega_j}\frac{\partial g_j}{\partial(x + v_y/\Omega_j)}\right\} \quad (3.1.15)$$

where $k^2 = k_y^2 + k_z^2$. This is the general integro-differential dispersion equation which we will investigate further in the succeeding sections in order to determine the dispersion properties of the plasma.

3.2 Unperturbed Orbit Equations

In order to proceed further with our analysis of the integro-differential dispersion equation (3.1.15), we need to know the unperturbed particle orbits, i.e., the characteristics of (3.1.1). The unperturbed orbits are defined by (3.1.2) and (3.1.3) which, when we change the time variable from t' to $\tau+t$ to conform to the desired form of the orbits, become

$$\frac{d\underline{v}'}{d\tau} = G_j \underline{i}_x + \frac{q_j}{m_j c} \underline{v}' \times \underline{B} \qquad (3.2.1)$$

$$\frac{d\underline{x}'}{d\tau} = \underline{v}' \qquad (3.2.2)$$

subject to the initial conditions

$$\underline{x}'(\tau = 0) = \underline{x} \qquad (3.2.3)$$

$$\underline{v}'(\tau = 0) = \underline{v} \ . \qquad (3.2.4)$$

In (3.2.1) we have utilized the fact that for our plasma model the only external force field is in the x direction and representable by the gravity force. Writing out the component parts of (3.2.1) explicitly, we have

$$\frac{dv_x'}{d\tau} = \Omega_j v_y' + G_j \qquad (3.2.5)$$

$$\frac{dv'_y}{d\tau} = - \Omega_j v'_x \qquad (3.2.6)$$

$$\frac{dv'_z}{d\tau} = 0 \qquad (3.2.7)$$

where as before $\Omega_j = q_j |\underline{B}|/m_j c$ = the cyclotron frequency for the j^{th} species of particles. The solution of (3.2.7) subject to the v_z component of condition (3.2.4) is simply

$$v'_z = v_z \, . \qquad (3.2.8)$$

Substituting v'_x from (3.2.6) into (3.2.5), we find that the equation which we must solve for v'_y is

$$\frac{d^2 v'_y}{d\tau'} + \Omega_j^2 \, v'_y = -G_j \, \Omega_j \, . \qquad (3.2.9)$$

The homogeneous part of this differential equation describes the oscillatory motion in the y direction caused by the spiraling of the particles around the magnetic field lines. The gravity dependent inhomogeneous term accounts for the $\underline{F} \times \underline{B}/q_j B^2$ type of drift (3.2) in the y direction caused by the gravity force in the x direction. At this point it is convenient to introduce a cylindrical coordinate system for the unprimed velocity

space coordinates. For such a coordinate system we define an azimuthal angle θ such that

$$\theta = \tan^{-1} v_y/v_x$$

and a velocity perpendicular to the magnetic field as

$$v_\perp = (v_x^2 + v_y^2)^{1/2} . \qquad (3.2.10)$$

The velocity in the z or magnetic field direction remains unchanged. In this cylindrical coordinate systems v_x and v_y are given by

$$v_x = v_\perp \cos\theta \qquad (3.2.11)$$

$$v_y = v_\perp \sin\theta . \qquad (3.2.12)$$

With these definitions we find that the solution of (3.2.9) subject to the initial condition given by the v_j component of condition (3.2.4) is

$$v_y' = v_\perp \sin(\theta - \Omega_j\tau) - \frac{G_j}{\Omega_j}(1-\cos\Omega_j\tau) . \qquad (3.2.13)$$

Differentiating this result with respect to τ and using (3.2.6), we find that

$$v_x' = v_\perp \cos(\theta - \Omega_j \tau) + \frac{G_j}{\Omega_j} \sin \Omega_j \tau \quad . \qquad (3.2.14)$$

The general solution of (3.2.2) is

$$\underline{x}' = \int d\tau \, \underline{v}' + \underline{c} \qquad (3.2.15)$$

where $\underline{c}$ is a constant vector determined by the initial conditions. Using the results obtained for v_x', v_y' and v_z', and applying initial condition (3.2.3), we find that the particle orbits are given by

$$x' = x - \frac{v_\perp}{\Omega_j}\left[\sin(\theta - \Omega_j\tau) - \sin\theta\right] + \frac{G_j}{\Omega_j^2}(1 - \cos\Omega_j\tau) \qquad (3.2.16)$$

$$y' = y + \frac{v_\perp}{\Omega_j}\left[\cos(\theta - \Omega_j\tau) - \cos\theta\right] - \frac{G_j}{\Omega_j}\left(\tau - \frac{1}{\Omega_j}\sin\Omega_j\tau\right) \qquad (3.2.17)$$

$$z' = z + v_z\tau. \qquad (3.2.18)$$

In (3.2.16) we see that the x component of the unperturbed particle orbit is given by its position x at $\tau = 0$ plus oscillatory terms which vanish at $\tau = 0$. The pair of terms proportional to $v_\perp/\Omega_j$ describe the x component of the spiraling motion of the particle around a magnetic field line. Since the magnitude of the sine function never exceeds unity, the magnitude of this pair of terms never

exceeds twice the Larmor radius of the particle under consideration. The last pair of terms represent the x component of the oscillatory "wiggle" in the gravity-force-induced drift in the y direction which was discussed previously in connection with (3.2.9). This oscillatory contribution to the orbit is usually ignored, but our analysis will show that retaining it leads to further restrictions on the magnitude of the gravity force (see following section). In the y component of the unperturbed orbit (3.2.17), the gravity induced drift is the source of the $G_j\tau/\Omega_j$ term, and the oscillatory terms are of the same origin as those in the x orbit. The z component of the unperturbed orbit (3.2.18) is simply the position at $\tau = 0$ plus the particle translation $v_z\tau$ which has occurred since that time.

In deriving these simple particle orbits, we have implicitly made two assumptions which are worth mentioning here. First, based upon the fact that we are only concerned with low β plasmas, we know that the equilibrium magnetic field gradients are much smoother than the density gradients, and so we have neglected the magnetic field gradients. Second, in allowing magnetic field curvature effects to be represented simply by the gravity force, we have neglected various terms which would arise due to the other, less dominant (usually oscillatory) effects of the magnetic field curvature. With these remarks in mind we

wish to add a note of caution about the conclusions reached in later parts of this work. Since we are neglecting these and perhaps other "small" effects which are presumably expandable effects (i.e., their effects can be expanded in a perturbation series), we would not expect that the conclusions reached would be drastically modified by their inclusion. However, there is one notable exception to this statement. If we conclude on the basis of our approximate analysis that a given plasma is very nearly marginally stable, we do not know a priori whether the inclusion of "small" effects would change our conclusion as to the plasma's stability or instability. However, we usually know the frequency and wavelength ranges in which the small effects of relevance for any particular real plasma could become important, and hence we can have confidence in our conclusions, except possibly in these particular ranges.

3.3 Dispersion Relation: General $\langle f \rangle$

We now return to the task of finding the dispersion relation. Substituting the orbits found in the preceding section into the integro-differential dispersion equation (3.1.15), we obtain

$$\left[\frac{d^2}{dx^2} - k^2\right]\phi(x) = -2\phi(x)\sum_j \omega_{pj}^2 \int d^3v \frac{\partial\langle f_j\rangle}{\partial(v_\perp^2 - 2G_j x)} - i\sum_j \omega_{pj}^2 \int d^3v \int_{-\infty}^{0} d\tau\, \phi(x')$$

$$\times \exp\left\{ i\left[\frac{k_y v_\perp}{\Omega_j}\left(\cos(\theta - \Omega_j\tau) - \cos\theta\right) - \frac{k_y G_j}{\Omega_j}\left(\tau - \frac{1}{\Omega_j}\sin\Omega_j\tau\right) + k_z v_z \tau - \omega\tau\right]\right\}$$

$$\times \left\{ k_z \frac{\partial\langle f_j\rangle}{\partial v_z} - 2(k_z v_z - \omega)\frac{\partial\langle f_j\rangle}{\partial(v_\perp^2 - 2G_j x)} - \frac{k_y F_j}{\Omega_j}\frac{\partial g_j}{\partial(x + v_y/\Omega_j)}\right\}. \tag{3.3.1}$$

To further simplify this equation, we will use the Bessel function identities

$$e^{i\gamma\cos(\theta-\alpha)} = \sum_{n=-\infty}^{\infty} J_n(\gamma)\, e^{-in(\theta-\alpha-\pi/2)}$$

$$e^{-i\gamma\cos\theta} = \sum_{\ell=-\infty}^{\infty} J_\ell(\gamma)\, e^{i\ell(\theta-\pi/2)}$$

$$e^{i\beta\sin\delta} = \sum_{m=-\infty}^{\infty} J_m(\beta)\, e^{im\delta}$$

which are derivable from similar ones given by Watson (3.3). Next we note that since we have an inhomogeneous plasma, the equilibrium distribution function which is dependent on the guiding center position is anisotropic in velocity space in the plane perpendicular to the magnetic field direction. That is, the equilibrium distribution function depends explicitly on the velocity space azimuthal angle θ. For our particular plasma model, around $x = 0$ this dependence is given by (2.2.4) with v_y being defined in (3.2.12):

$$\langle f_j \rangle = F_j \left(1 + \frac{v_\perp \sin\theta}{\Omega_j} \frac{\partial g_j}{\partial (x + v_y/\Omega_j)} \right)_{x \approx 0} . \tag{3.3.2}$$

This explicit dependence of $\langle f_j \rangle$ on the azimuthal angle θ is usually neglected, since the contribution of the resultant terms is important only for high frequencies (of the order of the ion cyclotron frequency and its harmoincs), but will be retained here since we will consider instabilities for such high frequencies (see Chapter 7). In later calculations in this section we will need spatial derivatives of $\langle f_j \rangle$. In computing such derivatives we will assume (only in this section) that $\partial g_j / \partial (x + v_y/\Omega_j)$ is sufficiently dependent on x to account for the rest of the Taylor series expansion of g_j (2.2.4) appropriate for the particular plasma density

profile under consideration. That is, we represent the entire functional dependence of g_j on x by the first two terms in its Taylor series expansion. Using the form of the equilibrium distribution function given by (3.3.2) and the Bessel function identities listed above, in the region close to x = 0 we can write the integro-differential dispersion equation as

$$\left[\frac{d^2}{dx^2} - k^2\right]\phi(x) = -2\phi(x)\sum_j \omega_{pj}^2 \int d^3v \frac{\partial \langle f_j \rangle}{\partial(v_\perp^2 - 2G_j x)}$$

$$-i\sum_j \omega_{pj}^2 \int d^3v \int_{-\infty}^{0} d\tau\, \phi(x') \sum_{n=-\infty}^{\infty}\sum_{\ell=-\infty}^{\infty}\sum_{m=-\infty}^{\infty} J_n\left(\frac{k_y v_\perp}{\Omega_j}\right) J_\ell\left(\frac{k_y v_\perp}{\Omega_j}\right) J_m\left(\frac{k_y G_j}{\Omega_j^2}\right)$$

$$\times \exp\left\{i\left[(k_z v_z + (n+m)\Omega_j - \frac{k_y G_j}{\Omega_j} - \omega)\tau - (\theta - \pi/2)(n-\ell)\right]\right\}\left\{k_z \frac{\partial}{\partial v_z}\left[F_j\left(1\right.\right.\right.$$

$$\left.\left.\left. + \frac{v_\perp \sin\theta}{\Omega_j}\frac{\partial g_j}{\partial(x + v_y/\Omega_j)}\right)\right] - 2(k_z v_z - \omega)\left[\frac{\partial F_j}{\partial(v_\perp^2 - 2G_j x)} + \frac{v_\perp \sin\theta}{\Omega_j}\frac{\partial}{\partial(v_\perp^2 - 2G_j x)} F_j \frac{\partial g_j}{\partial(x + v_y/\Omega_j)}\right] - \frac{k_y F_j}{\Omega_j}\frac{\partial g_j}{\partial(x + v_y/\Omega_j)}\right\}_{x\approx 0}. \quad (3.3.3)$$

In order to proceed further we need to consider the potential $\phi(x)$ in more detail. At this point in the derivation, it is commonly assumed that the potential is roughly a constant and the dispersion relation readily follows. This is the so-called "local approximation". In this work we will make such an approximation later, but for the moment we will consider the parametric ranges in which this procedure is reasonably correct.

Were it not for the inhomogeneity of the plasma, we would simply Fourier analyze the potential fluctuations in the x direction as we have done for the other directions. However, since we cannot do this, we try the next best thing--which is to consider the question of whether or not we can neglect the x dependence of the potential. Clearly we could not do so if the potential depended on the properties of the plasma far from the region of interest. Therefore we see that the potential must be localized in the x direction in the vicinity of $x = 0$. That is, a solution of the integro-differential dispersion equation which is localized around the region $x \approx 0$ must exist.

In order to examine this question of localization of the potential, we expand the potential $\phi(x')$ in a Taylor series about $x' = x$:

$$\phi(x') = \phi(x) + (x'-x)\phi'(x) + \frac{1}{2!}(x'-x)^2 \phi''(x) + \ldots \quad .$$

Keeping only the terms through the second derivative in this expression, upon substituting it into (3.3.3), using the x' unperturbed orbit given by (3.2.16) and employing the general identity

$$\int_0^{2\pi} d\theta \int_{-\infty}^{0} d\tau \sum_{n=-\infty}^{\infty} \sum_{\ell=-\infty}^{\infty} \sum_{m=-\infty}^{\infty} J_n\left(\frac{k_y v_\perp}{\Omega_j}\right) J_\ell\left(\frac{k_y v_\perp}{\Omega_j}\right) J_m\left(\frac{k_y G_j}{\Omega_j^2}\right) \exp\left\{ i\left[\left(k_z v_z + (n+m)\Omega_j - \frac{k_y G_j}{\Omega_j} - \omega\right)\tau - i\left(\theta - \pi/2\right)(n-\ell)\right]\right\}$$

$$\begin{Bmatrix} 1 \\ \sin\theta \\ \sin(\theta - \Omega_j \tau) \\ \sin^2\theta \\ \sin\theta \sin(\theta - \Omega_j \tau) \\ \cos\Omega_j \tau \\ \sin\theta \cos\Omega_j \tau \end{Bmatrix} = \frac{1}{i} \int_0^{2\pi} d\theta \sum_{\ell=-\infty}^{\infty} \sum_{m=-\infty}^{\infty} \frac{J_\ell^2\left(\frac{k_y v_\perp}{\Omega_j}\right) J_m\left(\frac{k_y G_j}{\Omega_j^2}\right)}{k_z v_z + (\ell+m)\Omega_j - k_y G_j/\Omega_j - \omega} \begin{Bmatrix} 1 \\ \ell\Omega_j / k_y v_\perp \\ \ell\Omega_j / k_y v_\perp \\ \left(\frac{\ell\Omega_j}{k_y v_\perp}\right)^2 - \frac{\Omega_j}{k_y v_\perp} \frac{J_\ell'(k_y v_\perp/\Omega_j)}{J_\ell(k_y v_\perp/\Omega_j)} \\ \left(\ell\Omega_j / k_y v_\perp\right)^2 \\ m\Omega_j^2 / k_y G_j \\ \left(m\Omega_j^2 / k_y G_j\right)\left(\ell\Omega_j / k_y v_\perp\right) \end{Bmatrix}$$

$$Im(\omega) > 0$$

(3.3.4)

we obtain the following integro-differential dispersion equation:

$$\left[\frac{d^2}{dx^2} - k^2\right]\phi(x) = -2\phi(x)\sum_j \omega_{pj}^2 \int d^3v \frac{\partial \langle f_j \rangle}{\partial(v_\perp^2 - 2G_j x)}$$

$$- \sum_j \omega_{pj}^2 \int d^3v \sum_{n=-\infty}^{\infty}\sum_{m=-\infty}^{\infty} \frac{J_n^2(k_y v_\perp/\Omega_j) J_m(k_y G_j/\Omega_j^2)}{k_z v_z + (n+m)\Omega_j - k_y G_j/\Omega_j - \omega}$$

$$\times \left\{ k_z \frac{\partial}{\partial v_z} F_j \left[\phi(x) + \mathcal{O}\left(a_j^2 + \frac{G_j^2}{\Omega_j^4}\right)\phi''(x) + \left\{\phi(x)\frac{n}{k_y} + \phi'(x)\left[\frac{n}{k_y}\frac{G_j}{\Omega_j^2}\left(1 - \frac{m\Omega_j^2}{k_y G_j}\right)\right.\right.\right.\right.$$

$$\left.\left.\left.\left. - \frac{v_\perp}{k_y \Omega_j}\frac{J_n'(k_y v_\perp/\Omega_j)}{J_n(k_y v_\perp/\Omega_j)}\right]\right\}\frac{\partial g_j}{\partial(x + v_y/\Omega_j)}\right] - 2(k_z v_z - \omega)\left[\left\{\phi(x) + \mathcal{O}\left(a_j^2 + \frac{G_j^2}{\Omega_j^4}\right)\phi''(x)\right\}\frac{\partial F_j}{\partial(v_\perp^2 - 2G_j x)}\right.$$

$$\left. + \left\{\phi(x)\frac{n}{k_y} + \phi'(x)\left[\frac{n}{k_y}\frac{G_j}{\Omega_j^2}\left(1 - \frac{m\Omega_j^2}{k_y G_j}\right) - \frac{v_\perp}{k_y \Omega_j}\frac{J_n'(k_y v_\perp/\Omega_j)}{J_n(k_y v_\perp/\Omega_j)}\right]\right\}\frac{\partial}{\partial(v_\perp^2 - 2G_j x)} F_j \frac{\partial g_j}{\partial(x + v_y/\Omega_j)}\right]$$

$$\left. + \frac{k_y F_j}{\Omega_j}\frac{\partial g_j}{\partial(x + v_y/\Omega_j)}\left[\phi(x) + \mathcal{O}\left(a_j^2 + \frac{G_j^2}{\Omega_j^4}\right)\phi''(x)\right]\right\}_{\substack{x \approx 0 \\ Im(\omega) > 0}}$$

(3.3.5)

where $\mathcal{O}(a_j^2 + \frac{G_j^2}{\Omega_j^4})$ means terms of order $a_j^2 + G_j^2/\Omega_j^4$ in which a_j is the mean Larmor radius for the j^{th} species of plasma particles, i.e.,

$$a_j = \frac{\alpha_{\perp_j}}{\Omega_j} \quad . \tag{3.3.6}$$

Since the largest Larmor radius is normally that of the ions, hereafter we will usually take the ion Larmor radius as the representative one. In the general identity (3.3.4), the restriction Im $\omega > 0$ is necessary so that the time integral converges, and this specifies the region of the complex ω plane in which our dispersion relation is defined. Henceforth this restriction will be understood to always apply unless we specifically state that we are analytically continuing the dispersion relation to other regions. We were able to do the time integrals separately from the $v_\perp, v_z$ velocity integrals here since the terms in braces in (3.3.3) are either fixed coordinates or conserved quantities and hence independent of time.

In (3.3.5) the terms proportional to $\phi'(x)$ represent an "average" displacement of the instantaneous position x' of the particle about position x, along the unperturbed helical particle trajectory. Since the plasma is nearly uniform in the x direction, we expect that this average displacement must be small and proportional to the density gradient as is observed in (3.3.5). The terms proportional to $\phi''(x)$ on the right side of (3.3.5) are not likewise proportional to the density gradient since in this case we are finding the average of the square of the displacement which is of the order of the maximum displacement squared irrespective of the nonuniformity of the plasma.

Next we note that (3.3.5) can be put in the form

$$\frac{d^2\phi(x)}{dx^2} + A(x,\omega)\frac{d\phi(x)}{dx} - Q(x,\omega)\phi(x) = 0 \qquad (3.3.7)$$

where $Q(x,\omega)$ is similar to but somewhat more general than the quantity $q(x)$ specified by Krall and Rosenbluth (3.4) and $A(x,\omega)$ is, as described implicitly in the preceding paragraph, "small" and inversely proportional to the characteristic inhomogeneity length. In particular, considering the various terms in (3.3.5) we see that, neglecting for the moment the usually small n/k_y terms, the terms of $A(x,\omega)$ are of the order of the Larmor radius squared divided by the characteristic inhomogeneity length times the similar terms contributing to $Q(x,\omega)$. Within the limitations of the present derivation, the n/k_y terms can never be very large. This is because if the $(n/k_y)\partial g_j/\partial(x+v_y/\Omega_j)$ terms were of the order of or larger than unity, it would be necessary to include higher order derivative terms in the Taylor series expansion of g_j (see (2.2.4)). Physically, large n/k_y would imply wave resonance with particles having such large v_y that their Larmor radius would be comparable to the characteristic inhomogeneity length, in which case keeping only two terms in the Taylor series expansion of g_j is obviously insufficient. Therefore, in this work we restrict the values of n/k_y of interest to

$$n/k_y << L$$

where L is the characteristic inhomogeneity length (i.e., $\left[\partial g_j / \partial (x + v_y/\Omega_j)\right]^{-1}$). Using this condition on the magnitude of n/k_y, we find that the terms of $A(x,\omega)$ are of the order of $(a_j + G_j/\Omega_j^2)a_j/L$ compared to the corresponding terms contributing to $Q(x,\omega)$. Physically the gravity length G_j/Ω_j^2 is the distance that particles drifting with an $\underline{F} \times \underline{B}/q_j B^2$ velocity of G_j/Ω_j travel in one cyclotron period. It is also the spatial extent of the oscillatory "wiggle" in the gravity-induced motion. Therefore G_j/Ω_j^2 is the scale length of the charge separation caused by the gravity-induced particle drifts in the y direction.

Now, except for the "small" $d\phi/dx$ term, equation (3.3.7) is exactly the same as that considered by many authors (3.4 - 3.15) in discussing the localization of the potential $\phi(x)$. Since the coefficient of the $d\phi(x)/dx$ term is "small" in our case, it seems reasonable to try to transform (3.3.7) into an equation having no first derivative. Such a transformation can be accomplished by the general substitution (3.16)

$$\phi(x) = \Psi(x) \exp\left\{-\frac{1}{2}\int^{x} A(x',\omega)dx'\right\} . \qquad (3.3.8)$$

Substituting in this Ansatz, the differential equation of (3.3.7) becomes

$$\frac{d^2 \Psi(x)}{dx^2} - q(x,\omega)\, \Psi(x) = 0 \qquad (3.3.9)$$

where

$$q(x,\omega) = Q(x,\omega) + \frac{A^2(x,\omega)}{4} + \frac{A'(x,\omega)}{2}$$

in which the prime on $A(x,\omega)$ denotes differentiation with respect to x. In general the term $Q(x,\omega)$ is of the order of k^2 or $1/\lambda_D^2$ (λ_D = the Debye length), whichever is larger (3.4). Assuming that $A'(x,\omega) \sim A(x,\omega)/L$ and recalling our previous discussion about the magnitude of $A(x,\omega)$ compared to $Q(x,\omega)$, we see that in $q(x,\omega)$ the $A(x,\omega)$ terms are smaller than the corresponding $Q(x,\omega)$ terms by approximately the ratio $(a_j + G_j/\Omega_j^2)a_j/L^2$. Therefore the $A(x,\omega)$ terms in $q(x,\omega)$ may be neglected as long as

$$(a_j + G_j/\Omega_j^2)a_j/L^2 << 1 \quad ,$$

a condition which is consistent with our intention of treating only slightly inhomogeneous media in this work. From (3.3.8) we also note that when this condition is satisfied the potential is nearly equal to $\Psi(x)$ for x not more than a few Larmor radii from x = 0.

Having shown that our general integro-differential dispersion equation can be approximated by (3.3.9) in which $\Psi(x)$ is approximately the potential $\phi(x)$, we now consider the conditions under which a localized solution for the potential $\phi(x)$ can exist. In order to have a localized solution, $\Psi(x)$ must be bounded as $x \longrightarrow \pm \infty$. For such a solution to exist it can easily be shown (3.5 - 3.8) that $q(x,\omega)$ must have at least one zero for some value of x. Since equation (3.3.9) is reminiscent of the time-independent Schroedinger equation for an arbitrary potential well (3.17) whose solutions are commonly found by the WKB method (3.18), it seems reasonable to attempt to use this method here. However, in contrast to the usual Schroedinger equation case, $q(x,\omega)$ is, in general, a complex quantity as $x \longrightarrow \pm \infty$. Many authors (3.6, 3.8 - 3.10) have shown that in this case "localized" potential solutions can exist only if there are at least two zeros or "turning points" of $q(x,\omega)$ which, in general, occur at complex values of x. Furthermore, the solution is only localized if the usual WKB phase integral condition on q is satisfied between these complex turning points, i.e.,

$$\int_{x_1}^{x_2} \left[-q(x,\omega)\right]^{1/2} dx = (n + \tfrac{1}{2})\pi \ , \ n=0,1,\ldots \qquad (3.3.10)$$

where x_1, x_2 are the complex turning points, i.e., in general complex values of x such that

$$q(x_1,\omega) = 0$$
$$q(x_2,\omega) = 0 \quad . \tag{3.3.11}$$

As in the quantum mechanical case, such a solution can exist only if $q(x,\omega)$ represents a density (plasma pressure) "hill" on the x direction. Here we interpret the plasma model described in Section 1.3 as representing only one side of the density "hill" with the maximum density gradient occurring locally at $x \approx 0$, and we imagine that there is a similar density gradient in the opposite direction far off to the left of the origin in Fig. 1.1. Some special cases in which equations (3.3.10) and (3.3.11) can be simultaneously solved for particular density distributions have been discussed by Silin (3.9). In general, however, simultaneously satisfying these three equations for each frequency ω of interest is a formidable task. Therefore we go on from these results and ask under what conditions the simultaneous satisfaction of these three equations gives approximately the same result as that obtained by using the local approximation, i.e., $q(x \approx 0,\omega) = 0$ or approximately $Q(x \approx 0,\omega) = 0$. For a somewhat simpler function Q, Krall and Rosenbluth (3.4)

have shown that the local approximation closely approximates the simultaneous solution of equations (3.3.10) and (3.3.11) as long as

$$a_i/L << 1 \qquad (3.3.12)$$

where L is the characteristic inhomogeneity length of $Q(x,\omega)$, and the a_i results from the $\mathcal{O}(a_i^2 + G_i^2/\Omega_i^4)$ terms in (3.3.5) with the G_i^2/Ω_i^4 term being neglected. It is implicitly assumed in their derivation that the Debye length is much smaller than the ion Larmor radius. If this is not the case, then a_i should be replaced by $\sqrt{a_i^2 + \lambda_D^2}$ in (3.3.12). Also, it is assumed that successive spatial derivatives of $Q(x,\omega)$ (up to second order) and hence of the plasma pressure are approximately given by the quantity being differentiated divided by the characteristic inhomogeneity length, i.e.,

$$Q'(x,\omega) \sim Q(x,\omega)/L \; ; \; Q''(x,\omega) \sim Q'(x,\omega)/L \sim Q(x,\omega)/L^2 \; .$$

A case in which this last assumption is not true has been considered by Hoh (3.10). Putting in the usually neglected gravity length and allowing for the possibility that the Debye length may be comparable to or larger than the ion Larmor radius, we see that the most general condition under which the local approximation dispersion relation for our

case gives a good representation of the simultaneous solution of equations (3.3.10) and (3.3.11) is

$$\frac{\sqrt{a_i^2 + \lambda_D^2 + G_i^2/\Omega_i^4}}{L} << 1 . \qquad (3.3.13)$$

This criterion simply specifies that for the local approximation to be valid the inhomogeneity length of the plasma must be long compared to the "fine structure" lengths in the plasma. We also note that as long as condition (3.3.13) is satisfied, $q(x,\omega)$ is very nearly equal to $Q(x,\omega)$ and $\psi(x)$ is very nearly just the potential $\phi(x)$.

Condition (3.3.13) gives another usually unrecognized condition on the magnitude of the gravity or external force. In contrast to the restriction found in Section 2.4, here the condition arises irrespective of whether or not the gravity force is representing magnetic field curvature and hence applies to all force fields in the x direction. Tracing the G_j/Ω_j^2 gravity length term back through the derivation, we find that this restriction arises due to the inclusion of the usually neglected oscillatory "wiggle" in the unperturbed particle orbits resulting from the gravity induced drift in the y direction (see preceding section).

In addition to the approximate WKB analysis method of solution, it should also be mentioned that other methods

have been used to solve (3.3.9). For a very simple particular plasma density distribution with no gravity force present, Pearlstein (3.11) has succeeded in solving the equation exactly. For this simple example Pearlstein concludes that under the assumption that condition (3.3.13) holds (with $G_j = 0$), the WKB solution and local approximation solution closely match the exact solution. Another case in which the exact and WKB method results are nearly identical has been reported by Chen (3.12). In addition, Rutherford and Frieman (3.13) have performed an analysis based on the propagation of wave packets in the x direction. They conclude that the local approximation is adequate to determine the initial growth rates of the instabilities, i.e., the complex frequencies ω. The localization of the potential in a cylindrical geometry has been considered by Shima and Fowler (3.14). By examining the kernal of the appropriate integral equation, they obtain a "local" approximation under conditions which are consistent with (3.3.13). A similar method involving an examination of the kernal of the integral equation was also used earlier by Krall and Rosenbluth (3.15) in studying a slab model case.

Having established the conditions under which we can use the local approximation for $\phi(x)$, we will now assume that those conditions are satisfied and then, taking $\phi(x)$ to be a constant as implied by the local approximation,

we can easily obtain the dispersion relation:

$$k^2 = 2\sum_j \omega_{P_j}^2 \int d^3v \frac{\partial \langle f_j \rangle}{\partial(v_\perp^2 - 2G_j x)} + \sum_j \omega_{P_j}^2 \int d^3v \sum_{n=-\infty}^{\infty} \sum_{m=-\infty}^{\infty} \frac{J_n^2(k_y v_\perp/\Omega_j)\, J_m(k_y G_j/\Omega_j^2)}{k_z v_z + (n+m)\Omega_j - k_y G_j/\Omega_j - \omega}$$

$$\times \left\{ k_z \frac{\partial}{\partial v_z}\left[F_j \left(1 + \frac{n}{k_y} \frac{\partial g_j}{\partial(x + v_y/\Omega_j)} \right) \right] - 2(k_z v_z - \omega) \frac{\partial}{\partial(v_\perp^2 - 2G_j x)} \left[F_j \left(1 + \frac{n}{k_y} \frac{\partial g_j}{\partial(x+v_y/\Omega_j)} \right) \right] + \frac{k_y F_j}{\Omega_j} \frac{\partial g_j}{\partial(x+v_y/\Omega_j)} \right\}_{x \approx 0}.$$

(3.3.14)

Rearranging this equation by completing the denominator in the term proportional to $(k_z v_z - \omega)$, combining the resultant term with the first term on the right side of (3.3.14) and defining n = n-m to reorder the n summation so that all of the resonances near a given cyclotron harmonic are grouped in a single term of the n summation, we may write the dispersion relation as

$$k^2 = \sum_j \omega_{P_j}^2 \int d^3v \sum_{n=-\infty}^{\infty} \sum_{m=-\infty}^{\infty} \frac{J_{n-m}^2(k_y v_\perp/\Omega_j)\, J_m(k_y G_j/\Omega_j^2)}{k_z v_z + n\Omega_j - k_y G_j/\Omega_j - \omega}$$

$$\times \left\{ k_z \frac{\partial}{\partial v_z}\left[F_j \left(1 + \frac{n-m}{k_y} \frac{\partial g_j}{\partial x} \right) \right] + \left(\frac{n\Omega_j}{v_\perp} - \frac{k_y G_j}{v_\perp \Omega_j} \right) \frac{\partial}{\partial v_\perp} \left[F_j \left(1 + \frac{n-m}{k_y} \frac{\partial g_j}{\partial x} \right) \right] + \frac{k_y F_j}{\Omega_j} \frac{\partial g_j}{\partial x} \right\}_{x \approx 0}$$

(3.3.15)

where, having performed the time integration, we have simplified the derivatives of the distribution function. Equation (3.3.15) is the general dispersion relation from which all further work in this thesis will derive.

We will now consider some general properties of this dispersion relation. First, we note that it has a branch line defined by $Re(k_z) = 0$. In order to see this, we divide the singular denominator in (3.3.15) through by k_z. Then, in this form it is easy to see that the prescription $Im(\omega) > 0$ for the evaluation of the v_z integral leads to different representations of the integral for positive and negative $Re(k_z)$. (See Appendix B for a discussion of an example of these singular v_z integrals.) Either representation may be analytically continued to the other half-plane of k_z; however, the two representations will not be equal in the resultant overlapping regions. The two different representations are joined along the line $Re(k_z) = 0$, which is therefore a branch line. They are equal at the branch point, $Re(k_z) = Im(k_z) = 0$.

As a matter of convenience, we would like to consider only $Re(k_z) > 0$ and thus avoid crossing this branch line. In order to justify restricting ourselves to this region of k_z space, we need to consider the symmetries of the dispersion relation with respect to sign changes in k_y, k_z, ω, n and m. In discussing these symmetries we will refer to the function which is formed by putting the terms on the right of (3.3.15) to the left of the equal sign as the dielectric function. As we shall discuss in Chapters 6 and 7, we will only be concerned in this work with real k_y, but, in general, with complex ω and k_z. For complex ω and k_z if we simultaneously change the signs of k_y, n

and m and the real parts of k_z and ω, the dielectric function is unchanged, except for the sign of its imaginary part. However, in order to have a solution of the dispersion relation, the imaginary part of the dielectric function must vanish. Therefore solutions of the dispersion relation for negative $Re(k_z)$ can be obtained from solutions for positive $Re(k_z)$ simply by changing the signs of k_y and the real part of ω. Recalling that the Bessel functions $J_n^2(k_y v_\perp / \Omega_j)$ are even functions of k_y, we see from the general dispersion relation that, instead of changing the sign of k_y, mathematically we could change the directions of the spatial inhomogeneity of the plasma and the gravity force. In any case we see that we can restrict our consideration of complex k_z modes to those whose real parts of k_z are positive (or zero).

When all of the equilibrium distribution functions $F_j(v_\perp, v_z)$ are even functions of v_z, a further symmetry exists. Then, for complex ω and k_z if we simultaneously change the signs of n, k_y, m, v_z, the real part of ω and the imaginary part of k_z, the dielectric function is as before unchanged, except for the sign of its imaginary part. Therefore we can obtain the solutions of the dispersion relation having negative k_y by simply changing the signs of the real part of ω and the imaginary part of k_z of the solutions we have found with positive k_y. In much of the subsequent work in this thesis, we will restrict

ourselves to cases in which all of the equilibrium distribution functions $F_j(v_\perp, v_z)$ are even functions of v_z (i.e., $v_{o_j} = 0$). For such cases we can restrict our search for solutions of the dispersion relation to positive k_y and k_z's having a positive real part. However, in general, we consider frequencies ω with both positive and negative real parts.

At this point in our consideration of dispersion relation (3.3.15), it is convenient to introduce a "reference species" of plasma particles. This species will really be a fictitious species since no reference species particles need exist in the plasma. The reference species will be denoted by a subscript zero and will usually be taken to be the ions (with a Maxwellian velocity distribution), although it is not necessary to do so. The reason for introducing such a reference species here is to allow us to write the dispersion in a particularly useful dimensionless form. It will be even more useful in the following section where we will write all quantities in the dispersion relation in dimensionless groups by using the properties of the reference species. The particular form in which we wish to write the dispersion relation here is

$$D(\omega,k) = \lambda - H(\omega,k) \qquad (3.3.16)$$

where

$$\lambda = \Omega_o^2/\omega_{p_o}^2 \tag{3.3.17}$$

$$H(\omega,k) = \frac{\Omega_o^2}{k^2}\sum_j \frac{\omega_{p_j}^2}{\omega_{p_o}^2}\int d^3v \sum_{n=-\infty}^{\infty}\sum_{m=-\infty}^{\infty} \frac{J_{n-m}(k_y v_\perp/\Omega_j) J_m^2(k_y G_j/\Omega_j^2)}{k_z v_z + n\Omega_j - k_y G_j/\Omega_j - \omega}$$

$$\times\left\{k_z \frac{\partial}{\partial v_z}\left[F_j\left(1+\frac{n-m}{k_y}\frac{\partial q_j}{\partial x}\right)\right] + \left(\frac{n\Omega_j}{v_\perp} - \frac{k_y G_j}{v_\perp \Omega_j}\right)\frac{\partial}{\partial v_\perp}\left[F_j\left(1+\frac{n-m}{k_y}\frac{\partial q_j}{\partial x}\right)\right] + \frac{k_y F_j}{\Omega_j}\frac{\partial q_j}{\partial x}\right\}_{x\approx 0}. \tag{3.3.18}$$

Here and throughout the rest of this work we will commonly use the symbol k as a shorthand notation denoting k_y, k_z or one or the other of the wave vector compoments when it only denotes the functional dependence of H. In the separation of the terms of the dispersion relation, we note that λ is <u>independent</u> of ω and k, but inversely proportional to the over-all plasma density. In contrast $H(\omega,k)$, which we will call the "dispersion function", is dependent on the ratio of the plasma frequency of a given species to that of the reference species and hence on the relative densities of each species, but is <u>independent of the over-all plasma density</u>. We shall make great use of this property of being able to separate out the density dependent term in the stability analysis of the succeeding chapters. In fact, it is this particular separation property which affords us the opportunity of arriving at a simple procedure for determing the density for transition to absolute instability (see Section 5.2).

Referring back to our discussion in Section 3.1, we can understand the physical significance of each of the terms enclosed in braces in our general dispersion relation (3.3.15). From that discussion it is readily apparent that the term proportional to k_z represents the destruction of the v_z constant of the motion. Similarly, $(k_y F_j/\Omega_j) \cdot \partial g_j/\partial x$ is the term which represents the destruction of the guiding center constant of the motion. Finally, the destruction of the constant of the motion which is analogous to the magnetic moment (see Section 2.1) is represented by the term containing $(n\Omega_j/v_\perp - k_y G_j/v_\perp \Omega_j)$. Since in the absence of a gravity force this last term is proportional to n, we see that for perturbations whose frequencies are much less than the ion cyclotron frequency and whose wavelengths k_y^{-1} are long compared to the ion Larmor radius (see Section 6.1), the magnetic moment is conserved. That this is true in general for such perturbations has been shown by Taylor (3.19). The gravity force term does not similarly vanish for low frequencies but does become small for wavelengths long compared to the ion Larmor radius. The reason it does not vanish for low frequencies is that the gravity force causes a uniform v_y drift of the particles irrespective of the frequency of the electric field fluctuation. In the general dispersion relation (3.3.15), the terms proportional to $\frac{n-m}{k_y} \frac{\partial g_j}{\partial x}$ result from the averaging of the particle trajectory

orbits over the velocity space anisotropy caused by the density gradient. As we have discussed previously in this section, these $\frac{(n-m)}{k_y} \frac{\partial g_j}{\partial x}$ terms must always be small compared to unity for our analysis to be valid.

The physical significance of the terms in the singular or resonant denominator of (3.3.15) is also worth considering. The essence of the entire denominator $k_z v_z + n\Omega_j - k_y G_j/\Omega_j - \omega$ is that it gives the effective frequency of the wave as seen by the particles. Thus we note that with ω being the true frequency of the electrostatic wave there are three "correction" terms. First there is the correction of $k_z v_z$ which is the Doppler shift due to the motion of the particle in the z direction. Next, as long as $k_y \neq 0$, there is the correction of $n\Omega_j$ accounting for the resonance of the wave with the n^{th} harmonic of the basic frequency of the helical motion of the particles around the magnetic field lines, the cyclotron frequency. Finally, there is the $k_y G_j/\Omega_j$ Doppler shift correction for the motion of the particles in the y direction since in this direction there is a gravity-force-induced uniform drift velocity of $v_{D_y} = G_j/\Omega_j$ (see preceding section). Note that the "drift's" v_{o_j}, $\langle v_\perp \rangle /\sqrt{2}$ and those arising from the density-gradient-induced diamagnetic current do not appear explicitly in the resonant denominator of the dispersion relation since they are macroscopic drifts associated with the equilibrium

state of the plasma. Rather, they enter through the dependence of the dispersion relation on the equilibrium distribution. The Bessel function multiplier terms give the appropriate weighting factors to account for the degree of spatial coherence of the wave propagation perpendicular to the magnetic field with the helical motion of the particles around the magnetic field lines for coupling with each particular harmonic of the cyclotron frequency.

The over-all effects of the terms which contribute to the dispersion relation are often referred to by particular names. Since a homogeneous plasma with a Maxwellian velocity distribution is known to be stable against microinstabilities (see Section 1.1), the terms which contribute to the dispersion relation must have either a damping effect or no effect at all on the waves propagating in such a plasma. The damping contributions due to the $k_z \partial \langle f_j \rangle / \partial v_z$ terms are commonly referred to as " Landau" or "collisionless" damping (3.20). When Landau damping is the major damping mechanism and even it is nearly negligible, the slightly damped waves which propagate are called "plasma" waves or "plasma oscillations" (3.21). The $\frac{n \Omega_j}{v_\perp} \frac{\partial \langle f_j \rangle}{\partial v_\perp}$ terms are the source of what is called "cyclotron" damping (3.22). The waves which are slightly damped only by this last mechanism (or not affected at all

if $\omega \simeq n\Omega_i$) are referred to as "cyclotron" waves (3.23). The contributions to the dispersion relation accounting for inhomogeneities of a plasma have no similar names indicating damping mechanisms since they usually have a destabilizing influence on a plasma. However, the waves excited or driven by plasma inhomogeneities are commonly referred to as "drift" waves for reasons which are discussed in Section 7.1.

In addition to this brief description of the terms in the general dispersion relation, we note some of its limiting forms. First, if we have no gravity force and no plasma inhomogeneities, then we see that our general dispersion relation reduces to the Harris dispersion relation (3.24). If we were to keep, in addition, the plasma inhomogeneity terms but neglect the usually small $\frac{n-m}{k_y} \frac{\partial g_j}{\partial x}$ terms, we would have a general form of the dispersion relation for drift cyclotron waves, which was first derived by Mikhailovskii and Timofeev (3.25). Considering only low frequencies in this simplified dispersion relation and thus neglecting the $n\Omega_j/v_\perp$ magnetic moment destruction term, we are left with the usual dispersion relation for drift waves in an inhomogeneous plasma (3.4). Specializing that dispersion relation to waves whose wavelengths perpendicular to the magnetic field are much longer than the ion Larmor radius, we obtain the

dispersion relation which results from the so-called drift kinetic approximation (3.26).

3.4 Dispersion Relation: Special $\langle f \rangle$

Having found the dispersion relation for general $\langle f \rangle$, we will now work out the dispersion relation for our particular equilibrium distribution function. In doing this we need only work out the "dispersion function" $H(\omega,k)$ since λ, the other part of the dispersion relation, is independent of the choice of equilibrium distribution function. While we will include both gravity and non-zero ℓ contributions to $H(\omega,k)$ in the following equations, we remind the reader that considering a combination of these parameters is probably not a reasonable way to examine magnetic field curvature effects on a plasma which has a loss-cone distribution (see Section 2.2). For the general equilibrium distribution function discussed in detail in Chapter 2, the dispersion function may be written as

$$H(\omega,k) = \frac{\Omega_o^2}{k^2}\sum_j \frac{\omega_{pj}^2}{\omega_{po}^2}\int_{-\infty}^{\infty} dv_z \sum_{n=-\infty}^{\infty}\sum_{m=-\infty}^{\infty} \frac{J_m(k_y G_j/\Omega_j^2)}{k_z v_z + n\Omega_j - k_y G_j/\Omega_j - \omega} \frac{e^{-(v_z-v_{oj})^2/\alpha_{zj}^2}}{\sqrt{\pi}\,\alpha_{zj}}$$

$$\times \int_0^{\infty} 2\pi v_\perp dv_\perp J_{n-m}^2\left(\frac{k_y v_\perp}{\Omega_j}\right)\left\{ -\frac{2(v_z-v_{oj})}{\alpha_{zj}^2} k_z\left[1 + \frac{n-m}{k_y}\left(-\epsilon_j' + \delta_{\perp j}\alpha_{\perp j}^{-2} v_\perp^2 + \delta_{zj}\left\{\alpha_{zj}^{-2}(v_z-v_{oj})^2 - 1\right\}\right)\right] F_{\perp j}^{\ell}\right.$$

$$+ \left[\frac{n\Omega_j}{v_\perp} - \frac{k_y G_j}{v_\perp \Omega_j}\right]\left[\left\{1 + \frac{n-m}{k_y}\left(-\epsilon_j' + \delta_{\perp j}\alpha_{\perp j}^{-2} v_\perp^2 + \delta_{zj}\alpha_{zj}^{-2}(v_z-v_{oj})^2\right)\right\}\frac{dF_{\perp j}^{\ell}}{dv_\perp} + 2\delta_{\perp j}\alpha_{\perp j}^{-2} v_\perp F_{\perp j}^{\ell}\right]$$

$$\left. + \frac{k_y}{\Omega_j}\left[-\epsilon_j' + \delta_{\perp j}\alpha_{\perp j}^{-2} v_\perp^2 + \delta_{zj}\alpha_{zj}^{-2}(v_z-v_{oj})^2\right] F_{\perp j}^{\ell}\right\}. \qquad (3.4.1)$$

In this equation we note that we have integrals of $J_n^2(k_y v_\perp/\Omega_j)$ times the perpendicular velocity distribution $F_{\perp j}^{\ell}$ and its derivative. In Appendix A the integrals of interest are discussed in detail and related to the C,D functions defined by Guest and Dory (3.27). Here we list only the relevant results found there:

$$\int_0^{\infty} 2\pi v_\perp dv_\perp J_n^2\left(\frac{k_y v_\perp}{\Omega_j}\right) F_{\perp j}^{\ell} = C_{nj}^{\ell}(\lambda_j)$$

$$\int_0^{\infty} 2\pi v_\perp dv_\perp J_n^2\left(\frac{k_y v_\perp}{\Omega_j}\right) v_\perp^2 F_{\perp j}^{\ell} = (\ell+1)\alpha_{\perp j}^2 C_{nj}^{\ell+1}(\lambda_j)$$

$$\int_0^\infty 2\pi v_\perp dv_\perp \, J_n^2\left(\frac{k_y v_\perp}{\Omega_j}\right)\left[\frac{1}{v_\perp}\frac{dF_{\perp j}^{\ell}}{dv_\perp}\right] = -\frac{2}{\alpha_{\perp j}^2} D_{n_j}^{\ell}(\lambda_j)$$

$$\int_0^\infty 2\pi v_\perp dv_\perp \, J_n^2\left(\frac{k_y v_\perp}{\Omega_j}\right) v_\perp^2\left[\frac{1}{v_\perp}\frac{dF_{\perp j}^{\ell}}{dv_\perp}\right] = -2\left[(\ell+1)D_{n_j}^{\ell+1}(\lambda_j) + C_{n_j}^{\ell}(\lambda_j)\right]$$

where

$$\lambda_j \equiv (k_y a_j)^2/2 = k_y^2 \alpha_{\perp j}^2/2\,\Omega_j^2 \quad .$$

Using these results in (3.4.1) we obtain

$$H(\omega,k) = \frac{\Omega_0^2}{k^2}\sum_j \frac{\omega_{pj}^2}{\omega_{p0}^2}\sum_{n=-\infty}^{\infty}\sum_{m=-\infty}^{\infty} J_m\left(\frac{k_y G_j}{\Omega_j v_2}\right)\frac{1}{\sqrt{\pi}}\int_{-\infty}^{\infty} d\left(\frac{v_z}{\alpha_{zj}}\right)\frac{e^{-(v_z-v_{0j})^2/\alpha_{zj}^2}}{k_z v_z + n\Omega_j - \frac{k_y G_j}{\Omega_j} - \omega}$$

$$\times\left\{-\frac{2(v_z-v_{0j})}{\alpha_{zj}^2}k_z\left[C_{n-m_j}^{\ell} + \frac{n-m}{k_y}\left(-\epsilon_j' C_{n-m_j}^{\ell} + \delta_{\perp j}(\ell+1)C_{n-m_j}^{\ell+1} + \delta_{zj}\left\{\alpha_{zj}^{-2}(v_z-v_{0j})^2 - 1\right\}C_{n-m_j}^{\ell}\right)\right]\right.$$

$$-\frac{2}{\alpha_{\perp j}^2}\left[n\Omega_j - \frac{k_y G_j}{\Omega_j}\right]\left[D_{n-m_j}^{\ell} + \frac{n-m}{k_y}\left(-\epsilon_j' D_{n-m_j}^{\ell} + \delta_{\perp j}(\ell+1)D_{n-m_j}^{\ell+1} + \delta_{zj}\alpha_{zj}^{-2}(v_z-v_{0j})^2 D_{n-m_j}^{\ell}\right)\right]$$

$$\left.+\frac{k_y}{\Omega_j}\left[-\epsilon_j' C_{n-m_j}^{\ell} + \delta_{\perp j}(\ell+1)C_{n-m_j}^{\ell+1} + \delta_{zj}\alpha_{zj}(v_z-v_{0j})^2 C_{n-m_j}^{\ell}\right]\right\} \qquad (3.4.2)$$

where the argument λ_j of the C,D function has been omitted for simplicity in notation. In carrying out the remaining v_z integration, we encounter integrals of the form

$$\int_{-\infty}^{\infty} du \; \frac{u^{n_e} - u^2}{u - w_n}$$

where $w_n = \dfrac{-n\,\Omega_j + k_y G_j/\Omega_j + \omega}{k_z \alpha_{z_j}} - \dfrac{v_{o_j}}{\alpha_{z_j}}$. In the definition of these integrals we must remember that the dispersion relation was derived for $\mathrm{Im}\,\omega > 0$ and hence for $\mathrm{Im} w_n > 0$ (for $\mathrm{Re}(k_z) > 0$). The singular integrals which arise here are related to the plasma dispersion function (3.28) and are discussed in detail in Appendix B, where we define

$$Z_n(w) = \frac{1}{\sqrt{\pi}} \int_{-\infty}^{\infty} \frac{u^{n_e} - u^2}{u - w} \, du \quad .$$

Using this definition and forming dimensionless groups of all variables through the use of the reference species introduced in the preceding section, we can write the dispersion function as ($\mathrm{Re}(k_z) > 0$)

$$H(\omega,k) = -\frac{2}{(ka_o)^2}\sum_j \frac{\omega_{p_j}^2}{\omega_{p_o}^2}\frac{\alpha_{z_o}^2}{\alpha_{z_j}^2}\sum_{n=-\infty}^{\infty}\sum_{m=-\infty}^{\infty} J_m\left[(k_y a_o)\left(\frac{G_j}{a_o\Omega_j^2}\right)\right]$$

$$\times\left\{\left\{Z_1(w_n)\left[C^{\ell}_{n-m_j} + \frac{n-m}{(k_y a_o)}\left(-(\epsilon_j' a_o)\,C^{\ell}_{n-m_j} + (\ell+1)(\delta_{\perp_j} a_o)\,C^{\ell+1}_{n-m_j}\right)\right] + \frac{n-m}{(k_y a_o)}(\delta_{z_j} a_o)\left[Z_3(w_n) - Z_1(w_n)\right]C^{\ell}_{n-m_j}\right\}\right.$$

$$+\frac{1}{(k_z a_o)}\left(\frac{a_o}{a_j}\right)\left(\frac{\alpha_{z_j}}{\alpha_{\perp_j}}\right)\left[n-(k_y a_o)\left(\frac{G_j}{a_o\Omega_j^2}\right)\right]\left\{Z_o(w_n)\left[D^{\ell}_{n-m_j} + \frac{n-m}{(k_y a_o)}\left(-(\epsilon_j' a_o)D^{\ell}_{n-m_j} + (\ell+1)(\delta_{\perp_j} a_o)D^{\ell+1}_{n-m_j}\right)\right]\right.$$

$$\left.+ Z_2(w_n)\frac{n-m}{(k_y a_o)}(\delta_{z_j} a_o)D^{\ell}_{n-m_j}\right\} - \frac{(k_y a_o)}{2(k_z a_o)}\left(\frac{a_j}{a_o}\right)\left(\frac{\alpha_{z_j}}{\alpha_{\perp_j}}\right)\left\{Z_o(w_n)\left[-(\epsilon_j' a_o)\,C^{\ell}_{n-m_j} + (\ell+1)(\delta_{\perp_j} a_o)C^{\ell+1}_{n-m_j}\right]\right.$$

$$\left.\left.+ Z_2(w_n)(\delta_{z_j} a_o)\,C^{\ell}_{n-m_j}\right\}\right\} \qquad (3.4.3)$$

in which

$$w_n = \frac{\left(\frac{\omega}{\Omega_o}\right)\left(\frac{\alpha_{z_o}}{\alpha_{z_j}}\right) - \left(\frac{a_o}{a_j}\right)\left(\frac{\alpha_{\perp_j}}{\alpha_{z_j}}\right)\left[n-(k_y a_o)\left(\frac{G_j}{a_o\Omega_j^2}\right)\right]}{(k_z a_o)} - \left(\frac{v_{o_j}}{\alpha_{z_o}}\right)\left(\frac{\alpha_{z_o}}{\alpha_{z_j}}\right).$$

In writing this equation for the dispersion function, we have assumed that $\alpha_{z_o} = a_{\perp_o}$, i.e., all reference species have Maxwellian velocity distributions. The terms in (3.4.3) are written in the same order as those in (3.3.15) so we can easily discern the physical significance of each term. In addition, we note that the symbols ϵ', $\delta_\perp$, δ_z

represent respectively the gradients of density, and temperature transverse and parallel to the magnetic field so we can easily identify the effects of each of these parts of the plasma inhomogeneity. In (3.4.3) the resonant denominator of (3.3.15) is represented by w_n. Physically we interpret w_n to be the phase velocity of the wave, as seen by the particles for coupling with the n^{th} cyclotron harmonic of the particle motion, divided by the thermal velocity of the particles. It is therefore an "effective" dimensionless wave phase velocity as seen by the particles.

While we will not further manipulate the dispersion function at this point, in Appendix C we put it in a rapidly convergent form which is more suitable for numerical computations. In Appendix C we also discuss the very general computer programs which were developed in this work to investigate the stable and unstable (convective and absolute) waves characterized by the dispersion relation given in (3.3.16) with the general dispersion function being that defined by (3.4.3).

Before proceeding to a discussion of instability criteria, there are some general properties of the dispersion relation as worked out in this section which are worth discussing here. First, we note that when k_z is real but nonzero the dispersion function $H(\omega,k)$ is a sum of entire functions of the complex frequency ω (see Appendix B). Thus, in this case it is analytic over the

entire finite complex ω-plane. When $k_z = 0$, the dispersion function's only singularities are simple poles which occur for frequencies ω equal to harmonics of the cyclotron frequency. Therefore for all k_z the dispersion function $H(\omega,k)$ is an entire function over the upper half complex ω-plane.

Another property is that for $|Im(k_z)| > |Re(k_z)|$ the dispersion function $H(\omega,k)$ is undefined (infinite). We will refer to the region of k_z space for which the dispersion function is undefined as the "divergence" region. That the dispersion function becomes infinite can be seen from the fact that for arbitrarily large n and k_z in the "divergence" region, the arguments of the plasma dispersion function moments have arbitrarily large negative imaginary parts. For such arguments we see from equations (B.7) and (B.13) that the plasma dispersion function moments become arbitrarily large in magnitude, thus causing the dispersion function to diverge. Two factors apparently contribute to the divergence of the dispersion function. These are the lack of convergence of the Bessel function expansion and the inclusion of particles moving at arbitrarily large velocities, as evidenced by the fact that the divergent terms are far off resonance (large n and large effective wave phase speed). It can be shown (3.29) that the divergence occurs even when the Bessel function expansion is not made. Therefore it seems

that the divergence is the result of the inclusion of particles moving at arbitrarily large velocities (e.g., greater than the velocity of light).

One way to avoid this divergence difficulty is simply to ignore the contributions to the dispersion function from all terms except that representing the wave resonance with the closest cyclotron harmonic. The dispersion function which results from this procedure might closely approximate the exact one if the divergence is indeed due to the inclusion of particles moving faster than the velocity of light. However, in this work we will avoid the divergence region difficulties by confining ourselves to a consideration of unstable modes whose k_z's are not in the divergence region. This restriction is not severe, but does limit us to absolute instabilities with small temporal growth rates (see Sections 6.2, 7.2). We should also note that just outside the divergence region the off-resonance terms vanish exponentially. Therefore we expect that the dispersion function we have derived in this section is an accurate representation of the exact dispersion function for k_z outside the divergence region.

4. REAL-k INSTABILITY ANALYSIS

4.1 Marginal Stability Analysis

In this chapter we will be concerned with determining the parametric conditions under which a given wave (mode) in a plasma can be unstable. We defer the problem of determining whether the unstable mode is of the convective or absolute type to the next chapter. As we have discussed previously (Section 1.1), the key parameter of interest here is the density. Thus we will be looking mainly for the threshold density, that is the density at which a particular mode first becomes unstable.

In order to find the parametric ranges of instability it is customary to carry out a marginal stability analysis. In such an analysis we determine the parametric conditions under which a given wave in a plasma is marginally stable, i.e. the point at which if the parametric conditions were changed incrementally in some particular way the mode would become unstable. Clearly the characteristics of a marginally stable mode are that it must not be growing either temporally or spatially and hence it must have a real frequency ω and a real wave vector $\underline{k}$. Therefore the essence of the marginal stability analysis is that we must find the parametric conditions for which solutions of the dispersion relation can exist for real ω, $\underline{k}$. However, in

doing so, depending on the dispersion relation, we must remember that not all allowed modes which have real ω, $\underline{k}$ are necessarily marginally stable modes. As an example we note that for many "cold plasma" dispersion relations (4.1) such modes may be merely undamped propagating modes which would be damped in a real collisionless plasma due to the presence of Landau ("collisionless") damping (4.2) or perhaps due to collisions themselves. The ambiguity concerning the nature of the real ω, $\underline{k}$ modes can be avoided by restricting our study to those modes which, for a slight change in parameters, can have frequencies with an infinitesimal positive imaginary part and hence are truly marginally stable modes. However, in this work we employ "hot plasma" dispersion relations which include Landau damping and thus know that all allowed modes with real ω, $\underline{k}$ are marginally stable modes.

In addition to the above qualification on the interpretation of real ω, $\underline{k}$ modes there are two other questions left unanswered by a marginal stability analysis. First, knowing the marginal stability boundary in parameter space, there is the question of which side of the boundary represents unstable modes and which side stable modes. This question is usually quite easily answered by physical arguments (e.g. consideration of free energy sources) or by a simple calculation of the sign of the imaginary part

of the frequency as we move incrementally away from the marginal stability boundary. Second and more serious is the question as to whether or not the parametric regions of instability predicted by the marginal stability analysis constitute all of the possible regions of instability. A related question is whether or not the plasma is stable outside the predicted regions of instability.

For an infinite homogeneous plasma with no magnetic field present, these questions have been answered for exponentially growing waves by the derivation of necessary and sufficient conditions for instability (4.3-4.5). That the lack of satisfaction of these conditions is sufficient to guarantee stability against nonexponential growths as well has been shown by Penrose (4.4). We begin our discussion of these criteria by specifying the dispersion relation for a homogeneous unmagnetized plasma. For a general equilibrium distribution function, the dispersion relation in this case is (4.5)

$$k^2 = \sum_j \omega_{p_j}^2 \int d^3v \, \frac{k \, \partial F_j / \partial v_z}{k v_z - \omega} \; ; \; \mathrm{Im}(\omega) > 0 \qquad (4.1.1)$$

where the direction of propagation is chosen to be in the z direction.

Defining

$$F(u) \equiv \sum_j \omega_{pj}^2 \int d^3v \; F_j(\underline{v})\,\delta(u - \underline{v}\cdot\underline{k}/k), \qquad (4.1.2)$$

we can write this dispersion relation as

$$k^2 = H(\omega/k) \qquad (4.1.3)$$

where

$$H(\omega/k) = \int_{-\infty}^{\infty} du \; \frac{F'(u)}{u-\omega/k} \qquad (\mathrm{Im}(\omega)>0)$$

$$= \mathcal{P}\int_{-\infty}^{\infty} du \; \frac{F'(u)}{u-\omega/k} + \pi i F'(\omega/k) \quad (\mathrm{Im}(\omega)=0^+). \qquad (4.1.4)$$

In this last expression $\mathcal{P}$ denotes the Cauchy principal value operator, i.e.

$$\mathcal{P}\int_{-\infty}^{\infty} du = \lim_{\varepsilon\to 0}\left\{ \int_{-\infty}^{a-\varepsilon} du + \int_{a+\varepsilon}^{\infty} du \right\}.$$

In deriving necessary and sufficient conditions for instability we need to determine the conditions under which unstable modes can exist in a plasma. The unstable modes are those solutions of the dispersion relation which can exist in the upper half ω-plane, that is with $\mathrm{Im}(\omega)>0$. The dispersion relation of interest here (4.1.3) has the form of a positive definite constant k^2 (k is real here) being equal to a transcendental function of the wave phase

velocity. Note however that the transcendental function $H(\omega/k)$ is independent of the magnitude of k for a fixed wave phase velocity. A convenient method of analyzing the solutions of this type of dispersion relation is by a conformal mapping procedure (4.7) similar to that used in the Nyquist diagram technique (4.8). Basically in this approach the entire upper half ω-plane is mapped into the $H(\omega/k)$ plane and then the question of instability reduces

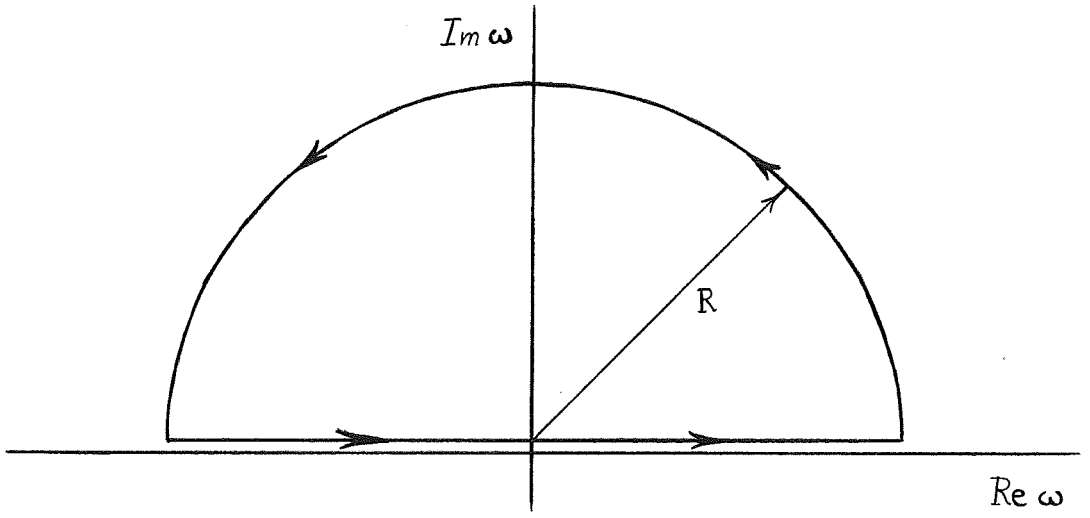

Figure 4.1. Mapping Contour for Nyquist Diagram Technique ($R \to \infty$).

to the question of whether or not $H(\omega/k)$ can take on positive real values within the mapped region. In order to perform the mapping it is convenient to use the ω-plane contour shown in Fig. 4.1. The contour goes from $-\infty$ to $+\infty$ in Re ω just above the real axis and is closed in the upper half ω-plane by a semicircle at infinity. It can easily

be seen from (4.1.4) that $H(\omega/k)$ vanishes along the semi-circle.

Typical mappings of this contour into the $H(\omega/k)$ plane and the respective plots of $F'(\omega/k)$ for a stable plasma and two characteristic types of unstable plasmas are shown in Fig. 4.2. The directions of the arrows in these mappings correspond to those along the contour shown in Fig. 4.1. From the theory of complex variables (4.7) we know that the interior of the mapped contours (i.e. to our left as we proceed along the contour) corresponds to the interior of the contour being mapped. In our case it is the upper half ω-plane which is being mapped and its interior maps into the shaded regions of Fig. 4.2. The cases displayed will be discussed in more detail later in this section.

Now, in order to have an instability we must satisfy the dispersion relation given by (4.1.3) in the upper half ω-plane. To do so it is clearly necessary for the H-plane mapping of the upper half ω-plane to encompass part of the positive real $H(\omega/k)$ axis. Considering the form of $H(\omega/k)$ displayed in the second part of (4.1.4), we see that this is possible if and only if there is a speed u_o such that the imaginary part of the dispersion relation vanishes and the real part can be satisfied by a positive definite value of k^2 (4.3-4.5, 4.9):

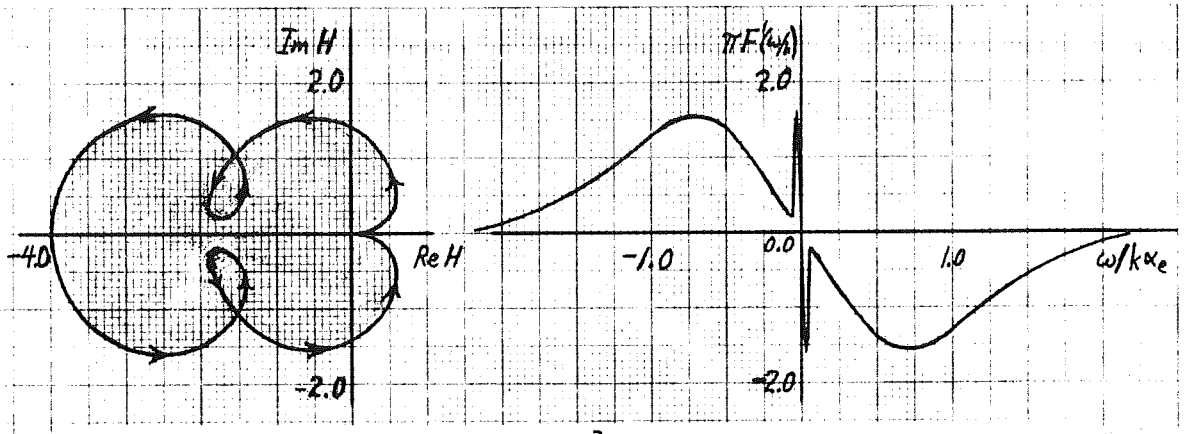

a.) Stable Plasma: $\langle f_e \rangle = (\sqrt{\pi}\alpha)^{-3} \exp[-v^2/\alpha^2]$

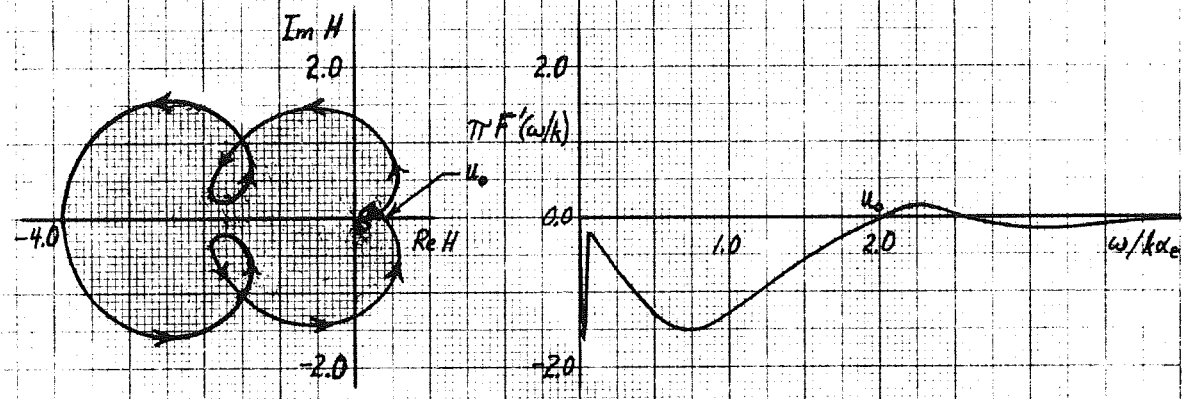

b.) "Bump-on-Tail" Instability: $\langle f_e \rangle = (\sqrt{\pi}\alpha)^{-3} \left\{ 0.95 \exp[-v^2/\alpha^2] + 0.05 \exp[-(v-2.5\alpha)^2/\alpha^2] \right\}$

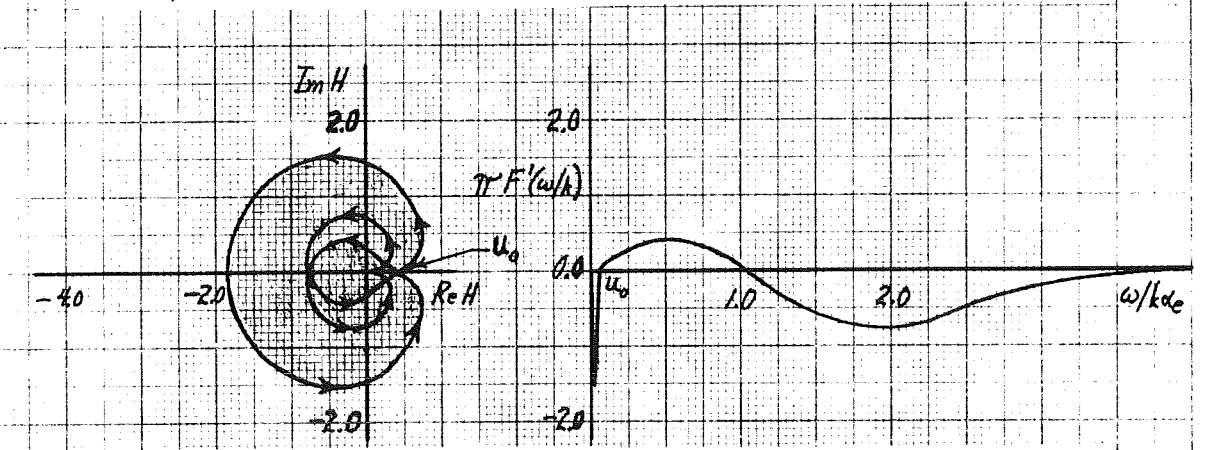

c.) "Two-Stream" Instability: $\langle f_e \rangle = \frac{1}{2} (\sqrt{\pi}\alpha)^{-3} \left\{ \exp[-(v-\alpha)^2/\alpha^2] + \exp[-(v+\alpha)^2/\alpha^2] \right\}$

Figure 4.2. Nyquist and F'(ω/k) Plots for Various Types of Stable and Unstable Plasmas.

$$F'(u_o) = 0, \text{ with} \begin{cases} F'(u_o+\varepsilon) > 0 \\ F'(u_o-\varepsilon) < 0 \end{cases} \quad \text{(necessary condition)} \quad (4.1.5)$$

$$\mathcal{P}\int_{-\infty}^{\infty} \frac{F'(u)}{u-u_o}\, du > 0 \qquad \text{(sufficiency condition)} \quad (4.1.6)$$

These necessary and sufficient conditions for instability of exponentially growing waves have been derived in a more rigorous fashion by Penrose (4.4), who has also shown that when these conditions are not satisfied the plasma is stable against all types of growing modes (within the limits of the linear theory). For that analysis to apply, F'(u) and its derivative must be bounded and square integrable. Finally, the question of instability when F'(u) has a second or higher order zero was also considered by Penrose (4.4). The instability conditions given by (4.1.5) and (4.1.6) are often referred to as the "Penrose conditions."

Considering conditions (4.1.5) and (4.1.6) we see that unstable modes can exist in a plasma only if there is a minimum of F(u) which is sufficiently "deep." We also note that since

$$\lim_{u\to\infty} F'(u) = 0^- \qquad (4.1.7)$$

$$\lim_{u\to-\infty} F'(u) = 0^+, \qquad (4.1.8)$$

condition (4.1.5) reduces simply to the requirement that F'(u) have more than one zero in the finite range of real u. A consequence of this reduction is the fact that all equilibrium distributions F(u) which are "single-humped" must be stable, a result which has been obtained by many authors (e.g. 4.3, 4.8).

In Section 1.1 we noted that Rowlands (4.10) has shown that a homogeneous unmagnetized plasma for which the velocity distribution of each species of plasma particles is a continuous,but not necessarily monotonic, function of the single particle energy is nonlinearly stable against microinstabilities. Since one might think that a velocity distribution which is not a monotonically decreasing function of the energy could give rise to a "two-stream" type of instability, it would appear that Rowland's conclusion contradicts the results which would be obtained from an application of the instability conditions given by (4.1.5) and (4.1.6)--the Penrose conditions. However as we shall now show, this is not the case. Let us consider F'(u) for equilibrium distribution functions which are continuous functions of v^2--the single particle energy here. For these types of equilibria, from (4.1.2) we see that

$$F'(u) = 2u \sum_j \omega_{p_j}^2 \int_0^\infty \pi d(v_\perp^2) \frac{dF_j(v_\perp^2 + u^2)}{d(v_\perp^2 + u^2)}$$

in which the $\perp$ subscript denotes directions perpendicular to the wave propagation direction. Changing the variable of integration to $y = v_\perp^2 + u^2$, we obtain a perfect differential and thus have

$$F'(u) = 2\pi u \sum_j \omega_{p_j}^2 F_j(y) \Big|_{u^2}^{\infty} .$$

However all F_j must vanish at $u^2 = \infty$ so that they are normalizable and so this becomes simply

$$F'(u) = -2\pi u \sum_j \omega_{p_j}^2 F_j(u^2) .$$

Since by definition $F_j(u) \geq 0$, we see from this last result that $F'(u)$ has at most one first order zero. Therefore the Penrose conditions also predict stability for this case in agreement with the proof by Rowlands (4.10).

For an unstable plasma characterized by dispersion relation (4.1.1), the speed u_o which satisfies conditions (4.1.5) and (4.1.6) is the phase velocity of the marginally stable mode. The appropriate frequency ω and wave number k for the marginally stable mode are determined by the value of k given by solving (4.1.3), i.e.

$$k_o = \sqrt{H(u_o)} = \sqrt{\mathcal{P} \int_{-\infty}^{\infty} \frac{F'(u)}{u-u_o}\, du} \quad . \qquad (4.1.9)$$

Note that we can solve the dispersion relation for k in this manner only because,while $H(\omega/k)$ is dependent on the phase velocity,it is independent of the magnitude of k. After once crossing the real $H(\omega/k)$ axis at $u = u_o$, the H-plane mapping may or may not cross the positive real $H(\omega/k)$ axis again. Therefore in order to determine the range of k for the unstable modes, we must find the next zero of the imaginary part of the dispersion relation (the next maximum of F(u)) for $|u| > |u_o|$. Supposing that this occurs for $u = u_1$, the range of real k for which unstable waves occur in the plasma is given by

$$k_i < |k| < k_o$$

where

$$k_1 \equiv \begin{cases} \sqrt{H(u_1)}, & H(u_1) > 0 \\ 0, & H(u_1) \leq 0. \end{cases}$$

In the preceding paragraph we have seen that the phase velocities of unstable modes in a plasma are always greater than the velocity u_o at a minimum of F(u) and less than the velocity u_1 at the next maximum of F(u) ($|u_1| > |u_o|$). We will refer to such regions of u as "positive-slope" regions since, at least for positive velocities u, F(u) has a positive slope in these regions. Waves whose phase velocities are in the "positive-slope" regions may be

expected to be unstable since, as is known from quasilinear theory (4.11), the presence of any wave in this region causes diffusion of the particles "downhill" in velocity space which in this case corresponds to particles losing kinetic energy. The conservation of energy then demands that the wave gain energy at the expense of the particles' kinetic energy and hence that the wave is unstable. We may also note that the "positive-slope" region is a region in which we expect the plasma to have "free energy" which can feed an instability since there the effective distribution function F(u) is not a monotonically decreasing function of the energy (see Section 1.1). We therefore see that the "positive-slope" regions of F(u) correspond to the unstable phase velocity regions for very physical reasons. Throughout the remainder of this work we shall find the concept of "positive-slope" regions of effective distributions quite useful in identifying phase velocity regions in which unstable modes may exist.

As examples of the application of the necessary and sufficient conditions for instability, consider the three cases shown in Fig. 4.2. In all three cases the leftmost heart-shaped curves in the Nyquist plots and the very narrow spikes in the F'(u) plots represent the effects of the ions. The more slowly varying parts of the F'(u) plots and the remainder of the Nyquist plots are due to the effects of the electrons. For the stable plasma case

(Fig. 4.2a) it is obvious that F'(u) has only one zero which corresponds to a maximum of F(u) and hence the plasma is indeed stable. This of course can also be seen from the fact that the mapping of the upper half ω-plane does not encompass any part of the positive real $H(\omega/k)$ axis (the Nyquist curve asymptotically approaches the Re(H) axis). In the last two cases shown in Fig. 4.2 the plasma is unstable. In these cases F'(u) is only plotted for positive u since the plot for negative u is easily ascertained from the data shown for these cases and the stable plasma case. In the "bump-on-tail" instability case F'(u) has three zeros and consideration of the corresponding Nyquist plot shows that the zero marked with a u_o satisfies both the necessary and sufficient conditions for instability. Likewise, in the "two-stream" instability case F'(u) has five zeros, of which two of the respective values of u (with the same magnitudes but opposite signs) satisfy the necessary and sufficient conditions for instability. Note that, as we would expect, the "positive-slope" regions occur for phase velocities which are less than the "drift" velocities in the unstable plasmas.

All of the preceding remarks in this chapter have applied only to a uniform plasma in the absence of a magnetic field. The general necessary and sufficient conditions for instability have been extended to a homogeneous

plasma in a uniform magnetic field by McCune (4.12). We will not discuss that analysis here since in the next section we employ nearly the same procedure to obtain criteria further generalized to include the slight plasma inhomogeneity and gravity force which are included in the dispersion relation derived in the preceding chapter.

4.2 General Instability Criterion

In this section we will show how we can put our general dispersion relation (3.3.15) into a form in which we can apply the necessary and sufficient conditions for instability given in the preceding section. In addition we will put these conditions in a form in which the threshold density is readily determined.

In order to obtain an appropriate form of the dispersion relation, we follow the general procedure used by McCune (4.12) in the uniform magnetic field case. In terms of our notation, we make the substitution ($k_z \neq 0$)

$$ku = k_z v_z + n\Omega_j - k_y G_j/\Omega_j \tag{4.2.1}$$

for each j, n; we can then write the "dispersion function" $H(\omega,k)$ as

$$H(\omega,k) = \int_{-\infty}^{\infty} \frac{P(u)}{u-\omega/k}\, du \tag{4.2.2}$$

where

$$P(u) \equiv \frac{\Omega_o^2}{k^3} \sum_j \frac{\omega_{p_j}^2}{\omega_{p_o}^2} \int d^3v \sum_{n=-\infty}^{\infty} \sum_{m=-\infty}^{\infty} J_{n-m}^2(k_y v_\perp/\Omega_j)\, J_m(k_y G_j/\Omega_j^2)$$

$$\times \left\{ \left[k_z \frac{\partial}{\partial v_z} + \left(\frac{n\Omega_j}{v_\perp} - \frac{k_y G_j}{v_\perp \Omega_j} \right) \frac{\partial}{\partial v_\perp} \right] \left[F_j \left(1 + \frac{n-m}{k_y} \frac{\partial g_j}{\partial x} \right) \right] + \frac{k_y F_j}{\Omega_j} \frac{\partial g_j}{\partial x} \right\}$$

$$\times \delta \left(v_z - \frac{ku - n\Omega_j + k_y G_j/\Omega_j}{k_z} \right) . \qquad (4.2.3)$$

The transformation given by (4.2.1) reduces the dispersion function $H(\omega,k)$ from a sum of a countable infinity of singular integrals over various derivatives of the smooth equilibrium distribution function into a singular integral over a single, albeit complicated, function. Therefore the transformation in a sense transforms the complicated magnetic field case into a familiar simple case with a "projected" distribution function $\int_{-\infty}^{u} P(u')\, du'$ which although very complicated is in principle much like that of the analogous $F(u)$ for two-stream or many-stream distribution functions in an unmagnetized plasma. The transformation can of course only be performed if $k_z \neq 0$. However as we shall see later in this section, when $k_z = 0$ the instability analysis is similar to that for nonzero k_z, k_y. We also note that for real ω, k, $P(\omega/k)$ is simply the imaginary part of the dispersion function divided by π. Since in a marginal stability analysis one usually fixes k, we can write $P(\omega/k)$ as $P(\omega/\Omega_o)$ or what is usually the same $P(\omega/\Omega_i)$.

Recalling the general form of our dispersion relation (3.3.16) and using (4.2.2) we can write the dispersion

relation as

$$\lambda = \frac{\Omega_o^2}{\omega_{p_o}^2} = \int_{-\infty}^{\infty} \frac{P(u)}{u-\omega/k}\, du \qquad (4.2.4)$$

in which we must remember that P(u) is explicitly dependent on k_y, k_z. At first sight one might think that the results of the preceding section could not be applied to the more general dispersion relation considered in this work since P(u) does depend explicitly on the wave vector components. However, from the form of (4.2.4) we see that the k^2 of (4.1.3) in the unmagnetized plasma case has been replaced here by $\Omega_o^2/\omega_{p_o}^2$ which is a positive definite quantity dependent on the plasma density. Likewise the k-independent F'(u) has been replaced by P(u) which is <u>independent of the overall plasma density</u> (see Section 3.3). Here and throughout the remainder of this work we will refer to a parameter which has this property that it can be separated out from the rest of the dispersion relation (in an additive sense) as a "free parameter." With this definition in mind we see that whereas previously the wave number k was a "free parameter," here it is λ or the overall plasma density which is the "free parameter." The overall plasma density is a "free parameter" for a homogeneous unmagnetized plasma as well.

With these remarks in mind we see that we can equally well apply the Nyquist diagram technique used in the preceding section to the present case as long as P(u) and its derivative are bounded and square integrable and $k_z \neq 0$. It is easy to see from (4.2.3) that these conditions on P(u) are satisfied for sufficiently well behaved equilibrium distribution functions. Therefore the conditions for a given mode characterized by k_y, k_z to be unstable are that there must exist a u_o such that

$$P(u_o) = 0, \text{ with } \begin{cases} P(u_o+\varepsilon) > 0 \\ P(u_o-\varepsilon) < 0 \end{cases} \text{ (necessary condition)} \tag{4.2.5}$$

$$\mathcal{P}\int_{-\infty}^{\infty} \frac{P(u)}{u-u_o}\, du > 0 \quad \text{(sufficiency condition).} \tag{4.2.6}$$

For the special case of a homogeneous plasma in a uniform magnetic field these conditions were first given by McCune (4.12) for a slightly different form of P(u)*. When these

* The original derivation of conditions (4.2.5) and (4.2.6) given by McCune (4.12) involved unnecessarily complicated arguments showing that P(u) is independent of the magnitude of k, although it is dependent on ω/k, Ω_j/k. The fact that the density is a free parameter analogous to k in the original Penrose analysis, which allows the simple type of analysis carried out here, was pointed out to the author by McCune (4.13). Ozawa, Kaji and Kito (4.14) have also used a substitution like that given in (4.2.1) to obtain a dispersion relation for a homogeneous plasma in a uniform magnetic field which depends only on a function that is essentially $k^2 P(u)$. These authors use potential theory (4.5) to derive instability conditions which for some cases are identical with those given here, but in general are incorrect due to an improper consideration of the sufficiency condition for instability (4.2.6).

necessary and sufficient conditions for instability are satisfied and the plasma is unstable for <u>some</u> plasma densities, then the density at which the plasma first becomes unstable to the given mode (the threshold density) is specified by

$$\lambda_o = \frac{\Omega_o^2}{\omega_{p_o}^2} = \mathrm{Re}[H(ku_o,k)] = \mathcal{P}\int_{-\infty}^{\infty} \frac{P(u)}{u-u_o}\,du \,. \qquad (4.2.7)$$

Therefore in checking the sufficiency condition for instability, we simultaneously determine the "critical" λ and hence the threshold density for instability for given k_y, k_z, <u>etc</u>. As in the unmagnetized homogeneous plasma case, the range of the free parameter for which unstable modes occur may be limited due to the fact that the H-plane mapping may again intersect the real $H(\omega,k)$ axis on the positive side for $|u| > |u_o|$. Taking this possibility into account, we find that the range of plasma densities for which the given mode under consideration is unstable is specified by

$$\lambda_i < \lambda = \frac{\Omega_o^2}{\omega_{p_o}^2} < \lambda_o \qquad (4.2.8)$$

where

$$\lambda_1 \equiv \begin{cases} \mathrm{Re}[H(ku_1,k)] = H(ku_1,k), & H(ku_1,k) > 0 \\ 0, & H(ku_i,k) \leq 0 \end{cases} \qquad (4.2.9)$$

in which u_1 is defined to be the next zero of P(u) which occurs for $|u| > |u_o|$. Conditions (4.2.5), (4.2.6) and (4.2.8) comprise respectively the necessary and sufficient conditions for the existence of exponentially growing (unstable) waves in a plasma and the range of λ and hence plasma density for which the given mode (i.e. given k) is unstable. It is interesting to note that since for real and nonzero k_Z the dispersion function $H(\omega,k)$ is bounded for all finite ω (see Section 3.4), (4.2.7) and (4.2.8) show us that any plasma will be stable against exponentially growing modes having any given nonzero k_Z for sufficiently low densities.

Having derived necessary and sufficient conditions for the existence of exponentially growing modes, we would like to know if, in the absence of such modes, the plasma is stable against growing modes of all types. The derivation given by Penrose (4.4) showing that this is the case for an unmagnetized plasma is based upon the fact that the linearized Vlasov equation can be put into a one-dimensional form, i.e. a form which depends only on F'(u)--the velocity-space derivative of the equilibrium distribution function along the direction of wave propagation. The fact that here we are able to obtain the one-dimensional function P(u) which is directly analogous to F'(u) of the Penrose analysis implies that the linearized Vlasov equation can also be put into a one-dimensional form even for the complicated plasma model considered in this work. For the

simpler case of a homogeneous plasma in a magnetic field, McCune (4.13) has directly demonstrated that a one-dimensional form of the linearized Vlasov exists. With these remarks in mind we conjecture that the proof by Penrose (4.4) that the plasma is stable in the absence of exponentially growing modes applies to the more complicated plasma model considered in this work as well. Therefore, we expect that the necessary and sufficient conditions for stability are that the necessary and sufficient conditions for instability, (4.2.5) and (4.2.6), not be satisfied for any mode of the plasma.

From the instability conditions we have seen that for unstable modes to occur, P(u) must have more than one zero and u must be in the range between two successive zeros of P(u), the first of which must correspond to a minimum of the function $\int_{-\infty}^{u} P(u')du'$. This range of u is a "positive-slope" region of $\int_{-\infty}^{u} P(u')du'$ and has the same physical significance as that discussed in the preceding section for F(u). The function P(u) is thus the "effective" velocity-space derivative of the equilibrium distribution function in the direction of wave propagation for waves propagating at any angle other than 90° with respect to the magnetic field, and is directly analogous to F'(u) in all ways. In many directions of propagation it is easy to understand the physical significance of the dominant

contributions to P(u). In the later parts of this work we will find an understanding of these contributions and the concept of "positive-slope" regions to be very powerful tools in identifying the phase velocity regions (in both the y and z directions) for which unstable waves can exist in a plasma.

It is worth noting that the necessary and sufficient conditions for instability are simply those which arise in a marginal stability analysis. Thus what we have shown here is that the usual marginal stability analysis in which we take real ω, k and search for zeros of the imaginary part of the dispersion relation (P(u) in this case) is rigorously correct. In the marginal stability analysis an ambiguity in the range of density for which a given mode is unstable arises when the dispersion relation can be satisfied for realistic plasma densities at any two successive zeros of P(u). This ambiguity is resolved as a natural consequence of the Nyquist diagram technique employed here (condition (4.2.8)).

The general conditions for instability given by (4.2.5), (4.2.6) and (4.2.8) are applicable only for non-zero k_z. When $k_z = 0$ the dispersion function $H(\omega,k)$ becomes an algebraic function of ω, with singularities at harmonics of the cyclotron frequency (see appendix C). Unstable solutions of this dispersion relation occur when there is a local minimum of $H(\omega,k_y,k_z=0)$ between two

cyclotron harmonics. The unstable modes occur for λ less than the local minimum of H. The conditions for instability when $k_z = 0$ are thus

$$\left.\frac{\partial H(\omega,k_y,k_z=0)}{\partial \omega}\right|_{\omega=\omega_o} = 0 \qquad \text{(necessary condition)} \tag{4.2.10}$$

$$\lambda_o \equiv H(\omega_o,k_y,k_z=0) > 0 \quad \text{(sufficiency condition)}. \tag{4.2.11}$$

When unstable modes exist, the density range for instability is given by

$$\lambda < \lambda_o . \tag{4.2.12}$$

In view of the similarity of conditions (4.2.5), (4.2.6) and (4.2.8) to (4.2.10), (4.2.11) and (4.2.12) we find that when $k_z=0$ a convenient definition of P(u) is

$$P(u) = \frac{\partial H(ku,k_y,k_z=0)}{\partial u} . \tag{4.2.13}$$

With this definition the instability conditions for zero and nonzero values of k_z become nearly synonymous.

At this point we wish to make a distinction between two different approaches to finding unstable modes of a plasma. Basically the two approaches derive from whether we wish to satisfy the necessary or the sufficient condition for instability first. Often a combination of both

approaches is useful in determining the conditions for instability (see Chapters 6 and 7). In the following discussion we limit ourselves to nonzero k_z in which case the approaches are distinguished by whether we satisfy the real or the imaginary part of the dispersion relation first. However, with appropriate interpretations of the real and imaginary parts of the dispersion relation in terms of the instability conditions, the same general remarks apply for $k_z=0$.

If we satisfy the imaginary part of the dispersion relation first, we search for zeros of P(u) and then determine the threshold density for instability (if one exists) for those zeros by considering the sufficiency condition for instability (4.2.6). This approach has the advantage that we are seeking zeros of a transcendental function P(u). Therefore we can be quite sure mathematically (or numerically) whether or not the necessary condition for instability is satisfied.

Alternatively we may try to satisfy the real part of the dispersion relation first. This can be done by reverting to making Nyquist plots. While at first sight this procedure would seem to be quite difficult, in many cases it is easy to rapidly sketch Nyquist plots. The reason for this is that for cases in which there are no temperature gradients along the magnetic field, we can

easily see from (3.4.3) that $H(\omega,k)$ is a simple linear combination of the transcendental functions $-2Z_0(w)$, $-2Z_1(w)$. The behavior of these basic functions for the Nyquist plotting contour of Fig. 4.1 is plotted in Fig. 4.3. Both $-2Z_0(w)$ and $-2Z_1(w)$ tend toward the real axis asymptotically as they approach the origin in such a way that the origin is not enclosed by either mapping. Also, both functions vanish along the semicircle at infinity in Fig. 4.1. The numbers along the curves in Fig. 4.3 give the value of w at that point. We recall that in the present notation $-2Z_1(w)$ is the same as the more familiar function $Z'(w)$ (see appendix B).

Since the dispersion function $H(\omega,k)$ is a simple weighted sum of the functions $-2Z_0(w)$ and $-2Z_1(w)$ with differing arguments for each cyclotron harmonic and each species of plasma particle, we can easily obtain its Nyquist plot by appropriately combining the curves shown in Figs. 4.3a and 4.3b. We have already seen examples of such combinations in Fig. 4.2. There, as we might expect from comparing Figs. 4.2 and 4.3, the heart-shaped curves are due to the $-2Z_1(w)$ function. The physical significance of this function is that it gives the appropriate contribution to the dispersion relation for one species of particles having a Maxwellian velocity distribution in an unmagnetized plasma. In the limit of large phase velocity this function leads to a Landau or colli-

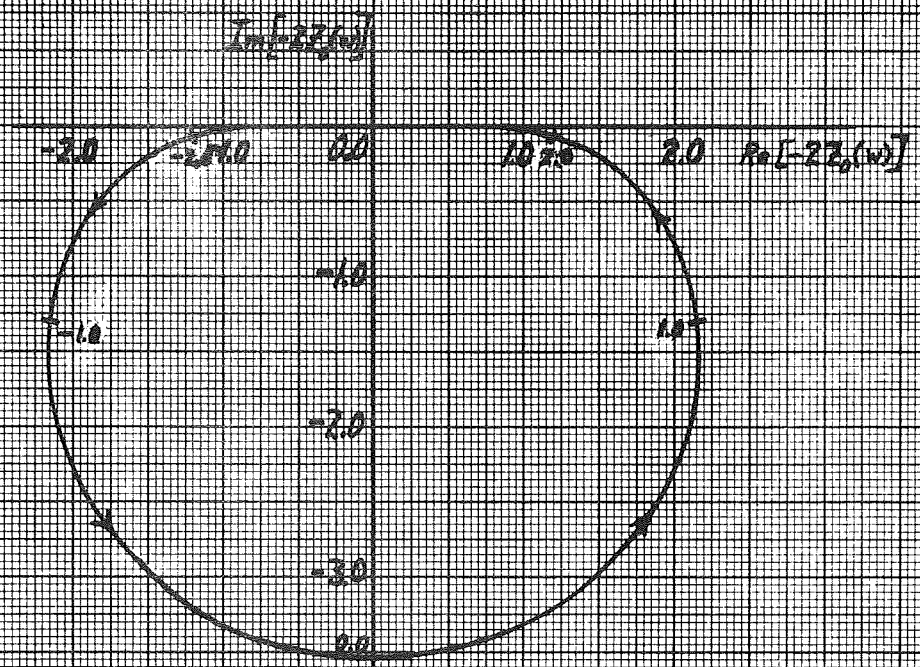

a.) The Function $-2Z_0(w)$

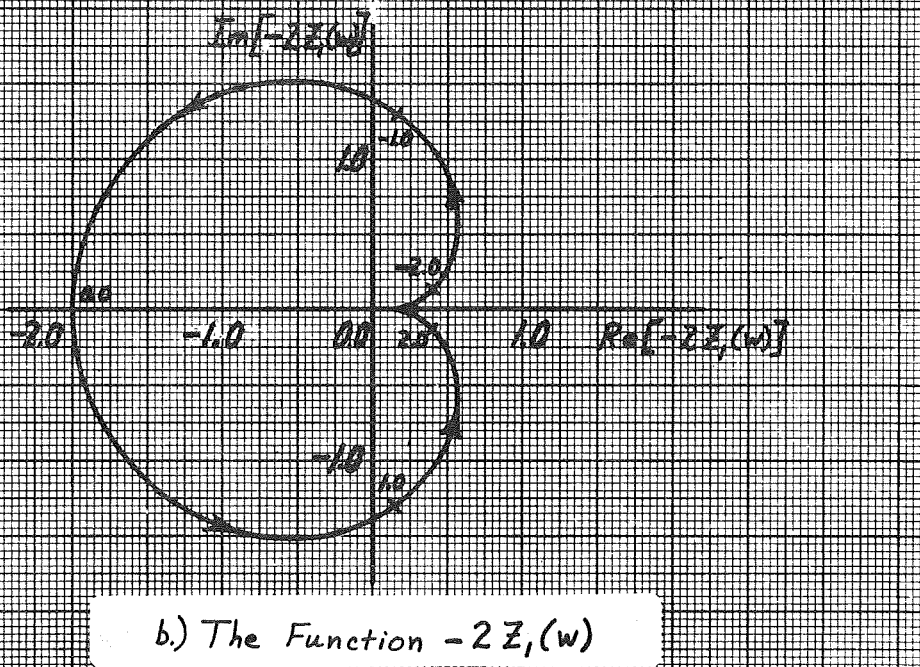

b.) The Function $-2Z_1(w)$

Figure 4.3. Behavior of the Functions $-2Z_0(w)$ and $-2Z_1(w)$ for Real w.

sionless damping contribution. Since we are usually interested only in the behavior of the Nyquist plot in the vicinity of the positive real axis, we can normally simplify the plotting procedure by restricting our attention to that portion of the Nyquist plot.

In order to further clarify these different approaches, we consider a particular example. The case we consider is that introduced by Beasley (4.15) in modeling the "central peak" plasma of the DCX-2 machine (4.16). The relevant parameters for this homogeneous plasma example are $T_{z_i}/T_{\perp_i} = 10^{-3}$, $T_{z_e}/T_{z_i} = 0.05$, and $\ell = 1$ for the type of $v_\perp$ distribution (see Eq. (1.3.1)). Here the principal source of free energy is the ion velocity distribution anisotropy due to the large difference between the mean velocities along and transverse to the magnetic field. The "loss-cone" nature of the $v_\perp$ distribution constitutes in comparison a nearly negligible source of free energy (see Section 6.1) We refer to the plasma instabilities which are driven mainly by the source of free energy associated with the inequality of mean velocities along and transverse to the magnetic field as "temperature-anisotropy" instabilities (see Section 6.1). For the present we only wish to illustrate the possible methods of finding plasma instabilities and so we will defer discussion of the simplifications of the general dispersion relation (3.3.15) for this case and of the physics

of this instability to Chapter 6. The mode which we will consider here is that which has $k_y a_i = 2.0$ and $k_z a_i = 0.75$.

In Fig. 4.4 the Nyquist and P(u) plots for this case are displayed. In Figs. 4.4a and 4.4b these plots are shown on a scale in which only the electron contribution is seen. Since we can distinguish only one zero of $P(\omega/\Omega_i)$ and no enclosure of the positive real axis by the Nyquist plot in these plots, we might think that the plasma is stable to this mode. However this is not the case. In Figs. 4.4c and 4.4d we magnify the scale of the Nyquist and $P(\omega/\Omega_i)$ plots around the origin of the Nyquist plot to the scale of the ion contributions to the dispersion relation. The latter plots are only shown for positive frequencies since for this case the real and imaginary parts of the dispersion function are respectively symmetric and antisymmetric functions of the frequency. Thus the corresponding plots for negative frequencies are easily found from those shown for positive frequencies.

In one approach to finding the unstable modes, we examine the imaginary part of the dispersion relation first. From Fig. 4.4d we observe that $P(\omega/\Omega_i)$ has eight zeros for $0 < \omega/\Omega_i < 4.5$. Four of these zeros satisfy the necessary condition for instability. The real part of the dispersion function at each of these four zeros can be ascertained from Fig. 4.4c which shows that the sufficiency condition for instability is satisfied for all four zeros.

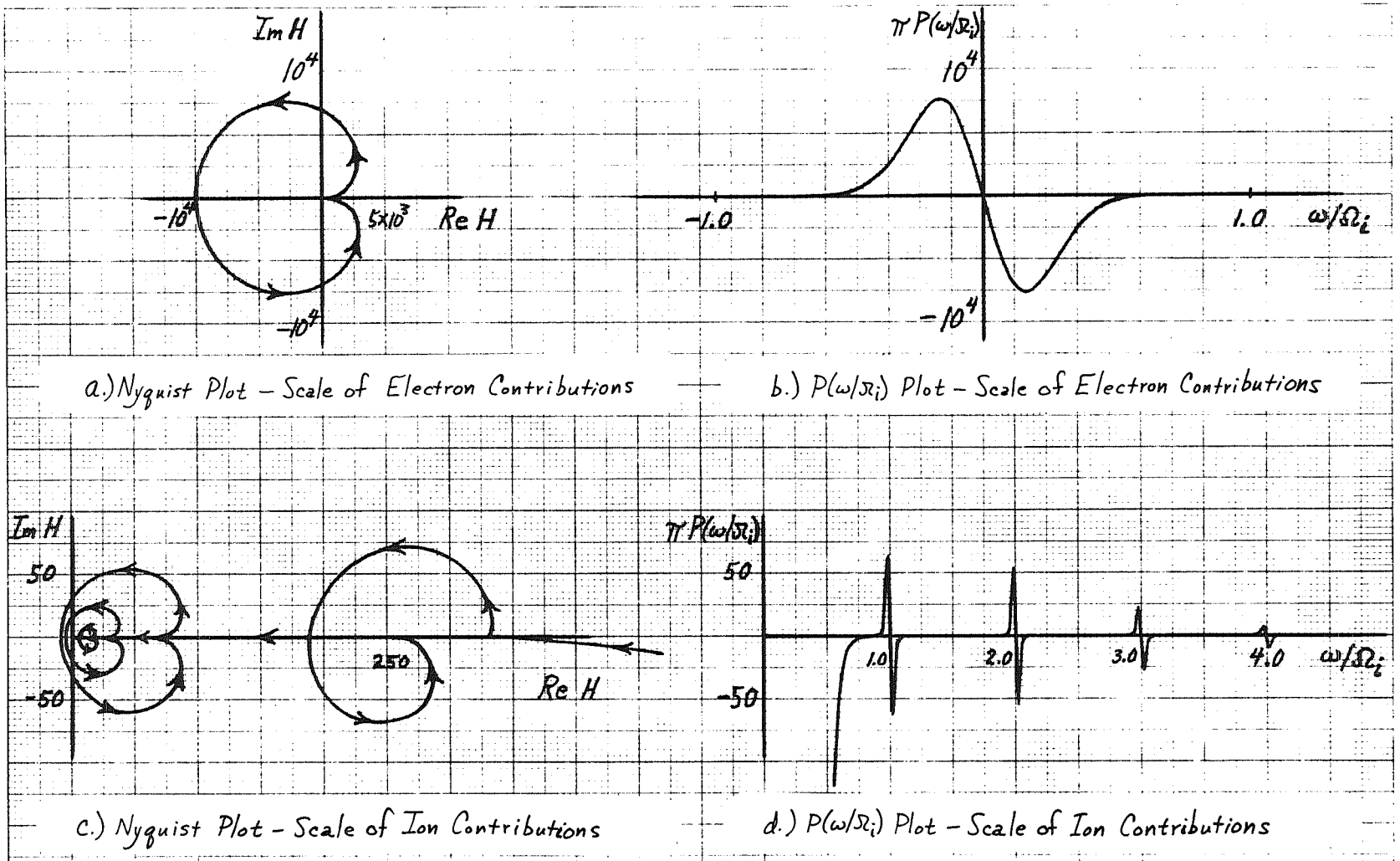

a.) Nyquist Plot – Scale of Electron Contributions

b.) $P(\omega/\Omega_i)$ Plot – Scale of Electron Contributions

c.) Nyquist Plot – Scale of Ion Contributions

d.) $P(\omega/\Omega_i)$ Plot – Scale of Ion Contributions

Figure 4.4. Nyquist and $P(\omega/\Omega_i)$ Plots for Temperature-Anisotropy Instability Case ($T_{z_i}/T_{\perp_i}=10^{-3}$, $T_{z_e}/T_{z_i}=\frac{1}{20}$, $l=1$, $k_y a_i=2.0$, $k_z a_i=0.75$).

In the alternative approach we discover that the plasma is unstable to this mode (for sufficiently high density) by directly considering the Nyquist plot shown in Fig. 4.4c. Here it is obvious that a portion of the positive real H axis is enclosed by the contour and hence that the mode can be unstable at least for a range of plasma densities. In Fig. 4.4c it is readily apparent that the Nyquist plot is simply constructed from a superposition of many of the heart-shaped curves characteristic of the $-2Z_1(w)$ functions (see Fig. 4.2b). Examples in which the $Z_o(w)$ functions dominate the ion contributions to the dispersion relation are considered in Section 4.4 and Chapters 6 and 7. Viewing Figs. 4.2 and 4.4 it is easy to see how with only a meager knowledge of the coefficients of the Z_o and Z_1 functions we could plot Nyquist plots for other cases of interest. In particular we note that as long as $k_y \alpha_e / \Omega_e << 1$ (see Section 6.1), the electron "background" part is always nearly the same and it is only the shape of the curves which represent the ion contributions which changes according to the type of free energy source which is present.

We conclude this section with some remarks on the advantages and disadvantages of these two different approaches to determining whether a given mode is unstable. While finding the zeros of a transcendental function such

as $P(\omega/\Omega_o)$ is a relatively simple matter on a computer, finding them by hand can be very laborious. In contrast, the development of the computer program logic necessary to follow complicated Nyquist plots (e.g. Fig. 4.4) and determine the points at which such curves cross the positive real axis can be very difficult. We also note that while $P(\omega/\Omega_i)$ is generally a rapidly convergent series due to its transcendental nature, the real part of the dispersion function is a relatively slowly convergent series due to its algebraic nature. Therefore for computer calculations it is best to avoid evaluating the real part of the dispersion function $H(\omega,k)$ and hence Nyquist plot points as much as possible. However, in contrast to these considerations of computational difficulty, we have seen that for many cases of interest it is fairly easy to sketch a Nyquist plot. We thus conclude that the technique of finding zeros of $P(\omega/\Omega_i)$ is best suited for computing machines, while a judgment as to the possibility of a given instability is often most readily ascertained from a rough sketch of the appropriate Nyquist plot.

4.3 Temporal Growth Rates

In this section we address ourselves to the problem of determining the temporal growth rate of an instability once the plasma density exceeds the threshold density. As we have mentioned previously (Section 1.1), we really should be interested first in determining whether the instability is of the absolute or convective type. However, for the purposes of this section we will assume that the waves are propagating in an infinite homogeneous (in the directions of wave propagation) medium and that there is a uniform density of random noise sources inducing instability uniformly throughout the plasma. Under these conditions there is no intrinsic difference between absolute and convective instabilities, and we are only concerned with the temporal growth rates of the instabilities for real wave numbers $\underline{k}$.

The usual method used to determine the temporal growth rate (the positive imaginary part of a complex frequency ω) of an instability is to follow the trajectory of the complex ω root of the dispersion relation for real wave numbers $\underline{k}$. In particular, for a given plasma density we generally begin at the $\omega,\underline{k}$ values corresponding to a marginally stable mode and change $\underline{k}$ by small increments until it reaches another marginal stability point. We follow the corresponding complex ω root by solving the

dispersion relation with the Newton-Raphson (4.17) or another suitable iteration technique at each successive value of the real wave number $\underline{k}$, using the previous result as an estimate of the location of the new root. Fairly accurate estimates of the location of roots are required for most iteration schemes. Therefore the root following procedure of determining temporal growth rates usually requires that at least a moderately accurate marginal stability analysis be carried out to provide reasonable starting values of $\omega,\underline{k}$ at each density of interest.

A completely different method of finding complex ω solutions of the dispersion relation, which does not rely upon the marginal stability analysis, has been described by McCune (4.18). This method, which we will call the Cauchy integral method, is derived from an application of Cauchy's integral theorems (4.19). For a function $\phi(z)$ which has zeros at $a_1,a_2,\ldots$ of multiplicity $r_1,r_2,\ldots$respectively and poles at $b_1,b_2,\ldots$of multiplicity $s_1,s_2,\ldots$respectively within a given contour C, and a function f(z) which is analytic within the same region, we know from the calculus of residues (4.19) that

$$\frac{1}{2\pi i}\oint_C f(z)\,\frac{\phi'(z)}{\phi(z)}\,dz = \sum_i r_i\, f(a_i) - \sum_i s_j\, f(b_j). \qquad (4.3.1)$$

In the simple case of $f(z) = 1$ this general equation reduces to the familiar theorem for counting the number of zeros and poles of a given function $\phi(z)$ within a contour C:

$$\oint_C \frac{\phi'(z)}{\phi(z)}\, dz = N - P.$$

We can also use the same general integral to locate zeros of the dispersion relation in the complex ω plane by taking $f(z)$ to be equal to z and $\phi(z)$ to be the dispersion relation. Then, noting that the general dispersion relation has no poles for $k_z \neq 0$ (it is analytic over the entire finite complex ω-plane--see Section 3.4) and assuming for the moment that only one zero of the dispersion relation falls within the contour C, we can write ($z \equiv \omega/\Omega_o$)

$$\left.\frac{\omega}{\Omega_o}\right|_{D=0} = \frac{1}{2\pi i} \oint_C z\, \frac{H'(\Omega_o z, k)}{H(\Omega_o z, k) - \lambda}\, dz \qquad (4.3.2)$$

where the prime denotes differentiation with respect to z. For $k_z = 0$ the dispersion function $H(\omega,k)$ has poles for frequencies ω equal to harmonics of the cyclotron frequency. In this case as long as the contour C does not encircle any of these poles, (4.3.2) is still valid.

In practice it may be difficult to choose a contour which encircles only one zero of the dispersion relation.

However, even when more than one zero falls within the contour we can determine the location of each of the zeros (4.20). In order to do so it is convenient to define

$$I_b(C) \equiv \frac{1}{2\pi i} \oint_C z^b \frac{\phi'(z)}{\phi(z)} dz \qquad (4.3.3)$$

in which here we take ϕ to be the dispersion relation, i.e. $H(\Omega_o z,k)-\lambda$. For a given contour C, $I_o(C)$ gives the number of complex zeros of ϕ which are encircled by the contour. In order to solve for all the zeros we need at least $I_o(C)$ independent complex equations relating the complex zeros. Since $I_1(C)$, $I_2(C)$, etc. give respectively the sum of the zeros, the sum of the squares of the zeros, etc., the required equations to solve for all zeros within the contour can be obtained by calculating the integral given in (4.3.3) for $b = 1,2,\ldots,I_o(C)$. In addition to these considerations of simple zeros within the contour, it is easily shown (4.13) that for branch zeros, $I_o(C)$ gives the order of the branch zero. Therefore we see that in general all simple zeros and branch zeros of the dispersion relation can be computed by evaluating a sufficient number of the moment-integrals defined in (4.3.3).

Note that in the contour integrals given by (4.3.2) and (4.3.3) we are keeping k a constant, but can simulta-

neously calculate (on a computer) the complex frequency ω for a variety of λ's (densities) as long as the contour C encloses all of the roots of interest. This reduction in effort required to find any one zero is possible only because the density is a "free parameter" of the dispersion relation. Similar economies can of course be achieved for variation in any other "free parameters" of the dispersion relation if they exist.

Clearly a major difficulty with the Cauchy integral method is the selection of an appropriate contour C. In practice the contour is relatively easy to select if we have done a marginal stability analysis for a given k, since then we know the limits on the real ω axis between which the plasma may be unstable. However, it is not really necessary to have this marginal stability information. This is particularly true when the Cauchy integral method is used in conjunction with an "on-line" computer in which the "Nyquist" plot of the dispersion relation along the contour C can be visually examined to see if it encircles the origin, thus demonstrating that a zero of the dispersion relation lies within the contour. The feasibility of using the Cauchy integral method on an "on-line" computer has been demonstrated by McCune and Fried (4.20).

We have computed temporal growth rates useing both of the methods discussed above for the plasma model of DCX-2 which we used as an example in the preceding section. Typical results for these temperature-anisotropy instabilities are shown in Fig. 4.5. In Fig. 4.5a we show the growth rates for a given k_z and varying λ (plasma density) which were computed by the Cauchy integral method. The relevant values of $\lambda = \Omega_i^2/\omega_{p_i}^2$ are listed along the curves. Similarly in Fig. 4.5b where we find the growth rates for fixed λ (that which corresponds to a density 2.57 times the minimum threshold density) and varying k_z by following the trajectory of the complex ω roots, the numbers listed along the curves are the relevant values of $k_z a_i$. As we see from Fig. 4.5, the temporal growth rates of these instabilities are significant fractions of the ion cyclotron frequency for very moderate plasma densities, an obvious indication of the threat which the temperature-anisotropy instabilities pose to plasma confinement.

Generally for a thorough analysis of a given instability, we would like to know its maximum temporal growth rate for a given density. Since the normal method of following the trajectory of the complex ω roots of the dispersion relation for a given density naturally yields such a result, this method seems best for a thorough study of a given plasma instability. However, this method is heavily dependent

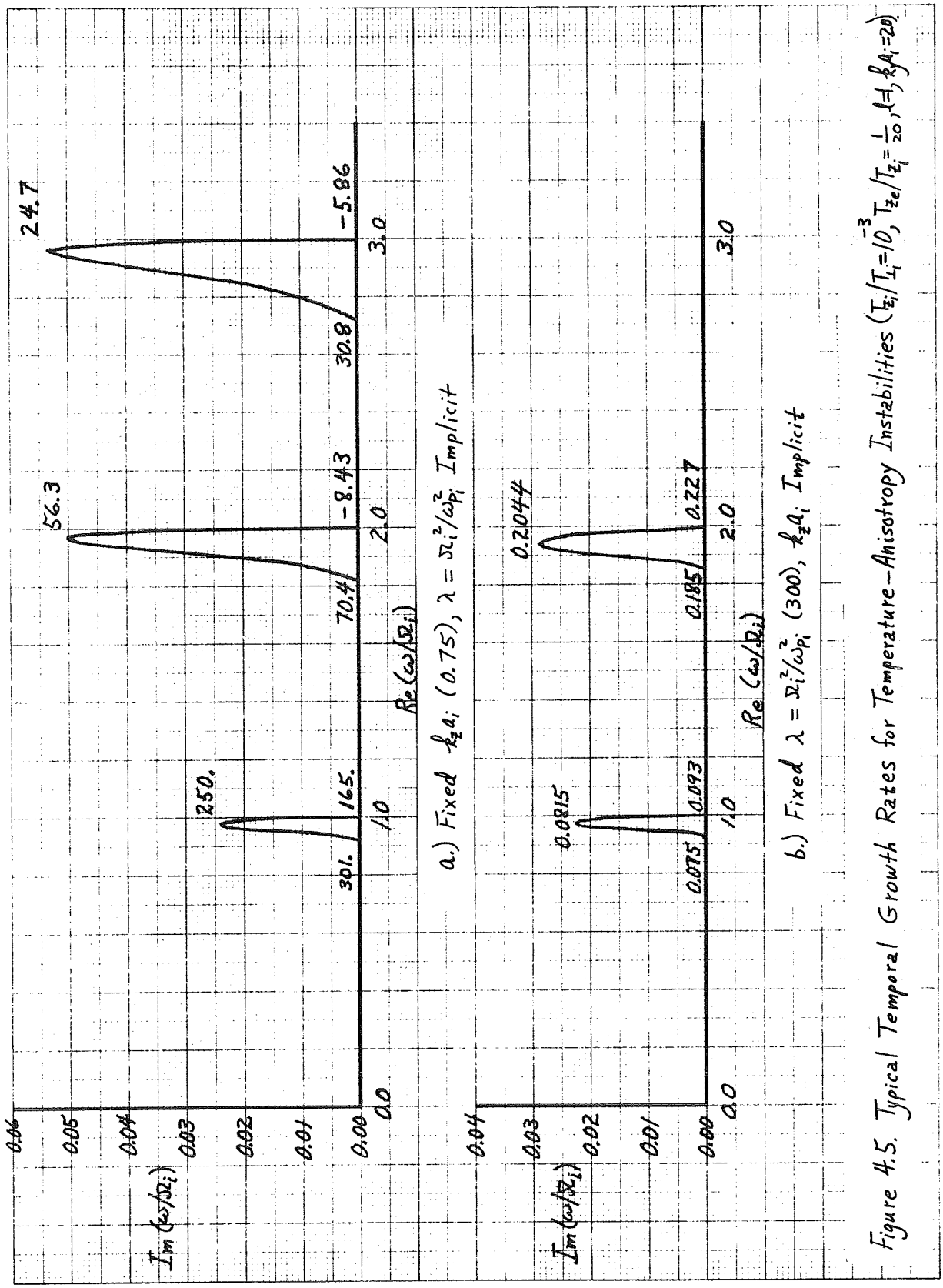

Figure 4.5. Typical Temporal Growth Rates for Temperature-Anisotropy Instabilities ($T_{\perp i}/T_{\parallel i}=10^{-3}$, $T_{\perp e}/T_{\parallel i}=\frac{1}{20}$, $\beta_i=1$, $k_y\rho_i=2.0$)

upon the results of a marginal stability analysis which must provide the precise regions of instability and starting values for complex ω root following iterations. In contrast, as long as one has an on-line computer available and can adjust contours in the complex ω-plane relatively easily, the Cauchy integral method does not require any estimate as to the location of the roots of the dispersion relation, although certainly even a crude guess is helpful. However, to determine the maximum temporal growth rate for a given density by the Cauchy integral method we must carry out many contour integrations for varying k.

The time required to find temporal growth rates on a computer is governed by the number of times it is necessary to calculate the plasma dispersion function $H(\omega,k)$. This is because it is very time-consuming to sum up the infinite sum of Bessel and plasma dispersion functions. The determination of the temporal growth rates shown in Fig. 4.5 for the unstable mode having $\omega/\Omega_i \simeq 2$ requires approximately the same number of evaluations (100) of the dispersion function for both the complex-ω root following and Cauchy integral methods. In this given amount of computer time, from the complex-ω root following method we have already determined the maximum temporal growth rate at the density given by $\Omega_i^2/\omega_{p_i}^2 = 300$. In contrast, for

the Cauchy integral method we must cross-plot a number of curves such as that shown in Fig. 4.5a to determine the maximum temporal growth rate for any given density. However, from Fig. 4.5a we are able to see how the temporal growth rate changes with density for a given axial wavelength. Thus we conclude that if we only want to look at some general characteristics of a few unstable modes and do not wish to bother with a marginal stability analysis, it is probably easiest to obtain the results by using the Cauchy integral method on an on-line computer. However, if it is desirable to do a thorough analysis of a given instability or we wish to use normal computer batch processing, then it is probably best to use the complex-ω root following method.

4.4 A Simple Example

In order to illustrate the use of the general instability criteria developed in Section 4.2 we consider a simple example in somewhat greater detail. A second reason for displaying such results here is to provide background information for the study of convective and absolute instabilities in the following section.

The special case we study here is an example of a "loss-cone" instability (see Section 6.2). We prescribe the homogeneous plasma case of interest by the following parameters: $T_e/T_i = 10^{-2}$, $T_{\perp i}/T_{z_i} = 1.0$, $\ell = 1$ (the $v_\perp$ distribution is thus of the loss-cone type) and $k_y a_i = 5.0$. Here, since $T_{\perp_i} = T_{z_i}$, there can be no free energy arising from dissimilar mean velocities perpendicular and parallel to the magnetic field. Rather, the source of free energy in this case is due strictly to the loss-cone nature of the $v_\perp$ distribution. As for the temperature-anisotropy instability, we defer a detailed discussion of the simplifications of the dispersion relation (3.3.15) and the physics of the instability to Chapter 6.

Examples of the $P(\omega/\Omega_i)$ and Nyquist plots for the loss-cone instability are shown in Fig. 4.6. As in the temperature-anisotropy instability case considered previously, it is necessary to make these plots on two different scales: that of the electrons (Figs. 4.6a, 4.6b) and that of the

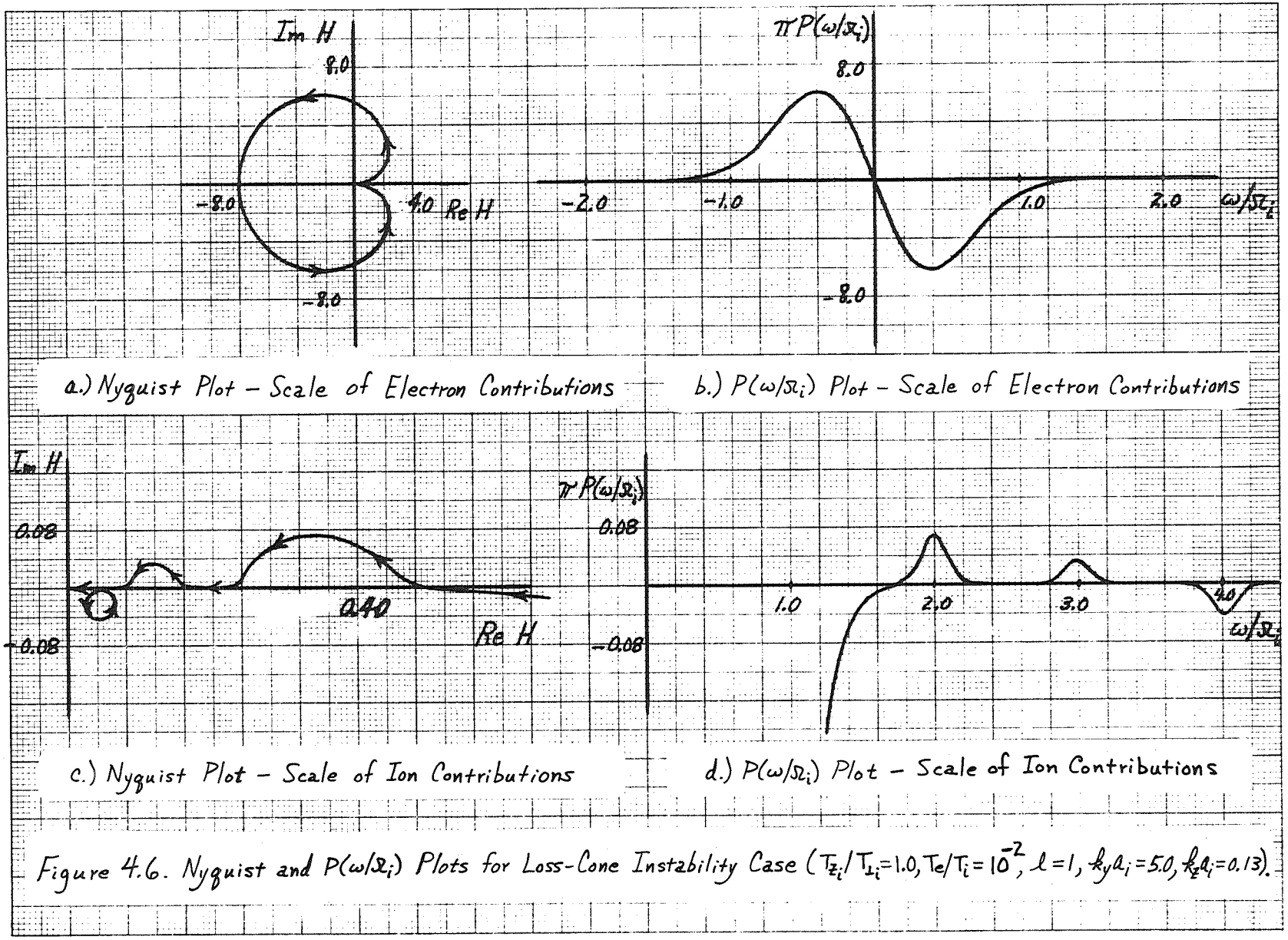

Figure 4.6. Nyquist and $P(\omega/\Omega_i)$ Plots for Loss-Cone Instability Case ($T_{z_i}/T_{\perp_i}=1.0$, $T_e/T_i=10^{-2}$, $\ell=1$, $k_y a_i=5.0$, $k_z a_i=0.13$).

ions (Figs. 4.6c, 4.6d). In both the $P(\omega/\Omega_i)$ and Nyquist plots it is readily apparent that the structure of the ion contribution differs from that of the temperature-anisotropy case shown in Fig. 4.4. In the present loss-cone case we note that the ion contribution is characteristic of the function $-2Z_o(w)$ (with a negative coefficient --see Fig. 4.3). We recall that for the temperature-anisotropy case the ion contribution was characteristic of the function $-2Z_1(w)$. This interesting difference in the nature of the ion contributions is related to the type of free energy source driving the instability and will be discussed further in Chapter 6.

For comparison with previous results we also display examples of the complex-ω solutions of the dispersion relation for the loss-cone instability case in Fig. 4.7. These curves are to be compared with those shown in Fig. 4.5. As before we display temporal growth rates found for varying λ (density), given k_z and varying k_z, given λ (here for a density equal to 1.91 times the minimum threshold density), with the numbers along the curves indicating the relevant value of the implicit parameter. The temporal growth rates of these instabilities are significant fractions of the ion cyclotron frequency for rather moderate plasma densities, an obvious indication of the threat which the loss-cone instabilities pose to plasma

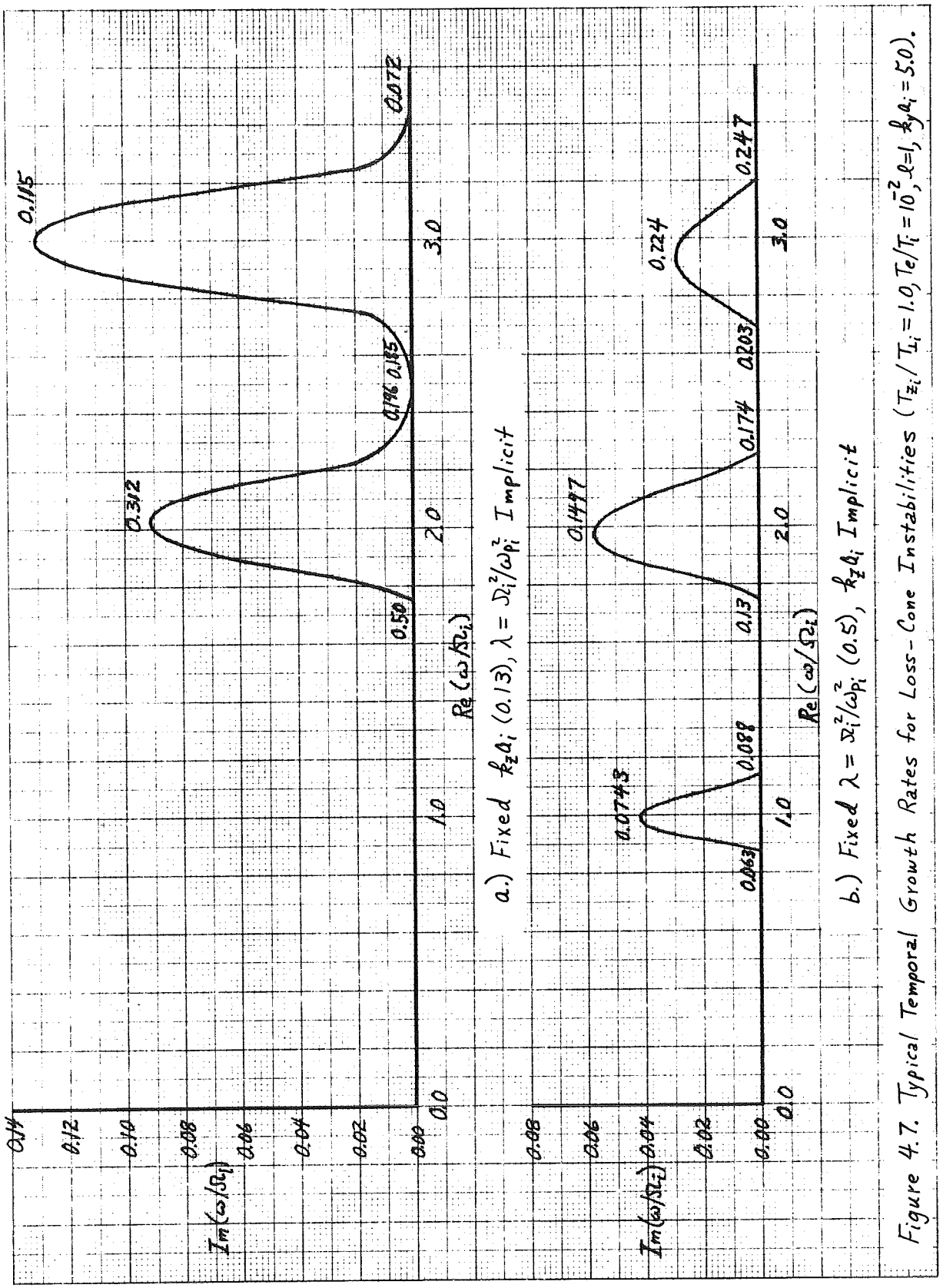

Figure 4.7. Typical Temporal Growth Rates for Loss-Cone Instabilities ($T_{z_i}/T_{\perp_i} = 1.0$, $T_e/T_i = 10^{-2}$, $\ell=1$, $k_y a_i = 5.0$).

confinement.

In order to arrive at a stability map for the $k_y a_i = 5.0$ set of modes, we apply the necessary and sufficient conditions for instability over the relevant range of k_z. For each mode (given $k_z a_i$) which satisfies these conditions, we find the range of plasma densities for which the mode is unstable from (4.2.8). Assembling all these results for varying k_z, we obtain the marginal stability curve displayed in Fig. 4.8. Above and outside the three humps in the figure the plasma is stable. Hence, the plasma is stable against the loss-cone instabilities with $k_y a_i = 5.0$ for sufficiently low densities ($\omega_{p_i}^2 \lesssim \Omega_i^2$). Inside the humps and hence for sufficiently high densities the plasma is unstable. The numerical values listed along the curve in the figure give the values of $k_z a_i$ on the marginal stability boundary.

The three separate humps in Fig. 4.8 correspond to resonance of the wave with the first three harmonics of the ion cyclotron frequency. While one might expect the three humps to correspond to three separate sets of unstable modes, we see from the figure that this is not the case since no region of overlapping is observed. Thus at any given density for which the plasma is unstable, as the frequency of the instability varies from 1.5 to 4 times the ion cyclotron frequency, the mode is always a member

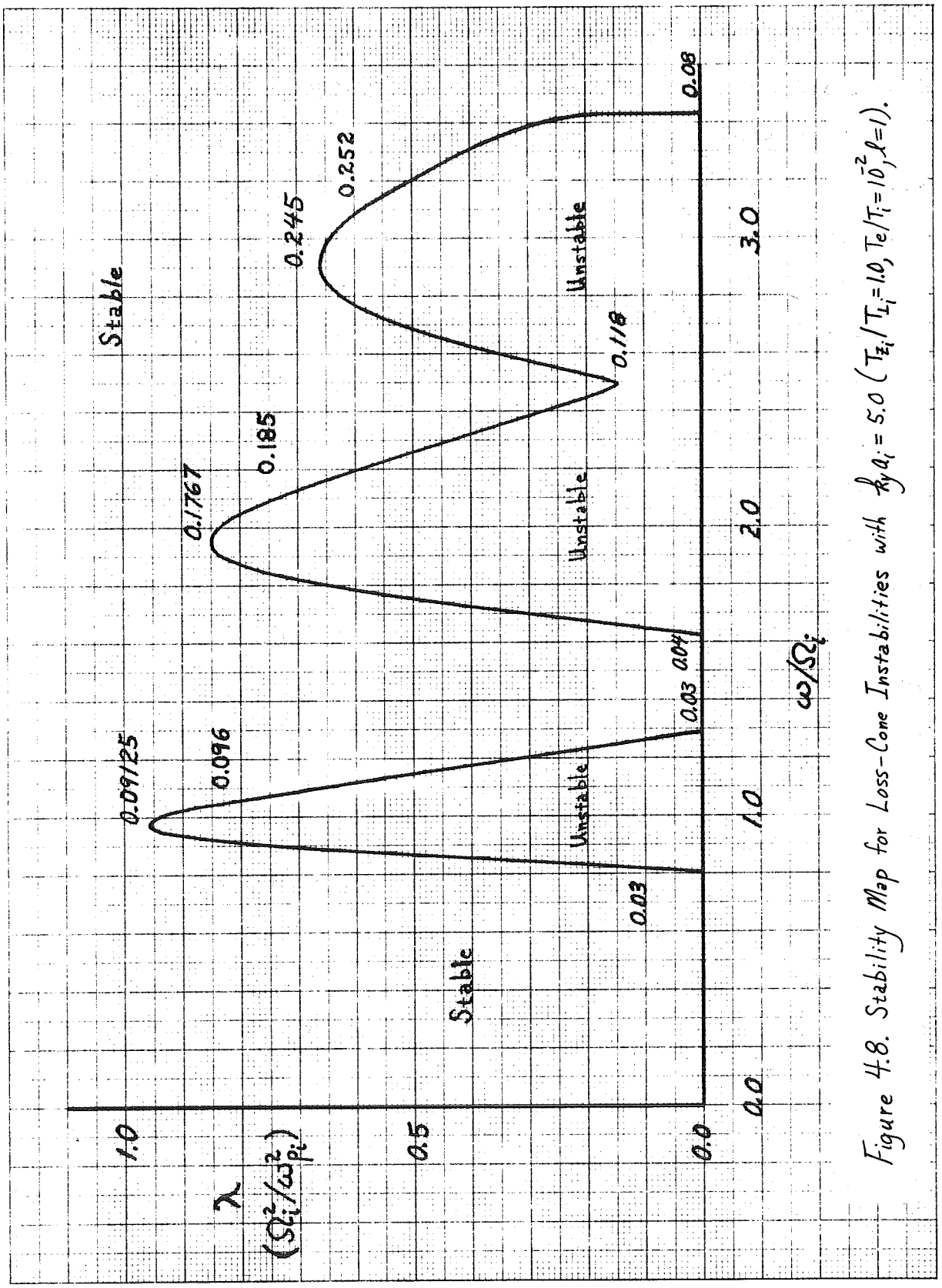

Figure 4.8. Stability Map for Loss-Cone Instabilities with $k_y a_i = 5.0$ ($T_{z_i}/T_{L_i}=1.0$, $T_e/T_i=10^{-2}$, $\ell=1$).

of the same set of unstable modes. If this were not the case then in Fig. 4.8 for $\lambda < 0.15$ and $\omega/\Omega_i \simeq 2.45$ there would be two overlapping marginal stability curves. When all the unstable modes of one or more groups belong to the same set as they do here, we will call them an "isolated" set of unstable modes. An equivalent but more complete definition of an "isolated" set of unstable modes is that such modes all lie on a single Riemann sheet of the solutions of the dispersion relation. A group of unstable modes of a plasma will be members of an "isolated" set if the marginal stability boundary in λ versus ω space is a single continuous curve, or there is a set of such curves which do not intersect each other. Note that by this last criterion there are two isolated sets of modes in Fig. 4.8: those having $\omega/\Omega_i \simeq 1$ and $1.6 \leq \omega/\Omega_i \leq 3.4$. In all but one of the many cases considered in this work, all the unstable modes were found to be members of isolated sets. In the one case in which some overlapping of the sets of unstable modes was found ($T_{z_i}/T_{\perp_i} = 1.0$, $T_e/T_i = 10^{-3}$, $\ell = 1$, $k_y a_i = 2.50$), the region of overlap occured for high plasma densities and frequencies about midway between two successive harmonics of the ion cyclotron frequency. For the purposes of the next chapter, it is important to note that while unstable modes may not all be members of an isolated set, the question of

whether or not overlapping sets of unstable modes do in fact occur, as well as the regions of overlap, can easily be ascertained from a thorough marginal stability analysis.

5. CONVECTIVE VERSUS ABSOLUTE INSTABILITY

5.1 Distinguishing Between Convective and Absolute Instabilities

In the preceding chapter we have discussed the problem of determining the parametric regions of instability of a given plasma. In particular, we have given a prescription for determining the plasma density at which a given mode (given k_y, k_z) becomes unstable, i.e. its threshold density. In this chapter we consider the question of the type of instability which occurs as the density is increased above this threshold density.

Sturrock (5.1) first drew attention to the fact that just knowing that an instability exists is not enough in many cases and that we must distinguish between two types of instabilities, namely convective and absolute (nonconvective) instabilities. The physical distinction between these two types of instabilities is best visualized by considering the response of a plasma to a small perturbation which is localized in both space and time. The two different characteristic types of response are displayed in Fig. 5.1. For the convective type of instability, the disturbance grows fastest in a frame of reference moving at a speed near the phase velocity of the unstable mode in such a way that, after a long time the response of the

plasma at any given point (including the point of the original disturbance) becomes vanishingly small; the instability is "convected" away. In contrast, for the absolute instability while the disturbance may still grow most rapidly in a moving frame, it grows at all

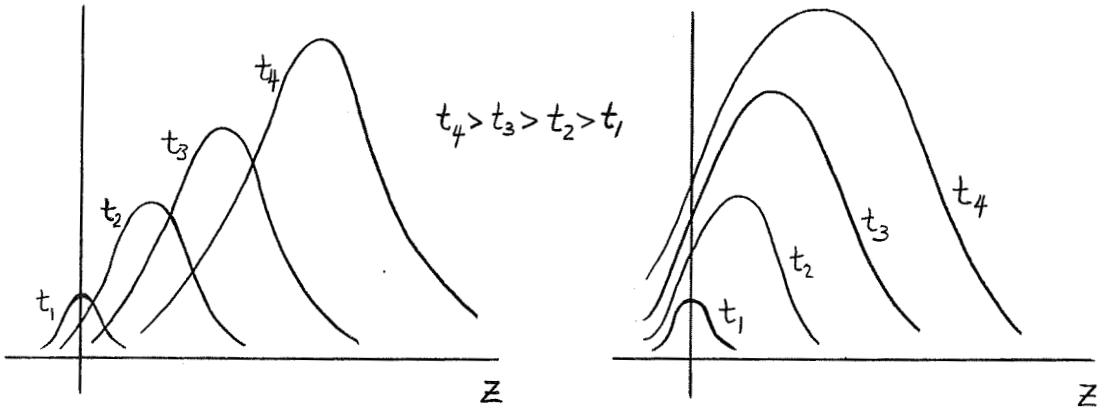

a.) Convective Instability b.) Absolute Instability

Figure 5.1. Envelopes of Time Development of Convective and Absolute Instabilities.

points in space in the time asymptotic limit. Intuitively we would expect that a disturbance which grows continuously in the vicinity of the original perturbation must be a nonpropagating or zero group-velocity mode of the plasma. We shall later see that this is indeed the case.

In order to further clarify the distinctions between convective and absolute instabilities, we will discuss a physical model of an absolute instability. We imagine a source localized near the origin from which a single wave

packet emanates. Physically we can think of this wave packet as having been developed by thermal fluctuations in the plasma. Let us suppose that as the wave packet moves in the positive z direction it is amplified. Generally, as the wave packet moves through any given small volume of the plasma located at $z > 0$, in addition to being amplified, it is dispersed. Therefore a portion of the original wave packet can be thought of as being "reflected" from this small volume and propagating back toward the origin, presumably being damped in the process. If any particular Fourier component of the "reflected" part of the wave packet arrives back at the origin with a net amplification and is in phase with the original Fourier component, then an absolute instability is possible. Otherwise the plasma is only convectively unstable. From this model we see that in addition to rapid spatial amplification, the appearance of an absolute instability requires that there be a sufficient amount of dispersion of wave packets moving in the plasma. We can also interpret this model as requiring that there be a sufficient amount of internal feedback from the bulk of the plasma to the region of the initial disturbance as has been discussed by Sudan (5.2). Finally, we note that for an absolute instability to occur it is crucial that waves can propagate in both directions, even if they are heavily damped in one direction, since otherwise we cannot transmit the dispersed or "reflected" part of a wave packet back to the origin.

As we have discussed previously (Section 4.3), for a truly infinite, homogeneous plasma the distinction between convective and absolute instabilities is not significant since a uniform distribution of disturbances in such a plasma leads to an "absolute" type of instability in both cases. However, when we attempt to use the infinite homogeneous plasma theory to study a finite plasma, the differences between convective and absolute instabilities becomes very important. This is because while the absolute instabilities are relatively unaffected by the finiteness of the plasma (as long as their wavelength "fits" into the finite length plasma--see Section 5.4), the ultimate effect of convective instabilities on plasma confinement is critically dependent on the degree of reflection and absorption of the unstable waves from the pressure gradients _etc_. at the edges of the plasma. In addition, it may be very difficult to observe convective instabilities experimentally in a finite plasma if their absorption at the edges of the plasma is large and their spatial growth rates small.

The relevance of these statements has been dramatically demonstrated by experimental results from the DCX-2 (5.3) and Pheonix II (5.4) machines. In both cases it has been found that the plasma is apparently stable and relatively quiescent for densities significantly exceeding the threshold density. Such results imply that either the

marginal stability analysis or our model is inappropriate. However, more detailed theoretical calculations (5.5, 5.4 respectively) have shown that for the conditions of the above experiments, the plasmas were only convectively unstable with relatively long spatial growth lengths. It is therefore unlikely that any instability of the plasma would have been observed. If, on the other hand, the expected instabilities become absolute at some higher density, we would expect them to be observable above this density. The plasma densities attained in the previously mentioned experiments are reasonably consistent with the calculated densities for the onset of absolute instabilities. From these observations we conclude that in order to make useful comparisons between theory and experiment, it is imperative to have detailed information about the convective versus absolute nature of microinstabilities.

With this brief introduction, we will now discuss criteria for distinguishing between convective and absolute instabilities. In doing so we follow principally the development given by Bers and Briggs (5.6). Implicit in our discussion of these criteria is the assumption that the plasma is infinite and homogeneous in the direction of wave propagation. As we have seen earlier in this section, in determining the type of instability which is present we need to consider the response of a plasma to an initial disturbance which is localized in space. In order to do

this it is only necessary to know the dispersion relation for the modes of interest. Now, since the dispersion relation, when appropriately normalized, is simply the inverse of the Fourier (z) - and Laplace (t) - transformed Green's function of the system, the response of a general unidimensional system is given by

$$\psi(z,t) = \frac{1}{(2\pi)^2} \int_L d\omega \int_F dk \; e^{i(kz-\omega t)} \frac{S(k,\omega)}{D(k,\omega)} \qquad (5.1.1)$$

$$\equiv \frac{1}{2\pi} \int_L d\omega \; e^{-i\omega t} \; I(\omega, z)$$

where $S(k,\omega)$ is the Fourier-Laplace transform of the initial disturbance. Since the response to any spatially localized pulse can be constructed from a superposition of the response to a delta function, we will restrict ourselves to delta function sources in space. The temporal behavior of the initial disturbance will be assumed to either be sinusoidal in time ($S(k,\omega) \sim (\omega-\omega_{dist.})^{-1}$), or to be localized in which case we need only consider the response to a delta function source in time at $t = 0$ ($S(k,\omega) = 1$). In any case $S(k,\omega)$ will always be an analytic function in the upper half ω-plane. More general types of initial disturbances are discussed by Briggs (5.6). Here, for simplicity, we are only considering the spatial response in a given direction (z) since the generalization to more spatial dimensions is straightforward (5.7).

The inverse Fourier transform contour F in (5.1.1) is along the entire real k-axis since we have assumed spatial homogeneity in the z direction. The inverse Laplace transform contour L is along the line $-\infty+i\sigma$ to $\infty+i\sigma$ where σ is taken to be sufficiently large so that the Laplace contour passes above all of the singularities of the integrand $I(\omega,z)$ (or, $D(\omega,k)^{-1}$ for real k). That such a σ must exist may be looked upon as a causality condition (5.6), since if a finite σ did not exist then the plasma would have a nonvanishing response for $t<0$, i.e. before the disturbance is initiated.

For a particular frequency ω along the Laplace contour L, the roots of the dispersion relation (poles of the Green's function) in the k-plane are shown schematically as crosses in Fig. 5.2. Note that the roots are located on one or the other side, but not on the real k-axis since by definition the Laplace contour is above all the singularities for real k. In addition, since by the same argument no roots can cross the Fourier contour as the Laplace contour is raised to even higher Im ω, we can determine uniquely in which half of the k-plane (upper or lower) each of the singularities of the Green's function of the plasma belongs. Therefore for the Laplace contour shown in Fig. 5.2a, the inverse Fourier transform $I(\omega,z)$ is well-defined with the Fourier contour taken along the real k-axis.

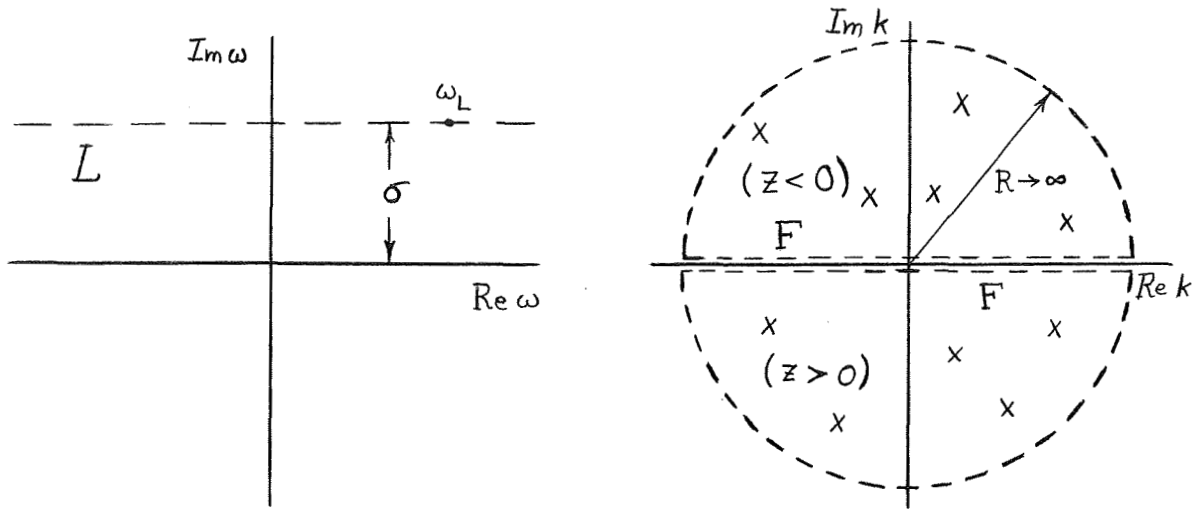

a.) Laplace Inverse Transform Contour.

b.) Fourier Inverse Transform Contour.

Figure 5.2. Laplace and Fourier Inverse Transform Integration Contours.

To determine $I(\omega,z)$ we can close the Fourier contour in the upper half plane for $z > 0$ and in the lower half plane for $z < 0$ as shown in Fig. 5.2b, providing the Green's function $D(k,\omega)^{-1}$ is sufficiently well behaved as $|k| \to \infty$. (The fact that the dispersion function employed in this work diverges for $|\text{Im } k_z| > |\text{Re } k_z|$ (see Section 3.4) does not cause any problem here since this just assures convergence of the integral (5.1.1) in the "divergence" region of k space. Note also that the branch point at $k_z = 0$ in our dispersion relation (see Section 3.3) causes no difficulty since the integral of the inverse of the dispersion relation along the entire Fourier contour is well defined as long as we take into account the change

in representation as we pass through the branch point.) Thus, for values of ω with imaginary parts greater than or equal to σ , the roots of the dispersion relation in the upper half k-plane contribute to the response of the plasma for $z > 0$ whereas those in the lower half contribute for $z < 0$. For frequencies on the Laplace contour the location of the roots in the k-plane indicate that all of the modes are spatially evanescent. Physically, this means that a localized source whose strength grows exponentially with time will cause a response which decays spatially in either direction away from the source.

If we now vary the frequency away from values on the Laplace contour toward the real ω-axis, the roots in the k-plane must still contribute to the response of the plasma for the same z-direction irrespective of whether or not they cross the real k-axis (see below). If any roots do cross the real k-axis they will correspond to spatially growing modes of the plasma for the appropriate z-direction at some frequency ω with $0 < \mathrm{Im}(\omega) < \sigma$.

We can in principle find the total response of the plasma from equation (5.1.1) by taking into account all of the solutions of the dispersion relation $D(\omega,k) = 0$. However, here we are really only interested in the time-asymptotic limit of the response. This is especially true since we are looking for instabilities of a plasma. Therefore since modes whose frequencies ω have negative

imaginary parts are damped out in the time-asymptotic limit, we need only concern ourselves with modes which can have frequencies ω with positive or zero imaginary parts, i.e. unstable or marginally stable modes. As we have seen (Chapter 4), the marginal stability analysis enables us to identify unstable or growing modes. However, in the present development we will use another approach. With reference to Eq. (5.1.1), the most obvious way to discover which are growing modes within the framework of the present development is to analytically

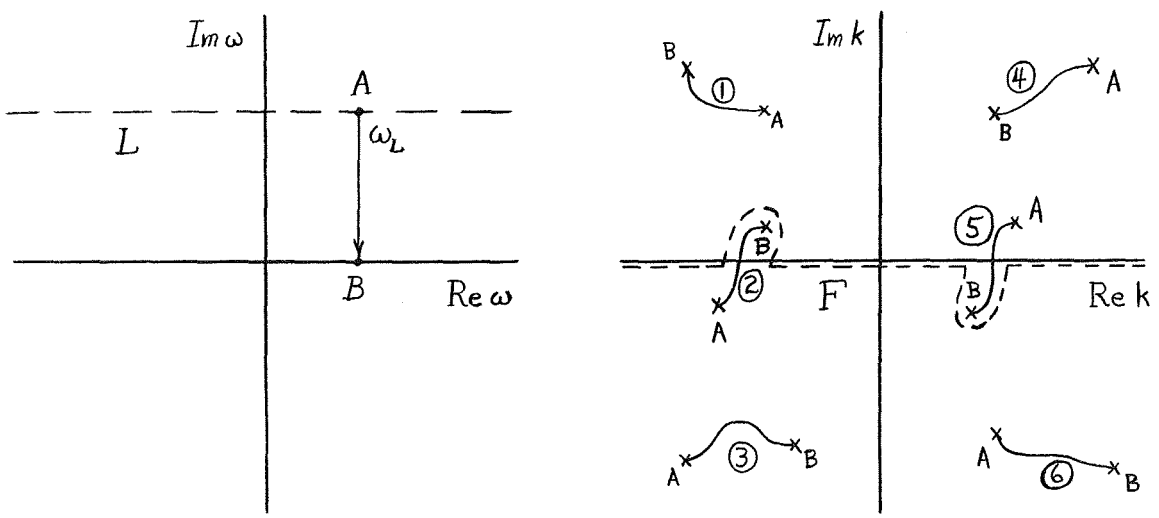

a.) Laplace Contour Change for a Given Real Frequency.

b.) Fourier Contour Deformations as Singularities Move in the k-plane

Figure 5.3. Movement of Singularities in the k-plane as the Laplace Contour is Analytically Continued Down to the real ω-axis (② and ⑤ are Convectively Unstable Modes).

continue $I(\omega,z)$ in the ω-plane by deforming the Laplace contour down towards the real ω-axis and observe the corresponding motion of the roots of the dispersion relation

in the k-plane. In order to properly analytically continue $I(\omega,z)$ we must deform the Fourier contour F if any roots cross the real k-axis* so that the contributions of these roots are always included in the proper half of the k-plane. This analytical continuation of $I(\omega,z)$ is illustrated in Fig. 5.3 for a particular point on the Laplace contour. Since roots (2) and (5) cross the real k-axis as the imaginary part of ω decreases to zero, these two roots correspond to spatially growing modes when driven by a source of real frequency. In contrast, roots (1), (3), (4), (6) correspond to spatially evanescent modes since they do not cross the real k-axis.

If the movement of the singularities in the k-plane were as simple as that pictured in Fig. 5.3 for all frequencies on the Laplace contour, then we could deform the entire Laplace contour all the way to the real ω-axis. In this case we would conclude that all unstable modes present are convective since the asymptotic response of the plasma would be that due to a set of spatially growing modes with no temporal growth or decay. In fact, there would be a time-asymptotic response at finite z in this case only if there is a continuing source of disturbance.

---

* Note that such crossing requires that there exist roots of $D = 0$ for real k with $\sigma > \mathrm{Im}(\omega) \geq 0$, which are unstable modes according to the marginal stability analysis.

However, the situation is not always as simple as that indicated in Fig. 5.3. An additional complicating feature which can occur is that the k-plane roots of the dispersion relation from opposite half planes may coalesce from some frequency with a positive or zero imaginary part. This possibility is illustrated in Fig. 5.4. Since the two coalesced modes from opposite half k-planes constitute a combined mode which has nonvanishing contributions for all finite spatial points and a temporal growth rate given by the imaginary part of ω_B, such a merged mode corresponds to an absolute instability. Physically, this can be thought of as a "resonance" of the system since in this case there is an asymptotic response

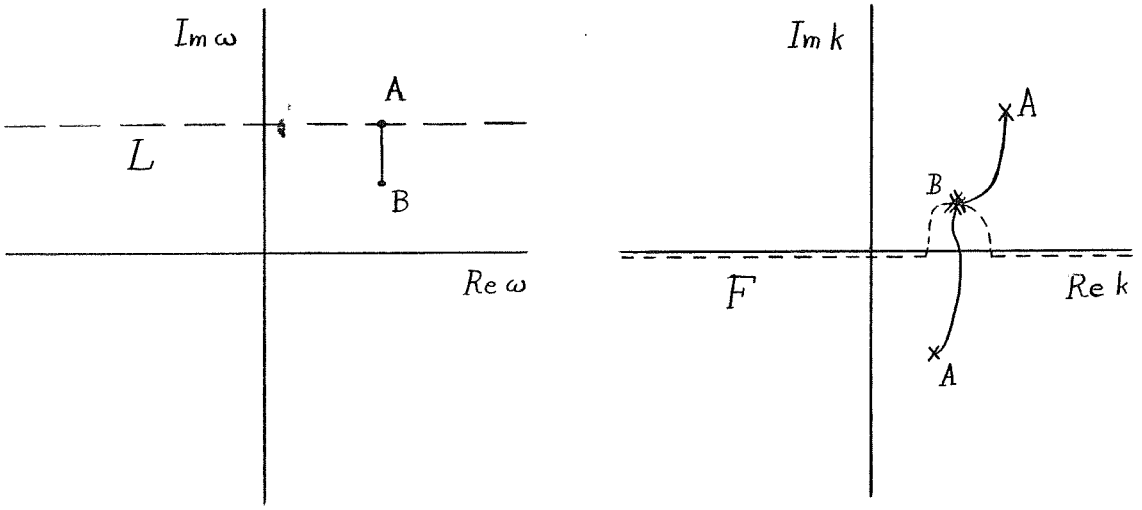

a.) Laplace Contour Change for a Given Real Frequency.

b.) Fourier Contour Deformation as Singularities Coalesce for some ω_B.

Figure 5.4. Movement of Singularities in the k-plane as the Laplace Contour is Analytically Continued Down to the Real ω-axis (Coalescence of ① and ② at ω_B Indicates an Absolutely Unstable Mode).

of the system even after the initiating disturbance is turned off.

Mathematically we see that such a coalescence of modes leads to a singularity in $I(\omega,z)$ in that the Fourier contour defining $I(\omega,z)$ must pass between two modes which have merged in the k-plane. This is commonly referred to as a "pinching" of the Fourier contour. In the vicinity of any point where two roots of the dispersion relation merge, we have

$$(k-k_B)^2 \sim (\omega-\omega_B) \tag{5.1.2}$$

or,

$$(k-k_B) \sim (\omega-\omega_B)^{1/2}. \tag{5.1.3}$$

Therefore we see that the coalescence of two modes gives rise to a saddle point in the $\omega(k)$ plane and a branch point in the $k(\omega)$ plane. Returning to Eq. (5.1.1), we find that this circumstance implies that the inner (Fourier) integral $I(\omega,z)$ has a branch point at $\omega=\omega_B$ of the type $I \sim (\omega-\omega_B)^{-1/2}$. Since a branch point in $I(\omega,z)$ occurs at ω_B, we cannot deform the Laplace contour past ω_B without special consideration of this point. By first performing the k integration in (5.1.1) through the saddle point and afterwards the ω integration, it is easily shown that this coalescence of two modes through the Fourier contour F indicates an absolute instability (5.6). On the other hand, it is important to note that the merging of two modes from

the same side of the real k-axis in the k-plane, no matter where in the k-plane they may merge, does not give rise to an absolute instability since then the Fourier inversion contour can be deformed around the merging point and $I(\omega,z)$ remains regular. Instead of being an absolute instability, such a coalescence only indicates a special double-root type of convective instability. In terms of our physical model, this circumstance corresponds to the coalescence of two waves which are moving to the right (say), rather than to the coalescence of one wave moving to the right and one to the left. This simple picture of the merging of poles through the Fourier contour F can readily be generalized to coalescence of more than two poles (5.6). For mergings of more than two poles, the essential condition for an absolute instability to occur is that of all the poles merging, at least one must have come from the upper half k-plane and at least one must have come from the lower half k-plane.

We will now summarize what we have learned about the conditions necessary for the appearance of an absolute instability with the statement of a criterion for absolute instability. We note that the necessity of the merging in the k-plane of two or more roots of the dispersion relation can be written simply as

$$D(\omega,k) = 0 \qquad (5.1.4)$$

$$\frac{\partial D(\omega,k)}{\partial k} = 0 . \qquad (5.1.5)$$

With the meaning of these equations in mind, we see that the necessary and sufficient conditions for a given instability to be an absolute instability may be stated as follows:

> An absolute instability can occur only if there exists an ω_B with positive imaginary part such that
>
> $$D(\omega_B, k_B) = 0 \qquad (\alpha)$$
>
> $$\frac{\partial D(\omega_B, k)}{\partial k}\bigg|_{k=k_B} = 0.$$
>
> When condition (α) is satisfied, the merged mode corresponds to an absolute instability if of the two or more modes which coalesce at ω_B, k_B, there is at least one on each side of the real axis of the k-plane when the modes are evaluated for $Re(\omega)=\omega_B$, $Im(\omega) \geq \sigma$. (β)

If conditions (α) and (β) are not both satisfied, then the instability is of the convective type.

The above criterion is essentially a restatement or distillation of the original Bers and Briggs criterion (5.6). Dysthe (5.7) has derived essentially the same criterion and numerous variations of it by a different procedure. In order to interpret the criterion physically, we note that if we take the total derivative of the dispersion relation

and solve the resultant equation for the group velocity, we obtain

$$\frac{d\omega}{dk} = - \frac{\partial D/\partial k}{\partial D/\partial \omega} \quad . \tag{5.1.6}$$

Therefore we see that condition (α) is equivalent to requiring the existence of a zero group-velocity mode in the plasma, provided $\partial D/\partial \omega$ is bounded. For the dispersion relations employed in this work D is an entire function of ω as long as $k_z \neq 0$ and $\partial D/\partial \omega$ is thus bounded for all finite ω (see Section 3.4). The case $k_z = 0$ is not important here since such a case, when unstable at all, is already implicitly an "absolute" instability in the z direction (the only direction in which we will consider the convective versus absolute nature of the instabilities --see Section 6.1). Condition (α) is thus a confirmation of our intuitive feeling that a mode which grows at all points in space simultaneously must be a nonpropagating or zero group-velocity mode.

From the preceding discussion in this section we know that condition (β) ensures that the zero group-velocity mode satisfying condition (α) is composed of individual modes which propagate in opposite directions from the initial perturbation so that the disturbance can, in fact, spread out and grow at all points in space while growing in time. When, as is usually the case, the imaginary part of k_B is nonzero, condition (β) simply requires that of the modes coalescing at least one be a spatially growing

mode and at least one be an evanescent mode. This confirms our physical picture of absolute instabilities since what condition (β) thus implies is that one mode grow spatially say for $z > 0$ and a "reflected" or dispersed part of it with precisely the same spatial dependence is damped in propagating back to the origin in such a way that it always arrives with just the right phase to reinforce the original disturbance.

Through a derivation which is similar to that of Bers and Briggs (5.6) in that the importance of distinguishing the types of merging modes is emphasized, Sudan (5.2) has derived a criterion for absolute instability which is applicable to slightly inhomogeneous plasmas, i.e. those in which the characteristic inhomogeneity length in the direction of propagation is longer than the wavelength of the instability. For homogeneous media Sudan's criterion is basically the same as the Bers and Briggs criterion as given in our conditions (α) and (β). Briggs (5.6) has reviewed the merits and limitations of other earlier derivations of criteria for absolute instability.

In addition to these derivations based upon following roots which merge through the Fourier contour, criteria for absolute instability have also been derived by utilizing other information about the set of unstable modes of a plasma. A conceptually useful way of proceeding is to plot solutions of the dispersion relation (for some given set of plasma parameters including the density) in the

complex ω-plane for real k. Such a plot is illustrated for a simple case in Fig. 5.5a. In this sketch the curve labeled with A denotes the real k solutions and that labeled with B the real ω solutions. Note that if this were the only set of unstable modes, the σ which defines the Laplace contour would only have to be larger than ${}^{\omega}I_{max}$. In addition, for such a simple case the region of the complex ω-plane enclosed by the curve A-B is the only region in which absolute instability condition (β) can be satisfied since only there can a growing mode of the

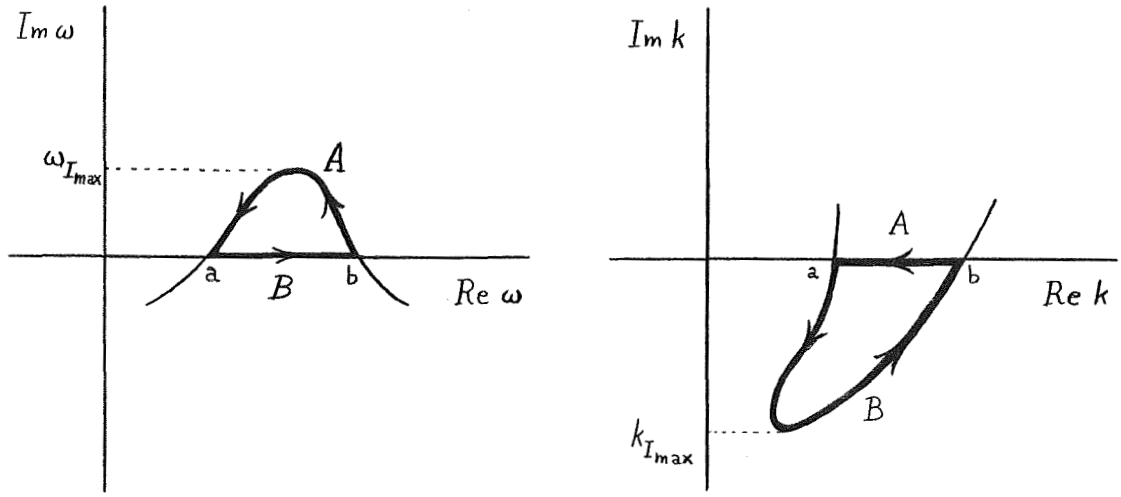

a.) Complex ω Solutions of the Dispersion Relation.

b.) Complex k Solutions of the Dispersion Relation.

Figure 5.5. Complex ω and k Solutions of the Dispersion Relation for a Set of Unstable Modes.

plasma exist. Therefore in this case we can restrict the portion of the complex ω-plane in which we look for satisfaction of condition (α) to this same region. The same conclusion has been arrived at in an independent way by

Baldwin and Rowlands (5.8). For convenience we will henceforth refer to the contour A-B in Fig. 5.5a as the Baldwin-Rowlands or simply the B-R contour since to the author's knowledge they were the first authors to introduce it. Some examples of this contour for our standard loss-cone instability example will be displayed in Section 5.3. We should also note that Fainberg et al. (5.9) have arrived at essentially the same criterion as Baldwin and Rowlands except that instead of satisfying our condition (α) with the B-R contour they require that there be a saddle point in $\omega(k)$ (i.e. $d\omega/dk=0$) within the contour. As we have noted previously, the condition $d\omega/dk=0$ is usually equivalent to condition (α) so the criterion of Fainberg et al. is usually the same as that of Baldwin and Rowlands.

In considering the work of Baldwin and Rowlands and Fainberg et al. we have been assuming that there is only one set of unstable modes as illustrated in Fig. 5.5. The preceding remarks also apply as long as the set of unstable modes under consideration is an "isolated" set of modes in the sense defined in Section 4.4. However, if there are sets of unstable modes which overlap each other, then we cannot directly assure that condition (β) is satisfied within the B-R contour. This is because it is then possible that two growing modes may coalesce to satisfy condition (α) with the B-R contour. As we have previously noted, the merging of two growing modes does not constitute an

absolute instability. Therefore the Fainberg et al. (5.9) and Baldwin and Rowlands (5.8) criteria for absolute instability can be valid only for "isolated" sets of unstable modes. This point has been discussed at greater length by Briggs (5.6). We should also note that it is possible for two evanescent modes (usually for large Im(k)) to coalesce within the B-R contour. Such a coalescence does not lead to an absolute instability as would be predicted by the criteria of Baldwin and Rowlands and Fainberg et al. However, this latter circumstance would seem to be quite unlikely and could easily be discriminated against by making sure that one of the modes which merges is a member of the set of unstable modes for which the B-R contour is drawn. In any case, having once found an absolute instability "candidate" by these methods, we can always trace the roots of the dispersion relation for increasing $\mathrm{Im}(\omega)$ away from the saddle point to make sure that the merged mode satisfies condition (β). In spite of the limitations mentioned above, we will find the Baldwin-Rowlands picture to be very useful in considering absolute instabilities.

In addition to the B-R contour displayed in Fig. 5.5a, we can also make use of mappings of the B-R contour into the complex k-plane as shown in Fig. 5.5b. As long as the instability is convective the contour is closed and does have a definite maximum $|\mathrm{Im}\ k|$ as shown by $k_{I_{max}}$. The parameter $k_{I_{max}}$ is of interest for convective instabilities

since it gives the maximum spatial growth rate of the set of convectively unstable modes. If an absolute instability occurs there is a branch point within the mapping of the B-R contour into the k-plane. Then, the mapping in the k-plane is an open contour. We could in principle use this property of absolute instabilities to discover merged modes satisfying condition (α), but this is generally not practicable since it is very difficult to design computer programs which are capable of faithfully following roots of the dispersion relation in the vicinity of a branch point. However, as we shall see in the following section, it is very useful to use contour plots such as that illustrated in Fig. 5.5b to "follow" a growing or unstable mode into the merged root to ensure that a given merged root in fact satisfies condition (β).

Absolute instability conditions (α) and (β) are of course applicable only in a specified coordinate system. Here, implicitly, the coordinate system is that in which the dispersion relation was derived. We will now consider some aspects of the problem of absolute versus convective instability in other coordinate systems. Since for densities only slightly exceeding the threshold density the plasma is presumably not very dispersive, we would expect that the unstable modes would be most rapidly growing in a frame of reference which moves at approximately the phase velocity of the wave. In such a frame of reference the instability would appear as an absolute instability.

Usually, however, for plasma microinstabilities as the density is increased sufficiently far above the threshold density the plasma becomes dispersive enough to permit zero group-velocity modes in the original frame of reference and hence absolute instabilities in that frame (5.4, 5.10).

Many authors (e.g. 5.6, 5.8, 5.11) have discussed the problem of determining the nature of an instability in any given frame of reference. Going somewhat further than most treatments, Hall and Heckrotte (5.11) have given a method for finding absolute instability modes (in the laboratory frame) which depends upon finding an absolute instability mode in a given frame of reference (namely that in which condition (α) is easily satisfied--see (5.11)) and then transforming to the laboratory frame, making sure in the process that the mode is still an absolutely unstable mode. The transformation is carried out by solving (numerically) differential equations relating velocity frames moving at slightly different velocities. An important by-product of this type of analysis is that one obtains the spatial shape of the time-asymptotic behavior of the response of the plasma (5.11).

As an alternative to the procedures discussed above, we could find absolutely unstable modes by using the Cauchy integral method (see Section 4.3). To do so we would take the hint given by Baldwin and Rowlands (5.8) and see if any merged modes occured within the B-R contour. This could be

accomplished by defining the function $\phi(z)$ in (4.3.1) to be

$$\phi(\omega) = \frac{\partial H(\omega,k)}{\partial k}\Bigg|_{k=k(\omega)}$$

in which $k(\omega)$ is the solution of the dispersion relation (5.1.4). Choosing an appropriate density, we would use the Cauchy integral method to find the complex ω at which absolute instability condition (α) is satisfied within the B-R contour. From (5.1.3) we know that it is quite likely that the solutions found will be branch points. However, as we have discussed previously (Section 4.3) this presents no problem for the Cauchy integral method as long as the function ϕ vanishes at the branch point, as happens here. Note that since this use of the Cauchy integral method is dependent on the Baldwin and Rowlands (5.8) or Fainberg et al. (5.9) criteria for absolute instability, it has the same limitations. Therefore, in general, after locating modes satisfying condition (α) we must separately check that these merged modes satisfy condition (β).

This Cauchy integral method would be about as efficient as the methods described previously in this section in determining the absolute instability growth rate for a given density. If, in addition to the zero group-velocity absolute instability modes, the temporal growth rates of absolutely unstable modes for a set of velocities of moving frames are desired, then the Cauchy integral method can be

more efficient. This is because for the appropriate definition of $\phi(z)$, the reference frame velocity would be a "free" parameter. Thus we would need to compute ϕ and ϕ' along only one B-R contour to determine the temporal growth rates of absolute instabilities for a given set of velocities. However, one difficulty which arises in the application of the Cauchy integral method with the dispersion relation employed in this work is that often the appropriate contours go into the region of the k-plane in which the dispersion relation "diverges." Therefore while such a technique is not useful for the present work, it may be useful for dispersion relations which have no "divergence" regions.

Hall and Heckrotte (5.11) and to a lesser degree Baldwin and Rowlands (5.8) emphasize the importance of viewing the response of the plasma in an arbitrary velocity frame. Probably the most important justification for this emphasis is the fact that there may be very rapidly growing convective instabilities which have very small but nonzero group-velocities and thus are essentially "absolute" instabilities due to the fact that they propagate to the ends of the plasma so slowly. Therefore the relevant question is whether or not the special case of zero group-velocity (absolute instability) is reasonably representative of convectively unstable modes with very small group velocities. While this may not be the case for low frequency modes ($\omega << \Omega_i$), for the high

frequency modes ($\omega \gtrsim \Omega_i$) considered in this work the typical phase velocity in the direction of propagation (along the magnetic field) is usually much larger than the electron thermal velocity. Now, since the typical group velocities are presumably equal to the phase velocities to within an uncertainty of perhaps the electron thermal velocity, it is likely that the convectively unstable modes normally propagate to the ends of the plasma very rapidly. Therefore, we presume that for the cases considered in this work (Chapters 6, 7), zero group-velocity modes are reasonably representative of rapidly growing, convectively unstable modes which have small group-velocities. Hence we will only be concerned with determining the parametric conditions for which zero group-velocity modes can occur in the laboratory or rest frame.

5.2 Determining the Transition Density

In the preceding section we have discussed the general criterion for distinguishing between convective and absolute instabilities and the various methods which have been proposed to implement it. A common feature of all these methods is that they seek to determine whether a specified plasma with a fixed density in excess of the threshold density is convectively or absolutely unstable. Therefore, using these methods, repeated application of the entire procedure is necessary to determine, for example, the density at which an absolute instability first appears, that is the "transition density." In this section we develop a direct method which is much more efficient in determining the transition density than any of the above procedures. The new technique determines the transition density directly by making use of the same property which allowed us to readily determine the threshold density from the marginal stability analysis, namely that the plasma density is a "free" parameter in the dispersion relation. In addition, this method makes maximum use of the results of the marginal stability analysis.

In order to determine the transition density directly, we first consider how we might satisfy absolute instability condition (α). Using the form of the dispersion relation given by (3.3.16), condition (α) reduces to finding simultaneous solution of the equations

$$\lambda - H(\omega,k) = 0 \qquad (5.2.1)$$

$$\partial H(\omega,k)/\partial k = 0. \qquad (5.2.2)$$

We recall that $\lambda \equiv \Omega_o^2/\omega_{p_o}^2$ and is thus positive and real. Since (5.2.2) is independent of λ (density) we solve it first. Its general solution for a range of frequencies is

$$k=K(\omega). \tag{5.2.3}$$

This solution (or any set of such solutions) is physically meaningless except when it simultaneously satisfies the dispersion relation. A convenient way of ensuring this for some value of λ (some density) is to find the point, or points (if any) where the imaginary part of $H(\omega,k)$ vanishes along the trajectory given in (5.2.3). If this occurs at ω_B, $K(\omega_B)$, the appropriate value of λ (density) for which the dispersion relation is satisfied is given immediately by

$$\lambda_B = \text{Re}\ \{H[\omega_B,\ K(\omega_B)]\} = H[\omega_B, K(\omega_B)] \tag{5.2.4}$$

provided $\text{Re}\{H[\omega_B,K(\omega_B)]\}$ is positive. This procedure gives us a simple method for determining the characteristics ω_B, $K(\omega_B)$, λ_B of a merged mode of the plasma which satisfies condition (α). The method requires only that the density or some other relevant parameter be a "free" parameter in the dispersion relation (see Section 4.2). While most dispersion relations for uncoupled electrostatic or transverse electromagnetic waves seem to have this property, the full three-by-three determinant dispersion relation (see Section 1.2) which is relevant when the electrostatic and transverse modes are significantly coupled does not. However, if the modes are only weakly coupled, we could presumably develop an iterative method for the more general

case based upon these same ideas.

Let us now consider the characteristics of the absolute instability mode at the transition density. We recall that the existence of an absolute instability requires the plasma to be highly dispersive. We therefore expect an absolute instability mode to first appear at a density above the threshold density (Section 4.2) and, by analogy with the marginal stability analysis, to be neither decaying nor growing temporally at this "transition" density. The mode would be expected to exhibit temporal growth as the density is increased above the transition density. In other words, at the transition density we expect the absolute instability mode to be "marginally stable" and hence have a real frequency ω. Its wave number k will in general be complex.

Unfortuantely, in contrast to the marginal stability analysis, it is not a priori obvious that the absolute instabilities will first appear in this way. Note that if the absolute instability always has a real frequency at the transition density, then the merged root comes into the B-R contour in Fig. 5.5a only through the real ω-axis (curve B). While this is certainly the most probable circumstance, it is not obvious that the merged root cannot come in through the real k mapping (curve A) or even suddenly appear inside the B-R contour.

In order to justify ruling out these latter possibilities, we need to consider the circumstances under which

absolute instabilities may occur in more detail. As we have noted in the previous section, condition (α) implies that a saddle point in $\omega(k)$ must exist ($d\omega/dk=0$), provided $\partial D/\partial\omega$ remains finite. In the following analysis we will assume that $\partial D/\partial\omega$ is finite for all ω (as is the case here for $k_z \neq 0$--see Section 3.4) or at least that $\partial D/\partial\omega$ is finite at the point where $d\omega/dk=0$. Next, we note that a saddle point in $\omega(k)$ can only occur on the surface of a single Riemann sheet. That is, the intersection of two Riemann sheets cannot give rise to a saddle point in $\omega(k)$ since it instead leads to the condition $dk/d\omega \to \infty$, i.e. a branch point in $\omega(k)$. Thus in our consideration of modes which satisfy condition (α), we can restrict our attention to those modes which lie on a single Riemann sheet.

Of the modes which lie on a single Riemann sheet there will of course be some stable modes and some unstable modes. From the results of a marginal stability analysis we already have a considerable amount of information about the unstable modes. In general the unstable modes occur only for limited ranges of $Re(\omega)$, $Re(k)$ and the density (see Section 4.2), and in "isolated" sets. Note that an isolated set of modes is by definition a set whose members all lie on the same Riemann sheet. In light of these observations about the unstable modes, in the following we will assume that for the modes under consideration the ranges of $Re(\omega)$, $Re(k)$ for instability are finite. Under this assumption we see that the $Im(\omega)$ surfaces of an

isolated set of modes in the complex k-plane must be topologically similar to those shown in Fig. 5.6. In this figure ω_I, k_R, k_I are respectively Im[$\omega(k)$], Re(k), Im(k) and λ_t is the value of λ at the transition density. The subscripts 1, 2, on λ_t refer to the first and second groups of modes (in terms of increasing k_R) shown in the figure.

For all points except those where $d\omega/dk=0$ (i.e. those where condition (α) is satisfied), the Cauchy-Riemann conditions show us that $\omega_I(k_R,k_I)$ can have no local finite maximum or minimum and that the contours $\omega_I>0$ must map (in the k-plane) inside the contours $\omega_I=0$ as shown in Fig. 5.6 b, d, f. We recall that in Section 4.2 we have shown that for sufficiently low densities the plasma is always stable, in which case ω_I is negative for all k_R. As we increase the density to a value slightly above the threshold density, but still below the transition density, we obtain the disposition of stable and unstable modes shown in Fig. 5.6a, b. Here curve B of Fig. 5.5b must be closed to indicate a convective instability and any saddle point must be below the $\omega_I = 0$ plane. We recall that condition (β) requires, if a given saddle point is to imply absolute instability, the merging of an "unstable" mode with a "stable" mode. Since Eqs. (5.2.1) and (5.2.2) are very well-behaved functions of λ (inverse density), as the density is changed incrementally there is no reason to expect discontinuities in the general structure of the Riemann surface. Now, as

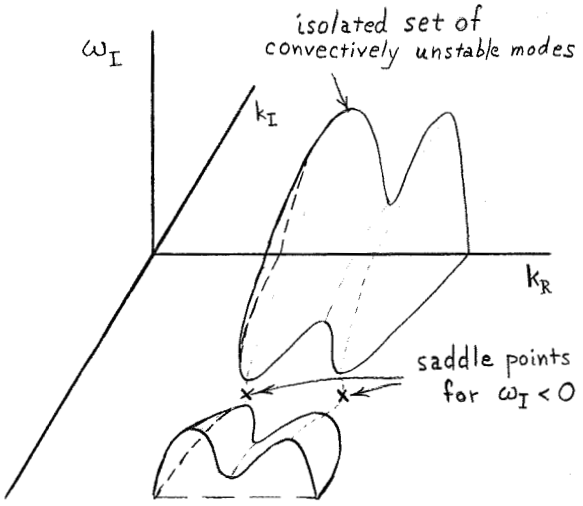

a.) $\lambda > \lambda_t$

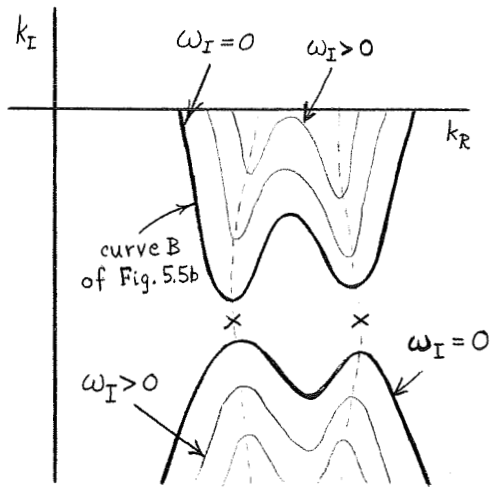

b.) $\lambda > \lambda_t$

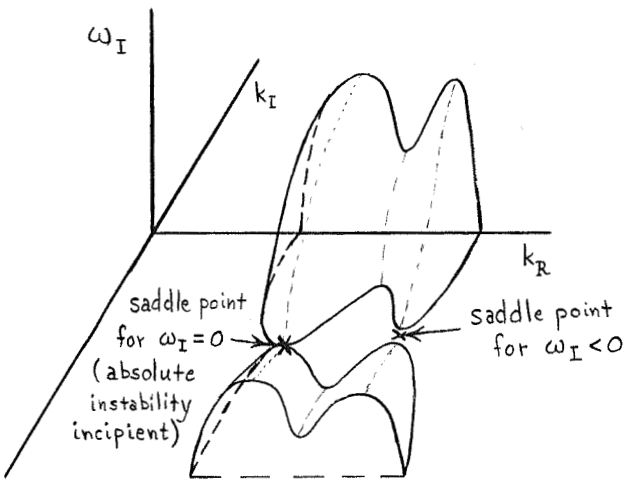

c.) $\lambda = \lambda_{t_1}$

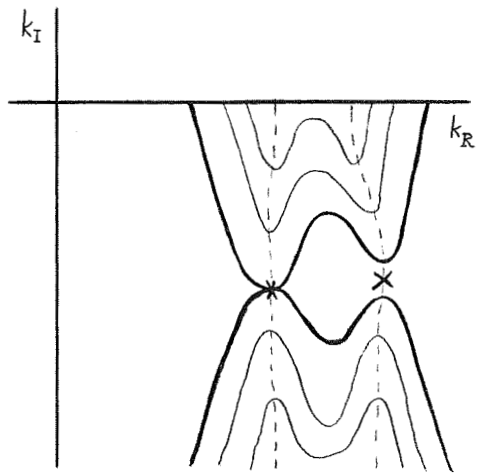

d.) $\lambda = \lambda_{t_1}$

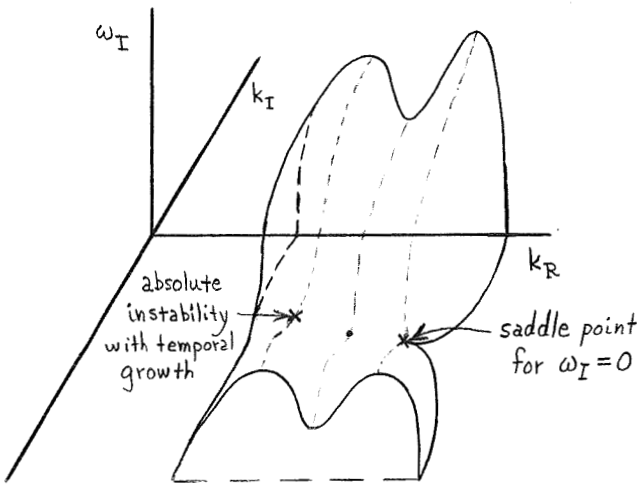

e.) $\lambda = \lambda_{t_2} < \lambda_{t_1}$

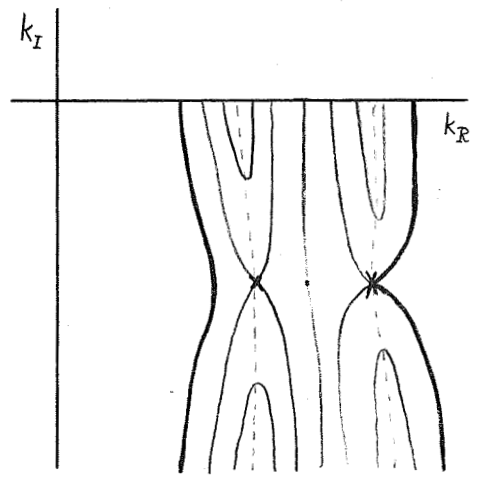

f.) $\lambda = \lambda_{t_2} < \lambda_{t_1}$

Fig. 5.6. Appearance of an Absolute Instability as the Density Increases (λ Decreases).

we increase the density (decrease λ) and hence presumably bring the sets of stable and unstable modes closer together in the k-plane, we note that since the ω_I contours are nested, when the stable and unstable modes first come together for $Im(\omega) \geq 0$ (if they ever do), they must do so for $Im(\omega) = 0$. Thus, as the density is increased towards the transition density, the saddle point must emerge into the B-R contour through the real ω-axis, i.e. through curve B of Fig. 5.5a. Hence, just at the transition density we expect the absolute instability to have a real frequency ω and to have a complex k (in general) which lies arbitrarily close to the value for one of the convectively unstable modes associated with $\lambda \geq \lambda_{t_{1,2}}$.

However, the above must remain only a "plausibility argument" in that we have assumed, from the simple dependence of Eqs. (5.2.1) and (5.2.2) on λ, that a given saddle point does not simply disappear as λ is increased slightly above λ_t, but instead moves slightly in the ω-plane to a point just outside the corresponding B-R contour and loses significance. With this assumption and the application of the Cauchy-Riemann conditions we see (Fig. 5.6) that a saddle point must move into the lower half ω-plane as the density decreases below the transition density.

As we have discussed previously, we can tell whether condition (α) is satisfied anywhere within the B-R contour by checking that its mapping is an open contour in the complex k-plane. Since from the preceding analysis it seems

only a remote possibility that the merged root will enter the B-R contour anywhere except on the real ω-axis, in this work we will assume that at the transition density the absolute instability mode does have real ω. Then, after having found a transition density we choose a slightly lower density and check that the k-plane mapping of the B-R contour is a closed curve implying convective instability. Using such a procedure, the merged mode was indeed found to enter the B-R contour through the real ω-axis in all of the examples treated in the remainder of this work.

Using this property of the absolute instability mode at the transition density, we begin a study of such modes by restricting our search for solutions of condition (α) to real frequencies ω. Hence, we need only determine solutions $K(\omega)$ of (5.2.3) for real ω. An example of such a solution and the real and imaginary parts of $H[\omega,k(\omega)]$ along the trajectory is shown in Fig. 5.7. The case considered here is that pertaining to the isolated set of unstable modes near the first ion cyclotron harmonic of the loss-cone example considered in Section 4.4. As is conventional for such cases (see Section 6.1) we consider the convective versus absolute nature of the instability only along the magnetic field direction. The numbers on the $K(\omega)$ curve in the figure give the respective values of ω/Ω_i along the trajectory. The dashed lines indicate the boundaries of the region in which the dispersion function

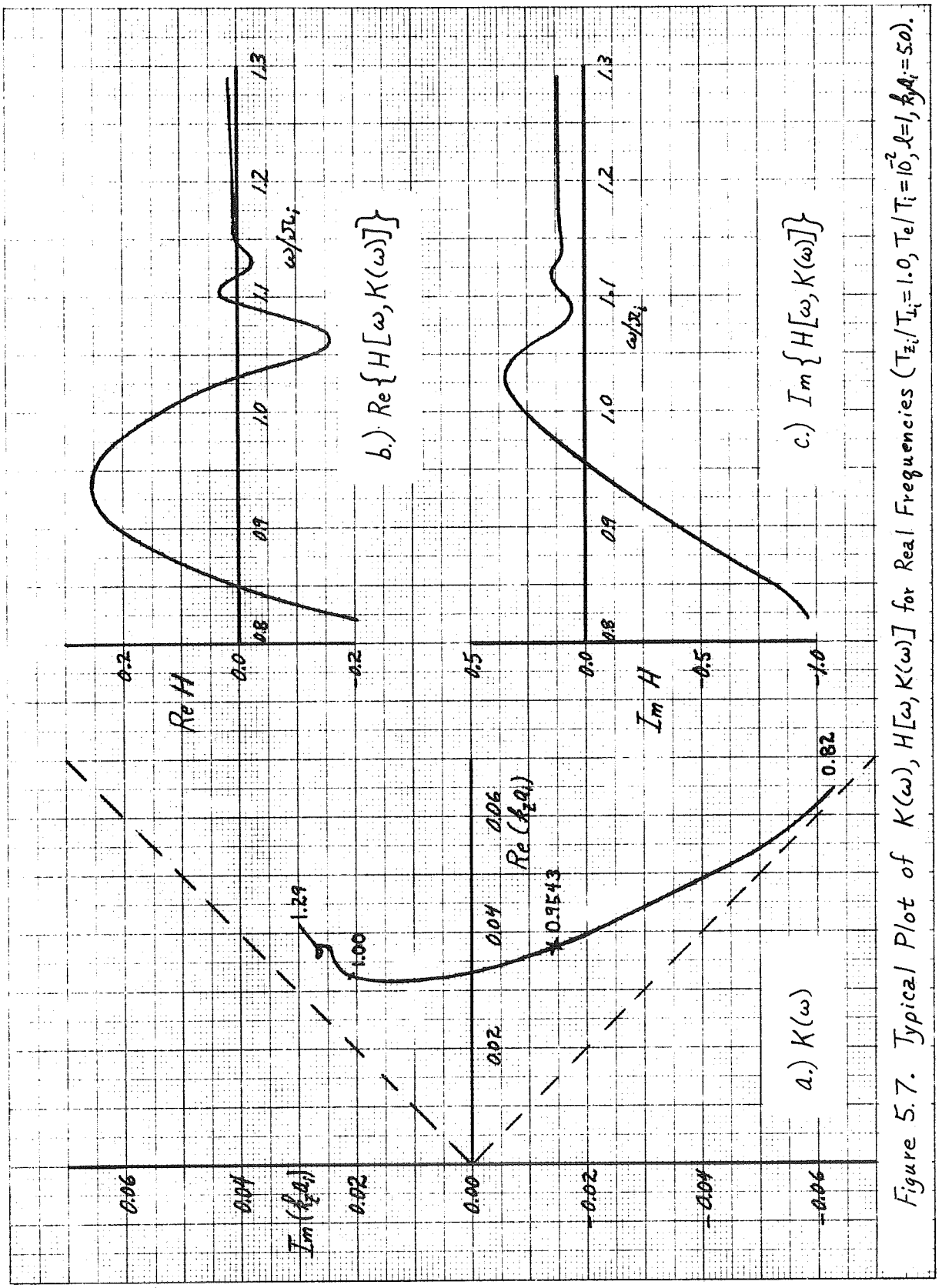

Figure 5.7. Typical Plot of $K(\omega)$, $H[\omega, K(\omega)]$ for Real Frequencies ($T_{z_i}/T_{i_i}=1.0$, $T_e/T_i=10^{-2}$, $\lambda=1$, $k_y A_i=.50$).

H "diverges" (see Section 3.4). From Figs. 5.7b, c we see that at $\omega/\Omega_i = 0.9543$ the imaginary part of $H[\omega,K(\omega)]$ vanishes and at that point the real part of H is positive and equal to 0.2448. Therefore this point satisfies the dispersion relation and hence condition (α) for $\lambda = 0.2448$. Comparing Figs. 4.8 and 5.7 we note that the density at which this merged mode occurs is about a factor of four higher than the threshold density.

Having found a pair of modes which merge to satisfy absolute instability condition (α) for a real frequency ω, we now wish to see whether these modes also satisfy condition (β). In examining this question we go one step further than in the preceding section and note that as long as $Im(k_B)$ is nonzero, in order to satisfy condition (β) it is sufficient to show that only one of the modes which have merged to satisfy condition (α) is an unstable or growing mode. (In the very rare cases where the merged mode has real k_B, it is sufficient to show that only one of the modes lies on a continuous marginal stability curve.) In the following analysis we will use this restricted interpretation of condition (β) since it is sufficient for our purposes.

As a first consideration of the constraints imposed by absolute instability condition (β), we must certainly only be concerned with those merged modes satisfying condition (α) which have their real frequency ω in a region in which unstable or growing modes can exist. These are the

real frequency regions which have been previously identified by a marginal stability analysis. (They are also the portions of the B-R curves (for all densities) labeled as curve B in Fig. 5.5a.) For the example shown in Fig. 4.8 these ranges are those bounded by the marginal stability curve. Note that the real frequency ranges from the marginal stability analysis are applicable here since we are looking for the transition density which occurs for a real frequency ω. We should also note that since in this case (i.e. that shown in Fig. 4.8) the marginal stability results give a unique boundary in real ω between the maps of the upper and lower half k-planes, they also define the sign of Im(k) for the unstable or growing modes within the frequency ranges of interest. (We are dealing here with an "isolated" set of unstable modes, e.g. the leftmost set in Fig. 4.8). Therefore absolute instability criterion (β) requires as a necessary condition that the merged mode have its real frequency in the unstable regions identified by the marginal stability analysis and have the same sign of Im(k) as the unstable modes.

In the example shown in Fig. 4.8, the unstable real frequency region under the marginal stability curve is found to encompass a part of the lower half k-plane. Thus, for this case it is at least necessary for the sign of Im(k) to be negative and for the real frequency to lie under the marginal stability curve in Fig. 4.8 for a mode which satisfies condition (α) to be an absolute instability.

It is readily apparent from Figs. 4.8 and 5.7 that these conditions are met by the merged mode found at $\omega/\Omega_i=0.9543$. (In other cases considered later in this work it is sometimes found that the imaginary part of $H[\omega,k(\omega)]$ also vanishes at pairs of points for $(\omega-n\Omega_i)/\Omega_i \sim +0.1$. Many times $H[\omega, k(\omega)]$ is positive and real for one of these points. The $K(\omega)$, $H[\omega,k(\omega)]$ plots for these cases are similar to those displayed in Fig. 5.7. At first sight one might expect that such merged modes, which satisfy condition (α) within the appropriate real frequency range, correspond to absolute instabilities. However, since Im(k) turns out to be of the wrong sign for these merged modes, we may immediately conclude that they do not satisfy condition (β). They simply represent the merging of two evanescent modes. Therefore these special merged modes at $(\omega-n\Omega_i)/\Omega_i \sim +0.1$ do not correspond to absolute instabilities and we omit them from consideration in all examples discussed in the following chapters.)

In the preceding paragraphs we have indicated two ways in which some of the constraints implied by condition (β) can be applied immediately to show whether or not certain classes of merged modes which satisfy condition (α) can be absolutely unstable modes. However, we have not yet shown that the classes of merged modes which do satisfy these rudimentary applications of condition (β) are in fact "marginally stable" absolute instability modes. We could of course assure that they are by going back to

the strictest interpretation of condition (β) and simply increase the imaginary part of ω until it exceeds σ, following in the k-plane the individual modes which have merged to make sure that they return to opposite sides of the real k-axis. However, in this work we will check for satisfaction of condition (β) in a manner which is more in keeping with our emphasis on the use of marginal stability results.

As we have noted previously, in order to satisfy condition (β) we need to show that <u>one</u> and <u>only one</u> growing mode coalesces into the merged mode which satisfies condition (α). If only two modes are merging (the usual case), the alternate possibilities are of course that two stable or two unstable modes merge. We have already noted an easily identified case in which two evanescent modes merge for real ω to satisfy condition (α) but not (β). Therefore, in general, we expect that we must in fact be prepared to discriminate against the merging of two stable modes.

In contrast, at least under certain circumstances, we can show that it is impossible for two growing or unstable modes to merge. As in a previous discussion we will assume (for the moment) that we are only concerned with a single "isolated" set of unstable modes and that the range of k_R for instability at $k_I=0$ is finite. For such a case, a potential merging of two unstable modes of the same set is shown in Fig. 5.8. However, as we have pre-

viously noted, the Cauchy-Riemann conditions show us that $\omega_I(k_R,k_I)$ can have no local maximum or minimum. Therefore the "lake" shown in Fig. 5.8b cannot exist and hence it is impossible for two unstable modes in the same isolated set to merge to form a saddle point, i.e. to satisfy condition (α).

On the other hand if there are overlapped sets of unstable modes, then a branch point may occur in $\omega(k)$. In this case, at least in the region of overlap (previously identified from a marginal stability analysis since here we are only concerned with real ω), we may not always be able to apply the Cauchy-Riemann conditions and hence

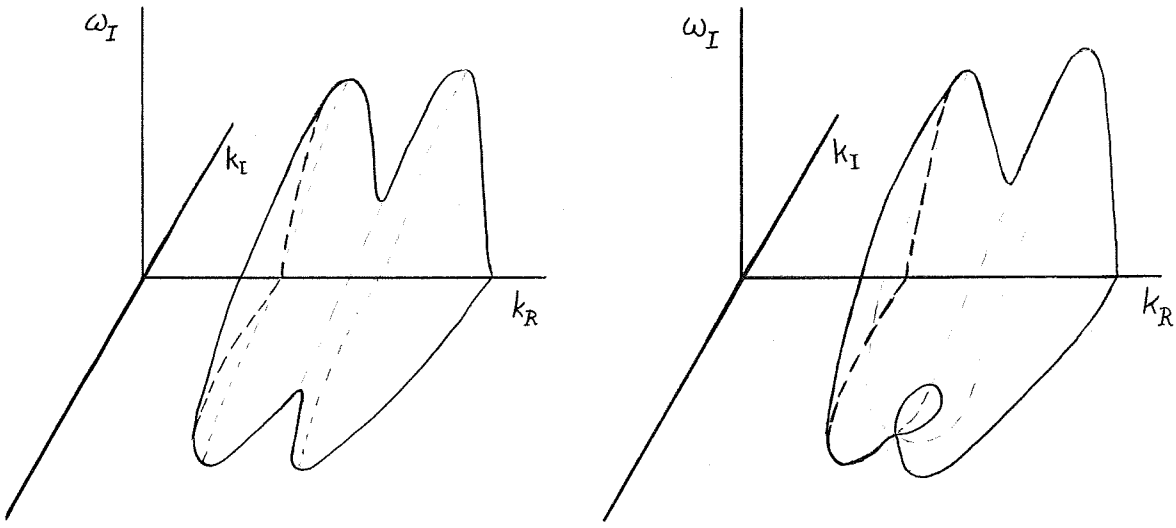

a.) Isolated Set of Convectively Unstable Modes.

b.) Not Possible from Cauchy-Riemann Conditions.

Figure 5.8. Impossibility of Merging of Two Unstable Modes from a Given Isolated Set.

condition (α) may be satisfied by the merging of two unstable modes.

Thus, in order to be certain that a given merged mode which satisfies condition (α) is an absolute instability, in general, we must demonstrate that <u>one</u> and <u>only one</u> of of the merged modes is a growing or unstable mode. The way we ensure this is to make complex k - real ω plots of the unstable modes, such as that shown in Fig. 5.5b, for densities increasing successively from the threshold density up to the density at which the merged mode exists. If the merged modes is to satisfy condition (β), then these complex-k curves of the set of growing modes must be closed for $\lambda > \lambda_B$ and some point on these curves must come arbitrarily close to the merged point as the density becomes arbitrarily close to the density at which the merged mode occurs ($\lambda \to \lambda_B$). If there are overlapped sets of unstable modes, then condition (β) is satisfied if <u>only one</u> set of such curves comes arbitrarily close to the merged mode. In practice it is not really necessary to plot the complex k curves in detail since they tend to be fairly strongly peaked functions of the frequency and the merged modes tend to occur very near the extrema of the imaginary part of k. Therefore in order to ensure satisfaction of condition (β), we usually need only follow the real frequencies for which $\max|\mathrm{Im}(k)|$ occurs for densities from the threshold density up to that at which the merged mode occurs. An important by-product of this procedure is that we obtain the maximum spatial growth rates of the convectively unstable modes. A knowledge of the properties of these convec-

tively unstable modes which have the largest spatial growth rates is also useful in making an initial guess at the solution $K(\omega)$ in (5.2.2).

We should also note that we could use a somewhat simpler procedure to show that merged modes which satisfy condition (α) also satisfy condition (β). Since we need to show that only one of the merged modes is an unstable mode, we can ensure satisfaction of condition (β) by checking that the merged mode is contained once and only once in the complex k - real ω mapping of the unstable modes (Fig. 5.5b) at the density for which the merged mode of interest occurs. The points at which the mapping intersects the real k-axis must of course be on the marginal stability boundary at the appropriate density. Note that this procedure of satisfying condition (β) is very analogous to the normally used "pole-pinch" analysis in which one follows the merged roots away from the saddle point for increasing $Im(\omega)$. In either of the ways discussed above we verify that only one of the modes which merged at ω_B, $K(\omega_B)$, λ_B is a growing mode and hence that the merged mode is an absolute instability mode.

In addition to the preceding discussion concerning determination of the transition density in the frame of reference in which the dispersion relation was derived, we note that the same procedures can be applied to find the densities for transition to absolute instability in arbitrary frames of reference. Since the question of

stability versus instability is independent of the frame of reference, the marginal stability analysis remains unchanged. However, the absolute instability analysis does change in that instead of solving (5.2.2) for a $K(\omega)$ trajectory, we now must solve

$$\frac{\partial H}{\partial k} + V \frac{\partial H}{\partial \omega} = 0 \qquad (5.2.5)$$

which is, as before, a density-independent equation. In carrying out the same procedure as before, with (5.2.5) now defining the trajectory $K(\omega)$, we determine the transition density in a frame of reference moving with velocity V relative to the laboratory frame. While such results are interesting in themselves, they would not directly allow us to make plots of the spatial shape of the time-asymptotic response of the plasma as Hall and Heckrotte (5.11) do, since our results would not all be for the same plasma density.

In order to illustrate the procedures outlined above, we consider the problem of determining the transition densities (in the rest frame only) for each of the groups of unstable modes ($\omega/\Omega_i \sim 1,2,3$) of the simple loss-cone example considered in Section 4.4. Using the computer programs discussed in appendix C which implement these procedures, we obtain the results displayed in Fig. 5.9 (here $k_\perp = k_y$) and Table 5.1. In the figure the dashed lines indicate the real frequency for which max $|\mathrm{Im}(k_z)|$ occurs at densities for which the instability remains

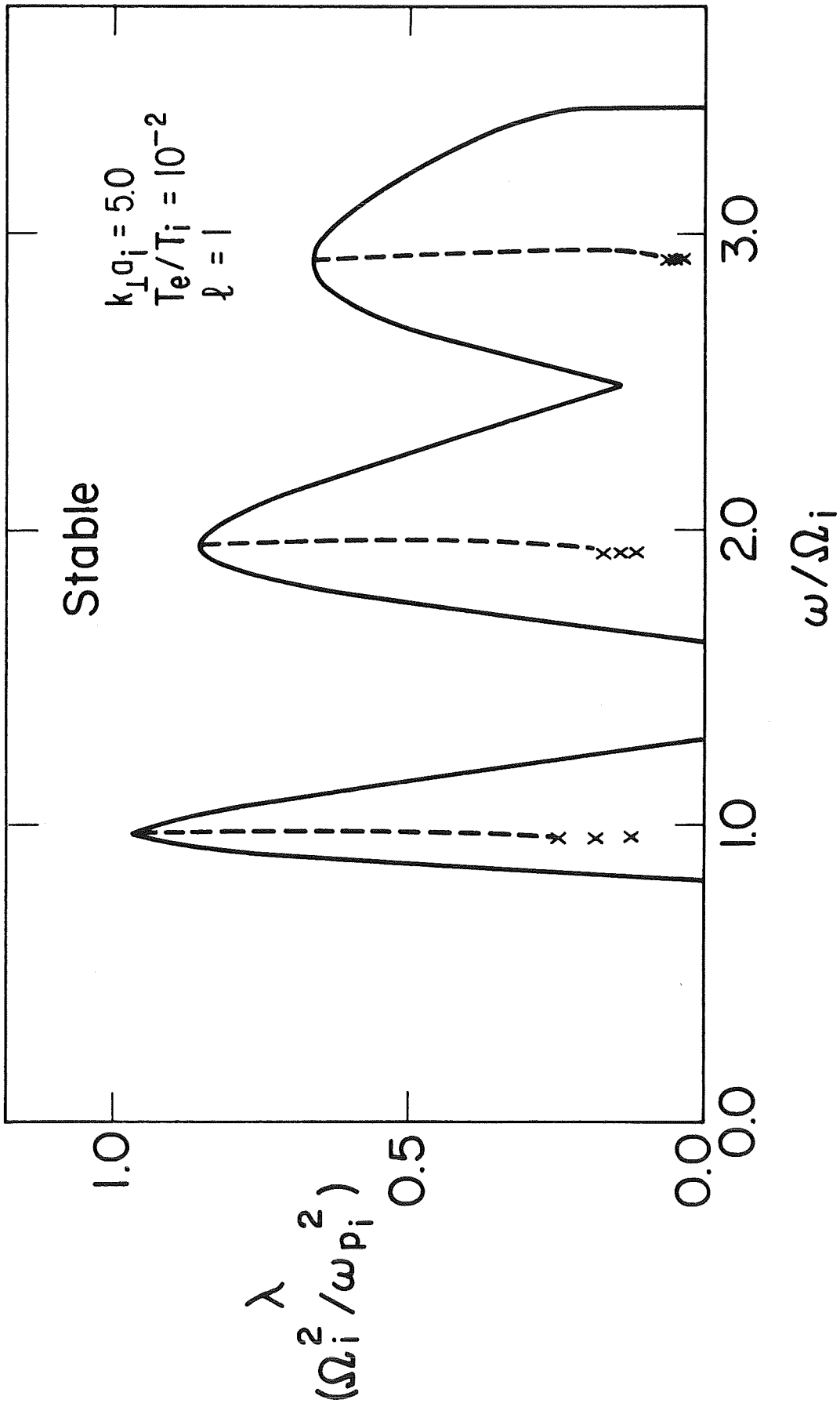

Figure 5.9. Simple Loss-Cone Instability Case.

Table 5.1. Properties of the Unstable Modes for the Simple Loss-Cone Instability Case ($T_e/T_i=10^{-2}$, $\ell=1$, $k_y a_i=5.0$).

	$\mathrm{Re}(\omega/\Omega_i)$	$\mathrm{Im}(\omega/\Omega_i)$	$\lambda=\Omega_i^2/\omega_{p_i}^2$	$\mathrm{Re}(k_z a_i)$	$\mathrm{Im}(k_z a_i)$	$\omega_{p_i}^2/\Omega_i^2$
instability threshold	0.9708	0.00	0.9568	0.09125	0.00	1.045
	1.944	0.00	0.8498	0.1767	0.00	1.177
	2.911	0.00	0.6608	0.245	0.00	1.513
"marginally stable" absolute instability mode	0.9543	0.00	0.2448	0.03747	-0.01431	4.085
	1.920	0.00	0.1692	0.06581	-0.02534	5.910
	2.915	0.00	0.05745	0.06994	-0.02733	17.41
absolute instability mode	0.9559	0.01	0.1812	0.03127	-0.01588	5.519
	1.922	0.01	0.1415	0.05951	-0.02671	7.067
	2.918	0.01	0.04514	0.06339	-0.02850	22.15
absolute instability mode	0.9572	0.02	0.1248	0.02510	-0.01825	8.013
	1.923	0.02	0.1155	0.05317	-0.02847	8.658
	2.920	0.02	0.03354	0.05678	-0.03003	29.82

convective. The cross at highest λ (lowest density) for each of the groups of unstable modes indicates the "marginally stable" absolute instability mode (i.e. the transition density) found by the method just described. The crosses at lower λ (higher density) indicate the densities at which the plasma is absolutely unstable with temporal growth rates of 1%, 2%, etc. of the ion cyclotron frequency. The latter results are found by an obvious variation of the above procedure in which we follow $K(\omega)$ trajectories for ω having the appropriate positive imaginary part. The details of this procedure are discussed in the following section.

From the tabulation of the important numerical results in Table 5.1 we see that the "marginally stable" absolute instability mode has a negative imaginary part of k_z which is the appropriate sign here for a growing mode. In addition, from Fig. 5.9 we see that the dashed curves indicating the real frequency for which max $|\mathrm{Im}(k_z)|$ occurs do indeed closely approach the merged mode which satisfies condition (α). Detailed plots of the complex k-real ω solutions of the dispersion relation (corresponding to contour B of Fig. 5.5b) for varying densities confirm that the merged modes include one and only one growing mode. For this example we have also used an independent "pole-pinch" analysis, in which as previously described one follows the merged roots away from the saddle point for increasing $\mathrm{Im}(\omega)$, to directly demonstrate that each of the merged modes satisfies condition (β). Therefore from all this evidence, we conclude that the modes denoted by crosses are indeed absolutely unstable modes.

5.3 Absolute Instability Temporal Growth Rates

Having developed a method for determining the density at which a "marginally stable" absolute instability mode exists, we will now discuss in more detail how we compute the temporal growth rate of the absolute instability as the density is increased above the transition density. As we have already pointed out, the obvious procedure is to carry through the same method as described in the preceding section, determining $K(\omega)$ as a function of the real part of the frequency with the imaginary part held constant at some positive value, say γ. By such a process we determine the density at which an absolute instability has a temporal growth rate of γ.

While most of the analysis is the same as for the real frequency case ($\gamma=0$), here we cannot use the marginal stability analysis to ensure satisfaction of condition (β) since that analysis is applicable only for real frequencies. Rather, we will ensure satisfaction of condition (β) by checking that the absolute instability mode of interest always remains within the appropriate B-R contour as the density is increased. We have previously noted that in using the B-R contour to check for absolute instabilities, we generally must separately check for satisfaction of condition (β) by the merged mode. However, as long as we increase the growth rate γ only incrementally from one computation to the next, we can be sure that we are following the absolute instability mode which has previously been

shown to satisfy condition (β). Then, to ensure satisfaction of condition (β) we need only check that the merged mode does not go outside the B-R contour, or coalesce with another absolutely unstable mode in which case a "pinch" dissolution could occur (5.11).

In order to illustrate these points, we consider their application to the simple example discussed in Sections 4.4 and 5.2. From Fig. 5.9 it is readily apparent that as the density increases above the transition density the separate absolute instability modes do not coalesce and thus pinch dissolution cannot occur. The B-R contour plots for a set of densities and a range of frequencies around the first ion cyclotron harmonic are displayed in Fig. 5.10. From these plots it is apparent that the merged mode we are following does remain within the B-R contours as the density is increased. Therefore, we conclude that the merged mode remains an absolute instability mode for the temporal growth rates and densities shown.

Since the inside of the B-R contour represents a map of a portion of the upper or lower half k-plane, we would expect that an indication of a merged mode moving out of the B-R contour would be a change in the sign of Im(k). However, this conclusion only applies for simple contours such as that shown in Fig. 5.5a in which curve A of this figure does not intersect itself. A particular case in which the contour does intersect itself is illustrated in Fig. 5.11. The only difference between this case and the

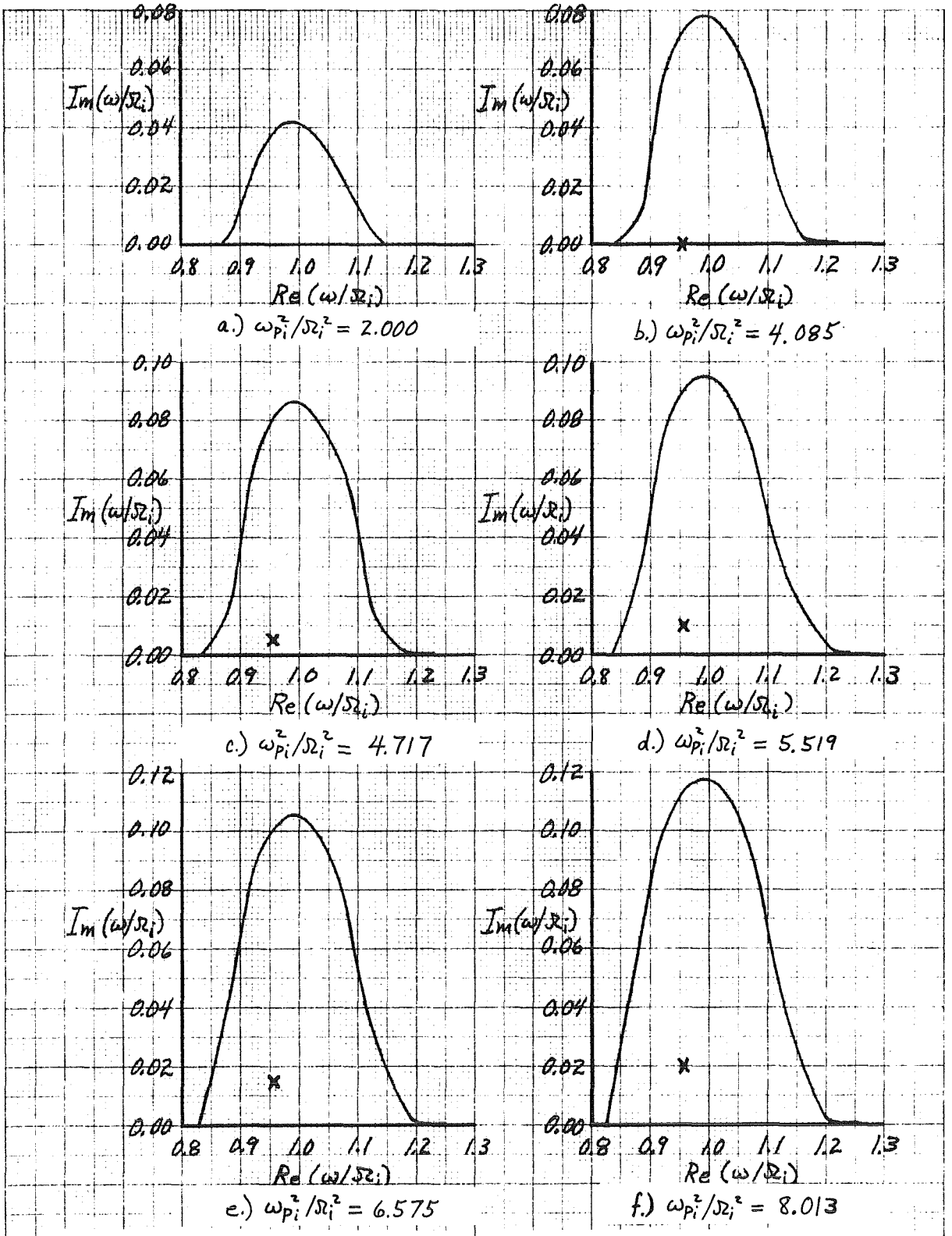

Figure 5.10. B-R Contours for Simple Loss-Cone Instability Case ($T_e/T_i = 10^{-2}$, $\ell = 1$, $k_y a_i = 5.0$). Crosses Indicate Absolute Instability Mode.

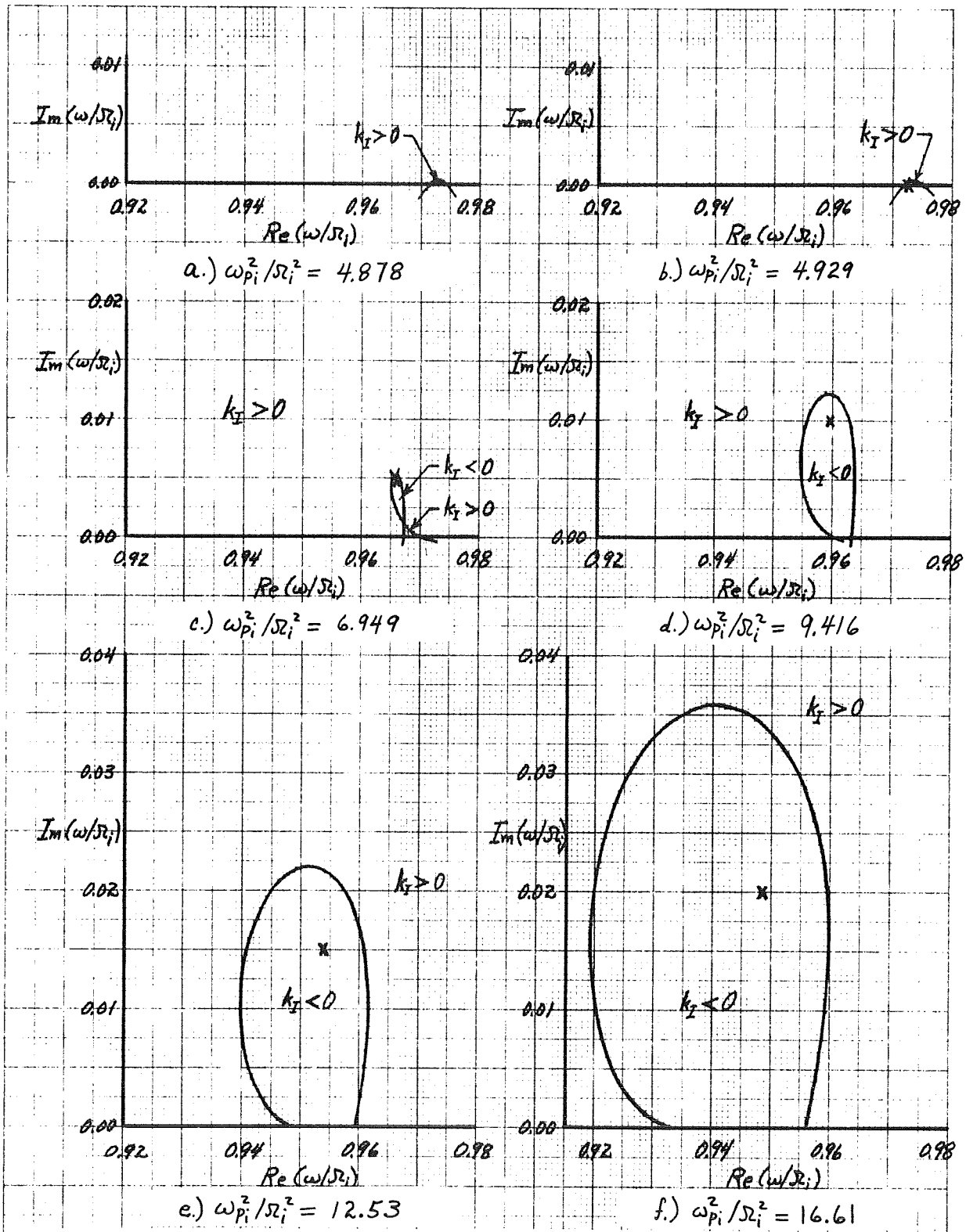

Figure 5.11. B-R Contours for a Loss-Cone Instability Case ($T_e/T_i = 1.0$, $\ell = 1$, $k_y a_i = 5.0$). Crosses Indicate Absolute Instability Mode. k_I Denotes $Im(k_z)$.

simple loss-cone example which we have been considering is that T_e/T_i has been increased to a value of unity. In considering the present case it is found that $Im(k_z)$ of the merged mode changes sign from positive to negative as γ is increased from zero to $0.005\Omega_i$. As we have indicated above, ordinarily such a change of sign would be an indication that the merged mode has moved out of the B-R contour. However, as can be seen from Fig. 5.11 in which the respective regions of mappings of the k-plane are indicated by $k_I(Im(k_z))$, the B-R contour "turns itself inside out" as the density is increased in such a way that the merged root always remains within the B-R contour. As in the simple loss-cone case (Figs. 4.8 and 5.9), no other absolute instability modes coalesce with this merged mode. Therefore we conclude that the merged modes do remain absolutely unstable modes as the density is increased. We have also verified this conclusion by using a "pole-pinch" analysis to directly demonstrate that condition (ß) is satisfied for these modes.

In this $T_e/T_i=1$ case the physical significance of the B-R contour "turning itself inside out" is that as the density increases above the transition density, the instability changes from one characteristic type to another. Note however that all of the unstable modes belong to a single "isolated"set since there exists only one continuous B-R contour. This unusual phenomenon is also indicated by the marginal stability analysis where it is found that the

marginal stability curve intersects itself. These points will be discussed in more detail in the next chapter.

Incidentally, we may also note that the results displayed in Figs. 5.10 and 5.11 show that the real-k temporal growth rates are not at all representative of the temporal growth rates of the absolute loss-cone instabilities. In addition, comparing Table 5.1, Fig. 5.9 and Fig. 4.7 and viewing Figs. 5.10a, b and 5.11a, b we see that even when the instability remains convective and is often experimentally unobservable (see next section), the real-k temporal growth rates may be appreciable. Thus the real-k temporal growth rates can be very misleading in the assesment of an instability. This observation further strengthens our conclusion that the convective versus absolute nature of the instabilities must be examined in detail.

5.4 Realistic Stability Criteria for Finite Plasmas

In all of the preceding work we have assumed that the plasma is infinite and homogeneous in the directions of wave propagation. Following the procedures we have developed, we can find the parametric ranges of stability and instability (both absolute and convective). In this section we discuss the application of the results obtained from studying an infinite homogeneous plasma model to the problem of predicting the instabilities of real laboratory plasmas which are finite in the directions of wave propagation.

A first step in the adaptation of an infinite homogeneous theory to a finite plasma is to make sure that the unstable modes of interest have wavelengths which can "fit" into the finite plasma in some sense. In order to know the precise wavelengths of the modes which can occur in a given plasma, we must of course take into account the details of plasma inhomogeneities throughout the plasma and at its boundaries. However, as a rough guide (in some cases very rough), we can say that a half-wavelength of the relevant unstable modes can be no longer than the length of the plasma in the direction of wave propagation. Many of the microinstabilities which we will consider in the next two chapters only occur if their wavelengths along the magnetic field exceed a certain length. Hence we will find this implication of the infinite plasma model to be useful in deciding how short an experimental machine should

be in order to avoid certain microinstabilities.

When the wave vector component in a given direction vanishes, the implication of the preceding discussion is that the mode can exist only in a plasma which is infinite and homogeneous in this direction. However, in this special case other considerations prevail. The vanishing of a wave-vector component in a given direction really means that there is no wave propagation in this direction. We may thus think of this as a case in which we have found a "local" solution of the dispersion relation in the sense discussed in Section 3.3. Therefore, when a given wave-vector component vanishes, as long as the plasma is longer than a few "fine-structure" scale lengths (the Debye length, Larmor radius, etc.) in this direction, we expect the mode to "fit" into the finite plasma. We also note that the instability of a mode which does not propagate in a given direction is presumably rather insensitive to inhomogeneities in that direction.

One such particular case with which we will be concerned is where instabilities occur which have no propagation in the axial direction ($k_z=0$) and frequencies which are usually of the order of the ion cyclotron frequency and its harmonics. These modes are called flute-like modes since they are similar to the low-frequency flute modes which we are assuming have been stabilized (Section 1.1). As with the flute modes, magnetic wells and "line-tying" at the ends of the plasma may be helpful in suppressing

these modes. However, since the frequencies are so much higher for the flute-like modes, it is questionable if particles could carry charge perturbations to the ends of the plasma fast enough to make "line-tying" truly effective. Therefore, we expect that when flute-like modes are predicted by the infinite homogeneous plasma model, they will appear in most finite plasmas as well.

The next step in the application of our infinite plasma model results to a finite plasma is the consideration of the convective versus absolute nature of the instabilities. As we have noted in this chapter, microinstabilities are usually convective for densities only slightly exceeding the threshold density and become absolute only at higher densities. When the instability is convective, the relevant measure of its potency is the distance over which the unstable mode grows by a factor of e -- the growth length. If we neglect reflection of convective modes from the ends of the plasma, then for waves initiated by thermal fluctuations to grow to experimentally observable amplitudes (and thereby to be able to destroy confinement), the plasma must be many growth lengths long. However, if there is even a small amount of reflection, then whether or not a convective instability causes a finite plasma to be unstable is usually determined by the magnitude of the reflection coefficient as well as the length of the plasma in terms of growth lengths.

Many authors (5.12-5.17) have considered the problem of computing the reflection coefficient for plasma waves impinging upon density gradients. The reflection coefficient is generally thought to be very small due to the appearance of strong Landau damping as the electron density decreases (5.12). Calculations based upon a fluid model (5.13) and upon a WKB type solution of the Vlasov equation (5.14, 5.15) have shown that the reflection coefficient is generally small as long as the wavelength or the ion Larmor radius is small compared to the characteristic inhomogeneity length. These conclusions based upon approximate treatments have been verified by numerically integrating the Vlasov equation and Poisson's equation for waves propagating into the density gradient region (5.16). In the above treatments the reflection arises from the scattering of the wave off of the gradual changes in the sheath potential and dielectric constant of the plasma. For certain cases in which the plasma sheath potential varies rapidly with the spatial position, Baldwin (5.17) has shown that the reflection coefficient may be of order unity. The essential point in the latter calculation is that the particles which are reflected almost ballistically from a sharp sheath gradient maintain the phase coherence of the wave. However, as Baldwin notes, for typical loss-cone and temperature-anisotropy instabilities, there will be some phase mixing due to the finite wavelengths of the modes transverse to the magnetic field. We

thus conclude that in general the reflection coefficient must be estimated separately for each plasma of interest.

In the next two chapters we will find that for convectively unstable modes to render a finite plasma unstable before an absolute instability appears, the reflection coefficient must be about 0.285 or greater. Therefore, since the above studies indicate that the reflection coefficient is usually less than this value, or apparently can be made so, we do not expect convective instabilities to cause experimentally observable instabilities of finite plasmas which are reasonably well represented by the plasma model studied here.

In contrast to a convective instability, an absolute instability is relatively unaffected by the reflection properties at the ends of the plasma, i.e. only the slight damping effects of the ends will have any significant effect on the absolute instabilities.. Therefore as a rough guide, we would expect the instability criterion of a finite plasma to be that a half-wavelength of the absolutely unstable mode "fit" into the plasma and that the plasma density exceed the transition density (as opposed to the threshold value). For a plasma with a finite lifetime, the absolute instability will be experimentally observable only if the instability can grow appreciably within the plasma lifetime. This of course requires a density somewhat larger than the transition density.

In addition to these rudimentary considerations, recently the effects on absolute instabilities of variations

of magnetic field strength (5.18) and other parameters (5.19) along the magnetic field direction have been considered. The calculations are carried out through a WKB type analysis in which the wavelength of the modes is assumed to be small compared to the scale length of the inhomogeneities. These studies are still in progress. At present it is not unequivocally clear whether small magnetic field, density etc. variations have stabilizing or destabilizing effects on the absolute instabilities. Physically we might expect the magnetic field variation to be a stabilizing effect due to the fact that the local ion cyclotron frequency changes along the magnetic field, thereby perhaps "detuning" the absolute instability. Similarly plasma inhomogeneities could "detune" an absolute instability by changing the relevant frequency and wave number of the instability. However, we should also note that any inhomogeneities will introduce an additional amount of dispersion or "refelction" into the plasma. From the standpoint of our physical model of an absolute instability (Section 5.1), this effect of the inhomogeneities might be destabilizing since it may provide more feedback of wave energy to the point of the original disturbance than that provided by a similar infinite homogeneous plasma. Finally we note that even if the overall effect of the slowly varying inhomogeneity is in the direction of stabilizing the plasma, it would probably only increase the density at which the absolute instability

appears, i.e. it would not prevent the absolute instability from ever occuring. Then, the important question is how much the transition density has been increased.

We should also note that in contrast to the preceding discussion, the more typical situation in a real plasma is that the characteristic inhomogeneity length is of the order of or shorter than the wavelength of the instability, at least near the ends of the plasma. To the author's knowledge the effects of inhomogeneities in this case have not been considered in any detailed manner, although some effects due to the finite lengths of plasmas have been considered by Cotsaftis (5.20).

In addition to the preceding considerations of the effects of a finite geometry, the instabilities may also have their wave amplitudes limited by nonlinear effects. For convenience we will divide the known nonlinear effects into three categories: quasilinear, strong turbulence and mode-coupling. The quasilinear theory (5.21) is the necessary addition to the linear theory to ensure energy conservation as it describes the limiting of wave amplitudes due to the absorption (by the waves) of all the free energy driving the instability. The transfer of energy takes place by action of the waves causing particle diffusion in such a direction as to reduce the sources of free energy. The "strong turbulence" theory (5.22) accounts for the limiting of wave growth of a large amplitude wave or a narrow spectrum of such waves due to the "trapping"

of a large group of particles in velocity space such that the average of the growth rate over the group vanishes, i.e. the group includes particles which damp the wave as well as those which feed the wave. Finally, the mode-coupling theory (5.23) takes into account the limitations of wave amplitude due to wave-wave interactions with damped modes and nonresonant particles. It is important to note that while quasilinear effects are mainly dependent on the local amount of free energy available, strong turbulence and mode-coupling effects are primarily dependent on the local wave amplitude. Therefore we would not expect quasilinear effects to be important in limiting a convective instability since the waves sample virgin spatial regions as the convectively unstable wave packet moves. However, if a high level of homogeneous turbulence is present in the plasma, then we would expect the normal quasilinear effects to be relevant even for a convectively unstable plasma. With this one qualification, all of the nonlinear effects would seem to apply directly to convectively and absolutely unstable plasmas. However, nearly all of the nonlinear theories have been developed on the basis of a real k-complex ω analysis, thereby completely ignoring the convective or absolute nature of the instabilities. An exception is that the quasilinear theory of a plasma which has only convectively unstable modes has been formulated by Drummond (5.24). In convectively and absolutely unstable plasmas the motion and spatial growth

of wave packets, which is usually ignored in the nonlinear theories, is presumably very important. Therefore, before nonlinear calculations can be realistically applied to finite plasmas in which the type of instability is important, it is imperative to consider the extent to which the nonlinear effects as presently conceived would actually occur in a convectively or absolutely unstable plasma.

6. VELOCITY-SPACE ANISOTROPY INSTABILITIES

6.1 Introduction; Temperature-Anisotropy Instabilities

In the preceding two chapters we have developed and rigorously justified methods for determining the parametric regions of stability, convective instability and absolute instability. In this chapter we will apply these methods to the study of microinstabilities caused by velocity-space anisotropies of a homogeneous plasma. First, however, we review the literature concerning these instabilities. The majority of this review is concerned with instabilities driven principally by the sources of free energy (see Section 1.1) associated with either the inequality of mean velocities along and transverse to the magnetic field or a nonmonotonic ("loss-cone") type of $v_\perp^2$ distribution. We refer to these two major types of homogeneous plasma instabilities as temperature-anisotropy and loss-cone instabilities respectively. After this review, we study loss-cone instabilities in detail. The main part of the study is concerned with determining the convective versus absolute nature of the loss-cone instabilities for relatively low densities ($\omega_{pi}^2 \sim \Omega_i^2$) and moderate wavelengths transverse to the magnetic field $k_\perp a_i \gtrsim 1$). However, in addition we consider a high density and very short transverse wavelength case ($k_\perp a_i = 25.0$). The principal purpose in considering the latter case is to examine the range of applicability of a "continuum" limit

(very short transverse wavelengths, $k_\perp a_i >> 1$) of the dispersion relation which has been derived by Rosenbluth and Post (6.1).

The starting point for studies of velocity-space anisotropy instabilities is the dispersion relation given by (3.3.15) with the inhomogeneity and gravity terms omitted:

$$k^2 = \sum_j \omega_{pj}^2 \int d^3v \sum_{n=-\infty}^{\infty} \frac{J_n^2(k_\perp v_\perp/\Omega_j)}{k_z v_z + n\Omega_j - \omega} \left\{ k_z \frac{\partial F_j}{\partial v_z} + \frac{n\Omega_j}{v_\perp} \frac{\partial F_j}{\partial v_\perp} \right\}. \tag{6.1.1}$$

Here, we have taken k_y to be $k_\perp$ since in a homogeneous plasma, equilibrium considerations demand that there be azimuthal symmetry in velocity space with respect to the magnetic field direction and hence invariance of the Vlasov equation under rotation about $\underline{B}$. We can in this case think of $k_\perp$ as being either the azimuthal or the radial component of the wave-vector in magnetic mirror machine type plasmas. We will usually take it to be the radial component. We recall that in this work we are considering "low β" plasmas in which only electrostatic waves are important (see Section 1.2). The general dispersion relation for propagation of electrostatic and transverse waves in a uniform magnetized plasma has been derived by Bernstein (6.2). Harris (6.3) specialized that general dispersion relation to the case of electrostatic waves and first put it in the convenient form given by (6.1.1). Therefore (6.1.1) is usually referred to as the Harris dispersion relation.

In examining solutions of the Harris dispersion relation for a given equilibrium distribution function, we will concern ourselves with the convective versus absolute nature of the unstable waves only along the magnetic field. In this direction the phase velocities of the waves we consider are typically large compared to the electron thermal velocity. We may thus expect that the modes will be convectively unstable ones which are only slightly dispersed by the plasma and that the group velocity is approximately equal to the phase velocity. As we have noted in Section 5.1, when the typical modes of the plasma are convective modes with large group velocities as is true here, then the zero group-velocity absolute modes are intrinsically different from all but very small group-velocity convective modes. Therefore we may expect that the parametric regions in which convective and absolute modes propagate in the magnetic field direction will usually be different and should be examined in detail.

In contrast, there are reasons to believe that the convective versus absolute nature of the propagation transverse to the magnetic field may not be too important. If we think of $k_\perp$ as being the azimuthal wave-vector component, this is obvious since then $k_\perp$ must be real. When $k_\perp$ is taken to be the radial wave-vector component, the situation is more complicated. Since most plasmas are surrounded by highly conducting walls, if the wavelength of an unstable mode is of the order of the dimensions of

the system, we might expect the wall reflections to bring about radial standing wave normal modes for which $k_\perp$ is discrete and real (an "absolute" type of instability). However, this spatial constraint is not applicable for many of the instabilities considered in this work since, as we shall later see, the unstable modes occur only if the transverse wavelength is shorter than a certain critical length which is often much smaller than the dimensions of any conceivable system. Concerning shorter wavelengths, we will find that the phase velocities of the unstable modes transverse to the magnetic field direction are typically small compared to the mean ion velocity. Therefore the typical group velocities will also (presumably) be small and thus the distinctions between convective and absolute instabilities may not be too important (see Section 5.1). We also note that we would expect these small phase velocity modes to be very strongly dispersed by the ion thermal motions. Thus zero group-velocity (absolute instability) modes in the direction transverse to the magnetic field will presumably exist in the plasma even for densities which only barely exceed the threshold density for instability. The preceding observations imply that in determining the characteristics of the instabilities, it is perhaps sufficient to consider only real values of the wave vector component $k_\perp$. These conjectures should of course be examined by a detailed consideration of the absolute versus convective nature of the propagation of unstable modes in the

plane perpendicular to the magnetic field. Such an investigation would require consideration of complex values of $k_\perp$. However, in this work we will content ourselves with a study of the Harris dispersion relation for complex wave-vector components k_z, but allow only real values of $k_\perp$. Thus we examine the convective versus absolute nature of the unstable modes only in the axial or z direction.

For real $k_\perp$, it is readily apparent that the Harris dispersion relation is independent of the sign of $k_\perp$. This observation coupled with previous ones (Section 3.3) concerning the symmetry properties of the general dispersion relation (3.3.15) show us that we can restrict our consideration of solutions of the Harris dispersion relation (6.1.1) to those having positive values of $k_\perp$, $\mathrm{Re}(k_z)$ and $\mathrm{Re}(\omega)$. Note that in arriving at this conclusion we have assumed that all $F_j(v_\perp, v_z)$ are even functions of v_z (see Section 3.3).

As a first consideration of solutions of the Harris dispersion relation, we review some limiting cases (6.4). When there is propagation only along the magnetic field ($k_\perp = 0$), we see that (6.1.1) reduces to the dispersion relation for a homogeneous unmagnetized plasma, i.e. the dispersion relation given by (4.1.1). In this limiting case the electrostatic modes are stable under the same conditions as those in a plasma with no magnetic field (see Section 4.1). The fact that equilibrium distribution functions which are dependent solely on the single particle

kinetic energy of the particles are nonlinearly stable as well against transverse electromagnetic waves propagating along the magnetic field has been noted by Rowlands (6.5). A proof by Kammash and Heckrotte (6.6) that in a plasma in which the ions have a bi-Maxwellian velocity distribution ($T_\perp \neq T_Z$) and the electrons a Maxwellian distribution, electrostatic waves propagating along the magnetic field are stable follows from the work of Rowlands (6.5) as well as from an application of the Penrose stability criterion (see Section 4.1) which applies in such cases.

The case of propagation purely transverse to the magnetic field ($k_Z = 0$) is of greater interest. By definition if any such unstable modes exist they are called flute modes if $\omega << \Omega_i$ and flute-like modes if $\omega \sim n\Omega_i$, n being an integer. For $k_Z = 0$, the dispersion relation (6.1.1) is a symmetric function of ω. Therefore referring back to instability conditions (4.2.10) and (4.2.11) which are appropriate for $k_Z = 0$ modes, we see that at the onset of a flute mode ($\omega << \Omega_i$) in a homogeneous plasma, the frequency would vanish and the instability criterion (4.2.12) would reduce to

$$\frac{\omega_{Pi}^2}{\Omega_i^2} > \left\{ \frac{\Omega_i^2}{k^2} \sum_j \frac{\omega_{Pj}^2}{\omega_{Pi}^2} \int d^3v \left[1 - J_o^2(k_\perp v_\perp / \Omega_j) \right] \frac{\partial F_j}{\partial v_\perp^2} \right\} > 0$$

(instability). (6.1.2)

In writing the instability condition in this form we have made use of the Bessel function identity given in Eq. (A.22).

Reductions of this instability condition have been noted by Dory, Guest and Harris (6.7) and Wimmel and Saison (6.8). It is easy to see from (6.1.2) that all plasmas for which each species has a $v_\perp$ distribution which is a monotonically decreasing function of $v_\perp^2$ are stable against flute modes. This observation is in agreement with work by Kammash and Heckrotte (6.6, 6.9) who have shown that purely growing modes ($Re(\omega)=0$) cannot exist in a plasma which has a bi-Maxwellian ion velocity distribution and a Maxwellian electron distribution. However, flute modes can occur in plasmas which have a nonmonotonic ("loss-cone") $v_\perp^2$ distribution for at least one species of particles. For a plasma in which the ions have a loss-cone type of $v_\perp$ distribution, by examining the values of $k_\perp$ for which (6.1.2) can be satisfied, it is easy to see that, in general $\omega_{p_i}^2/\Omega_i^2$ must significantly exceed unity for flute instabilities to occur, irrespective of the details of the $v_\perp$ distribution. For a delta function distribution, Harris (6.10) discusses the conditions under which flute modes can occur and the earlier literature on the subject. For the more general $v_\perp$ distributions employed in this work, Dory, Guest and Harris (6.7) have shown that both flute and flute-like unstable modes occur only if $\ell \geq 3$, i.e. the $v_\perp$ distribution is peaked sharply enough about a nonzero velocity. These authors also discuss instability criteria for the flute-like modes. An approximate formula for the temporal growth rates of the flute modes in a homogeneous plasma has been given by

Brambilla (6.11). Using exact collisionally equilibriated loss-cone distributions appropriate for magnetic mirror machines instead of the idealized distributions employed in this work (see Section 1.3), Post and Rosenbluth (6.12) conclude that the flute instability occurs only for a mirror ratio (magnetic field at the mirror divided by that at the midplane) which is near unity and even then requires a very high plasma density ($\omega_{pi}^2/\Omega_i^2 >> 1$). The implication of all these remarks is thus that for a homogeneous plasma with a loss-cone type of velocity distribution, the flute or flute-like modes are not important as long as the $v_\perp$ distribution is not too sharply peaked or $\omega_{p_i}^2/\Omega_i^2$ is not too large compared to unity. In the next section we will see that even when flute and flute-like modes can occur, they do not appear until the density is much higher than the threshold and transition densities for unstable modes propagating at large angles (but less than 90°) to the magnetic field. That waves propagating neither exactly along nor exactly transverse to the magnetic field should become unstable at lower plasma densities than either limiting case was first noted by Harris (6.3).

The above remarks concerning flute-like modes apply to their appearance in a plasma with a single ion species. Pearlstein, Rosenbluth and Chang (6.13), using a short wavelength limit ($k_\perp a_i >> 1$) of the Harris dispersion relation (see Section 6.3), have shown that flute-like modes may be unstable if there exists the combination of

some cold ions or electrons together with a hot component of ions or electrons, respectively, which has even a very well thermalized (high mirror ratio) loss-cone distribution. For a plasma with two such ion species, these analytical results have been extended to all physically permissible wavelengths through numerical computations by Farr and Budwine (6.14). Post and Rosenbluth (6.12), also using the short transverse wavelength limit of the dispersion relation, have shown that loss-cone modes can be unstable in inhomogeneous plasmas with loss-cone type ion velocity distributions. The latter instability will be discussed in Section 7.3 along with the absolute and convective instabilities which occur in such a plasma.

Having reviewed the limiting cases which have been studied, we now discuss the work which has been done for arbitrary directions of propagation with respect to the magnetic field and nonzero frequencies. The vast majority of all previous instability studies have been concerned only with determining the parametric regions of instability and do not consider the convective versus absolute nature of the instabilities. Therefore, for convenience, in the following discussion we will not specifically mention the type of instability analysis employed unless the convective versus absolute nature of the instabilities was considered.

Certain velocity-space anisotropy instabilities driven by the free energy source due to drifts along the magnetic

field (i.e. particle currents) have been considered. For example, Drummond and Rosenbluth (6.15) have shown that a sufficient current along the magnetic field ($v_{D_i} \gtrsim 5\alpha_{Z_i}$) can induce ion-cyclotron instabilities. Similarly Hall and Grewal (6.16) have studied the case of two counter-streaming species of ions having high temperature anisotropy ($T_{\perp_i} >> T_{Z_i}$).

In the remainder of this work we will be concerned only with instabilities driven by free energy sources other than particle drifts along the magnetic field. An exhaustive qualitative and semiquantitative discussion of many of the possible types of velocity-space anisotropy instabilities which can occur in the absence of particle drifts along the magnetic field is given by Hall, Heckrotte and Kammash (6.17). Among the instabilities discussed by these authors are the electron-cyclotron instabilities driven by a loss-cone type of velocity distribution. For delta function $v_\perp$ distributions, these instabilities have also been studied by Ozawa, Kaji and Kito (6.18) and Gruber, Klein and Auer (6.19). The latter work gives some indication of the real-k temporal growth rates of these electron-cyclotron instabilities. For more realistic loss-cone distributions, Korablev (6.20) discusses high frequency electron-cyclotron instabilities using the Rosenbluth and Post "continuum" limit (6.1) of the Harris dispersion relation. However, as we shall see in Section 6.3, this "continuum" limit is usually only applicable for rather

high frequencies ($\omega >> \Omega$), short transverse wavelengths ($k_\perp a >> 1$) and high plasma densities ($\omega_p^2/\Omega^2 >> 1$) so that Korablev's treatment would be applicable only at very high plasma densities.

Another type of instability discussed by Hall, Heckrotte and Kammash (6.17) is that which arises when hot ions with a loss-cone distribution or $T_\perp \neq T_z$ co-exist with a group of cold ions. Using the Rosenbluth and Post "continuum" limit of the dispersion relation (6.1), Hall and Heckrotte (6.21) have discussed the effect of adding cold plasma to a hot ion plasma which has a delta function $v_\perp$ distribution. Again, as we shall see in Section 6.3, since the "continuum" limit is rigorously valid only at very high plasma densities, this particular work of Hall and Heckrotte (6.21) is only applicable at very high plasma densities. These multicomponent plasma instabilities are presently being examined in more detail by Guest and co-workers (6.22). In the latter studies particular emphasis is being placed on the effect which the addition of a small amount of cold plasma has on the temperature-anisotropy and loss-cone instabilities.

The two velocity-space anisotropy instabilities of greatest current interest in controlled thermonuclear fusion research are the ion-electron instabilities with frequencies near the ion cyclotron frequency or harmonics thereof, which are driven by the ion free energy sources

associated with the inequality of mean velocities along and transverse to the magnetic field and/or nonmonotonic (loss-cone type) perpendicular velocity distributions. As we have previously noted, we refer to these instabilities as the temperature-anisotropy and loss-cone instabilities respectively. We begin our discussion of these two major types of instabilities with some general remarks which apply equally to both types of instability.

In order to illustrate the basic properties of these instabilities we will use the basic plasma model delineated in Section 1.3. This model only allows for cylindrically cut-out "loss-cone" distributions, however the results we obtain here should be indicative of all typesof "loss-cone" distributions since our rough examination of the dispersion relation is independent of the details of the ion velocity distribution. The Harris dispersion relation worked out for our plasma model is that given by (3.3.16) and (3.4.3) with the inhomogeneity and gravity terms omitted. We are not considering the effects of net particle drifts along the magnetic field here; hence the v_{o_j} terms will also be omitted. Since the frequencies of interest here are of the order of the ion cyclotron frequency, we can usually neglect all but the $n = 0$ term in the electron contributions to the dispersion relation. (Actually, upon working out the terms in detail, one finds that the contribution of the real part of the $n \neq 0$ electron terms to the dispersion relation is negligible only

if

$$\omega_{p_e}^2 > \Omega_e^2. \qquad (6.1.3)$$

We should also note that for cases in which condition (6.1.3) is not satisfied, it is likely that we can no longer safely neglect transverse electromagnetic waves -- see Section 1.2.) In the actual numerical calculations presented in this and the following chapter the contributions of all the (electrostatic) terms in the electron summation are taken into account exactly. However, for the purposes of the present discussion we will assume that the density is low enough to satisfy (6.1.3) and hence we need only keep the n = 0 contribution from the electrons. We also assume here that the mean electron velocity perpendicular to the magnetic field is small enough and the transverse wavelengths long enough so that

$$k_\perp a_e << 1, \qquad (6.1.4)$$

in which case the $C_{n_e}^{\circ} \approx 1$. In this approximation the only relevant electron temperature is that characterizing the electron velocity distribution along the magnetic field which we will label as T_e. In reducing our general dispersion relation for an arbitrary number of species to the ion-electron plasma of interest, we take the "reference" species (see Section 3.3) to be the ions except that we allow for inequalities of perpendicular and parallel ion

temperatures by allowing T_{Z_i} to be different from T_{Z_o}. Note that with this choice of reference species $T_{\perp_i} = T_{\perp_o} = T_{Z_o} \neq T_{Z_i}$. Using all of these assumptions and conventions, we can write the approximate dispersion relation as

$$\frac{\Omega_i^2}{\omega_{pi}^2} = -\frac{2}{(k a_i)^2}\left\{ \frac{T_{\perp i}}{T_e} Z_1\left[\frac{(\omega/\Omega_i)}{(k_z a_i)}\sqrt{\frac{m_e}{m_i}\frac{T_{\perp i}}{T_e}}\right] + \frac{T_{\perp i}}{T_{z_i}} \sum_{n=-\infty}^{\infty}\left[Z_1(w_n)\, C_{n_i}^{\ell} + \frac{n}{(k_z a_i)}\sqrt{\frac{T_{z_i}}{T_{\perp i}}}\, Z_o(w_n)\, D_{n_i}^{\ell}\right]\right\} \tag{6.1.5}$$

in which

$$w_n = \frac{(\omega/\Omega_i) - n}{(k_z a_i)}\sqrt{\frac{T_{\perp i}}{T_{z_i}}} \quad .$$

In this dispersion relation the first term in the braces represents the surviving electron contribution while the remaining terms account for the ion contributions.

For the present rudimentary analysis of unstable wave solutions of this dispersion relation we concern ourselves only with the satisfaction of the conditions for marginal stability, i.e. we seek solutions for real ω and k_Z. Therefore the arguments of the Z_o and Z_1 functions will be real. The behavior of these functions for all real arguments has been previously displayed in Fig. 4.3, from which we note that the magnitude of both functions never exceeds 3.6. We also note the neither the

individual C and D functions nor their summation over all harmonics exceed unity (see appendix B). From these facts plus knowing that $(k_Z a_i)$ is not infinitesimally small at the threshold density (see examples in Chapter 4), we can easily see from (6.1.5) that in general for $T_e < T_{Z_i}$ the electron term dominates the dispersion relation while for $T_e > T_{Z_i}$ the ion terms dominate.

We will first consider the case where $T_e < T_{Z_i}$. The Nyquist and $P(\omega/\Omega_i)$ plots for two such cases have already been displayed in Figs. 4.4 and 4.6. For $T_e < T_{Z_i}$, since the electron term (which is a stabilizing term--see Section 4.2) dominates the dispersion relation, we need to examine the conditions under which the electron term can be made comparable to the ion terms thereby allowing the ion free energy sources to drive an instability. The electron contributions to the dispersion relation can be made small only if the phase velocity of the wave along the magnetic field is large compared to the electron thermal velocity. The instabilities we shall find therefore arise from the coupling of the ion motions with electron plasma waves having high phase velocities along the magnetic field. (Restricting ourselves to large phase velocities along the magnetic field is equivalent to considering only the enlarged region near the origin of the Nyquist plot as displayed in Figs. 4.4c and 4.6c.). In the region of interest we can replace the Z_1 function of the electron term in the dispersion relation by its asymptotic expansion

(see appendix B). Then, we can reduce the dispersion relation to the form

$$\frac{\Omega_i^2}{\omega_{pi}^2} = \frac{m_i}{m_e}\frac{(k_z a_i)^2}{(k a_i)^2}\left(\frac{\Omega_i}{\omega}\right)^2 - \frac{2 i\sqrt{\pi}}{(k a_i)^2}\frac{T_{\perp i}}{T_e}\,\zeta\, e^{-\zeta^2}$$

$$-\frac{2}{(k a_i)^2}\frac{T_{\perp i}}{T_e}\sum_{n=-\infty}^{\infty}\left[Z_1(w_n)C_{ni}^{\ell} + \frac{n}{(k_z a_i)}\sqrt{\frac{T_{z_i}}{T_{\perp i}}}\,Z_0(w_n)\,D_{ni}^{\ell}\right] \qquad (6.1.6)$$

where

$$\zeta = \sqrt{\frac{T_{\perp i}}{T_e}\frac{m_e}{m_i}}\,\frac{(\omega/\Omega_i)}{(k_z a_i)} = \frac{\omega}{k_z \alpha_e}\,.$$

Here, the first term on the right gives a contribution which is the same as the result of the low temperature fluid model for the electron dynamics, while the second term accounts for the electron Landau damping. The last two terms on the right of (6.1.6), as in (6.1.5), give the ion contributions to the dispersion relation.

The waves can absorb the free energy of the ions only if the wave frequencies are nearly resonant with the ion cyclotron frequency or harmonics thereof so that the wave can interact strongly with the particles in the ion distribution. Thus, we must have

$$\omega \sim n\Omega_i \qquad (6.1.7)$$

where n is the harmonic number of the ion cyclotron fre-

quency. Now, neglecting for the moment the ion contributions to the dispersion relation as well as the electron Landau damping ($T_e \to 0$) and realizing that k_z can be no larger than k^2, by solving the real part of the resultant dispersion relation we see that a very crude necessary condition for instability is that

$$\omega_{p_e} > n\Omega_i . \tag{6.1.8}$$

This minimum density required for instability (for n = 1) was first noted by Harris (6.3). Taking into account the fact that the frequency may deviate from a given harmonic of the ion cyclotron frequency by as much as half the cyclotron frequency, Dnestrovsky, Kostomarov and Pistunovich (6.23) have derived the slightly less restrictive necessary condition for instability given by

$$\omega_{p_e} > (n-1/2)\Omega_i .$$

These very crude limits can be improved upon by adding the requirement that there be only a small amount of electron Landau damping, i.e. taking the plasma to have a nonzero electron temperature. Electron Landau damping can be neglected in the imaginary part of the dispersion relation whenever the phase velocity of the wave along the magnetic field is about 2.5 times the electron thermal velocity or higher; i.e.

$$\frac{\omega}{k_z \alpha_e} = \frac{\omega/\Omega_i}{(k_z a_i)} \sqrt{\frac{T_{\perp i}}{T_e} \frac{m_e}{m_i}} \gtrsim 2.5 . \tag{6.1.9}$$

Or, employing (6.1.7) and rearranging this equation we have

$$(k_z a_i) \lesssim \frac{n}{2.5}\sqrt{\frac{T_{\perp i}}{T_e}\frac{m_e}{m_i}} \quad \text{(instability)}. \tag{6.1.10}$$

Using this limit on k_z and again solving the real part of the dispersion relation neglecting the ion contributions, we see that an approximate necessary condition for instability is

$$\frac{\omega_{pi}^2}{\Omega_i^2} \gtrsim 6\,(ka_i)^2\left(\frac{T_e}{T_{\perp i}}\right) \quad \text{(instability)}. \tag{6.1.11}$$

This limit is only applicable for values of T_e/T_i large enough (but still small compared to unity) so that it is not lower than that given by (6.1.8). We note that the approximate instability conditions given in (6.1.10) and (6.1.11) have been derived without reference to the type of ion free energy source. Our only concession to the ions has been the requirement that $\omega \sim n\Omega_i$. The nature of the ion free energy source determines the values of $k_\perp$ for which instability can occur. We should also note that (6.1.10) and (6.1.11) are approximate formulas for the appearance of velocity-space anisotropy instabilities of either the convective or absolute type and hence give us no indication of the transition density or required axial wavelength for the appearance of <u>absolute</u> instabilities.

Before describing the two basic mechanisms by which the waves we consider in this chapter can extract energy from the ion free energy sources, let us discuss the various means which have been employed to understand the physics of these instabilities. As pointed out in Chapter 4, we can view the unstable waves as extracting energy from particle motions by diffusing particles to lower energies when the phase velocities of the waves lie in the "positive-slope" portion of the effective velocity distribution of the particles. This is the description which we will employ throughout this work. For the waves in the "positive-slope" portion of the effective velocity distribution, the amount of energy in these waves increases as a result of their interaction with a damped wave or lossy medium. This apparent paradox of waves growing as a result of having energy extracted from them is resolved by realizing that the waves are "negative energy" waves (6.24, 6.25). The mechanisms of velocity-space anisotropy instabilities have been discussed in terms of the concepts of "negative energy" waves by Bers and Gruber (6.26) and Gruber (6.27). These authors show that a group of waves with frequencies slightly less than each of the ion cyclotron harmonics are "negative energy" waves while waves with frequencies slightly greater than the ion cyclotron harmonics are positive energy of "stable" waves. The physical mechanism of the velocity-space anisotropy instabilities is therefore identified as the coupling of the "negative energy"

waves with electron plasma waves (positive energy waves) along the magnetic field. A completely different approach to discussing the mechanism of these instabilities has been developed by Hall, Heckrotte and Kammash (6.17). In their approach the coupling of the particle motions to the electrostatic field oscillations is discussed through an approximate mechanical analysis in what are called "interaction models." The relation of these "interaction models" to "negative energy" wave concepts has been discussed by Hall and Heckrotte (6.28).

In order to discuss the mechanisms of velocity-space anisotropy instabilities in terms of "positive-slope" regions, we need to examine the conditions for which $P(\omega/\Omega_i)$ can have zeros (see Section 4.2). For the present homogeneous magnetized plasma case, making all of the same assumptions and omissions of terms that we have made to arrive at equations (6.1.1) and (6.1.6) as well as assuming that condition (6.1.10) is satisfied so that the electron contributions to $P(\omega/\Omega_i)$ can be ignored, we can reduce (4.2.3) to (for $|\omega| \gtrsim \Omega_i/2$, $k_\perp \neq 0$, $k_Z \neq 0$)

$$P(\omega/\Omega_i) = \frac{\Omega_i^2}{k^3}\int d^3v \sum_{n=-\infty}^{\infty} J_n^2\left(\frac{k_\perp v_\perp}{\Omega_i}\right)\left\{k_z \frac{\partial F_i}{\partial v_z} + \frac{n\Omega_i}{v_\perp}\frac{\partial F_i}{\partial v_\perp}\right\}\delta\left(v_z - \frac{\omega - n\Omega_i}{k_z}\right).$$

Or, making use of the properties of the delta function we can write this equation as

$$P(\omega/\Omega_i) = \frac{2\Omega_i^3}{k^3}\int d^3v \sum_{n=-\infty}^{\infty} J_n^2\left(\frac{k_\perp v_\perp}{\Omega_i}\right)\left\{(\omega - n\Omega_i)\frac{\partial F_i}{\partial v_z^2} + n\Omega_i \frac{\partial F_i}{\partial v_\perp^2}\right\}\delta\left(v_z - \frac{\omega - n\Omega_i}{k_z}\right). \tag{6.1.12}$$

For the purposes of the present marginal stability analysis, we are interested in the zeros of this function for real ω, $k_\perp$, k_Z. We have previously noted that for the work in this chapter we need only consider positive values of each of these quantities. For positive ω, zeros of $P(\omega/\Omega_i)$ will occur whenever there is a "positive-slope" region in the effective velocity distribution $\int_{-\infty}^{ku} P(\omega)\,d\omega$ (see Sections 4.1, 4.2), in which the function $P(\omega/\Omega_i)$ takes on positive values. Therefore, in looking for "positive-slope" regions, we need only examine the conditions under which $P(\omega/\Omega_i)$ can take on positive values for a range of positive ω. Note that if there is a small electron contribution to $P(\omega/\Omega_i)$, it will be negative and have a stabilizing influence. Indeed, it was through a consideration of the magnitude of the stabilizing influence of the electrons that we arrived at condition (6.1.10).

There are two different contributions to the function $P(\omega/\Omega_i)$ which may make it positive for a range of frequencies. First, we note that while $\partial F_i/\partial v_Z^2$ is a negative definite quantity for a Maxwellian ion distribution along the magnetic field, $(\omega-n\Omega_i)$ may take on either sign. Second, the $\partial F_i/\partial v_\perp^2$ term which is normally negative, can be positive if the $v_\perp$ distribution is not a monotonically decreasing function of $v_\perp^2$, i.e. if it is of the "loss-cone" type. We shall later see that it is the $\partial F_i/\partial v_\perp^2$ term which gives the dominant positive or destabilizing contribution for loss-cone instabilities while for the temperature-

anisotropy instabilities it is the $(\omega-n\Omega_i)\ \partial F_i/\partial v_Z^2$ term with $\omega < n\Omega_i$ which gives the principal destabilizing influence. However, as long as $T_e < T_{Z_i}$, even when one term is dominant, both terms usually contribute.

For any given $k_\perp$, since the maximum positive contribution from the $(\omega-n\Omega_i)$ term occurs for $\omega < n\Omega_i$, we expect that at the lowest threshold density for instability the frequency will be slightly less than a harmonic of the ion cyclotron frequency. In fact, since k_Z is limited by condition (6.1.10), it is easy to show that the minimum threshold density should occur for frequencies given by

$$(n - \omega/\Omega_i) \simeq (k_z a_i)\sqrt{\frac{T_{z_i}}{2T_{\perp_i}}} \lesssim \frac{n}{4}\sqrt{\frac{T_{z_i}}{T_e}\frac{m_e}{m_i}}\ , \qquad (6.1.13)$$

providing of course that this number is less than 1/2 so that it is realistic to consider the nth harmonic separately from all others. The applicability of this formula is borne out by the results shown in Fig. 4.8 and Table 5.1 and all other examples considered in this work for which $T_e < T_{Z_i}$.

Of the two basic types of velocity-space anisotropy instabilities, the first we will discuss in detail is that which is driven by the ion free energy source associated with unequal mean velocities along and transverse to the magnetic field, i.e. the temperature-anisotropy instabilities. As discussed in Section 3.3, the terms in braces in the

Harris dispersion relation and (6.1.12) are easily understood as those accounting for the destruction of the conservation of particle energy along ($\sim v_z^2$) and transverse to ($\sim v_\perp{}^2$ -- the magnetic moment here) the magnetic field. For distribution functions which are monotonically decreasing functions of the energies transverse and along the magnetic field we also recall that the destruction of these constants of the motion lead respectively to Landau and cyclotron damping. However, from the preceding consideration of "positive-slope" regions of the effective velocity distribution, we know that when the frequency is slightly less than a harmonic of the ion cyclotron frequency the $\partial F_i/\partial v_z^2$ term can be a destabilizing contribution to $P(\omega/\Omega_i)$. There is thus Landau damping for $\omega > n\Omega_i$, but Landau growth for $\omega < n\Omega_i$. Physically the ions stay nearly in phase with the wave for $\omega \sim \Omega_i$ by travelling a distance of one wavelength along the magnetic field in one cyclotron period. The temperature-anisotropy instability thus results from the coupling of electron plasma waves along the magnetic field with ion waves (along the magnetic field) having frequencies slightly less than harmonics of the ion cyclotron frequency.

If the ion velocity distribution is isotropic and a monotonically decreasing function of the particle energy, then we know from the general stability proofs noted in Section 1.1 that the plasma is stable. Therefore in this case the ion cyclotron damping is sufficient to overcome Landau growth at all frequencies and in particular for

frequencies just slightly less than harmonics of the ion cyclotron frequency. This fact can also be seen directly from a consideration of the "positive-slope" regions of the effective velocity distribution. Assuming a bi-Maxwellian ion velocity distribution, we can simplify the $P(\omega/\Omega_i)$ in (6.1.12) to

$$P(\omega/\Omega_i) = -\frac{2\Omega_i^2}{k^3}\int d^3v \sum_{n=-\infty}^{\infty} J_n^2\left(\frac{k_\perp v_\perp}{\Omega_i}\right) F_i \left\{ \frac{(\omega - n\Omega_i)}{T_z} + \frac{n\Omega_i}{T_\perp} \right\} \delta\left(v_z - \frac{\omega - n\Omega_i}{k_z}\right).$$

Now, this function can take on positive values for positive frequencies near a given harmonic of the ion cyclotron frequency and thus indicate a "positive-slope" region only if

$$\frac{\omega - n\Omega_i}{T_{z_i}} + \frac{n\Omega_i}{T_{\perp_i}} < 0, \quad n > 0 \qquad \text{(instability)}.$$

The frequency in this expression cannot deviate from a given harmonic by more than half the cyclotron frequency or it is unrealistic to consider only a single harmonic term. Therefore this instability condition can be reduced to

$$-\frac{1}{2T_{z_i}} + \frac{n}{T_{\perp_i}} < 0, n > 0 \qquad \text{(instability)}. \tag{6.1.14}$$

Clearly this condition cannot be satisfied for an isotropic plasma ($T_\perp = T_z$). However, if we increase the mean velocity transverse to the magnetic field relative to that

along the magnetic field, it is easy to see from the Harris dispersion relation (6.1.1) and all our subsequent reductions of it that the cyclotron damping term decreases in magnitude relative to the Landau damping or growth term. Solving (6.1.14) for $T_\perp$, we find that the "critical" value for which instability occurs is given by

$$T_{\perp i} > 2nT_{Z_i} \qquad \text{(instability)}. \qquad (6.1.15)$$

Timofeev (6.29) first showed that a plasma with a bi-Maxwellian ion distribution is unstable if $T_{\perp i} > 2T_{Z_i}$ and gave some indication of the effects of electron temperature for large T_e/T_{Z_i}. Dnestrovsky, Kostomarov and Pistunovich (6.23) extended that work to include all T_e/T_{Z_i} greater than unity and first noted the instability condition given by (6.1.15) and variations of it including the effects of electron temperature. Shima and Hall (6.30) have shown that a given plasma species with a bi-Maxwellian distribution can have a destabilizing influence on the plasma only if condition (6.1.15) is satisfied.

For very high degrees of temperature anisotropy ($T_\perp >> T_Z$), the ion cyclotron damping terms become negligible compared to the ion Landau growth or damping term. Physically this means that in this limit the magnetic moment of the ions is a conserved quantity for the electric field fluctuations in the plasma (see Section 3.1) and thus the detailed structure of the ion $v_\perp$ distribution has very little effect on the

dispersion relation (6.31). Therefore for large anisotropies, even for a plasma in which the ions have a loss-cone type of $v_\perp$ distribution, the velocity-space anisotropy instabilities are driven almost entirely by the free energy associated with the large anisotropy in the mean velocities along and transverse to the magnetic field. Indeed, this is why we call them temperature-anisotropy instabilities.

As indication of the effect of large anisotropy can be seen in Fig. 4.4 which displays typical Nyquist and $P(\omega/\Omega_i)$ plots for a plasma having $T_{\perp_i} = 10^{+3}\ T_{Z_i}$ and a loss-cone type of $v_\perp$ distribution (ℓ=1). We recall that the ion contributions to these plots are those shown in the enlarged portions labeled 4.4c, d. For this case it is obvious that the ion contributions to the Nyquist plot are characteristic of the Z_1 functions (compare Figs. 4.3b and 4.4c) so that the ion Landau growth or damping term for $\omega \sim n\Omega_i$ completely overwhelms the ion cyclotron damping term. The same conclusion can also be arrived at by comparing the plot of $P(\omega/\Omega_i)$ in Fig. 4.4d with its analytical form given by (6.1.12). Further, we note that the fact that these modes have real-k temporal growth rates only for $\omega \lesssim n\Omega_i$ (see Fig. 4.5) is also indicative of the domination of the temperature-anisotropy source of free energy (see instability condition preceding (6.1.14)).

Next, we consider the limitations imposed on the transverse wave number $k_\perp$ so that the temperature-anisotropy instabilities can occur. Since we only require that there be some interaction of the ions with the wave for $\omega \sim n\Omega_i$ (i.e. $C_{n_i}^{\ell} \neq 0$), it is clear that there are no critical conditions on $k_\perp a_i$ for instability. However, we expect the strongest interaction to occur when the transverse wavelength is comparable to the ion Larmor diameter (see next section), i.e. in general when

$$k_\perp a_i \sim n\pi. \tag{6.1.16}$$

Since $(k_z a_i)$ is limited as per (6.1.10) to be generally much less than n, we see from (6.1.11) that the density threshold for the appearance of these temperature-anisotropy instabilities is usually a strong function of the particular $k_\perp a_i$ we choose. However, when $k_\perp a_i$ becomes comparable to or smaller than $k_z a_i$, its choice is no longer important in the determination of ka_i and hence of the threshold density. Therefore, the value of (ka_i) which determines the threshold density for the temperature-anisotropy instabilities is usually the smaller of either a.) the $k_\perp a_i$ representing the maximum radial wavelength which can "fit" into any given plasma of interest, or b.) the maximum value of $(k_z a_i)$ which satisfies condition (6.1.10).

With these remarks delineating the general features of the temperature-anisotropy instabilities, we will now

survey the analyses of these instabilities which have been carried out. Some early, very extensive computations of the marginal stability boundaries for the temperature-anisotropy modes were done by Dnestrovsky, Kostomarov and Pistunovich (6.23). In that work the effects of changes in the parameters $T_{\perp_i}/T_{Z_i}$, $k_\perp a_i$, $k_Z a_i$ and T_{Z_i}/T_{Z_e} on the threshold density were considered. As would be expected from (6.1.11), these authors have observed that increasing the electron temperature increases the threshold density. Soper and Harris (6.32) have also investigated the marginal stability boundaries for temperature-anisotropy instabilities, principally for conditions of very high anisotropy and small electron temperatures which roughly approximate the experimental conditions in the DCX-1, OGRA and ALICE machines. In considering velocity-space anisotropy modes driven by a combination of temperature-anisotropy and loss-cone sources of free energy, Guest and Dory (6.33) treat one case ($T_\perp/T_Z = 10$) in which the ion temperature-anisotropy dominates over the loss-cone source of free energy. Davydova, Dnestrovsky and Kostomarov (6.34) have determined the threshold density for the instabilities of a plasma which has both a high density of anisotropy and a loss-cone distribution under conditions appropriate to the OGRA-2 machine. In the latter work, particular emphasis was placed upon calculating the threshold density for a given axial wavelength

which is determined by the physical length of the OGRA-2 machine. Similar calculations have been carried out for the M.M.I.I. machine by Hennion (6.35) with a delta function $v_\perp$ distribution centered about a nonzero velocity, again with high temperature anisotropy dominating the free energy sources. In general the theoretical results obtained by all these authors for $T_e < T_{z_i}$ are consistent to within about an order of magnitude with the conditions given by (6.1.8), (6.1.10), (6.1.11), (6.1.13) and (6.1.15), at least where simple checks can be made.

In all of the studies cited above, only the threshold density for instability of any type was determined and the convective versus absolute nature of the instabilities was ignored. However, as we have noted in Section 5.1, in order to make useful theoretical and experimental comparisons it is necessary to consider the distinction. The first calculations considering the distinctions between convective and absolute temperature-anisotropy instabilities were carried out by Cordey (6.36), who showed that a plasma having a delta function ion $v_\perp$ distribution and a high degree of temperature anisotropy does exhibit absolute instabilities. The previously cited (Section 5.1), somewhat more detailed absolute instability calculations carried out at about the same time by Beasley (6.37) in demonstrating theoretical agreement with experiment were concerned with conditions appropriate for the highly anisotropic "central peak plasma of the DCX-2 machine. More extensive computations concerning the effect of varying $T_{z_i}/T_{\perp_i}$ on the convective and absolute instabilities ($\omega \lesssim \Omega_i$) of a plasma with

an $\ell = 1$ type $v_\perp$ distribution (see Section 1.3) and relatively cool electrons ($T_e/T_{z_i} = 0.05$) have been carried out by Beasley and Cordey (6.38). A portion of those results have been replotted here in Fig. 6.1. Here and throughout the remainder of this work we denote the marginal stability or threshold density boundary with a solid line and the "marginally stable" absolute instability or transition density boundary with a long dash and dot or center line. In the figure the values of $k_z a_i$ shown are the real part of $k_z a_i$ appropriate for the "marginally stable" absolute instability modes. Over the range of $T_{\perp_i}/T_{z_i}$ shown, the spatial growth length of the absolute instabilities and hence the minimum growth length of the convective instabilities just below the absolute instability transition density (see discussion following (6.2.8)) is roughly constant at 2.6 times the wavelength of the relevant unstable mode. The values of $k_z a_i$ on the marginal stability boundary are not shown, but are typically a factor of 2.5-3 above those shown for the absolute instability modes and agree roughly with condition (6.1.10). The density threshold for the appearance of instabilities (convective) is in reasonable agreement with conditions (6.1.11) and (6.1.15) (see below).

Unfortunately, we do not have any corresponding simple conditions for the absolute instability characteristics at the transition density (however, see end of Section 6.2 for some relevant comments). However, we observe from Fig. 6.1 that the transition density and axial wavelengths for the absolute instability tend to vary with $T_{\perp_i}/T_{z_i}$ in much the same way as the corresponding marginal stability (convective)

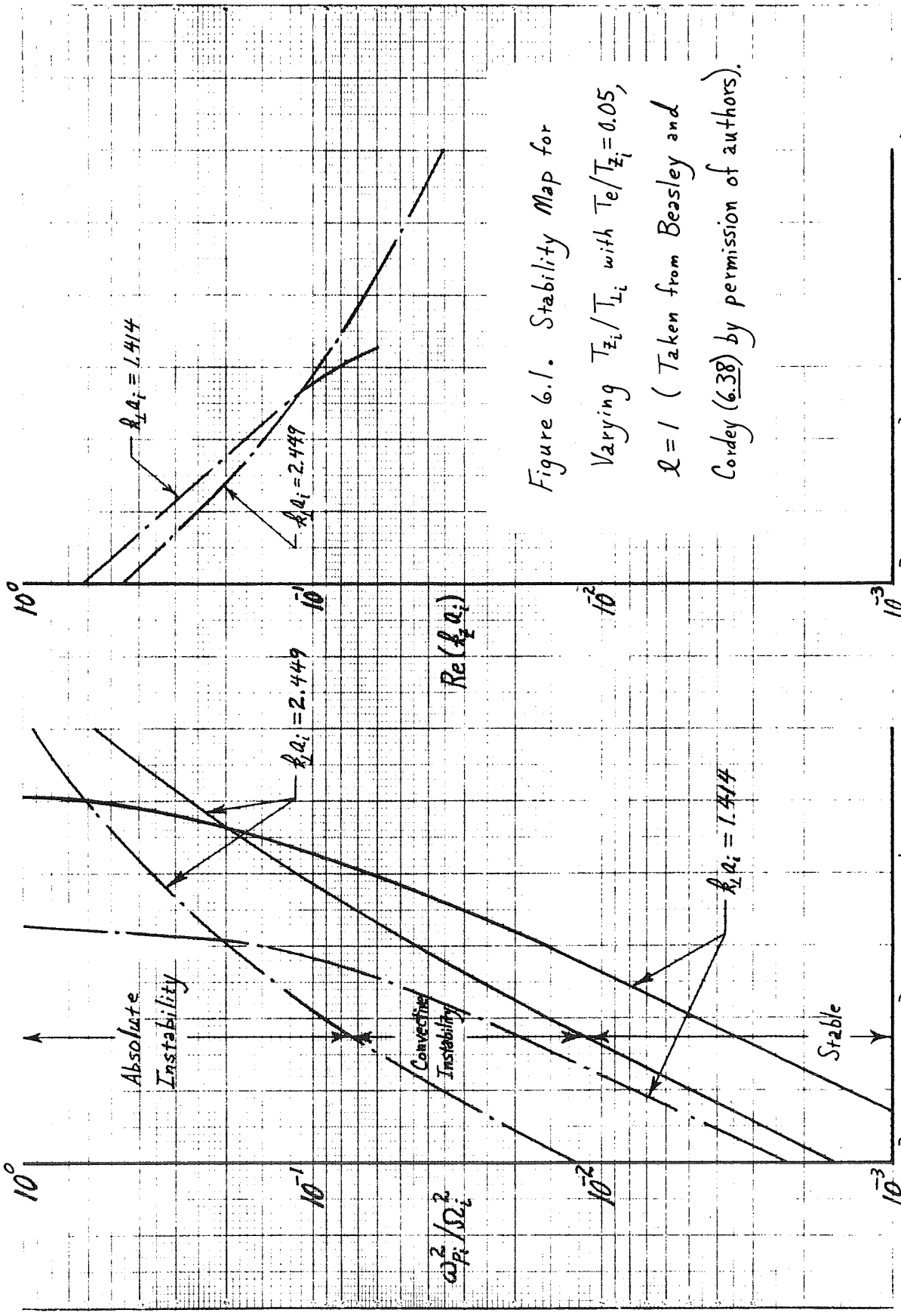

Figure 6.1. Stability Map for Varying $T_{z_i}/T_{\perp_i}$ with $T_e/T_{z_i} = 0.05$, $\ell = 1$ (Taken from Beasley and Coroley (6.38) by permission of authors).

characteristics. With respect to the data displayed in the figure, Beasley and Cordey (6.38) also note that the transition density for absolute instability is nearly independent of the electron temperature over a large range of ratios of T_e/T_{z_i}, presumably all less than unity (see Section 6.2--Fig. 6.8).

Comparing the results displayed in Fig. 4.5 with the $T_{z_i}/T_{\perp_i} = 10^{-3}$ results displayed in Fig. 6.1, we see that the real-k temporal growth rates of an instability can be misleading. For the density at which the real-k analysis (Fig. 4.5) indicates a maximum temporal growth rate of about 2% of the ion cyclotron frequency (a fairly large growth rate), from Fig. 6.1 we see that the unstable mode is of the convective type. Therefore we know from our discussion in Section 5.4 that it is unlikely that this supposedly rather potent unstable mode would even be observed in such an experimental plasma. This observation further strengthens our conclusion that the convective versus absolute nature of the instabilities must be examined in detail.

In Fig. 6.1 we note that instability of the plasma (both convective and absolute) persists as $T_{\perp_i} \to T_{z_i}$ for sufficiently large $k_\perp a_i$, seemingly in contradiction to condition (6.1.15). However, these calculations by Beasley and Cordey (6.38) were carried out for a distribution which not only has temperature anisotropy, but is also of the loss-cone type. In such a case condition (6.1.15) is not the relevant instability criterion as $T_{\perp_i} \to T_{z_i}$ since then the dominant source of free energy is due

to the loss-cone. The conditions under which loss-cone type $v_\perp$ distributions are unstable for $T_{\perp_i} = T_{z_i}$ are discussed in the next section. However, considering only the data shown in Fig. 6.1, we see that the loss-cone instabilities ($T_{\perp_i} = T_{z_i}$) appear to have higher threshold and transition densities and longer axial wavelengths than the temperature-anisotropy instabilities ($T_{\perp_i} > T_{z_i}$). We would therefore tentatively expect the loss-cone instabilities to be less detrimental to plasma confinement than the temperature-anisotropy instabilities, if the latter can occur. The results we obtain from a thorough study of the loss-cone instabilities (see next section) confirm this expectation.

For a <u>strictly</u> <u>bi-Maxwellian</u> plasma, Beasley (<u>6.39</u>) has shown that an absolute instability can occur only if

$$T_{\perp_i} \gtrsim 125\, T_{z_i} \quad \text{(absolute instability)}. \tag{6.1.17}$$

This condition is relevant for the appearance of an absolute instability with a frequency slightly less than the ion cyclotron frequency. Thus, it should be compared with the instability condition for convectively unstable modes in a bi-Maxwellian plasma given by (6.1.15) with $n = 1$. The effects of varying the sharpness of the velocity-space anisotropy on the absolute instabilities of a plasma have been considered by Beasley, Cordey and Dory (<u>6.40</u>). In these studies a mixture of temperature anisotropy and loss-cone distribution sources of free energy are considered, with the dominant source of free energy nearly always being that due to the temperature anisotropy.

In the next section we will discuss the loss-cone instabilities in detail for $T_e < T_{z_i}$. However, before proceeding to that work, we conclude this section with a discussion of some properties of velocity-space anisotropy instabilities of all types when $T_e > T_{z_i}$. In this case the contributions of the electrons to the dispersion relation and hence to the instabilities becomes small or negligible. The instabilities which can occur are then due to exchanges of energy between the perpendicular and parallel motions of the ions alone (6.17). Since the coupling is between orthogonal motions of a single species of particles, these ion instabilities are similar to the electron velocity-space anisotropy instabilities which we have previously surveyed. The exchange of energy occurs through the coupling of ion-waves along the magnetic field with ion cyclotron waves transverse to the magnetic field. Note that, in contrast, for $T_e/T_{z_i} < 1$ the coupling is with electron plasma waves moving in the magnetic field direction. The relevant frequencies of the ion-waves are however shifted to the vicinity of harmonics of the ion cyclotron frequency. For bi-Maxwellian velocity distributions, instability condition (6.1.15) applies for $T_e > T_{z_i}$ as well as for the $T_e < T_{z_i}$ case we have been considering. In addition, in the work of Dnestrovsky, Kostomarov and Pistunovich (6.23) and Davydova, Dnestrovsky and Kostomarov (6.34) the effects of electron temperatures in excess of the parallel ion temperature on the threshold density for instability were considered. In those studies it was found that increasing the electron

temperature increased the threshold density. To the author's knowledge, no similar work concerning the effect of electron temperature when $T_e > T_{z_i}$ on the properties of the absolute temperature-anisotropy instabilities has been considered. However, for an absolute instability driven principally by the loss-cone source of free energy, an investigation of the effects of electron temperature for $T_e > T_{z_i}$ has been undertaken by Guest and co-workers (6.22).

6.2 Loss-Cone Instabilities

In this section we consider velocity-space anisotropy instabilities driven by the free energy associated with a nonmonotonic ("loss-cone") $v_\perp^2$ distribution. In order to eliminate the temperature-anisotropy instabilities as much as possible, we equate the mean velocities along and transverse to the magnetic field. Here we will only consider the loss-cone instabilities in the lowest density regime in which they can appear. We defer consideration of the high density Rosenbluth and Post "continuum" limit (6.1) to the next section.

As in most of our discussion of temperature-anisotropy instabilities in the preceding section, we will assume that $T_e < T_{z_i}$. We recall that in this case the electron contributions dominate the dispersion relation except when the phase velocity of the wave along the magnetic field is large compared to the electron thermal velocity. In the present case the only source of ion free energy driving the instability is that associated with the nonmonotonic nature of the $v_\perp$ distribution. Therefore in looking for the parametric regions of loss-cone instability, we must look for "positive slope" regions of the effective velocity distribution for waves moving nearly perpendicular to the magnetic field (see below).

In the preceding section we have seen that the "positive-slope" regions occur when the function $P(\omega/\Omega_i)$ defined by (6.1.12) is positive for a range of positive ω. If T_e is not too much less than T_i, the value of $k_z a_i$ at the threshold and higher densities is quite small (see (6.1.10)). Then, the wave resonatesvery strongly with a given harmonic and the contributions of the nonresonant harmonics to $P(\omega/\Omega_i)$ are negligible. The instability condition that $P(\omega/\Omega_i)$ be positive for a range of ω can thus be written as

$$\int d^3v \, J_n\left(\frac{k_\perp v_\perp}{\Omega_i}\right)\left\{\left(\frac{k_z v_z}{\Omega_i}\right)\frac{\partial F_i}{\partial v_\perp^2} + n\,\frac{\partial F_i}{\partial v_\perp^2}\right\}\delta\left(v_z - \frac{\omega - n\Omega_i}{k_z}\right) > 0$$

(instability). (6.2.1)

Recalling that for the present case $T_{\perp_i} = T_{z_i}$ and using the fact that $k_z a_i$ is small once more, we can reduce this condition to

$$\int d^3v \, J_n^{\,2}\left(k_\perp v_\perp / \Omega_i\right)\frac{\partial F_i}{\partial v_\perp^2} \gtrsim 0$$

(instability). (6.2.2)

for each n of interest. This criterion for instability is a bit awkward to use and so we will seek a simpler form.

We will develop a simpler criterion in a very physical manner based on ideas introduced by Rosenbluth and Post (6.1)--see Section 6.3. If there were no magnetic field constraining the particle motions in the plane perpendicular to the magnetic field, the effective velocity distribution seen by waves moving in say the y direction would be given by

$$\tilde{F}_i(v_y) \equiv \int dv_x dv_z F_i(v_\perp, v_z). \qquad (6.2.3)$$

Ignoring the presence of the magnetic field once again, by analogy with the uniform unmagnetized plasma work (see Section 4.1), we would expect that a necessary condition for instability of a wave with frequency ω and wave-vector $k_\perp = k_y \simeq k$ ($k_z << k_y$ here) would be

$$\left.\frac{\partial \tilde{F}_i}{\partial v_y}\right|_{v_y = \omega/k_y} = \int d^3v \, \frac{\partial F_i(v_\perp, v_z)}{\partial v_y} \delta(v_y - \omega/k_y) > 0 \qquad (6.2.4)$$

(instability).

Of course, in contrast to what we have been assuming here, the ions are not really free to move transverse to the magnetic field. However, for waves whose frequencies are near harmonics of the ion cyclotron frequency, we expect that the waves would be able to interact strongly with the particles in such a way that the magnetic field has very little constraining influence on the ion motions. Therefore we expect that when (6.2.4) is satisfied for some wave with a frequency

near a harmonic of the cyclotron frequency, such a wave may be unstable. Conversely, if (6.2.4) is not satisfied we expect the wave to be damped. Then, since the plasma has no other source of free energy, the plasma would be stable.

Besides these heuristic arguments, there are other reasons to believe that (6.2.4) is a reasonable instability condition. First, we note that in the limit of large $k_\perp a_i$ compared to n (the limit of greatest interest here), this condition can be shown to approach that given by (6.2.2). Next, we observe that the simple instability criterion given by (6.2.4) can be obtained by taking the "continuum" limit (see next section) of the $P(\omega/\Omega_i)$ given by (6.1.12) using the prescription given by Rosenbluth (6.41). The major assumptions in such a derivation are that $T_e < T_i$, $k_z << k_\perp$ and $Im(\omega/\Omega_i) \gtrsim 1$, the last assumption being highly dubious here since we are doing marginal stability calculations for which both the frequency and wave vector are real. In spite of the dubious methods by which we have arrived at (6.2.4), we will find (see below) that in many cases it is a very useful and accurate instability condition. It is, however, important to note that if there are distinct groups of ions which have dissimilar velocity distributions along the magnetic field, then it may not be realistic to consider only the velocity distribution perpendicular to the magnetic field. That is, in such cases we cannot necessarily expect either (6.2.2) or (6.2.4) to be correct and in general must

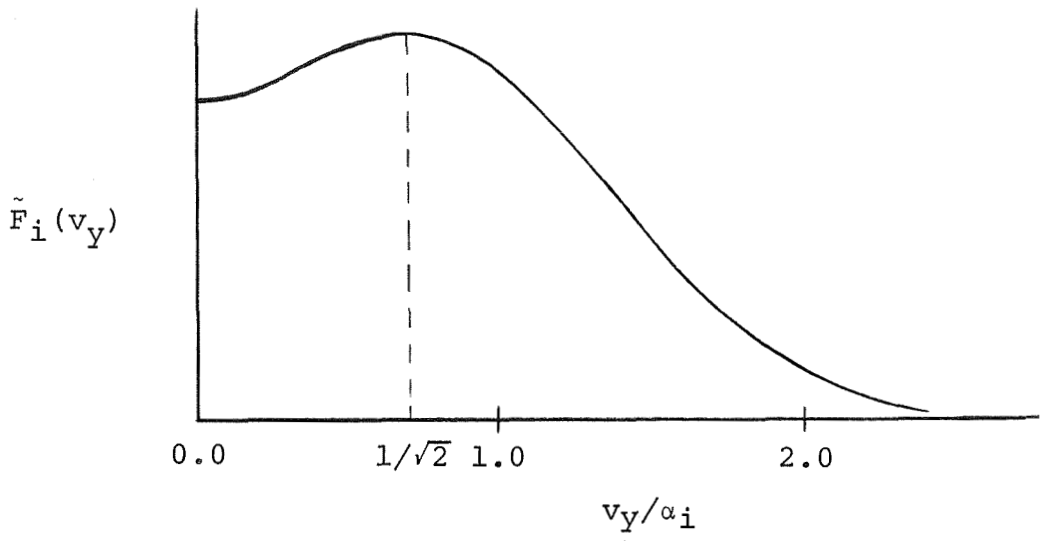

Figure 6.2 Effective Velocity Distribution in a Given Direction Perpendicular to the Magnetic Field Direction (Homogeneous Plasma, $\ell = 1$).

instead return to a consideration of the more general $P(\omega/\Omega_i)$ given by (6.1.12).

For the $\ell = 1$ or most thermally spread of the cylindrically cut-out "loss-cone" distributions employed in this work, $\tilde{F}_i(v_y)$ is displayed in Fig. 6.2. Note that this function is always a symmetric function of v_y due to the isotropy of the homogeneous plasma about the magnetic field direction as required by equilibrium considerations. The most general characteristic of $\tilde{F}_i(v_y)$ is that it is peaked (twice) about a nonzero v_y-velocity and thus indicates that there are net "drift" velocities in the plasma transverse to the magnetic field direction. Since $\tilde{F}_i(v_y)$ is an even function of v_y, it in effect has two counterstreaming groups of particles, a situation which is very analogous to that which causes the classic "two-stream" instability. Rosenbluth (6.41)

has shown that $\tilde{F}_i(v_y)$ has the same general characteristics for true collisionally equilibrated loss-cone distributions.

For the $\tilde{F}_i(v_y)$ distribution shown in Fig. 6.2, the phase velocities which are in the "positive-slope" region and hence satisfy condition (6.2.4) are given by

$$0 < \omega/k_y = \omega/k_\perp < \alpha_i/\sqrt{2} \qquad \text{(instability)}. \tag{6.2.5}$$

Recalling that in general the frequency must be near a harmonic of the cyclotron frequency for a strong wave-particle interaction to occur, we can rewrite (6.2.5) to indicate the range of $k_\perp a_i$ for which the plasma can be unstable:

$$k_\perp a_i > \frac{\omega}{\Omega_i}\sqrt{2} \simeq n\sqrt{2} \qquad \text{(instability)}. \tag{6.2.6}$$

Then, using this inequality in (6.1.11) we see that the density threshold for loss-cone instabilities over the entire range of $k_\perp a_i$ is given roughly by

$$\frac{\omega_{p_i}^2}{\Omega_i^2} \gtrsim 12n^2\left(\frac{T_e}{T_{\perp i}}\right) \qquad \text{(instability)}. \tag{6.2.7}$$

For values of $k_\perp a_i$ greatly in excess of $n\sqrt{2}$, the density threshold for that particular mode remains that given by (6.1.11).

In order to illustrate the validity of instability condition (6.2.4) and those derived from it, we will consider a particular example. We consider loss-cone instabilities in a plasma characterized by the parameters $\ell = 1$,

$T_e/T_i = 10^{-2}$, i.e. the most thermally spread $v_\perp$ distribution of the loss-cone type which we have available and "cool" electrons. Throughout the remainder of this chapter we refer to this as the "standard" loss-cone case and we will make all parametric changes away from this case. In Sections 4.4 and 5.2 we have already considered this "standard" case in detail for the perpendicular wavelength given by $k_\perp a_i = 5.0$. From Fig. 4.8 we note that for this case waves with frequencies higher than $3.428\Omega_i$ are always stable. This observation is in agreement with the instability condition given by (6.2.6). The results of examining our standard case for the maximum frequency for which waves can be unstable (usually occuring at high densities) over a large range of values of $k_\perp a_i$ are shown in Fig. 6.3. This figure shows that the condition given by (6.2.6) is remarkably good in predicting the frequencies for which instability occurs, including those which lie between harmonics of the ion cyclotron frequency.

From the instability conditions noted above, we see that loss-cone instabilities can occur only if the $\partial F_i/\partial v_\perp^2$ term of the Harris dispersion relation becomes positive. Thus the usual cyclotron damping term has become a cyclotron "growth" term. The loss-cone instability therefore results from the coupling of an unstable ion-cyclotron wave with a damped electron plasma wave moving along the magnetic field by wave propagation at an

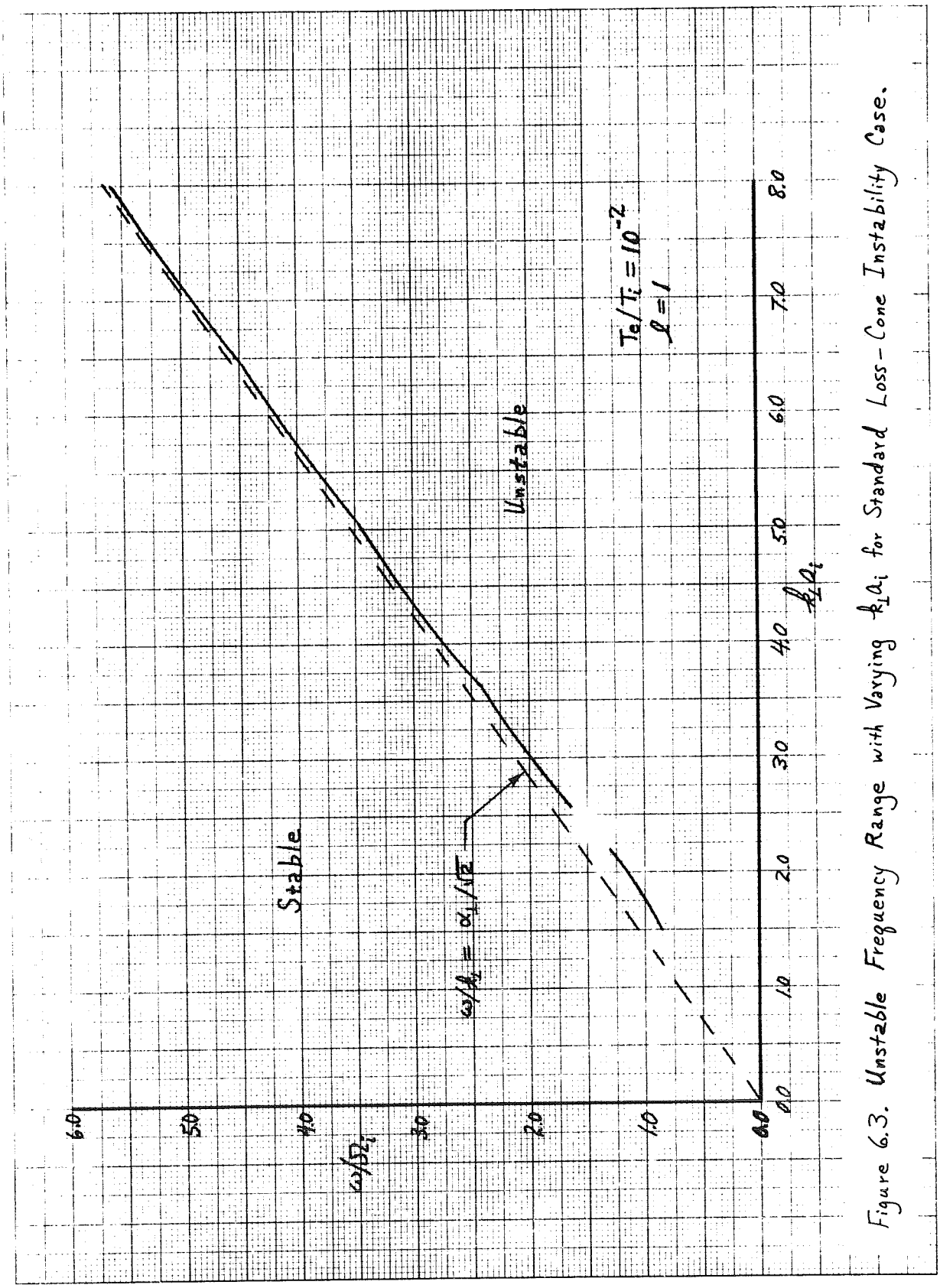

Figure 6.3. Unstable Frequency Range with Varying $k_\perp \rho_i$ for Standard Loss-Cone Instability Case.

angle other than 90^{o} to the magnetic field. Since the $\partial F_i/\partial v_\perp$ term is so important in the dispersion relation, the constancy of the magnetic moment of the ions is rapidly destroyed. As a matter of fact, it is this change (reduction) in the magnetic moment of the particles in the "positive-slope" region that releases the source of free energy driving the instability.

Note that this description of the loss-cone instability is considerably different from the explanation which we gave of the dynamics of the temperature-anisotropy instabilities. Here, as has been noted by Hall, Heckrotte and Kammash (6.17), the nature of the $v_\perp$ distribution is very critical in determining the characteristics of the instability. Also, in contrast to the temperature-anisotropy instabilities, for the loss-cone instabilities it is the ion Landau damping (or growth) term which is nearly negligible. This fact can be seen from the typical Nyquist and $P(\omega/\Omega_i)$ plots for the loss-cone case displayed in Fig. 4.6. In Fig. 4.6c we find that the ion contributions to the dispersion relation are characteristic of the Z_0 functions (see Fig. 4.3a) which we see from (6.1.5) are indicative of the ion cyclotron damping or growth terms. The ion contributions shown in the Nyquist plots of Figs. 4.4.c and 4.6c are therefore intrinsically different and in fact their differences are directly related to the differences in the mechanisms of the temperature-anisotropy

and loss-cone instabilities. Similarly we note that the $P(\omega/\Omega_i)$ plots (Figs. 4.4d and 4.6d) and real-k temporal growth rate curves (Figs. 4.5 and 4.7) for the two types of instabilities are different for the same reason.

Having delineated the general features of the loss-cone instabilities, we will now survey the analyses of these instabilities which have been carried out. Dnestrovsky (6.31) was the first to study the velocity-space anisotropy instabilities driven by the free energy associated with nonmonotonic $v_\perp^2$ distributions. After discussing the instabilities in a general way for arbitrary but nonmonotonic $v_\perp^2$ distributions, he considers a plasma having a delta function $v_\perp$ distribution. The main emphasis of the work by Dnestrovsky is on demonstrating that, in contrast to the temperature-anisotropy instabilities, the loss-cone instabilities persist even when the mean velocities along and transverse to the magnetic field are equal. Davydova (6.42) has considered loss-cone instabilities for ion $v_\perp$ distributions given by

$$F_i(v_\perp) \sim \exp\left[-(v_\perp - v_0)^2/v_0^2 A^2\right]$$

in which A is adjusted to give the desired "sharpness" of the distribution. Upon considering the effects of varying A, Davydova (6.42) concludes that spreading the $v_\perp$ distribution stabilizes the plasma against the loss-cone instabilities to a limited degree. The results found in this

work (see Fig. 6.11) are in agreement with this conclusion. The loss-cone instabilities for $v_\perp$ distributions of the type employed in this work have been considered by Guest and Dory (6.33). In the latter work, the effect of electron temperature on the instabilities is considered over a broad range of T_e/T_{z_i} values, all less than unity. Guest and Dory (6.33) have also given slightly more exact formulas for the threshold density and maximum axial wavelength for instability than those given in (6.2.7) and (6.1.10) respectively. In addition to these studies, some of the works (6.34, 6.35) which we cited in surveying the literature of temperature-anisotropy instabilities have employed nonmonotonic $v_\perp^2$ distributions. However, in those studies, the dominant source of free energy was from the inequality of mean velocities along and transverse to the magnetic field and not from the loss-cone type distribution.

The studies of the loss-cone instabilities discussed above have all been concerned with determining the parametric regions of instability and completely ignore the convective versus absolute nature of the instabilities. The work of Beasley and Cordey (6.38) which we discussed in the preceding section and which does consider the nature of the instabilities is carried out for a loss-cone type distribution ($\ell = 1$). However, in their work (see Fig. 6.1) the dominant free energy source is due to $T_\perp \neq T_z$ except when $T_\perp \simeq T_z$. Therefore that work is

not really for loss-cone instabilities. Very recently Guest and co-workers (6.22) have undertaken a study of the effect of electron temperature on absolute loss-cone instabilities for T_e/T_{z_i} in the range of 0.1 to 10. They find that over this range, increasing the electron temperature has a slight stabilizing influence on the plasma in that the temporal growth rates of the absolute instabilities are reduced and the axial wavelengths increased. The results of the calculations in this work are in general agreement with this conclusion (see Fig. 6.8).

We will now discuss the extensive calculations of the loss-cone instabilities which we have carried out. First, we will consider the general characteristics of the loss-cone instabilities for our "standard" case ($T_e/T_i=10^{-2}, \ell=1$). In all the computations throughout this work we take $m_i/m_e = 1836$. We examine the general characteristics of the loss-cone instabilities by computing the lowest threshold density, the transition density for absolute instability and the densities corresponding to certain temporal growth rates for the absolute instabilities, using the procedures already described for the case $k_\perp a_i = 5.0$ (see Figs. 4.8, 5.9). Carrying these procedures out over a range of values of $k_\perp a_i$ and cross-plotting the results, we obtain the stability map shown in Fig. 6.4 (see also Table 7.3). As in Fig. 6.1, we adopt the convention that a solid line denotes the marginally stable modes (threshold density) while the

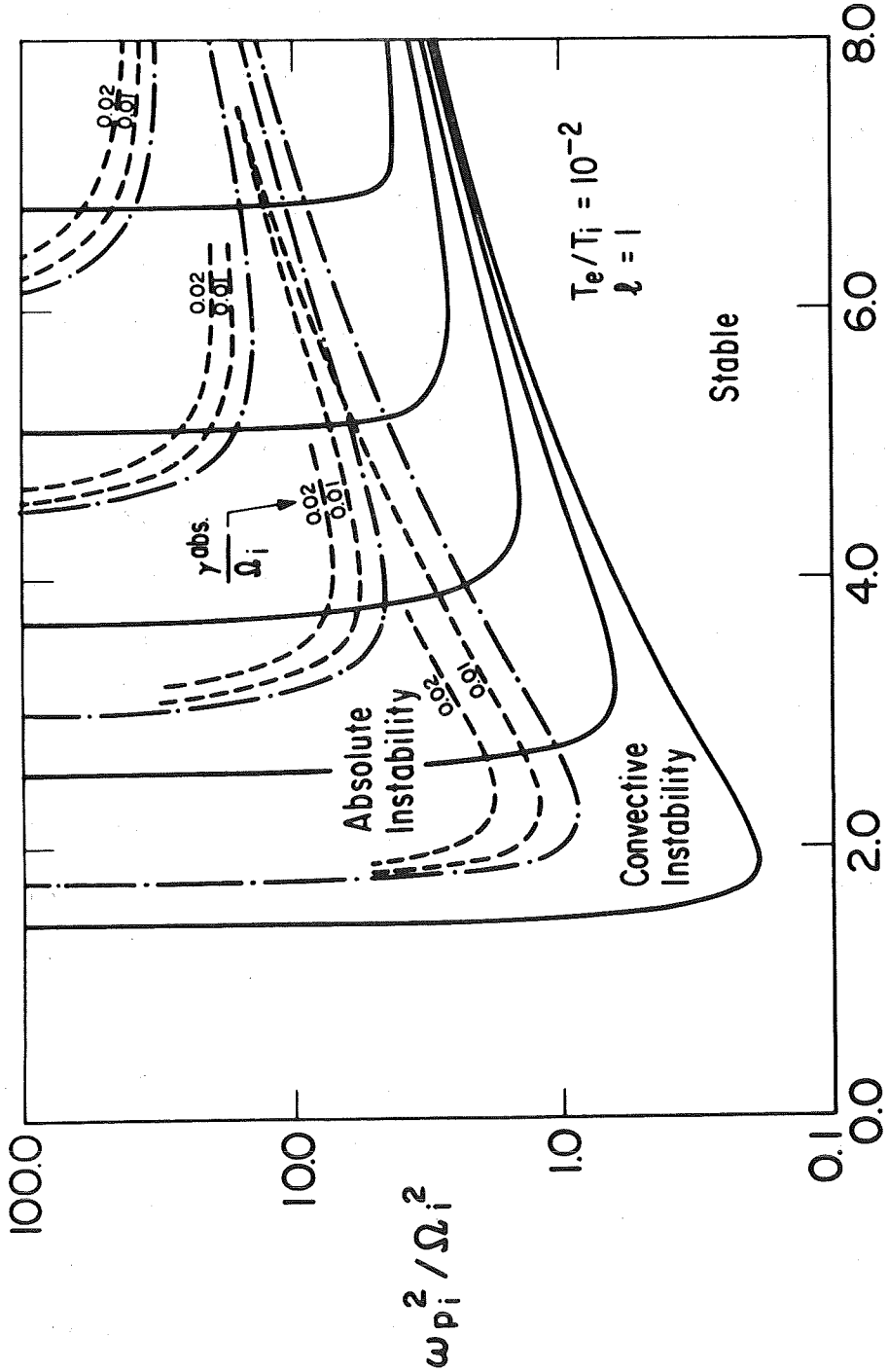

Figure 6.4. Effect of Varying $k_\perp a_i$ on Loss-Cone Instabilities.

dash-dot line indicates the "marginally stable" absolute instability modes (transition density). Here we have added dashed lines to denote the absolutely unstable modes with given temporal growth-rates of γ^{abs}. In this graph and throughout the remainder of this work these dashed lines indicate successively temporal growth rates of 1%, 2%, etc. of the ion cyclotron frequency. We are limited to such small growth rates here because as the temporal growth rates increase, the k_z of the absolutely unstable modes moves toward and eventually becomes lost into the "divergence" region (see Table 5.1 and Section 3.4).

The nested sets of curves in Fig. 6.4 represent instabilities with frequencies near the ion cyclotron frequency and its first, second, etc. harmonics with each succeeding harmonic becoming unstable as $k_\perp a_i$ increases. The values of $k_\perp a_i$ (increasing from the left) for which the successive harmonics become unstable are in reasonable agreement with condition (6.2.6), lending further support to the heuristic arguments from which this condition was derived. For large $k_\perp a_i$ the deviations of the results shown in Fig. 6.4 from condition (6.2.6) are due to the fact that then the frequency at which the instability occurs is significantly less than a harmonic of the cyclotron frequency (see (6.1.13) and Fig. 6.7). For all cases examined in this work the more exact instability condition given by (6.2.5) is satisfied. The minimum threshold density is predicted by instability

condition (6.2.7) for each harmonic to within a factor of two. We also observe that as $k_\perp a_i$ becomes large compared to the value necessary to satisfy (6.2.6), the instabilities near the various cyclotron harmonics do tend to have nearly the same threshold density, a result which is consistent with instability condition (6.1.11). These comparisons with our approximate instability criteria confirm their usefulness with respect to predicting the onset of convective instabilities.

From Fig. 6.4 we observe that the loss-cone instabilities do become absolute in nature for our standard loss-cone case when $k_\perp a_i$ exceeds about 1.75. While the general shapes of the marginal stability and absolute instability curves are similar, the simple formulas which predict the marginal stability characteristics do not accurately predict the absolute instability characteristics. However, the transition density does scale with $k_\perp a_i$ in a manner which is roughly consistent with our simple instability condition formulas.

Along the absolute instability transition-density curve we find empirically that for all $k_\perp a_i$

$$-\frac{\mathrm{Im}(k_z a_i)}{\mathrm{Re}(k_z a_i)} = 0.387 \pm 0.005. \qquad (6.2.8)$$

This result is indicative of the maximum spatial growth rate of the convective instabilities since at the transition density the absolute instability is "marginally stable" (temporally). It does not give the maximum spatial growth rate precisely since the two modes which are merging do not generally merge

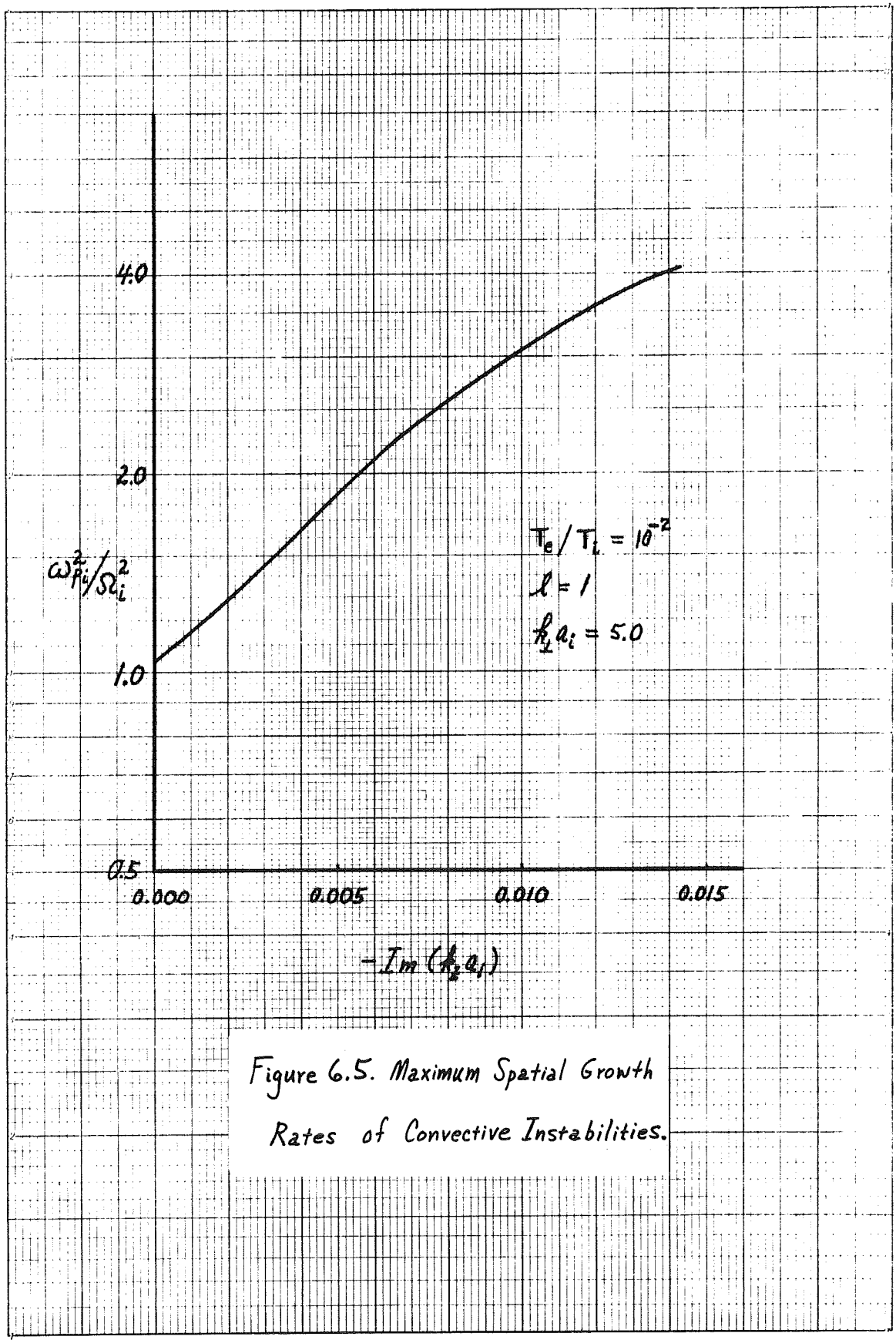

Figure 6.5. Maximum Spatial Growth Rates of Convective Instabilities.

precisely at $k_{I_{max}}$ (see Section 5.2). However, the deviation of the true maximum spatial growth rate from that indicated in (6.2.8) is usually of the order of the uncertainty in its value and so we may neglect it. A typical plot of the spatial growth rate versus density for the convectively unstable modes is shown in Fig. 6.5. From this graph we note that the maximum spatial growth rate of the convective instabilities increases roughly linearly with the logarithm of the density.

Returning to Fig. 6.4, we observe that the instability whose frequency is near the ion cyclotron frequency is the "most unstable" mode in that it has the lowest threshold and transition densities for all $k_\perp a_i$. However, as we have noted in Section 5.4, before we conclude that this truly is the "most unstable" mode, we must check that the wavelength of the unstable mode "fits" into the plasma of interest. In the radial or perpendicular direction, we see from Fig. 6.4 that there is no "cutoff" for short wavelengths so that any of the unstable modes can "fit" into the plasma.

However, for the axial or parallel wavelengths there is a short wavelength "cutoff" for any given group of unstable modes. This effect is shown in Fig. 6.6 in which we have plotted the values of $Re(k_z a_i)$ along the threshold and transition density curves of Fig. 6.4. In this figure $k_\perp a_i$ is an implicit parameter and increases from left to right on the curves. In Fig. 6.6 as in Fig. 6.4 the nested sets of

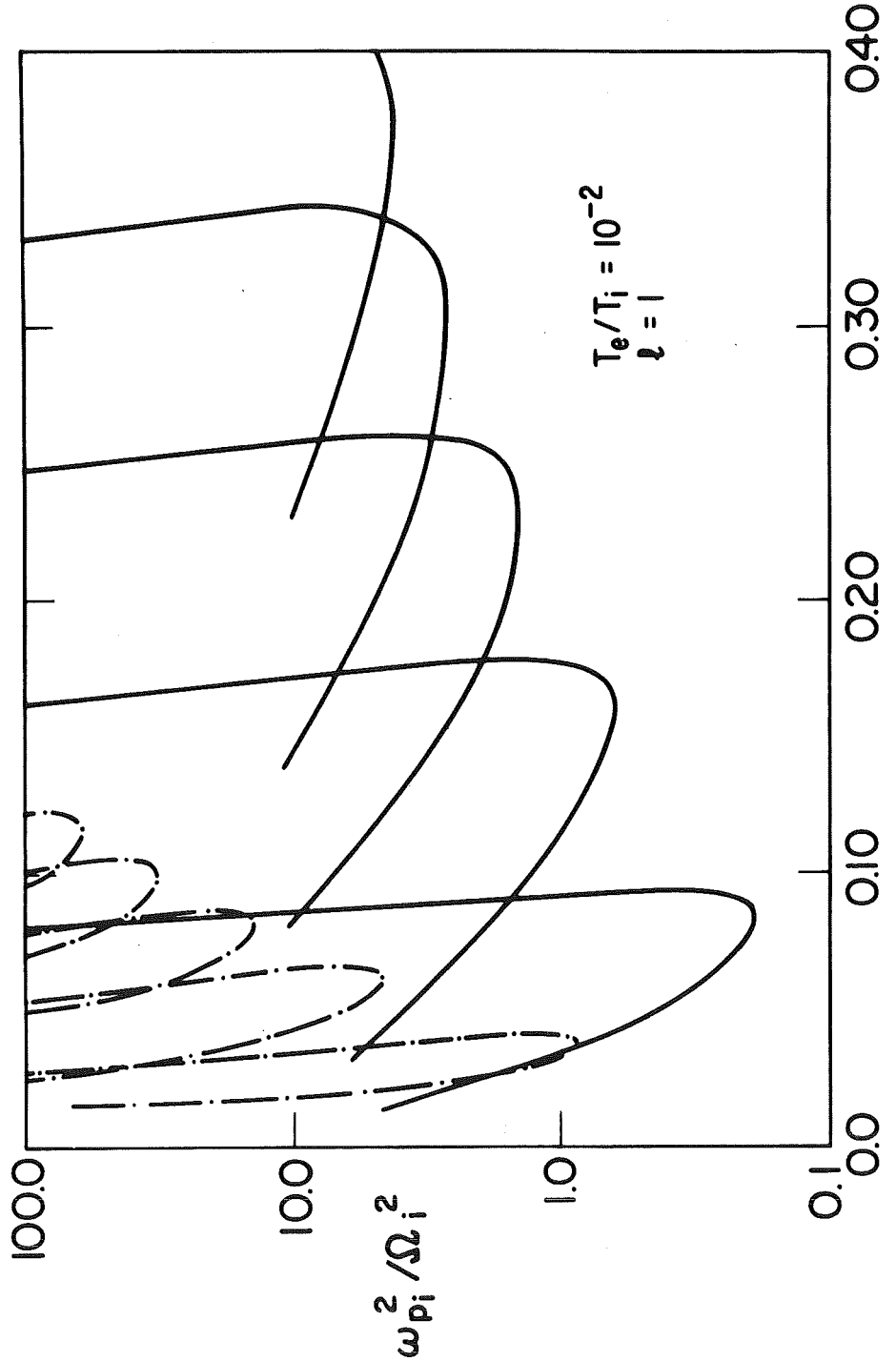

Figure 6.6. Variation of $\mathrm{Re}(k_z a_i)$ Along Curves in Fig. 6.4.

curves correspond to instabilities having $\omega/\Omega_i \sim 1,2,$ etc., with those curves at the lowest densities representing instability for the lowest harmonics of the ion cyclotron frequency. Since the values of $k_z a_i$ along the marginal stability curve in Fig. 6.6 are those for which the minimum threshold density occurs, they are not necessarily the maximum values for which instability occurs for any given harmonic (see Fig. 4.8). However, the deviation of the maximum $k_z a_i$ for instability from that shown in Fig. 6.6 rarely exceeds 5% (except for $T_e \sim T_i$ -- see Fig. 6.8) and so we will neglect it henceforth.

The maximum $k_z a_i$ for which instability of any kind occurs is predicted quite accurately by condition (6.1.10), which we recall was derived by requiring that there not be excessive electron Landau damping of the instability. We also see that the $\mathrm{Re}(k_z a_i)$ values appropriate for the absolute instabilities are much smaller than the values for the convective instabilities, but do scale with the harmonic number n in roughly the same manner. The absolute instabilities thus have considerably longer wavelengths than the convective instabilities and hence much longer plasmas are required for their appearance. For example, for the "most unstable" mode of Fig. 6.4 ($\omega/\Omega_i \sim 1$), the plasma must be a rather long 83 ion Larmor radii in length for a half-wavelength of the absolute instability to "fit" into the plasma. Therefore the maximum $k_z a_i$ for which a given

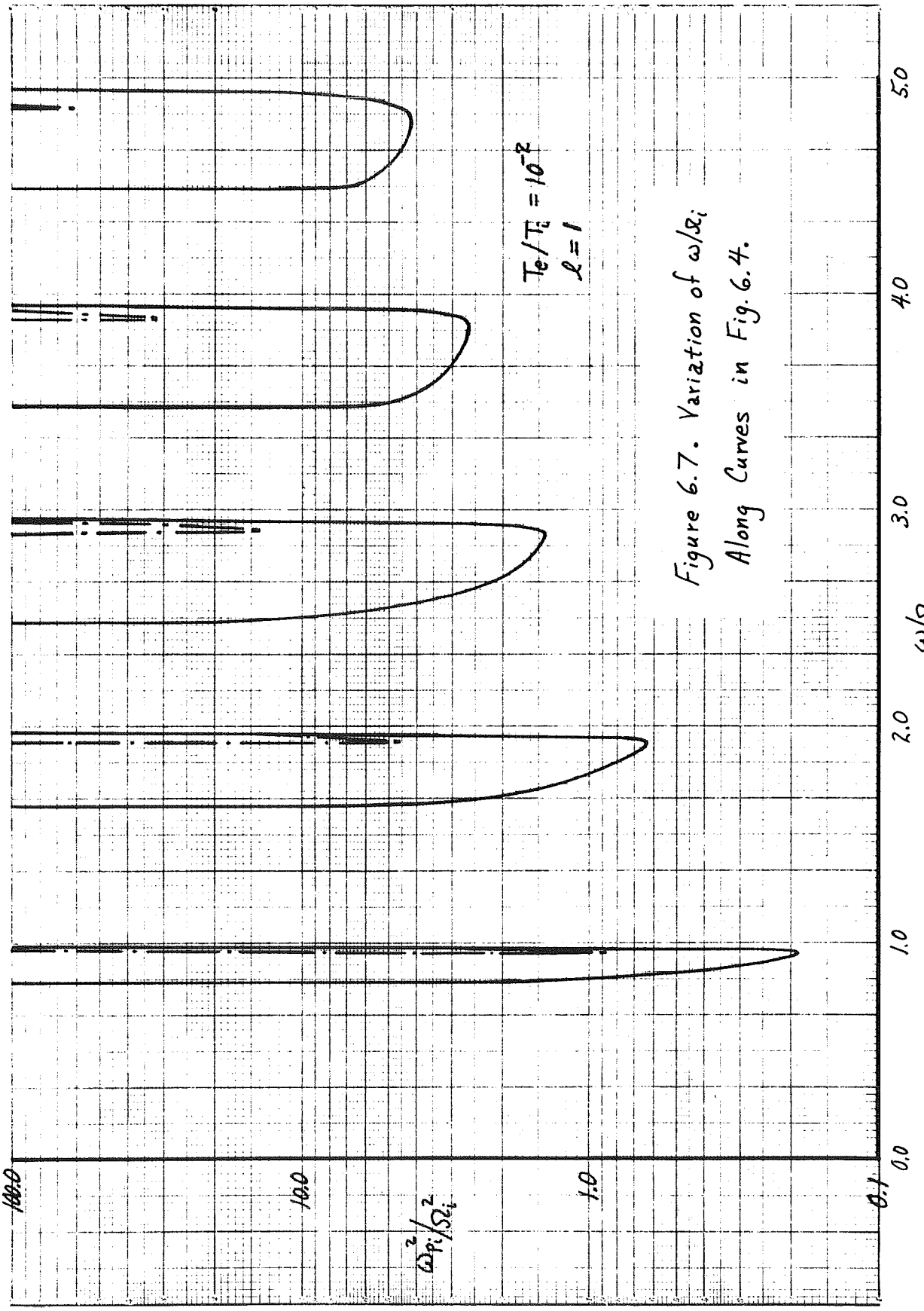

Figure 6.7. Variation of ω/Ω_i Along Curves in Fig. 6.4.

unstable mode occurs can be as important a consideration in predicting the appearance of an instability as the plasma density at which the unstable mode first appears.

As a final examination of the effects of varying $k_\perp a_i$, we exhibit in Fig. 6.7 the values of ω/Ω_i along the threshold and transition density curves of Fig. 6.4. Here as in Fig. 6.6 $k_\perp a_i$ increases from left to right along the threshold density curves, but increases in the opposite direction along the transition density curve. The frequencies along the marginal stability curve agree reasonably well with (6.1.13) except for small $k_\perp a_i$. The disagreement at small $k_\perp a_i$ is due to the constraints of condition (6.2.5). The variation of the real part of the frequency of the absolute instabilities for a given temporal growth rate is even less than that shown for the "marginally stable" absolute instability mode. From the results shown we see that the frequency of the unstable modes does not deviate very much from harmonics of the ion cyclotron frequency; this is particularly true for the absolute instability modes.

Next, we investigate the effect which varying the electron temperature has on the loss-cone instabilities. We do this by first considering the properties of the unstable mode having $\omega/\Omega_i \sim 1$. This is the mode which we have found from the $k_\perp a_i$ analysis to be the "most unstable" mode in that it has the lowest threshold and transition densities. In

determining the properties of this "most unstable" mode as T_e/T_i changes, we minimize the threshold and transition densities with respect to variations in $k_\perp a_i$. The results are displayed in Fig. 6.8. (The absolute instability temporal growth rate curves were not iterated for the lowest density at which the given temporal growth rate occurs. Rather, since we see from Fig. 6.4 that the temporal growth rates we consider are not a strong function of $k_\perp a_i$ near the lowest transition density, we compute the absolute instability temporal growth rates for the particular $k_\perp a_i$ which yields the lowest transition density.) The variations of $-\mathrm{Im}(k_z a_i)/\mathrm{Re}(k_z a_i)$, $k_\perp a_i$ and ω/Ω_i along the curves in Fig. 6.8 are shown in Fig. 6.9.

From the results shown in Fig. 6.8 we see that the absolute and convective instabilities are affected by changes in the electron temperature in very different ways. The convective instabilities are seen to be strongly influenced by the electron temperature. For T_e/T_i less than about 0.1, the threshold density for convectively unstable modes roughly satisfies instability condition (6.2.7). Likewise the values of $k_z a_i$ at which the convective instabilities appear (solid line in Fig. 6.8) are given approximately by (6.1.10). The deviations of the convective instability results from the approximate formulas we have derived are due to slight variations in the amount of electron Landau damping which is required to balance the ion growth terms at the threshold density.

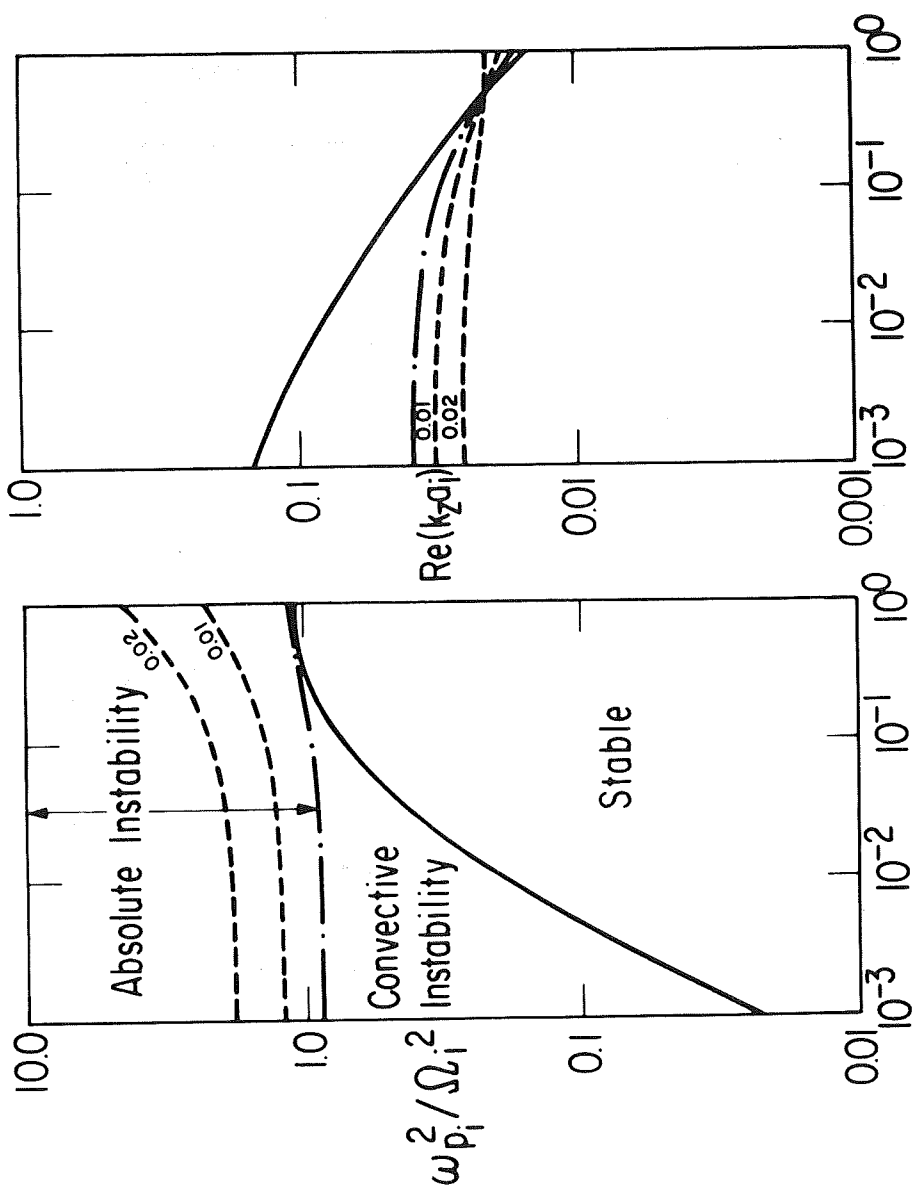

Figure 6.8 Effect of Varying T_e/T_i on Loss-Cone Instabilities (ℓ=1).

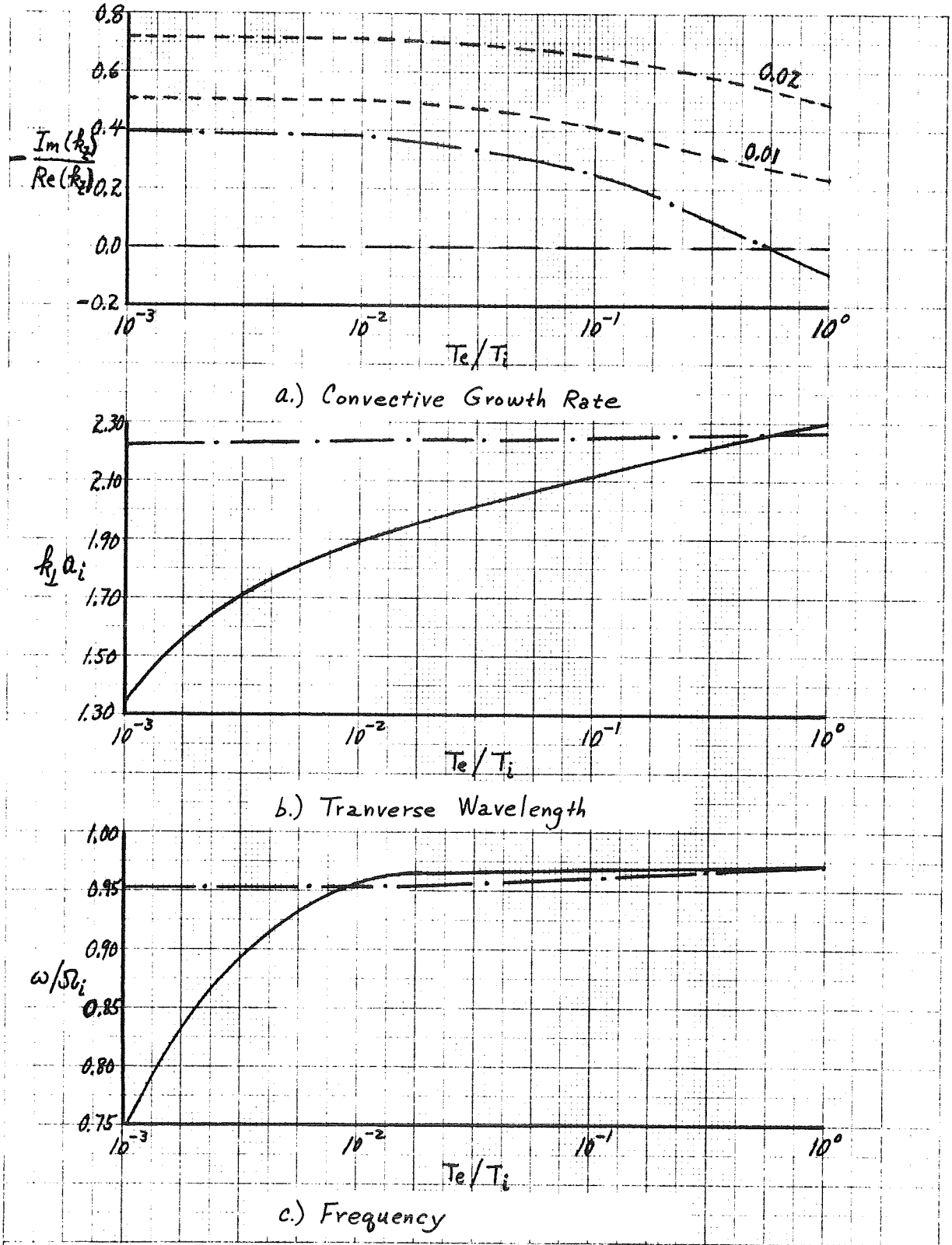

Figure 6.9. Changes in Implicit Parameters for Varying T_e/T_i ($\ell=1$).

In contrast to the convective instabilities, the absolute instabilities are relatively unaffected by variations in the electron temperature except when T_e/T_i approaches unity. For a given plasma density in excess of the transition density, as T_e/T_i increases toward unity we see from Fig. 6.8 that the absolute instability temporal growth rates decrease slightly. In addition, we note that the axial wavelengths of the absolute instabilities increase slightly with T_e/T_i, but again only for T_e/T_i near unity. Guest and co-workers (6.22) have found that these trends persist as T_e/T_i is increased above unity. On the basis of these observations we might expect to achieve a slight degree of stabilization of the absolute loss-cone instabilities by heating the electrons up to or above the ion temperature. On the other hand, we also note from Fig. 6.8 that as T_e/T_i becomes larger than about 0.60, the higher density and larger temporal growth rate absolute modes have successively higher values of $Re(k_z a_i)$ thereby indicating that they can exist in successively shorter plasmas. It thus seems that we gain very little in continuing to increase the electron temperature above $T_e/T_i \simeq 0.60$. However, this conclusion requires further investigation including perhaps a consideration of the finite length effects we have discussed in Section 5.4.

Another very important fact we note concerning the effect of T_e/T_i variations is that the real part of $k_z a_i$ of the absolute loss-cone instabilities asymptotically approaches a

maximum of about 0.04 as $T_e/T_i \to 0$. In this same limit the maximum convective growth rate (just before an absolute instability occurs) asymptotically approaches a maximum specified by

$$-\frac{\mathrm{Im}(k_z a_i)}{\mathrm{Re}(k_z a_i)} \lesssim 0.40 \qquad (6.2.9)$$

(cf. Fig. 6.9a).

In the preceding section we have noted that the nature of the instability is different as T_e/T_i changes from a small to a large number (compared to unity). We recall that the basic difference in these cases is whether the ion cyclotron waves moving transverse to the magnetic field couple respectively to electron plasma or ion waves along the magnetic field. In Figs. 6.8, 6.9 we see evidences of this phenomenon. In particular, from Fig. 6.9a we note that for $T_e/T_i \simeq 0.60$ the imaginary part of $k_z a_i$ for the absolute instability changes sign. From our discussion in Chapter 5 we know that this means that of the two merging modes, what was the growing mode has become the evanescent mode and vice versa. However, we see from Fig. 6.9a that as the density increases, the identification of the growing and evanescent modes reverts to that for low T_e/T_i. The satisfaction of absolute instability condition (β) for such cases has already been discussed in Section 5.3.

For small T_e/T_i we note from Fig. 6.9b,c that for the "most unstable" (convective) modes the frequency becomes significantly less than the ion cyclotron frequency and $k_\perp a_i$ decreases substantially. These effects arise from the large

ion Doppler shifts due to the large values of $k_z a_i$ relevant for these cases (cf. (6.1.10)). Then, condition (6.2.5) can be satisfied for smaller $k_\perp a_i$, and condition (6.1.11) shows us that this results in a lower threshold density.

In addition to investigating the effects of electron temperature on the "most unstable" mode, we have considered as a typical case these same effects on the instabilities for $k_\perp a_i = 5.0$. These results are shown in Fig. 6.10. We observe here the same general characteristics as those displayed in Fig. 6.8, i.e. for the "most" unstable modes. It is interesting to note that for small T_e/T_i each of the three convectively unstable modes have nearly the same threshold density while for $T_e/T_i \sim 1$ their respective threshold densities are distinctly different and each approximate the transition density for the corresponding absolute instability mode. The variations of $\mathrm{Re}(k_z a_i)$, the maximum convective growth rate and ω/Ω_i with T_e/T_i in this case are similar to those shown in Figs. 6.8 and 6.9.

Let us now consider the effect of varying the sharpness of the $v_\perp$ distribution by changing the parameter ℓ. As we have noted in Section 1.3, as ℓ varies the mean velocity (really the most probable velocity) perpendicular to the magnetic field is given by

$$\langle v_\perp \rangle = \alpha_{\perp i} \sqrt{\ell} \ . \qquad (6.2.10)$$

For convenience, here we will keep the mean velocity $\langle v_\perp \rangle$ a constant as we vary ℓ. Therefore we assume a given value of

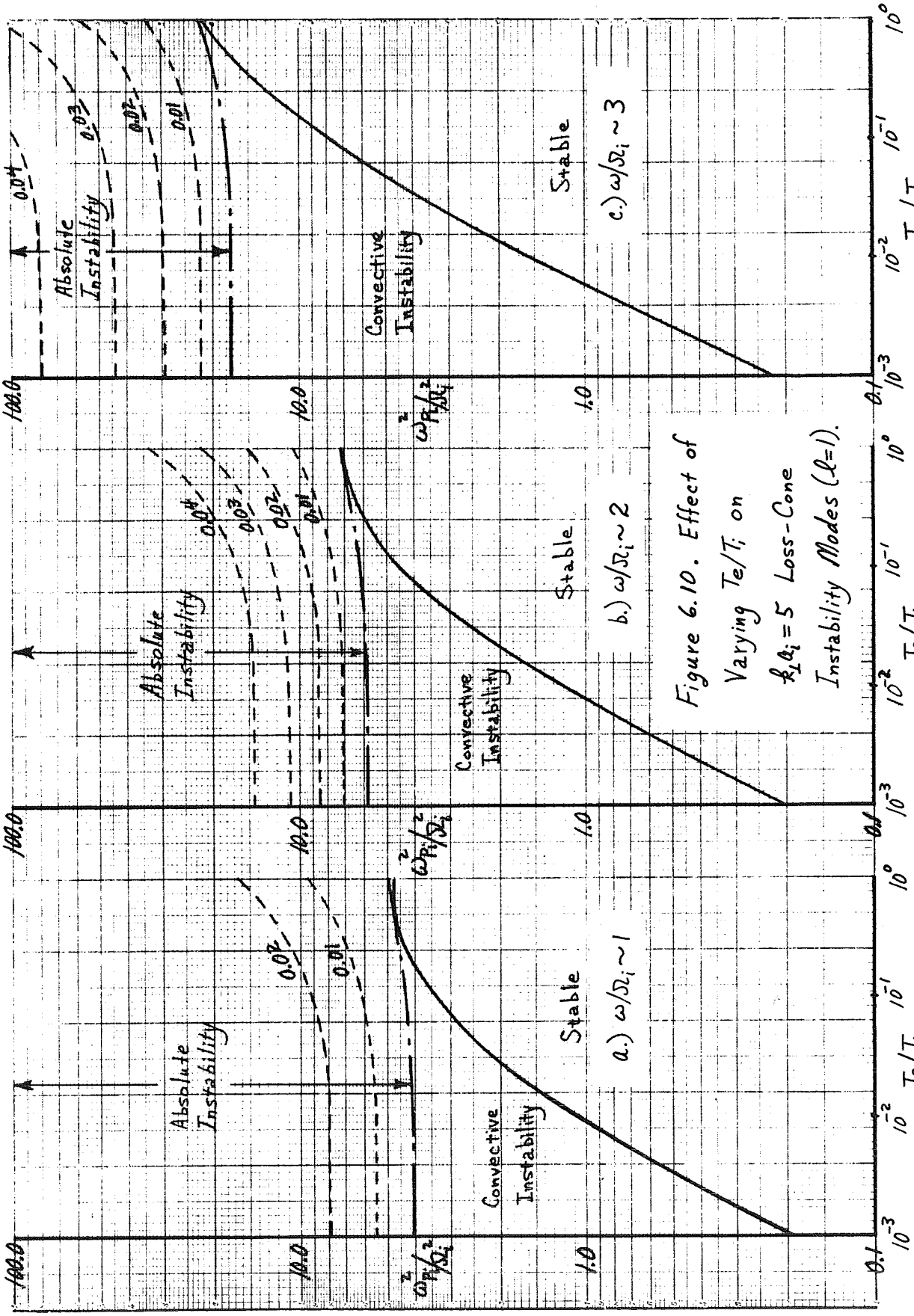

Figure 6.10. Effect of Varying T_e/T_i on $k_\perp a_i = 5$ Loss-Cone Instability Modes ($\ell=1$).

$\langle v_\perp \rangle$ and define

$$\alpha_{\perp_i} \equiv \langle v_\perp \rangle / \sqrt{\ell} \ . \qquad (6.2.11)$$

With this convention the mean ion Larmor radius is given by $\langle v_\perp \rangle / \Omega_i$. Having taken $\langle v_\perp \rangle$ to be constant, in varying ℓ we are changing the thermal spread in the $v_\perp$ distribution according to the relation

$$\frac{(\delta v_\perp)^2}{\langle v_\perp \rangle^2} = \frac{1}{\ell} \qquad (6.2.12)$$

in which $\delta v_\perp$ is roughly the velocity spread at half-maximum. The parameter $1/\ell$ is thus a measure of the thermal spread relative to the net "drift" energy of the $v_\perp$ distribution.

Following this procedure of keeping the mean perpendicular velocity $\langle v_\perp \rangle$ and hence the mean ion Larmor radius a constant, we have considered the properties of the unstable modes having $\omega/\Omega_i \sim 1$ (i.e. the "most unstable" modes) for varying ℓ. Minimizing the threshold and transition densities with respect to $k_\perp \langle v_\perp \rangle / \Omega_i$ for $\ell = 1, 2, 3, \infty$, we obtain the results displayed in Fig. 6.11. Here and in future graphs concerning the effects of thermal spread we have connected the discrete points at $1/\ell = 1, \frac{1}{2}, 1/3, 0$ by straight line segments to facilitate visualization of trends in the results. As with the T_e/T_i computations, the densities at which the absolute instabilities have certain temporal growth rates are not minimized with respect to $k_\perp$. Rather, they are computed for the $k_\perp$ at which the minimum transition density occurs, but are

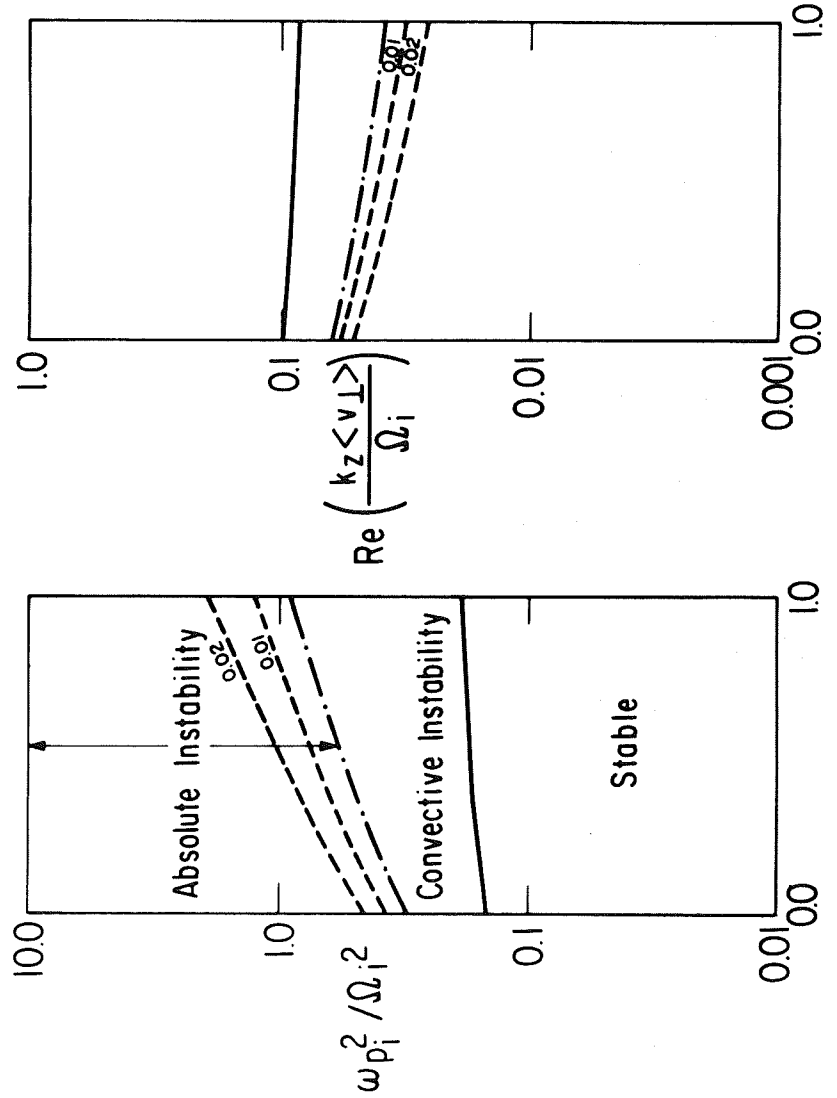

Figure 6.11. Effect of Varying the Thermal Spread in $v_\perp$ Distribution on Loss-Cone Instabilities ($T_e/T_i = 10-2$).

nonetheless fairly representative. The variations of $-Im(k_z)/Re(k_z)$, $k_\perp \langle v_\perp \rangle /\Omega_i$ and ω/Ω_i for the values of ℓ considered in Fig. 6.11 are displayed in Fig. 6.12.

Since a delta function distribution has more free energy than the same group of particles centered about the same mean velocity with some thermal spread, we expect that the plasma will have the greatest tendency toward instability when the $v_\perp$ distribution has zero thermal spread ($\ell = \infty$). From Fig. 6.11 we see that this is indeed the case. In contrast to the variations with T_e/T_i, the threshold density for convective instability is seen to be relatively independent of the spread in the $v_\perp$ distribution. On the other hand, the transition density for absolute instability is moderately affected by the thermal spread in the $v_\perp$ distribution. It is interesting to note that increasing the thermal spread increases the stability of the plasma by increasing the axial wavelengths of the "most unstable" modes as well as both the threshold and transition densities. Likewise the temporal growth rates of the absolute instabilities increase less rapidly with density as the thermal spread is increased. However, it is important to note that in spreading the $v_\perp$ distribution from zero spread up to the well spread case of $\ell = 1$, the transition density increases by only a factor of 2.86 while the wavelength of the absolute instability mode increases by only a factor of 1.65. Thus we conclude that experimentally increasing the thermal spread in the $v_\perp$ distribution would stabilize the loss-cone instabilities to only a very limited degree.

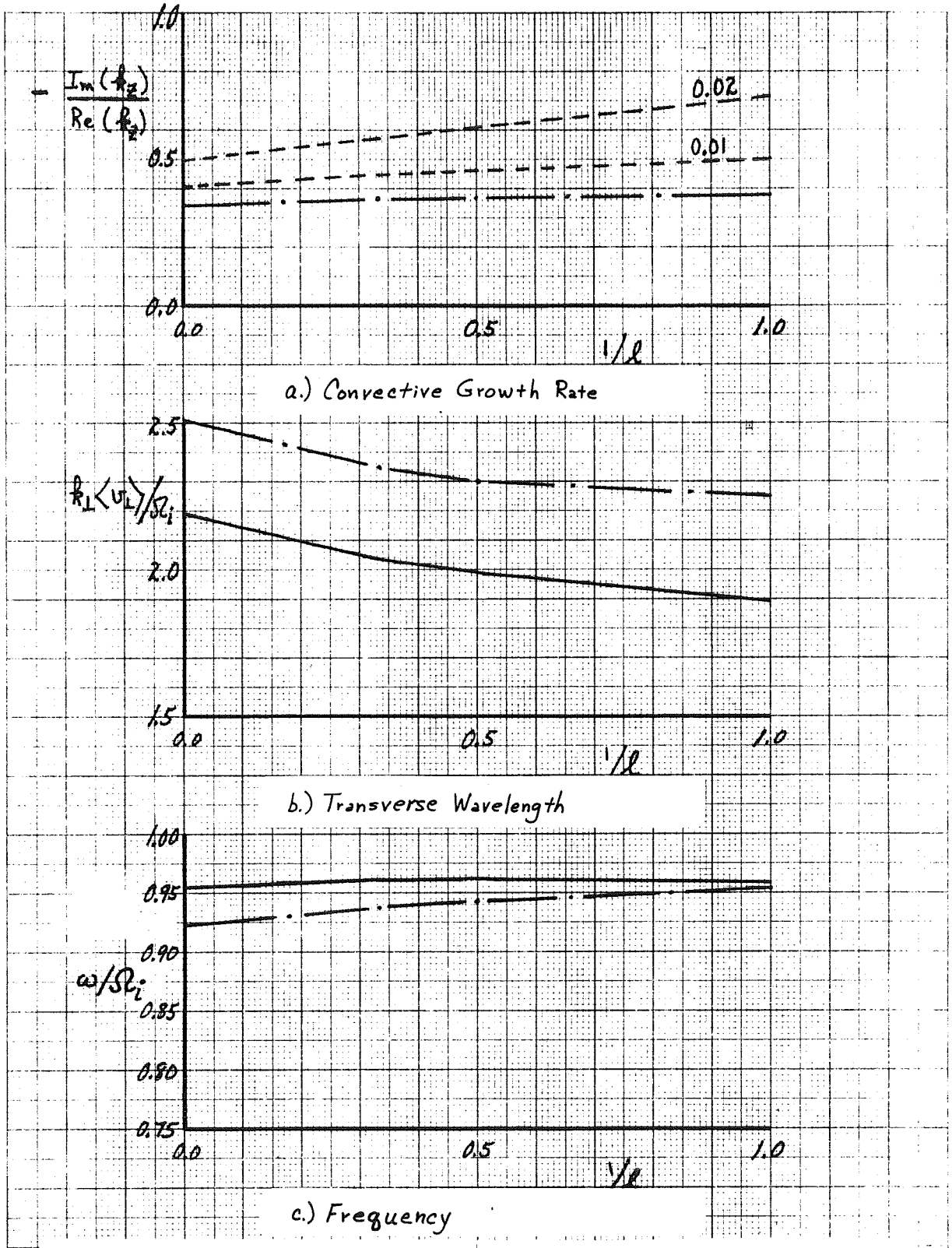

Figure 6.12. Changes in Implicit Parameters for Varying ℓ ($T_e/T_i = 10^{-2}$).

We may also compare the absolute and convective loss-cone instabilities shown in Fig. 6.11 with the flute and flute-like modes discussed in the preceding section. As we have noted previously, Dory, Guest and Harris (6.7) have shown that the $k_z = 0$ modes are unstable only if $\ell \geq 3$. Here we find that the density at which the flute modes ($k_z = 0$, $\omega/\Omega_i \sim 0$) appear are given by $\omega_{p_i}^2/\Omega_i^2 = 746.7$, 16.98 for $\ell = 3, \infty$ respectively. These values are in agreement with those reported by Dory, Guest and Harris (6.7). The flute-like modes ($\omega \sim n\Omega_i$) have similar density thresholds (6.7). Therefore the flute and flute-like modes occur only at much higher densities than the convective or absolute loss-cone instabilities. However, the nonzero k_z instabilities may of course be forbidden by plasma length considerations. In any case since even a moderate amount of thermal spreading of the $v_\perp$ distribution stabilizes the flute and flute-like instabilities, they presumably do not present a very important threat to plasma containment (see also Section 6.1).

Since the convective instability threshold densities and values of $k_z a_i$ do not vary much with ℓ, we find general agreement of these results with the approximate instability conditions given by (6.2.7) and (6.1.10). However, there remain some subtle points which should be discussed. Recalling definition (6.2.11), we note that the value of v_y for which the effective velocity distribution $\tilde{F}_i(v_y)$ has its

maximum, increases monotonically from $\langle v_\perp \rangle/2$ for $\ell = 1$ to $\langle v_\perp \rangle$ for $\ell = \infty$. Therefore as ℓ increases up to infinity, instability condition (6.2.5) becomes

$$0 < \omega/k_\perp < \langle v_\perp \rangle \quad (\ell \to \infty, \text{ instability}) \tag{6.2.13}$$

which in turn changes condition (6.2.6) to

$$k_\perp \langle v_\perp \rangle /\Omega_i > \omega/\Omega_i \sim n \quad (\ell \to \infty, \text{ instability}). \tag{6.2.14}$$

On the basis of the latter condition and the fact that the threshold density is generally lowest near the smallest value of $k_\perp$ permissible (see (6.1.11)), we would expect that as ℓ increases, the value of $k_\perp$ at which the lowest threshold density occurs would decrease. However, from Fig. 6.12b we see that this is not the case. Examining the maximum frequency for which instability can occur for a given $k_\perp$, we find that increasing ℓ does allow higher frequency modes to be unstable, although with frequencies not quite as large as (6.2.13) would allow. We therefore conclude that our arguments about the phase velocity perpendicular to the magnetic field being in a "positive-slope" region are still valid.

This being the case, we must consider why it is that (6.1.11) is inapplicable here. The reason is that as the $v_\perp$ distribution has its thermal spread reduced, certain wavelengths transverse to the magnetic field exchange energy with the sharply peaked $v_\perp$ distribution of particles much more effectively than others. When $\ell = 1$, the $v_\perp$ distribution

is sufficiently thermalized (see Fig. 6.2) so that nearly any wave which satisfies (6.2.5) can resonate well with some group of particles. However, from a consideration of the interaction between plane waves and particles moving transverse to the magnetic field (carried to first order corrections in the perturbed electric fields), we can easily see that if all the ions had the same perpendicular velocity ($\ell = \infty$), then for $\omega/\Omega_i \sim 1$ the interaction is strongest when the wavelength is nearly equal to the Larmor diameter. In general we find that for $\omega/\Omega_i \sim 1$ the interaction is strongest if

$$\frac{\Omega_i \lambda_\perp}{4 \langle v_\perp \rangle} \simeq \frac{1}{2}, \frac{1}{4}, \frac{1}{6}, \ldots, \qquad (6.2.15)$$

while for

$$\frac{\Omega_i \lambda_\perp}{4 \langle v_\perp \rangle} \simeq \frac{1}{1}, \frac{1}{3}, \frac{1}{5}, \ldots \qquad (6.2.16)$$

there is virtually no interaction at all. The values of $k_\perp \langle v_\perp \rangle / \Omega_i$ for which the interaction is strongest are therefore

$$\frac{k_\perp \langle v_\perp \rangle}{\Omega_i} \simeq \pi, 2\pi, 3\pi, \ldots . \qquad (6.2.17)$$

As can be seen from our general instability conditions (see Section 4.2 and (6.1.12)), the exact values of $k_\perp \langle v_\perp \rangle / \Omega_i$ for the strongest interaction are given by the minima of the

function D_l^{∞}, which is really just the function $J_l J_l'$ (see Appendix A). The values of $k_\perp \langle v_\perp \rangle / \Omega_i$ given by (6.2.17) are simply those for which $J_l J_l'$ has its maximum negative value as $k_\perp \langle v_\perp \rangle / \Omega_i$ becomes arbitrarily large, i.e. in the asymptotic limit. The reasons why the Bessel functions arise here and the details of the wave-particle coupling interactions are discussed by Hall, Heckrotte and Kammash (6.17).

From (6.2.17) we see that the smallest value of $k_\perp \langle v_\perp \rangle / \Omega_i$ for which strong wave-particle interactions occur is π. Therefore the reason $k_\perp$ increases at the lowest threshold density as we decrease the thermal spread of the $v_\perp$ distribution is that the value of $k_\perp \langle v_\perp \rangle / \Omega_i$ for strongest wave-particle interaction is increasing. The value of $k_\perp \langle v_\perp \rangle / \Omega_i$ does not increase all the way to π because as (6.1.11) shows, the minimum $k_\perp$ for which an appreciable interaction occurs is the one for which the instability has the lowest threshold density. It is interesting to note from Fig. 6.12b that as ℓ varies, the $k_\perp$ for which the lowest transition density for absolute instability occurs scales in the same manner as that for the threshold density for convective instabilities.

We have also considered the effects of changes in ℓ on modes with a particular $k_\perp$, viz. $k_\perp \langle v_\perp \rangle / \Omega_i = 5.0$. The results of these computations are shown in Fig. 6.13. For the $\omega/\Omega_i \sim 1$ mode, we note that when $\ell = \infty$ this

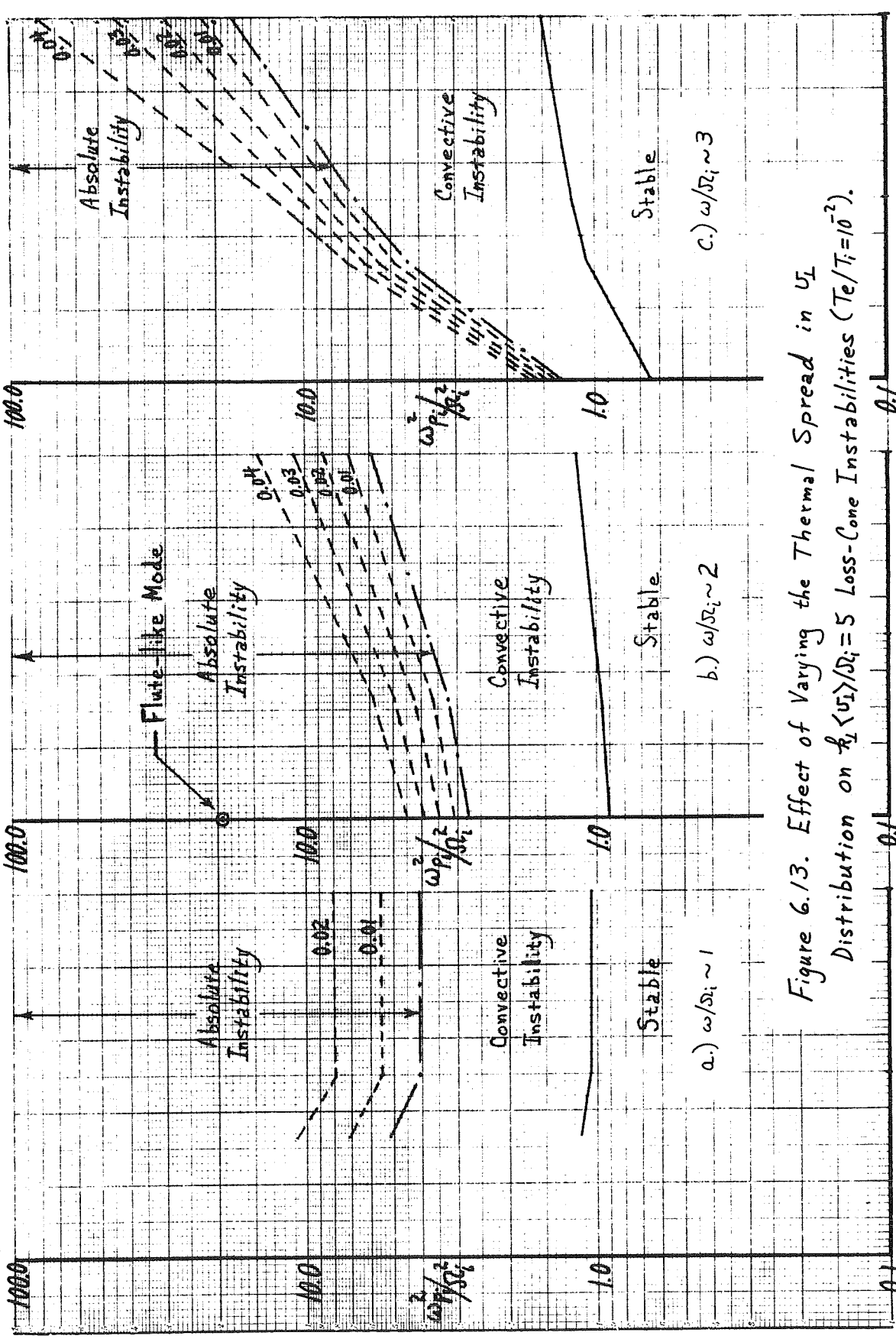

Figure 6.13. Effect of Varying the Thermal Spread in $v_\perp$ Distribution on $k_\perp \langle v_\perp \rangle / \Omega_i = 5$ Loss-Cone Instabilities ($T_e/T_i = 10^{-2}$).

mode is not unstable. Since our value of $k_\perp \langle v_\perp \rangle / \Omega_i = 5.0$ is near $3\pi/2$, which is one of the points for which virtually no wave-particle interaction occurs (see (6.2.16)), we would not expect such a mode to be unstable. The $\omega/\Omega_i \sim 2$ mode has characteristics which are similar to the "most unstable" mode (see Fig. 6.11). However, we note that the $\omega/\Omega_i \sim 3$ modes and particularly these absolute instability modes are quite sensitive to changes in the thermal spread in the $v_\perp$ distribution. Referring back to Fig. 6.4 we see that this sensitivity arises from the fact that this mode lies in a very rapidly changing portion of the transition density curve. Therefore we conclude that this strong variation is not typical. This observation emphasizes the fact that we should be very careful in interpreting the results of a single calculation with one parameter fixed, since as we have seen here, the results from a single calculation may not be very representative.

In concluding this section we will summarize what we have learned about loss-cone instabilities and make comparisons between the loss-cone and temperature-anisotropy instabilities. For both types of instabilities we have found that for $T_e/T_{z_i} \lesssim 1$ just before the absolute instabilities appear the minimum growth length of the convective instabilities is always greater than 2.5 times the wavelength of the unstable mode (see Section 6.1, (6.2.8), (6.2.9) and Fig. 6.12a). Therefore, if we presume that absolute instabilities can "fit"

into a plasma whose length is equal to a half-wavelength of the unstable mode, then the convectively unstable modes are a serious threat to plasma containment only if the reflection coefficient at the ends exceeds 0.285 and even then only for small T_e/T_i (see Fig. 6.9a). Since such a high reflection coefficient seems improbable or at least avoidable (see Section 5.4), we expect that only absolute loss-cone or temperature-anisotropy instabilities will limit confinement of experimental plasmas.

In this section we have found that the absolute loss-cone instabilities are relatively unaffected by changes in the electron temperature and only moderately affected by changes in the thermal spread of the $v_\perp$ distribution. Even under the most severe circumstances they can occur only if the plasma density is high enough so that $\omega_{p_i}^2/\Omega_i^2 \gtrsim 0.3$ (see Fig. 6.11). In contrast, Beasley and Cordey (6.38 -- see Fig. 6.1) have shown that for large $T_{\perp_i}/T_{z_i}$, the plasma density required for absolute temperature-anisotropy instabilities is lower by a factor of roughly $T_{z_i}/T_{\perp_i}$. Their results also indicate that as $T_{\perp_i}/T_{z_i}$ is increased (above unity) the axial wavelengths of the unstable modes decrease roughly as the square root of $T_{z_i}/T_{\perp_i}$ (see Fig. 6.1). Therefore we expect that whenever the temperature-anisotropy instabilities are possible by virtue of there being an inequality of the mean velocities along and transverse to the magnetic field, they will be the dominant instabilities which

inhibit confinement of high density experimental plasmas. The purpose of this work has been to investigate the ultimate situation in which the sources of free energy driving the temperature-anisotropy instabilities have been removed (by having $T_\perp \sim T_z$) and we are left with "only" the loss-cone instabilities in an open-ended confinement system.

For sufficiently high plasma densities we have found that the loss-cone instabilities are always of the absolute type. This fact alone is perhaps one of the most important results found in this thesis since earlier work ((6.1)-- see next section) had indicated that the loss-cone instabilities were always of the convective type. The absolute loss-cone instabilities have rather long axial wavelengths and therefore may be amenable to stabilization by keeping experimental plasmas relatively short. The successively higher cyclotron harmonic modes have shorter axial wavelengths, but fortunately do not occur until successively higher plasma densities have been reached. Analyzing our results on an empirical basis, we find that we can stabilize an experimental plasma against these absolute loss-cone instabilities only if

$$L \lesssim \frac{25\pi a_i}{n^{2/3}} \qquad \text{(stability)}, \qquad (6.2.18)$$

$$\frac{\omega_{p_i}^{\ 2}}{\Omega_i^{\ 2}} \lesssim 0.8\, n^{8/3} \qquad \text{(stability)} \qquad (6.2.19)$$

in which L is the axial legnth of an experimental plasma and n is the harmonic number of the absolute instability mode. In obtaining the length criterion we have assumed that if the plasma is a half-wavelength long the corresponding absolute instability mode "fits" into the plasma (see Section 5.4). Our results also indicate that neither heating the electrons (up towards the ion temperature) nor increasing the thermal spread of the $v_\perp$ distribution will be very helpful in suppressing these absolute loss-cone instabilities. The relevant transverse wavelengths of the absolute loss-cone modes having the lowest transition densities are given roughly by

$$k_\perp a_i \gtrsim 2n \ . \qquad (6.2.20)$$

Since for high harmonic numbers the relevant modes have very short transverse wavelengths, they will undoubtedly grow rapidly into the nonlinear regime where they may be limited in amplitude. The resultant effects of these absolute loss-cone instability modes is then presumably a high level of turbulent diffusion. To the author's knowledge the only calculation of nonlinear limiting processes for the loss-cone instabilities is that carried out by Galeev (6.43), who has used the quasilinear theory to consider their effects on the particle velocity distributions. However, in addition to making the seemingly inconsistent approximations of $\mathrm{Im}(\omega)/\Omega_i \ll 1$ for the validity of the quasilinear theory and $\mathrm{Im}(\omega)/\Omega_i \gg 1$ for the validity of the "continuum" limit of the dispersion relation (see next section), his calculations ignore the convective versus absolute

nature of the loss-cone instabilities. Therefore it is difficult to see how those calculations would be applicable to the loss-cone instabilities we have discussed in this work.

Finally, we will discuss the understanding of the physics of the absolute loss-cone and temperature-anisotropy instabilities which we can gain from the results of our numerical computations. First, we note that for small T_e/T_i the phase velocity of the absolute instability modes along the magnetic field is very large compared to the electron thermal velocity. For $T_e/T_i \sim 1$ it becomes only slightly larger than the electron thermal velocity. Thus we expect that the thermal motions of the electrons will cause little dispersion of the waves unless $T_e/T_i \sim 1$. The truth of this conjecture can be seen from Fig. 6.8 where we find that the absolute instabilities, whose presence requires a significant amount of dispersion (see Section 5.1), are practically unaffected by changes in the electron temperature except for $T_e/T_i \sim 1$. In general, the necessary dispersion for the existence of zero group-velocity (i.e. absolute instability) modes is supplied by the ions. As evidence of this fact, we note that (see for example Tables 5.1, 6.1) at the transition density for absolute instability the "effective" phase velocity of the absolute instability mode along the magnetic field for the dominant ion contribution to the dispersion relation (see Section 3.4) is only slightly greater than the ion thermal velocity in this direction (for both the loss-cone and temperature-anisotropy modes). This is

of course precisely the effective phase velocity which would be expected to result in the greatest amount of dispersion of the waves by the thermal motions of the ions. Using essentially only the physical facts we have noted in this paragraph, Rosenbluth and Horton (6.44) have analytically shown that for absolute loss-cone instabilities, in the limit of small T_e/T_i, the transition density should scale as $n^{8/3}$ and the value of k_z as $n^{2/3}$, both scalings being independent of the electron temperature; these results agree with (6.2.18) and (6.2.19). We should also note that under almost the same assumptions, Beasley and Cordey (6.38) have analytically obtained the relevant values of ω and k_z for the absolute temperature-anisotropy modes. The conclusion of the preceding remarks is thus that while the coupling of the electron motions along the magnetic field to the transverse ion motions is responsible for the appearance of convective instabilities, it is the ion motions along the magnetic field which are primarily responsible for the dispersion of the waves (with frequencies near harmonics of the ion cyclotron frequency) and hence the absolute instabilities.

6.3 The Rosenbluth-Post "Continuum" Limit

In this section we will discuss the "continuum" limit (very short transverse wavelengths, $k_\perp a_i >> 1$) of the Harris dispersion relation which has been derived by Rosenbluth and Post (6.1, 6.41). After deriving this and another large $k_\perp a_i$ limit, we survey the work which has been carried out using the resultant forms of the dispersion relation. Then, to see how applicable the "continuum" limit is, we consider in detail a particular very short transverse wavelength case ($k_\perp a_i = 25$) using the exact Harris dispersion relation.

As we have seen in the preceding section, except for the higher harmonic, higher density modes, the loss-cone instabilities have rather long wavelengths along the magnetic field and hence occur only in relatively long experimental plasmas. Therefore we expect that in relatively short experimental plasmas the only loss-cone instabilities which occur have frequencies which are high harmonics of the ion cyclotron frequency. At the same time, we note from the results of the preceding section (see for example Fig. 6.3) that these high harmonic numbers imply that

$$k_\perp a_i >> 1 \ . \qquad (6.3.1)$$

Therefore we expect that in fairly short experimental plasmas the perpendicular wavelengths of the unstable modes will be much less than the ion Larmor radius. This being the case, if the unstable modes were to grow in times like the ion cyclotron period, the ions could be considered to have straight-line

orbits transverse to the magnetic field direction, i.e. be unconstrained by the magnetic field in their motions. Making this very physical assumption (which we have also used in obtaining (6.2.4)), Rosenbluth and Post (6.1) have derived the dispersion relation for waves moving in such a dense plasma which has an arbitrary ion velocity distribution. Since the ion cyclotron frequency and ion Larmor radius drop out of the dispersion relation in this case, due to the very high frequencies and short transverse wavelengths, we refer to this limit as the "continuum" limit of the Harris dispersion relation. We will not derive this dispersion relation based upon straight-line ion orbits directly. Rather, we will follow a procedure which has been given by Rosenbluth (6.41) for algebraically reducing the ion contributions to the Harris dispersion relation to this "continuum" limit. This procedure has the advantage that the conditions under which the "continuum" limit should be applicable emerge from it quite naturally.

In deriving the "continuum" limit we are only concerned with the ion contribution to the dispersion relation which we will call R_i:

$$R_i \equiv \omega_{Pi}^2 \int d^3v \sum_{n=-\infty}^{\infty} \frac{J_n^2(k_\perp v_\perp/\Omega_i)}{k_z v_z + n\Omega_i - \omega} \left\{ k_z \frac{\partial F_i}{\partial v_z} + \frac{n\Omega_i}{v_\perp} \frac{\partial F_i}{\partial v_\perp} \right\} . \quad (6.3.2)$$

Completing the numerator in the $\partial F_i/\partial v_\perp$ term, for F_i distributions which vanish for $v_\perp = 0$ (the only ones of interest here), we can rewrite R_i as

$$R_i = \omega_{pi}^2 \int d^3v \sum_{n=-\infty}^{\infty} \frac{J_n^2(k_\perp v_\perp/\Omega_i)}{k_z v_z + n\Omega_i - \omega} \left\{ k_z \frac{\partial F_i}{\partial v_z} + \frac{\omega - k_z v_z}{v_\perp} \frac{\partial F_i}{\partial v_\perp} \right\}$$

$$= i\omega_{pi}^2 \int d^3v \sum_{n=-\infty}^{\infty} \int_{-\infty}^{0} d\tau \exp\left\{ i(k_z v_z + n\Omega_i - \omega)\tau \right\}$$

$$\times J_n^2(k_\perp v_\perp/\Omega_i) \left\{ k_z \frac{\partial F_i}{\partial v_z} + \frac{\omega - k_z v_z}{v_\perp} \frac{\partial F_i}{\partial v_\perp} \right\}.$$

Then, using the Bessel function identity (6.45)

$$J_0\left[z\sqrt{2(1-\cos\phi)}\right] = \sum_{m=-\infty}^{\infty} e^{im\phi} J_m^2(z),$$

we have

$$R_i = i\omega_{pi}^2 \int d^3v \left\{ k_z \frac{\partial F_i}{\partial v_z} + \frac{\omega - k_z v_z}{v_\perp} \frac{\partial F_i}{\partial v_\perp} \right\}$$

$$\times \int_{-\infty}^{0} d\tau \; e^{i(k_z v_z - \omega)\tau} J_0\left[\frac{k_\perp v_\perp}{\Omega_i} \sqrt{2(1-\cos\Omega_i\tau)} \right].$$

Now, assuming that

$$\mathrm{Im}(\omega/\Omega_i) > 1 , \qquad (6.3.3)$$

only times τ less than Ω_i^{-1} will contribute significantly to the τ integration and so

$$1 - \cos\Omega_i\tau \simeq \tfrac{1}{2}\Omega_i^2\tau^2 .$$

Using this result and the Bessel function integral identity (6.46)

$$\int_0^\infty e^{ibt} J_0(at)\,dt = \frac{i}{\left(b^2-a^2\right)^{\frac{1}{2}}}$$

we finally obtain

$$R_i \simeq \omega_{pi}^2 \int d^3v \left\{ k_z \frac{\partial F_i}{\partial v_z} + \frac{\omega - k_z v_z}{v_\perp} \frac{\partial F_i}{\partial v_\perp} \right\} \frac{1}{\left[(\omega - k_z v_z)^2 - k_\perp^2 v_\perp^2\right]^{1/2}} \quad (6.3.4)$$

In contrast to the original expression (6.3.2), we see that the ion cyclotron frequency and indeed all indications of the ion cyclotron resonance have disappeared from this last approximate form of R_i. Note that in deriving this result, the only approximation which was made was that of (6.3.3). However, since the temporal growth rate of an unstable mode seldom exceeds its real frequency and large values of $k_\perp a_i$ are required for high harmonic number modes to be unstable, we see that condition (6.3.3) implies that condition (6.3.1) be satisfied as well.

In addition to the assumption in (6.3.3), we will also assume, as is customary, that (for the ions)

$$k_z v_z << \omega \,. \quad (6.3.5)$$

Then, since for the loss-cone instabilities the mean velocities along and transverse to the magnetic field are nearly equal, all terms containing k_z can be set to zero and we obtain the desired result (6.1, 6.41):

$$R_i \simeq \omega_{p_i}^2 \int d^3v \, \frac{1}{v_\perp} \frac{dF_i}{dv_\perp} \, \frac{1}{\left[1 - \frac{k_\perp^2 v_\perp^2}{\omega^2}\right]^{\frac{1}{2}}} \qquad (6.3.6)$$

in which as usual the singular denominator is defined for $\mathrm{Im}(\omega) > 0$. Equation (6.3.6) is the form of the ion contributions to the dispersion relation from which we obtain instability condition (6.2.4) (see (6.1)). For the most thermally spread of our $v_\perp$ distributions ($\ell = 1$), we find that this ion contribution is given by*

$$R_i \simeq \frac{2\omega_{p_i}^2}{\alpha_{\perp_i}^2} \left[\tfrac{1}{2} Z_1(\omega/k_\perp v_\perp) - Z_3(\omega/k_\perp v_\perp)\right] \qquad (6.3.7)$$

where the functions Z_1 and Z_3 are plasma dispersion function moments which we discuss in Appendix B.

Using the "continuum" limit of the ion contributions to the dispersion relation, Rosenbluth and Post (6.1) arrive at many interesting conclusions about loss-cone driven instabilities. First, they note that there are no flute or flute-like ($k_z = 0$) unstable modes. However, as we have discussed in Section 6.1, both flute and flute-like modes can become unstable if the $v_\perp$ distribution is sufficiently sharply peaked about a nonzero velocity. The reason the continuum limit does not give the proper answer here is due to the fact that for sufficiently sharp $v_\perp$ distributions, only certain transverse

*In performing the required integrations, it is easiest to convert (6.3.6) into a form in which the singular denominator involves only the v_y velocity component (see (6.1)).

wavelengths can resonate strongly with the transverse motions of the particles (see preceding section) and in the continuum limit we smooth out such discreteness effects. A second prediction which Rosenbluth and Post make from the continuum limit of the dispersion relation is that for the most unstable modes

$$\mathrm{Re}(\omega) \simeq \mathrm{Im}(\omega) \simeq k_\perp \alpha_{\perp_i} \simeq \omega_{p_i} \simeq k_z \alpha_{\perp_i} (m_i/m_e)^{\frac{1}{2}} . \quad (6.3.8)$$

We will examine these conditions later in a numerical example.

Finally, Rosenbluth and Post (6.1) note that the unstable modes predicted by the continuum limit of the dispersion relation are all only convectively unstable modes, i.e. absolute instability modes do not occur. With this observation they then estimate convective growth lengths and reflection coefficients, thereby arriving at critical machine lengths below which the plasma should be stable against these convective instabilities (see Section 5.4). We have seen from Section 5.1 that in order to show that unstable modes are of the convective type, we must be able to solve the dispersion relation for complex k and real frequencies. However, the continuum limit of the dispersion relation is not rigorously valid for real frequencies (see (6.3.3)) and so the conclusion derived from it that the loss-cone instabilities are of the convective type would seem to be a very dubious conclusion. Indeed, we have already seen that the loss-cone instabilities can be of the absolute type for values of $k_\perp a_i$ up to 8. We extend those calculations up to a value of $k_\perp a_i$ of 25 later in this

section and find that the loss-cone instabilities still may be of the absolute type for sufficiently dense plasmas. From the discussion at the end of the preceding section concerning the physics of the absolute loss-cone instabilities, we have seen that it is the cyclotron resonance of the unstable wave with ion motions along the magnetic field which gives rise to the required dispersion for absolute instabilities. However, these cyclotron resonances are precisely the effects which have been "smoothed out" by the process of taking the "continuum" limit. Therefore it is not at all surprising that, in contrast to the actual case, the continuum limit of the dispersion relation predicts that the loss-cone instabilities are never of the absolute type.

We will now survey the work which has been carried out using the continuum limit of the ion contribution to the dispersion relation. The first such work was by Krasovitskii and Stepanov (6.47) who used a delta function distribution for the ions. The work of these authors actually preceded the apparently independent work of Rosenbluth and Post (6.1). However, in the former work the continuum limit was derived only for a delta function distribution. Hall and Heckrotte (6.21) have carried the work with delta function distributions somewhat further and in addition have used the continuum limit of the ion terms to discuss the high frequency instabilities of a two-component ion plasma when the electron contributions to the dispersion relation are negligible ($T_e/T_{\perp_i} > 1$). Also, as we

will discuss in more detail later, McCune and Fried (6.48) have used a delta function ion $v_\perp$ distribution to numerically calculate and compare the real-k temporal growth rates from the continuum limit and exact dispersion relations. Using the exact collisionally equilibriated loss-cone distributions, Post and Rosenbluth (6.12) have carried out very extensive numerical computations of the critical machine lengths as determined by the convective growth lengths predicted from the continuum limit of the dispersion relation. These results are quite optimistic in that they predict rather long critical machine lengths even for fairly dense plasmas. However, again we note that these conclusions are based upon the dubious procedure of deducing properties of the unstable modes for real frequencies where the continuum limit of the dispersion relation is not rigorously valid and that in contrast to the continuum limit predictions, serious absolute instabilities do appear. Brambilla and Schmidt (6.49) have also used the continuum limit form of the dispersion relation to do a marginal stability analysis of electrostatic instabilities of a plasma in which only a single species of plasma particles contribute to the dispersion relation (e.g. the ions if $T_e/T_i >> 1$). However, again we wonder if the results of such a study are to be believed since the marginal stability analysis relies upon evaluations of the dispersion relation for real frequencies and real wave-numbers, which is precisely where the continuum limit contributions are not rigorously valid.

As we have previously noted, Korablev (6.20) has also used the continuum limit to study electron-cyclotron instabilities of a two-component electron plasma with one component having a loss-cone type $v_\perp$ distribution.

In addition to the continuum limit of the ion contributions to the dispersion relation which we have derived above, there is another limit which can be derived by taking large $k_\perp a_i$ when $k_z = 0$. In this case we evaluate the Bessel functions in their asymptotic limit and set

$$J_n^2 (k_\perp v_\perp / \Omega_i) \simeq 2\Omega_i / (\pi k_\perp v_\perp) \quad . \tag{6.3.9}$$

Then, using the identity

$$\sum_{n=-\infty}^{\infty} \frac{1}{n-\omega/\Omega_i} = -\pi \cot(\pi \frac{\omega}{\Omega_i}) \quad , \tag{6.3.10}$$

we can write the ion contribution to the dispersion relation as

$$R_i \simeq \omega_{p_i}^2 \left(\pi \frac{\omega}{\Omega_i}\right) \cot \left(\pi \frac{\omega}{\Omega_i}\right) \int d^3v \, \frac{1}{v_\perp} \frac{dF_i}{dv_\perp} \quad . \tag{6.3.11}$$

Aamodt (6.50) has derived a more general continuum limit for our $\ell = 1$ $v_\perp$ distribution which includes both (6.3.6) and (6.3.11) and from which we can in principle derive higher order corrections to these two limiting cases. The limiting form given by (6.3.11) has been used by Post and Rosenbluth (6.12) to study flute-like modes which occur in a plasma which has both loss-cone and density inhomogeneity sources of free energy. In that work the approximate results were also compared with the results obtained from using the exact

dispersion relation. In general, Post and Rosenbluth (6.12) found agreement between the exact and approximate results as long as condition (6.3.1) was satisfied. We will discuss these flute-like instabilities in detail in Section 7.3. As we have previously noted, Pearlstein, Rosenbluth and Chang (6.13) have also used the limiting form of the ion term given by (6.3.11) to investigate flute-like instabilities in plasmas which have both hot and cold components of the same species of plasma particles, with the hot component having a loss-cone type $v_\perp$ distribution.

We will now investigate the applicability of the continuum limit of the ion contributions to the dispersion relation given by (6.3.6). We have already seen in the preceding section that in some ways it is applicable and is indeed very useful. This is because since condition (6.2.4) is directly derivable from (6.3.6), we see that the instability conditions given by (6.2.5), (6.2.6) and (6.2.7) are really based upon the "continuum" limit of the ion contributions to the dispersion relation. The latter instability conditions have of course been found to be quite adequate to predict the onset of convective instabilities for the cases we have considered. In fact, the results displayed in Fig. 6.3 are really a direct verification of the applicability of the continuum limit in predicting the value of $k_\perp$ for the onset of instabilities of a given frequency for the particular case of $T_e/T_i = 10^{-2}$, $\ell = 1$. However, it is important to note that

if, in contrast to the cases considered here, there are groups of ions in a plasma which have dissimilar velocity distributions along the magnetic field, then it is certainly not a priori obvious that we could reduce the exact necessary condition for instability (see Section 4.2) to the approximate result given by (6.2.4), with the ion distribution being simply the sum of the individual ion components. Rather, we would expect that it would be very important to take account of the differing velocity distributions of the ions along the magnetic field. Thus we conclude (more or less empirically) that the continuum limit of the ion contributions to the dispersion relation is quite applicable for calculations of parametric conditions for the onset of convective instabilities, at least for plasmas having only a single ion component.

In addition to the preceding discussion, we wish to see under what conditions inequality (6.3.3) can be satisfied and to what extent the loss-cone instabilities are of the absolute type as $k_\perp a_i$ becomes large. We have already noted that for the satisfaction of condition (6.3.3) we need to go to large $k_\perp a_i$. The question of how large $k_\perp a_i$ must be has been considered by McCune and Fried (6.48). Using a delta function ion $v_\perp$ distribution peaked about a nonzero velocity, these authors numerically compute the real-k temporal growth rates from both the continuum limit and exact dispersion relation and compare them. McCune and Fried (6.48) conclude that, for

any given $k_\perp a_i$ less than or equal to 20, merely increasing the plasma density does not bring the continuum limit results arbitrarily close to the exact results. Rather, they note that the continuum limit results are only moderately representative of the exact results when $k_\perp a_i$ is 20 even though the real-k temporal growth rates reach about $4\Omega_i$, but that the agreement would be better for larger values of $k_\perp a_i$. We thus observe that as far as the prediction of real-k temporal growth rates are concerned, it seems that condition (6.3.3) must be well satisfied in order for the continuum limit results to be reasonably correct.

With regard to the question of the occurence of absolute loss-cone instabilities, we have already found them for $k_\perp a_i$ values up to 8. Therefore the way in which we investigate the region of applicability in this regard is to ask how large we must make $k_\perp a_i$ so that the continuum limit applies (i.e. where there are no absolute instabilities). In this work we will take $k_\perp a_i = 25$ (the largest value our computer programs can conveniently handle) and investigate the applicability of the continuum limit of the dispersion relation. For this value of $k_\perp a_i$ the transverse wavelength is about ¼ of the ion Larmor radius and we would thus expect this case to closely approach the continuum limit. The plasma we consider will be that of our standard loss-cone case ($T_e/T_i = 10^{-2}$, $\ell = 1$). Using the methods described in Chapters 4 and 5, we obtain the marginal stability and absolute instability results displayed

in Fig. 6.14 (see also Table 7.3). The characteristics of the absolute instability modes shown in this figure are listed in Table 6.1.

Table 6.1. Properties of the "Marginally Stable" Absolute Instability Modes for $k_\perp a_i = 25$, Loss-Cone Instability Case ($T_e/T_i \cong 10^{-2}$, $\ell = 1$).

ω/Ω_i	$k_z a_i$	$\omega_{p_i}^2/\Omega_i^2$
0.9718	0.02321-0.009089i	275.5
1.944	0.04620-0.01808i	278.7
2.917	0.06876-0.02688i	286.5
3.890	0.09065-0.03538i	299.3
4.864	0.1117-0.04354i	317.4
5.840	0.1316-0.05122i	342.8
6.817	0.1503-0.05841i	376.8
7.797	0.1673-0.06497i	424.1
8.778	0.1827-0.07091i	489.0
9.762	0.1958-0.07603i	585.1
10.749	0.2066-0.08034i	731.5
11.740	0.2142-0.08353i	987.2
12.735	0.2184-0.08549i	1518.
13.736	0.2176-0.08559i	3373.
14.745	0.2109-0.08345i	∞
15.766	0.1939-0.07736i	∞
16.810	0.1574-0.06353i	∞

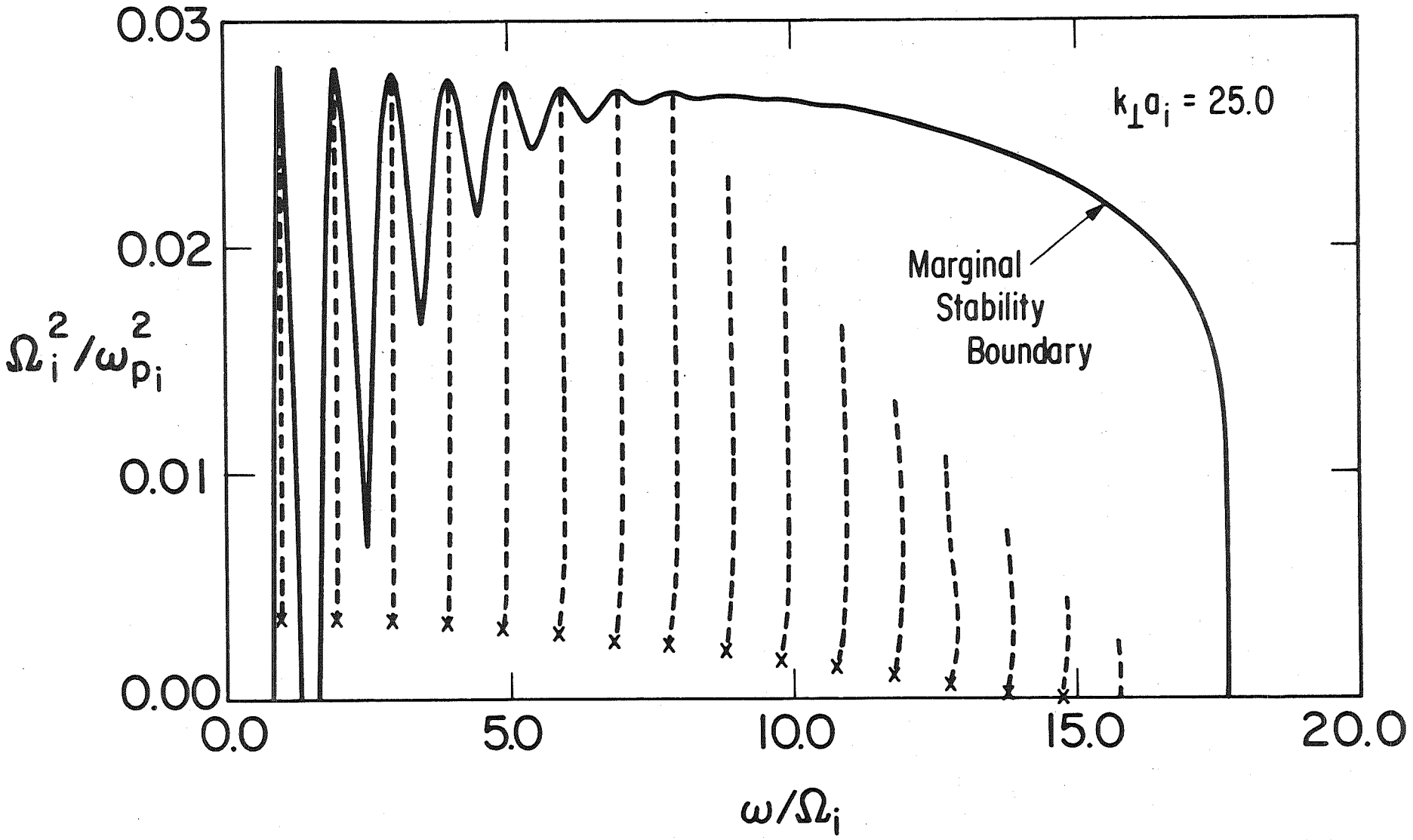

Figure 6.14. Stability Map for $k_\perp a_i = 25$ Loss-Cone Instability Case ($T_e/T_i = 10^{-2}$, $\ell=1$).

Figure 6.14 is plotted in the same manner as the $k_\perp a_i = 5$ case displayed in Figs. 4.8, 5.9 and comparing these two graphs we note many interesting similarities and differences. First, while for $k_\perp a_i = 5$ only wave frequencies up to $3.428\Omega_i$ may be unstable, for $k_\perp a_i = 25$ frequencies out to $17.66\Omega_i$ are unstable. The latter unstable frequency range is precisely that predicted by condition (6.2.5). Next, we note that in going from 5 to 25 in the value of $k_\perp a_i$, the threshold density for say the $\omega/\Omega_i \sim 1$ modes increases by a factor of about 34.2 which is roughly consistent with instability condition (6.1.11).

In the $k_\perp a_i = 25$ case, for densities exceeding the minimum threshold density but less than the lowest transition density, we see that the plasma is convectively unstable over a broad frequency range encompassing many cyclotron harmonic resonances, in apparent agreement with the continuum limit predictions. However, it is very important to observe that in the $k_\perp a_i = 25$ case, as in the $k_\perp a_i = 5$ case, absolute loss-cone instabilities do occur for sufficiently high plasma densities which is in contrast to the predictions of the continuum limit of the dispersion relation. The transition density for the appearance of these absolute instabilities increases by a factor of about 67.4 in going from 5 to 25 in the value of $k_\perp a_i$. In comparing this change with that in the threshold density, we see that the transition density is becoming proportionally larger than the threshold density as

we increase $k_\perp a_i$. An indication of this trend can also be seen from Fig. 6.4. Therefore we see that if we took sufficiently large $k_\perp a_i$, we could eventually reach a situation where the absolute instability transition densities would be many orders of magnitude above the convective instability threshold density. However, since we have increased $k_\perp a_i$ by a factor of 5 here and observed that the ratio of transition to threshold density increases by only a factor of about 2, in this regard the approach to the "continuum" limit (where there are only convective instabilities) seems to be very slow.

In spite of the apparent overlapping of cyclotron resonances shown in Fig. 6.14, there is still considerable ion cyclotron resonance structure even in the convectively unstable region. In Fig. 6.15 we plot the spatial growth rates versus real frequency for a density just below the minimum transition density. Here it is readily apparent that the first 15 ion cyclotron harmonic resonances are easily distinguishable, i.e. not overlapped. This observation coupled with the fact that the convectively unstable modes merge into the absolute instability modes near the $\mathrm{Im}(k_z)$ corresponding to the maximum spatial growth rate shows us why we still get many easily distinguishable absolute instability modes. One reason why the continuum limit results do not predict the appearance of absolute instabilities is that the fine structure in Fig. 6.15 is lost. The fine structure is due principally to

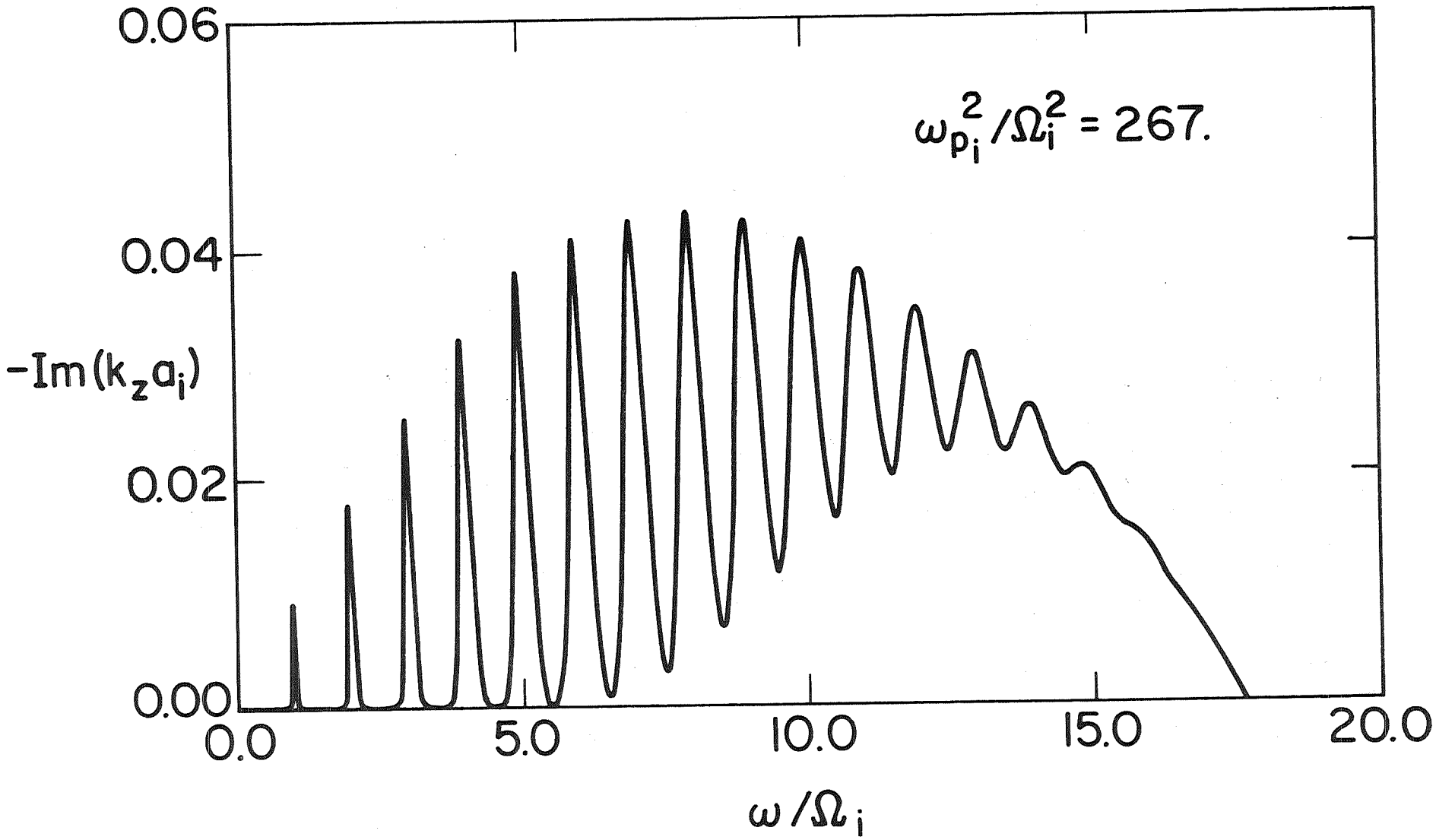

Figure 6.15. Spatial Growth Rates of Convective Loss-Cone Instabilities for $k_\perp a_i = 25$ ($T_e/T_i = 10^{-2}$).

the fact that for frequencies near harmonics of the ion cyclotron frequency, the wave resonates with the ion motions along the magnetic field (see Section 6.1). For the large $k_z a_i$ which occur near the threshold density (e.g. up to 1.26 in Fig. 6.14), these effects would of course be minimal due to the overlapping of many resonances. However, as we go to higher densities, we can see directly from the "fluid contribution" of the electrons (see Section 6.1) that the value of k_z for instability simultaneously decreases (see Fig. 6.16). Therefore as we observe here, eventually we reach a density at which we can easily distinguish the individual ion cyclotron harmonic resonances (see Fig. 6.15).

Next we compute the real-k_z temporal growth rates of the loss-cone instabilities for this $k_\perp a_i = 25$ case. The results obtained are shown in Fig. 6.16 for a density just below the lowest transition density for absolute instability, then densities which are factors of 2,4 and 8 higher and finally the case of infinite density. The last case is of course physically impossible and would definitely be a case in which we could not neglect the transverse electromagnetic waves (see Section 1.2). However, we include it here since it is the mathematical limiting case of our electrostatic dispersion relation. In Fig. 6.16 we immediately see that when $\mathrm{Im}(\omega)/\Omega_i < 1$ the ion cyclotron harmonic structure is distinguishable. (At large $k_z a_i$ and $\mathrm{Im}(\omega/\Omega_i) < 1$ the structure tends to disappear not due to

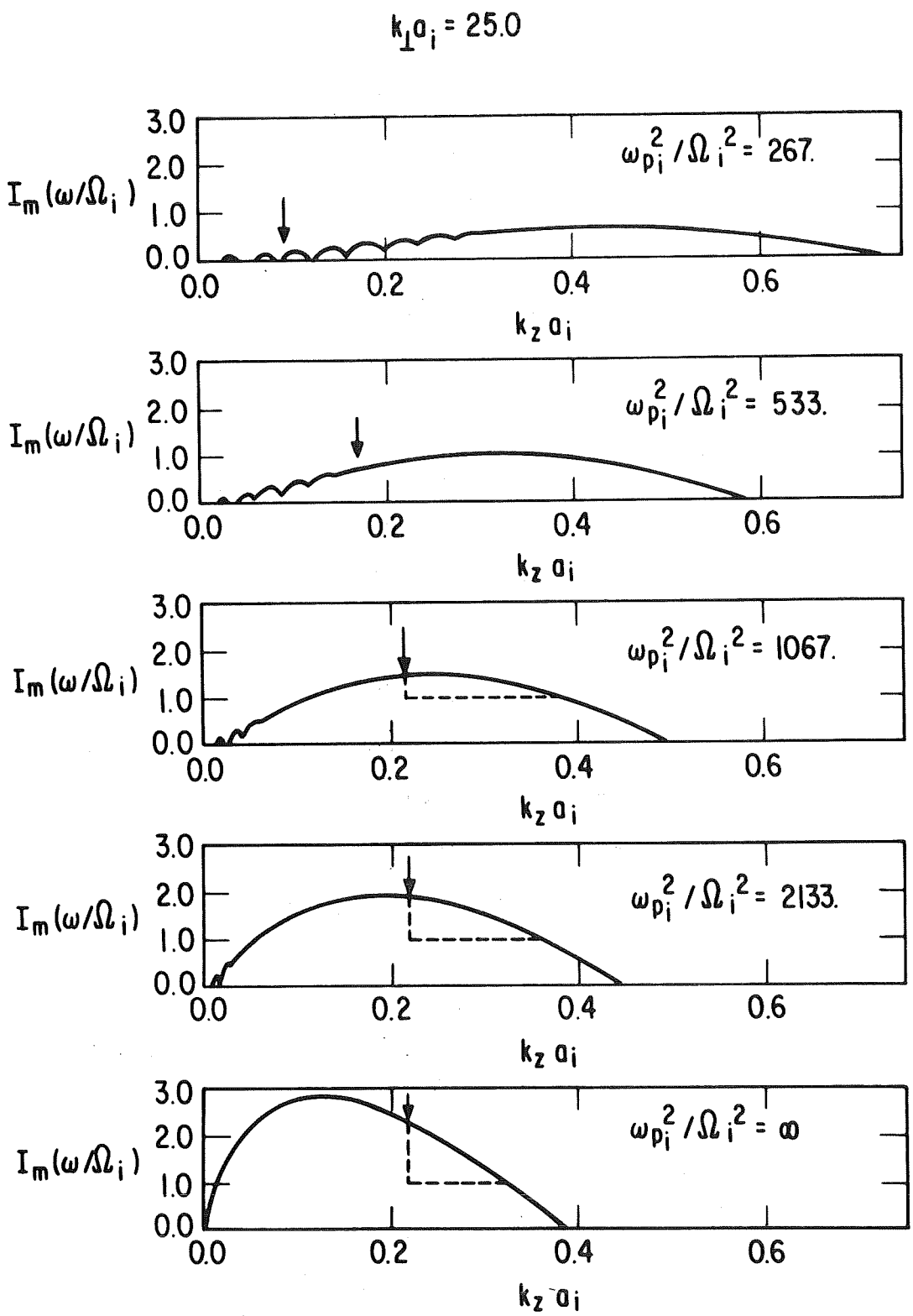

Figure 6.16. Real-k_Z Temporal Growth Rates of $k_\perp a_i=25$ Loss-Cone Instabilities ($T_e/T_i=10^{-2}$, $\ell=1$).

$\mathrm{Im}(\omega) > 0$, but rather due to the fact that the individual ion cyclotron resonances overlap because of the large $k_z v_z$ ion Doppler shifts.) However, for $\mathrm{Im}(\omega)/\Omega_i \gtrsim 1$ we see that the ion cyclotron harmonic structure disappears altogether in agreement with condition (6.3.3) and thus the continuum limit.

In Fig. 6.16 we have also indicated with an arrow the relevant value of $\mathrm{Re}(k_z a_i)$ for which an absolute instability occurs for each of the densities considered. Since any plasma which would admit unstable waves with $\mathrm{Re}(k_z a_i)$ less than those particular values would presumably admit the absolute instability modes as well, the arrows indicate the smallest value of $\mathrm{Re}(k_z a_i)$ for which the continuum limit can be applicable. Assuming then that, as we have previously discussed, the continuum limit is only applicable for $\mathrm{Im}(\omega) > \Omega_i$, we have denoted the resultant combined region of applicability with dashed lines in Fig. 6.16. Since these regions of applicability are relatively small, we conclude that at $k_\perp a_i = 25$ we still have not yet reached the regime of extensive applicability of the continuum limit.

We may summarize these results by ordering the set of approximate equalities given in (6.3.8) into a proper set of inequalities. In general we find that for modes with the largest real-k_z temporal growth rates

$$\mathrm{Im}(\omega) < k_z \alpha_{\perp i} \left(\frac{m_i}{m_e}\right)^{\frac{1}{2}} < \mathrm{Re}(\omega) < k_\perp \alpha_{\perp i} < \omega_{p_i} . \qquad (6.3.12)$$

The fact that $Im(\omega)$ is the smallest of all these quantities is indicative of the difficulty we have in reaching the continuum limit whose validity requires that $Im(\omega)$ be larger than Ω_i.

We will now discuss what effect changes in the parameters T_e/T_i and ℓ might have on the above results for the $k_\perp a_i = 25$ case. As we have seen in the preceding section, varying T_e/T_i changes the ranges of $k_z a_i$ for which convective instability can occur but has practically no effect on the absolute instabilities. Therefore for smaller T_e/T_i than that used here, the $k_z a_i$ ranges of instability in Fig. 6.16 would expand to somewhat larger values of $k_z a_i$. At the same time the arrows indicating the $Re(k_z a_i)$ values for the absolute instabilities would remain nearly unchanged. Similarly the maximum temporal growth rates would be nearly unaffected by changing T_e/T_i (electron Landau damping is nearly negligible for these instabilities at high densities). Therefore for values of T_e/T_i less than 10^{-2}, the region of applicability of the continuum limit would be expanded somewhat, mainly to larger $k_z a_i$. Conversely, we note by the same reasoning that if T_e/T_i is increased above 10^{-2} the range of applicability shrinks. Since most experimental plasmas are characterized by values of T_e/T_i larger than that of our "standard" case, our conclusions with respect to Fig. 6.16 are probably more optimistic about the applicability of the continuum limit than is actually the case in experimental plasmas of interest.

We expect that decreasing the thermal spread in the $v_\perp$ distribution by increasing ℓ will increase the temporal growth rates at any given density due to the fact that we are increasing the free energy of the plasma. We have already seen an indication of this in the preceding section where we found that decreasing the thermal spread led to increased absolute instability temporal growth rates at any given density. The fact that McCune and Fried (6.48) found real-k_z temporal growth rates which were slightly larger than ours for a smaller value of $k_\perp a_i$ is a consequence of their having used a delta function distribution as opposed to our well-thermalized loss-cone distribution. However, while decreasing the thermal spread does increase the real-k_z temporal growth rates of the unstable modes slightly, we note from Fig. 6.11 that it also increases the value of $\mathrm{Re}(k_z a_i)$ for the absolute instabilities. Finally, as we have previously discussed, increasing ℓ tends to accentuate the resonance of the waves with certain ranges of $k_\perp a_i$ and hence presumably it also accentuates the ion cyclotron resonance structure of the dispersion relation. We therefore conclude that as the thermal spread in the $v_\perp$ distribution decreases (ℓ increases), the range of extensive applicability of the continuum limit probably does increase, but not very substantially. With these remarks in mind, we see that the only way we can substantially increase the range of applicability of the continuum limit is to continue to increase $k_\perp a_i$, going beyond 25.

In summary, we note that in the $k_\perp a_i = 25$ case we see many characteristics of the continuum limit but apparently are as yet at too small a value of $k_\perp a_i$ for it to be completely valid. Since the general features of Figs. 6.14-6.16 are indicative of smoothly varying functions upon which a great deal of structure is imposed, the continuum limit may well be sufficient for doing very rough calculations of stability, nonlinear effects, etc. where the details of the ion contribution to the dispersion relation are relatively unimportant. However, at least for $k\, a_i \lesssim 25$ and $\omega_{p_i}^2/\Omega_i^2 \lesssim 10^3$, any detailed calculations of the loss-cone instabilities must certainly be carried out using the exact Harris dispersion relation and the role of absolute instabilities must be considered. Therefore while the continuum limit is derived from very appealing physical arguments and is very helpful in guiding our intuition and in doing approximate calculations, it does not seem to have a wide enough range of applicability for detailed instability calculations including the convective versus absolute nature of loss-cone instabilities. Indeed, perhaps the most surprising aspect of the results presented in this section is that even for the very large value of $k_\perp a_i$ of 25, we still appear to be relatively far from a region of extensive applicability of the continuum limit.

7. "UNIVERSAL" INSTABILITIES

7.1 Introduction; Low Frequency Drift Instabilities

In the preceding chapter we were concerned with instabilities driven by the free energy source associated with velocity-space anisotropies. These sources of free energy arise only in certain types of plasma confinement or plasma injection schemes, e.g. in magnetic mirror confinement or neutral beam injection methods respectively. A more general reservoir of free energy is that associated with the spatial inhomogeneity of a confined plasma. Instabilities driven by this source of free energy are loosely referred to as "universal" instabilities since they presumably occur in any confined plasma. However, as we shall later see, this is a misnomer because these instabilities can be prevented from occurring, or at least suppressed in many types of plasmas.

In this chapter we consider the two basic types of "universal" instabilities. First, in the present section we discuss the low frequency drift instabilities ($\omega << \Omega_i$) with the objectives being to give the essential features of these modes for later comparisons and to briefly review the work which has been done on them. In the following sections we investigate in detail the drift-cyclotron instabilities ($\omega \sim n\Omega_i$). These modes were first discussed by Mikhailovskii and Timofeev (7.1) and are very analogous to the velocity-space anisotropy instabilities (see Section 7.2). The previous work on drift-cyclotron instabilities is reviewed in Section 7.2. In the same section we compute the parametric regions of convective and absolute instability for the nonzero k_z drift-cyclotron

modes and compare them with the concomitant flute-like ($k_z=0$, $\omega \sim n\Omega_i$) modes. Those calculations are carried out for a Maxwellian velocity distribution. Then, having considered the loss-cone and drift-cyclotron instabilities separately, in the final section of this chapter we consider the instabilities which occur when the plasma has both velocity-space anisotropy (loss-cone) and density gradient sources of free energy.

In studying the electrostatic instabilities of an inhomogeneous plasma in a magnetic field, the basic starting point is the dispersion relation given by (3.3.15) with the normally small $(n-m)/k_y$ terms (see Section 3.3) neglected, in which case the m summation is trivial and we obtain simply

$$k^2 = \sum_j \omega_{Pj}^2 \int d^3v \sum_{n=-\infty}^{\infty} \frac{J_n^2(k_y v_\perp/\Omega_j)}{k_z v_z + n\Omega_j - k_y G_j/\Omega_j - \omega} \left\{ k_z \frac{\partial F_j}{\partial v_z} + \left(\frac{n\Omega_j}{v_\perp} - \frac{k_y G_j}{v_\perp \Omega_j} \right) \frac{\partial F_j}{\partial v_\perp} + \frac{k_y F_j}{\Omega_j} \frac{\partial q_j}{\partial x} \right\}_{x=0.} \tag{7.1.1}$$

In this work the $(n-m)/k_y$ terms are retained in the numerical computations, but we will ignore them for the purposes of the present discussion. In addition to ignoring these small terms, when the gravity terms are relevant, it is customary (7.2, 7.3) to consider only those cases for which

$$k_y G_j/\Omega_j^2 \ll 1. \tag{7.1.2}$$

The reason for restricting oneself to such small gravity forces and/or long transverse wavelengths is that the dispersion relation is normally derived under this assumption. In the dispersion relation thus derived (7.2, 7.3), the m summation over Bessel functions in (3.3.15) is replaced by unity and m set to zero, i.e.

(7.1.1) is obtained. However, in our own work we have derived precisely the same dispersion relation without assuming that condition (7.1.2) is satisfied. Therefore what we have found is that as long as the $(n-m)/k_y$ terms are negligible, it is not necessary to satisfy condition (7.1.2) in order for the dispersion relation given by (7.1.1) to be valid. As we have noted in Section 3.3, if the $(n-m)/k_y$ terms are not negligible, our density gradient expansion breaks down and we must seek alternative forms of the dispersion relation. Thus, within the limitations of this work (i.e. when the density gradient expansion does not break down), the dispersion relation given by (7.1.1) is valid whether or not condition (7.1.2) is satisfied.

The basic source of free energy driving the "universal" instabilities is of course the inhomogeneity of the plasma. As we have seen in Sections 2.3 and 2.4, in order for an equilibrium to exist the inhomogeneity of the confining magnetic field must be balanced by the magnetic field produced by a diamagnetic current flowing in the inhomogeneous plasma. The diamagnetic current is produced by net or macroscopic "drift" velocities of each of the species of plasma particles which are given by

$$V_{D_j} = \int d^3v \; v_y \langle f_j \rangle_{x \simeq 0}$$

$$= \frac{1}{2} a_j \left[\frac{1}{n_j} \frac{dn_j}{dx} - \frac{1}{(\ell+1)} \frac{1}{T_{\perp_j}} \frac{dT_{\perp_j}}{dx} - \frac{1}{(\ell+1)} \frac{2G_j}{\alpha^2_{\perp_j}} \right] \alpha_{\perp_j} . \tag{7.1.3}$$

Note that the drifts are in opposite directions for oppositely charged species of particles. The way in which we expect to be able to release the free energy of inhomogeneous plasmas is through

waves which resonate with particles in the "positive-slope" regions of the effective velocity distributions having the net drift velocities given by (7.1.3), i.e.

$$0 < \omega/k_y < V_{D_j} \quad , \quad V_{D_j} > 0,$$

$$0 > \omega/k_y > V_{D_j} \quad , \quad V_{D_j} < 0. \qquad (7.1.4)$$

That the waves in these phase velocity regions are the only ones which can be unstable is easily shown from a consideration of the necessary condition for instability, i.e. $P(\omega/\Omega_i)$ (see below). These waves which resonate with the drift velocities in the plasma and hence are potentially unstable are usually referred to as drift waves. A number of the physical mechanisms by which these drift waves can become unstable are discussed by Chen (7.4).

For frequencies much smaller than the ion cyclotron frequency ($\omega << \Omega_i$), the instabilities resulting from coupling of the potentially unstable drift waves with particle motions along the magnetic field are commonly called drift instabilities. From (7.1.4) and (7.1.3) we immediately see that the phase velocities and presumably also the group velocities transverse to the magnetic field direction are usually much less than the ion thermal velocity and hence quite small. Since the drift waves usually couple to ion waves along the magnetic field (see below), the phase velocities along the magnetic field are typically somewhat larger than the mean ion velocity along the magnetic field, but less than the mean electron velocity in the same direction. Therefore their phase velocities and also presumably their group velocities along the magnetic field are much less than those encountered in the velocity-space anisotropy instabilities discussed in the

preceding chapter. The group velocities of the low frequency drift instabilities are thus presumably "small" in both directions of propagation. For such small group velocity cases, we have previously noted (Sections 5.1, 6.1) that the distinctions between convective and absolute instabilities can be investigated on the basis of a real-k analysis and their convective versus absolute nature ignored. This conjecture should of course be checked by detailed numerical computations of the convective versus absolute nature of the instabilities including a consideration of the group velocities of the unstable modes in both directions of propagation. However, in this work this will not be done for the low frequency drift instabilities. Rather, we content ourselves with a brief discussion of the parametric regions of instability for these modes.

For $k_z=0$ and the standard hydrodynamic approximations ($k_y a_i = k a_i \to 0$), the drift instabilities become flute or hydrodynamic interchange instabilities (7.5). This particular type of mode is essentially the well-known Rayleigh-Taylor instability, requiring both a density gradient and an unfavorable gravity (or curvature). This is in contrast to the low-frequency "drift modes" described above (and in more detail below) which exist and can be unstable even with $G_j=0$ (7.6). As we have previously noted, by the term flute instabilities we mean those instabilities which have $k_z=0$ and $\mathrm{Re}(\omega)$ very, very small if not zero. A direct derivation of the flute or hydrodynamic interchange instability from dispersion relation (7.1.1) is given by Rosenbluth (7.6). A major contribution to the theory of flute instabilities was made by Rosenbluth, Krall and Rostoker (7.7) who discussed the finite ion Larmor radius ($k_y a_i$ small, but nonzero) stabilization effects for relatively dense

plasmas ($\omega_{pi}^2 >> \Omega_i^2$). A comprehensive review of work on flute instabilities for arbitrary $k_y a_i$ is given by Mikhailovskii (7.8).

In this work we are assuming that the hydromagnetic interchange and also presumably all flute modes have been stabilized by some appropriate confinement scheme (Section 1.1). Therefore any low frequency ($\omega << \Omega_i$) instabilities which remain have nonzero k_z and a description of them must include the dynamics of the particle motions along the magnetic field. The earliest work on low frequency drift instabilities with nonzero k_z was done by Tserkovnikov (7.9) and Rudakov and Sagdeev (7.10, 7.11). More extensive studies have been carried out by Kadomtsev and Timofeev (7.12), Galeev, Oraevskii and Sagdeev (7.13) and Krall and Rosenbluth (7.2). Early comprehensive reviews of work on drift instabilities were made by Mikhailovskii (7.8), Kadomtsev (7.14), Rukhadze and Silin (7.15), and Hoh (7.16). A very useful discussion of the types of instabilities obtained from dispersion relation (7.1.1) has been given by Rosenbluth (7.6).

Here we will only discuss some rudimentary facts about these low frequency drift instabilities. In order to do so, we will consider the necessary condition for instability (see Section 4.2), i.e. $P(u)$ or as we will label it here, $P(\omega)$. For frequencies much less than the ion cyclotron frequency, only the n=0 terms in both the ion and electron Bessel function summations contribute significantly to $P(\omega)$ since the low frequency plane waves do not couple appreciably to the cyclotron orbit motions. Thus, assuming a Maxwellian, isothermal ($T_e = T_i$) plasma, we find that (4.2.3) can be reduced to

$$P(\omega) = -\frac{\Omega_i^2}{k^2}\left(\frac{k_y}{k}\right)\left\{(\omega/k_y - V_{D_e})\, e^{-(\omega/k_z\alpha_e)^2}\right.$$

$$\left. + (\omega/k_y - V_{D_i})\, e^{-(\omega/k_z\alpha_i)^2}\, I_0(\lambda_i) e^{-\lambda_i}\right\} \qquad (7.1.5)$$

where as in Section 3.4,

$$\lambda_i \equiv (k_y a_i)^2/2$$

and in which we have assumed that $k_y a_e << 1$. The first term in braces in this expression gives the electron contribution while the second gives the ion contribution. Note that since we have assumed that $T_e = T_i$, the electron and ion drift velocities (V_{D_e}, V_{D_i} respectively) are equal in magnitude although opposite in sign. We recall from Section 4.2 that in order for instability to be possible, $P(\omega)$ must have more than one zero. Thus, we see that the ion or electron contributions are not destabilizing by themselves, although the combination of them may be. Note also that, in general, only those phase velocities in the "positive-slope" regions of the effective velocity distribution transverse to the magnetic field direction (see (7.1.4)) can lead to destabilizing contributions to the dispersion relation. In fact, since the mean electron velocity α_e is much larger than the mean ion velocity α_i, it is easy to see that the only waves which can be unstable are those for which ω/k_y is of the same sign, but smaller in magnitude than V_{D_e}, i.e. those which propagate in the direction of the electron drifts and hence opposite to the direction of the diamagnetic current. Thus, these particular drift instabilities are often referred to as electron-drift instabilities.

We also note from (7.1.5) that for large $\omega/k_z\alpha_e$ (i.e. large phase velocities along the magnetic field compared to the electron

thermal velocity), $P(\omega)$ becomes very small and hence the instability, even if it occurs, would be expected to have a small temporal growth rate (7.17). On the other hand, for small $\omega/k_z\alpha_i$ (i.e. small phase velocities along the magnetic field compared to the ion thermal velocity), the exponential factors approach unity and the destabilizing drift terms cancel. Therefore the electron-drift instability is most dangerous for

$$\alpha_i < \omega/k_z < \alpha_e \,. \qquad (7.1.6)$$

The properties of the electron-drift instabilities which we have discussed above are illustrated graphically in Fig. 7.1 in which we have plotted a typical pair of Nyquist and $P(\omega/\Omega_i)$ curves. Comparing the plots in Fig. 7.1 with the corresponding ones for the temperature-anisotropy, loss-cone and drift-cyclotron instabilities (Figs. 4.4, 4.6, and 7.4 respectively), we find few if any similarities, a result which is indicative of the intrinsic differences in the instability mechanisms. Here, as usual, the slowly varying function of ω in the $P(\omega/\Omega_i)$ plot represents the electron contributions to the dispersion relation while the rapidly varying part represents the ion contributions. In the Nyquist plot the dashed lines indicate where the curve would go in the absence of cyclotron damping near harmonics of the ion cyclotron frequency. These cyclotron damping contributions are much larger in magnitude and cannot be plotted on the scale used in Fig. 7.1. In Fig. 7.1a, the small heart-shaped curve near the origin is, as usual, the electron contribution. Here it is distorted slightly due to the electron diamagnetic drift. From Fig. 7.1 we see that the unstable

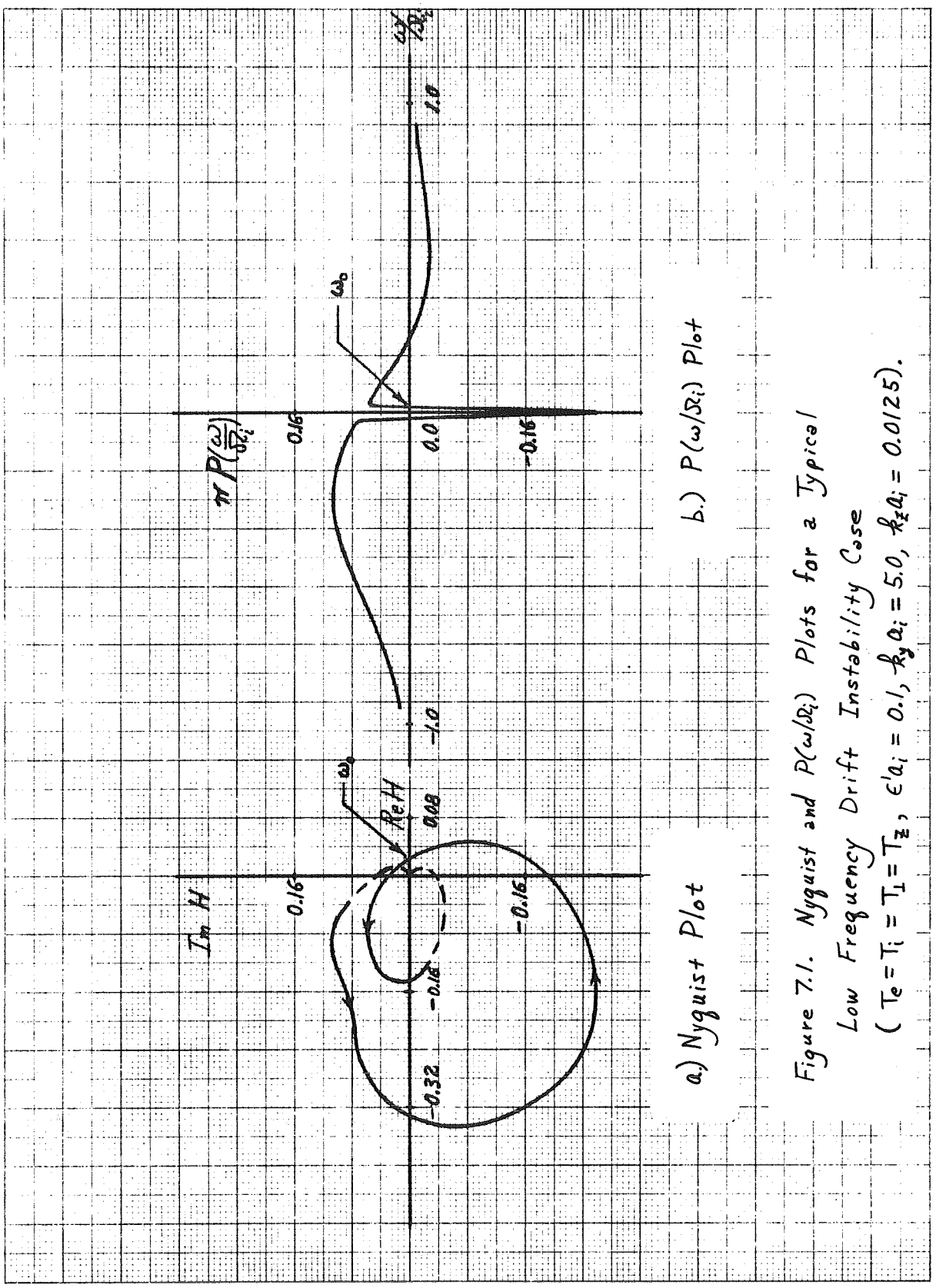

a.) Nyquist Plot

b.) $P(\omega/\Omega_i)$ Plot

Figure 7.1. Nyquist and $P(\omega/\Omega_i)$ Plots for a Typical Low Frequency Drift Instability Case
($T_e = T_i = T_\perp = T_z$, $\epsilon' a_i = 0.1$, $k_y a_i = 5.0$, $k_z a_i = 0.0125$).

modes (those near ω_0) have positive frequencies and recalling the definitions given by (7.1.3) and (2.2.7), we see that they do propagate in the direction of the electron diamagnetic drift velocity. In Fig. 7.1 it is readily apparent that the unstable modes lie within the range specified by (7.1.6).

If we combine the left most of the conditions in (7.1.6) with the condition given by (7.1.4) (for the electrons), we see that the k_z for which instability can occur is limited by

$$k_z < \frac{k_y V_{D_e}}{\alpha_i} \qquad \text{(instability)}. \quad (7.1.7)$$

In the limit of large k_y, this condition implies that k_z is unlimited in magnitude. However, from (7.1.5) we note that as k_y becomes large, the ion term becomes small due to the reduction in magnitude of the Bessel function coefficient $I_0(\lambda_i)e^{-\lambda_i}$. Taking this reduction into account and also considering the limitations of the sufficiency condition for instability, the fundamental frequency of the drift oscillations, $k_y V_{D_e}$ (see (7.1.4)), becomes multiplied by a factor of (7.14)

$$\frac{I_0(\lambda_i)e^{-\lambda_i}}{2-I_0(\lambda_i)e^{-\lambda_i}} .$$

Physically this correction to the fundamental drift frequency is due to the averaging of the wave field over the ion Larmor radius (7.14). Using this finite Larmor radius correction and evaluating the Bessel function in the limit of large $k_y a_i$, we find that drift instabilities occur only if

$$(k_z a_i) < \frac{1}{4\sqrt{\pi}} \left(\frac{a_i}{n_i} \frac{dn_i}{dx} \right) \qquad \text{(instability)}.$$

This approximate result has been noted by Rosenbluth (7.6).

The variation of k_z for which instability occurs for varying $k_y a_i$, $T_\perp$, T_z, T_e, T_i and plasma density has been considered in detail by Krall and Rosenbluth (7.2). They find that if

$$(k_z a_i) < \frac{\pi}{20.6}\left(\frac{a_i}{n_i}\frac{dn_i}{dx}\right)\left(\frac{T_{\perp_i}}{T_{z_i}}\right)^{1/2} 2\left(1 + \frac{T_{\perp_i}}{T_{z_e}} + \frac{(ka_i)^2}{2}\frac{\Omega_i^2}{\omega_{p_i}^2}\frac{T_{\perp_i}}{T_{z_i}}\right)^{-1}$$

(instability) (7.1.8)

instability can occur, generally for values of $k_y a_i$ significantly in excess of unity. The effect of varying $k_y a_i$ is displayed graphically by these authors. Imposing the condition that the plasma be at least a half wavelength in length for the unstable mode to occur, Krall and Rosenbluth (7.2) note that a given plasma will be stable against these low frequency electron-drift instabilities if

$$L < 20.6\left(\frac{1}{n_i}\frac{dn_i}{dx}\right)^{-1}\frac{1}{2}\left(1 + \frac{T_{\perp_i}}{T_{z_e}} + \frac{(ka_i)^2}{2}\frac{\Omega_i^2}{\omega_{p_i}^2}\frac{T_{\perp_i}}{T_{z_i}}\right)\left(\frac{T_{z_i}}{T_{\perp_i}}\right)^{1/2}$$

(stability) (7.1.9)

in which L is the axial length of the plasma.

For a particular case ($T_e=T_i=T_\perp=T_z$, $\ell=0$, $\varepsilon' a_i = 0.1$, $k_y a_i = 5.0$) we have investigated the variation of $k_z a_i$ with plasma density ($\omega_{p_i}^2/\Omega_i^2$) for the marginally stable modes and found the results to agree with condition (7.1.8) to within about 5%. The slight discrepancy is in the appropriate direction for the noninfinite value

of $k_y a_i$ considered here and presumably is due solely to this effect. We therefore conclude that our results confirm the plasma density dependence of instability condition (7.1.8).

The preceding remarks have applied only to density gradient driven instabilities and even among those only to the ones whose phase velocities along the magnetic field lie within the range given in (7.1.6). The effects which temperature gradients, a "cold" component added to a "hot" plasma and currents along the magnetic field have on these instabilities have been discussed by Krall and Rosenbluth (7.2). The temperature gradient drift instabilities were first considered by Mikhailovskaya and Mikhailovskii (7.18). The work on drift instabilities in the presence of a current flowing along the magnetic field has been reviewed by Mikhailovskii (7.19). For all these different types of low frequency drift instabilities, a condition similar to (7.1.8) remains applicable (7.2).

It is of interest to compare the critical lengths for which the low frequency drift instabilities can occur with those obtained in chapter six for the velocity-space anisotropy instabilities. This can be done by making a comparison of conditions (7.1.8) and (6.1.10). For $m_i/m_e=1836$, condition (6.1.10) can be written approximately as

$$(k_z a_i) \lesssim \frac{n}{100}\left(\frac{T_{\perp i}}{T_e}\right)^{1/2} \quad \text{(instability)}. \qquad (7.1.10)$$

We recall that the general dispersion relation was derived under the assumption that the characteristic inhomogeneity length is much larger than an ion Larmor radius, i.e.

$$\frac{a_i}{n_i}\frac{dn_i}{dx} \ll 1 . \qquad (7.1.11)$$

Therefore, upon comparing conditions (7.1.8) and (7.1.10) (for $T_e/T_{z_i} \lesssim 1$, since conditions (6.1.10) and (7.1.10) are only applicable for these values of T_e), we see that the two are comparable only when $T_{\perp_i}/T_{z_i} \sim 1$, $T_{\perp_i}/T_e \sim 1$ and even then only for the n=1 velocity-space anisotropy modes. (We have also found in chapter six that the value of $\mathrm{Re}(k_z a_i)$ for which absolute instability occurs is smaller than that given by condition (7.1.10). However, for $T_e/T_{\perp_i} \sim 1$ the difference is very slight.) For smaller electron temperatures ($T_e/T_{\perp_i} \lesssim 1$) or a higher harmonic number n, the low frequency drift instabilities only occur for smaller k_z and hence only in longer plasma machines than the velocity-space anisotropy instabilities. Therefore we conclude that in most open-ended confinement devices (e.g. magnetic mirror machines) which have loss-cone or other velocity-space anisotropy sources of free energy, as long as the plasma inhomogeneity is sufficiently gentle to satisfy condition (7.1.11), the velocity-space anisotropy instabilities will be the more dangerous ones in limiting plasma containment. For confinement schemes which have closed field lines (e.g. stellerators) in which there is no prominent loss-cone source of free energy, as long as the temperatures along and transverse to the magnetic field lines are nearly equal (see(6.1.15)), the low-frequency drift instabilities will presumably be the most detrimental to plasma containment. However, in principle the latter instabilities may be stabilized by a number of means which we will now discuss.

In general what is found in all studies of the low frequency drift instabilities satisfying condition (7.1.6) is that for

instability, k_z must be very small as indicated by condition (7.1.8). Since k_z is thus much smaller than k_y for instability, any "uncertainty" in k_z caused by a sheared magnetic field would presumably stabilize the instability (see (7.8)). Many authors have considered this effect and a short review of that work and the limitations of these simple concepts is given by Rutherford and Frieman (7.20). Another subject of considerable interest in this regard are the recent demonstrations (7.21-7.23) that the temperature-gradient-driven drift instabilities are relatively unaffected by a sheared magnetic field structure. Similarly it has been noted (7.24) that a drift instability due to impurity ions is not influenced by shear.

Another possible stabilizing effect on the drift instabilities is that of collisions, due to the fact that the drift frequency is so small. The earliest considerations of collisional drift instabilities have been reviewed by Kadomtsev (7.14). The most recent work has been done by Mikhailovskii and Pogutse (7.25) who develop the dispersion relation using the BGK collision model (7.26), by Hendel et al. (7.27) and by Jukes (7.23) who considers the effects of collisions on the temperature-gradient-driven drift instability in the presence of a sheared magnetic field structure.

For plasma densities large enough to give collision frequencies of the order of the drift frequency, the parameter β of the plasma may be larger than that specified by (1.2.24). In this case the electron thermal velocity may become comparable with the Alfvén speed (7.8) and transverse electromagnetic waves must be considered (see Section 1.2). The first work on transverse wave-low frequency drift

modes was carried out by Mikhailovskii and Rudakov (7.28) who found that a sufficiently high value of β (still less than unity) stabilizes the plasma against drift modes and by Krall and Rosenbluth (7.29). These and other studies of transverse modes are surveyed by Mikhailovskii (7.8), Kadomtsev (7.14), Rukhadze and Silin (7.15) and Galeev, Moiseev and Sagdeev (7.30).

A quite different means of stabilizing the drift instabilities is through favorable curvature in the confining magnetic field structure. This stabilization has been considered by Krall and Rosenbluth (7.2). As we have discussed in Section 2.4, the magnetic field curvature can be represented to a limited degree by the gravity force. Representing the curvature in this way, we see immediately from (7.1.3) that the effect of the curvature is to modify the drift velocities in the plasma. Since the drifts constitute the source of free energy driving the instability, the direction of favorable curvature is that for which the effective drift velocities are reduced. This favorable curvature direction is also synonymous with that for the stabilization of the hydrodynamic interchange instabilities (7.2). In addition to this rudimentary consideration of the stabilization due to magnetic field curvature, Laval et al. (7.31) have considered the effects in more detail by accounting for the fact that the curvature affects particles of dissimilar velocities slightly differently (see equation preceding (2.4.11)). This velocity dispersion effect on the constant "gravity" commonly used to represent magnetic field curvature effects was found to dramatically improve the stabilization of the drift instabilities for favorable curvature situations (7.31).

The nonlinear stabilization of low frequency drift instabilities has been the subject of many studies. The literature concerning this work is very extensive and we will not attempt to survey it here. An early introduction to the nonlinear work is contained in Kadomtsev's book (7.14). The various types of nonlinear limiting mechanisms are discussed and appropriate references noted in Section 5.4.

The experimental observations of drift instabilities have recently been reviewed by Lehnert (7.32). In that review Lehnert notes that no experimental evidence of shear stabilization of drift waves has been found. Very recently Grove et al. (7.33) have demonstrated that, at least for the small amounts of shear presently available in the C-stellarator, a collisionless plasma is stabilized somewhat by the introduction of magnetic field shear. In addition, very good agreement between theory and experiment has recently been reported by Hendel et al. (7.27) for a drift instability in which collisions are important.

Finally in our discussion of low frequency drift instabilities, we should mention a class of modes whose phase velocities along the magnetic field do not satisfy condition (7.1.6). Rather, these modes satisfy the condition

$$\omega/k_z << \alpha_{z_i}, \alpha_{z_e}$$

and are thus typically very low frequency instabilities having axial wavelengths shorter than those satisfying condition (7.1.8). They can therefore occur in plasmas which are shorter than those admitting the low frequency drift instabilities we have previously discussed. However, as observed by Galeev et al. (7.13) and Kogan and Moiseev

(7.34), their appearance in an inhomogeneous plasma in a nearly uniform magnetic field requires the satisfaction of rather special and unlikely conditions, e.g. that the ratio of temperature to density gradient satisfy the condition

$$\frac{d\ell nT_i}{d\ell nn_i} > 2 \qquad \text{(instability)}.$$

When a varying magnetic field curvature is considered, Coppi et al. (7.35) have shown that drift modes can be localized in unfavorable curvature regions and be unstable under less stringent conditions than those given above. Coppi, Rosenbluth and Yoshikawa (7.36) have discussed the localized ("ballooning") modes which arise in multipole configurations and which include drift modes localized in the regions of unfavorable curvature. In addition, Kadomtsev and Pogutse (7.37) and Rosenbluth (7.38) have discussed flute instabilities which can occur due to the trapping of particles in the unfavorable curvature regions between local magnetic mirrors in complex magnetic field geometries. The latter instabilities are referred to as "trapped particle" instabilities. Finally, we should note that presently there are in progress many investigations of low frequency drift and flute or trapped particle instabilities in very general magnetic field configurations (7.39-7.42).

7.2 Drift-Cyclotron Instabilities

Having briefly reviewed the dominant features of the low frequency drift instabilities, we will now discuss the so-called drift-cyclotron instabilities (7.1) in much greater detail. In this section we restrict our consideration of the drift-cyclotron instabilities to those which occur in a spatially inhomogeneous plasma (density gradients only) which has a Maxwellian velocity distribution with equal temperatures along and transverse to the magnetic field direction. We defer a discussion of the high frequency ($\omega \sim n\Omega_i$) instabilities that occur in a plasma which has both loss-cone and density gradient sources of free energy to the next section.

The appropriate dispersion relation for studying the drift-cyclotron instabilities is that given by (7.1.1) with the gravity term omitted:

$$k^2 = \sum_j \omega_{p_j}^2 \int d^3v \sum_{n=-\infty}^{\infty} \frac{J_n^2(k_\perp v_\perp/\Omega_j)}{k_z v_z + n\Omega_j - \omega}$$

$$\times \left\{ k_z \frac{\partial F_j}{\partial v_z} + \frac{n\Omega_j}{v_\perp} \frac{\partial F_j}{\partial v_\perp} + \frac{k_y F_j}{\Omega_j} \frac{\partial q_j}{\partial x} \right\}_{\chi \simeq 0}.$$

(7.2.1)

While in omitting the gravity term we omit all consideration of magnetic field curvature effects, later in this section we review other studies of these effects which have been carried out. As in the calculations carried out in Chapter 6, we will only consider the convective versus absolute nature of the unstable modes in the z or magnetic field direction. As long as $T_e < T_{z_i}$, we will find that, as with the velocity-space anisotropy modes, in the z or axial direction the drift-cyclotron modes typically have phase velocities much larger than the electron thermal velocity and hence the distinctions between absolute and convective modes in this direction will be expected to be important. For the drift-cyclotron instabilities, we will also find (see(7.2.14)) that the phase velocity of the unstable modes transverse to the magnetic field must always be considerably less than that given by (6.2.5) for the loss-cone instabilities and certainly less than the ion thermal velocity. Therefore, our arguments in Section 6.1 for

neglecting the absolute versus convective nature of the instabilities in the y direction would seem to be even better justified for the drift-cyclotron instabilities. Assuming these arguments to be valid, we need only consider solutions of the dispersion relation for real k_y. However, as usual we consider k_z and ω to be complex in general. With these assumptions, we have previously seen from a consideration of the symmetry properties of the general dispersion relation (see Section 3.3) that we need only consider positive k_y and values of k_z having positive real parts, but real parts of ω of either sign.

Carrying out the indicated integrations in the dispersion relation given by (7.2.1) for the plasma model of interest here, we obtain the dispersion relation given by (3.3.16) and (3.4.3) with the n/k_y, gravity and temperature gradient terms omitted and the variables V_{0_j} set to zero. Making the same approximations in the electron contributions to the dispersion relation as we did in Section 6.1 (namely $\omega_{p_e}^2 < \Omega_e^2$, $k_\perp a_e << 1$, $T_e < T_{z_i}$) and making the further assumption that $T_{\perp_i} = T_{z_i}$, we may write the resultant dispersion relation as

$$\frac{\Omega_i^2}{\omega_{p_i}^2} = \frac{m_i}{m_e}\frac{(k_z a_i)^2}{(k a_i)^2}\left(\frac{\Omega_i}{\omega}\right)^2 + \frac{k_y a_i}{(k a_i)^2}\frac{(\epsilon' a_i)}{(\omega/\Omega_i)} + \frac{i\sqrt{\pi}}{(k a_i)^2}\frac{T_i}{T_e}\left[\zeta - \frac{(k_y a_i)}{(k_z a_i)}(\epsilon' a_i)\sqrt{\frac{T_e}{T_i}\frac{m_e}{m_i}}\right] e^{-\zeta^2}$$

$$- \frac{2}{(k a_i)^2}\sum_{n=-\infty}^{\infty} \Gamma_n^0(\lambda_i)\left[Z_1(w_n) + \frac{Z_0(w_n)}{(k_z a_i)}\left(n + \frac{(\epsilon' a_i)(k_y a_i)}{2}\right)\right] \qquad (7.2.2)$$

where

$$\zeta = \frac{(\omega/\Omega_i)}{(k_z a_i)}\sqrt{\frac{T_i}{T_e}\frac{m_e}{m_i}} \; ; \qquad w_n = \frac{(\omega/\Omega_i) - n}{(k_z a_i)} \; ; \qquad \lambda_i = (k_y a_i)^2/2 .$$

Here the first two terms on the right give the fluid model contributions of the electrons with the second of these representing the effect of the electron density gradient. Similarly the two terms enclosed in the first set of brackets account for the coupling of the wave with electron motions along the magnetic field in which the dominant contribution comes from the electron Landau damping term (the first term). Finally, the terms summed over n give the ion contributions to the dispersion relation. The latter terms account for the free energy which drives the drift-cyclotron instabilities (see below). As with the velocity-space anisotropy instabilities, in order for waves to interact strongly with the particles and tap this source of free energy, their frequency must be near a multiple of the cyclotron frequency, i.e.

$$\omega \sim n\Omega_i \quad . \tag{7.2.3}$$

The drift-cyclotron instabilities were first studied by Mikhailovskii and Timofeev (7.1) who showed that both flute-like ($k_z = 0$) and "convective" ($k_z \neq 0$) modes can be unstable. The term "convective" here is used to imply motion of the wave along the magnetic field and is common in the Russian literature. It does not necessarily imply that the mode is of the convective type in the sense of our discussion in chapter five and so in order to avoid confusion we will refrain from further use of the word "convective" to describe modes with nonzero k_z. A very extensive study of the drift-cyclotron instabilities under varying plasma conditions has been carried out by Mikhailovskii (7.43). Very brief discussions of the general features of the drift-cyclotron instabilities can be

found in the review works by Kadomtsev (7.14), Mikhailovskii (7.8) and Rosenbluth (7.6).

Taking the $k_z = 0$ limit of dispersion relation (7.2.2) and adding the term m_e/m_i to the left of the resultant equation to account for the lowest order $n \neq 0$ electron contributions to the exact electrostatic dispersion relation, the flute-like modes can be shown to be unstable only if (see (7.1, 7.6), or use the instability criterion given in Section 4.2 for such cases)

$$|\varepsilon' a_i| > 2n \left[\frac{m_e}{m_i} + \frac{\Omega_i^2}{\omega_{p_i}^2}\right]^{1/2} \qquad \text{(instability)} .$$

For a plasma of sufficiently low density so that $\omega_{p_e}^2 < \Omega_e^2$ * this criterion can be reduced to

$$\frac{\omega_{p_i}^2}{\Omega_i^2} > \frac{4n^2}{(\varepsilon' a_i)^2} \qquad \text{(instability)} . \quad (7.2.4)$$

In our numerical calculations of the threshold density for the flute-like drift-cyclotron instabilities (see below) in which we retain the exact electron contributions to the electrostatic dispersion relation, we find this latter criterion to be quite adequate for estimating the threshold density.

Next, we will discuss the drift-cyclotron instabilities having nonzero k_z. Owing to the similarity of the dispersion relation

*If this condition is not satisfied, then it is not a priori obvious that the plasma will have a sufficiently low value of β to warrant our neglect of transverse electromagnetic waves (see Section 1.2).

given by (7.2.2) to that studied in connection with the velocity-space anisotropy instabilities -- (6.1.6), we will follow the same general procedure as that in Section 6.1 in discussing the $k_z \neq 0$ drift-cyclotron instabilities and refer the reader to that section for the details of the brief arguments presented here. As before, it is important to note that the ion contributions to the dispersion relation are of order unity. Omitting these contributions for the moment and setting k_z equal to k, we find that for instability to occur we certainly must have

$$\omega_{p_i} > n\Omega_i \, (m_e/m_i) \qquad (7.2.5)$$

in which we have employed (7.2.3). Next, we note that in order for the destabilizing ion terms to be able to contribute significantly to the dispersion relation, the electron Landau damping must be made "small" by considering only those waves whose phase velocities along the magnetic field are large compared to the electron thermal velocity. As before, we write this requirement in terms of a condition reflecting the values of k_z which may be unstable:

$$(k_z a_i) \lesssim \frac{n}{2.5}\sqrt{\frac{T_i}{T_e}\frac{m_e}{m_i}} \qquad \text{(instability)}. \quad (7.2.6)$$

Using this limit on k_z and again solving the real part of the dispersion relation omitting the ion contributions, we see that an approximate necessary condition for instability is

$$\frac{\omega_{p_i}^2}{\Omega_i^2} \gtrsim \frac{6(ka_i)^2\left(\frac{T_e}{T_i}\right)}{1 - 6\frac{(\varepsilon' a_i)}{n}(ka_i)\left(\frac{T_e}{T_i}\right)} \qquad \text{(instability)}. \quad (7.2.7)$$

This limit is only applicable for values of T_e/T_i large enough (but still small compared to unity) so that it is not lower than that given by (7.2.5). However, in general this limit is usually considerably less restrictive on the plasma density than condition (7.2.5). Now, with the exception of the density dependent term in the denominator of (7.2.7) which is negligible for small T_e/T_i or very weak spatial gradients, we note that conditions (7.2.6) and (7.2.7) are identical with the corresponding ones derived in the preceding chapter for velocity-space anisotropy instabilities. The reason for this lack of prominent differences is that we have yet to consider any aspects of the ion free energy source that drives the drift-cyclotron instability (except for assumption (7.2.3)) and which is somewhat different from that of the velocity-space anisotropy instabilities.

The drift-cyclotron instabilities are driven by the source of free energy associated with the inhomogeneity of the plasma, which as we have discussed in the preceding section manifests itself in net or macroscopic particle drifts in the y direction. Considering a plasma having only a density gradient, the net drift velocity for the ions is given by (see (7.1.3))

$$V_{D_i} = \frac{\alpha_{\perp_i}}{2}\left[\frac{a_i}{n_i}\frac{dn_i}{dx}\right] = -\frac{\alpha_{\perp_i}}{2}(\varepsilon' a_i) \quad . \qquad (7.2.8)$$

The ion drift velocity is most relevant here since we will be considering (cyclotron) waves which couple energy out of the ion motions transverse to the magnetic field.

In order to discuss the mechanism of the drift-cyclotron instabilities in terms of "positive-slope" regions, we examine

the zeros of the function $P(\omega/\Omega_i)$. For the present inhomogeneous magnetized plasma case, making all of the same assumptions and omissions of terms that we have made to arrive at equations (7.2.1) and (7.2.2) as well as assuming that condition (7.2.6) is satisfied so that the electron contribution to $P(\omega/\Omega_i)$ can be ignored, we can reduce (4.2.3) to (for $|\omega| \gtrsim \Omega_i/2$, $k_y \neq 0$, $k_z \neq 0$)

$$P(\omega/\Omega_i) = \frac{\Omega_i^2}{k^2} \int d^3v \sum_{n=-\infty}^{\infty} J_n^2(k_y v_\perp/\Omega_i) \left\{ k_z \frac{\partial F_i}{\partial v_z} + \frac{n\Omega_i}{v_\perp} \frac{\partial F_i}{\partial v_\perp} + \frac{k_y F_i}{\Omega_i} \frac{\partial g_i}{\partial x} \right\} \left(v_z - \frac{\omega - n\ell_i}{k_z}\right) . \qquad (7.2.9)$$

For the purposes of the present marginal stability analysis, the zeros of this function are to be found for real $\omega, k_\perp, k_z$. We have noted previously that we need only consider positive values of each of these quantities except ω. However, we need only consider positive ω if we allow for spatial gradients in either direction, i.e. of either sign (see Section 3.3). Zeros of $P(\omega/\Omega_i)$ will occur whenever there is a "positive-slope" region (see Sections 4.1, 4.2). For positive ω, $P(\omega/\Omega_i)$ has positive values in this region. In (7.2.9), in addition to the terms which are present for a homogeneous plasma, we have the plasma inhomogeneity term $(k_y/\Omega_i)F_i \partial g_i/\partial x$. Since, as we have previously discussed (Section 6.1), for a Maxwellian plasma the homogeneous plasma contributions both have stabilizing effects, it is the inhomogeneity term which must lead to the destabilization here. We also note that due to the similarities of the relevant terms in the dispersion relation and $P(\omega/\Omega_i)$ for the velocity-space anisotropy and drift-cyclotron modes, the frequency of the drift-cyclotron mode at the lowest threshold density would be expected to

be that given by (6.1.13). The validity of this assertion is borne out by all of our numerical calculations of drift-cyclotron instabilities having nonzero k_z and $T_e/T_i \lesssim 1$.

If T_e is not too much less than T_i, the value of $k_z a_i$ at and above the threshold density is quite small (see (7.2.6)). As before, we note that in this case the resonance of the wave is primarily with a given harmonic of the ion cyclotron frequency and the contributions of the nonresonant harmonics to $P(\omega/\Omega_i)$ are negligible. Then, again using the fact that $k_z a_i$ is small, we can reduce the instability condition that $P(\omega/\Omega_i)$ from (7.2.9) be positive for positive ω to

$$\int d^3v \, J_n^2 \left(\frac{k_y v_\perp}{\Omega_i}\right) \left\{ n\Omega_i \frac{\partial F_i}{\partial v_\perp^2} + \frac{k_y F_i}{2\Omega_i} \frac{\partial g_i}{\partial x} \right\} \gtrsim 0 \qquad \text{(instability)} \quad (7.2.10)$$

for each positive n of interest. Working out this criterion for a Maxwellian velocity distribution, we find that it becomes simply

$$\frac{n\Omega_i}{k_y} \lesssim V_{D_i} \qquad \text{(instability)} \quad (7.2.11)$$

Recalling assumption (7.2.3), we see that this result is very indicative of a resonance of the wave with particles in the "positive-slope" portion of an effective ion velocity distribution which takes into account the ion diamagnetic drift velocity (see below).

If, instead of using the procedure described in the preceding paragraph, we make the same physical arguments as those made in Section 6.2 regarding the effective velocity distribution transverse to the magnetic field, we would define it here as

$$\tilde{F}_i(v_y) \equiv \int dv_x dv_z \left\langle f_i(x, \underline{v}) \right\rangle_{x \approx 0}. \qquad (7.2.12)$$

Then, as before, we would conclude that the appropriate instability criterion for waves having a component in the y direction would be

$$\left.\frac{d\tilde{F}_i(v_y)}{dv_y}\right|_{v_y = \omega/k_y} = \int d^3v \left.\frac{\partial\langle f_i(x,\underline{v})\rangle}{\partial v_y}\right|_{x=0} (v_y - \omega/k_y) > 0. \tag{7.2.13}$$

For $\omega = n\Omega_i$, at least in the limit of small gradients, this last criterion is equivalent in the present case to (7.2.11). We should also note that (7.2.13) can be obtained by taking the "continuum" limit of $P(\omega/\Omega_i)$ given by (7.2.9) using the prescription given by Rosenbluth (7.6) (see Sections 6.2, 6.3 for the details of this procedure). In subsequent calculations we will find that (7.2.13) is quite adequate for predicting the ranges of frequencies for which instability of a mode with given k_y can occur and in fact is a more accurate instability criterion than that given by (7.2.11). As with the similar criterion developed in Section 6.2, it is important to note that if there are distinct groups of ions which have dissimilar velocity distributions along the magnetic field, then it may not be very realistic to consider only the effective velocity distribution perpendicular to the magnetic field. That is, in such cases we do not necessarily expect either (7.2.10) or (7.2.13) to be correct and in general must return to a consideration of the more general $P(\omega/\Omega_i)$ given by (7.2.9).

A typical plot of $\tilde{F}_i(v_y)$ for an inhomogeneous plasma with a Maxwellian velocity distribution is shown in Fig. 7.2. From this figure we see that the spatial inhomogeneity of the plasma effectively gives rise to a velocity-space anisotropy. Viewing the

figure and considering (7.2.13), we see that the phase velocities specified by

$$0 < \omega/k_y < V_{D_i} = \frac{\alpha_{\perp i}}{2}\left(\frac{a_i}{n_i}\frac{dn_i}{dx}\right) = -\frac{(\varepsilon' a_i)}{2}\alpha_{\perp_i} \qquad (7.2.14)$$

are in the "positive-slope" region of the effective velocity distribution $\tilde{F}_i(v_y)$ and hence correspond to potentially unstable waves. Note that those waves having negative ω/k_y are necessarily stable waves.

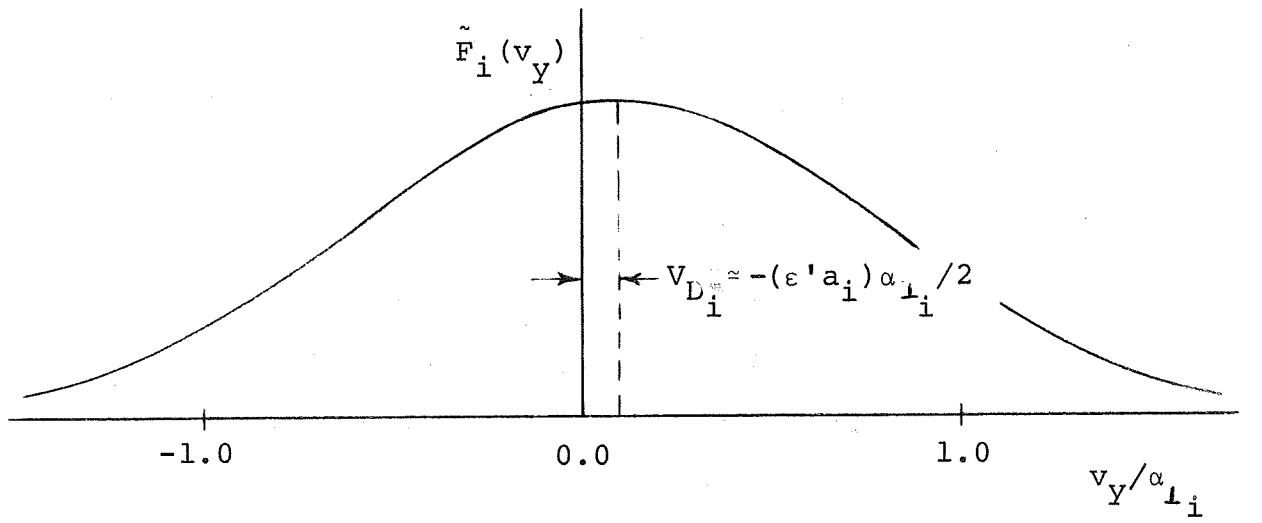

Figure 7.2. Effective Velocity Distribution in the y Direction (Inhomogeneous Plasma, $\frac{a_i}{n_i}\frac{dn_i}{dx} = -\varepsilon' a_i = 0.2$).

As in the preceding chapter, in order to demonstrate the validity of (7.2.14), we will consider a particular example. The case we investigate is that which is characterized by $T_e/T_i = 10^{-2}$ and $\frac{a_i}{n_i}\frac{dn_i}{dx} = -\varepsilon' a_i = 0.2$. This case will be the "standard" drift-cyclotron instability case, away from which we will make all variations of T_e/T_i and $\varepsilon' a_i$. Strictly speaking, this choice of density gradient scale length of $a_i/L = 0.2$ is on the borderline of being acceptable as far as the satisfaction of condition (3.3.13)

for the validity of our dispersion relation. While it would perhaps be better to choose a somewhat smaller value of this parameter, we use the value of 0.2 since within the limitations of our computer programs ($k_y a_i \lesssim 28$), it allows us the greatest possible flexibility in varying $k_y a_i$ (see below). Later when we consider the influence of variations in the density gradient parameter, we will find that this choice for our "standard" case does yield results which are qualitatively equivalent to those found for smaller values of $\varepsilon' a_i$ which more closely satisfy condition (3.3.13) (see Fig. 7.9).

Considering this standard case, for a given $k_y a_i$ we find stability curves such as those displayed in Figs. 4.8, 5.9 for positive frequencies. For negative frequencies we do not find any instabilities, a result which is in agreement with (7.2.14) and which tells us that unstable waves propagate only in the ion drift or diamagnetic current direction. Again, as in the case of the loss-cone instabilities, we find that for each given $k_y a_i$ there is a maximum frequency wave (typically for a fairly high density) which can be unstable in the plasma. The variation with $k_y a_i$ of this maximum frequency for which instability can occur is displayed in Fig. 7.3. From these results and the fact that waves with negative ω are always stable for this case, we conclude that condition (7.2.14) is a valid condition for instability for all frequencies, including those which lie between harmonics of the ion cyclotron frequency.

Having established the validity of (7.2.14), we will now use it to derive a more accurate stability criterion than that given by (7.2.7). Recalling that in general the frequency must be near

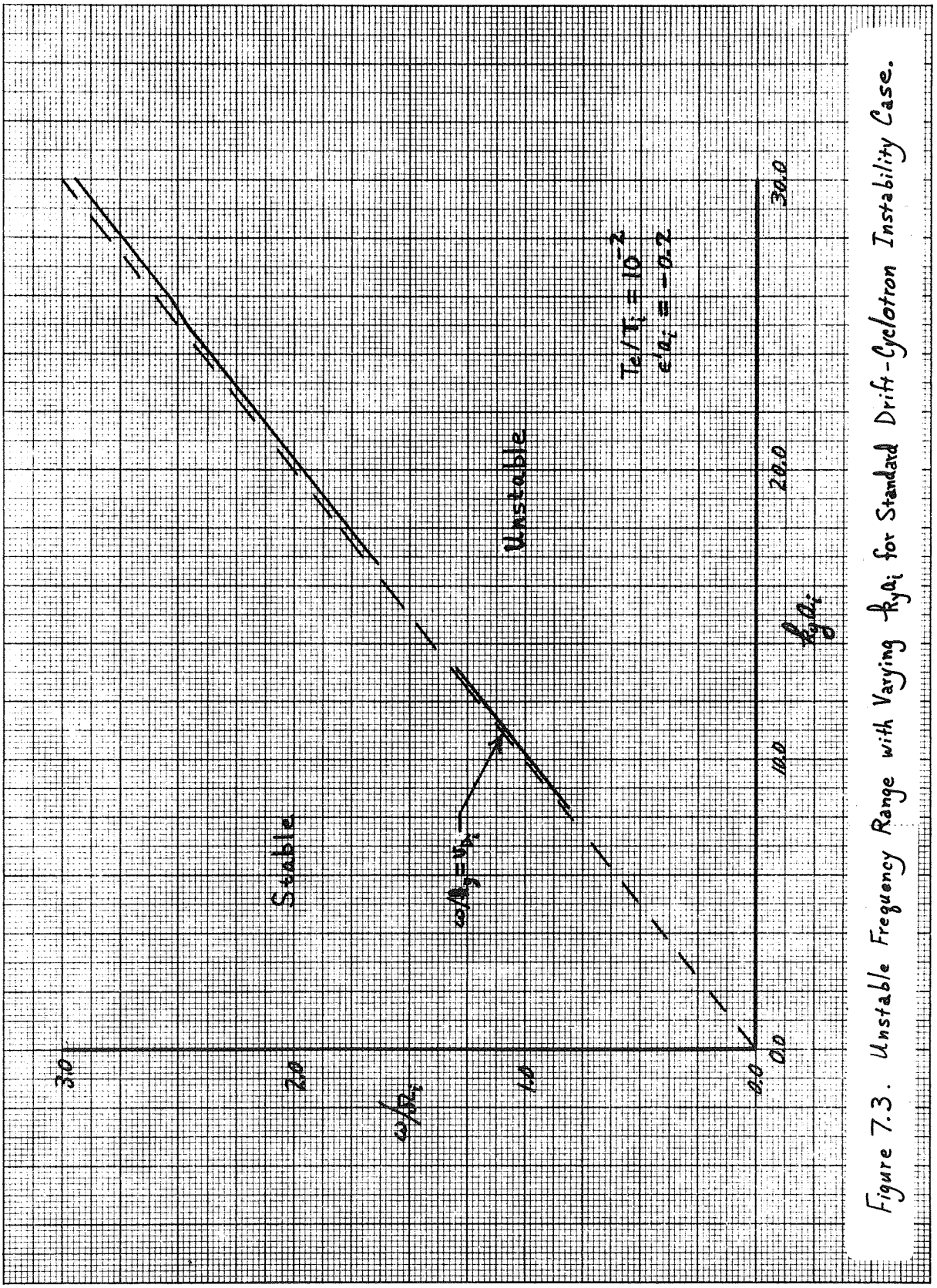

Figure 7.3. Unstable Frequency Range with Varying $k_y \rho_i$ for Standard Drift-Cyclotron Instability Case.

a cyclotron harmonic for a strong wave-particle interaction to occur, we can rewrite (7.2.14) to indicate the range of $k_y a_i$ for which the plasma can be unstable:

$$k_y a_i > \left| n \frac{\alpha_{\perp_i}}{v_{D_i}} \right| = \left| \frac{2n}{(\varepsilon' a_i)} \right| . \qquad (7.2.15)$$

Then, using this relation in (7.2.7), we find that the density threshold over the entire range of $k_y a_i$ for which drift-cyclotron instabilities can occur is given roughly by:

$$\frac{\omega_{p_i}}{\Omega_i^2} \gtrsim \frac{6n^2}{1 + 12\ (T_e/T_i)} \frac{T_e}{T_i} \left(\frac{\alpha_{\perp_i}}{v_{D_i}} \right)^2 = \frac{24n^2}{1 + 12\ (T_e/T_i)}$$

$$\frac{T_e}{T_i} \frac{1}{(\varepsilon' a_i)^2} \quad \text{(instability)}. \qquad (7.2.16)$$

For $k_y a_i$ values greatly in excess of $n\, \alpha_{\perp_i}/v_{D_i}$, the density threshold for instability of that particular mode remains that given by (7.2.7).

In the derivation of the dispersion relation we required the satisfaction of condition (3.3.13) which here is given by:

$$2 \left| \frac{v_{D_i}}{\alpha_{\perp_i}} \right| = |\varepsilon' a_i| \ll 1. \qquad (7.2.17)$$

Therefore we immediately see from conditions (7.2.15) and (7.2.16) that a consequence of this smallness of the drift velocity for inhomogeneous plasmas is that the drift-cyclotron instabilities occur only for very short transverse wavelengths and relatively high plasma densities. They can therefore be prevented at any given plasma density by requiring that the plasma have a sufficiently gentle density gradient.

Recalling condition (7.2.15) for a negative value of $\varepsilon' a_i$, we can readily see from the dispersion relation and $P(\omega/\Omega_i)$ that the combination of the $\partial \langle f_i \rangle / \partial v_\perp$ and $\partial \langle f_i \rangle / \partial x$ terms is positive near a given harmonic of the ion cyclotron frequency when the drift-cyclotron instability occurs. Thus, here as for the loss-cone instability, the normal cyclotron damping has become a cyclotron growth. The drift-cyclotron instability (with nonzero k_z) therefore results from the coupling of a potentially unstable ion-cyclotron wave with a damped electron plasma wave moving along the magnetic field by wave propagation at an angle other than 90° to the magnetic field. We also note that since the $\partial \langle f_i \rangle / \partial x$ term gives the destabilizing contribution to the dispersion relation, the x component of the guiding center of the ions is rapidly destroyed as a constant of the motion. As a matter of fact, it is this change in the guiding center in the "positive-slope" region which releases the source of free energy driving the instability.

The statements made in the preceding paragraph can be illustrated by considering the Nyquist and $P(\omega/\Omega_i)$ plots for the drift-cyclotron instabilities. A typical set of such graphs is displayed in Fig. 7.4. As in the case of the velocity-space anisotropy instabilities, since we are considering a case with $T_e << T_{z_i}$, the

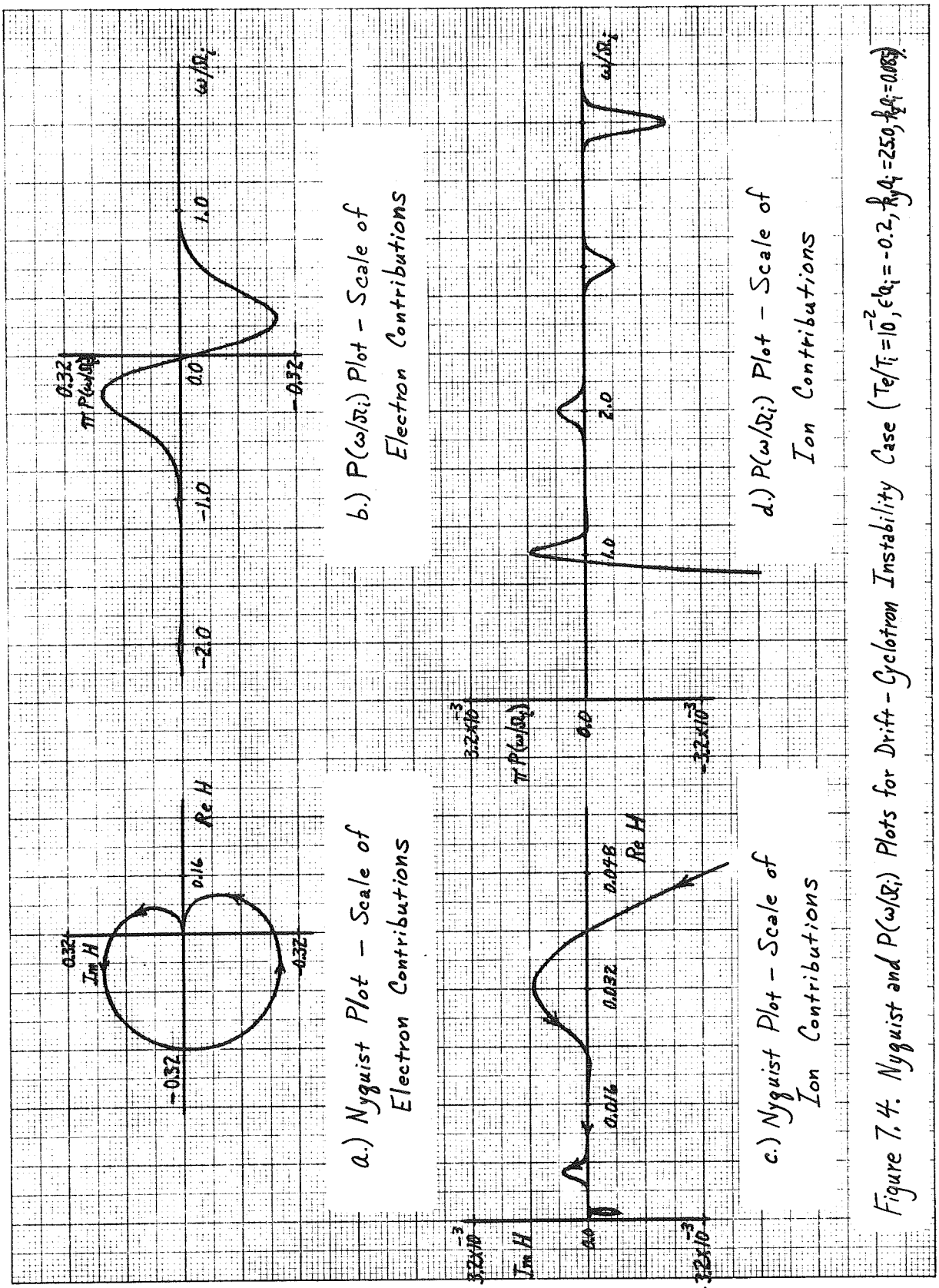

Figure 7.4. Nyquist and $P(\omega/\Omega_i)$ Plots for Drift-Cyclotron Instability Case ($T_e/T_i = 10, \epsilon^2 k_i = -0.2, k_y \rho_i = 2.50, k_z \rho_i = 0.085$).

electron and ion contributions to the dispersion relation are in general on vastly different scales. The Nyquist and $P(\omega/\Omega_i)$ plots on the electron scale are displayed in Fig. 7.4 a,b. As usual the electron contribution is characteristic of the Z_1 function (see Fig. 4.3b) although here there is a slight deviation from this simple function due to the presence of the electron drift velocity. For negative frequencies we note from Fig. 7.4b that there is cyclotron damping of waves with frequencies near integer multiples of the ion cyclotron frequency. This damping persists for all negative frequencies, a fact which can be seen directly from dispersion relation (7.2.2) or $P(\omega/\Omega_i)$ as given by (7.2.9). However, as we can see from the Nyquist and $P(\omega/\Omega_i)$ plots on the scale of the ion contributions to the dispersion relation (Fig. 7.3 c,d), for positive frequencies there is cyclotron growth at least for $\omega/\Omega_i \sim 1,2$ in this case. For higher harmonics the ion contributions have stabilizing effects. We also note that irrespective of whether the ion contributions have stabilizing or destabilizing effects, they are always characteristic of the Z_o functions (cf. Fig. 4.3a).

Comparing Fig. 7.4 with the corresponding figure for loss-cone instabilities (Fig. 4.6), we see a great number of similarities. As we have previously discussed, the electron contributions differ only by the small electron drift velocity effects. In both cases the ion contributions (stabilizing and destabilizing) are nearly identical except that for the drift-cyclotron instabilities the destabilizing effects occur only for positive frequencies and hence positive phase velocities transverse to the magnetic field.

This is a consequence of the directionality of the diamagnetic particle drifts in an inhomogeneous plasma. In contrast, the "loss-cone" v_i distribution has net particle "drifts" in all directions in the plane perpendicular to the magnetic field and hence permits destabilizing effects for all wave directions in this plane. Thus, except for the directionality and perhaps the magnitudes of the "drift" velocities, the drift-cyclotron and loss-cone instabilities are very similar and we would expect many of their instability characteristics to be similar as well. It is also interesting to note that while the drift-cyclotron instabilities tap the free energy source associated with the spatial inhomogeneity of the plasma, they do so by taking energy from the velocity-space anisotropy resulting from the density-gradient-induced diamagnetic particle drifts. Therefore in a sense, they are really just velocity-space anisotropy instabilities like those we have discussed in the preceding chapter.

With this introduction to the general properties of the drift-cyclotron instabilities, we will now discuss the calculations we have carried out concerning these instabilities. We begin by considering the effects of variations of $k_y a_i$ on the unstable drift-cyclotron modes for our standard case ($T_e/T_i=10^{-2}$, $\varepsilon' a_i = -0.2$). In all of the computations presented here and elsewhere in this work, we take $m_i/m_e = 1836$. As in considering the loss-cone instabilities, we first make instability plots for a given $k_y a_i$ of the type displayed in Figs. 4.8 and 5.9. Then, cross-plotting the minimum densities for which instability occurs for each $k_y a_i$, we obtain the instability map displayed in Fig. 7.5.

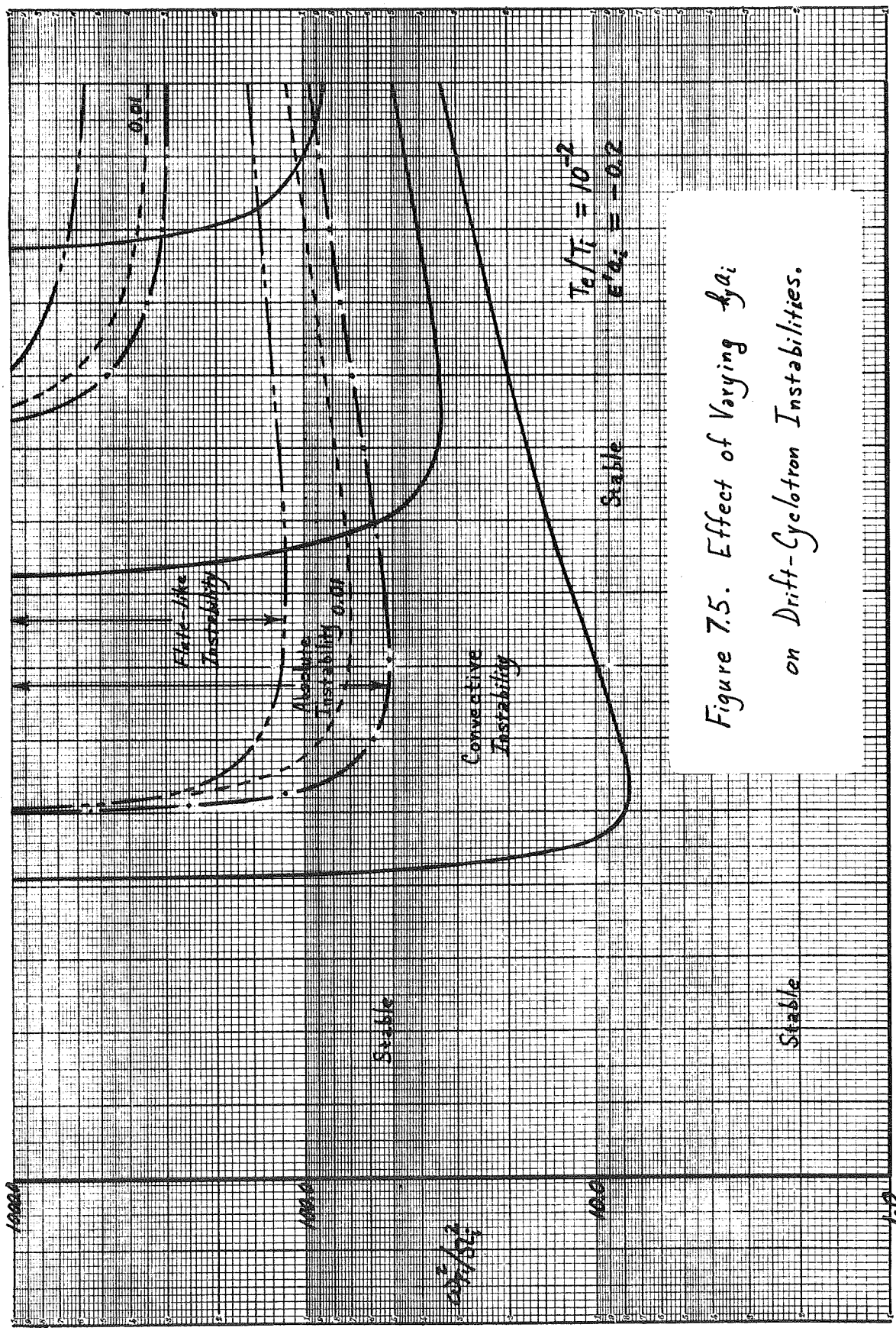

Figure 7.5. Effect of Varying $k_y a_i$ on Drift-Cyclotron Instabilities.

As in the graphs in the preceding chapter, a solid line denotes the marginally stable modes (threshold density), a dash-dot or center line indicates the "marginally stable" absolute instability modes (transition density) and the dashed lines indicate the absolute instability modes with given temporal growth rates. The new lines having long dashes separated by two short dashes which we introduce in this graph denote the flute-like (k_z=0) modes. In this section the single dashed lines which are displayed will always indicate absolute instability temporal growth rates of 1% of the ion cyclotron frequency. We recall that we are limited to such small temporal growth rates since as they increase, the k_z of the absolute instability modes moves toward and eventually becomes lost into the "divergence" region (see Section 3.4).

In Fig. 7.5 the nested sets of curves represent drift-cyclotron instabilities with frequencies near the first, second, etc. harmonics of the ion cyclotron frequency with each successive harmonic becoming unstable as we increase $k_y a_i$. The values of $k_y a_i$ for which the consecutive harmonics are unstable are in reasonable agreement with condition (7.2.15), a result which gives further support to the arguments from which this condition was derived. The deviations of the results shown from condition (7.2.15) are due to the fact that the frequency at which the instability has its lowest threshold density is somewhat less than a harmonic of the cyclotron frequency (see Fig. 7.6). For all the cases considered in this work, the more exact instability condition given by (7.2.14) is always satisfied. The minimum threshold density for instability of each of the cyclotron harmonic modes is found to be predicted

by instability condition (7.2.16) within roughly a factor of 1.5. We also observe that as $k_y a_i$ becomes large compared to the value necessary to satisfy (7.2.15), the instabilities near the various cyclotron harmonics tend to have nearly the same threshold density, as indicated by instability condition (7.2.7). These confirmations of our approximate instability criteria exhibit their usefulness with respect to predicting the onset of convective instabilities.

From Fig. 7.5 we observe that the drift-cyclotron instabilities do become absolute in nature when $k_y a_i$ exceeds 10. While the general shapes of the marginal stability and absolute instability curves are obviously similar, the simple formulas which predict the marginal stability characteristics do not accurately predict the absolute instability characteristics. However, the density at which the transition to absolute instability occurs does scale with $k_y a_i$ in a manner which is roughly consistent with our simple instability condition formulas. Along the absolute instability transition density curve we find empirically that for all $k_y a_i$, the ratio of the imaginary part of k_z to its real part is roughly the same as that given by (6.2.8) for the corresponding loss-cone instability case. The degree to which the values of Im (k_z) along the same curve faithfully represent the maximum spatial growth rate of the convective instabilities is roughly the same as for the loss-cone instabilities (see Section 6.2). The maximum spatial growth rate for the convective drift-cyclotron instabilities as a function of density is typically the same as that displayed in Fig. 6.5 for the loss-cone instabilities.

It is interesting to note that the flute-like drift-cyclotron instabilities only appear for densities in excess of those for which the nonzero k_z instabilities of both the convective and absolute type are present. However, unlike the nonzero k_z modes, the flute-like modes are not generally restricted to occur only in sufficiently long plasmas (see Section 5.4 and Fig. 7.6). Comparing the results shown in Fig. 7.5 with instability condition (7.2.4), we find that the density threshold for flute-like instabilities is quite accurately predicted by that instability condition.

Over all $k_y a_i$ for which the drift-cyclotron modes can be unstable, we observe from Fig. 7.5 and condition (7.2.16) that the mode whose frequency is near the ion cyclotron frequency is the "most unstable" mode in that the threshold density, transition density for absolute instability and the density at which the flute-like instability first appears are all lowest for this mode. However, at least for the nonzero k_z modes, before we can conclude that this mode is the most detrimental to plasma containment, we must consider the length of plasma required for the existence of these modes. Since the transverse wavelengths $2\pi\ k_y^{-1}$ are much smaller than the transverse dimension of any conceivable plasma, the waves can always "fit" into the plasma in the direction perpendicular to the magnetic field.

However, the parallel or axial wavelengths $2\pi\ k_z^{-1}$ for which the drift-cyclotron instability occurs are usually quite long and so the length of the plasma in this direction is a major consideration in determining which unstable modes can occur in a given plasma. This effect is displayed in Fig. 7.6 in which

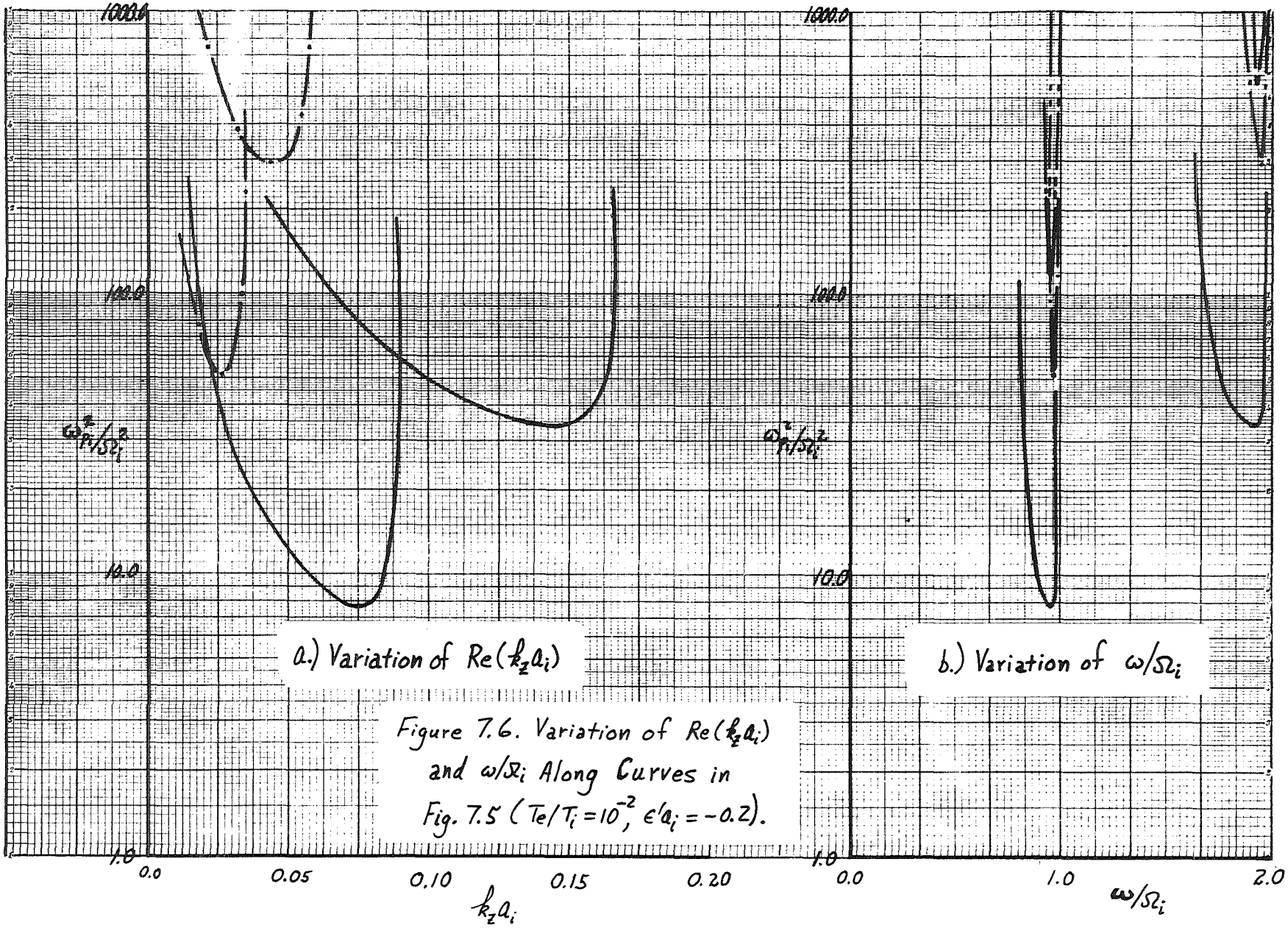

Figure 7.6. Variation of $Re(k_z a_i)$ and ω/Ω_i Along Curves in Fig. 7.5 ($T_e/T_i = 10^{-2}$, $\epsilon' a_i = -0.2$).

we display the variations of $Re(k_z a_i)$ and ω/Ω_i along the marginal stability, absolute instability and flute-like instability curves in Fig. 7.5. In this figure $k_y a_i$ is an implicit parameter and increases in value from left to right on all curves, except the frequency curves for the absolute and flute-like instability modes in which $k_y a_i$ increases in the opposite direction. As with the loss-cone instabilities (see Section 6.2), we see from Fig. 7.6b that the variation of the frequency along the marginal stability curve is small compared to the ion cyclotron frequency and in rough agreement with (6.1.13) -- see discussion in Section 6.2. We also note that frequency variations along the absolute and flute-like instability curves are small compared to the ion cyclotron frequency. The deviations of the values of $(k_z a_i)$ shown in Fig. 7.6a from the maximum $(k_z a_i)$ for which instability (convective) can occur at any density is, as in the case of the loss-cone instabilities, small and we ignore it. Comparing the results shown in Fig. 7.6a with instability condition (7.2.6), we find excellent agreement for the convective instabilities. However, as we would expect, the $Re(k_z a_i)$ values shown for the absolute instabilities are not accurately predicted by (7.2.6), although they do scale with harmonic number n in a manner which is consistent with (7.2.6). Since the absolute drift-cyclotron instabilities have considerably longer wavelengths than the corresponding convective instabilities, they require much longer plasmas for their appearance. The axial wavelength of the non-zero k_z modes is thus a very important consideration in determining whether the drift-cyclotron instabilities occur in a given experimental plasma.

Next we will investigate the effect which varying T_e/T_i (i.e. the electron temperature) has on the drift-cyclotron instabilities. From the preceding $k_y a_i$ analysis, we have found that the "most unstable" modes in the sense of having the lowest density for each type of instability are those modes whose frequencies are near the ion cyclotron frequency. In examining the effects of varying T_e/T_i we will only consider the influence which this parameter has on the "most unstable" modes. In determining the properties of these "most unstable" modes as T_e/T_i varies, we minimize the threshold and transition densities and the density at which the flute-like modes first appear with respect to variations in $k_y a_i$. The results of these computations for $\varepsilon' a_i = -0.2$ are displayed in Fig. 7.7. The variations of $-\mathrm{Im}(k_z)/\mathrm{Re}(k_z)$, $k_y a_i$ and ω/Ω_i along the curves in Fig. 7.7 are shown in Fig. 7.8.

Comparing Figs. 6.8, 6.9 and 7.7, 7.8, we find that as we expected, the effects of varying the electron temperature for the drift-cyclotron instabilities are nearly the same as for the loss-cone instabilities. Since the effects of electron temperature are so similar in the two cases, the remarks which we have made previously for the loss-cone instabilities (see Section 6.2) apply equally to the drift-cyclotron instabilities. We recall that the most important point about the effects of varying T_e/T_i was that while the convective instabilities abey the approximate instability criteria which we have derived (here (7.2.6), (7.2.16)), the absolute instabilities are relatively unaffected by changes in T_e/T_i except when this parameter approaches unity. This result is important since it implies that in general, heating the electrons will not substantially affect the confinement of a plasma

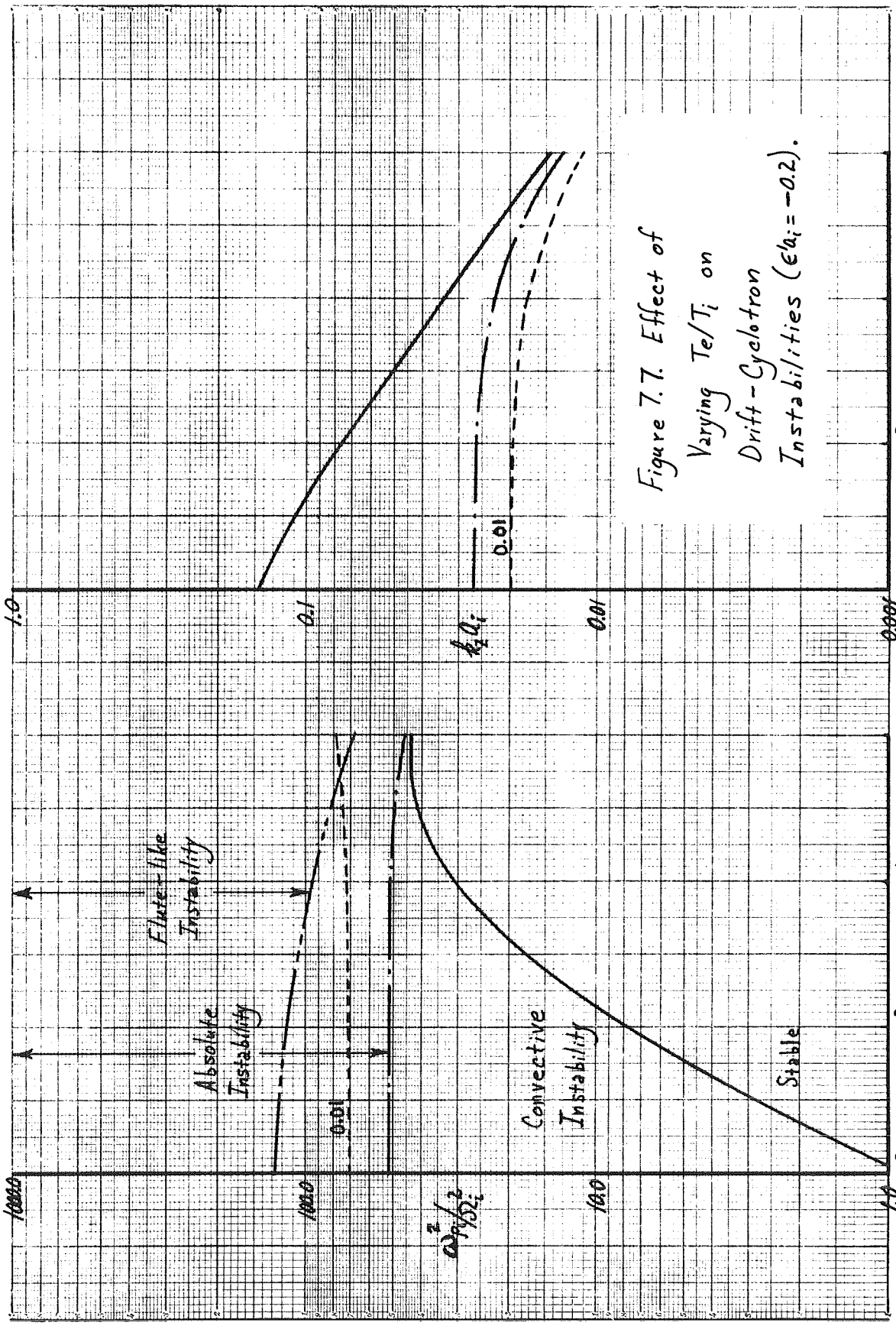

Figure 7.7. Effect of Varying T_e/T_i on Drift-Cyclotron Instabilities ($\epsilon' a_i = -0.2$).

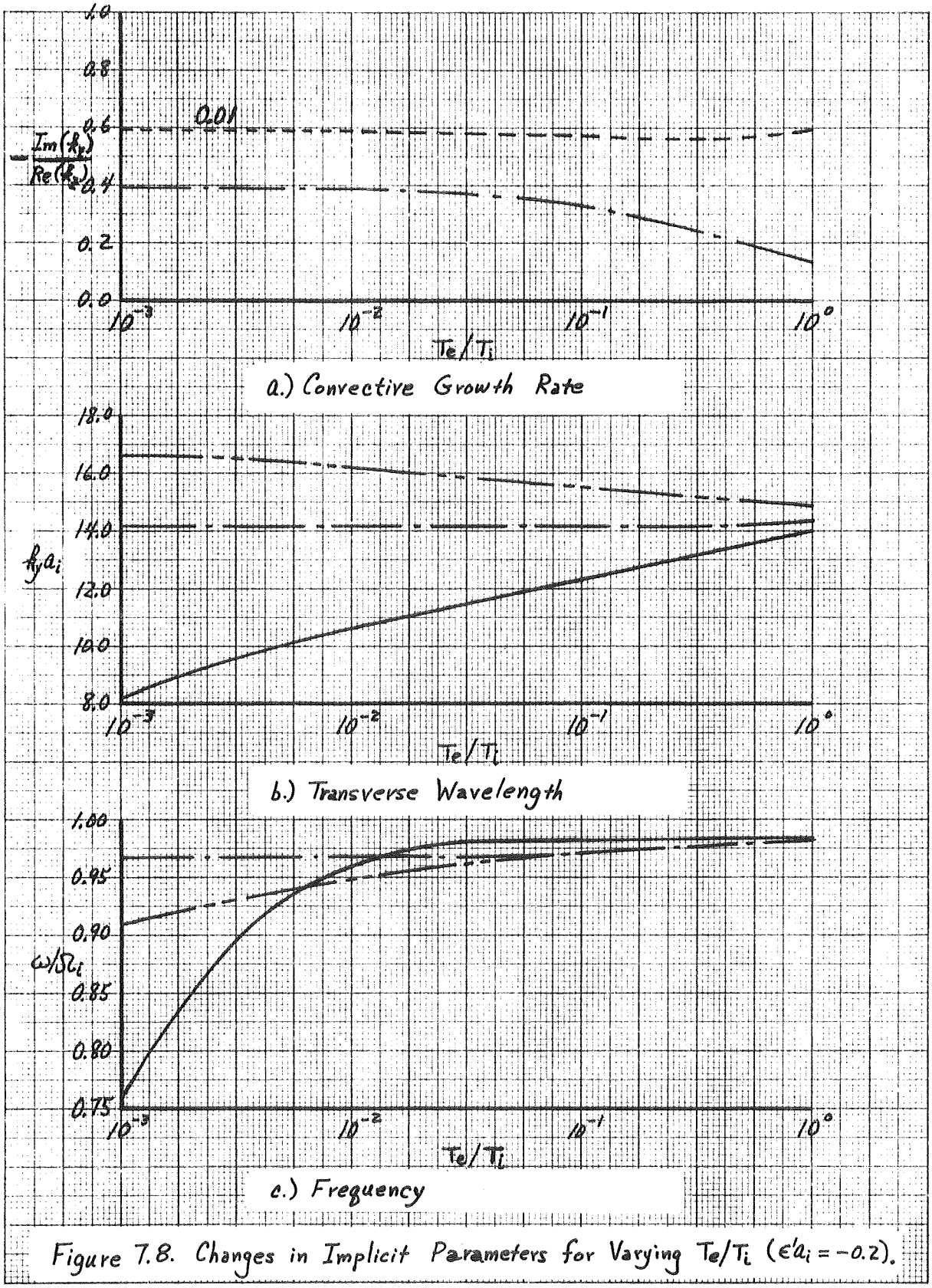

Figure 7.8. Changes in Implicit Parameters for Varying T_e/T_i ($\epsilon' a_i = -0.2$).

which is limited in density due to an absolute drift-cyclotron instability. However, as with the loss-cone instabilities, we should note that it may be important to consider the effects due to the finite length of experimental plasmas (see Section 5.4).

The variation of the threshold density for the flute-like (k_z=0) modes with changing T_e/T_i, even though slight, is surprising at first glance since the electron temperature parallel to the magnetic field disappears from the dispersion relation for k_z=0. However, noting from Fig. 7.8b that $k_y a_i$ for these modes is about 16, we see that as T_e/T_i approaches unity the assumption that $k_y a_e << 1$ becomes invalid. In the calculations the exact electrostatic dispersion relation given by (7.2.1) is used and so all the electron contributions are retained exactly. Therefore the observed slight variation of the threshold density for the flute-like modes is due to the finite electron Larmor radius effects.

Finally, we will investigate the effect which changes in the density gradient scale length have on the "most unstable" drift-cyclotron instabilities. As always, we minimize the various instability threshold densities with respect to variations in $k_y a_i$, $k_z a_i$ and ω/Ω_i for each case. The results of computations for $T_e/T_i=10^{-2}$ and density gradient scale lengths given by $-\varepsilon' a_i$ = 0.1, 0.2, 0.5 are displayed in Fig. 7.9. The variations of $-Im(k_z)/Re(k_z)$, $k_y a_i$ and ω/Ω_i along the curves in Fig. 7.9 are shown in Fig. 7.10. For the $\varepsilon' a_i = -0.1$ case the absolute and flute-like instabilities have their lowest transition and threshold densities respectively for values of $k_y a_i$ larger than those we can conveniently handle in the computer programs. We

obtain these points by an extrapolation procedure, the approximate error of which is indicated by the size of the circles in Fig. 7.10b. We also note that, strictly speaking, $\varepsilon' a_i = -0.5$ does not satisfy condition (7.2.17) which is required for the validity of the dispersion relation we are using. We include this case here as a mathematical rather than physical limiting case. In these computations with varying density gradient scale lengths we have restricted ourselves to values of $|\varepsilon' a_i|$ equal to or greater than 0.1 since for smaller values of this parameter the values of $k_y a_i$ for the unstable modes become larger than 28, which is the largest value we can conveniently handle in the computer programs. The trends in the relevant quantities for smaller values of $\varepsilon' a_i$ can easily be ascertained by extrapolating the data shown in Figs. 7.9, 7.10.

The most striking result from the variations of the density gradient scale length is the very strong influence which it has on the threshold density for the various types of instability (convective, absolute and flute-like). Comparing the marginal stability and flute-like instability threshold density curves with the respective instability conditions of (7.2.4) and (7.2.16), we find excellent agreement. We also observe that while the absolute instability transition density is not well predicted by either of these instability conditions, it does scale with the density gradient scale length in nearly the same manner as these two conditions. It is interesting to note that for sharper density gradients, in addition to occurring at lower plasma densities, the drift-cyclotron modes have

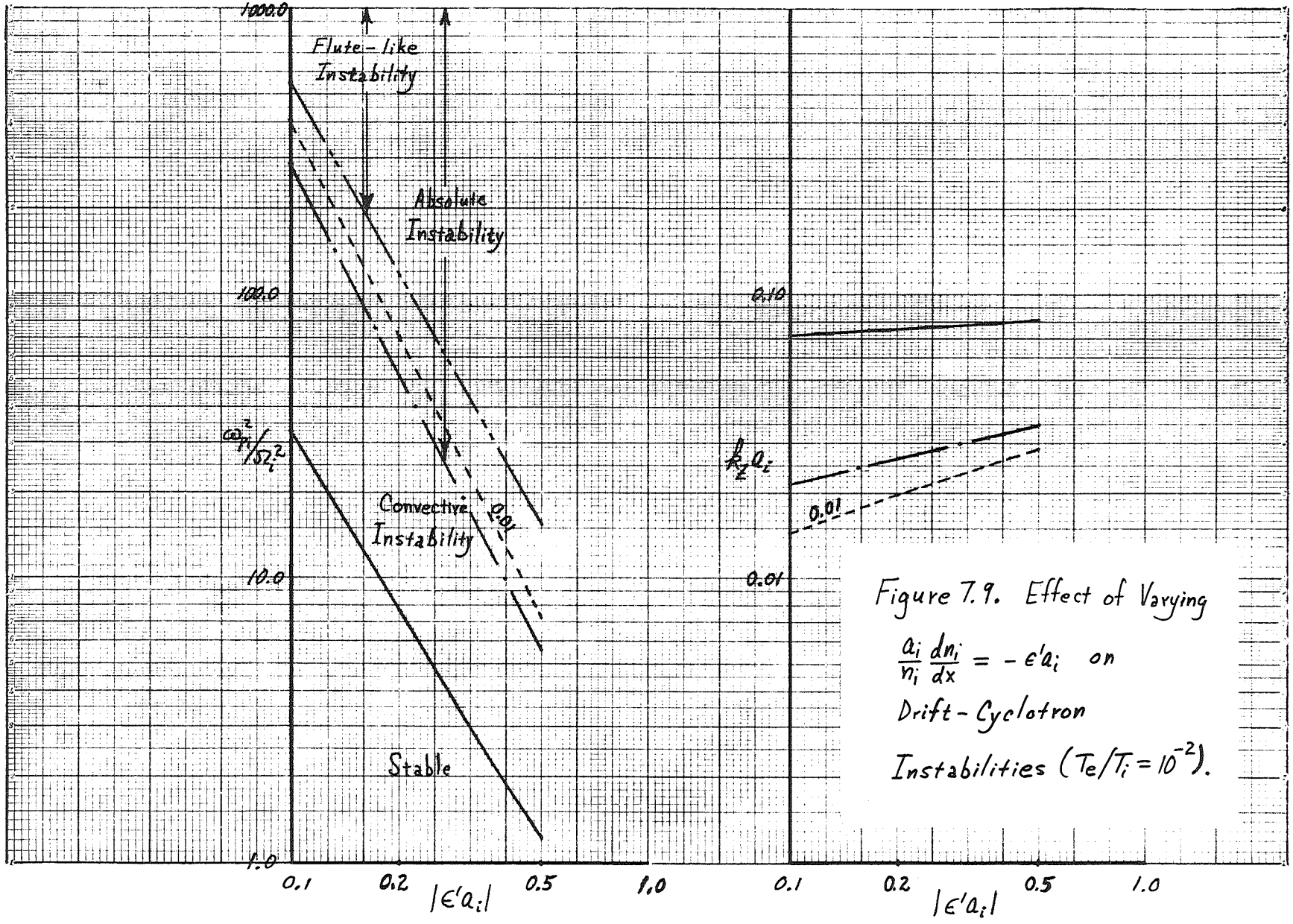

Figure 7.9. Effect of Varying $\frac{a_i}{n_i}\frac{dn_i}{dx} = -\epsilon' a_i$ on Drift-Cyclotron Instabilities ($T_e/T_i = 10^{-2}$).

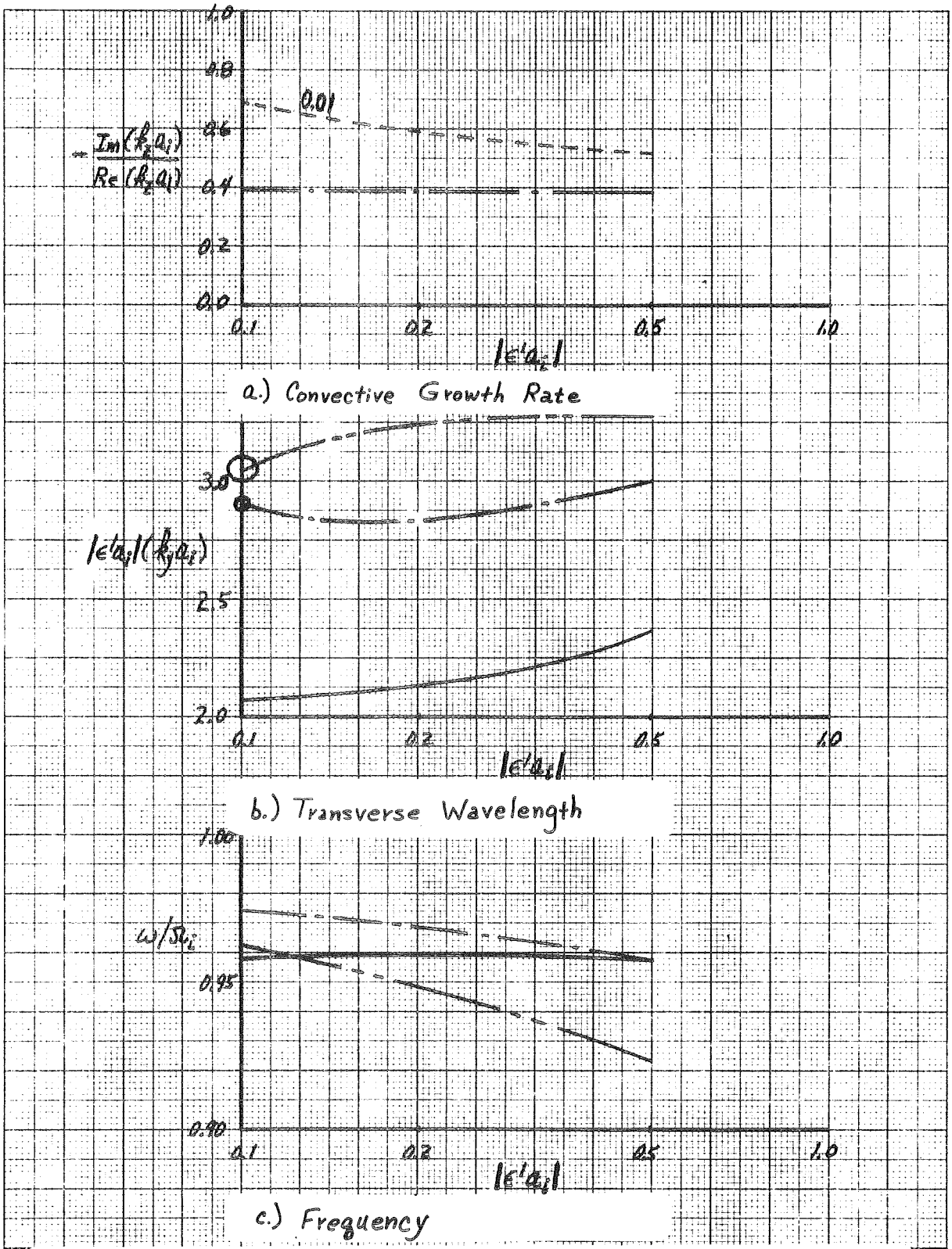

Figure 7.10. Changes in Implicit Parameters for Varying $\frac{a_i}{n_i}\frac{dn_i}{dx} = -\epsilon' a_i$ $(T_e/T_i = 10^{-2})$.

shorter axial wavelengths and hence are also more detrimental to confinement in that they may occur in shorter plasmas.

From the data presented here, it is obvious that the most effective way to prevent drift-cyclotron instabilities in any given experimental situation is to make plasmas which have sufficiently gentle density gradients. We will now examine just how gentle the density gradients must be. Considering Figs. 7.8a and 7.10a and our previous remarks concerning the absolute instability modes in Fig. 7.5, we find that the maximum spatial growth rate of the convective instabilities which occur before the appearance of absolute drift-cyclotron instabilities is in agreement with condition (6.2.9). Therefore, as with the loss-cone instabilities (see Section 6.2), if we assume that absolute instabilities can "fit" into any plasma which is at least a half-wavelength in length, we would expect the convective instabilities to be detrimental to plasma containment only if the reflection coefficient for waves moving axially in the plasma exceeds about 0.285 and even then only for small T_e/T_i (see Fig. 7.8a). As we have discussed in Section 5.4, such a high reflection coefficient seems unlikely or at least avoidable and so we will presume that we need only be concerned with the absolute drift-cyclotron instabilities.

As with the loss-cone instabilities, our results imply that at least up to $T_e \sim T_i$, heating the electrons does not have an important stabilizing effect on the absolute drift-cyclotron instabilities. Analyzing our data empirically (and recalling the similarities between the loss-cone and drift-cyclotron

instabilities), we find that the absolute drift-cyclotron instabilities obey the following stability criterion:

$$\frac{\omega_{p_i}^2}{\Omega_i^2} \lesssim \frac{n^{8/3}}{2}\left(\frac{\alpha_{\perp_i}}{v_{D_i}}\right)^2 = \frac{2n^{8/3}}{(\varepsilon' a_i)^2} \quad \text{(stability)} \qquad (7.2.18)$$

in which we recall that $\varepsilon' a_i$ is the ratio of the ion Larmor radius to the density gradient scale length. Presuming that a plasma which is a half-wavelength long admits an absolute drift-cyclotron instability mode, we obtain the following condition on the plasma length L for stability:

$$L \lesssim \frac{35\pi\, a_i}{n^{2/3}} \quad \text{(stability).} \qquad (7.2.19)$$

The relevant transverse wavelengths for the absolute drift-cyclotron modes with the minimum transition density are given roughly by:

$$(k_y a_i) \approx \frac{3n}{2\,|\varepsilon' a_i|} \,. \qquad (7.2.20)$$

The discussion of the physical mechanism of the <u>absolute</u> loss-cone instabilities at the end of Section 6.2 applies to the absolute drift-cyclotron instabilities as well.

Comparing conditions (7.2.18) and (7.2.19) with the corresponding ones for loss-cone instabilities (6.2.19) and (6.2.18) and recalling condition (7.2.17), we see that if a loss-cone type of $v_\perp$ distribution is present, the absolute loss-cone instabilities

will be more detrimental to plasma containment than the absolute drift-cyclotron instabilities in that they have transition densities which are smaller by a factor of $\frac{1}{2}\left(\frac{a_i}{n_i}\frac{dn_i}{dx}\right)^2$. However, we should also note that when the plasma has a density gradient, then flute-like drift-cyclotron instabilities which are not particularly subject to a length condition (see Section 5.4) as the absolute instabilities are, can appear. Considering the plasma to have only a density inhomogeneity source of free energy, the instability criterion for the flute-like modes is given by (7.2.4). (The case in which both loss-cone and density inhomogeneity sources of free energy are present is discussed in the next section.) It is conceivable that low harmonic number absolute drift-cyclotron modes ($k_z \neq 0$) may be forbidden in a given machine by condition (7.2.19), in which case the flute-like drift-cyclotron instabilities would occur at lower plasma densities than the absolute instabilities and thus presumably be more detrimental to plasma containment. However, as we will now discuss, the flute-like drift-cyclotron instabilities can be stabilized by (among other things) the introduction of a moderate amount of favorable magnetic field curvature.

The effect of magnetic field curvature on drift-cyclotron instabilities was first considered by Mikhailovskii (7.43) who concluded that these instabilities are not stabilized by curvatures with radii longer than or approximately equal to the density gradient scale length. Krall and Fowler (7.3) have reconsidered this problem including the effect of magnetic field curvature on the effective drift velocity (see (7.1.3)) which

was neglected by Mikhailovskii. For the flute-like drift-cyclotron instabilities, Krall and Fowler (7.3) find that a moderate amount of favorable magnetic field curvature (curvature length not too much in excess of the density gradient scale length) is sufficient to effectively stabilize these modes. The essential stabilization mechanisms here are the reduction in the effective ion drift velocity of (7.1.3) by the favorable curvature and a downward shift in the frequency of the instability. Krall and Fowler (7.3) also conclude that the nonzero k_z modes are not significantly affected by the introduction of magnetic field curvature. Using the general computer programs developed in this work, we have found that, as we would expect from the way in which we derive the approximate instability conditions given by (7.2.14), (7.2.15) and (7.2.16), in at least one nontrivial case the magnetic field curvature effects (represented by the "gravity" force) do have a significant effect on the instability of the nonzero k_z drift-cyclotron modes. Thus this last conclusion of the work by Krall and Fowler seems questionable to us.

In all of the preceding work cited the magnetic field curvature effects have been taken into account through a velocity-independent gravity term (see Section 2.4). However, as we have noted previously, Laval et al. (7.31) have shown that the velocity dispersion effects of the magnetic field curvature have an important stabilizing influence on the low frequency drift instabilities. We would expect that these effects would also be important in the consideration of drift-cyclotron instabilities. Bhadra (7.44) has carried out a numerical calculation in which the dispersive effects of the magnetic field curvature on the flute-like drift-cyclotron

instabilities have been considered for a specific case. While no attempt was made to determine the stabilizing effects of the velocity-dependent as opposed to the velocity-independent curvature effects, Bhadra (7.44) does indicate that in the strong curvature case considered, a larger shift in the frequency of the flute-like instability than that obtained from velocity-independent curvature calculations is found. There is thus an indication that the velocity dispersion effects of curvature do have a significant effect on the drift-cyclotron instabilities. From this observation and the fact that the inclusion of the velocity dependence of the curvature drifts does have a stabilizing effect on the low-frequency drift instabilities (7.31), we conjecture that it may likewise have a stabilizing effect on the drift-cyclotron instabilities.

The effect which collisions have on the drift-cyclotron instabilities has also been considered. Pogutse (7.45) first considered these effects using the BGK collision model (7.26) from which he concluded that while collisions do reduce the real-k temporal growth rates somewhat, they do not markedly affect the stability of the drift-cyclotron instabilities. This work by Pogutse has been criticized by Bogdankevich and Rukhadze (7.46) who note that the work by Pitaevskii (7.47) has indicated that the essentially hydrodynamic BGK model is inadequate for the very short transverse wavelengths encountered in the drift-cyclotron instabilities. Using a Landau-type collision model (7.48) the latter authors find the drift-cyclotron instabilities can be stabilized by a moderate number

of collisions, but that as the collisions are introduced, it becomes possible for the potentially more dangerous drift-dissipative instability (7.14) to occur. We thus conclude that it is unlikely that the introduction of particle collisions is a reasonable means of stabilizing the drift-cyclotron instabilities.

In addition to the effects discussed above, Mikhailovskii (7.43) has also considered the effects on the drift-cyclotron instabilities of temperature gradients, "cold" plasma at the ends of the "hot" plasma, inhomogeneities in the magnetic field both along and transverse to the magnetic field and finally magnetic shear. Among these effects only the magnetic shear and introduction of cold plasma at the ends (by "line-tying" effects - see Section 1.1 for references) are found to significantly stabilize these instabilities. In other work, Mikhailovskii (7.49) has considered the nonlinear limiting of the drift-cyclotron instabilities for $T_e >> T_i$. Finally, we should note that a transverse electromagnetic ($\underline{k} \cdot \delta\underline{E} = 0$) drift-cyclotron instability has been predicted and discussed by Mikhailovskii (7.50).

A brief discussion of experiments in which the drift-cyclotron instability may be occurring is given by Lehnert (7.32). A definitive observation of flute-like drift-cyclotron instabilities in a multipole machine has recently been made by Ohkawa and Yoshikawa (7.51). In that work the dispersion characteristics of the unstable mode were found to be similar to those of the drift-cyclotron modes and the unstable modes were observed to propagate in the direction of the diamagnetic current, in agreement with theoretical predictions. However, the frequency was found

experimentally to be only a small fraction of instead of nearly equal to the ion cyclotron frequency. This latter discrepancy is, for the most part, explained by the large magnetic field curvature effect in the experimental machine (7.51) and has been carefully investigated theoretically by Bhadra (7.44).

7.3 Combination Loss-Cone and Drift-Cyclotron Instability

Having considered the loss-cone and drift-cyclotron instabilities separately in Sections 6.2 and 7.2 respectively, we will now discuss the instabilities of a plasma which has both loss-cone and spatial inhomogeneity sources of free energy. In this work we restrict ourselves to instabilities with occur near harmonics of the ion cyclotron frequency in such a plasma. In doing so we omit from consideration the low frequency drift and flute modes which might have different characteristics from the corresponding modes we have previously discussed which have only one of these two sources for free energy. To the author's knowledge these combination modes have never been investigated. However, a consideration of the characteristics of such low frequency modes ($\omega << \Omega_i$) is beyond the scope of the present work.

For convenience in discussing these instabilities driven by a combination of loss-cone and spatial inhomogeneity sources of free energy, we refer to them as "drift-cone" instabilities, a name given to them by Mikhailovskii (7.52). For a delta function $v_\perp$ distribution (peaked about a nonzero velocity), the drift-cone instabilities having $k_z=0$ were first discussed by Mikhailovskii (7.43). However, in that work the instabilities near harmonics

of the ion cyclotron frequency were found to be only slightly affected by the spatial inhomogeneity and persisted even in the limit of spatial homogeneity of the plasma. This particular set of modes discussed by Mikhailovskii are really just the flute-like loss-cone instabilities, which we have discussed in Sections 6.1 and 6.2, with slight corrections arising from the plasma inhomogeneity. Mikhailovskii (7.43) also discusses the high-frequency limit of the flute-like drift-cone instabilities. (This limit is equivalent to the "continuum" limit discussed in Section 6.3, whose validity requires that condition (6.3.3) be satisfied.) The effect of taking this limit in this case is to "smooth-out" the resonances of the waves moving transverse to the magnetic field direction with the individual cyclotron harmonic motions of the ions, thereby removing from consideration the flute-like instabilities driven by only the loss-cone source of free energy (see Section 6.3). Understandably, in the limit of spatial homogeneity of the plasma, Mikhailovskii (7.43) predicts that the drift-cone modes are stable. However, when a density gradient is present, Mikhailovskii finds that the flute-like drift-cone modes are unstable for sufficiently high plasma densities.

A much more exhaustive treatment of the flute-like drift-cone instabilities is given by Post and Rosenbluth (7.53). In contrast to Mikhailovskii (7.43), in analytical work they use a large $k_y a_i$ limit of the dispersion relation (see Section 6.3). The latter limit is valid for all complex ω, but "smooths out" the strengths of the individual cyclotron resonances so that the

flute-like instabilities driven by only the loss-cone source of free energy are again removed from consideration. In this limit of large $k_y a_i$, Post and Rosenbluth find that the flute-like drift-cone modes are unstable for a given density plasma if:

$$\left(\frac{\langle a_i \rangle}{n_i}\frac{dn_i}{dx}\right) > 0.38\left(\frac{m_e}{m_i} + \frac{\Omega_i^2}{\omega_{p_i}^2}\right)^{2/3} \qquad \text{(instability)} \quad (7.3.1)$$

in which

$$\langle a_i \rangle \equiv \left[\Omega_i^3 \int \frac{\langle f_i \rangle}{v_\perp^3} d^3v\right]^{-1/3} \approx a_i .$$

Now, for low densities ($\omega_{p_e}^2 < \Omega_e^2$ -- see footnote at bottom of p.344) the instability condition can be written approximately as:

$$\frac{\omega_{p_i}^2}{\Omega_i^2} \gtrsim \left|\frac{a_i}{n_i}\frac{dn_i}{dx}\right|^{-3/2} \qquad \text{(instability).} \quad (7.3.2)$$

Comparing this criterion with (7.2.4), we immediately conclude that the flute-like drift-cone instabilities are intrinsically different from the flute-like drift-cyclotron instabilities, but are in a sense an average of the flute-like loss-cone and drift-cyclotron instabilities. For a delta function $v_\perp$ distribution, Mikhailovskii (7.43) has also derived (7.3.2). However, it is important to note that (7.3.2) applies and flute-like drift-cone

instabilities can occur for any loss-cone type of $v_\perp$ distribution as long as $F_i(v_\perp, v_z)\Big|_{v_\perp=0} = 0$ (7.53). Post and Rosenbluth (7.53) have also carried out extensive numerical calculations of the critical density gradient for instability of these flute-like drift-cone modes using the exact dispersion relation and compared them with the approximate criterion given by (7.3.1). In these computations exact collisionally equilibrated $v_\perp$ distributions found in magnetic mirror machines are used and the effect of varying the magnetic mirror ratio is discussed. In general it is concluded that condition (7.3.1) is appropriate as long as $\left(\frac{\langle a_i \rangle}{n_i}\frac{dn_i}{dx}\right)$ is less than about 0.1, which in turn implies that $k_y a_i$ be greater than about three. We should also note with respect to the flute-like drift-cone instabilities that Mikhailovskii (7.54) has considered some aspects of their nonlinear effects.

To the author's knowledge the drift-cone instabilities having nonzero k_z have never been investigated. From our previous discussions of the nonzero k_z loss-cone and drift-cyclotron instabilities, it is easy to ascertain the general characteristics of the drift-cone instabilities. In comparing the loss-cone and drift-cyclotron instabilities we have found that the only fundamental difference between them is the range of phase velocities transverse to the magnetic field for which the ion contributions are destabilizing and thus lead to instability. For the loss-cone instabilities, those waves with phase velocities less than roughly the mean ion velocity transverse to the magnetic field are potentially unstable. In contrast, for the drift-cyclotron

modes the unstable waves have phase velocities which are less than the ion diamagnetic drift velocity and propagate only in the direction of the ion drift. Now, since within the approximations employed in this work (see (7.2.17)) the ion diamagnetic drift velocity is much less than the mean ion velocity, the phase velocity ranges in which the loss-cone and drift-cyclotron instabilities occur are usually quite different. Therefore we expect that the characteristics of the drift-cone instability will generally be governed by the range in which the phase velocity transverse to the magnetic field lies. If it is sufficiently small and in the direction of the ion diamagnetic drift, we expect the drift-cone instability to be like the drift-cyclotron instability. Likewise, when the phase velocity transverse to the magnetic field lies outside this small region but is still somewhat less than the mean ion velocity, the drift-cone instability would be expected to be like the loss-cone instability. Finally, we note that when the phase velocity is outside the regions for which a loss-cone instability can occur, we expect that the drift-cone modes will be stable.

In order to illustrate these points we will now discuss some calculations of the drift-cone instability which we have carried out. For convenience in comparing the results to the loss-cone and drift-cyclotron instabilities we choose the plasma parameters as follows: $T_e/T_i=10^{-2}$, $T_{\perp_i}=T_{z_i}$, $\ell=1$, $\varepsilon' a_i = -0.2$. With this choice of parameters we have computed the effects of varying $k_y a_i$ on the drift-cone instabilities in the usual manner (see Sections 6.2, 7.2). The results of these calculations are displayed in

Fig. 7.11, Tables 7.1, 7.2 and 7.3. In Fig. 7.11 the marginal stability and absolute instability characteristics are only plotted for the unstable drift-cone modes having frequencies near the ion cyclotron frequency. However, the flute-like drift-cone instabilities are shown for $\omega/\Omega_i \sim 1,2$.

For $\omega/\Omega_i \sim 1$ and $k_y a_i < 10$, the transverse phase velocity of the modes is greater than the ion diamagnetic drift velocity and so we expect that in this range the drift-cone instability will be like the loss-cone instability. Comparing the $\omega \sim \Omega_i$ instabilities in Fig. 7.11 with those in Fig. 6.4, we find that this is indeed the case. However, there are also two very important differences between the loss-cone and drift-cone modes in this regime.

First, we note that as we have discussed earlier in this section, there is a flute-like drift-cone instability even for the $\ell=1$ or most thermalized $v_\perp$ distribution for which the flute-like loss-cone modes are stable (see Section 6.1). Comparing the results displayed in Figs. 7.5 and 7.11, we see that the combination of loss-cone and spatial inhomogeneity sources of free energy induces a flute-like instability which occurs at a much lower density than that required in a comparable plasma with the source of free energy due to the loss-cone type of $v_\perp$ distribution removed. Even though we are out of the range in which instability condition (7.3.1) or (7.3.2) has been found by Post and Rosenbluth (7.53) to apply, we find that it is correct to within approximately a factor of 3 in the plasma density. The minimum density for instability of the flute-like drift-cone modes shown in Fig. 7.11 is consistent with the numerical calculations of Post and Rosenbluth (7.53).

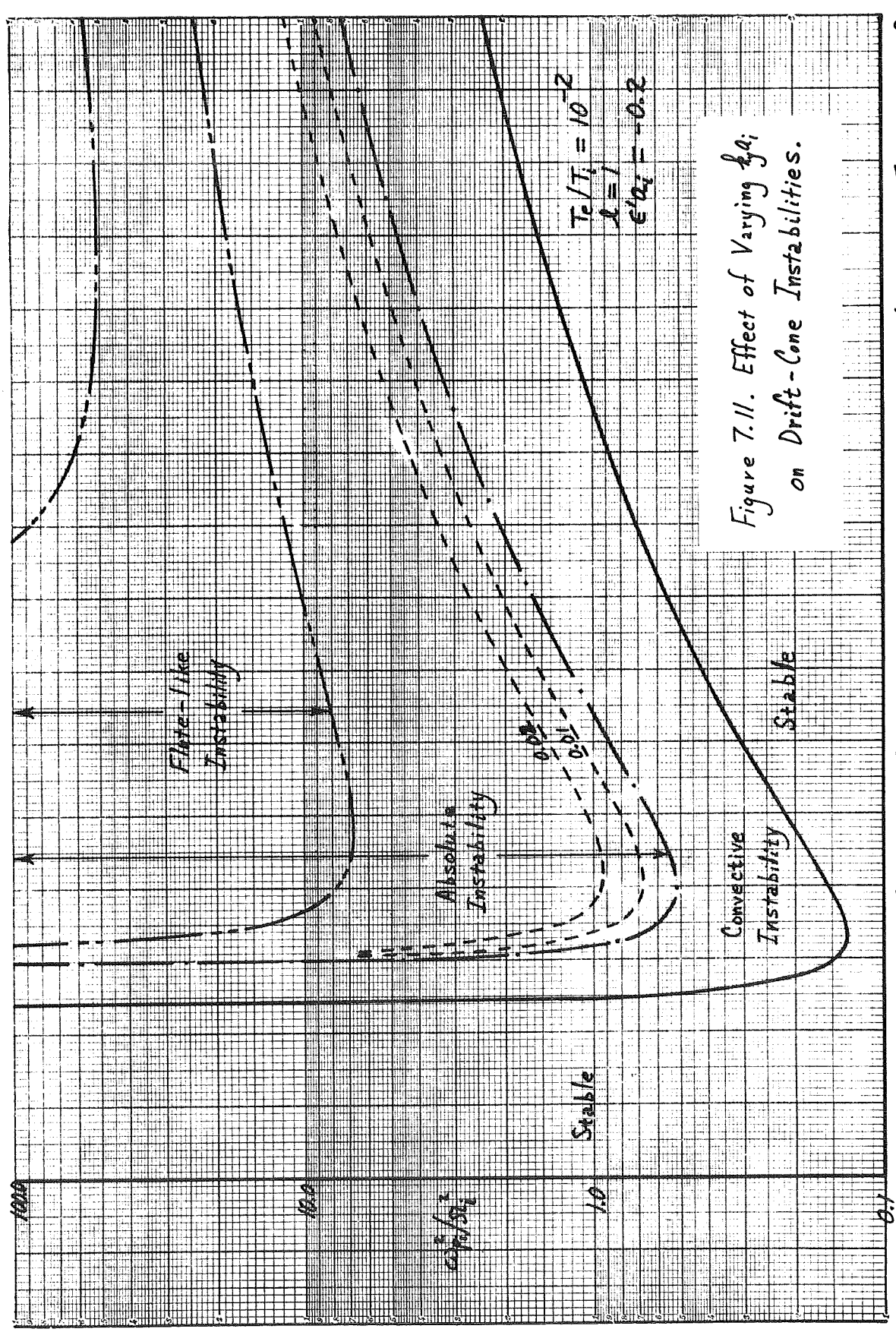

Figure 7.11. Effect of Varying $k_y a_i$ on Drift-Cone Instabilities.

The second major difference between the drift-cone and loss-cone instabilities in this regime is that in contrast to the loss-cone instabilities, the drift-cone instabilities have different characteristics for positive and negative frequencies. This difference is due to the directionality of the ion diamagnetic drift which has an effect on the drift-cone instabilities even in this essentially loss-cone instability regime. In order to demonstrate this effect, in Table 7.1 we have tabulated some properties of the drift-cone instabilities. Here we see that in the direction of diamagnetic current or ion diamagnetic drift (positive frequency) the instability is generally enhanced in that it occurs for lower densities and shorter axial wavelengths. In the opposite direction it is generally suppressed in these same respects. It is also important to note that the flute-like drift-cone modes, like the flute-like drift-cyclotron modes, are unstable only when they propagate in the direction of the ion diamagnetic drift.

Next, we consider the properties of the drift-cone instabilities for $\omega/\Omega_i \sim 1$ and $k_y a_i \gtrsim 10$ in which case the transverse phase velocity is of the order of or smaller than the ion diamagnetic drift velocity. As we have noted previously, we then expect the drift-cone instabilities to have properties which are similar to the drift-cyclotron instabilities. In order to make an appropriate comparison, we have computed the properties of the drift-cone instabilities for $k_y a_i = 10, 17$ and 25. The results of these computations are shown in Table 7.2. Similar results for the loss-cone instability are given in Table 7.3. Comparing the data shown in Table 7.2 with that displayed in

Table 7.1. Sample Properties of Drift-Cone Instabilities for $k_y a_i < 10$ ($T_e/T_i = 10^{-2}$, $\ell = 1$, $\varepsilon' a_i = -0.2$).

$k_y a_i$	ω/Ω_i	$(\omega_{pi}^2/\Omega_i^2)_{min}$	$k_z a_i$
Flute-Like Modes (k_z=0)			
2.50	0.7679	6.807	
3.02	0.7795	7.610	
3.50	0.7942	8.749	
Marginal Stability Analysis			
2.50	0.9639	0.2185	0.0957
	-0.9678	0.3272	0.08585
3.02	0.9652	0.3135	0.0961
	-0.9722	0.4460	0.0882
3.50	0.9662	0.4230	0.09585
	-0.9739	0.6035	0.0882
Absolute Instability Transition Densities			
2.50	0.9439	0.6345	0.04583-0.01709i
	-0.9635	2.279	0.03004+0.01165i
3.02	0.9436	0.8905	0.04605-0.01716i
	-0.9601	2.560	0.03278+0.01265i
3.50	0.9444	1.209	0.04540-0.01695i
	-0.9605	3.560	0.03245+0.01253i

Table 7.2. Sample Properties of Drift-Cone Instabilities for $k_y a_i \geq 10$ ($T_e/T_i = 10^{-2}$, $\ell = 1$, $\epsilon' a_i = -0.2$).

$k_y a_i$	ω/Ω_i	$(\omega_{pi}^2/\Omega_i^2)_{min}$	$k_z a_i$
Flute-Like Modes (k_z=0)			
10.0	0.8958	31.32	
17.0	0.9267	59.84	
25.0	0.9424	94.16	
Marginal Stability Analysis			
10.0	0.9741	3.724	0.09225
17.0	0.9760	10.67	0.0907
25.0	0.9762	22.18	0.08975
Absolute Instability Transition Densities			
10.0	0.9534	11.48	0.03820-0.01456i
17.0	0.9567	31.23	0.03547-0.01361i
25.0	0.9586	59.70	0.03399-0.01309i
Absolute Instabilities with Temporal Growth Rates			
10.0	0.9550+0.01i	14.18	0.03199-0.01609i
	0.9563+0.02i	17.93	0.02580-0.01839i
17.0	0.9585+0.01i	37.40	0.02918-0.01508i
	0.9599+0.02i	45.29	0.02291-0.01738i
25.0	0.9604+0.01i	69.40	0.02763-0.01449i
	0.9620+0.02i	80.97	0.02129-0.01674i

Table 7.3. Sample Properties of Loss-Cone Instabilities for $k_y a_i \geq 10$, for comparison with Table 7.2 ($T_e/T_i = 10^{-2}$, $\ell = 1$, $\varepsilon' a_i = 0.0$).

$k_y a_i$	ω/Ω_i	$(\omega_{pi}^2/\Omega_i^2)_{min}$	$k_z a_i$
Marginal Stability Analysis			
10.0	0.9798	4.794	0.0880
17.0	0.9842	15.38	0.08525
25.0	0.9864	35.78	0.0833
Absolute Instability Transition Densities			
10.0	0.9624	24.38	0.03089-0.01196i
17.0	0.9682	98.62	0.02623-0.01023i
25.0	0.9718	275.5	0.02321-0.009089i
Absolute Instabilities with Temporal Growth Rates			
10.0	0.9641+0.01i	35.01	0.02457-0.01358i
	0.9653+0.02i	64.43	0.01842-0.01620i
17.0	0.9698+0.01i	151.1	0.01985-0.01192i
	0.9708+0.01844i	246.5	0.01468-0.01427i
25.0	0.9735+0.01i	450.0	0.01680-0.01085i
	0.9742+0.01526i	633.5	0.01356-0.01230i

Figs. 7.5, 7.6 for the drift-cyclotron instabilities and that displayed in Table 7.3 for the loss-cone instabilities, we find that in this regime, as we expected, the drift-cone instabilities are most like the drift-cyclotron instabilities and that the similarity increases with increasing $k_y a_i$.

We have thus seen that for the most part the drift-cone instability is simply a "superposition" of the loss-cone and drift-cyclotron instabilities. Since the T_e/T_i characteristics of these two different types of instabilities are nearly the same, we expect that the drift-cone modes will have these same characteristics for varying T_e/T_i. As we have seen there are two major contradictions to this "superpositioning" of the loss-cone and drift-cyclotron instabilities.

First, there is the appearance of the flute-like drift-cone mode at much lower densities and values of $k_y a_i$ than found for the drift-cyclotron instabilities in a regime in which no flute-like loss-cone instabilities occur. The appearance of this drift-cone mode has very important implications on the possibility of containment of high density loss-cone type plasmas since in contrast to the drift-cone modes with nonzero k_z, the flute-like mode appears in plasmas of nearly any length (see Section 5.4). It is thus much more dangerous. We also note that in the case considered here it occurs at a fairly low plasma density. As with the flute-like modes which we have previously discussed, we may be able to suppress the flute-like drift-cone instability by the introduction of cold plasma at the ends of the hot plasma region ("line-tying" effect), or of curvature of the magnetic

field. It may also be controlled by making the density gradients and $v_\perp$ distribution sufficiently gentle (7.53). Therefore while these flute-like drift-cone instabilities would appear to be very detrimental to the containment of high density plasmas, it appears that we may be able to control them to a reasonable degree.

The other major contradiction to the "superpositioning" of the loss-cone and drift-cyclotron instabilities is that the ion diamagnetic drift introduces a preferential direction in which the drift-cone modes move. An important implication of this observation is that the unstable "high frequency" modes (with frequencies near harmonics of the ion cyclotron frequency) in any finite plasma with a loss-cone type of $v_\perp$ distribution would be expected to preferentially propagate in the direction of the diamagnetic current. This property could presumably be helpful in identifying the instabilities of an experimentally unstable plasma.

8. CONCLUSION

8.1 Summary

We have already given a synopsis of the topics discussed in each of the chapters of this thesis in Section 1.4. In this section we summarize the important results obtained in this work. Some extensions of this work which are worthy of consideration are noted in the following section.

In the first three chapters we have come to some conclusions of perhaps only minor importance which are, however, worth noting here. First, in Section 1.2 we have concluded that in order to justify neglecting the effects of transverse (electromagnetic) waves in a plasma, the β of the plasma must be much less than m_e/m_i, or unity for wave frequencies much less than, or of the order of the ion cyclotron frequency respectively. In Section 2.4 we have found that, strictly speaking, in order to satisfy this condition on β and have a self-consistent equilibrium when there is magnetic field curvature but no static electric field component along the magnetic field, the characteristic curvature length must in general be long compared to the characteristic scale length for plasma inhomogeneities. Finally, in Section 3.3 we have determined that the "local" approximation (in the direction of plasma inhomogeneities) to the exact dispersion relation, which is used in this and many other works, is reasonably valid only if the characteristic plasma inhomogeneity length

is long compared to not only the ion Larmor radius as noted by Krall and Rosenbluth (8.1), but also to two other "fine-structure" lengths in the plasma, namely the Debye length and G_i/Ω_i^2 (the scale length of charge separations due to the presence of a gravity force transverse to the magnetic field).

The conclusions and results obtained in the following chapters are of greater importance. In Chapter 4 we have rigorously derived very general necessary and sufficient conditions for instability of a slightly inhomogeneous plasma in a magnetic field. In general, these criteria justify and elucidate the commonly used marginal stability analysis. As a further conclusion in this chapter, we have noted that while the Cauchy integral method (8.2) can be extremely useful in finding real-k temporal growth rates of unstable modes if an "on-line" computer is available, in general if we want to thoroughly investigate the real-k temporal growth rates of a given instability or wish to use normal computer "batch" processing, it is probably best to use the usual iterative root following techniques.

In the fifth chapter we have reviewed the criteria which have been derived for distinguishing between convective and absolute instabilities and have summarized that work for our purposes with the statement of a single criterion for absolute instability. By exploiting the fact that the dispersion relation can be written in a form in which the density is a "free parameter" and the results of a marginal stability analysis,

we have developed a new and very efficient method for implementing the criterion for absolute instability to directly determine the transition density for the onset of absolute instability. We have also discussed how we can use essentially the same method to directly determine the density at which an absolute instability has a given temporal growth rate.

In the following chapters we have applied the techniques developed in this work to the study of two very general classes of microinstabilities. First, in Chapter 6 we have considered the instabilities of a homogeneous plasma in a magnetic field which are driven by the free energies associated with velocity-space anisotropies. Using the general instability criterion of Chapter 4 as a guide, we have reviewed the literature concerning these instabilities.

With this review as an introduction, we have undertaken an extensive study of the velocity-space anisotropy instabilities driven by the source of free energy associated with a loss-cone type of $v_\perp$ distribution, i.e. the loss-cone instabilities. The effects which variations in the electron temperature and sharpness of the $v_\perp$ distribution have on loss-cone instabilities for all relevant wave numbers and frequencies have been considered. The convective versus absolute nature of these unstable modes along the axial or magnetic field direction has been thoroughly investigated. In contrast to previous indications (8.3), we find that the loss-cone instabilities can be of the absolute type and in fact as a general rule

are so for relevant plasma conditions. Assuming that absolute instabilities can "fit" into any plasma which is at least a half-wavelength long, we have found that the convective loss-cone instabilities can be a serious detriment to plasma containment before the appearance of an absolute instability only if the reflection coefficient for waves moving axially in the plasma exceeds about 0.285 and even then only for small T_e/T_i. Since such a large reflection coefficient seems unlikely or at least avoidable (see Section 5.4), we conclude that only the absolute loss-cone instabilities will be important in limiting plasma containment in an experimental device.

Within the limits of a consideration of the infinite homogeneous plasma theory, we have found that neither heating the electrons (up to $T_e \sim T_i$) nor increasing the thermal spread in the $v_\perp$ distribution (up to a spread roughly equal to the mean displacement) significantly stabilize the absolute loss-cone instabilities. The relevant criteria for the appearance of the absolute loss-cone instabilities have been found to be

$$\frac{\omega_{p_i}^2}{\Omega_i^2} > 0.8\, n^{8/3} \qquad \text{(instability)} \qquad (8.1.1)$$

$$L > \frac{25\pi a_i}{n^{2/3}} \qquad \text{(instability)} \qquad (8.1.2)$$

in which n is the ion cyclotron harmonic number of the

unstable mode, a_i is the mean ion Larmor radius and L is the axial length of the plasma. In arriving at the length condition we have assumed that an absolute instability mode "fits" into the plasma if L is greater than a half-wavelength of the mode. The threshold densities for both flute and flute-like loss-cone instabilities are generally higher than that given by inequality (8.1.1) -- see Section 6.2.

We have also employed the techniques developed in this work to examine the applicability of the "continuum" limit (short transverse wavelengths, $k_\perp a_i >> 1$) of the dispersion relation which has been derived by Rosenbluth and Post (8.3) for studying loss-cone instabilities. In this regard, we have considered a case in which $k_\perp a_i = 25$ in great detail. We conclude that while the "continuum" limit is derived from very appealing physical arguments and is very helpful in guiding our intuition and in doing approximate calculations, it does not seem to have a wide enough range of applicability for detailed instability calculations which must include a consideration of the convective versus absolute nature of the loss-cone instabilities.

The second general application of the techniques we have developed in this work has been to the study of "universal" or drift instabilities (see Chapter 7), i.e. those driven by the source of free energy associated with the inhomogeneity of confined plasmas. In this regard, we have briefly surveyed the literature concerning low frequency drift instabilities and

employed the instability criteria developed in this work to derive a simple version of a general instability criterion for these modes which has been given by Krall and Rosenbluth (8.1). By comparing the instability criteria for low frequency drift modes with those for the loss-cone instabilities, we conclude that the loss-cone modes generally occur in shorter plasmas and are thus potentially more detrimental to plasma containment.

As a second major application of the techniques developed in this work, we have undertaken an extensive study of the drift-cyclotron instabilities (those drift instabilities which have frequencies of the order of the ion cyclotron frequency or its harmonics). This study includes a review of the literature on these instabilities and an examination of their convective versus absolute nature in the axial or magnetic field direction. The effects which variations in the electron temperature and density gradient have on drift-cyclotron instabilities for all relevant wave numbers and frequencies have been considered. We find that, as with the loss-cone instabilities, the drift-cyclotron instabilities can be of the absolute type and that the convective drift-cyclotron instabilities would be expected to be detrimental to plasma containment only if the reflection coefficient at the axial ends of the plasma exceeds about 0.285. Thus, as before, we conclude that only the absolute drift-cyclotron instabilities will be of importance in experimental plasmas. These absolute instabilities have been found

to be relatively unaffected by variations in the electron temperature (up to $T_e \sim T_i$), but strongly affected by changes in the density gradient. The criteria for the appearance of absolute drift-cyclotron instabilities were found to be

$$\frac{\omega_{p_i}^2}{\Omega_i^2} > 2n^{8/3} \left[\frac{a_i}{n_i}\frac{dn_i}{dx}\right]^{-2} \qquad \text{(instability)} \qquad (8.1.3)$$

$$L > \frac{35\pi a_i}{n^{2/3}} \qquad \text{(instability)} \qquad (8.1.4)$$

in which the corresponding symbols have the same meanings as in (8.1.1) and (8.1.2). The corresponding instability criterion for the appearance of the flute-like drift-cyclotron instabilities is (see Section 7.2)

$$\frac{\omega_{p_i}^2}{\Omega_i^2} > 4n^2 \left[\frac{a_i}{n_i}\frac{dn_i}{dx}\right]^{-2} . \qquad (8.1.5)$$

Comparing the respective criteria for the appearance of absolute loss-cone and absolute and flute-like drift-cyclotron instabilities, we conclude that the loss-cone instabilities pose the greater threat to plasma confinement.

Finally, in Section 7.3 we have discussed the instabilities which occur when both loss-cone and spatial inhomogeneity sources of free energy are present. We have found that these instabilities are just a "superposition" of the loss-cone and drift-cyclotron instabilities in all but two respects. First,

we have observed that the flute-like instabilities which occur in such a plasma (8.4, 8.5) have characteristics which are different from either the flute-like loss-cone or drift-cyclotron instabilities although they do represent some sort of an average of those characteristics. However, it is important to note that the combination flute-like modes generally have a lower threshold density than either of the separate modes (see Section 7.3). Second, we have found that the introduction of the density gradient causes the instabilities to have a preferred direction of propagation, namely in the direction of the diamagnetic current. This latter property may be useful in experimentally identifying these unstable modes.

In short, the methods we have developed to study the stability and absolute versus convective instability of weakly inhomogeneous plasmas immersed in a magnetic field have been found to be of sufficient generality and efficiency to allow us to thoroughly examine for the first time the absolute versus convective nature and potency of the loss-cone and drift-cyclotron instabilities.

8.2 Suggestions for Further Study

While we have restricted our applications of the general techniques developed in this work to detailed studies of the loss-cone and drift-cyclotron instabilities, the techniques can presumably be fruitfully applied to many other types of instabilities as well. Within the limitations of the computer programs developed in this work, in addition to the effects considered here, we could consider: multi-component plasmas, inequality of mean velocities along and transverse to the magnetic field, particle currents along the magnetic field, temperature gradients along and transverse to the magnetic field, magnetic field curvature effects at least in bi-Maxwellian plasmas (see Sections 2.2, 2.4), or any desired combination of these effects. Of particular interest would be a study of the effects of the introduction of a small number of "warm" ions having a Maxwellian distribution into a "hot" plasma whose ions have a loss-cone type $v_\perp$ distribution since this procedure has been proposed (8.6) as a method of "filling in" the loss-cone and thereby stabilizing the loss-cone instabilities.

With respect to the loss-cone and drift-cyclotron instabilities which we have studied in great detail, there are a number of subsidiary questions worth considering which may result in modifications of the conclusions we have arrived at in this work. First, it is very important to know if the loss-cone instabilities of a plasma having a true collisionally equilibriated loss-cone distribution would have the same

qualitative features as those we have found using idealized "loss-cone" distributions. Next, it would be of great interest to study the nonzero, but real, group-velocity loss-cone and drift-cyclotron instability modes to ascertain if, as we have conjectured, the zero group-velocity (absolute instability) modes are indeed representative of the small group-velocity modes and that the absolute versus convective nature of the unstable modes transverse to the magnetic field direction is of little importance. Also of interest would be a study of the nonlinear effects on the absolute instabilities which, as we have noted in Section 5.4, must presumably take account of the motion and spatial growth of wave packets of unstable modes. Of perhaps greatest importance would be a study of the effects which the finite length of any given plasma may have on both the convective and absolute instabilities, including those cases where the scale length of the plasma or magnetic field inhomogeneity is of the order of the wavelength of the unstable modes.

Finally, we may note studies which have been implicitly suggested in our derivation and analysis of the general dispersion relation. From the fact that we have seen that transverse (electromagnetic) waves cannot be ignored in very dense plasmas (see Section 1.2), we observe that a study of these waves and their coupling to the electrostatic waves considered here would be of interest in such plasmas. The rudimentary level of our discussion of the effects of

magnetic field curvature, particularly with loss-cone type $v_\perp$ distributions, is indicative of the present theoretical treatments of this subject. A study of these effects including their dependence on particle velocities (see Sections 2.4, 7.1) and a careful consideration of the establishment of a realistic and self-consistent equilibrium would be of considerable interest with regard to applications of this work to a theoretical study of plasmas such as those found in the Van Allen belts. It would also be interesting to derive a one-dimensional form of our general dispersion relation (see Chapter 4) directly from the Vlasov equation. Such a derivation would allow us to show directly that the necessary and sufficient conditions for stability are that the necessary and sufficient conditions for instability not be satisfied for any mode in the plasma. It would also presumably give us further insight into the nature of the "local" approximation used in deriving the dispersion relation. Finally, it would be of interest to further elucidate (see Section 5.2) the conditions under which absolute instability modes at the lowest densities for which they can occur have real frequencies.

ACKNOWLEDGEMENT

The author wishes to thank Professor J. E. McCune for his guidance and friendship throughout the course of this study. Professor McCune was the author's major thesis advisor and his invaluable suggestions and his diligence in working with the author are gratefully acknowledged. The author sincerely appreciates the many generosities shown by Professor McCune during the course of this investigation.

It is a pleasure to thank Professor T. H. Dupree for his continuing interest and for a number of provocative discussions of this work. The author also wishes to thank Professors D. J. Rose and L. M. Lidsky for their consideration and guidance during the author's graduate studies at M.I.T. Professor Rose served as the Thesis Reader, carefully read the thesis, and made a number of valuable suggestions.

The typing of the final manuscript was capably handled by Misses D. Burns and A. Carbone and AID, Inc., whom the author wishes to thank. Particular thanks are due Miss D. Burns who quickly and cheerfully made final corrections to and assembled the final manuscript.

The author is grateful for the financial support of his graduate studies at M.I.T. which was supplied by: the Atomic Energy Commission through its Special Fellowship Program in Nuclear Science and Engineering which is

administered by the Oak Ridge Institute of Nuclear Studies (2 years); the National Science Foundation through its Graduate Fellowship program (1 year); and the Nuclear Engineering Department through a Research Assistantship (1 semester). Finally, the author wishes to express his gratitude to Professor M. N. Rosenbluth and the Institute for Advanced Study for their financial support and hospitality during the four months preceding the completion of this document.

The author also acknowledges the primary support for this research which was extended to the Massachusetts Institute of Technology by the National Aeronautics and Space Administration under Contract NsG-496 with the Center for Space Research. In addition, partial support was derived from the National Science Foundation under Contract GK-1165 with the Research Laboratory of Electronics. The numerical computations in this work were carried out at the M.I.T. Computation Center as problem M5107.

VITA

The author was born on [redacted] in [redacted] and received the majority of his elementary and secondary education there, graduating from Wichita High School North in 1958. He received his undergraduate education at Kansas State University from which he graduated Cum Laude in June, 1962 with a B.S. in Nuclear Engineering. The author held a Putnam Scholarship during his undergraduate years, participated in student activities and was a member of the varsity swimming team for two years. The national honor societies of which the author is a member include: Sigma Xi, Phi Kappa Phi, Blue Key, Tau Beta Pi, Sigma Tau and Pi Mu Epsilon.

After completing his undergraduate work the author studied and did research on boiling water reactor coolant problems for one year at the Technische Hogeschool Te Eindhoven, Eindhoven, Netherlands on a Fulbright Fellowship. Then, he returned to Kansas State University at which he held an AEC Fellowship and from which he graduated with an M.S. degree in Nuclear Engineering (Fission) in August, 1964. The author's master's thesis was entitled, "The Spherical Harmonics Method for Critical Spheres" and was supervised by Dr. J. O. Mingle.

In September, 1964 the author came to M.I.T. During the course of his graduate studies at M.I.T. he has held AEC Fellowships (2 years), an NSF Graduate Fellowship

(1 year) and a Research Assistantship (1 semester). He passed the general examination in the fall of 1965 and began this study shortly thereafter. During the final 4 months of this work he was in residence at the Institute for Advanced Study.

The professional experience of the author includes approximately one year of part-time computer programming at Kansas State University and a summer at Avco-Everett Research Laboratory where he did research on electron-rich plasmas dominated by space charge effects under the supervision of Dr. R. H. Levy. The author is a co-author of the journal publications

"The Diocotron Instability in a Quasi-Toroidal Geometry," Phys. Fluids 8, 2298 (1965) (with R. H. Levy),

"Spherical Harmonics Convergence Studies for Critical Spheres," J. Nucl. Energy 22, 173 (1968) (with J. O. Mingle)

and is the author or co-author of 4 scientific meeting presentations and 4 technical reports.

With the completion of the author's doctoral work, he will be supported by an NSF Postdoctoral Fellowship to carry out research at the Institute for Advanced Study, Princeton, New Jersey under the direction of Professor M. N. Rosenbluth.

REFERENCES

1.1 For a recent survey of plasma instabilities of all types see: B. Lehnert, Plasma Physics 9, 301 (1967).

1.2 J.B. Taylor, Phys. Fluids 6, 1529 (1963); Phys. Fluids 7, 161 (1964); see also J. Androeoletti, Comptes Rendus Acad. Sci. 257, 1033 (1963); H.P. Furth, Phys. Rev. Letters 11, 308 (1963); M.N. Rosenbluth and N.A. Krall, Phys. Fluids 8, 1004 (1965); T.K. Fowler, Phys. Fluids 9, 1437 (1966).

1.3 For a magnetic mirror geometry see: Yu. B. Gott, M.S. Ioffe and V.G. Telkovsky, Nuclear Fusion: 1962 Supplement, Pt. 3, 1045 (1962) (in Russian); Yu. T. Baiborodov, M.S. Ioffe, V.M. Petrov and R.I. Sobolev, Atom Energiya (USSR) 14, 443 (1963) (Translations: Soviet J. At. Energy 14, 459 (1964) and J. Nucl. Energy, Pt. C: Plasma Physics 5, 409 (1963)); W. Bernstein, V.V. Chechkin, L.G. Kuo, E.G. Murphy, M. Petravic, A.C. Riviere and D.R. Sweetman in Plasma Physics and Controlled Nuclear Fusion Research (International Atomic Energy Agency, Vienna, 1966), Vol. II, p. 23 and references cited therein. For a toroidal multipole geometry see: T. Ohkawa, A.A. Schupp, Jr., H.G. Voorhies and M. Yoshikawa, ibid., Vol. II, p. 531; R.A. Dory, D.W. Kerst, D.M. Meade, W.E. Wilson and C.W. Erickson, Phys. Fluids 9, 997 (1966). For a high density arc plasma in a magnetic mirror geometry see F. Schwirzke, Phys. Fluids 10, 183 (1967).

1.4 B. Coppi and M.N. Rosenbluth, Plasma Physics and Controlled Nuclear Fusion Research (International Atomic Energy Agency, Vienna, 1966), Vol. I, p. 617; H.P. Furth, J. Killeen, M.N. Rosenbluth and B. Coppi, ibid., p. 103 and references cited therein.

1.5 D.H. Birdsall, R.J. Briggs, S.A. Colgate, H.P. Furth and C.W. Hartman, ibid., Vol. II, p. 291; D.J. Grove, E.B. Meservey, W. Stodiek and K.M. Young, Bull. Am. Phys. Soc. 13, 286 (1968).

1.6 C.W. Hartman, Phys. Fluids 9, 821 (1966); W.B. Kunkel and J.U. Guillory in Proceedings of the Seventh International Conference on Phenomena in Ionized Gases (Gradevinska Knjiga Publishing House, Beograd, Yugoslavia, 1966), Vol. II, p. 702 and references cited therein.

1.7 For a survey of microinstabilities see: M.N. Rosenbluth, "Microinstabilities" in Plasma Physics (International Atomic Energy Agency, Vienna, 1965), p. 485.

1.8 T.K. Fowler, Phys. Fluids 8, 459 (1965); (Erratum) Phys. Fluids 8, 2120 (1965); Phys. Fluids 7, 249 (1964); J. Math. Phys. 4, 559 (1963).

1.9 G. Rowlands, Phys. Fluids 9, 2528 (1966).

1.10 For small perturbations see: M.N. Rosenbluth, "Microinstabilities," article in Riso Report No. 18, Danish Atomic Energy Commission Research Establishment Riso, International Summer Course in Plasma Physics (1960); in Advanced Plasma Theory, M.N. Rosenbluth, Ed. (Academic Press, New York, 1964), p. 137; and reference 1.7. For a nonlinear proof see C.S. Gardner, Phys. Fluids 6, 839 (1963) and reference 1.8.

1.11 J.E. McCune, Phys. Rev. Letters 15, 398 (1965); (Erratum) Phys. Rev. Letters 15, 684 (1965).

1.12 P.A. Sturrock, Phys. Rev. 112, 1488 (1958); P.A. Sturrock in Plasma Physics, J.E. Drummond, Ed. (McGraw-Hill, New York, 1961), p. 124.

1.13 J.E. McCune and J.D. Callen, Bull. Am. Phys. Soc. 13, 282 (1968) (to be published).

1.14 J.D. Callen and J.E. McCune, Bull. Am. Phys. Soc. 13, 282 (1968) (to be published).

1.15 D.C. Montgomery and D.A. Tidman, Plasma Kinetic Theory (McGraw-Hill, New York, 1964), p. 41 et seq.

1.16 C.R. Wylie, Advanced Engineering Mathematics (McGraw-Hill, New York, 1951), p. 34.

1.17 See for example: I.B. Bernstein, Phys. Rev. 109, 10 (1958), Eq. (21); and reference 1.15, p. 134, Eq. (10.35); or follow through the general procedures of Chapter 3 of this work for a nearly homogeneous plasma keeping the perturbed magnetic field $\delta\underline{B}$ and with the appropriate coordinate system for the electric field vector $\delta\underline{E}$. See also D.E. Baldwin, I.B. Bernstein and M.P.H. Weenick, "Kinetic Theory of Plasma Waves in a Magnetic Field" (to be published in Nuclear Fusion).

1.18 See for example: T.H. Stix, The Theory of Plasma Waves (McGraw-Hill, New York, 1962), pp. 10, 33.

1.19 L.I. Rudakov and R.Z. Sagdeev, Dokl. Akad. Nauk SSSR 138, 581 (1961) (Translation: Soviet Phys. - Doklady 6, 415 (1961)).

1.20 N.A. Krall and M.N. Rosenbluth, Phys. Fluids 8, 1488 (1965).

1.21 W.E. Drummond and M.N. Rosenbluth, Phys. Fluids 5, 1507 (1962).

1.22 B.B. Kadomtsev, Plasma Turbulence (Academic Press, London, 1965), p. 81.

1.23 A.B. Mikhailovskii, "Oscillations of an Inhomogeneous Plasma," in Reviews of Plasma Physics, M.A. Leontovich, Ed. (Consultants Bureau, New York, 1967), Vol. 3, p. 159.

1.24 P.H. Rutherford and E.A. Frieman, Phys. Fluids 10, 1007 (1967) and references cited therein.

1.25 R.A. Dory, G.E. Guest and E.G. Harris, Phys. Rev. Letters 14, 131 (1965).

1.26 R.F. Post and M.N. Rosenbluth, Phys. Fluids 9, 730 (1966).

1.27 J.D. Jackson, Classical Electrodynamics (Wiley, New York, 1962), p. 3.

1.28 M.N. Rosenbluth and R.F. Post, Phys. Fluids 8, 547 (1965).

1.29 A.B. Mikhailovskii and A.V. Timofeev, Zh. Eksperim. i Teor. Fiz. 44, 919 (1963) (Translation: Soviet Phys. - JETP 17, 626 (1963)).

2.1 H. Goldstein, Classical Mechanics (Addison-Wesley, Reading, Mass., 1959), p. 48.

2.2 N.A. Krall and M.N. Rosenbluth, op. cit. 1.20.

2.3 D.J. Rose and M. Clark, Plasmas and Controlled Fusion (MIT Press, Cambridge, Mass., 1961), p. 264.

3.1 R. Courant and D. Hilbert, Methods of Mathematical Physics, Vol. II, Partial Differential Equations by R. Couvant (Interscience, New York, 1962), p. 62.

3.2 D.J. Rose and M. Clark, op. cit. 2.3, p. 200.

3.3 G.N. Watson, The Theory of Bessel Functions (Cambridge Univ. Press, Cambridge, England, 1962), 2nd Ed., p. 22.

3.4 N.A. Krall and M.N. Rosenbluth, op. cit. 1.20.

3.5 L.I. Rudakov and R.Z. Sagdeev, op. cit. 1.19.

3.6 N.A. Krall and M.N. Rosenbluth, Phys. Fluids 6, 254 (1963). See also A.A. Rukhadze and V.P. Silin, Usp. Fiz. Nauk 82, 499 (1964) (Translation: Soviet Phys. Usp. 7, 209 (1964)).

3.7 A.B. Mikhailovskii and L.I. Rudakov, Zh. Eksperim. i Teor. Fiz. 44, 912 (1963) (Translation: Soviet Phys. - JETP 17, 621 (1963)).

3.8 A.A. Galeev, Zh. Eksperim. i Teor. Fiz. 44, 1920 (1963) (Translation: Soviet Phys. - JETP 17, 1292 (1963)); Dokl. Akad. Nauk SSSR 150, 503 (1963) (Translation: Soviet Phys. - Doklady 8, 444 (1963)).

3.9 V.P. Silin, Zh. Eksperim. i Teor. Fiz. 44, 1271 (1963) (Translation: Soviet Phys. - JETP 17, 857 (1963)).

3.10 F.C. Hoh, Phys. Fluids 8, 1741 (1965).

3.11 L.D. Pearlstein, Phys. Fluids 8, 1743 (1965).

3.12 F.F. Chen, Phys. Fluids 9, 965 (1966).

3.13 P.H. Rutherford and E.A. Frieman, op. cit. 1.24.

3.14 Y. Shima and T.K. Fowler, Phys. Fluids 8, 2245 (1965).

3.15 N.A. Krall and M.N. Rosenbluth, Phys. Fluids 5, 1435 (1962).

3.16 J. Mathews and R.L. Walker, Mathematical Methods of Physics (Benjamin, New York, 1965), p. 12.

3.17 See for example: A. Messiah, Quantum Mechanics (Wiley, New York, 1961), Vol. I, p. 77.

3.18 L.I. Schiff, Quantum Mechanics (McGraw-Hill, New York, 1955), pp. 184 ff. See also: P.M. Morse and H. Feshbach, Methods of Theoretical Physics (McGraw-Hill, New York, 1953), Vol. II, pp. 1092 ff. and N. Fröman and P.O. Fröman, JWKB Approximation (North-Holland Pub. Co., Amsterdam, 1965).

3.19 J.B. Taylor, Phys. Fluids 10, 1357 (1967).

3.20 For the original theoretical work see: L.D. Landau, J. Phys. (USSR) 10, 25 (1946). For a discussion of the physics of Landau damping see: T.H. Stix, op. cit. 1.18, p. 132; D.C. Montgomery and D.A. Tidman, op. cit. 1.15, p. 265. For the original experimental work confirming the existence of Landau damping see: A.Y. Wong, N. D'Angelo and R.W. Motley, Phys. Rev. 133, A436 (1964); J.H. Malmberg and C.B. Wharton, Phys. Rev. Letters 13, 184 (1964); J.H. Malmberg, C.B. Wharton and W.E. Drummond, Plasma Physics and Controlled Nuclear Fusion Research (International Atomic Energy Agency, Vienna, 1966), Vol. I, p. 485. For a recent summary of experimental verifications of Landau damping see: I. Alexeff, W.D. Jones and D. Montgomery, Phys. Rev. Letters 19, 422 (1967).

3.21 I.B. Bernstein, S.K. Trehan and M.P.H. Weenick, Nuclear Fusion 4, 61 (1964); D.C. Montgomery and D.A. Tidman, op. cit. 1.15, p. 60.

3.22 For a discussion of the physics of cyclotron damping see: T.H. Stix, op. cit. 1.18, p. 159. For experimental work see: C.B. Wharton and J.H. Malmberg, Proc. 7th International Conf. on Phenomena in Ionized Gases, Beograd, Aug. 22-27, 1965 (Gradevinska Knjiga Pub. House, Beograd, 1966), Vol. II, p. 256. See also J.A. Tataronis and F.W. Crawford, ibid., Vol. II, p. 244.

3.23 I.B. Bernstein, Phys. Rev. 109, 10 (1958); T.H. Stix, op. cit. 1.18, p. 41.

3.24 E.G. Harris, Phys. Rev. Letters 2, 34 (1959); J. Nucl. Energy, Pt. C: Plasma Physics 2, 138 (1961).

3.25 A.B. Mikhailovskii and A.V. Timofeev, Zh. Eksperim. i Teor. Fiz. 44, 919 (1963) (Translation: Soviet Phys. - JETP 17, 626 (1963)).

3.26 F.C. Hoh, Phys. Fluids 8, 968 (1965).

3.27 G.E. Guest and R.A. Dory, Phys. Fluids 8, 1853 (1965).

3.28 B.D. Fried and S.D. Conte, The Plasma Dispersion Function (Academic Press, New York, 1961).

3.29 J.E. McCune (private communication).

4.1 See for example: W.P. Allis, S.J. Buchsbaum and A. Bers, Waves in Anisotropic Plasmas (M.I.T. Press, Cambridge, Mass., 1963). Or, take the limit of $\alpha_{\perp_j}$ and α_{z_j} going to zero with $\alpha_{\perp_j}/\alpha_{z_j} \to 1$ in the dispersion relations derived in this work.

4.2 op. cit. 3.20.

4.3 J.D. Jackson, J. Nucl. Energy, Pt. C: Plasma Physics 1, 171 (1960).

4.4 O. Penrose, Phys. Fluids 3, 258 (1960).

4.5 P.D. Noerdlinger, Phys. Rev. 118, 879 (1960).

4.6 See for example: D.C. Montgomery and D.A. Tidman, op. cit. 1.15, p. 63. Or, specialize our general dispersion relation (3.3.15) to a homogeneous plasma with no magnetic field present by first setting $k_y=0$, then taking the limit $|\underline{B}|=0$.

4.7 E.T. Copson, Theory of Functions of a Complex Variable (Oxford Univ. Press, New York, 1935), pp. 180, 182.

4.8 See for example: H.M. James, N.B. Nichols and R.S. Philips, Eds., Theory of Servomechanisms (McGraw-Hill, New York, 1947), p. 70; T.H. Stix, op. cit. 1.18, p. 148.

4.9 P.L. Auer, Phys. Rev. Letters 1, 411 (1958). Auer gave the necessary condition but not the sufficiency condition.

4.10 G. Rowlands, op. cit. 1.9.

4.11 A.A. Vedenov, E.P. Velikhov and R.Z. Sagdeev, Nuclear Fusion 1, 82 (1961); 1962 Supplement, Part 2, p. 465; W.E. Drummond and D. Pines, ibid., Part 3, p. 1049.

4.12 J.E. McCune, op. cit. 1.11.

4.13 J.E. McCune (private communication).

4.14 Y. Ozawa, I. Kaji and M. Kito, J. Nucl. Energy, Pt. C: Plasma Physics 4, 271 (1962).

4.15 C.O. Beasley, Phys. Fluids 10, 466 (1967).

4.16 P.R. Bell, R.A. Dory, G.E. Guest, G.G. Kelley, N.H. Lazar, J.F. Lyon and R.F. Stratton, Phys. Rev. Letters 16, 1162 (1966).

4.17 M. Abromowitz and I.A. Stegun, Eds., Handbook of Mathematical Functions (Dover, New York, 1965), p. 18.

4.18 J.E. McCune, Phys. Fluids 9, 2082 (1966).

4.19 E.T. Whittaker and G.N. Watson, Modern Analysis (Cambridge Univ. Press, Cambridge, England, 1950), 4th Ed., p. 119.

4.20 J.E. McCune and B.D. Fried, "The Canchy-Integral Root-Finding Method and the Plasma 'Loss-Cone' Instability," M.I.T. Center for Space Research, CSR TR-67-1, Jan., 1967 (to be published); B.D. Fried, J.E. McCune and C.L. Hedrick, Bull. Am. Phys. Soc. 13, 282 (1968).

5.1 P.A. Sturrock, op. cit. 1.12.

5.2 R.N. Sudan, Phys. Fluids 8, 1899 (1965).

5.3 P.R. Bell et al., op. cit. 4.16.

5.4 W. Calvert, L.G. Kuo-Petravic, E.G. Murphy, M. Petravic, D.R. Sweetman and E. Thompson, Bull. Am. Phys. Soc. 13, 281 (1968).

5.5 C.O. Beasley, op. cit. 4.15.

5.6 A. Bers and R.J. Briggs, R.L.E. Quarterly Progress Report No. 71, p. 122, M.I.T. (1963); A. Bers and R.J. Briggs, Bull. Am. Phys. Soc. 9, 304 (1964); R.J. Briggs, Electron-Stream Interaction with Plasmas, Research Monograph No. 29 (M.I.T. Press, Cambridge, Mass., 1964), p. 19 et seq.

5.7 K.B. Dysthe, Nuclear Fusion 6, 215 (1966).

5.8 D.E. Baldwin and G. Rowlands (to be published).

5.9 Ya. B. Fainberg, V.I. Kurilko and V.D. Shapiro; Zh. Techn. Fiz. 31, 633 (1961) (Translation: Soviet Phys. - Tech. Phys. 6, 459 (1961)).

5.10 C.O. Beasley and J.G. Cordey, "Convective and Absolute Ion Cyclotron Instabilities in Homogeneous Plasmas" (to be published in Plasma Physics).

5.11 L.S. Hall and W. Heckrotte, Phys. Rev. 166, 120 (1968).

5.12 T.H. Stix, op. cit. 1.18, chapt. 10.

5.13 R.E. Aamodt and D.L. Book, Phys. Fluids 9, 143 (1966).

5.14 H.L. Berk, M.N. Rosenbluth and R.N. Sudan, Phys. Fluids 9, 1606 (1966).

5.15 H.L. Berk, C.W. Horton, M.N. Rosenbluth and R.N. Sudan, Phys. Fluids 10, 2003 (1967).

5.16 C.W. Horton, Jr., Bull. Am. Phys. Soc. 13, 313 (1968) (to be published in Physics of Fluids).

5.17 D.E. Baldwin, Phys. Rev. Letters 18, 1119 (1967). See also H.L. Berk, C.W. Horton, M.N. Rosenbluth, D.E. Baldwin and R.N. Sudan, Phys. Fluids 11, 365 (1968).

5.18 M.N. Rosenbluth, H. Berk and L.D. Pearlstein, Bull. Am. Phys. Soc. 13, 297 (1968).

5.19 R.J. Briggs, R.L.E. Quarterly Report No. 88, p. 186, M.I.T. (1968).

5.20 M. Cotsaftis, Nuclear Fusion 7, 3 (1967); Phys. Letters 25A, 170 (1967).

5.21 op. cit. 4.11.

5.22 T.H. Dupree, Phys. Fluids 9, 1773 (1966); 10, 1049 (1967).

5.23 For a recent review of the mode-coupling theory see V.N. Tsytovich, Usp. Fiz. Nauk 90, 435 (1966) (Translation: Soviet Phys. Usp. 9, 805 (1967)).

5.24 W.E. Drummond, Phys. Fluids 7, 816 (1964).

6.1 M.N. Rosenbluth and R.F. Post, op. cit. 1.28.

6.2 I.B. Bernstein, op. cit. 3.23.

6.3 E.G. Harris, op. cit. 3.24.

6.4 For a more complete discussion of limiting cases and the approach of them, see: D.E. Baldwin, I.B. Bernstein and M.P.H. Weenink, op. cit. 1.17.

6.5 G. Rowlands, op. cit. 1.9.

6.6 T. Kammash and W. Heckrotte, Phys. Rev. 133, A132 (1964).

6.7 R.A. Dory, G.E. Guest and E.G. Harris, Phys. Rev. Letters 14, 131 (1965).

6.8 H.K. Wimmel and R. Saison, Z. Naturforsch. 21, 1953 (1966); Phys. Letters 23, 449 (1966).

6.9 T. Kammash and W. Heckrotte, Phys. Rev. 131, 2129 (1963).

6.10 See reference 3.24 and the remark concerning that work in reference 6.7.

6.11 M. Brambilla, Phys. Letters 23, 334 (1966).

6.12 R.F. Post and M.N. Rosenbluth, op. cit. 1.26.

6.13 L.D. Pearlstein, M.N. Rosenbluth and D.B. Chang, Phys. Fluids 9, 953 (1966).

6.14 W.M. Farr and R.E. Budwine, Bull. Am. Phys. Soc. 12, 629 (1967); "High-Frequency Flute-like Instabilities in Multicomponent Plasmas," ORNL Semiannual Progress Report, Thermonuclear Division, April 30, 1967, p. 19.

6.15 W.E. Drummond and M.N. Rosenbluth, op. cit. 1.21.

6.16 L.S. Hall and M.S. Grewal, Phys. Fluids 10, 1523 (1967).

6.17 L.S. Hall, W. Heckrotte and T. Kammash, Phys. Rev. Letters 13, 603 (1964); Phys. Rev. 139, A1117 (1965).

6.18 Y. Ozawa, I. Kaji and M. Kito, op. cit. 4.14.

6.19 S. Gruber, M.W. Klein and P.L. Auer, Phys. Fluids 8, 1504 (1965).

6.20 L.V. Korablev, Zh. Eksperim. i Teor. Fiz. Pis'ma 5, 137 (1967) (Translation: Soviet Phys. - JETP Letters 5, 111 (1967)).

6.21 L.S. Hall and W. Heckrotte, Proc. 7th International Conf. on Phenomena in Ionized Gases, Beograd, Aug. 22-27, 1965 (Gradevinska Knjiga Pub. House, Beograd, 1966), Vol. II, p. 624.

6.22 G.E. Guest (private communication); Bull. Am. Phys. Soc. 13, 282 (1968).

6.23 Yu. N. Dnestrovsky, D.P. Kostomarov and V.I. Pistunovich, Nuclear Fusion 3, 30 (1963).

6.24 P.A. Sturrock, J. Appl. Phys. 31, 2052 (1960).

6.25 B.B. Kadomtsev, A.B. Mikhailovskii and A.V. Timofeev, Zh. Eksperim. i Teor. Fiz. 47, 2266 (1965) (Translation: Soviet Phys. - JETP 20, 1517 (1965)).

6.26 A. Bers and S. Gruber, Appl. Phys. Letters 6, 27 (1965).

6.27 S. Gruber, Proc. 7th International Conf. on Phenomena in Ionized Gases, Beograd, Aug. 22-27, 1965 (Gradevinska Knjiga Pub. House, Beograd, 1966), Vol. II, p. 621.

6.28 L.S. Hall and W. Heckrotte, Phys. Fluids 9, 1496 (1966).

6.29 A.V. Timofeev, Zh. Eksperim. i Teor. Fiz. 39, 397 (1960) (Translation: Soviet Phys. - JETP 12, 281 (1961)).

6.30 Y. Shima and L.S. Hall, Phys. Rev. 139, A1115 (1965).

6.31 Yu. N. Dnestrovsky, Nuclear Fusion 3, 259 (1963).

6.32 G.K. Soper and E.G. Harris, Phys. Fluids 8, 984 (1965).

6.33 G.E. Guest and R.A. Dory, Phys. Fluids 8, 1853 (1965).

6.34 T.A. Davydova, Yu. N. Dnestrovsky and D.P. Kostomarov, Nuclear Fusion 7, 123 (1967).

6.35 F. Hennion, "Study of Microinstabilities Due to an Anisotropic Velocity Distribution Function of the Particles of a Homogeneous Plasma," CEA-R3074 (EUR-3002f), Centre d'Etudes Nucleaires, Fontenay aux Roses, France (Sept., 1966) (in French).

6.36 J.G. Cordey, Phys. Letters 23, 228 (1966).

6.37 C.O. Beasley, op. cit. 4.15.

6.38 C.O. Beasley and J.G. Cordey, "Convective and Absolute Ion Cyclotron Instabilities in Homogeneous Plasmas" (to be published in Plasma Physics).

6.39 C.O. Beasley (private communication).

6.40 C.O. Beasley, J.G. Cordey and R.A. Dory, Bull. Am. Phys. Soc. 13, 281 (1968).

6.41 M.N. Rosenbluth, op. cit. 1.7.

6.42 T.A. Davydova, Zh. Techn. Fiz. 35, 1024 (1965) (Translation: Soviet Phys. - Tech. Phys. 10, 787 (1965)).

6.43 A.A. Galeev, J. Plasma Physics 1, 105 (1967).

6.44 M.N. Rosenbluth and C.W. Horton, Jr. (private communication).

6.45 G.N. Watson, op. cit. 3.3, p. 359.

6.46 M. Abromowitz and I.A. Stegun, op. cit. 4.17, p. 487.

6.47 V.B. Krasovitskii and K.N. Stepanov, Zh. Techn. Fiz. 34, 1013 (1964) (Translation: Soviet Phys. - Tech. Phys. 9, 786 (1964)).

6.48 J.E. McCune and B.D. Fried, "The Cauchy-Integral Root-Finding Method and the Plasma 'Loss-Cone' Instability," M.I.T. Center for Space Research, CSR TR-67-1 (Jan., 1967) (to be published).

6.49 M. Brambilla and G. Schmidt, Phys. Letters 22, 155 (1966).

6.50 R.E. Aamodt, Plasma Physics 9, 573 (1967).

7.1 A.B. Mikhailovskii and A.V. Timofeev, op. cit. 1.29.

7.2 N.A. Krall and M.N. Rosenbluth, op. cit. 1.20.

7.3 N.A. Krall and T.K. Fowler, Phys. Fluids 10, 1526 (1967).

7.4 F.F. Chen, Scientific American 217, No. 1, p. 76 (1967).

7.5 M.N. Rosenbluth and C.L. Longmire, Ann. Phys. 1, 120 (1957).

7.6 M.N. Rosenbluth, op. cit. 1.7.

7.7 M.N. Rosenbluth, N.A. Krall and N. Rostoker, Nuclear Fusion: 1962 Supplement, Part 1, p. 143.

7.8 A.B. Mikhailovskii, op. cit. 1.23.

7.9 Yu. A. Tserkovnikov, Zh. Eksperim. i Teor. Fiz. 32, 67 (1957) (Translation: Soviet Phys. - JETP 5, 58 (1957)).

7.10 L.I. Rudakov and R.Z. Sagdeev, op. cit. 1.19.

7.11 L.I. Rudakov and R.Z. Sagdeev, Nuclear Fusion: 1962 Supplement, Part 2, p. 481.

7.12 B.B. Kadomtsev and A.V. Timofeev, Dokl. Akad. Nauk SSSR 146, 581 (1962) (Translation: Soviet Phys. - Doklady 7, 826 (1963)).

7.13 A.A. Galeev, V.N. Oraevskii and R.Z. Sagdeev, Zh. Eksperim. i Teor. Fiz. 44, 903 (1963) (Translation: Soviet Phys. - JETP 17, 615 (1963)).

7.14 B.B. Kadomtsev, op. cit. 1.22, pp. 78-106.

7.15 A.A. Rukhadze and V.P. Silin, op. cit. 3.6.

7.16 F.C. Hoh, Phys. Fluids 8, 968 (1965).

7.17 A. Simon, "Linear Oscillations," in Plasma Physics (International Atomic Energy Agency, Vienna, 1965), pp. 163-195.

7.18 L.V. Mikhailovskaya and A.B. Mikhailovskii, Zh. Techn. Fiz. 33, 1200 (1963) (Translation: Soviet Phys. - Tech. Phys. 8, 896 (1964)).

7.19 A.B. Mikhailovskii, J. Nucl. Energy, Pt. C: Plasma Physics 8, 705 (1966) (Translation of Atom.Energiya 20, 103 (1966)).

7.20 P.H. Rutherford and E.A. Frieman, op. cit. 1.24.

7.21 B. Coppi, M.N. Rosenbluth and R.Z. Sagdeev, Phys. Fluids 10, 582 (1967).

7.22 O.P. Pogutse, Zh. Eksperim. i Teor. Fiz. 52, 759 (1967) (Translation: Soviet Phys. - JETP 25, 498 (1967)).

7.23 J.D. Jukes, Phys. Fluids 10, 1107 (1967).

7.24 B. Coppi, H.P. Furth, M.N. Rosenbluth and R.Z. Sagdeev, Phys. Rev. Letters 17, 377 (1966).

7.25 A.B. Mikhailovskii and O.P. Pogutse, Dokl. Akad. Nauk SSSR 156, 64 (1964) (Translation: Soviet Phys. - Doklady 9, 379 (1964)); Zh. Techn. Fiz. 36, 205 (1966) (Translation: Soviet Phys. - Tech. Phys. 11, 153 (1966)).

7.26 P.L. Bhatnagar, E.P. Gross and M. Krook, Phys. Rev. 94, 511 (1954); E.P. Gross and M. Krook, Phys. Rev. 102, 593 (1956).

7.27 H.W. Hendel, B. Coppi, F. Perkins and P.A. Politzer, Phys. Rev. Letters 18, 439 (1967).

7.28 A.B. Mikhailovskii and L.I. Rudakov, Zh. Eksperim. i Teor. Fiz. 44, 912 (1963) (Translation: Soviet Phys. - JETP 17, 621 (1963)).

7.29 N.A. Krall and M.N. Rosenbluth, op. cit. 3.6.

7.30 A.A. Galeev, S.S. Moiseev and R.Z. Sagdeev, J. Nucl. Energy, Pt. C: Plasma Physics 6, 645 (1964) (Translated from Atom. Energiya 15, 451 (1963)).

7.31 G. Laval, E.K. Maschke, R. Pellat and M. Vuillemin, Phys. Rev. Letters 19, 1309 (1967).

7.32 B. Lehnert, op. cit. 1.1.

7.33 D.J. Grove, et al., op. cit. 1.5.

7.34 E. Ya. Kogan and S.S. Moiseev, Zh. Techn. Fiz. 37, 805 (1967) (Translation: Soviet Phys. - Tech. Phys. 12, 579 (1967)).

7.35 B. Coppi, G. Laval, R. Pellat and M.N. Rosenbluth, Plasma Physics 10, 1 (1968).

7.36 B. Coppi, M.N. Rosenbluth and S. Yoshikawa, Phys. Rev. Letters 20, 190 (1968).

7.37 B.B. Kadomtsev and O.P. Pogutse, Zh. Eksperim. i Teor. Fiz. 51, 1734 (1966) (Translation: Soviet Phys. - JETP 24, 1172 (1967)).

7.38 M.N. Rosenbluth, "Low Frequency Limit of Interchange Instability," General Atomic, San Diego, California, Report No. GA-8177, Jan. 15, 1967 (to be published in Phys. Fluids).

7.39 P.H. Rutherford and E.A. Frieman, Phys. Fluids 11, 569 (1968).

7.40 M.N. Rosenbluth, Bull. Am. Phys. Soc. 13, 302 (1968).

7.41 R.J. Hastie and J.B. Taylor, Bull. Am. Phys. Soc. 13, 291 (1968).

7.42 P.H. Rutherford and E.A. Frieman, Phys. Fluids 11, 252 (1968).

7.43 A.B. Mikhailovskii, Nuclear Fusion 5, 125 (1965) (in Russian).

7.44 D. Bhadra, Phys. Rev. 161, 126 (1967).

7.45 O.P. Pogutse, Zh. Eksperim. i Teor. Fiz. 47, 941 (1964) (Translation: Soviet Phys. - JETP 20, 630 (1965)).

7.46 L.S. Bogdankevich and A.A. Rukhadze, Zh. Eksperim. i Teor. Fiz. 51, 628 (1966) (Translation: Soviet Phys. - JETP 24, 418 (1967)).

7.47 L.P. Pitaevskii, Zh. Eksperim. i Teor. Fiz. 44, 969 (1963) (Translation: Soviet Phys. - JETP 17, 658 (1963)).

7.48 L.D. Landau, Zh. Eksperim. i Teor. Fiz. 7, 206 (1936).

7.49 A.B. Mikhailovskii, Dokl. Akad. Nauk SSSR 158, 1068 (1964) (Translation: Soviet Phys. - Doklady 9, 901 (1965)).

7.50 A.B. Mikhailovskii, Zh. Eksperim. i Teor. Fiz. 44, 1552 (1963) (Translation: Soviet Phys. - JETP 17, 1043 (1963)).

7.51 T. Ohkawa and M. Yoshikawa, Phys. Rev. Letters 17, 685 (1966).

7.52 A.B. Mikhailovskii, Dokl. Akad. Nauk SSSR 169, 554 (1966) (Translation: Soviet Phys. - Doklady 11, 603 (1967)).

7.53 R.F. Post and M.N. Rosenbluth, op. cit. 1.26.

7.54 A.B. Mikhailovskii, Dokl. Akad. Nauk SSSR 169, 554 (1966) (Translation: Soviet Phys. - Doklady 11, 603 (1967)).

8.1 N.A. Krall and M.N. Rosenbluth, op. cit. 1.20.

8.2 J.E. McCune, op. cit. 4.18.

8.3 M.N. Rosenbluth and R.F. Post, op. cit. 1.28.

8.4 A.B. Mikhailovskii, op. cit. 7.43.

8.5 R.F. Post and M.N. Rosenbluth, op. cit. 1.26.

8.6 R.F. Post, Proc. Int. Conf. on Plasmas in Open-Ended Geometry, J.C. Dunlap, Editor, Gatlinburg, Tenn., Nov. 1-3, 1967 (to be published).

A.1 G.E. Guest and R.A. Dory, op. cit. 3.27.

A.2 G.N. Watson, op. cit. 3.3, p. 395.

A.3 J.D. Jackson, loc. cit. 1.27.

A.4 M. Abromowitz and I.A. Stegun, op. cit. 4.17, p. 363.

B.1 B.D. Fried and S.D. Conte, op. cit. 3.28.

B.2 M. Abromowitz and I.A. Stegun, op. cit. 4.17, p. 785.

B.3 M. Abromowitz and I.A. Stegun, op. cit. 4.17, p. 801.

C.1 IBM System/360 FORTRAN IV Language, Form C28-6515-4 (IBM Corp., Poughkeepsie, N.Y., 1966). See also D.D. McCracken, A Guide to FORTRAN IV Programming (J. Wiley and Sons, New York, 1965).

C.2 N.A. Krall and M.N. Rosenbluth, op. cit. 1.20.

C.3 J.E. McCune and B.D. Fried, op. cit. 4.20.

C.4 C.O. Beasley, op. cit. 4.15.

C.5 C.O. Beasley and J.G. Cordey, op. cit. 5.10.

C.6 P. Diamant, Phys. Fluids 10, 470 (1967).

C.7 I.A. Stegun and M. Abromowitz, M.T.A.C. 11, 255 (1957). See also H. Goldstein and R.M. Thaler, M.T.A.C. 13, 102 (1959).

C.8 M. Abromowitz and I.A. Stegun, loc. cit. 4.17.

C.9 B.D. Fried and S.D. Conte, op. cit. 3.28.

C.10 M. Abromowitz and I.A. Stegun, op. cit. 4.17, p. 886.

C.11 P.A. Crisman, Ed., The Compatible Time-Sharing System A Programmer's Guide (M.I.T. Press, Cambridge, Mass., 1966), 2nd Ed.

APPENDIX A: The Functions C and D

In the derivation of the dispersion relation in Section 3.4, integrals of the form

$$2\pi \int_0^\infty v_\perp dv_\perp \; J_n^2(k_y v_\perp/\Omega) \begin{Bmatrix} F_\perp^\ell \\ v_\perp^2 F_\perp^\ell \\ \left[\frac{1}{v_\perp}\frac{dF_\perp^\ell}{dv_\perp}\right] \\ v_\perp^2\left[\frac{1}{v_\perp}\frac{dF_\perp^\ell}{dv_\perp}\right] \end{Bmatrix}$$

are encountered. Here, for convenience, the species subscript has been suppressed since we will only be considering one species at a time. In the above expression $F_\perp^\ell$ is the part of the equilibrium distribution function prescribing the $v_\perp$ distribution, Eq. (1.3.1), i.e.

$$F_\perp^\ell(v_\perp) = \frac{1}{\pi\alpha_\perp^2 \ell!}\left(\frac{v_\perp^2}{\alpha_\perp^2}\right)^\ell e^{-v_\perp^2/\alpha_\perp^2}. \tag{A.1}$$

Following Guest and Dory (A.1), we define

$$C_n^\ell(\lambda) \equiv 2\pi \int_0^\infty v_\perp dv_\perp \; J_n^2(k_y v_\perp/\Omega)\; F_\perp^\ell \tag{A.2}$$

$$\hat{D}_n^\ell(\lambda) \equiv 2\pi \int_0^\infty v_\perp dv_\perp \; J_n^2(k_y v_\perp/\Omega)\left[\frac{1}{v_\perp}\frac{dF_\perp^\ell}{dv_\perp}\right] \tag{A.3}$$

where $\lambda = (k_y\alpha_\perp)^2/2\Omega^2$. Noting that

$$v_\perp^2 \, F_\perp^\ell = (\ell+1) \, \alpha_\perp^2 \, F_\perp^{\ell+1} \tag{A.4}$$

$$v_\perp^2 \left[\frac{1}{v_\perp} \frac{dF_\perp^\ell}{dv_\perp}\right] = (\ell+1) \, \alpha_\perp^2 \left[\frac{1}{v_\perp} \frac{dF_\perp^\ell}{dv_\perp}\right] - 2F_\perp^\ell \tag{A.5}$$

we see that the other integrals of interest can be specified in terms of (A.2) and (A.3) as

$$2\pi \int_o^\infty v_\perp dv_\perp \; J_n^2 \, (k_y v_\perp / \Omega) v_\perp F_\perp^\ell = (\ell+1) \, \alpha_\perp^2 \, C_n^{\ell+1} \tag{A.6}$$

$$2\pi \int_o^\infty v_\perp dv_\perp \; J_n^2 (k_y v_\perp / \Omega) v_\perp^2 \left[\frac{1}{v_\perp} \frac{dF_\perp^\ell}{dv}\right] = (\ell+1) \alpha_\perp^2 \hat{D}_n^{\ell+1} - 2C_n^\ell. \tag{A.7}$$

Having expressed all of the relevant integrals in terms of the C, D functions we will now list some of the important properties of these functions. First, we note that we can define a set of linear operators $\underline{Q}_\ell$ given by

$$\underline{Q}_\ell = 1 + \frac{\alpha_\perp^2}{\ell} \frac{\partial}{\partial \alpha_\perp^2} \tag{A.7}$$

which when operating on $F_\perp^\ell$ raise the index by one, that is,

$$F_\perp^{\ell+1} = \underline{Q}_\ell \, F_\perp^\ell . \tag{A.8}$$

Since the integrals of interest are independent of $\alpha_\perp$ except for the dependence through $F_\perp^\ell$, these operators can equally well be applied to the C, D functions. Applying the set of operators $\underline{Q}_\ell$ a sufficient number of times to the functions C_n°, $\hat{D}_n^\circ$ we can obtain C_n^ℓ, $\hat{D}_n^\ell$.

The former functions are known integrals which can be written in terms of the modified Bessel functions of the first kind (A.2):

$$C_n^{\circ}(\lambda) = I_n(\lambda)e^{-\lambda} \tag{A.9}$$

$$\hat{D}_n^{\circ}(\lambda) = -\frac{2}{\alpha_\perp^2} I_n(\lambda)e^{-\lambda}. \tag{A.10}$$

For convenience we renormalize the $\hat{D}$'s so that they are dimensionless by defining D_n^ℓ as

$$D_n^\ell = -\frac{\alpha_\perp^2}{2} \hat{D}_n^\ell. \tag{A.11}$$

With this definition, integrals (A.3) and (A.5) become

$$2\pi \int_0^\infty v_\perp dv_\perp \; J_n^2(k_y v_\perp/\Omega) \left[\frac{1}{v_\perp}\frac{dF_\perp^\ell}{dv_\perp}\right] = -\frac{2}{\alpha_\perp^2} D_n^\ell \tag{A.12}$$

$$2\pi \int_0^\infty v_\perp dv_\perp \; J_n^2(k_y v_\perp/\Omega) \; v_\perp^2 \left[\frac{1}{v_\perp}\frac{dF_\perp^\ell}{dv_\perp}\right] = -2[(\ell+1)D_n^{\ell+1} + C_n^\ell]. \tag{A.13}$$

Next, using the operator definition (A.7) and the renormalization definition (A.11) we can write the ℓ recursion relations for the C, D functions as

$$C_n^{\ell+1} = C_n^\ell + \frac{\lambda}{\ell+1}\frac{dC_n^\ell}{d\lambda} \tag{A.14}$$

$$D_n^{\ell+1} = \frac{1}{\ell+1}\left[\ell D_n^\ell + \lambda \frac{dD_n^\ell}{d\lambda}\right]. \tag{A.15}$$

These recursion relations can be simplified by noting that

$$\left[\frac{1}{v_\perp}\frac{dF_\perp^\ell}{dv_\perp}\right] = -\frac{2}{\ell}\frac{\partial}{\partial \alpha_\perp^2} F_\perp^{\ell-1}.$$

Using this formula we see from (A.3) and (A.11) that

$$D_n^{\ell+1} = \frac{\lambda}{\ell+1} \frac{d}{d\lambda} C_n^{\ell} \tag{A.16}$$

and then the other ℓ recursion relation becomes simply

$$C_n^{\ell+1} = C_n^{\ell} + D_n^{\ell+1}. \tag{A.17}$$

Considering the latter forms and (A.9), (A.10) we see that in general we can write

$$C_n^{\ell} = [P_n^{\ell}(\lambda) I_n(\lambda) - Q_n^{\ell}(\lambda) I_n'(\lambda)] e^{-\lambda} \tag{A.18}$$

$$D_n^{\ell} = [p_n^{\ell}(\lambda) I_n(\lambda) - q_n^{\ell}(\lambda) I_n'(\lambda)] e^{-\lambda} \tag{A.19}$$

where P_n^{ℓ}, Q_n^{ℓ}, p_n^{ℓ}, q_n^{ℓ} are polynomials in λ of order ℓ or less. The recursion relations of these polynomials can be shown to be given by

$$p_n^{\ell+1} = \frac{\lambda}{\ell+1} \left[\frac{dP_n^{\ell}}{d\lambda} - P_n^{\ell} - Q_n^{\ell} \left(1 + \frac{n^2}{\lambda^2} \right) \right]$$

$$q_n^{\ell+1} = \frac{\lambda}{\ell+1} \left[\frac{dQ_n^{\ell}}{d\lambda} - P_n^{\ell} - Q_n^{\ell} \left(1 + \frac{1}{\lambda} \right) \right]$$

$$P_n^{\ell+1} = p_n^{\ell+1} + P_n^{\ell}$$

$$Q_n^{\ell+1} = q_n^{\ell+1} + Q_n^{\ell}.$$

For future reference we list the first few of the polynomials:

$$P_n^{\circ} = 1 \qquad p_n^{\circ} = 1$$

$$Q_n^{\circ} = 0 \qquad q_n^{\circ} = 0$$

$$P_n^1 = 1 - \lambda \qquad p_n^1 = -\lambda$$

$$Q_n^1 = -\lambda \qquad q_n^1 = -\lambda$$

$$P_n^2 = \lambda^2 - 2\lambda + 1 + \frac{n^2}{2} \qquad p_n^2 = \lambda^2 - \lambda + \frac{n^2}{2}$$

$$Q_n^2 = \lambda^2 - \frac{3\lambda}{2} \qquad q_n^2 = \lambda^2 - \frac{\lambda}{2}$$

$$P_n^3 = -\left[\frac{2\lambda^3}{3} - \frac{17\lambda^2}{6} + \lambda\left(3+\frac{n^2}{2}\right) - (1+n^2)\right]$$

$$p_n^3 = -\left[\frac{2\lambda^3}{3} - \frac{11\lambda^2}{6} + \lambda\left(1+\frac{n^2}{2}\right) - \frac{n^2}{2}\right]$$

$$Q_n^3 = -\left[\frac{2\lambda^3}{3} - \frac{5\lambda^2}{2} + \lambda\left(\frac{11}{6} + \frac{n^2}{6}\right)\right] \qquad q_n^3 = -\left[\frac{2\lambda^3}{3} - \frac{3\lambda^2}{2} + \lambda\left(\frac{1}{3} + \frac{n^2}{6}\right)\right].$$

For $\ell \to \infty$ the distribution function $F_\perp^\ell$ approaches a Dirac delta function (A.3) centered at $v_\perp = \alpha_\perp$ and then the C, D functions can be shown to be

$$C_n^\infty = J_n^2(\sqrt{2\lambda}) \tag{A.20}$$

$$D_n^\infty = \lambda \frac{d}{d\lambda} J_n^2(\sqrt{2\lambda}) \ . \tag{A.21}$$

Finally, we list some useful summation formulas for the C, D functions. For $J_n^2(x)$ a summation rule given by Abromowitz and Stegun (A.4) is

$$\sum_{n=-\infty}^{\infty} J_n^2(x) = 1 \ . \tag{A.22}$$

In addition, we note from the second Bessel function identity following (3.3.1) that we can write

$$1 = \sum_{n=-\infty}^{\infty} \sum_{m=-\infty}^{\infty} J_n(x) J_m(x) e^{i\theta(n-m)} e^{-i\frac{\pi}{2}(n-m)} \ .$$

Multiplying this equation by sin θ and integrating θ from 0 to 2π we find that

$$0 = \sum_{n=-\infty}^{\infty} n\, J_n^2(x) . \tag{A.23}$$

Using the addition theorems of (A.22) and (A.23) we see immediately from (A.2) and (A.3) that

$$\sum_{n=-\infty}^{\infty} C_n^{\ell} = 1, \quad \ell = 0, 1, 2, \ldots \tag{A.24}$$

$$\sum_{n=-\infty}^{\infty} D_n^{\ell} = \delta_{\ell o} , \quad \ell = 0, 1, \ldots \tag{A.25}$$

$$\sum_{n=-\infty}^{\infty} n\, D_n^{\ell} = 0 , \quad \ell = 0, 1, \ldots \tag{A.26}$$

where $\delta_{\ell o}$ is the Kronecker delta function, previously defined in Eq. (2.2.7).

APPENDIX B: Plasma Dispersion Function Moments

In the derivation of the general dispersion relation in Section 3.4, singular integrals of the form

$$\int_{-\infty}^{\infty} \frac{u^n e^{-u^2}}{u-w}\, du$$

are encountered. These singular integrals are defined for w having a positive imaginary part. The simplest of these integrals (that with n=0) is proportional to the plasma dispersion function

$$Z(w) = \frac{1}{\sqrt{\pi}} \int_{-\infty}^{\infty} \frac{e^{-u^2}}{u-w}\, du \qquad (B.1)$$

which has been tabulated by Fried and Conte (B.1). In the succeding analysis we will show that all of the integrals of interest here can be simply related to this function and its derivatives.

Taking successive derivatives of the plasma dispersion function we note that in general

$$\frac{d^n Z(w)}{dw^n} = \frac{n!}{\sqrt{\pi}} \int_{-\infty}^{\infty} \frac{e^{-u^2} du}{(u-w)^{n+1}} . \qquad (B.2)$$

Integrating the right side of this equation by parts a total of n times we find that

$$\frac{d^n Z(w)}{dw^n} = \frac{1}{\sqrt{\pi}} \int_{-\infty}^{\infty} \frac{\frac{d^n}{du^n}\left(e^{-u^2}\right) du}{u-w} . \qquad (B.3)$$

Next we note from the Rodrigues' formula (B.2) for the

Hermite polynomials $H_n(x)$ that

$$\frac{d^n}{dx^n}\left(e^{-x^2}\right) = (-1)^n \quad e^{-x^2} \quad H_n(x). \tag{B.4}$$

Using this relation in (B.3) we see that a simple expression for the n^{th} derivative of the plasma dispersion function is

$$\frac{d^n Z(w)}{dw^n} = \frac{(-1)^n}{\sqrt{\pi}} \int_{-\infty}^{\infty} \frac{H_n(u) e^{-u^2}}{u-w} du. \tag{B.5}$$

In our work we encounter integrals in which the Hermite polynomials are replaced by simple powers of u. To find simple expressions for the latter integrals we note that we may express any power of a variable x in terms of a series of Hermite polynomials with orders up to and including the power of x. That is, in general

$$x^n = \frac{1}{2^n} \sum_{m=0}^{[n/2]} d_m(n) \; H_{n-2m}(x)$$

where $d_m(n)$ are coefficients given by Abromowitz and Stegun (B.3) and the notation [ ] denotes the bracket operator, i.e. [x] equals the largest integer less than or equal to x. With these remarks we see that the desired integrals, which we define as $Z_n(w)$ according to

$$Z_n(w) = \frac{1}{\sqrt{\pi}} \int_{-\infty}^{\infty} \frac{u^n e^{-u^2}}{u-w} du, \tag{B.6}$$

may be written as

$$Z_n(w) = \frac{1}{2^n} \sum_{m=0}^{[n/2]} (-1)^{\ell-2m} \, d_m(n) \, \frac{d^{n-2m} Z(w)}{dw^{n-2m}} \quad . \tag{B.7}$$

The first four of these functions are

$$Z_o(w) = Z(w) \tag{B.8}$$

$$Z_1(w) = -\frac{1}{2} Z'(w) \tag{B.9}$$

$$Z_2(w) = \frac{1}{4} [2Z(w)+Z''(w)] \tag{B.10}$$

$$Z_3(w) = -\frac{1}{8} [6Z'(w)+Z'''(w)] \tag{B.11}$$

where the prime denotes differentiation with respect to the argument.

Having shown that the singular integrals of interest can be written in terms of the plasma dispersion function and its derivatives, we will now list some of the important properties of the plasma dispersion function. For $Im(w)>0$ $Z(w)$ can be shown to satisfy the Cauchy-Riemann conditions and hence is an analytic function of w in the upper half complex w-plane. In addition, by deforming the integration contour in (B.1) so that it always passes below the point w in the complex w-plane, we can analytically continue the plasma dispersion function into the lower half w-plane. Therefore, when properly defined, the plasma dispersion function $Z(w)$ is an analytic function of w over the entire w-plane. The power series expansion of $Z(w)$ is (B.1)

$$\begin{aligned} Z(w) &= i\sqrt{\pi} \, e^{-w^2} - 2w\left[1 - \frac{2w^2}{3} + \frac{4w^4}{15} - \frac{8w^6}{105} + \ldots\right] \\ &= i\sqrt{\pi} \, e^{-w^2} - 2w \sum_{n=0}^{\infty} \frac{(-2w^2)^n}{(2n+1)!!} \end{aligned} \tag{B.12}$$

where the symbol !! means double factorial, i.e.

$$n!! = \begin{cases} n(n-2)(n-4)\ldots 1, & n \text{ odd} \\ n(n-2)(n-4)\ldots 2, & n \text{ even.} \end{cases}$$

The plasma dispersion function also has an asymptotic expansion which is given by (B.1)

$$Z(w) \simeq i\sqrt{\pi}\,\sigma\, e^{-w^2} - \frac{1}{w}\left[1+\frac{1}{2w^2} + \frac{3}{4w^4} +\ldots\right]$$

$$= i\sqrt{\pi}\,\sigma\, e^{-w^2} - \frac{1}{w}\sum_{n=0}^{\infty} \frac{(2n-1)!!}{(2w^2)^n} \qquad \text{(B.13)}$$

where

$$\sigma = \begin{cases} 0, & \text{Im } w > 0 \\ 1, & \text{Im } w = 0 \\ 2, & \text{Im } w < 0. \end{cases}$$

Note that for Im $w > 0$ and $|w| >> 1$, $Z(w)$ goes approximately $-1/w$. Another very useful formula concerning the plasma dispersion function is its differential equation:

$$Z'(w) = -2\,[1 + wZ(w)]. \qquad \text{(B.14)}$$

APPENDIX C: Description of Computer Programs

The group of programs discussed here have been used to obtain all of the results displayed in this thesis. In general, the programs calculate the properties of the instabilities of a plasma characterized by the dispersion relation given by (3.3.16) and (3.4.3). In particular, depending on the input data, these programs compute: the threshold density for a given k_y, k_z; the real-k temporal growth rates by the Cauchy integral method (see Section 4.3); the real-ω spatial growth rates (complex k_z) by a root following technique; the real-k temporal growth rates by a root following technique; the transition density for absolute instability; the density at which an absolute instability has any given temporal growth rate. In addition, if desired, the programs will print out data for Nyquist and $P(\omega/\Omega_0)$ plots and the results of some intermediate calculations. While the programs were originally written for an IBM 360/65 computer in the FORTRAN IV (G level) language (C.1), they are written in a manner which should make them easy to adapt to other machines which have FORTRAN IV compilers. The most important parameters for such an adaptation are ALOW and EXPMAX (specified in MICRO1, MICRO2, MICRO3 and MICRO4) which should be given respectively as 10^8 times the minimum nonzero number on the machine of interest and the maximum power to which the number e may be raised on the machine. Many of the individual subprograms which we have written are

of sufficient generality and efficiency to warrant their use in other applications.

The programs are divided into two different sets of packages. In general, the first set (MICRO1, MICRO3 and MICRO4) carries out a marginal stability analysis, computes real-k temporal growth rates by the Cauchy integral method and provides data for Nyquist and $P(\omega/\Omega_0)$ plots. The second set carries out the remaining procedures noted in the preceding paragraph by complex root following techniques. The first set has three different packages or versions, two of which (MICRO3, MICRO4) are essentially abbreviated versions of the most general one (MICRO1). The following list indicates the order in which the subprograms are arranged within each of the packages (indentations indicate general calling sequence of programs):

```
MICRO1          MICRO2          MICRO3          MICRO4
   INPUT           SINPUT          INPUT           SINPUT
   SETUP           SETUP           SETUP           SETUP
     CDCOMP          CDCOMP          CDCOMP          CDCOMP
     BESSEL          BESSEL          BESSEL          BESSEL
   FIND            FOLLOW          FIND            P
     P               LOCATE          P             ROOT
     ROOT            RESULT          ROOT          DISP
   DISP              FUNC          DISP              MOMENT
     DISPF           ROOT            DISPF           ZETA
     MOMENT        DISPF             MOMENT
     ZETA            MOMENT          ZETA
   GROWTH            ZETA
     INTEG
     LINE
     PHASE
   NYQUIS
```

A FORTRAN listing of each of these programs appears at the end of this appendix. Each of these four packages is a separate, independent program.

The input data for the programs is divided into two parts. First, there is the control program data which is read by MICRO1, MICRO2, MICRO3 and MICRO4. The first part of this data for each of these programs except MICRO4 is NCASES, NSUBS, the number of cases to be run and the number of subcases in the first case respectively. The remainder of the input data specifying the instability analysis to be performed is discussed below in conjunction with a discussion of some of the individual programs.

In addition to the data noted above, there is the data specifying the case to be considered, which is read by either subprogram INPUT or SINPUT. The proper sequence for loading the latter set of data is given in Table C-1. Format specifications and implicit DO loop conventions employed there are as per the FORTRAN IV language (C.1). The first species specified in the input data for a given case is assumed to be the species which is most like the reference species and determines the minimum step sizes in ω/Ω_o etc. which we consider. The value of JMAX is limited to a maximum of 3 in the present programs, but could be made larger by changing some DIMENSION statements in the programs. The maximum value of $k_y a_j$ is limited to about 28.2 by the BESSEL routine (see below). The value of ℓ is as specified in Section 1.3 except that for plasmas having no temperature gradients, ℓ greater than 3 is taken to be infinite, while for plasmas having temperature gradients, ℓ greater than 2 is taken to be infinite. After reading in the data which defines the case to be considered,

Table C-1. Input Data Specifying Case to be Considered (Read in by INPUT or SINPUT).

Format	Symbol	Explanation
3I5	JMAX	no. of species of particles in this case
	NTYPE	type of case (see below)
	NVZERO	key parameter for particle currents along magnetic field (if none set to zero)
2E14.8	(CAPK(I),I=1,2)	$k_y a_o, k_z a_o$ (in SINPUT, only $k_y a_o$ is read in here)

for each J of the JMAX species, the following data:

5E14.8,I2	(CHAR(I,J), I=1,5),L(J)	The constants m_j/m_o, n_j/n_o, q_j/q_o, T_{z_j}/T_{z_o}, $T_{\perp j}/T_{\perp o}$ and ℓ for this species, respectively

if NTYPE > 3

3E14.8	(GRAD(I,J),I=1,3)	$(\varepsilon'_j a_o)$, $(\delta_{\perp j} a_o)$, $(\delta_{z_j} a_o)$

if 1 < NTYPE < 3

E14.8	GRAD(1,J)	$(\varepsilon'_j a_o)$

if NTYPE is odd

E14.8	GRAD(4,J)	$G_j a_o / \Omega_j^2$

if NVZERO ≠ 0

E14.8	GRAD(5,J)	v_{o_j} / α_{z_o}

then, in INPUT if NNYQUS ≠ 0

E14.8	FRQNYQ	$\mathrm{Im}(\omega/\Omega_o)$ for "Nyquist" plot

a synopsis of the relevant parameters is printed.

The specification of the case to be considered constitutes the first subcase for the MICRO1 and MICRO3 packages. The remaining subcases for all programs are specified by cards following the block of data delineated in Table C-1. For MICRO1 and MICRO3 each subcase has the form of a key parameter NDIFF in I5 format on one card followed by the new pieces of data in 3E14.8 format on a succeeding card. The key parameter prescribes the nature of the new data. For NDIFF equal to 1, 2, 3, 4 the new piece or pieces of data are presumed to be: $k_z a_o$; ((GRAD(I,J), I=1,3), GRAD(5,J), J=1, JMAX); FRQNYQ; F. The symbols used here are defined in Table C-1 except for F which is defined by

$$(k_z a_o) = F\sqrt{\frac{m_2}{m_1}\,\frac{T_{\perp i}}{T_{z_2}}}\,(k_y a_o) \qquad (C.1)$$

in which the subscripts 1, 2 refer respectively to the first and second species in the input data to INPUT or SINPUT. The reason for allowing for this last possibility is that, as we can see from (6.1.10), for values of F ranging from zero to about n (the harmonic number of the relevant mode) it gives $k_z a_o$ the appropriate magnitude for the marginally stable modes. For MICRO3 only values of NDIFF of 1 and 4 are allowed. The subcase specifications for MICRO2 and MICRO4 will be discussed below.

The printed output from the programs is generally self-explanatory. All frequencies and wave-vector components

listed in the output are in units of Ω_o and a_o respectively. For cases in which k_y is zero (no magnetic field influence) $\Omega_o \equiv k\alpha_o$. That output which requires some clarification is discussed below along with the program from which it emanates.

The accuracy of the computer results was ensured by the following procedure. First, where practicable, the numerical results from each of the programs computing Bessel functions, the plasma dispersion function etc. were compared with the respective tables of these functions. Then, hand calculations of some particular solutions of the dispersion relation were compared with the numerical results. Real-k temporal growth rates found by the Cauchy integral method were compared with an approximate formula for the temporal growth rates of drift instabilities given by Krall and Rosenbluth (C.2) and with the loss-cone instability numerical calculations carried out by McCune and Fried (C.3). Finally, our numerical results were compared with some of the threshold and transition density results for loss-cone and temperature-anisotropy instabilities given by Beasley (C.4) and Beasley and Cordey (C.5). The programs were "debugged" until all of these checks yielded satisfactory agreement.

The speed of all but the marginal stability calculations is critically dependent upon the time required to calculate the dispersion function $H(\omega,k)$ and its derivatives. It therefore behooves us to calculate this function in its most rapidly convergent form. Considering the form

of $H(\omega,k)$ given by (3.4.3) and the asymptotic forms of the plasma dispersion function moments (see Appendix B), we observe that for off-resonance harmonics, the cyclotron harmonic expansion converges only as $1/w_n$ as $w_n \to \infty$ (w_n is defined after (3.4.3)). This rather slow convergence can, however, be improved upon. To do so we first note that for nonzero w_n we can write

$$Z_o(w_n) = -\frac{1}{w_n} + \frac{Z_1(w_n)}{w_n} \tag{C.2}$$

$$Z_2(w_n) = -\frac{1}{2w_n} + \frac{Z_3(w_n)}{w_n} \quad . \tag{C.3}$$

Then, putting these forms into (3.4.3), rewriting the separate $1/w_n$ terms as

$$\frac{1}{w_n} = \frac{1}{nw_c} - \frac{w_n - nw_c}{nw_c w_n}$$

in which

$$w_c \equiv \frac{a_o}{a_j} \frac{\alpha_{\perp j}}{\alpha_{Zj}} \frac{1}{(k_z a_o)} ,$$

we find that (by using the addition theorems given by (A.24)-(A.26)) we can perform the summations over n on the $1/nw_c$ terms and ultimately that $H(\omega,k)$ can be written as

$$H(\omega,k) = -\frac{2}{(ka_o)^2} \sum_j \left(\frac{\omega_{p_j}}{\omega_{p_o}}\right)^2 \left(\frac{\alpha_{Z_o}}{\alpha_{Z_j}}\right)^2 \left\{ \left[\left(\frac{\alpha_{Z_j}}{\alpha_{\perp_j}}\right)^2 \left[J_o\left[(k_y a_o)\left(\frac{G_j}{a_o \Omega_j}\right)^2\right] D^{\ell}_{o_j} \right.\right.\right.$$

$$\left.\left.\left. + 2 \sum_{m=1}^{\infty} D^{\ell}_{2mj} \; J_{2m}\left[(k_y a_o)\left(\frac{G_j}{a_o \Omega_j}\right)^2\right] - \delta_{\ell o} \right] + \sum_{m=-\infty}^{\infty} J_m\left[(k_y a_o)\left(\frac{G_j}{a_o \Omega_j}\right)^2\right] \right.$$

$$x \sum_{n=-\infty}^{\infty} \left\{ \left(\frac{a_o}{a_j}\right)\left(\frac{\alpha_{Z_j}}{\alpha_{\perp_j}}\right) \left[(1-\delta_{no}) \frac{w_n + n w_c}{w_c} - (k_y a_o)\left(\frac{G_j}{a_o \Omega_j^2}\right) \right] [D^{\ell}_{n-mj} \right.$$

$$+ \frac{(n-m)}{(k_y a_o)} \left(- (\varepsilon'_j a_o) D^{\ell}_{n-mj} + (\ell+1)(\delta_{\perp_j} a_o) D^{\ell+1}_{n-mj} + 1/2 (\delta_{Z_j} a_o) D^{\ell}_{n-mj} \right)]$$

$$+ \frac{(k_y a_o)}{2} \left(\frac{a_j}{a_o}\right)\left(\frac{\alpha_{Z_j}}{\alpha_{\perp_j}}\right)$$

$$\left. x [- (\varepsilon'_j a_o) C^{\ell}_{n-mj} + (\delta_{\perp_j} a_o)(\ell+1) C^{\ell+1}_{n-mj} + 1/2 (\delta_{Z_j} a_o) C^{\ell}_{n-mj}] \frac{1}{(k_Z a_o) w_n} \right]$$

$$- \left[\sum_{n=-\infty}^{\infty} \left\{ \{ Z_1(w_n) [C^{\ell}_{n-mj} + \frac{(n-m)}{(k_y a_o)} \left(- (\varepsilon'_j a_o) C^{\ell}_{n-mj} + (\ell+1)(\delta_{\perp_j} a_o) C^{\ell+1}_{n-mj} \right)] \right.\right.$$

$$+ \frac{(n-m)}{(k_y a_o)} (\delta_{Z_j} a_o) [Z_3(w_n) - Z_1(w_n)] C^{\ell}_{n-mj} \} + \left(\frac{a_o}{a_j}\right)\left(\frac{\alpha_{Z_j}}{\alpha_{\perp_j}}\right) [n - (k_y a_o)\left(\frac{G_j}{a_o \Omega_j^2}\right)]$$

$$\{ \frac{Z_1(w_n)}{(k_Z a_o) w_n} [D^{\ell}_{n-mj} + \frac{(n-m)}{(k_y a_o)} \left(- (\varepsilon'_j a_o) D^{\ell}_{n-mj} + (\ell+1)(\delta_{\perp_j} a_o) D^{\ell+1}_{n-mj} \right)]$$

$$\left. + \frac{Z_3(w_n)}{(k_Z a_o) w_n} \frac{(n-m)}{(k_y a_o)} (\delta_{Z_j} a_o) D^{\ell}_{n-mj} \right\}$$

$$- \frac{(k_y a_o)}{2} \left(\frac{a_j}{a_o}\right)\left(\frac{\alpha_{Z_j}}{\alpha_{\perp_j}}\right) \left\{ \frac{Z_1(w_n)}{(k_Z a_o) w_n} [- (\varepsilon'_j a_o) C^{\ell}_{n-mj} + (\delta_{\perp_j} a_o)(\ell+1) C^{\ell+1}_{n-mj}] \right.$$

$$\left.\left.\left. + \frac{Z_3(w_n)}{(k_Z a_o) w_n} (\delta_{Z_j} a_o) C^{\ell}_{n-mj} \right\} \right] \right\} . \qquad (C.4)$$

With respect to this particular form of $H(\omega,k)$, it is of interest to note that the terms enclosed in the first set of large brackets are the only ones which remain in the limit that k_z goes to zero. In (C.4) we see that while the simple algebraic sum enclosed in the first set of large brackets converges only as $1/w_n$, because of its algebraic simplicity it can be rapidly summed. The other more complicated part of $H(\omega,k)$ enclosed in the second set of large brackets converges as $1/w_n^2$, i.e. more rapidly than before.

In numerical computations of the dispersion function, we have found that for the standard loss-cone case considered in this work (see Section 5.2), the form given by (C.4) generally converges at least three times faster than that given by (3.4.3). Further reductions in the time required to evaluate the dispersion function may be realizable by employing methods discussed by Diamant (C.6). For the IBM 360/65 computer which has multiply, add and access times of roughly 5,2 and 0.75 μ sec, we have found that about 0.1 second is required to evaluate the dispersion function for the standard loss-cone case with moderate $k_y a_i$. Approximately 5 minutes of computer time was required to produce the results shown in Figs. 4.8, 5.9 and Table 5.1.

At the end of this appendix we display a FORTRAN listing of the computer programs developed in this work. Within the listing of each individual program there are COMMENT statements which describe most of the program's important objectives, features and limitations. In the

following paragraphs we discuss some other features of the programs which are not covered in the COMMENTs. The order in which we discuss the programs is, for the most part, in the order of their appearance in the FORTRAN listing.

The main program MICRO1 is the control program for the first package of programs. The order and format of input data other than that already explained is easily ascertained from the FORTRAN listing of MICRO1. The key parameters NGROW, NNYQUS, NPPLOT, NEXTR1 which are used there should each be nonzero respectively if real-k temporal growth rates by the Cauchy integral method, data for a Nyquist plot, data for a $P(\omega/\Omega_o)$ plot, or all roots found by the Cauchy integral method (i.e. those having negative as well as positive imaginary parts) are desired. If it is desired to bypass any one of these procedures, then the corresponding parameter should be set to zero. The key parameter KMAX gives the number (up to a maximum of 20) of values of λ (density) for which the temporal growth rates are to be found by the Cauchy integral method (see Section 4.3). The key parameters NPRINT and FRACT are discussed in the comments in the FORTRAN listing of LINE. The parameter ERROR is to be given as the minimum accuracy to which the real-k temporal growth rates and Nyquist plot data are to be determined. The accuracy of the temporal growth rates obtained by the Cauchy integral method is usually much better than ERROR (see below) and for reasonable economy in computer time it is recommended that ERROR not be specified as less than 10^{-2} when NGROW is nonzero. In subprograms INPUT and SINPUT, if the input data does not satisfy the charge neutrality condi-

tions given by (2.3.2) and (2.3.3), an appropriate error message is printed and program execution is terminated.

The subprogram SETUP supervises the calculations of the C and D functions of all orders and is called only once for each case which is considered. The evaluations of the C and D functions in subprogram CDCOMP are carried out by the formulas given in Appendix A. For arguments x less than 0.1, the BESSEL subprogram computes the functions $J_n(x)$ and $I_n(x)$ by evaluating the respective series expansions of these functions. For larger arguments the Bessel functions of all orders are computed by a very accurate and efficient recursion relation method which has been suggested by Stegun and Abromowitz (C.7). Since the DIMENSION statement in BESSEL only allows for Bessel functions up to order 400, the maximum argument which can be accomodated by this subprogram is limited to something less than 400 by the fact that in the recursion relation method we must store the Bessel functions of all orders up to at least the point where the order exceeds the argument. For $\ell = 1$, this limitation imposes the requirement that $k_y a_i$ be less than about 28.2 since the argument of the $I_n(x)$ Bessel functions is $(k_y a_i)^2/2$ (see Appendix A). If it is desired to compute the Bessel functions for even larger arguments, we would suggest that they be computed from their asymptotic expansions.

In subprogram FIND, the zeros of P(u) for nonzero k_z are found by evaluating P(u) at discrete points whose separation corresponds to a change of 1/2 in the effective

wave phase speed w_n (see Section 3.4) for the first species specified in the input data. For $k_Z=0$ the step size is taken as 1/20th of the cyclotron frequency of the reference species. For any two successive points for which P(u) has opposite signs, thereby indicating that a zero of P(u) lies between them, we iterate for the exact position of the zero by a Regula Falsi method (C.8) by calling subprogram ROOT. The printed output of FIND includes the results of the marginal stability calculations and the data for a $P(\omega/\Omega_o)$ plot, if desired. In this output, u is measured in units of ω/Ω_o, LAMBDA is $\lambda \equiv \Omega_o^2/\omega_{p_o}^2$, H is $(ka_o)^2/2$ times the $H(\omega,k)$ defined in (3.4.3) and P(u) for nonzero k_Z is $-2\pi^{-1/2}/((ka_o)^2|k_Z a_o|)$ times the P(u) defined by (4.2.3), and for $k_Z = 0$ is $-2/(ka_o)^2$ times the P(u) defined by (4.2.13). The latter normalizations for P(u) also represent the forms in which they are computed in subprogram P.

The subprogram DISPF computes the dispersion function $H(\omega,k)$ by the formula given in (C.4) when the magnitude of the smallest w_n for a given species is greater than 1/4 and otherwise reverts to evaluating this function as given by (3.4.3) to avoid round-off errors in the result when $|w_n|$ is very small. In both the P and DISPF subprograms, for each species of plasma particles, the series of cyclotron harmonic terms is summed beginning from the term which has the smallest value of w_n and hence is presumably the largest in magnitude. The plasma dispersion function moments

$Z_m(w_n)$ (or their counterparts $z_{m+1}(w_n)/w_n$ defined by the expansions given by (C.2) and (C.3)) and the derivatives $\partial/\partial(k_z a_o)$, $\partial^2/\partial(k_z a_o)^2$, $\partial/\partial(\omega/\Omega_o)$ and $\partial^2/\partial(\omega/\Omega_o)\,\partial(k_z a_o)$ of them for the nth harmonic are computed by subprogram MOMENT and stored in the complex array labeled ZMOM in the form ZMOM $(m, Z_m(w_n)$ and its derivatives in the order listed above).

The evaluation of the plasma dispersion function (C.9) and its first three derivatives for subprogram MOMENT is carried out in subprogram ZETA by the most effieicnt and accurate means possible. For complex arguments which have magnitudes larger than 4, the third derivative of the plasma dispersion function is computed from its asymptotic expansion (see Appendix B). We evaluate the third derivative directly in the asymptotic region since, if we evaluated it from recursion relations relating it to the plasma dispersion function itself, there would be substantial round-off errors. For smaller arguments for which the magnitude of the imaginary part exceeds unity, we evaluate the plasma dispersion function by the continued fraction method (C.9). Finally, for all remaining arguments we evaluate the plasma dispersion function by its power series expansion (see Appendix B) using double precision (15 place) arithmetic. The remaining derivatives of the plasma dispersion function are computed by using recursion relations derived from its differential equation.

Subprogram GROWTH is the control program for the computation of real-k temporal growth rates by the Cauchy integral method (see Section 4.3). In the printed output of this program, w refers to the frequency of the unstable mode measured in units of Ω_o, ER is the value of $I_o(C)-1$ which gives an indication of the uncertainty in the results (see Section 4.3), and D is the residual error when the appropriate root is substituted into the dispersion relation. The basic building block of the Cauchy integral calculations is subprogram LINE which computes the line integrals, four of which make up $I_b(C)$ as defined by (4.3.3), by Bode's fourth order integration rule (C.10). If the estimated error in the integral over any finite interval is larger than the accuracy prescribed by ERROR or the change in the phase of the complex integrand between any two points in the interval being integrated is greater than $\pi/2$, then the integration over that interval is redone with a reduced spacing of points. In this way, the accuracy of the results is ensured to be at least as good as that prescribed by ERROR.

Subprogram NYQUIS computes and prints out the data for a Nyquist plot of the dispersion relation. In the printed output, H and DHDW are $(ka_o)^2/2$ times the dispersion function defined in (3.4.3) and its derivative with respect to ω/Ω_o, respectively. Each block of data in the print-out is for frequencies equally spaced between two harmonics of the cyclotron frequency of the reference species.

The main program MICRO2 is the control program for the package of programs which employ interative complex root following techniques to find the complex ω and k_Z roots of the dispersion relation and the saddle points of $\omega(k_Z)$ (i.e. the absolute instability modes--see Sections 5.1, 5.2). The input parameters ACCUR and ERROR are to be given as the accuracy desired,respectively,of the iterated results and of the dispersion function when used in the calculations. Recommended values for these parameters are 10^{-3} and 10^{-5} respectively. The order and meaning of the remaining imput data for this program is easily ascertained from the FORTRAN listings of this program and FOLLOW. The latter listing explains in detail the data to be given for each of the subcases to be considered.

Subprogram FOLLOW supervises the complex root following iterations and prints out the results. In the printed output, the column labeled NUMBER OF ITERATIONS gives a lower limit on the number of iterations which were required to find the respective root. If this number is consistently larger than about 5 in any given set of calculations, it may be advisable to increase the value of the input parameter NSTEPS. In general, if the iteration for any given complex root converges too slowly or not at all, the program automatically cuts the step size and attempts the iteration again. This interval cutting procedure is carried out until the interval is not numerically

significant in comparison with the parameter being changed. In the printed output, the points labeled by MAX and MAXIMUM indicate the points for which max $(\mathrm{Im}(\omega/\Omega_o))$, max $(-\mathrm{Im}(k_z))$ or the absolute instability modes occur (i.e. where $\mathrm{Im}[H(\omega,K(\omega))] = 0$), depending on the type of calculation being performed. The location of these points are iterated to the accuracy prescribed by the input parameter ACCUR.

Certain error messages which indicate numerical difficulties are occasionally written by subprograms FOLLOW and FUNCT. The coding of the parameter IERROR which is printed in some of these error messages is discussed in the FORTRAN listing of subprogram LOCATE. The error messages occur most often at the end of a list of data and indicate that the complex root which is being followed has migrated into the "divergence" region of the complex k_z plane (see Section 3.4). If the error messages occur before any results are printed, it is likely that the initial guess for the location of the root is not sufficiently accurate and it is a good idea to carefully examine the input data. The iterations to find the complex roots are carried out in subprogram LOCATE which uses the simple Newton-Raphson formula for complex variables (C.8).

Main program MICRO3 is an abbreviated version of MICRO1. The input data required for this program is easily ascertained from the FORTRAN listing of MICRO3 and our previous remarks about MICRO1. If, exclusive of MICRO2,

only marginal stability calculations are to be performed, then it is more advantageous to use MICRO3 than MICRO1 since the former is much shorter and hence requires less computer loading time.

Main program MICRO4 is the control program for a version of the marginal stability analysis which is suitable for the M.I.T. Compatible Time-Sharing System (C.11). The latter system is commonly referred to by the acronym CTSS. The key differences between normal "batch" processing and CTSS are that the latter affords some degree of operator intervention from a remote console and gives results "instantly." MICRO4 takes advantage of these features by allowing the user to supply certain key parts of the input data from the console. We should also note that the present CTSS system has no provision for complex arithmetic in its FORTRAN processor, a limitation which necessitates some changes in adapting the subprograms which we use on "batch" processing to CTSS.

Prior to execution of MICRO4 it is necessary to prepare a psuedo-tape (C.11) which contains the majority of the input data. The psuedo-tape must be labeled .TAPE. 5 and must contain all of the data described in Table C.1 except for the values of $k_y a_o$ and $k_z a_o$, for each case of interest. The data for each of the cases to be considered is placed sequentially on .TAPE. 5 with no intervening data. Upon execution of MICRO4, the program requests that the user type in $k_y a_o$ (in format E 14.8) to begin the first case. After this request has been satisfied the program

requests that the user type in guesses for ω/Ω_o and $k_z a_o$ (in format 2E 14.8). This request initiates the consideration of the first subcase. When the request has been satisfied, the program searches for zeros of $P(\omega/\Omega_o)$ evaluated with k_y and k_z as previously supplied and for frequencies near the guess given for ω/Ω_o. To find the zeros for nonzero k_z, the program takes steps in the frequency such that the smallest w_n of the first species in the case being considered changes by 1/4. For k_z=0 the step size is taken to be 1/20th of the cyclotron frequency of the reference species. The program changes the frequency by these step sizes in the direction of decreasing the magnitude of $P(\omega/\Omega_o)$ until a change in the sign of $P(\omega/\Omega_o)$ occurs. When a change of sign is detected, the ROOT subprogram which uses a Regula Falsi method (C.8) is called upon to iterate the frequency for which the zero of $P(\omega/\Omega_o)$ occurs, to an accuracy of 3×10^{-7}. After finding the frequency for which $P(\omega/\Omega_o)$ vanishes, the program checks the sufficiency condition for instability (see Section 4.2) and prints the relevant results on the console. If no change of sign in $P(\omega/\Omega_o)$ is detected within 30 steps, or $P(\omega/\Omega_o)$ becomes less that the smallest number on the computer ($\sim 10^{-38}$), appropriate error messages are written on the console.

After completion of any given subcase, whether or not an answer was obtained, the program again requests guesses for ω/Ω_o and $k_z a_o$. If these data are supplied, the same

value of $k_y a_o$ and thus the same case remain under consideration. If it is desired to begin a new case, the frequency guess should be given as zero. Then, the program advances to the next case on .TAPE. 5 and requests a new value of $k_y a_o$. If it is desired to terminate the execution of MICRO4, the frequency guess should be given as 1.E+30. A synopsis of the parameters characterizing the cases which have been considered is written on .TAPE. 6 and may be printed by the usual procedures (C.11).

The listings of the subprograms SINPUT, SETUP, CDCOMP, BESSEL, P and ROOT in the FORTRAN listing immediately following MICRO4 are the CTSS versions of these programs. They differ from the "batch" versions of the same programs listed earlier mainly in that they have provisions to receive some data from and to print some key error messages on a remote console. The subprogram DISP in the FORTRAN listing following MICRO4 is a special version of the subprograms DISP, DISPF which computes the real and imaginary parts of the dispersion function $H(\omega,k)$ for real ω, k_z. This special version is necessary since, as we have previously noted, CTSS has no direct provision for complex arithmetic. Similarly, the version of MOMENT appearing after MICRO4 in the FORTRAN listing is a special abbreviated version of subprogram MOMENT for CTSS. In this version, the functions $Z_m(w_n)$ are stored in the real matrix ZMOM in the form ZMOM (m,i) where i = 1,2 for the real and imaginary

parts respectively. The subprogram ZETA which is used for the CTSS package was supplied by the R.L.E. Computing Group at M.I.T. and has essentially the same features as the ZETA subprogram discussed earlier. Copies of this program and details concerning its usage are available by writing: Application Group, Computation Center, M.I.T., Cambridge, Mass. 02139.

```
C             MICRO1
C           MAIN PROGRAM 1
C  CONTROL PROGRAM FOR STABILITY AND TEMPORAL GROWTH RATE COMPUTATIONS
C
      COMMON CCAPK,HATRP,DHATRP,CAPK,CONST,GRAD,C,D,GRAV,ROOTP
      COMMON ALOW,EXPMAX,FRACT,UMAX,EXTRA1,EXTRA2,EXTRA3
      COMMON JMAX,L,NTYPE,JPOS,JNEG,KMAX,MMAX,NEXTR1,NEXTR2,NEXTR3
      COMMON NEXTR4,NEXTR5,NEXTR6,NEXTR7
      DIMENSION CONST(4,3),GRAD(5,3),L(3),CAPK(3),CCAPK(3)
      DIMENSION C(2,400,3),D(2,400,3),GRAV(400,3)
      DIMENSION ROOTP(100,2),HATRP(100,2),DHATRP(100,2)
      COMPLEX CCAPK,HATRP,DHATRP
      DIMENSION CHAR(5,3)
    1 FORMAT(14I5)
    2 FORMAT(5E14.8)
      MMAX=3
      NMAX=400
      ALOW=1.E-65
      EXPMAX=150.
      READ(5,1)NCASES
      DO 400 NCASE=1,NCASES
      READ(5,1)NSUBS
      READ(5,1)NGROW,NNYQUS,NPPLOT,KMAX,NPRINT,NEXTR1
      KMAX=IABS(KMAX)
      IF(KMAX.GT.20)KMAX=20
      IF(KMAX.EQ.0)KMAX=10
      READ(5,2)ERROR,FRACT
      ERROR=ABS(ERROR)
      ERROR=AMAX1(ERROR,1.E-05)
      FRACT=AMAX1(FRACT,1.E-06/ERROR)
      DO 300 NSUB=1,NSUBS
      CALL INPUT(NCASE,NSUB,NGOOF,CHAR,NDIFF,NNYQUS,FRQNYQ)
      IF(NGOOF.NE.0)GO TO 450
      IF(NDIFF.EQ.3)GO TO 200
      IF(NSUB.EQ.1)CALL SETUP(NMAX,CHAR)
      UMAX=ABS(CONST(1,1)/CONST(3,1))
      CALL FIND(NPPLOT)
      IF(NGROW.NE.0.AND.JPOS+JNEG.GT.2)CALL GROWTH(NPRINT,ERROR)
  200 IF(NNYQUS.NE.0)CALL NYQUIS(FRQNYQ,ERROR)
  300 CONTINUE
  400 CONTINUE
  450 RETURN
      END


      SUBROUTINE INPUT(NCASE,NSUB,NGOOF,CHAR,NDIFF,NNYQUS,FRQNYQ)
C
C  THIS SUBPROGRAM READS THE MAJORITY OF THE INPUT DATA FOR EACH CASE
C    TO BE RUN AND PRINTS A SUMMARY OF THE RELEVANT PARAMETERS FOR THE
C    CASE BEING CONSIDERED.
C
      COMMON CCAPK,HATRP,DHATRP,CAPK,CONST,GRAD,C,D,GRAV,ROOTP
```

```
      COMMON ALOW,EXPMAX,FRACT,UMAX,EXTRA1,EXTRA2,EXTRA3
      COMMON JMAX,L,NTYPE,JPOS,JNEG,KMAX,MMAX,NEXTR1,NEXTR2,NEXTR3
      COMMON NEXTR4,NEXTR5,NEXTR6,NEXTR7
      DIMENSION CONST(4,3),GRAD(5,3),L(3),CAPK(3),CCAPK(3)
      DIMENSION C(2,400,3),D(2,400,3),GRAV(400,3)
      DIMENSION ROOTP(100,2),HATRP(100,2),DHATRP(100,2)
      COMPLEX CCAPK,HATRP,DHATRP
      DIMENSION CHAR(5,3)
    1 FORMAT(5I5)
    2 FORMAT(5E14.8,I2)
    3 FORMAT(1H1,10X4HCASE,I3,9H, SUBCASE,I3/1H0)
    4 FORMAT(1H0,6X45HREFERENCE LARMOR RADIUS TIMES THE WAVE VECTOR/1H0,
     19X3HK-Y,16X3HK-Z,17X1HK/1H0,3(1PE17.7,2X)/1H0)
    9 FORMAT(80X23HREFERENCE LARMOR RADIUS/1X7HSPECIES,16X29HRATIO TO RE
     1FERENCE SPECIES OF,22X33HDIVIDED BY THE GRADIENT LENGTH OF,4X7HGRA
     2VITY,5X7HCURRENT/2X6HNUMBER,5X4HMASS,7X7HDENSITY,5X6HCHARGE,6X6HTE
     3MP-Z,4X11HTEMP-'PERP',2X1HL,4X7HDENSITY,3X11HTEMP-'PERP',3X6HTEMP-
     4Z,2X2(3X9HPARAMETER)/1H )
   10 FORMAT(2XI3,3X1P5E12.3,I4,1P5E12.3)
   11 FORMAT(1H0,26HCHARGE NEUTRALITY VIOLATED)
   12 FORMAT(1H0,32HDENSITY GRADIENTS DO NOT BALANCE)
      NGOOF=0
      DERROR=1.E-04
      WRITE(6,3)NCASE,NSUB
      IF(NSUB.EQ.1)GO TO 90
C
C  THIS SECTION READS IN THE DESIRED CHANGES TO THE CASE PRESENTLY
C    BEING CONSIDERED.
C
      READ(5,1)NDIFF
      IF(NDIFF.LT.5.AND.NDIFF.GT.0)GO TO 50
      NGOOF=3
      RETURN
   50 GO TO (60,70,80,60),NDIFF
   60 READ(5,2)CAPK(2)
      IF(NDIFF.LT.4)GO TO 91
      CAPK(2)=CAPK(2)*SQRT(CHAR(1,2)*CHAR(5,1)/(CHAR(1,1)*CHAR(4,2)))*CA
     1PK(1)
      GO TO 91
   70 DO 75 J=1,JMAX
      IF(NTYPE.GT.3)READ(5,2)(GRAD(I,J),I=1,3)
      IF(NTYPE.GT.1.AND.NTYPE.LE.3)READ(5,2)GRAD(1,J)
      IF(NVZERO.NE.0)READ(5,2)GRAD(5,J)
   75 CONTINUE
      GO TO 110
   80 IF(NNYQUS.EQ.0)NGOOF=1
      READ(5,2)FRQNYQ
      RETURN
C
C  THIS SECTION READS IN THE NORMAL INPUT DATA TO DEFINE THE CASE
C    TO BE CONSIDERED.
C
   90 READ(5,1)JMAX,NTYPE,NVZERO
      READ(5,2)(CAPK(I),I=1,2)
   91 CAPK(3)=SQRT(CAPK(1)*CAPK(1)+CAPK(2)*CAPK(2))
      WRITE(6,4)(CAPK(I),I=1,3)
```

```
      IF(CAPK(3).NE.0.0)GO TO 92
      NGOOF=2
      RETURN
   92 DO 93 I=2,3
   93 CCAPK(I)=CAPK(I)
      IF(NSUB.GT.1)RETURN
      NDIFF=0
      DO 100 J=1,JMAX
      DO 99 I=1,5
   99 GRAD(I,J)=0.0
      READ(5,2)(CHAR(I,J),I=1,5),L(J)
      IF(NTYPE.GT.3)READ(5,2)(GRAD(I,J),I=1,3)
      IF(NTYPE.GT.1.AND.NTYPE.LE.3)READ(5,2)GRAD(1,J)
      IF(NTYPE-2*(NTYPE/2).NE.0)READ(5,2)GRAD(4,J)
      IF(NVZERO.NE.0)READ(5,2)GRAD(5,J)
  100 CONTINUE
      IF(NNYQUS.NE.0)READ(5,2)FRQNYQ
  110 WRITE(6,9)
      WRITE(6,10)(J,(CHAR(I,J),I=1,5),L(J),(GRAD(I,J),I=1,5),J=1,JMAX)
      SUM=0.0
      DO 120 J=1,JMAX
  120 SUM=SUM+CHAR(2,J)*CHAR(3,J)
      IF(ABS(SUM).LT.DERROR)GO TO 130
      NGOOF=1
      WRITE(6,11)
  130 IF(NTYPE.LT.1)GO TO 150
      SUM=0.0
      DO 140 J=1,JMAX
      SUM=SUM+CHAR(2,J)*CHAR(3,J)*(-GRAD(1,J)+FLOAT(L(J)+1)*GRAD(2,J)+0.
     15*GRAD(3,J)+2.0*GRAD(4,J)*FLOAT(1/(L(J)+1)))
  140 GRAD(4,J)=GRAD(4,J)*CHAR(5,J)*CHAR(1,J)/(CHAR(3,J)*CHAR(3,J))
      IF(ABS(SUM).LT.DERROR)GO TO 150
      NGOOF=1
      WRITE(6,12)
  150 RETURN
      END



      SUBROUTINE SETUP(NMAX,CHAR)
C
C  THIS SUBPROGRAM SETS UP THE RELEVANT MATRICES OF THE C AND D
C    COEFFICIENTS AS WELL AS THE SIMILAR GRAVITY COEFFICIENTS IF
C    NECESSARY.
C
      DIMENSION CONST(4,3),GRAD(5,3),L(3),CAPK(3),CCAPK(3)
      DIMENSION C(2,400,3),D(2,400,3),GRAV(400,3)
      DIMENSION ROOTP(100,2),HATRP(100,2),DHATRP(100,2)
      COMMON CCAPK,HATRP,DHATRP,CAPK,CONST,GRAD,C,D,GRAV,ROOTP
      COMMON ALOW,EXPMAX,FRACT,UMAX,EXTRA1,EXTRA2,EXTRA3
      COMMON JMAX,L,NTYPE,JPOS,JNEG,KMAX,MMAX,NEXTR1,NEXTR2,NEXTR3
      COMMON NEXTR4,NEXTR5,NEXTR6,NEXTR7
      COMPLEX CCAPK,HATRP,DHATRP
      DIMENSION CA(400,2),DA(400,2),EX(400),CHAR(5,3)
      DO 10 J=1,JMAX
      HOLD=SQRT(CHAR(1,J)/CHAR(4,J))
```

```
      CONST(1,J)=CHAR(3,J)*HOLD/CHAR(1,J)
      CONST(2,J)=CHAR(4,J)/CHAR(5,J)
      CONST(3,J)=HOLD
10    CONST(4,J)=CHAR(2,J)*(CHAR(3,J)**2)/CHAR(4,J)
      ITGRAD=1
      IF(NTYPE.GT.3)ITGRAD=2
      DO 20 J=1,JMAX
      X=0.5*((CAPK(1)/CHAR(3,J))**2)*CHAR(5,J)*CHAR(1,J)
      M=NMAX
      CALL CDCOMP(X,L(J),M,CA,DA,ALOW,ITGRAD)
      DO 20 I=1,ITGRAD
      DO 20 K=1,NMAX
      C(I,K,J)=CA(K,I)
20    D(I,K,J)=DA(K,I)
      IF(NTYPE-2*(NTYPE/2).EQ.0)GO TO 40
      DO 30 J=1,JMAX
      X=CAPK(1)*GRAD(4,J)
      K=NMAX
      CALL BESSEL(X,K,EX,-1.0,ALOW)
      DO 30 I=1,NMAX
30    GRAV(I,J)=EX(I)
40    RETURN
      END



      SUBROUTINE CDCOMP(X,L,N,C,D,ALOW,ITGRAD)

THIS SUBROUTINE COMPUTES THE CONSTANTS C(N,L,J) AND D(N,L,J) WHICH
  ARISE IN A CYLINDRICALLY CUT-OUT V 'PERP' DISTRIBUTION FUNCTION.
'L' = 0,1,2,3 ARE TREATED NORMALLY
'L' GREATER THAN 3 IS CONSIDERED TO BE INFINITE AND THUS THE V 'PERP'
  DISTRIBUTION FUNCTION IS A DELTA FUNCTION.
'N' IS TO BE GIVEN AS THE DIMENSION OF THE FIRST SUBSCRIPT OF C AND D
  AND IS RETURNED AS THE HIGHEST POSITION WHICH CONTAINS A NON-ZERO
  RESULT.
'ITGRAD' = 1, ONLY THE C AND D FUNCTIONS FOR L ARE COMPUTED
'ITGRAD' = 2, THE C AND D FUNCTIONS FOR BOTH L AND L+1 ARE COMPUTED
  (FOR 'ITGRAD' = 2, 'L' = 3 IS CONSIDERED TO BE INFINITE).

      DIMENSION C(400,2),D(400,2),ARRAY(400),PQ(4,2)
      DO 10 M=1,N
      DO 10 J=1,ITGRAD
      C(M,J)=0.0
10    D(M,J)=0.0
      IF(L.GT.3)GO TO 300
      IF(L.GT.2.AND.ITGRAD.GT.1)GO TO 300

NORMAL CALCULATION FOR L = 0,1,2,3

      CALL BESSEL(X,N,ARRAY,1.,ALOW)
      J=L+1
      GO TO (100,120,140,160),J
100   PQ(1,1)=1.0
      PQ(2,1)=0.0
      PQ(3,1)=1.0
```

```
      PQ(4,1)=0.0
      IF(ITGRAD.EQ.1)GO TO 200
      J=2
      GO TO 121
  120 J=1
  121 DO 122 M=1,4
  122 PQ(M,J)=-X
      PQ(1,J)=1.+PQ(1,J)
      IF(J.EQ.2)GO TO 200
      IF(ITGRAD.EQ.1)GO TO 200
      J=2
      GO TO 141
  140 J=1
  141 HOLD=X*(X-1.)
      PQ(1,J)=HOLD-X+1.0
      PQ(2,J)=HOLD-0.5*X
      PQ(3,J)=HOLD
      PQ(4,J)=HOLD+0.5*X
      IF(J.EQ.2)GO TO 200
      IF(ITGRAD.EQ.1)GO TO 200
      J=2
      GO TO 161
  160 J=1
  161 TWOTH=2./3.
      HOLD=-X*(X*(TWOTH*X-1./TWOTH)+0.5*TWOTH)
      PQ(4,J)=HOLD
      PQ(3,J)=HOLD+X*(X/3.-TWOTH)
      PQ(2,J)=HOLD+X*(X-1./TWOTH)
      PQ(1,J)=PQ(3,J)+X*(X-2.0)+1.0
  200 DO 240 M=1,N
      IF(M.NE.1)GO TO 210
      DO 201 J=1,ITGRAD
      C(1,J)=PQ(1,J)*ARRAY(1)-PQ(2,J)*ARRAY(2)
  201 D(1,J)=PQ(3,J)*ARRAY(1)-PQ(4,J)*ARRAY(2)
      GO TO 240
  210 IF(L.EQ.0)GO TO 220
      HOLD=FLOAT(M-1)-0.5
      GO TO (211,214,217),L
  211 IF(ITGRAD.EQ.1)GO TO 220
      J=2
      GO TO 215
  214 J=1
  215 PQ(1,J)=PQ(1,J)+HOLD
      PQ(3,J)=PQ(3,J)+HOLD
      IF(J.EQ.2)GO TO 220
      IF(ITGRAD.EQ.1)GO TO 220
      J=2
      GO TO 218
  217 J=1
  218 PQ(1,J)=PQ(1,J)-HOLD*(X-2.)
      PQ(2,J)=PQ(2,J)-X*HOLD/3.
      PQ(3,J)=PQ(3,J)-HOLD*(X-1.)
      PQ(4,J)=PQ(4,J)-X*HOLD/3.
  220 DO 221 J=1,ITGRAD
      C(M,J)=PQ(1,J)*ARRAY(M)-0.5*PQ(2,J)*(ARRAY(M-1)+ARRAY(M+1))
  221 D(M,J)=PQ(3,J)*ARRAY(M)-0.5*PQ(4,J)*(ARRAY(M-1)+ARRAY(M+1))
```

```
240 CONTINUE
    RETURN

 DELTA FUNCTION DISTRIBUTION FOR L GREATER THAN 3

300 HOLD=SQRT(2.*X)
    CALL BESSEL(HOLD,N,ARRAY,-1.,ALOW)
    J=HOLD
    C(1,1)=ARRAY(1)**2
    D(1,1)=-HOLD*ARRAY(1)*ARRAY(2)
    IF(ITGRAD.EQ.1)GO TO 3010
    C(1,2)=C(1,1)
    D(1,2)=D(1,1)
3010 M=2
    IF(X.EQ.0.0)GO TO 400
    CLOW=10.*SQRT(ALOW)/HOLD
 301 IF(ABS(ARRAY(M)).GT.CLOW)GO TO 302
    TWOTH=0.0
    IF(M.GT.J)GO TO 400
    GO TO 303
 302 TWOTH=ARRAY(M)**2
 303 C(M,1)=TWOTH
    D(M,1)=0.5*HOLD*ARRAY(M)*(ARRAY(M-1)-ARRAY(M+1))
    IF(ITGRAD.EQ.1)GO TO 304
    C(M,2)=TWOTH
    D(M,2)=D(M,1)
 304 M=M+1
    GO TO 301
 400 N=M-1
    RETURN
    END



    SUBROUTINE BESSEL(X,N,ARRAY,SIGNA,ALOW)

 THIS SUBROUTINE COMPUTES ALL ORDERS OF THE BESSEL FUNCTIONS J(M,X)
   OR I(M,X) FOR A GIVEN ARGUMENT X.
 USE 'SIGNA' = + 1. FOR I(M,X) AND
     'SIGNA' = - 1. FOR J(M,X).
 'ARRAY' IS THE VECTOR OF LENGTH 'N' IN WHICH THE RESULTS ARE TO BE
   PLACED.  'N' MUST BE GIVEN AND SHOULD BE THE MAXIMUM DIMENSION
   OF 'ARRAY'.
 AFTER EXECUTION OF THIS SUBPROGRAM, 'N' IS THE INDEX OF THE LAST
   ELEMENT OF 'ARRAY' WHICH CONTAINS A NON-ZERO RESULT.  THE M-TH
   ELEMENT OF 'ARRAY' CONTAINS J(M-1,X) OR I(M-1,X) DEPENDING ON THE
   SIGN OF SIGNA.
 ALOW IS TO BE GIVEN AS THE SMALLEST NUMBER POSSIBLE ON THE COMPUTER.

    DIMENSION ARRAY(400)
    NMAX=400
    BREAK=0.1
    SIGNT=1.0
    IF(X.LT.0.0) SIGNT=-SIGNT
    X=ABS(X)
    DO 99 I=1,N
```

```
   99 ARRAY(I)=0.0
   97 IF(X.GT.10.*EXP(0.5*ALOG(ALOW)))GO TO 101
      ARRAY(1)=1.0
      N=1
      RETURN
  101 IF(X.GE.BREAK) GO TO 200
C
C  SERIES METHOD - USED FOR X SMALLER THAN 0.1
C
      CLOW=10.*ALOW/X
       EXPX=1.0
      IF(SIGNA.LT.0.0)EXPX=EXP(X)
      I=1
      FMULT=X*X*SIGNA/4.0
      E=1.0
      GO TO 103
  102 E=E*(X/2.)/FLOAT(I-1)
  103 SUM=1.0
      ANPLUS=I
      AN=1.
      TERM=SUM
  104 SUME=SUM
      TERM=TERM*FMULT/(ANPLUS*AN)
      SUM=SUM+TERM
      ANPLUS=ANPLUS+1.0
      AN=AN+1.0
      IF(SUME-SUM.NE.0.0) GO TO 104
      ARRAY(I)=E*SUM/EXPX
      I=I+1
      IF(I.LE.N.AND.E.GT.CLOW)GO TO 102
      N=I-1
      GO TO 205
  150 WRITE(6,151)X
  151 FORMAT(50H ARGUMENT GIVEN TO BESSEL IS TOO LARGE, ARGUMENT =1PE15.
     17)
      CALL EXIT
C
C  RECURSION RELATION METHOD - USED FOR X LARGER THAN 0.1
C
  200 E=2.71828183
      CLOW=ALOG(1.E+08*ALOW)+X
      I=X
      IF(SIGNA.LT.0.0)I=2*I
  201 I=I+1
      AN=I
      IF((AN+0.5)*ALOG(E*X/(2.*AN)).GT.CLOW.AND.I.LT.N-1)GO TO 201
      IF(I.GT.NMAX)GO TO 150
      N=I
      ARRAY(I)=ALOW*1.E+08
      DO 202 I=2,N
      J=N-I+1
  202 ARRAY(J)=ARRAY(J+2)*SIGNA+2.0*FLOAT(J)*ARRAY(J+1)/X
      SUM=ARRAY(1)
      J=1
      IF(SIGNA.LT.0.0)J=2
      JLOW=J+1
```

```
      DO 203 I=JLOW,N,J
  203 SUM=SUM+2.0*ARRAY(I)
      DO 204 I=1,N
  204 ARRAY(I)=ARRAY(I)/SUM
  205 IF(SIGNT.GT.0.0)RETURN
      DO 206 I=2,N,2
  206 ARRAY(I)=-ARRAY(I)
      RETURN
      END



      SUBROUTINE FIND(NPPLOT)
C
C   THIS SUBPROGRAM FINDS THE ZERO'S OF P(U) AND HENCE THE CONDITIONS
C     UNDER WHICH THE DISPERSION RELATION HAS A VANISHING IMAGINARY PART.
C   'NPPLOT' = 0 FOR NO LISTING OF VALUES OF P(U) AS THEY ARE COMPUTED
C   'NPPLOT' = 1 FOR A LISTING OF THESE VALUES.
C
      COMMON CCAPK,HATRP,DHATRP,CAPK,CONST,GRAD,C,D,GRAV,ROOTP
      COMMON ALOW,EXPMAX,FRACT,UMAX,EXTRA1,EXTRA2,EXTRA3
      COMMON JMAX,L,NTYPE,JPOS,JNEG,KMAX,MMAX,NEXTR1,NEXTR2,NEXTR3
      COMMON NEXTR4,NEXTR5,NEXTR6,NEXTR7
      DIMENSION CONST(4,3),GRAD(5,3),L(3),CAPK(3),CCAPK(3)
      DIMENSION C(2,400,3),D(2,400,3),GRAV(400,3)
      DIMENSION ROOTP(100,2),HATRP(100,2),DHATRP(100,2)
      COMPLEX CCAPK,HATRP,DHATRP
      DIMENSION A(100,2),UMAT(5),PMAT(5)
      EXTERNAL P
    1 FORMAT(1+0/1H0/5(9X1HU,9X4HP(U),3X)/1H )
    2 FORMAT(5(1PE14.3,1PE12.3))
    3 FORMAT(1H )
    4 FORMAT(1H0/1H0/5X27HSOLUTIONS UZERO OF P(U) = 0,2X19H( SCALE OF UZ
     1ERO IS,1PE10.3,2H ))
    5 FORMAT(1H0,27X14HPOSITIVE UZERO)
    6 FORMAT(1H0,27X14HNEGATIVE UZERO)
    7 FORMAT(1H0,5HINDEX,6X5HUZERO,9X6HREAL H,5X6HIMAG H,3X9HREAL DHDW,2
     1X9HIMAG DHDW,9X9HFREQUENCY,9X6HLAMBDA,10X10HRECIPROCAL,6X4HSQRT/1H
     2 )
    8 FORMAT(1XI3,5X1PE10.3,3X1P4E11.2,3X0P2E17.8)
    9 FORMAT(1H+,105X1P2E13.3)
      DERROR=3.E-06
      ERROR=1.E-08
      IF(NPPLOT.NE.0)WRITE(6,1)
      HOLD=1.5*ABS(CAPK(1))+1.0
      NMAX=HOLD
      IF(CAPK(1).EQ.0.0)NMAX=8
      DUMIN=CAPK(2)/(2.0*CONST(3,1))
      IF(CAPK(2).NE.0.0)GO TO 70
      N=40
      GO TO 80
   70 N=ABS(UMAX/DUMIN)
      N=N+1
   80 DUMIN=UMAX/FLOAT(N)
      NNEG=1
   90 J=1
```

```
      K=-1
  100 I=1
      K=K+1
      U=FLOAT(K)*UMAX
      IF(NNEG.EQ.2)U=-U
      IF(CAPK(2).EQ.0.0.AND.K.NE.0)GO TO 150
      HOLD=P(U)
      SIGNH=SIGN(1.0,HOLD)
      IF(HOLD.EQ.0.0)SIGNH=0.0
  150 IF(NPPLOT.EQ.0)GO TO 200
      M=1
      UMAT(1)=U/UMAX
      PMAT(1)=HOLD
  200 U=U+DUMIN
      IF(CAPK(2).EQ.0.0.AND.I.EQ.N)GO TO 210
      TRY=P(U)
      SIGNT=SIGN(1.0,TRY)
      IF(TRY.EQ.0.0)SIGNT=0.0
  210 I=I+1
      IF(NPPLOT.EQ.0)GO TO 250
      IF(M.LT.5)GO TO 220
      WRITE(6,2)(UMAT(M),PMAT(M),M=1,5)
      M=0
  220 M=M+1
      UMAT(M)=U/UMAX
      PMAT(M)=TRY
  250 IF(CAPK(2).NE.0.0)GO TO 255
      IF(I.GT.N.OR.(I.EQ.2.AND.K.NE.0))GO TO 300
  255 HOLD=SIGNT*SIGNH
      IF(HOLD.GT.0.0.OR.(SIGNT.EQ.0.0.AND.SIGNH.EQ.0.0))GO TO 300
      IF(HOLD.LT.0.0)GO TO 260
      HOLD=U+DUMIN
      IF(SIGNH.EQ.0.0)HOLD=U-2.0*DUMIN
      IF(P(HOLD).EQ.0.0)GO TO 300
  260 HOLD=U
      ROOTP(J,NNEG)=ROOT(P,U-DUMIN,HOLD,0.0,DERROR)
      CALL DISP(CMPLX(ROOTP(J,NNEG),0.0),HATRP(J,NNEG),DHATRP(J,NNEG),ER
     1ROR)
      J=J+1
  300 HOLD=TRY
      SIGNH=SIGNT
      IF(I.LE.N)GO TO 200
      IF(NPPLOT.EQ.0)GO TO 330
      WRITE(6,2)(UMAT(I),PMAT(I),I=1,M)
      IF(M.EQ.5)WRITE(6,3)
  330 IF(K.LE.NMAX)GO TO 100
      IF(NNEG.NE.2)GO TO 350
      JNEG=J-1
      GO TO 500
  350 JPOS=J-1
      ISYM=0
      IF(NTYPE.NE.0)GO TO 390
      DO 380 J=1,JMAX
      IF(GRAD(5,J).NE.0.0)GO TO 390
  380 CONTINUE
      GO TO 400
```

```
  390 NNEG=2
      ISYM=1
      DUMIN=-DUMIN
      GO TO 90
  400 JNEG=JPOS
      DO 401 J=1,JPOS
      ROOTP(J,2)=-ROOTP(J,1)
      DHATRP(J,2)=CMPLX(-REAL(DHATRP(J,1)),AIMAG(DHATRP(J,1)))
  401 HATRP(J,2)=CONJG(HATRP(J,1))
  500 WRITE(6,4)UMAX
      IF(JPOS.EQ.0)GO TO 520
      DO 510 J=1,JPOS
  510 A(J,1)=ROOTP(J,1)/UMAX
  520 IF(JNEG.EQ.0)GO TO 540
      DO 530 J=1,JNEG
  530 A(J,2)=ROOTP(J,2)/UMAX
  540 I=1
      HOLD=0.5*CAPK(3)*CAPK(3)
      IF(JPOS.EQ.0)GO TO 620
      WRITE(6,5)
      JHIGH=JPOS
      GO TO 570
  560 IF(JNEG.EQ.0.OR.ISYM.EQ.0)RETURN
      WRITE(6,6)
      JHIGH=JNEG
  570 WRITE(6,7)
      DO 610 J=1,JHIGH
      U=REAL(HATRP(J,I))/HOLD
      WRITE(6,8)J,A(J,I),HATRP(J,I),DHATRP(J,I),A(J,I),U
      IF(U)610,580,590
  580 SIGNT=1.0/ALOW
      GO TO 600
  590 SIGNT=1.0/U
  600 SIGNH=SQRT(SIGNT)
      WRITE(6,9)SIGNT,SIGNH
  610 CONTINUE
  620 I=I+1
      IF(I.GT.2)RETURN
      GO TO 560
      END



      FUNCTION P(U)
C
C  THIS SUBPROGRAM COMPUTES THE VALUE OF THE IMAGINARY PART OF THE
C    DISPERSION FUNCTION H(W,K) WHICH IS CALLED P(U) HERE.
C
      DIMENSION CONST(4,3),GRAD(5,3),L(3),CAPK(3),CCAPK(3)
      DIMENSION C(2,400,3),D(2,400,3),GRAV(400,3)
      DIMENSION ROOTP(100,2),HATRP(100,2),DHATRP(100,2)
      COMMON CCAPK,HATRP,DHATRP,CAPK,CONST,GRAD,C,D,GRAV,ROOTP
      COMMON ALOW,EXPMAX,FRACT,UMAX,EXTRA1,EXTRA2,EXTRA3
      COMMON JMAX,L,NTYPE,JPOS,JNEG,KMAX,MMAX,NEXTR1,NEXTR2,NEXTR3
      COMMON NEXTR4,NEXTR5,NEXTR6,NEXTR7
      COMPLEX CCAPK,HATRP,DHATRP
```

```
      NMAX=400
      NOGRAV=NTYPE-2*(NTYPE/2)
      SCALE=ALOW*CONST(4,1)
      IF(SCALE.EQ.0.0)SCALE=ALOW
      IF(CAPK(2).EQ.0.0)SCALE=1.0
      THEMIN=ALOW/SCALE
      P=0.0
      IF(U.NE.0.0.OR.NTYPE.NE.0)GO TO 80
      DO 70 J=1,JMAX
      IF(GRAD(5,J).NE.0.0)GO TO 80
   70 CONTINUE
      RETURN
   80 DO 400 J=1,JMAX
      HOLD=CAPK(1)*GRAD(4,J)+CONST(3,J)*(U-CAPK(2)*GRAD(5,J))/CONST(1,J)
      SIGNT=0.5
      IF(HOLD.LT.0.0)SIGNT=-SIGNT
      N=HOLD+SIGNT
      IF(CAPK(1).EQ.0.0)N=0
      NPOS=1
      NNEG=-1
      NMOD=0
      HOLD=HOLD*CONST(1,J)
   90 S=HOLD-FLOAT(N+NMOD)*CONST(1,J)
      IF(IABS(N+NMOD).GE.NMAX)GO TO 165
      SSQ=S*S
      IF(CAPK(2).NE.0.0)GO TO 97
      IF(SSQ.NE.0.0)GO TO 94
      FMULT=1.E-08/ALOW
      GO TO 95
   94 FMULT=1./SSQ
   95 SSQ=0.5
      GO TO 98
   97 SSQ=SSQ/(CAPK(2)*CAPK(2))
      IF(SSQ.GT.EXPMAX)GO TO 165
      FMULT=EXP(-SSQ)
   98 GMULT=1.0
      MMOD=0
      IF(NOGRAV.EQ.0)GO TO 110
      MPOS=1
      MNEG=-1
  100 K=IABS(MMOD)+1
      SIGNT=1.0
      IF(MMOD.GE.0)GO TO 105
      IF(MMOD-2*(MMOD/2).NE.0)SIGNT=-SIGNT
  105 GMULT=GRAV(K,J)*SIGNT
      IF(ABS(GMULT).LT.ALOW)GO TO 155
  110 K=N+NMOD-MMOD
      A=FLOAT(K)
      IF(CAPK(1).NE.0.0)A=A/CAPK(1)
      K=IABS(K)+1
      C1=S
      IF(CAPK(2).EQ.0.0)C1=0.0
      D1=CONST(1,J)*CONST(2,J)*(FLOAT(N+NMOD)-CAPK(1)*GRAD(4,J))
      TERM=0.0
      IF(NTYPE.LT.2)GO TO 130
      TEMP1=-GRAD(1,J)
```

```
      IF(NTYPE.LT.4)GO TO 120
      TEMP1=TEMP1+SSQ*GRAD(3,J)
      TERM=GRAD(2,J)*FLOAT(L(J)+1)*(C(2,K,J)*(A*C1-0.5*CAPK(1)/CONST(1,J
     1))+A*D1*D(2,K,J))-A*C1*GRAD(3,J)*C(1,K,J)
  120 C1=C1*(1.0+A*TEMP1)-0.5*CAPK(1)*TEMP1/CONST(1,J)
      D1=D1*(1.0+A*TEMP1)
  130 TERM=GMULT*CONST(4,J)*(TERM+C1*C(1,K,J)+D1*D(1,K,J))
      TERM=TERM*(FMULT/SCALE)
      IF(ABS(TERM).LT.THEMIN)TERM=0.0
      IF((P+TERM)-P.EQ.0.0)GO TO 163
      P=P+TERM
      IF(NOGRAV.EQ.0)GO TO 180
  149 IF(MMOD)151,150,152
  150 MMOD=1
      GO TO 100
  151 IF(MPOS.EQ.0)GO TO 153
      MMOD=-MMOD+MPOS
      GO TO 100
  152 IF(MNEG.EQ.0)GO TO 154
      MMOD=-MMOD
      GO TO 100
  153 MMOD=MMOD+MNEG
      GO TO 100
  154 MMOD=MMOD+MPOS
      GO TO 100
  155 IF(MMOD)161,159,160
  159 IF(CAPK(2))165,149,165
  160 MPOS=0
      GO TO 162
  161 MNEG=0
  162 IF(MPOS.EQ.0.AND.MNEG.EQ.0)GO TO 180
      GO TO 149
  163 IF(NOGRAV.NE.0)GO TO 155
  165 IF(NMOD)170,300,169
  169 NPOS=0
      GO TO 171
  170 NNEG=0
  171 IF(NPOS.EQ.0.AND.NNEG.EQ.0)GO TO 400
  180 IF(NMOD)182,181,183
  181 NMOD=1
      GO TO 90
  182 IF(NPOS.EQ.0)GO TO 184
      NMOD=-NMOD+NPOS
      GO TO 90
  183 IF(NNEG.EQ.0)GO TO 185
      NMOD=-NMOD
      GO TO 90
  184 NMOD=NMOD+NNEG
      GO TO 90
  185 NMOD=NMOD+NPOS
      GO TO 90
  300 IF(CAPK(2).EQ.0.0)GO TO 180
  400 CONTINUE
      P=P*SCALE
      RETURN
      END
```

```
      FUNCTION ROOT(DUMMY,RFB,RFC,RFAE,RFRE)
C
C     THIS SUBPROGRAM COMPUTES A ROOT OF A GIVEN FUNCTION.
C       DUMMY IS THE NAME OF THE SUBPROGRAM WHICH REPRESENTS THE FUNC.
C       RFB IS THE LOWER LIMIT OF THE RANGE IN WHICH THE ROOT IS TO BE
C         FOUND.
C       RFC IS THE UPPER LIMIT OF THE SAME RANGE.
C       RFAE IS THE ABSOLUTE ACCURACY TO BE ITERATED TO.
C       RFRE IS THE RELATIVE ACCURACY TO BE ITERATED TO.
C
      JRFS=1
      RFFB=DUMMY(RFB)
      SIGNB=SIGN(1.0,RFFB)
      IF(RFFB.EQ.0.0)SIGNB=0.0
      RFFC=DUMMY(RFC)
      SIGNC=SIGN(1.0,RFFC)
      IF(RFFC.EQ.0.0)SIGNC=0.0
      IF(SIGNB*SIGNC.LE.0.0)GO TO 9122
 9102 WRITE(6,200)RFB,RFC
  200 FORMAT(1X76HLIMITS GIVEN TO ROOT FUNCTION GENERATE FUNCTIONAL VALU
     1ES WITH THE SAME SIGNS,11H,LIMITS ARE,1PE18.7,4X3HAND,E18.7)
      ROOT=0.0
      RETURN
 9122 RFA=RFC
      RFFA=RFFC
      SIGNA=SIGNC
 9123 IF(ABS(RFFB)-ABS(RFFA))9131,9131,9130
 9130 RFC=RFB
      RFB=RFA
      RFA=RFC
      RFFC=RFFB
      SIGNC=SIGNB
      RFFB=RFFA
      SIGNB=SIGNA
      RFFA=RFFC
      SIGNA=SIGNC
 9131 RFD=0.5*(RFB-RFA)
      RFT=RFAE+RFRE*ABS(RFB)
      IF(RFFB)9156,9135,9156
 9135 ROOT=RFB
      RETURN
 9156 IF(IRFK)9137,9157,9137
 9157 IRFK=3
 9138 RFV=RFD
      GO TO 9140
 9137 IF(RFFB-RFFC)9139,9138,9139
 9139 RFV=(RFB-RFC)*RFFB/(RFFB-RFFC)
 9140 IF(ABS(RFD)-RFT)9143,9143,9144
 9143 JRFS=2
      GO TO 9147
 9144 IF(ABS(RFV)-RFT)9149,9147,9147
 9147 IF((RFD-RFV)*RFV)9148,9152,9152
 9148 RFX=RFB-RFD
```

```
      GO TO 9153
 9149 IF(RFD)9151,9150,9150
 9150 RFV=RFT
      GO TO 9152
 9151 RFV=-RFT
 9152 RFX=RFB-RFV
 9153 GO TO (9101,9100),JRFS
 9100 ROOT=RFX
      RETURN
 9101 RFC=RFB
      RFB=RFX
      RFFC=RFFB
      SIGNC=SIGNB
      RFFB=DUMMY(RFX)
      SIGNB=SIGN(1.0,RFFB)
      IF(RFFB.EQ.0.0)SIGNB=0.0
      IF(SIGNA*SIGNB)9158,9131,9159
 9158 IRFK=IRFK-1
      GO TO 9123
 9159 IRFK=2
      GO TO 9122
      END



      SUBROUTINE DISP(W,H,HW,ERROR)
C
C   THIS SUBPROGRAM IS A DUMMY SUBPROGRAM WHICH SETS UP THE DISPERSION
C     FUNCTION AND ITS DERIVATIVE WITH RESPECT TO FREQUENCY BY CALLING
C     SUBPROGRAM DISPF.
C   THE ARGUMENTS ARE THE SAME AS THOSE SPECIFIED FOR DISPF WITH 'DERROR'
C     THERE AND 'ERROR' HERE BEING THE SAME ARGUMENTS.
C
      COMMON CCAPK,HATRP,DHATRP,CAPK,CONST,GRAD,C,D,GRAV,ROOTP
      COMMON ALOW,EXPMAX,FRACT,UMAX,EXTRA1,EXTRA2,EXTRA3
      COMMON JMAX,L,NTYPE,JPOS,JNEG,KMAX,MMAX,NEXTR1,NEXTR2,NEXTR3
      COMMON NEXTR4,NEXTR5,NEXTR6,NEXTR7
      DIMENSION CONST(4,3),GRAD(5,3),L(3),CAPK(3),CCAPK(3)
      DIMENSION C(2,400,3),D(2,400,3),GRAV(400,3)
      DIMENSION ROOTP(100,2),HATRP(100,2),DHATRP(100,2)
      COMPLEX CCAPK,HATRP,DHATRP
      COMPLEX W,H,HK,HKK,HW,HWK
      CALL DISPF(W,H,HK,HKK,HW,HWK,ERROR,4)
      HOLD=0.5*CAPK(3)*CAPK(3)
      H=H*HOLD
      HW=HW*HOLD
      RETURN
      END



      SUBROUTINE DISPF(W,H,HK,HKK,HW,HWK,DERROR,INDEX)
C
C   THIS SUBPROGRAM COMPUTES THE DISPERSION FUNCTION AND ITS DERIVATIVES.
C   'W' IS TO BE GIVEN AS THE DESIRED COMPLEX FREQUENCY ARGUMENT
C   'H' IS THE COMPLEX VALUE OF THE DISPERSION FUNCTION
```

```
C   'HK' IS THE COMPLEX K-Z DERIVATIVE OF THE DISPERSION FUNCTION
C   'HKK' IS THE COMPLEX SECOND DERIVATIVE OF THE DISPERSION FUNCTION
C     WITH RESPECT TO K-Z
C   'HW' IS THE DERIVATIVE OF THE DISPERSION FUNCTION WITH RESPECT TO THE
C     FREQUENCY
C   'HWK' IS THE DERIVATIVE OF 'HK' WITH RESPECT TO THE FREQUENCY.
C   'DERROR' IS TO BE GIVEN AS THE ACCURACY TO WHICH THE DISPERSION
C     FUNCTION AND THE DESIRED DERIVATIVES ARE TO BE COMPUTED.
C   'INDEX' IS TO BE GIVEN AS THE NUMBER OF QUANTITIES IN THE SEQUENCE
C     'H', 'HK', 'HKK', HW', 'HWK' WHICH ARE TO BE COMPUTED.
C
      DIMENSION CONST(4,3),GRAD(5,3),L(3),CAPK(3),CCAPK(3)
      DIMENSION C(2,400,3),D(2,400,3),GRAV(400,3)
      DIMENSION ROOTP(100,2),HATRP(100,2),DHATRP(100,2)
      COMMON CCAPK,HATRP,DHATRP,CAPK,CONST,GRAD,C,D,GRAV,ROOTP
      COMMON ALOW,EXPMAX,FRACT,UMAX,EXTRA1,EXTRA2,EXTRA3
      COMMON JMAX,L,NTYPE,JPOS,JNEG,KMAX,MMAX,NEXTR1,NEXTR2,NEXTR3
      COMMON NEXTR4,NEXTR5,NEXTR6,NEXTR7
      COMPLEX CCAPK,HATRP,DHATRP
      DIMENSION ZMOM(4,5)
      COMPLEX ZMOM
      COMMON ALAMB,ZMOM
      DIMENSION HF(5),HFHOLD(5)
      COMPLEX W,HOLD,TERM,Z,H,HK,HKK,HWK,HW,HFHOLD,HF,CKHOLD,D1
      THEMAG(Z)=ABS(REAL(Z))+ABS(AIMAG(Z))
      NMAX=400
      NOGRAV=NTYPE-2*(NTYPE/2)
      ITYPE=NTYPE-2
      DO 10 I=1,INDEX
   10 HF(I)=0.0
      CKHOLD=CCAPK(2)
      TCKHOL=THEMAG(CKHOLD)
      KZERO=1
      IF(THEMAG(CKHOLD).EQ.0.0)KZERO=0
      DO 400 J=1,JMAX
      ITIME=1
      IZERO=0
      DO 20 I=1,INDEX
   20 HFHOLD(I)=HF(I)
      C1=D(1,1,J)
      IF(L(J).EQ.0)C1=C1-1.0
      IF(NOGRAV.EQ.0)GO TO 72
      C1=C1*GRAV(1,J)
      N=1
   71 N=N+2
      A=2.0*GRAV(N,J)*D(1,N,J)
      C1=C1+A
      IF(ABS(A).GT.DERROR*ABS(C1))GO TO 71
   72 HF(1)=HF(1)+C1*CONST(2,J)*CONST(4,J)
      HOLD=CAPK(1)*GRAD(4,J)+CONST(3,J)*(W-CKHOLD*GRAD(5,J))/CONST(1,J)
      C1=REAL(HOLD)
      SIGNT=0.5
      IF(C1.LT.0.0)SIGNT=-SIGNT
      N=C1+SIGNT
      IF(CAPK(1).EQ.0.0)N=0
      HOLD=HOLD*CONST(1,J)
```

```
 80 IF(ITIME.GT.1)GO TO 81
    CCAPK(2)=0.0
    GO TO 82
 81 CCAPK(2)=CKHOLD
 82 NPOS=1
    NNEG=-1
    NMOD=0
 90 Z=HOLD-FLOAT(N+NMOD)*CONST(1,J)
    IF(IABS(N+NMOD).GE.NMAX)GO TO 165
    IF(ITIME.GT.1.OR.THEMAG(Z).GT.0.25*TCKHOL.OR.KZERO.EQ.0)GO TO 99
    IZERO=1
    DO 91 I=1,INDEX
 91 HF(I)=HFHOLD(I)
    GO TO 300
 99 CALL MOMENT(ITYPE,Z,J,ITIME,INDEX,IZERO)
    GMULT=1.0
    MMOD=0
    IF(NOGRAV.EQ.0)GO TO 110
    MPOS=1
    MNEG=-1
100 K=IABS(MMOD)+1
    SIGNT=1.0
    IF(MMOD.GE.0)GO TO 105
    IF(MMOD-2*(MMOD/2).NE.0)SIGNT=-SIGNT
105 GMULT=SIGNT*GRAV(K,J)
    IF(ABS(GMULT).LT.ALOW)GO TO 155
110 K=N+NMOD-MMOD
    A=FLOAT(K)
    IF(CAPK(1).NE.0.0)A=A/CAPK(1)
    K=IABS(K)+1
    THOLD=0.5*CAPK(1)/CONST(1,J)
    IERROR=0
    DO 145 I=1,INDEX
    TERM=FLOAT(N+NMOD)
    IF(ITIME.EQ.2)GO TO 115
    IF(I.NE.1.AND.I.NE.4.AND.GRAD(5,J).EQ.0.0)GO TO 145
    IF(REAL(TERM).EQ.0.0)GO TO 115
    IF(I.EQ.1)TERM=HOLD/CONST(1,J)
115 D1=CONST(1,J)*CONST(2,J)*(TERM-CAPK(1)*GRAD(4,J))
    TERM=0.0
    TEMP=1.0
    IF(NTYPE.LT.2)GO TO 130
    IF(NTYPE.LT.4)GO TO 120
    TERM=GRAD(2,J)*FLOAT(L(J)+1)*ZMOM(1,I)*(A*D1*D(2,K,J)-THOLD*C(2,K,
   1J))+GRAD(3,J)*ZMOM(3,I)*(A*D1*D(1,K,J)-THOLD*C(1,K,J))
    IF(ITIME.NE.1)TERM=TERM+GRAD(2,J)*FLOAT(L(J)+1)*C(2,K,J)*A*ZMOM(2,
   1I)+GRAD(3,J)*C(1,K,J)*A*(ZMOM(4,I)-ZMOM(2,I))
120 TEMP=1.0-A*GRAD(1,J)
    TERM=TERM+GRAD(1,J)*THOLD*C(1,K,J)*ZMOM(1,I)
130 IF(ITIME.NE.1)TERM=TERM+C(1,K,J)*ZMOM(2,I)*TEMP
    TERM=GMULT*CONST(4,J)*(TERM+D(1,K,J)*D1*TEMP*ZMOM(1,I))
140 HF(I)=HF(I)-TERM
    IF(ABS(REAL(TERM)).LE.DERROR*ABS(REAL(HF(I))).AND.ABS(AIMAG(TERM))
   1.LE.DERROR*ABS(AIMAG(HF(I))))GO TO 145
    IERROR=1
145 CONTINUE
```

```
      IF(IERROR.EQ.0)GO TO 163
      IF(NOGRAV.EQ.0)GO TO 180
  149 IF(MMOD)151,150,152
  150 MMOD=1
      GO TO 100
  151 IF(MPOS.EQ.0)GO TO 153
      MMOD=-MMOD+MPOS
      GO TO 100
  152 IF(MNEG.EQ.0)GO TO 154
      MMOD=-MMOD
      GO TO 100
  153 MMOD=MMOD+MNEG
      GO TO 100
  154 MMOD=MMOD+MPOS
      GO TO 100
  155 IF(MMOD)161,165,160
  160 MPOS=0
      GO TO 162
  161 MNEG=0
  162 IF(MPOS.EQ.0.AND.MNEG.EQ.0)GO TO 180
      GO TO 149
  163 IF(NOGRAV.NE.0)GO TO 155
  165 IF(NMOD)170,166,169
  166 IF(N)300,180,300
  169 NPOS=0
      GO TO 171
  170 NNEG=0
  171 IF(NPOS.EQ.0.AND.NNEG.EQ.0)GO TO 300
  180 IF(NMOD)182,181,183
  181 NMOD=1
      GO TO 90
  182 IF(NPOS.EQ.0)GO TO 184
      NMOD=-NMOD+NPOS
      GO TO 90
  183 IF(NNEG.EQ.0)GO TO 185
      NMOD=-NMOD
      GO TO 90
  184 NMOD=NMOD+NNEG
      GO TO 90
  185 NMOD=NMOD+NPOS
      GO TO 90
  300 ITIME=ITIME+1
      IF(ITIME.GT.2)GO TO 400
      IF(KZERO.NE.0)GO TO 80
  400 CONTINUE
      DO 410 I=1,INDEX
  410 HF(I)=2.0*HF(I)
      HOLD=1.0/(CCAPK(3)*CCAPK(3))
      H=HF(1)*HOLD
      IF(INDEX.EQ.1)RETURN
      HK=(HF(2)-2.0*CCAPK(2)*H)*HOLD
      IF(INDEX.EQ.2)RETURN
      HKK=(HF(3)-4.0*CCAPK(2)*HK-2.0*H)*HOLD
      IF(INDEX.EQ.3)RETURN
      HW=HF(4)*HOLD
      IF(INDEX.EQ.4)RETURN
```

```
      HWK=(HF(5)-2.0*CCAPK(2)*HW)*HOLD
      RETURN
      END


      SUBROUTINE MOMENT(ITYPE,Z,J,ITIME,INDEX,IZERO)
C
C   THIS SUBPROGRAM COMPUTES THE MOMENTS OF THE PLASMA DISPERSION
C     FUNCTION AND THEIR DERIVATIVES AS REQUIRED BY SUBPROGRAM DISPF.
C
      COMMON CCAPK,HATRP,DHATRP,CAPK,CONST,GRAD,C,D,GRAV,ROOTP
      COMMON ALOW,EXPMAX,FRACT,UMAX,EXTRA1,EXTRA2,EXTRA3
      COMMON JMAX,L,NTYPE,JPOS,JNEG,KMAX,MMAX,NEXTR1,NEXTR2,NEXTR3
      COMMON NEXTR4,NEXTR5,NEXTR6,NEXTR7
      DIMENSION CONST(4,3),GRAD(5,3),L(3),CAPK(3),CCAPK(3)
      DIMENSION C(2,400,3),D(2,400,3),GRAV(400,3)
      DIMENSION ROOTP(100,2),HATRP(100,2),DHATRP(100,2)
      COMPLEX CCAPK,HATRP,DHATRP
      DIMENSION ZMOM(4,5)
      COMPLEX ZMOM
      COMMON ALAMB,ZMOM
      COMPLEX Z,ZET,DZETA,DDZETA,DDDZET,TEMP,W,ZHOLD
      IF(ITIME.GT.1)GO TO 200
C
C   THIS SECTION COMPUTES THE RELEVANT QUANTITIES FOR THE K-Z EQUALS
C     ZERO CASE OR THE FIRST PART OF THE MORE RAPIDLY SUMMED FORM OF THE
C     DISPERSION FUNCTION.
C
      IF(ABS(REAL(Z))+ABS(AIMAG(Z)).NE.0.0)GO TO 110
      TEMP=CMPLX(1.E-08,1.E-08)/ALOW
      DO 100 I=1,INDEX
  100 ZMOM(1,I)=TEMP
      GO TO 124
  110 ZMOM(1,1)=-1.0/Z
      TEMP=CONST(3,J)/(Z*Z)
      GO TO (124,123,122,121,120),INDEX
  120 IF(GRAD(5,J).NE.0.0)ZMOM(1,5)=2.0*CONST(3,J)*GRAD(5,J)*TEMP/Z
  121 ZMOM(1,4)=TEMP
  122 IF(GRAD(5,J).NE.0.0)ZMOM(1,3)=-2.0*CONST(3,J)*(GRAD(5,J)**2)*TEMP/
     1Z
  123 IF(GRAD(5,J).NE.0.0)ZMOM(1,2)=-GRAD(5,J)*TEMP
  124 IF(ITYPE.LE.1)RETURN
      DO 130 I=1,INDEX
  130 ZMOM(3,I)=0.5*ZMOM(1,I)
      RETURN
  200 ZHOLD=Z
      Z=Z/CCAPK(2)
      CALL ZETA(Z,ZET,DZETA,DDZETA,DDDZET,EXPMAX)
      TEMP=(ZHOLD+GRAD(5,J)*CONST(3,J)*CCAPK(2))/(CCAPK(2)*CCAPK(2))
      IF(IZERO.NE.0)GO TO 300
C
C   THIS SECTION COMPUTES THE RELEVANT QUANTITIES FOR THE SECOND PART
C     OF THE DISPERSION FUNCTION IN ITS RAPIDLY CONVERGING FORM.
C
      DO 250 K=1,3,2
```

```
      IF(K.GT.1.AND.ITYPE.LE.1)GO TO 250
      IF(K.EQ.1)W=-0.5*DZETA
      IF(K.GT.1)W=-0.125*(6.0*DZETA+DDDZET)
      ZMOM(K,1)=W/ZHOLD
      ZMOM(K+1,1)=W
      IF(INDEX.EQ.1)GO TO 250
      IF(K.EQ.1)W=0.5*DDZETA
      IF(K.GT.1)W=-0.25*Z*DDDZET
      W=TEMP*W
      ZMOM(K,2)=W/ZHOLD
      IF(GRAD(5,J).NE.0.0)ZMOM(K,2)=ZMOM(K,2)+GRAD(5,J)*CONST(3,J)*ZMOM
     1K,1)/ZHOLD
      ZMOM(K+1,2)=W
      IF(INDEX.EQ.2)GO TO 250
      W=-2.0*W/CCAPK(2)
      IF(K.EQ.1)W=W-0.5*TEMP*TEMP*DDDZET
      IF(K.GT.1)W=W-0.25*TEMP*TEMP*((2.0*Z*Z-1.0)*DDDZET+6.0*Z*DDZETA)
      ZMOM(K,3)=W/ZHOLD
      IF(GRAD(5,J).NE.0.0)ZMOM(K,3)=ZMOM(K,3)+GRAD(5,J)*CONST(3,J)*2.0*
     1GRAD(5,J)*CONST(3,J)*ZMOM(K,1)+ZMOM(K+1,2))/(ZHOLD*ZHOLD)
      ZMOM(K+1,3)=W
      IF(INDEX.EQ.3)GO TO 250
      IF(K.EQ.1)W=-0.5*DDZETA
      IF(K.GT.1)W=0.25*Z*DDDZET
      W=CONST(3,J)*W/CCAPK(2)
      ZMOM(K,4)=(W-CONST(3,J)*ZMOM(K,1))/ZHOLD
      ZMOM(K+1,4)=W
      IF(INDEX.EQ.4)GO TO 250
      IF(K.EQ.1)W=-W+0.5*CONST(3,J)*TEMP*DDDZET
      IF(K.GT.1)W=-W+CONST(3,J)*TEMP*0.25*((2.0*Z*Z-1.0)*DDDZET+6.0*Z*D
     1ZETA)
      W=W/CCAPK(2)
      ZMOM(K,5)=(W-CONST(3,J)*ZMOM(K+1,2)/ZHOLD)/ZHOLD
      IF(GRAD(5,J).NE.0.0)ZMOM(K,5)=ZMOM(K,5)+GRAD(5,J)*CONST(3,J)*(ZMO
     1(K+1,4)-2.0*ZMOM(K,1)*CONST(3,J))/(ZHOLD*ZHOLD)
      ZMOM(K+1,5)=W
  250 CONTINUE
      RETURN
C
C  THIS SECTION COMPUTES THE RELEVANT QUANTITIES FOR THE NORMAL FORM OF
C    THE DISPERSION FUNCTION.
C
  300 ZMOM(1,1)=ZET/CCAPK(2)
      ZMOM(2,1)=-0.5*DZETA
      IF(INDEX.EQ.1)GO TO 350
      ZMOM(1,2)=-(TEMP*DZETA+ZMOM(1,1))/CCAPK(2)
      ZMOM(2,2)=0.5*TEMP*DDZETA
      IF(INDEX.EQ.2)GO TO 350
      ZMOM(1,3)=(TEMP*(TEMP*DDZETA+2.0*DZETA/CCAPK(2))-2.0*ZMOM(1,2))/C
     1APK(2)
      ZMOM(2,3)=-0.5*TEMP*(TEMP*DDDZET+2.0*DDZETA/CCAPK(2))
      IF(INDEX.EQ.3)GO TO 350
      ZMOM(1,4)=CONST(3,J)*DZETA/(CCAPK(2)*CCAPK(2))
      ZMOM(2,4)=-0.5*CONST(3,J)*DDZETA/CCAPK(2)
      IF(INDEX.EQ.4)GO TO 350
      ZMOM(1,5)=-CONST(3,J)*(TEMP*DDZETA+2.0*DZETA/CCAPK(2))/(CCAPK(2)*
```

```
     1CAPK(2))
      ZMOM(2,5)=0.5*CONST(3,J)*(TEMP*DDDZET+DDZETA/CCAPK(2))/CCAPK(2)
  350 IF(ITYPE.LE.1)RETURN
      ZMOM(3,1)=0.25*(2.0*ZET+DDZETA)/CCAPK(2)
      ZMOM(4,1)=-0.125*(6.0*DZETA+DDDZET)
      IF(INDEX.EQ.1)GO TO 400
      ZMOM(3,2)=-(0.25*TEMP*(2.0*DZETA+DDDZET)+ZMOM(3,1))/CCAPK(2)
      ZMOM(4,2)=-0.25*TEMP*Z*DDDZET
      IF(INDEX.EQ.2)GO TO 400
      ZMOM(3,3)=-(TEMP*TEMP*0.5*(2.0*DDZETA+Z*DDDZET)+2.0*ZMOM(3,2)/CCAP
     1K(2)+2.0*ZMOM(3,2))/CCAPK(2)
      ZMOM(4,3)=-(TEMP*TEMP*0.25*((2.0*Z*Z-1.0)*DDDZET+6.0*Z*DDZETA)+2.0
     1*ZMOM(4,2)/CCAPK(2))
      IF(INDEX.EQ.3)GO TO 400
      ZMOM(3,4)=CONST(3,J)*0.25*(2.0*DZETA+DDDZET)/(CCAPK(2)*CCAPK(2))
      ZMOM(4,4)=CONST(3,J)*0.25*Z*DDDZET/CCAPK(2)
      IF(INDEX.EQ.4)GO TO 400
      ZMOM(3,5)=(CONST(3,J)*TEMP*0.5*(2.0*DDZETA+Z*DDDZET)-2.0*ZMOM(3,4)
     1)/(CCAPK(2)*CCAPK(2))
      ZMOM(4,5)=(CONST(3,J)*TEMP*0.25*((2.0*Z*Z-1.0)*DDDZET+6.0*Z*DDZETA
     1)-ZMOM(4,4))/CCAPK(2)
  400 RETURN
      END



      SUBROUTINE ZETA(Z,ZETAOZ,DZETAZ,DDZETA,DDDZET,EXPMAX)
C
C  THIS SUBPROGRAM COMPUTES THE PLASMA DISPERSION FUNCTION AND ITS
C    FIRST THREE DERIVATIVES FOR A COMPLEX ARGUMENT Z.
C  'Z' = GIVEN ARGUMENT (COMPLEX)
C  'ZETAOZ' = PLASMA DISPERSION FUNCTION (COMPLEX)
C  'DZETAZ' = DERIVATIVE OF THE PLASMA DISPERSION FUNCTION (COMPLEX)
C  'DDZETA' = SECOND DERIVATIVE OF THE PLASMA DISPERSION FUNCTION
C  'DDDZET' = THIRD DERIVATIVE OF THE PLASMA DISPERSION FUNCTION
C
      COMPLEX Z,ZETAOZ,DZETAZ,TERM,FMULT,TERME,AN1,BN1,ZSQUAR,HOLD,
     1TEMP1,TEMP2,DDZETA,DDDZET
      DOUBLE PRECISION REALMU,IMAGMU,REALSU,IMAGSU,REALTE,IMAGTE,REALSE,
     1IMAGSE
      ERROR=1.E-06
      ZSQUAR=Z*Z
      X=REAL(Z)
      Y=AIMAG(Z)
      FN=REAL(ZSQUAR)
      IF(Y.GT.0.0)GO TO 99
      IF(ABS(FN).LT.EXPMAX.AND.ABS(AIMAG(ZSQUAR)).LT.5.E+04)GO TO 98
      IF(FN.GT.0.0)GO TO 97
    1 FORMAT(76H ARGUMENT Z OF SUBROUTINE ZETA HAS TOO LARGE A NEGATIVE
     1IMAGINARY PART, Z = ,1PE14.7,3H + ,1PE14.7,2H I)
      WRITE(6,1) Z
   97 HOLD=(0.0,0.0)
      GO TO 99
   98 HOLD=(0.0,1.772454)*CEXP(-ZSQUAR)
   99 IF(X*X+Y*Y.GT.16.0)GO TO 200
      IF(ABS(Y).GE.1.0)GO TO 300
```

```
C
C  POWER SERIES METHOD  -  DOUBLE PRECISION
C
      REALTE=-2.0*X
      IMAGTE=-2.0*Y
      REALMU=0.5*(IMAGTE*IMAGTE-REALTE*REALTE)
      IMAGMU=-IMAGTE*REALTE
      REALSU=REALTE
      IMAGSU=IMAGTE
      IF(X.EQ.0.0.AND.Y.EQ.0.0)GO TO 103
      FN=3.0
  100 REALSE=REALTE
      IMAGSE=IMAGTE
      REALTE=(REALSE*REALMU-IMAGSE*IMAGMU)/FN
      IMAGTE=(REALSE*IMAGMU+IMAGSE*REALMU)/FN
      REALSE=REALSU
      IMAGSE=IMAGSU
      REALSU=REALSU+REALTE
      IMAGSU=IMAGSU+IMAGTE
      FN=FN+2.0
      IF(SNGL(REALSE)-SNGL(REALSU).NE.0.0.OR.SNGL(IMAGSE)-SNGL(IMAGSU).N
     1E.0.0)GO TO 100
  103 X=REALSU
      FN=IMAGSU
      IF(Y.GT.0.0)HOLD=(0.0,1.772454)*CEXP(-ZSQUAR)
      ZETAOZ=CMPLX(X,FN)+HOLD
      GO TO 401
C
C  ASYMPTOTIC SERIES METHOD - COMPUTE THIRD DERIVATIVE
C
  200 FN=5.0
      DDDZET=6.0
      TERM=DDDZET
      FMULT=0.5/ZSQUAR
  201 TERME=TERM
      TERM=TERM*FMULT*FN*(FN-1.0)/(FN-3.0)
      ZETAOZ=TERM/TERME
      IF(ABS(REAL(ZETAOZ))+ABS(AIMAG(ZETAOZ)).GT.1.0)GO TO 250
      ZETAOZ=DDDZET
      DDDZET=DDDZET+TERM
      FN=FN+2.0
      IF(REAL(ZETAOZ).NE.REAL(DDDZET).OR.AIMAG(ZETAOZ).NE.AIMAG(DDDZET))
     1GO TO 201
  250 DDDZET=DDDZET/(ZSQUAR*ZSQUAR)
      IF(Y.GT.0.0)GO TO 260
      FN=1.0
      IF(Y.LT.0.0)FN=2.0
      DDDZET=DDDZET-4.0*FN*HOLD*Z*(2.0*ZSQUAR-3.0)
  260 DDZETA=-(4.0+(ZSQUAR-0.5)*DDDZET)/(Z*(2.0*ZSQUAR-3.0))
      DZETAZ=(2.0-Z*DDZETA)/(2.0*ZSQUAR-1.0)
      ZETAOZ=-(1.0+0.5*DZETAZ)/Z
      RETURN
C
C  CONTINUED FRACTION METHOD
C
C     (TERME=A(N-1), TERM=A(N), DZETAZ=B(N-1), FMULT=B(N))
```

```
300 IF(Y.LT.0.0)Z=CONJG(Z)
    TERME=(1.0,0.0)
    TERM=(0.0,0.0)
    DZETAZ=TERM
    FMULT=TERME
    N=0
    AN1=Z
    BN1=-Z*Z+0.5
301 TEMP1=BN1*TERM+AN1*TERME
    TEMP2=BN1*FMULT+AN1*DZETAZ
    ZETAOZ=TEMP1/TEMP2
    DZETAZ=(ZETAOZ-TERM/FMULT)/ZETAOZ
    IF(ABS(REAL(DZETAZ)).LT.ERROR.AND.ABS(AIMAG(DZETAZ)).LT.ERROR) GO
   1TO 302
    BN1=BN1+2.0
    N=N+1
    AN1=-0.5*FLOAT(N*(2*N-1))
    TERME=TERM
    DZETAZ=FMULT
    TERM=TEMP1
    FMULT=TEMP2
    IF(N.LT.30)GO TO 301
302 IF(Y.GE.0.0) GO TO 401
    ZETAOZ=CONJG(ZETAOZ)+2.0*HOLD
    Z=CONJG(Z)
401 DZETAZ=-2.0*(1.0+Z*ZETAOZ)
    DDZETA=-2.0*(ZETAOZ+Z*DZETAZ)
    DDDZET=-2.0*(2.0*DZETAZ+Z*DDZETA)
    RETURN
    END



    SUBROUTINE GROWTH(NPRINT,ERROR)
C
C  THIS SUBPROGRAM ORGANIZES THE DATA TO BE GIVEN TO SUBPROGRAM INTEG
C    FOR THE COMPUTATION OF REAL-K TEMPORAL GROWTH RATES FOR DENSITIES
C    EXCEEDING THE THRESHOLD DENSITY AT FIXED K-Z BY THE CAUCHY
C    INTEGRAL METHOD.
C  THIS SUBPROGRAM ALSO DECIDES AROUND WHICH OF THE CYCLOTRON HARMONICS
C    UNSTABLE MODES OCCUR AND THUS WHERE GROWTH RATES SHOULD BE COMPUTED
C  AFTER THE GROWTH RATES ARE COMPUTED THIS PROGRAM PRINTS A SUMMARY
C    OF THE RESULTS.
C
    COMMON CCAPK,HATRP,DHATRP,CAPK,CONST,GRAD,C,D,GRAV,ROOTP
    COMMON ALOW,EXPMAX,FRACT,UMAX,EXTRA1,EXTRA2,EXTRA3
    COMMON JMAX,L,NTYPE,JPOS,JNEG,KMAX,MMAX,NEXTR1,NEXTR2,NEXTR3
    COMMON NEXTR4,NEXTR5,NEXTR6,NEXTR7
    DIMENSION CONST(4,3),GRAD(5,3),L(3),CAPK(3),CCAPK(3)
    DIMENSION C(2,400,3),D(2,400,3),GRAV(400,3)
    DIMENSION ROOTP(100,2),HATRP(100,2),DHATRP(100,2)
    COMPLEX CCAPK,HATRP,DHATRP
    DIMENSION RESULT(20,3),SET(20),OTHER(20)
    DIMENSION NUMBER(20)
    COMPLEX RESULT,PHI,DPHIDZ
  1 FORMAT(1H1,4X34HRESULTS OF GROWTH RATE COMPUTATION,1X18H(ERROR REQ
```

```
     1UESTED =,1PE8.1,1H)/1H )
    2 FORMAT(1X,67HNO ZERO OF IMAG H WITH NEGATIVE REAL H CAN BE FOUND N
     1EAR THE ORIGIN)
    3 FORMAT(1X46HPART OF THE FOLLOWING SET OF DATA IS INCORRECT,2X9H(NE
     1RROR =,I5,1H))
    4 FORMAT(1XI3,4X1P3E12.3,6X1P2E12.3,3X2(3X,1P2E10.1),4XI3)
    5 FORMAT(1H0)
    6 FORMAT(1H0,5HINDEX,6X6HKSQLSQ,6X6HLAMBDA,4X10HRECIPROCAL,10X6HREAL
     1 W,6X6HIMAG W,11X7HREAL ER,3X7HIMAG ER,6X6HREAL D,4X6HIMAG D,4X6HN
     2 IN C/1H0)
    7 FORMAT(1H1)
    8 FORMAT(1H )
      DERROR=AMAX1(0.01*ERROR,1.E-06)
      WRITE(6,1)ERROR
      WRITE(6,6)
      ICOUNT=6
      NSET=KMAX
      ANORM=0.5*CAPK(3)*CAPK(3)
      ISYM=0
      IF(NTYPE.NE.0)GO TO 130
      DO 125 J=1,JMAX
      IF(GRAD(5,J).NE.0.0)GO TO 130
  125 CONTINUE
      INEG=1
      IF(REAL(HATRP(1,1)).GT.0.0)INEG=0
      ISYM=1
      GO TO 170
  130 IF(JNEG.EQ.0)GO TO 140
      INEG=0
      GO TO 170
  140 IF(JPOS.EQ.0)GO TO 150
      IF(REAL(HATRP(1,1)).LT.0.0)GO TO 160
  150 WRITE(6,2)
      RETURN
  160 INEG=1
  170 DO 310 JSIGN=1,2
      IF(JSIGN.EQ.2)GO TO 180
      MAX=JPOS
      JSTART=INEG+1
      GO TO 190
  180 JSTART=2-INEG
      IF(ISYM.NE.0)GO TO 310
      MAX=JNEG
  190 IF(MAX.LE.JSTART)GO TO 310
      DO 300 J=JSTART,MAX,2
      IF(REAL(HATRP(J,JSIGN)).LE.0.0)GO TO 300
      TKLMAX=REAL(HATRP(J,JSIGN))
      DIVIS=REAL(HATRP(J+1,JSIGN))
      AKMAX=NSET
      IF(DIVIS.LE.0.0)GO TO 200
      AKMAX=AKMAX+1.0
      TKLMAX=TKLMAX-DIVIS
  200 DO 210 I=1,NSET
      SET(I)=TKLMAX*FLOAT(I)/AKMAX
      IF(DIVIS.GT.0.0)SET(I)=SET(I)+DIVIS
      OTHER(I)=SET(I)/ANORM
```

```
  210 NUMBER(I)=0
      CALL INTEG(J,JSIGN,SET,NSET,RESULT,ERROR,NPRINT,NERROR,NUMBER)
      IF(NERROR.EQ.0)GO TO 280
      WRITE(6,3)NERROR
      ICOUNT=ICOUNT+1
  280 IF(NEXTR1.EQ.0)GO TO 290
      INDEX=0
      DO 285 I=1,NSET
      IF(NUMBER(I).NE.2)GO TO 285
      INDEX=1
      ICOUNT=ICOUNT+1
  285 CONTINUE
      IF(INDEX.EQ.0)GO TO 290
      WRITE(6,8)
      ICOUNT=ICOUNT+1
  290 ICOUNT=ICOUNT+2+NSET
      IF(ICOUNT.LE.60)GO TO 295
      ICOUNT=5+NSET
      WRITE(6,7)
      WRITE(6,6)
  295 DO 299 INDEX=1,NSET
      I=NSET+1-INDEX
      IF(NERROR.EQ.0)GO TO 296
      PHI=0.0
      GO TO 297
  296 CALL DISP(RESULT(I,2),PHI,DPHIDZ,DERROR)
      PHI=SET(I)-PHI
  297 RESULT(I,1)=(RESULT(I,1)-1.0)/UMAX
      RESULT(I,2)=RESULT(I,2)/UMAX
      IF(OTHER(I).NE.0.0)GO TO 298
      DIVIS=1.0/ALOW
      GO TO 299
  298 DIVIS=1.0/OTHER(I)
  299 WRITE(6,4)INDEX,SET(I),OTHER(I),DIVIS,RESULT(I,2),RESULT(I,1),PHI,
     1NUMBER(I)
      WRITE(6,5)
  300 CONTINUE
  310 CONTINUE
      RETURN
      END


      SUBROUTINE INTEG(J,JSIGN,SET,NSET,RESULT,ERROR,NPRINT,NERROR,NUMBE
     1R)
C
C  THIS SUBPROGRAM COMPUTES THE REAL-K GROWTH RATES FOR DENSITIES
C    EXCEEDING THE THRESHOLD DENSITY AT FIXED K-Z BY THE CAUCHY
C    INTEGRAL METHOD.
C  THE INTEGRAL OVER THE CONTOUR OF INTEREST (A RECTANGLE) IS SPLIT
C    UP INTO FOUR LINE INTEGRALS AND THESE ARE COMPUTED BY SUBPROGRAM
C    LINE.
C
      COMMON CCAPK,HATRP,DHATRP,CAPK,CONST,GRAD,C,D,GRAV,ROOTP
      COMMON ALOW,EXPMAX,FRACT,UMAX,EXTRA1,EXTRA2,EXTRA3
      COMMON JMAX,L,NTYPE,JPOS,JNEG,KMAX,MMAX,NEXTR1,NEXTR2,NEXTR3
```

```
      COMMON NEXTR4,NEXTR5,NEXTR6,NEXTR7
      DIMENSION CONST(4,3),GRAD(5,3),L(3),CAPK(3),CCAPK(3)
      DIMENSION C(2,400,3),D(2,400,3),GRAV(400,3)
      DIMENSION ROOTP(100,2),HATRP(100,2),DHATRP(100,2)
      COMPLEX CCAPK,HATRP,DHATRP
      DIMENSION RLINE(20,4,3),IHOLD(20),FHOLD(20),RHOLD(20,3),ICHANG(20)
      DIMENSION ISTART(20),FSTART(20),RESULT(20,3),SET(20),IJUMP(20)
      DIMENSION FJUMP(20),NUMBER(20)
      COMPLEX RLINE,DPHIDZ,PHI,GHOLD,TWOPI,FSTART,ZUPPER,ZLOWER,RESULT
      COMPLEX FHOLD,RHOLD,FJUMP
      EXTERNAL DISP
      TWOPI=CMPLX(0.0,1./6.282685)
      DERROR=AMAX1(0.01*ERROR,1.E-06)
      DO 90 ISET=1,NSET
      DO 90 M=1,MMAX
      RHOLD(ISET,M)=0.0
      DO 90 I=1,4
   90 RLINE(ISET,I,M)=0.0
      SIGNA=(-1.)**(JSIGN-1)
      IF(CAPK(2).EQ.0.0)GO TO 95
      CALL PHASE(DHATRP(J,JSIGN),IPHASE,0)
      IF(JSIGN.EQ.2)IPHASE=7-IPHASE
      CALL PHASE(DHATRP(J+1,JSIGN),N,0)
      N=-N
      IF(JSIGN.EQ.2)N=7-N
      IF(IPHASE.GT.N)IPHASE=N
      N=0.5+0.5*ABS((ROOTP(J,JSIGN)+ROOTP(J+1,JSIGN))/UMAX)
      AN=N
      WIDTH=ABS(CAPK(2)/CONST(3,1))
      SPACE=WIDTH/2.
      ZLOWER=CMPLX(ROOTP(J,JSIGN),-SPACE)
      ZUPPER=CMPLX(ROOTP(J+1,JSIGN),-SPACE)
      DZIMAG=ABS(ROOTP(J+1,JSIGN))+SPACE
      IF(IPHASE.EQ.7)GO TO 200
      IF(IPHASE.LT.4)GO TO 100
      IF(ABS(ROOTP(J,JSIGN))-SPACE.LT.WIDTH+UMAX*(AN-1.))GO TO 100
      IF(ABS(ROOTP(J+1,JSIGN)-ROOTP(J,JSIGN))+WIDTH.GT.1.0)GO TO 100
      ZLOWER=ZLOWER-SPACE*SIGNA
      ZUPPER=ZUPPER+SPACE*SIGNA
      GO TO 200
   95 SPACE=ABS(ROOTP(J,JSIGN))
      N=SPACE/UMAX+1.
      AN=N
      IF(SPACE.EQ.0.0)AN=0.5
      SPACE=0.05
      ZLOWER=UMAX*CMPLX((AN-1.0+SPACE)*SIGNA,SPACE)
      ZUPPER=UMAX*CMPLX((AN-SPACE)*SIGNA,SPACE)
      DZIMAG=UMAX*(AN+0.5+SPACE)
      GO TO 200
  100 HOLD=(AN-1.)*UMAX+WIDTH
      HOLD=AMIN1(HOLD,(AN-0.5)*UMAX)
      ZLOWER=CMPLX(SIGN(HOLD,SIGNA),-SPACE)
      HOLD=ABS(ROOTP(J+1,JSIGN))+SPACE
      HOLD=AMIN1(HOLD,(AN+0.5)*UMAX)
      ZUPPER=CMPLX(SIGN(HOLD,SIGNA),-SPACE)
  200 DZREAL=REAL(ZUPPER)-REAL(ZLOWER)
```

```
      KSET=NSET
      ILEFT=1
  205 CALL DISP(ZLOWER,PHI,DPHIDZ,DERROR)
      DO 210 ISET=1,KSET
      GHOLD=PHI-SET(ISET)
      CALL PHASE(GHOLD,ISTART(ISET),0)
      IHOLD(ISET)=ISTART(ISET)
      ICHANG(ISET)=IHOLD(ISET)
      FSTART(ISET)=DPHIDZ/GHOLD
      FHOLD(ISET)=FSTART(ISET)
      DO 210 M=1,MMAX
  210 RESULT(ISET,M)=0.0
      ISEG=1
      SIGNT=1.0
  220 CALL LINE(DISP,ZUPPER,ZLOWER,SET,KSET,ERROR,RESULT,NPRINT,NERROR,I
     1START,FSTART,FRACT,MMAX)
      IF(NERROR.NE.0)GO TO (350,450,550,650),ISEG
      I=SIGNA
      M=SIGNT
      DO 225 ISET=1,KSET
      ITRY=ISTART(ISET)-IHOLD(ISET)
      IF(I*M*ITRY.LT.0.AND.IABS(ITRY).GT.4)NERROR=(NSET+1-ISET)*1000+200
     1*ISEG+ITRY
  225 CONTINUE
      IF(NERROR.NE.0)GO TO (350,450,550,660),ISEG
      IF(ISEG.EQ.4)GO TO 700
  240 DO 260 ISET=1,KSET
      IHOLD(ISET)=ISTART(ISET)
      FHOLD(ISET)=FSTART(ISET)
      DO 250 M=1,MMAX
      RLINE(ISET,ISEG,M)=RESULT(ISET,M)-RHOLD(ISET,M)
  250 RHOLD(ISET,M)=RESULT(ISET,M)
  260 CONTINUE
      ISEG=ISEG+1
      GO TO (400,400,500,600),ISEG
  350 IF(CAPK(2).NE.0.0)RETURN
  400 ZLOWER=ZUPPER
      ZUPPER=ZLOWER+CMPLX(0.0,DZIMAG)
      IF(ILEFT.EQ.1)GO TO 220
      DO 410 ISET=1,KSET
      ISTART(ISET)=IJUMP(ISET)+IHOLD(ISET)
      FSTART(ISET)=FJUMP(ISET)
      DO 410 M=1,MMAX
  410 RESULT(ISET,M)=RESULT(ISET,M)+RLINE(ISET,4,M)
      GO TO 240
  450 RETURN
  500 ZLOWER=ZUPPER
      ZUPPER=ZLOWER-DZREAL
      GO TO 220
  550 RETURN
  600 ZLOWER=ZUPPER-CMPLX(0.0,DZIMAG)
      SIGNT=-1.0
      DO 610 ISET=1,KSET
      GHOLD=PHI-SET(ISET)
      IHOLD(ISET)=ICHANG(ISET)
      ICHANG(ISET)=ISTART(ISET)-ICHANG(ISET)
```

```
      ISTART(ISET)=IHOLD(ISET)
      FSTART(ISET)=DPHIDZ/GHOLD
      FHOLD(ISET)=FSTART(ISET)
      DO 610 M=1,MMAX
  610 RESULT(ISET,M)=-RESULT(ISET,M)
      GO TO 220
  650 RETURN
  660 ILEFT=2
      ZUPPER=ZLOWER
      DZREAL=UMAX*SIGNA
      ZLOWER=ZLOWER-DZREAL
      IF(REAL(ZLOWER)*SIGNA.LT.0.0)GO TO 700
      KSET=NERROR/1000
      DO 670 ISET=1,KSET
      IJUMP(ISET)=ISTART(ISET)-IHOLD(ISET)
      FJUMP(ISET)=FSTART(ISET)
      DO 670 M=1,MMAX
  670 RLINE(ISET,4,M)=RESULT(ISET,M)+RHOLD(ISET,M)
      GO TO 205
  700 DO 750 ISET=1,NSET
      ITRY=ICHANG(ISET)+IHOLD(ISET)-ISTART(ISET)
      NUMBER(ISET)=(IABS(ITRY)+4)/16
      DO 705 M=1,MMAX
  705 RESULT(ISET,M)=RESULT(ISET,M)*TWOPI
      IF(ITRY.GE.0)GO TO 720
      DO 710 M=1,MMAX
  710 RESULT(ISET,M)=-RESULT(ISET,M)
  720 IF(IABS(ITRY)-16.LE.1)GO TO 750
      IF(IABS(ITRY)-32.GT.1)GO TO 740
      RESULT(ISET,1)=RESULT(ISET,1)-2.
      GHOLD=CSQRT(2.*RESULT(ISET,3)-RESULT(ISET,2)*RESULT(ISET,2))
      ZUPPER=0.5*(RESULT(ISET,2)+GHOLD)
      ZLOWER=0.5*(RESULT(ISET,2)-GHOLD)
      IF(AIMAG(ZLOWER).GT.0.0)GO TO 730
      IF(AIMAG(ZUPPER).GT.0.0)GO TO 729
      IF(ABS(REAL(ZLOWER)).GT.ABS(REAL(ZUPPER)))GO TO 730
  729 RESULT(ISET,1)=RESULT(ISET,1)*(RESULT(ISET,3)-2.*ZLOWER*RESULT(ISE
     1T,2))/(ZUPPER-ZLOWER)
      RESULT(ISET,2)=ZUPPER
      GHOLD=ZLOWER
      GO TO 735
  730 RESULT(ISET,1)=RESULT(ISET,1)*(2.*ZUPPER*RESULT(ISET,2)-RESULT(ISE
     1T,3))/(ZUPPER-ZLOWER)
      RESULT(ISET,2)=ZLOWER
      GHOLD=ZUPPER
  735 RESULT(ISET,1)=RESULT(ISET,1)+1.
      IF(NEXTR1.EQ.0)GO TO 750
      HOLD=0.0
      PHI=(RESULT(ISET,1)-1.0)/UMAX
      GHOLD=GHOLD/UMAX
      ITRY=NSET+1-ISET
      WRITE(6,736)ITRY,SET(ISET),HOLD,GHOLD,PHI
  736 FORMAT(1X13,2(3X1P2E12.3),3X1P2E10.1)
      GO TO 750
  740 IF(NERROR.NE.0)GO TO 750
      NERROR=(NSET+1-ISET)*1000+ITRY
```

```
  750 CONTINUE
      RETURN
      END


      SUBROUTINE LINE(DUMMY,ZUPPER,ZLOWER,SET,NSET,RELERR,CROOT,NPRINT,N
     1ERROR,ISTART,FSTART,FRACT,MMAX)
C
C   THIS SUBPROGRAM COMPUTES THE LINE INTEGRAL (IN THE COMPLEX PLANE)
C     OF A FUNCTION SPECIFIED BY 'DUMMY' BETWEEN THE COMPLEX COORDINATES
C     'ZLOWER' AND 'ZUPPER' TO AN ACCURACY SPECIFIED BY 'RELERR'.
C   THE SUBPROGRAM 'DUMMY' MUST HAVE THE FORM DUMMY(Z,PHI,DPHIDZ,ERROR)
C     WHERE Z IS THE ARGUMENT SUPPLIED BY LINE, PHI IS THE FUNCTION OF
C     INTEREST, DPHIDZ ITS DERIVATIVE AND ERROR IS THE ACCURACY WHICH
C     THIS SUBPROGRAM REQUIRES OF PHI, DPHIDZ.
C     THE LINE INTEGRAL COMPUTED HERE IS THAT OF THE FUNCTION
C         (Z**M)*DPHIDZ/(PHI-SET(I))
C     IN WHICH M RANGES FROM 0 TO 'MMAX'-1 AND THE INDEX I OF 'SET'
C     RANGES FROM 1 TO 'NSET'.
C   THE COMPUTED RESULTS ARE STORED IN 'CROOT' IN THE FORM CROOT(I,M).
C   'NPRINT' = 0 FOR NO PRINTING OF INTERMEDIATE RESULTS OR ERROR
C     MESSAGES.
C   'NPRINT' = 1 OR GREATER FOR PRINTING OF THE ERROR MESSAGES.
C   'NPRINT' = 2 OR GREATER THAN 3 FOR A PRINTING OF A SHORT SUMMARY
C     OF INTERMEDIATE RESULTS.
C   'NPRINT' = 3 OR GREATER FOR A PRINTING OF DETAILED INTERMEDIATE
C     RESULTS.
C   UPON COMPLETION OF THIS CALCULATION
C   'NERROR' = 0,COMPUTATION WAS COMPLETED SUCCESSFULLY.
C   'NERROR' = 1,IN AT LEAST ONE LINE SEGMENT THE PHASE CHANGE OF THE
C     INTEGRAND WAS GREATER THAN PI/2.0 AND HENCE THE RESULTS MAY BE
C     INCORRECT.
C   'NERROR' = 2,THE ACCURACY CRITERION COULD NOT BE MET IN AT LEAST
C     ONE LINE SEGMENT AND HENCE THE RESULTS MAY BE INCORRECT.
C   'NERROR' = 3,4, 'NERROR' =1,2 CONDITIONS OCCURED AT LEAST 10 TIMES
C     AND THE CALCULATION WAS TERMINATED PREMATURELY AND HENCE THE
C     RESULTS ARE MOST LIKELY INCORRECT.
C   'ISTART' AND 'FSTART' ARE RESPECTIVELY THE PHASE AND VALUE OF THE
C     INTEGRAND WITH M = 0 AND MUST BE SUPPLIED TO THIS SUBPROGRAM AS
C     STARTING VALUES FOR ALL I, THAT IS FOR ALL VALUES OF SET(I).
C   'FRACT' IS TO BE GIVEN AS THE MINIMUM FRACTION INTO WHICH THE
C     INTERVAL (ZLOWER,ZUPPER) MAY DIVIDED IN ATTEMPTING TO SATISFY THE
C     DESIRED ACCURACY GIVEN BY 'RELERR'.
C   'MMAX' IS THE MAXIMUM NUMBER OF VALUES OF M (SEE INTEGRAND ABOVE)
C     STARTING FROM ZERO WHICH ARE TO BE COMPUTED.
C
      DIMENSION CROOT(20,3),SET(20),IPHASE(20,5),F(20,5,3),ISTART(20)
      DIMENSION FSTART(20)
      COMPLEX CROOT,PHI,DPHIDZ,HTRY,HMIN,H,GHOLD,AHOLD,F,FSTART,ZUPPER,
     1ZLOWER,ZHOLD,Z
      THEMAG(Z)=ABS(REAL(Z))+ABS(AIMAG(Z))
      TERROR=AMAX1(0.01*RELERR,1.E-06)
      ONEOER=1./RELERR
      IGOOF=0
      NSHORT=0
```

```
      NLONG=0
      IF(NPRINT.EQ.0)GO TO 90
      IF(NPRINT.EQ.2.OR.NPRINT.GT.3)NSHORT=1
      IF(NPRINT.GE.3)NLONG=1
   90 NERROR=0
      I3=0
      I5=0
      DO 100 ISET=1,NSET
      IPHASE(ISET,1)=ISTART(ISET)
      F(ISET,1,1)=FSTART(ISET)
      DO 100 M=2,MMAX
  100 F(ISET,1,M)=F(ISET,1,M-1)*ZLOWER
      ZHOLD=ZLOWER
      HTRY=0.25*(ZUPPER-ZHOLD)
      ITEST1=1
      HMIN=FRACT*RELERR*(ZUPPER-ZHOLD)
  200 IF(THEMAG(HTRY).LT.THEMAG(HMIN))HTRY=HMIN
      H=HTRY
      ITEST2=0
      GHOLD=ZUPPER-ZHOLD
      IF(THEMAG(4.0*H).LT.THEMAG(GHOLD).OR.ITEST1.EQ.1)GO TO 220
      H=0.25*(ZUPPER-ZHOLD)
      ITEST1=1
  220 Z=ZHOLD
      DERROR=AMAX1(TERROR,1.E-07)
      DO 260 I=2,5
      Z=Z+H
      IF(I.EQ.3.AND.I3.NE.0)GO TO 255
      IF(I.NE.5)GO TO 240
      IF(ITEST1.GT.0)Z=ZUPPER
      IF(I5.NE.0)GO TO 255
  240 CALL DUMMY(Z,PHI,DPHIDZ,DERROR)
      GHOLD=Z*DPHIDZ
      DO 250 ISET=1,NSET
      AHOLD=PHI-SET(ISET)
      IF(THEMAG(AHOLD).NE.0.0)GO TO 245
      NERROR=32000+ISET
      CROOT(ISET,1)=0.0
      CROOT(ISET,2)=Z
      IF(MMAX.LT.3)GO TO 244
      DO 243 M=3,MMAX
  243 CROOT(ISET,M)=Z*CROOT(ISET,M-1)
  244 RETURN
  245 CALL PHASE(AHOLD,IPHASE(ISET,I),IPHASE(ISET,I-1))
      F(ISET,I,1)=DPHIDZ/AHOLD
      F(ISET,I,2)=GHOLD/AHOLD
      IF(MMAX.LT.3)GO TO 250
      DO 249 M=3,MMAX
  249 F(ISET,I,M)=F(ISET,I,M-1)*Z
  250 CONTINUE
      GO TO 260
  255 DO 256 ISET=1,NSET
      CALL SPHASE(IPHASE(ISET,I),IPHASE(ISET,I-1))
  256 CONTINUE
  260 CONTINUE
      I3=0
```

```
      I5=0
      IJUMP=0
      ACCUR=0.0
      DO 270 ISET=1,NSET
      DO 261 M=1,MMAX
  261 F(ISET,4,M)=(14.*(F(ISET,1,M)+F(ISET,5,M))+64.*(F(ISET,2,M)+F(ISET
     1,4,M))+24.*F(ISET,3,M))/45.
      IF(NLONG.EQ.0)GO TO 264
  262 FORMAT(1X,7HZHOLD =,1P2E16.7,2H I,5X3HH =,1P2E16.7,2H I,5X6HISET =
     1,I5)
  263 FORMAT(5(2(1X,1PE9.2),1HI,I4,1X))
      WRITE(6,262)ZHOLD,H,ISET
      WRITE(6,263)(F(ISET,I,2),IPHASE(ISET,I),I=1,5)
  264 GHOLD=(2.*(F(ISET,1,2)+F(ISET,5,2))+8.*F(ISET,3,2))/3.-F(ISET,4,2)
      AHOLD=F(ISET,4,2)*RELERR
      ERROR1=0.0
      IF(REAL(AHOLD).NE.0.0)ERROR1=ABS(REAL(GHOLD)/REAL(AHOLD))
      ERROR2=0.0
      IF(AIMAG(AHOLD).NE.0.0)ERROR2=ABS(AIMAG(GHOLD)/AIMAG(AHOLD))
      ERROR=AMAX1(ERROR1,ERROR2)
      IF(ERROR.GT.ONEOER)GO TO 265
      GHOLD=H*F(ISET,4,2)
      AHOLD=(GHOLD+CROOT(ISET,2))*RELERR
      ERROR1=0.0
      IF(REAL(AHOLD).NE.0.0)ERROR1=ABS(REAL(GHOLD)/REAL(AHOLD))
      ERROR2=0.0
      IF(AIMAG(AHOLD).NE.0.0)ERROR2=ABS(AIMAG(GHOLD)/AIMAG(AHOLD))
      ERROR=AMIN1(ERROR,AMAX1(ERROR1,ERROR2))
  265 IF(ERROR.GT.ACCUR)ACCUR=ERROR
      DO 270 I=2,5
      ITRY=IABS(IPHASE(ISET,I)-IPHASE(ISET,I-1))
      IF(ITRY.GT.IJUMP)IJUMP=ITRY
  270 CONTINUE
      IF(NSHORT.EQ.0)GO TO 275
      WRITE(6,271)ZHOLD,H,HMIN,ACCUR,IJUMP
  271 FORMAT(1X7HZHOLD =,1P2E13.5,2H I,3X3HH =,1P2E10.2,2H I,3X6HHMIN =,
     11P2E10.2,2H I,7X7HACCUR =,1PE10.2,3X7HIJUMP =,I3)
  275 IF(ACCUR.LT.1.0.AND.IJUMP.LT.4)ITEST2=1
      IF(ITEST2.NE.0)GO TO 330
      HTRY=0.5*H
      TERROR=0.5*TERROR
      I5=5
      I3=2
      IF(ACCUR.LE.20.0)GO TO 285
      I3=0
      HTRY=0.5*HTRY
      TERROR=0.5*TERROR
  285 IF(ITEST1.EQ.0)GO TO 290
      IF(THEMAG(H).LE.THEMAG(HMIN))GO TO 310
      ITEST1=0
  290 IF(THEMAG(HTRY).LT.THEMAG(HMIN))GO TO 300
      H=HTRY
      I=I5-I3
      DO 295 ISET=1,NSET
      IF(I3.EQ.0)GO TO 292
      DO 291 M=1,MMAX
```

```
  291 F(ISET,5,M)=F(ISET,3,M)
      IPHASE(ISET,5)=IPHASE(ISET,3)
  292 DO 293 M=1,MMAX
  293 F(ISET,I,M)=F(ISET,2,M)
  295 IPHASE(ISET,I)=IPHASE(ISET,2)
      GO TO 220
  300 IF(THEMAG(H).EQ.THEMAG(HMIN))GO TO 310
      I3=0
      I5=0
      H=HMIN
      GO TO 220
  310 IF(NPRINT.NE.0)WRITE(6,320)H,ZHOLD,ACCUR,IJUMP
  320 FORMAT(1X53HINTEGRATION ROUTINE CANNOT GIVE DESIRED ACCURACY, H =,
     11P2E16.7,17H I  IS TOO SMALL./3X21HPROBLEM OCCURS AT Z =,1P2E16.7,
     22H I,26H  WHERE THE ERROR RATIO IS,1PE16.7,2X27HAND MAXIMUM PHASE
     3CHANGE IS,I3)
       IF(IJUMP.GE.4)NERROR=1
       IF(ACCUR.GT.1.0)NERROR=2
       IGOOF=IGOOF+1
       IF(IGOOF.LT.10)GO TO 335
       NERROR=NERROR+2
       RETURN
  330 IF(ITEST1.NE.0.OR.ACCUR.GE.0.1.OR.IJUMP.GT.1)GO TO 335
      HTRY=2.0*H
      TERROR=2.0*TERROR
      IF(ACCUR.GE.5.E-03)GO TO 335
      HTRY=2.0*HTRY
      TERROR=2.0*TERROR
  335 DO 340 ISET=1,NSET
      IPHASE(ISET,1)=IPHASE(ISET,5)
      DO 340 M=1,MMAX
      CROOT(ISET,M)=CROOT(ISET,M)+H*F(ISET,4,M)
  340 F(ISET,1,M)=F(ISET,5,M)
      ZHOLD=Z
      IF(ITEST1.EQ.0)GO TO 200
      DO 350 ISET=1,NSET
      ISTART(ISET)=IPHASE(ISET,5)
  350 FSTART(ISET)=F(ISET,5,1)
      RETURN
      END



      SUBROUTINE PHASE(Z,INEW,IOLD)
C
C  THIS SUBPROGRAM COMPUTES THE PHASE OF A COMPLEX VARIABLE 'Z' IN
C    SIXTEENTHS OF 2.0*PI. IT IS CALLED PRINCIPALLY BY LINE.
C  'INEW' IS THE PHASE FOUND.
C  'IOLD' IS THE PHASE OF A NEARBY COMPEX VALUE TO GIVE THE RELEVANT
C    NUMBER OF 2.0*PI'S TO WHICH THE NEW PHASE SHOULD BE REFERENCED.
C
      COMPLEX Z
      X=REAL(Z)
      Y=AIMAG(Z)
      IQUAD=0
      IF(Y.LT.0.0)IQUAD=3
```

```
      IF(X.LT.0.0)IQUAD=IQUAD+1
      IF(IQUAD.EQ.4)IQUAD=2
      Y=ABS(Y/X)
      IANGLE=0
      ICHANG=1
      IF(Y.LT.1.0)GO TO 100
      IANGLE=3
      Y=1.0/Y
      ICHANG=-1
  100 IF(Y.GE.0.4142136)IANGLE=IANGLE+ICHANG
      IF(IQUAD-2*(IQUAD/2).GT.0)IANGLE=3-IANGLE
      INEW=4*IQUAD+IANGLE
      GO TO 150
C
C  THIS ENTRY ALLOWS FOR CHANGING REFERENCING OF THE NUMBER OF 2.0*PI'S
C    WHEN THE RELATIVE PHASE OF THE COMPLEX VARIABLE IS ALREADY KNOWN.
C
      ENTRY SPHASE(INEW,IOLD)
      ICHANG=0
      IF(INEW.LT.0)ICHANG=-1
      INEW=INEW-16*(ICHANG+(INEW/16))
  150 IQUAD=IOLD/16
      IF(IOLD.LE.0)IQUAD=IQUAD-1
      INEW=INEW+16*IQUAD
      ICHANG=1
  200 IF(IABS(IOLD-INEW).LE.8)RETURN
      IF(ICHANG.LT.0)GO TO 250
      INEW=INEW+16
      ICHANG=ICHANG-2
      GO TO 200
  250 INEW=INEW-32
      RETURN
      END



      SUBROUTINE NYQUIS(FRQNYQ,ERROR)
C
C  THIS SUBPROGRAM COMPUTES THE DATA FOR A NYQUIST PLOT OF THE
C    DISPERSION FUNCTION.
C  'FRQNYQ' = THE IMAGINARY PART OF THE FREQUENCY AT WHICH THE NYQUIST
C    PLOT IS TO BE COMPUTED.
C  'ERROR' = THE ACCURACY TO WHICH THE DISPERSION FUNCTION IS TO BE
C    COMPUTED.
C
      COMMON CCAPK,HATRP,DHATRP,CAPK,CONST,GRAD,C,D,GRAV,ROOTP
      COMMON ALOW,EXPMAX,FRACT,UMAX,EXTRA1,EXTRA2,EXTRA3
      COMMON JMAX,L,NTYPE,JPOS,JNEG,KMAX,MMAX,NEXTR1,NEXTR2,NEXTR3
      COMMON NEXTR4,NEXTR5,NEXTR6,NEXTR7
      DIMENSION CONST(4,3),GRAD(5,3),L(3),CAPK(3),CCAPK(3)
      DIMENSION C(2,400,3),D(2,400,3),GRAV(400,3)
      DIMENSION ROOTP(100,2),HATRP(100,2),DHATRP(100,2)
      COMPLEX CCAPK,HATRP,DHATRP
      DIMENSION H(3),DH(3)
      COMPLEX H,DH,U
    1 FORMAT(1H1,5X17HNYQUIST PLOT DATA,1X9H(IMAG W =,1PE15.7,1H)/1H0/3(
```

```
     15X6HREAL H,5X6HIMAG H,4X7HREAL DH,3X7HIMAG DH,1X)/1X)
    2 FORMAT(3(2X,1P2E11.3,1P2E10.2))
    3 FORMAT(1H )
      IMAX=3
      WRITE(6,1)FRQNYQ
      AMAX=ROOTP(JPOS,1)
      IF(-ROOTP(JNEG,2).GT.AMAX)AMAX=ABS(ROOTP(JNEG,2))
      NMAX=AMAX/UMAX+3.0
      IF(CAPK(2).NE.0.0)GO TO 70
      LMAX=20
      GO TO 80
   70 DUMIN=CAPK(2)/(2.0*CONST(3,1))
      LMAX=ABS(UMAX/DUMIN)+1.0
   80 DUMIN=UMAX/FLOAT(LMAX)
      DO 200 JSIGN=1,2
      IF(JSIGN.NE.2)GO TO 90
      IF(NTYPE.NE.0)GO TO 85
      DO 84 I=1,JMAX
      IF(GRAD(5,I).NE.0.0)GO TO 85
   84 CONTINUE
      RETURN
   85 DUMIN=-DUMIN
   90 DO 190 N=1,NMAX
      I=1
      K=1
      AMAX=FLOAT(N-1)
      IF(JSIGN.EQ.2)AMAX=-AMAX
      U=UMAX*CMPLX(AMAX,FRQNYQ)
  100 CALL DISP(U,H(I),DH(I),ERROR)
      K=K+1
      I=I+1
      U=U+DUMIN
      IF(I.LE.IMAX)GO TO 120
      WRITE(6,2)(H(I),DH(I),I=1,IMAX)
      I=1
  120 IF(K.LE.LMAX)GO TO 100
      I=I-1
      IF(I.NE.0)WRITE(6,2)(H(J),DH(J),J=1,I)
      IF(I.EQ.0)WRITE(6,3)
  190 CONTINUE
  200 CONTINUE
      RETURN
      END



C              MICRO2
C            MAIN PROGRAM 2
C  CONTROL PROGRAM FOR COMPUTING GROWTH RATES AND THE ABSOLUTE
C     INSTABILITY DENSITY THRESHOLD
C
      COMMON CCAPK,HATRP,DHATRP,CAPK,CONST,GRAD,C,D,GRAV,ROOTP
      COMMON ALOW,EXPMAX,FRACT,UMAX,EXTRA1,EXTRA2,EXTRA3
      COMMON JMAX,L,NTYPE,JPOS,JNEG,KMAX,MMAX,NEXTR1,NEXTR2,NEXTR3
      COMMON NEXTR4,NEXTR5,NEXTR6,NEXTR7
      DIMENSION CONST(4,3),GRAD(5,3),L(3),CAPK(3),CCAPK(3)
```

```
      DIMENSION C(2,400,3),D(2,400,3),GRAV(400,3)
      DIMENSION ROOTP(100,2),HATRP(100,2),DHATRP(100,2)
      COMPLEX CCAPK,HATRP,DHATRP
      DIMENSION ZMOM(4,5)
      COMMON ALAMB,ZMOM,W,ITYPE,ACCUR,ERROR
      COMPLEX ZMOM,W
      DIMENSION CHAR(5,3)
      COMPLEX ZSTART
    1 FORMAT(14I5)
    2 FORMAT(5E14.8)
    3 FORMAT(1H1,10X4HCASE,I3,9H, SUBCASE,I3/1H0)
      NMAX=400
      ALOW=1.E-65
      EXPMAX=150.
      READ(5,1)NCASES
      DO 400 NCASE=1,NCASES
      READ(5,1)NSUBS
      READ(5,2)ACCUR,ERROR
      ACCUR=ABS(ACCUR)
      ERROR=ABS(ERROR)
      ACCUR=AMAX1(ACCUR,5.E-06)
      ERROR=AMAX1(ERROR,5.E-08)
      CALL SINPUT(NCASE,NGOOF,CHAR)
      IF(NGOOF.NE.0)RETURN
      CALL SETUP(NMAX,CHAR)
      DO 300 NSUB=1,NSUBS
      WRITE(6,3)NCASE,NSUB
      READ(5,1)ITYPE,NSTEPS,IPR
      NSTEPS=IABS(NSTEPS)
      IF(NSTEPS.EQ.0)NSTEPS=10
      READ(5,2)ALAMB,XSTART,XSTOP,ZSTART
      IF(ITYPE.LT.5.AND.ITYPE.GT.0)CALL FOLLOW(XSTART,XSTOP,NSTEPS,ZSTAR
     1T,IPR)
  300 CONTINUE
  400 CONTINUE
      RETURN
      END


      SUBROUTINE SINPUT(NCASE,NGOOF,CHAR)
C
C  THIS SUBPROGRAM READS MOST OF THE RELEVANT INPUT DATA FOR A GIVEN
C    CASE. IT IS AN ABBREVIATED VERSION OF SUBPROGRAM INPUT IN THAT
C    K-Z IS NOT INPUTTED BY THIS SUBPROGRAM. THIS SUBPROGRAM ALSO
C    PRINTS A SUMMARY OF THE RELEVANT INPUT PARAMETERS.
C
      DIMENSION CONST(4,3),GRAD(5,3),L(3),CAPK(3),CCAPK(3)
      DIMENSION C(2,400,3),D(2,400,3),GRAV(400,3)
      DIMENSION ROOTP(100,2),HATRP(100,2),DHATRP(100,2)
      COMMON CCAPK,HATRP,DHATRP,CAPK,CONST,GRAD,C,D,GRAV,ROOTP
      COMMON ALOW,EXPMAX,FRACT,UMAX,EXTRA1,EXTRA2,EXTRA3
      COMMON JMAX,L,NTYPE,JPOS,JNEG,KMAX,MMAX,NEXTR1,NEXTR2,NEXTR3
      COMMON NEXTR4,NEXTR5,NEXTR6,NEXTR7
      COMPLEX CCAPK,HATRP,DHATRP
      DIMENSION CHAR(5,3)
```

```
    1 FORMAT(5I5)
    2 FORMAT(5E14.8,I2)
    3 FORMAT(1H1,10X4HCASE,I3/1H0)
    4 FORMAT(1H0,45HREFERENCE LARMOR RADIUS TIMES THE WAVE VECTOR/1H0,21
     1X3HK-Y/1H0,16X1PE13.6/1H0)
    9 FORMAT(80X23HREFERENCE LARMOR RADIUS/1X7HSPECIES,16X29HRATIO TO RE
     1FERENCE SPECIES OF,22X33HDIVIDED BY THE GRADIENT LENGTH OF,4X7HGRA
     2VITY,5X7HCURRENT/2X6HNUMBER,5X4HMASS,7X7HDENSITY,5X6HCHARGE,6X6HTE
     3MP-Z,4X11HTEMP-'PERP',2X1HL,4X7HDENSITY,3X11HTEMP-'PERP',3X6HTEMP-
     4Z,2X2(3X9HPARAMETER)/1H )
   10 FORMAT(2XI3,3X1P5E12.3,I4,1P5E12.3)
   11 FORMAT(1H0,26HCHARGE NEUTRALITY VIOLATED)
   12 FORMAT(1H0,32HDENSITY GRADIENTS DO NOT BALANCE)
      NGOOF=0
      DERROR=1.E-04
      WRITE(6,3)NCASE
   90 READ(5,1)JMAX,NTYPE,NVZERO
      READ(5,2)CAPK(1)
      WRITE(6,4)CAPK(1)
      NDIFF=0
      DO 100 J=1,JMAX
      DO 99 I=1,5
   99 GRAD(I,J)=0.0
      READ(5,2)(CHAR(I,J),I=1,5),L(J)
      IF(NTYPE.GT.3)READ(5,2)(GRAD(I,J),I=1,3)
      IF(NTYPE.GT.1.AND.NTYPE.LE.3)READ(5,2)GRAD(1,J)
      IF(NTYPE-2*(NTYPE/2).NE.0)READ(5,2)GRAD(4,J)
      IF(NVZERO.NE.0)READ(5,2)GRAD(5,J)
  100 CONTINUE
  110 WRITE(6,9)
      WRITE(6,10)(J,(CHAR(I,J),I=1,5),L(J),(GRAD(I,J),I=1,5),J=1,JMAX)
      SUM=0.0
      DO 120 J=1,JMAX
  120 SUM=SUM+CHAR(2,J)*CHAR(3,J)
      IF(ABS(SUM).LT.DERROR)GO TO 130
      NGOOF=1
      WRITE(6,11)
  130 IF(NTYPE.LT.1)GO TO 150
      SUM=0.0
      DO 140 J=1,JMAX
      SUM=SUM+CHAR(2,J)*CHAR(3,J)*(-GRAD(1,J)+FLOAT(L(J)+1)*GRAD(2,J)+0.
     15*GRAD(3,J)+2.0*GRAD(4,J)*FLOAT(1/(L(J)+1)))
  140 GRAD(4,J)=GRAD(4,J)*CHAR(5,J)*CHAR(1,J)/(CHAR(3,J)*CHAR(3,J))
      IF(ABS(SUM).LT.DERROR)GO TO 150
      NGOOF=1
      WRITE(6,12)
  150 RETURN
      END


      SUBROUTINE FOLLOW(XSTART,XSTOP,NSTEPS,Z,IP)
C
C  THIS SUBPROGRAM 'FOLLOWS' SOLUTIONS OF THE DISPERSION RELATION OR
C    ITS K-Z DERIVATIVE.
C  ITYPE = 1 MEANS FOLLOW COMPLEX K FOR REAL OMEGA
```

```
C     (ALONG THE SOLUTION OF THE DISPERSION RELATION)
C   ITYPE = 2 MEANS FOLLOW COMPLEX OMEGA FOR REAL K
C     (ALONG THE SOLUTION OF THE DISPERSION RELATION)
C   ITYPE = 3 MEANS FOLLOW COMPLEX K FOR REAL OMEGA
C     (ALONG THE SOLUTION OF THE DERIVATIVE OF THE DISPERSION FUNCTION
C     SET TO ZERO)
C   ITYPE = 4 MEANS FOLLOW COMPLEX K AND LAMBDA FOR CHANGING IMAGINARY
C     OMEGA (ALONG SIMULTANEOUS SOLUTIONS OF THE DISPERSION RELATION
C     AND ITS DERIVATIVE)
C   FOR ITYPE = 1,2,3 'XSTART' IS THE STARTING VALUE OF REAL FREQUENCY,
C     K-Z, OR FREQUENCY RESPECTIVELY.
C   'XSTOP' IS THE CORRESPONDING FINAL VALUE TO WHICH THIS ROUTINE IS
C     TO 'FOLLOW' THE ROOT OF THE DISPERSION RELATION OR ITS DERIVATIVE.
C   FOR ITYPE = 4, 'XSTART','XSTOP' IS THE COMPLEX STARTING VALUE OF THE
C     FREQUENCY.
C   'NSTEPS' IS THE MINIMUM NUMBER OF STEPS WHICH THIS SUBPROGRAM IS
C     TO TAKE IN PROCEEDING FROM 'XSTART' TO 'XSTOP'.
C   'Z' IS TO BE GIVEN AS THE COMPLEX STARTING POINT FOR THE
C     COMPLEMENTARY VARIABLE TO THAT SPECIFIED BY 'XSTART','XSTOP'.
C   'IP' = 0 MEANS PRINT ONLY THE MAXIMUM OF THE ROOT BEING FOLLOWED
C   'IP' = 1 MEANS PRINT THE ROOT AS FOUND AT EACH STEP BETWEEN 'XSTART'
C     AND 'XSTOP'.
C   LAMBDA AS TRANSFERRED TO THIS SUBPROGRAM THROUGH COMMON DENOTES THE
C     APPROPRIATE DENSITY AT WHICH THE 'FOLLOW' IS TO BE DONE FOR
C     ITYPE = 1,2. LAMBDA IS NOT USED FOR ITYPE = 3. FOR ITYPE = 4
C     LAMBDA SPECIFIES THE TOTAL INTERVAL OF TEMPORAL GROWTH RATES OVER
C     WHICH THE ABSOLUTE INSTABILITY ROOTS ARE TO BE COMPUTED.
C
      COMMON CCAPK,HATRP,DHATRP,CAPK,CONST,GRAD,C,D,GRAV,ROOTP
      COMMON ALOW,EXPMAX,FRACT,UMAX,EXTRA1,EXTRA2,EXTRA3
      COMMON JMAX,L,NTYPE,JPOS,JNEG,KMAX,MMAX,NEXTR1,NEXTR2,NEXTR3
      COMMON NEXTR4,NEXTR5,NEXTR6,NEXTR7
      DIMENSION CONST(4,3),GRAD(5,3),L(3),CAPK(3),CCAPK(3)
      DIMENSION C(2,400,3),D(2,400,3),GRAV(400,3)
      DIMENSION ROOTP(100,2),HATRP(100,2),DHATRP(100,2)
      COMPLEX CCAPK,HATRP,DHATRP
      DIMENSION ZMOM(4,5)
      COMPLEX W,ZMOM
      COMMON ALAMB,ZMOM,W,ITYPE,ACCUR,ERROR,DXMIN
      COMPLEX H,HK,HKK,HW,HWK
      COMPLEX Z,ZHOLD,ZZERO,CK1,CK2,WHOLD
      EXTERNAL RESULT
    1 FORMAT(19X17HCOMPLEX FREQUENCY,20X19HCOMPLEX WAVE VECTOR,11X9HNUMB
     1ER OF)
    2 FORMAT(18X19HCOMPLEX WAVE VECTOR,20X17HCOMPLEX FREQUENCY,12X9HNUMB
     1ER OF)
    3 FORMAT(1H+,106X19HDISPERSION FUNCTION)
    4 FORMAT(1X5HINDEX,2(11X4HREAL,13X4HIMAG,6X),3X10HITERATIONS)
    5 FORMAT(1H+,105X4HREAL,13X4HIMAG)
    6 FORMAT(1H )
    8 FORMAT(1H0,2X63HTRAJECTORY OF THE SOLUTION OF THE DISPERSION RELAT
     1ION (LAMBDA =,1PE13.6,1H))
    9 FORMAT(1H0,2X71HTRAJECTORY OF THE SOLUTION OF THE DERIVATIVE OF TH
     1E DISPERSION FUNCTION)
   10 FORMAT(6X8H(ITYPE =,I2,22H, REQUESTED ACCURACY =,1PE8.1,1H)/1H0)
   11 FORMAT(I4,2(4X1P2E17.6),6XI5,6X1P2E17.6)
```

```
 12 FORMAT(1X44HNEWTON ITERATION DOES NOT CONVERGE (IERROR =,I2,6H), X
   1 =,1PE13.6,2X7HAND Z =,1P2E14.6,2H I)
 13 FORMAT(1H+,96X1P2E17.6)
 14 FORMAT(1X39HDDX IS TOO SMALL, PROBLEM OCCURS AT X =,1PE13.6,12H, W
   1ITH DDX =,1PE13.6,1X7HAND Z =,1P2E14.6)
 15 FORMAT(1X7HMAXIMUM,2(1P2E17.6,4X),2XI5,4X3HMAX)
 16 FORMAT(1X64HITERATION TO FIND ZERO OF IMAGINARY H DOES NOT CONVERG
   1E, ITRY4 =,I3)
    IMAX=0
    ITEND=10
    ITEND3=3*ITEND
    IF(ITYPE.LT.3)WRITE(6,8)ALAMB
    IF(ITYPE.GT.2)WRITE(6,9)
    WRITE(6,10)ITYPE,ACCUR
    IF(ITYPE.EQ.2)WRITE(6,2)
    IF(ITYPE.NE.2)WRITE(6,1)
    IF(ITYPE.GT.2)WRITE(6,3)
    WRITE(6,4)
    IF(ITYPE.GT.2)WRITE(6,5)
    WRITE(6,6)
110 X=XSTART
    IF(ITYPE.EQ.4)X=XSTOP
    XHOLD=X
    ZHOLD=Z
    ISTEP=0
    ICUT=0
    DX=(XSTOP-XSTART)/FLOAT(NSTEPS)
    IF(ITYPE.NE.4)GO TO 190
    DX=ALAMB/FLOAT(NSTEPS)
    W=CMPLX(XSTART,XSTOP)
190 DDX=DX
    DDXL=0.0
    GO TO 300
200 IF(ITYPE.LT.4)GO TO 210
    ITRY4=1
    IF(ITRY.GT.1)IT=IT+(ITRY-1)*ITEND
    IT=IT+ITHOLD
    ITRY=1
    ITHOLD=0
    HWK=W
    WHOLD=W
    CK1=CCAPK(2)
    CK2=CCAPK(3)
    Y=REAL(W)
    DYMIN=REAL(CCAPK(2))/(4.0*CONST(3,1))
    DY=DYMIN
    IMAX=0
    GO TO 220
210 IF(ISTEP.GT.0)TESTL=TEST
    DDX2L=DDXL
    DDXL=DDX
    IF(ITYPE.EQ.3)GO TO 220
    TEST=AIMAG(Z)
    IF(ITYPE.EQ.1)TEST=-TEST
    GO TO 230
220 CALL DISPF(W,H,HK,HKK,HW,HWK,ERROR,1)
```

```
      TEST=AIMAG(H)
      IF(ITYPE.EQ.4)GO TO 250
  230 IF(ISTEP.EQ.0)GO TO 250
      IF(ITYPE.EQ.3)GO TO 235
      IF(IMAX.EQ.1)GO TO 250
      IF(TEST.GT.TESTL.OR.TEST.LE.0.0)GO TO 250
      CK1=CCAPK(2)
      CK2=CCAPK(3)
      WHOLD=W
      IMAX=1
      A=X
      B=X-DDXL
      DXMIN=ABS(A+B)*ACCUR/2.0
      ZERO=FUNCT(B)
      IF(ZERO.EQ.0.0)GO TO 234
      IF(ZERO.GT.0.0)GO TO 236
      IF(DDX2L.EQ.0.0)GO TO 249
      A=A-DDXL
      B=B-DDX2L
      GO TO 236
  234 ZERO=B
      GO TO 237
  235 IF(TEST*TESTL.GT.0.0)GO TO 250
      A=X
      B=X-DDXL
      CK1=CCAPK(2)
      CK2=CCAPK(3)
      WHOLD=W
  236 ZERO=ROOT(FUNCT,A,B,0.0,ACCUR)
      IF(ZERO.EQ.0.0)GO TO 249
  237 GO TO (241,242,241,241),ITYPE
  241 W=CMPLX(ZERO,AIMAG(W))
      ZZERO=CCAPK(2)
      GO TO 243
  242 CCAPK(2)=ZERO
      CCAPK(3)=SQRT(ZERO*ZERO+CAPK(1)*CAPK(1))
      ZZERO=W
  243 CALL LOCATE(RESULT,ZZERO,ACCUR,ITEND,IERROR,ERROR,ITN)
      IF(IERROR.EQ.0)GO TO 244
      IF(IERROR.EQ.2.OR.ITYPE.LT.4)GO TO 2435
      IF(IMAX.EQ.1)GO TO 2435
      Y=Y-DY
      DY=DY/1.99995
      Y=Y+DY
      ITHOLD=ITHOLD+ITN
      ZZERO=Z
      ZERO=Y
      W=CMPLX(ZERO,AIMAG(W))
      IF(ABS(DY).GT.5.E-06*ABS(Y))GO TO 243
      WRITE(6,14)Y,DY,Z
 2435 WRITE(6,12)IERROR,ZERO,ZZERO
      RETURN
  244 IF(ITYPE.LT.4.OR.IMAX.EQ.1)GO TO 247
      Z=ZZERO
      HWK=W
      IT=ITN
```

```
      TESTL=TEST
      CALL DISPF(W,H,HK,HKK,HW,HWK,ERROR,1)
      TEST=AIMAG(H)
      ITRY4=ITRY4+1
      IF(TEST*TESTL.GT.0.0)GO TO 245
      IMAX=1
      A=Y
      B=Y-DY
      GO TO 236
  245 IF(ABS(TEST).LT.ABS(TESTL))GO TO 250
      IF(ITRY4.GT.2)GO TO 246
      W=WHOLD
      CCAPK(2)=CK1
      CCAPK(3)=CK2
      Y=Y-DY
      DY=-DY
      GO TO 250
  246 WRITE(6,16)ITRY4
      RETURN
  247 IF(ITYPE.GT.2)CALL DISPF(W,HK,H,HKK,HW,HWK,ERROR,1)
      HW=ZERO
      IF(ITYPE.EQ.4)HW=W
      WRITE(6,15)HW,ZZERO,ITN
      IF(ITYPE.GT.2)WRITE(6,13)HK
  249 IF(ITYPE.EQ.4)GO TO 250
      CCAPK(2)=CK1
      CCAPK(3)=CK2
      W=WHOLD
  250 IF(IP.EQ.0)GO TO 260
      IF(ITRY.GT.1)IT=IT+(ITRY-1)*ITEND
      IT=IT+ITHOLD
      HW=X
      IF(ITYPE.EQ.4)HW=HWK
      WRITE(6,11)ISTEP,HW,Z,IT
      IF(ITYPE.GT.2)WRITE(6,13)H
  260 IF(ITYPE.LT.4.OR.IMAX.EQ.1)GO TO 280
      IF(ITN+ITHOLD.LE.2.AND.ABS(DY).LT.ABS(DYMIN))DY=2.0*DY
      ITHOLD=0
      Y=Y+DY
      ZERO=Y
      IF(ITRY4.LT.ITEND3)GO TO 237
      GO TO 246
  280 ZHOLD=Z
      IF(ICUT.EQ.0)GO TO 290
      IF(IT.LE.2.AND.ITRY.EQ.1.AND.ABS((XHOLD-X)/DDX).GT.5.0)DDX=2.0*DDX
      X=X+DDX
      IF((XHOLD-X)*DDX.GT.0.0)GO TO 300
      DDX=DDX+XHOLD-X
      X=XHOLD
      ICUT=0
      GO TO 300
  290 X=X+DX
      DDX=DX
      ISTEP=ISTEP+1
      IF(ISTEP.GT.NSTEPS)RETURN
      IF(ITYPE.LT.4)GO TO 295
```

```
      IF(REAL(HK).LE.0.0)RETURN
      WRITE(6,6)
  295 IF(ISTEP.EQ.NSTEPS)X=XSTOP
      XHOLD=X
  300 ITHOLD=0
  305 ITRY=1
      GO TO (330,320,330,340),ITYPE
  320 CCAPK(2)=X
      CCAPK(3)=SQRT(X*X+CAPK(1)*CAPK(1))
      GO TO 400
  330 W=X
      GO TO 400
  340 W=CMPLX(REAL(W),X)
  400 CALL LOCATE(RESULT,Z,ACCUR,ITEND,IERROR,ERROR,IT)
      IF(IERROR.EQ.0)GO TO 200
      IF(IERROR.EQ.1)GO TO 420
      IF(IERROR.NE.2)GO TO 410
  401 WRITE(6,12)IERROR,X,Z
      RETURN
  410 ICUT=1
      IF(ISTEP.EQ.0)GO TO 401
  411 X=X-DDX
      DDX=DDX/1.95
      X=X+DDX
      Z=ZHOLD
      ITHOLD=ITHOLD+IT
      IF(ABS(DDX).GT.5.E-06*ABS(X))GO TO 305
      WRITE(6,14)X,DDX,Z
      RETURN
  420 ITRY=ITRY+1
      IF(ITRY.GT.3)GO TO 401
      GO TO 400
      END



      SUBROUTINE LOCATE(FUNCT,Z,EPS,ITEND,IERROR,ERROR,IT)
C
C  THIS SUBROUTINE LOCATES THE ZERO OF A FUNCTION WHOSE VALUE AND
C    DERIVATIVE ARE COMPUTED IN THE SUBROUTINE FUNCT BY THE NEWTON
C    ITERATION METHOD.
C  'FUNCT' IS TO BE GIVEN AS THE NAME OF THE SUBPROGRAM REPRESENTING THE
C    FUNCTION WHOSE ZERO IS DESIRED. THIS SUBPROGRAM MUST BE OF THE
C    FORM FUNCT(Z,F,DFDZ,ERROR) IN WHICH Z,F,DFDZ ARE ALL COMPLEX
C    QUANTITIES AND ERROR IS THE ACCURACY TO WHICH THE FUNCTION AND ITS
C    DERIVATIVE ARE TO BE COMPUTED.
C  'Z' IS TO BE GIVEN AS AN INITIAL GUESS FOR THE ROOT.
C  'EPS' IS THE RELATIVE ACCURACY TO WHICH THE ROOT IS TO BE DETERMINED.
C  'ITEND' IS TO BE GIVEN AS THE MAXIMUM NUMBER OF ITERATIONS ALLOWED
C    TO FIND THE ROOT.
C  ON COMPLETION OF THE CALCULATION
C  'IERROR' = 0 MEANS THAT THE ROOT WAS SUCCESSFULLY FOUND
C  'IERROR' = 1 MEANS THAT THE ITERATION DID NOT CONVERGE TO THE
C    DESIRED ACCURACY WITHIN 'ITEND' STEPS
C  'IERROR' = 2 MEANS THAT THE DERIVATIVE OF THE FUNCTION VANISHED
C    AT SOME POINT AND HENCE THAT THE ITERATION CANNOT PROCEED FURTHER
```

```
C   'IERROR' = 3 MEANS THAT THREE SUCCESSIVE CORRECTIONS TO THE PRESENT
C     GUESS WERE LARGER THAN THE PRECEDING ONES AND HENCE THAT THE
C     ITERATION DIVERGES FOR THIS CASE
C   'IERROR' = 4 MEANS THAT THE MAGNITUDE OF THE CORRECTION TO THE
C     GUESS IS LARGER THAN THE MAGNITUDE OF THE GUESS AND HENCE THAT THE
C     ITERATION IS PRESUMABLY DIVERGING
C   'IERROR' = 5 MEANS THAT THE IMAGINARY PART OF Z IS LARGER IN
C     MAGNITUDE THAN THE REAL PART AND HENCE THAT THE ROOT APPEARS
C     TO BE IN THE REGION IN WHICH THE DISPERSION FUNCTION IS INFINITE.
C   'ERROR' IS THE ACCURACY GIVEN TO 'FUNCT' INDICATING THE ACCURACY TO
C     WHICH THE FUNCTION AND ITS DERIVATIVE ARE TO BE COMPUTED
C   'IT' IS RETURNED AS THE NUMBER OF ITERATIONS REQUIRED TO LOCATE THE
C     ZERO.
C
      COMPLEX Z,F,DF,DZ,DDZ
      THEMAG(Z)=ABS(REAL(Z))+ABS(AIMAG(Z))
      IERROR=0
      IF(ITEND.LE.0)ITEND=10
      IDIVER=0
      IT=1
  100 CALL FUNCT(Z,F,DF,ERROR)
  110 IF(THEMAG(F).EQ.0.0)RETURN
      IF(THEMAG(DF).NE.0.0)GO TO 150
C
C  DERIVATIVE OF THE FUNCTION VANISHES
C
      IERROR=2
      RETURN
  150 DZ=F/DF
      IF(IT.EQ.1.OR.THEMAG(DZ).LT.THEMAG(DDZ))GO TO 160
      IDIVER=IDIVER+1
      IF(IDIVER.LT.4)GO TO 160
C
C  ITERATION IS DIVERGING
C
  155 IERROR=3
      RETURN
  156 IERROR=4
      RETURN
  157 IERROR=5
      RETURN
  160 IF(THEMAG(DZ).GT.THEMAG(Z))GO TO 156
      Z=Z-DZ
      IF(ABS(AIMAG(Z)).GT.ABS(REAL(Z)))GO TO 157
      IF(THEMAG(Z).GT.EPS)GO TO 200
C
C  Z IS NEARLY ZERO - TRY ZERO AS A SOLUTION
C
      DDZ=0.0
      CALL FUNCT(DDZ,F,DF,ERROR)
      IF(THEMAG(F).NE.0.0)GO TO 200
      Z=0.0
      RETURN
  200 IF(THEMAG(DZ).GT.EPS*THEMAG(Z))GO TO 210
      IERROR=0
      RETURN
```

```
  210 DDZ=DZ
      IT=IT+1
      IF(IT.LE.ITEND)GO TO 100
C
C   ITERATION DOES NOT CONVERGE IN ITEND STEPS
C
      IERROR=1
      RETURN
      END


      SUBROUTINE RESULT(Z,F,DF,DERROR)
C
C   THIS SUBPROGRAM IS A DUMMY SUBPROGRAM SETTING UP THE FUNCTION AND
C     ITS DERIVATIVE FOR THE PARTICULAR TYPE OF ITERATION BEING PERFORMED
C     AS SPECIFIED BY ITYPE FOR SUBPROGRAM LOCATE.
C
      COMMON CCAPK,HATRP,DHATRP,CAPK,CONST,GRAD,C,D,GRAV,ROOTP
      COMMON ALOW,EXPMAX,FRACT,UMAX,EXTRA1,EXTRA2,EXTRA3
      COMMON JMAX,L,NTYPE,JPOS,JNEG,KMAX,MMAX,NEXTR1,NEXTR2,NEXTR3
      COMMON NEXTR4,NEXTR5,NEXTR6,NEXTR7
      DIMENSION CONST(4,3),GRAD(5,3),L(3),CAPK(3),CCAPK(3)
      DIMENSION C(2,400,3),D(2,400,3),GRAV(400,3)
      DIMENSION ROOTP(100,2),HATRP(100,2),DHATRP(100,2)
      COMPLEX CCAPK,HATRP,DHATRP
      COMMON ALAMB,ZMOM,ZCOM,ITYPE
      DIMENSION ZMOM(4,5)
      COMPLEX ZMOM,ZCOM
      COMPLEX Z,F,DF,H,HK,HKK,HW,HWK
      IF(ITYPE.NE.2)GO TO 130
  120 INDEX=4
      ZCOM=Z
      GO TO 200
  130 INDEX=3
  131 CCAPK(2)=Z
      CCAPK(3)=CSQRT(Z*Z+CAPK(1)*CAPK(1))
  200 CALL DISPF(ZCOM,H,HK,HKK,HW,HWK,DERROR,INDEX)
      IF(ITYPE.GT.2)GO TO 330
      F=H-ALAMB
      GO TO (310,320),ITYPE
  310 DF=HK
      RETURN
  320 DF=HW
      RETURN
  330 DF=HKK
      F=HK
      RETURN
      END


      FUNCTION FUNCT(X)
C
C   THIS SUBPROGRAM COMPUTES THE RELEVANT QUANTITIES FOR DETERMINING
C     THE MAXIMUM IN SUBPROGRAM FOLLOW. FOR ITYPE = 1 THE NEGATIVE OF
```

```
C     THE IMAGINARY PART OF K-Z IS COMPUTED FOR THE REAL FREQUENCY
C     SPECIFIED BY 'X'. FOR ITYPE = 2 THE IMAGINARY PART OF THE FREQUENCY
C     IS COMPUTED FOR THE REAL K-Z SPECIFIED BY 'X'. FOR ITYPE=3,4 THE
C     IMAGINARY PART OF THE DISPERSION FUNCTION IS EVALUATED ALONG THE
C     SOLUTION OF THE EQUATION WITH THE DERIVATIVE OF THE DISPERSION
C     FUNCTION SET EQUAL TO ZERO WITH 'X' SPECIFYING THE REAL PART OF THE
C     FREQUENCY ON THE TRAJECTORY.
C
      COMMON CCAPK,HATRP,DHATRP,CAPK,CONST,GRAD,C,D,GRAV,ROOTP
      COMMON ALOW,EXPMAX,FRACT,UMAX,EXTRA1,EXTRA2,EXTRA3
      COMMON JMAX,L,NTYPE,JPOS,JNEG,KMAX,MMAX,NEXTR1,NEXTR2,NEXTR3
      COMMON NEXTR4,NEXTR5,NEXTR6,NEXTR7
      DIMENSION CONST(4,3),GRAD(5,3),L(3),CAPK(3),CCAPK(3)
      DIMENSION C(2,400,3),D(2,400,3),GRAV(400,3)
      DIMENSION ROOTP(100,2),HATRP(100,2),DHATRP(100,2)
      COMPLEX CCAPK,HATRP,DHATRP
      COMMON ALAMB,ZMOM,ZCOM,ITYPE,ACCUR,ERROR,DXMIN
      DIMENSION ZMOM(4,5)
      COMPLEX ZMOM,ZCOM
      COMPLEX Z,H,HK,HKK,HW,HWK,F,DF
      EXTERNAL RESULT
    1 FORMAT(1X44HNEWTON ITERATION DOES NOT CONVERGE (IERROR =,I2,6H), X
     1 =,1PE13.6)
      ITEND=10
      FUNCT=0.0
      ITRY=1
      IF(ITYPE.EQ.2)GO TO 120
      ZCOM=CMPLX(X,AIMAG(ZCOM))
      Z=CCAPK(2)
      GO TO 200
  120 Z=ZCOM
      CCAPK(2)=X
      CCAPK(3)=SQRT(X*X+CAPK(1)*CAPK(1))
  200 CALL LOCATE(RESULT,Z,ACCUR,ITEND,IERROR,ERROR,IT)
      IF(IERROR.EQ.0)GO TO 300
      IF(IERROR.EQ.1)GO TO 220
      IF(IERROR.EQ.2) GO TO 210
  210 WRITE(6,1)IERROR,X
      RETURN
  220 ITRY=ITRY+1
      IF(ITRY.GT.3)GO TO 210
      GO TO 200
  300 IF(ITYPE.GT.2)GO TO 400
      ITRY=1
      SIGNA=1.0
  301 Y=X-DXMIN*SIGNA/4.0
      GO TO (310,320),ITYPE
  310 CCAPK(2)=Z
      CCAPK(3)=CSQRT(Z*Z+CAPK(1)*CAPK(1))
      ZCOM=Y
      GO TO 350
  320 CCAPK(2)=Y
      CCAPK(3)=SQRT(Y*Y+CAPK(1)*CAPK(1))
      ZCOM=Z
  350 CALL RESULT(Z,F,DF,ERROR)
      FUNCT=FUNCT+SIGNA*AIMAG(F/DF)
```

```
      ITRY=ITRY+1
      SIGNA=-SIGNA
      IF(ITRY.EQ.2)GO TO 301
      FUNCT=2.0*FUNCT/DXMIN
      IF(ITYPE.EQ.1)FUNCT=-FUNCT
      RETURN
  400 CCAPK(2)=Z
      CCAPK(3)=CSQRT(Z*Z+CAPK(1)*CAPK(1))
      CALL DISPF(ZCOM,H,HK,HKK,HW,HWK,ERROR,1)
      FUNCT=AIMAG(H)
      RETURN
      END



C              MICRO3
C            MAIN PROGRAM 3
C  CONTROL PROGRAM FOR MARGINAL STABILITY ANALYSIS
C  THIS PROGRAM AND ITS ASSOCIATED SUBPROGRAMS ARE AN ABBREVIATED FORM
C    OF MICRO1 WHICH OMIT THE CAUCHY INTEGRAL METHOD GROWTH RATE
C    ANALYSIS AND THE POSSIBILITY OF OBTAINING NYQUIST PLOTS OF THE
C    DISPERSION FUNCTION.
C
      COMMON CCAPK,HATRP,DHATRP,CAPK,CONST,GRAD,C,D,GRAV,ROOTP
      COMMON ALOW,EXPMAX,FRACT,UMAX,EXTRA1,EXTRA2,EXTRA3
      COMMON JMAX,L,NTYPE,JPOS,JNEG,KMAX,MMAX,NEXTR1,NEXTR2,NEXTR3
      COMMON NEXTR4,NEXTR5,NEXTR6,NEXTR7
      DIMENSION CONST(4,3),GRAD(5,3),L(3),CAPK(3),CCAPK(3)
      DIMENSION C(2,400,3),D(2,400,3),GRAV(400,3)
      DIMENSION ROOTP(100,2),HATRP(100,2),DHATRP(100,2)
      COMPLEX CCAPK,HATRP,DHATRP
      DIMENSION CHAR(5,3)
    1 FORMAT(14I5)
    2 FORMAT(5E14.8)
    3 FORMAT(1H ,7HNDIFF =,I2,1X27HNOT ALLOWED IN THIS PROGRAM)
      NNYQUS=0
      NMAX=400
      ALOW=1.E-65
      EXPMAX=150.
      READ(5,1)NCASES
      DO 400 NCASE=1,NCASES
      READ(5,1)NSUBS
      READ(5,1)NPPLOT
      DO 300 NSUB=1,NSUBS
      CALL INPUT(NCASE,NSUB,NGOOF,CHAR,NDIFF,NNYQUS,FRQNYQ)
      IF(NGOOF.NE.0)GO TO 450
      IF(NDIFF.EQ.2.OR.NDIFF.EQ.3)GO TO 500
      IF(NSUB.EQ.1)CALL SETUP(NMAX,CHAR)
      UMAX=ABS(CONST(1,1)/CONST(3,1))
      CALL FIND(NPPLOT)
  300 CONTINUE
  400 CONTINUE
  450 RETURN
  500 WRITE(6,3)NDIFF
      RETURN
      END
```

```
C            MICRO4
C          MAIN PROGRAM 4
C  TIME-SHARING CONTROL PROGRAM FOR MARGINAL STABILITY ANALYSIS
C
      DIMENSION CONST(4,3),GRAD(5,3),L(3),CAPK(3),CCAPK(3)
      DIMENSION C(2,400,3),D(2,400,3),GRAV(400,3)
      DIMENSION ROOTP(100,2),HATRP(100,2),DHATRP(100,2)
      COMMON CCAPK,HATRP,DHATRP,CAPK,CONST,GRAD,C,D,GRAV,ROOTP
      COMMON ALOW,EXPMAX,FRACT,UMAX,EXTRA1,EXTRA2,EXTRA3
      COMMON JMAX,L,NTYPE,JPOS,JNEG,KMAX,MMAX,NEXTR1,NEXTR2,NEXTR3
      COMMON NEXTR4,NEXTR5,NEXTR6,NEXTR7
      DIMENSION CHAR(5,3)
    1 FORMAT(1X31HTYPE IN FREQUENCY, K-Z (2E14.8))
    2 FORMAT(2E14.8)
    3 FORMAT(1X61HUNDERFLOW OCCURS IN THE EVALUATION OF P(U), TRY ANOTHE
     1R GUESS//)
    4 FORMAT(/1X9HFOR K-Z =,1PE14.7,8H, FREQ =,1PE14.7,13H AND LAMBDA =
     1,1PE14.7,9H (RECIP =,1PE14.7,1H)///)
    5 FORMAT(1X50HZERO OF P(U) CANNOT BE FOUND NEAR GUESS, TRY AGAIN//)
    6 FORMAT(/////)
    7 FORMAT(///)
      NMAX=400
      ALOW=1.E-36
      EXPMAX=75.
      ERROR=3.E-07
      NCASE=1
   50 PRINT 6
      CALL SINPUT(NCASE,NGOOF,CHAR)
      NCASE=NCASE+1
      IF(NGOOF.NE.0)CALL EXIT
      PRINT 7
      CALL SETUP(NMAX,CHAR)
      UMAX=ABS(CONST(1,1)/CONST(3,1))
  100 PRINT 1
      READ 2,FREQ,CAPK(2)
      IF(FREQ.EQ.0.0)GO TO 50
      IF(FREQ.GT.1.E+29)CALL EXIT
      CAPK(3)=SQRT(CAPK(1)*CAPK(1)+CAPK(2)*CAPK(2))
      X=FREQ
      DX=CAPK(2)/(4.0*CONST(3,1))
      IF(CAPK(2).EQ.0.0)DX=UMAX/20.
      ITRY=1
      TESTL=P(X)
      SIGNL=SIGN(1.0,TESTL)
      IF(TESTL.EQ.0.0)SIGNL=0.0
      GO TO 210
  200 TESTL=TEST
      SIGNL=SIGNT
  210 X=X+DX
      TEST=P(X)
      SIGNT=SIGN(1.0,TEST)
      IF(TEST.EQ.0.0)SIGNT=0.0
      ITRY=ITRY+1
```

```
      HOLD=SIGNT*SIGNL
      IF(HOLD.GT.0.0)GO TO 250
      IF(HOLD.LT.0.0)GO TO 300
      IF(P(X+DX).NE.0.0)GO TO 300
      PRINT 3
      GO TO 100
  250 IF(ITRY.GT.30)GO TO 400
      IF(ABS(TEST).LT.ABS(TESTL))GO TO 200
      IF(ITRY.GT.2)GO TO 400
      X=X-DX
      DX=-DX
      GO TO 200
  300 A=X
      B=X-DX
      XCRIT=ROOT(P,A,B,0.0,ERROR)
      CCAPK(2)=CAPK(2)
      CCAPK(3)=CAPK(3)
      CALL DISP(XCRIT,A,B,ERROR)
      IF(A.LE.0.0)RECIP=1.0/ALOW
      IF(A.GT.0.0)RECIP=1.0/A
      PRINT 4,CAPK(2),XCRIT,A,RECIP
      GO TO 100
  400 PRINT 5
      GO TO 100
      END



      SUBROUTINE SINPUT(NCASE,NGOOF,CHAR)
C
C  SUBPROGRAM SINPUT FOR TIME-SHARING SYSTEM
C
      DIMENSION CONST(4,3),GRAD(5,3),L(3),CAPK(3),CCAPK(3)
      DIMENSION C(2,400,3),D(2,400,3),GRAV(400,3)
      DIMENSION ROOTP(100,2),HATRP(100,2),DHATRP(100,2)
      COMMON CCAPK,HATRP,DHATRP,CAPK,CONST,GRAD,C,D,GRAV,ROOTP
      COMMON ALOW,EXPMAX,FRACT,UMAX,EXTRA1,EXTRA2,EXTRA3
      COMMON JMAX,L,NTYPE,JPOS,JNEG,KMAX,MMAX,NEXTR1,NEXTR2,NEXTR3
      COMMON NEXTR4,NEXTR5,NEXTR6,NEXTR7
      DIMENSION CHAR(5,3)
    1 FORMAT(5I5)
    2 FORMAT(5E14.8,I2)
    3 FORMAT(1H1,10X4HCASE,I3//)
    4 FORMAT(/,1X45HREFERENCE LARMOR RADIUS TIMES THE WAVE VECTOR//,21
     1X3HK-Y//,16X1PE13.6//)
    9 FORMAT(80X23HREFERENCE LARMOR RADIUS/1X7HSPECIES,16X29HRATIO TO RE
     1FERENCE SPECIES OF,22X33HDIVIDED BY THE GRADIENT LENGTH OF,4X7HGRA
     2VITY,5X7HCURRENT/2X6HNUMBER,5X4HMASS,7X7HDENSITY,5X6HCHARGE,6X6HTE
     3MP-Z,4X11HTEMP-'PERP',2X1HL,4X7HDENSITY,3X11HTEMP-'PERP',3X6HTEMP-
     4Z,2X2(3X9HPARAMETER)/1H )
   10 FORMAT(2X13,3X1P5E12.3,I4,1P5E12.3)
   11 FORMAT(/,1X26HCHARGE NEUTRALITY VIOLATED)
   12 FORMAT(/,1X32HDENSITY GRADIENTS DO NOT BALANCE)
   13 FORMAT(1X11HTYPE IN K-Y)
      NGOOF=0
      DERROR=1.E-04
```

```
      WRITE(6,3)NCASE
   90 READ(5,1)JMAX,NTYPE,NVZERO
      PRINT 13
      READ 2,CAPK(1)
      WRITE(6,4)CAPK(1)
      NDIFF=0
      DO 100 J=1,JMAX
      DO 99 I=1,5
   99 GRAD(I,J)=0.0
      READ(5,2)(CHAR(I,J),I=1,5),L(J)
      IF(NTYPE.GT.3)READ(5,2)(GRAD(I,J),I=1,3)
      IF(NTYPE.GT.1.AND.NTYPE.LE.3)READ(5,2)GRAD(1,J)
      IF(NTYPE-2*(NTYPE/2).NE.0)READ(5,2)GRAD(4,J)
      IF(NVZERO.NE.0)READ(5,2)GRAD(5,J)
  100 CONTINUE
  110 WRITE(6,9)
      WRITE(6,10)(J,(CHAR(I,J),I=1,5),L(J),(GRAD(I,J),I=1,5),J=1,JMAX)
      SUM=0.0
      DO 120 J=1,JMAX
  120 SUM=SUM+CHAR(2,J)*CHAR(3,J)
      IF(ABS(SUM).LT.DERROR)GO TO 130
      NGOOF=1
      PRINT 11
  130 IF(NTYPE.LT.1)GO TO 150
      SUM=0.0
      DO 140 J=1,JMAX
      SUM=SUM+CHAR(2,J)*CHAR(3,J)*(-GRAD(1,J)+FLOAT(L(J)+1)*GRAD(2,J)+0.
     15*GRAD(3,J)+2.0*GRAD(4,J)*FLOAT(1/(L(J)+1)))
  140 GRAD(4,J)=GRAD(4,J)*CHAR(5,J)*CHAR(1,J)/(CHAR(3,J)*CHAR(3,J))
      IF(ABS(SUM).LT.DERROR)GO TO 150
      NGOOF=1
      PRINT 12
  150 RETURN
      END



      SUBROUTINE SETUP(NMAX,CHAR)
C
C SUBPROGRAM SETUP FOR TIME-SHARING SYSTEM

      DIMENSION CONST(4,3),GRAD(5,3),L(3),CAPK(3),CCAPK(3)
      DIMENSION C(2,400,3),D(2,400,3),GRAV(400,3)
      DIMENSION ROOTP(100,2),HATRP(100,2),DHATRP(100,2)
      COMMON CCAPK,HATRP,DHATRP,CAPK,CONST,GRAD,C,D,GRAV,ROOTP
      COMMON ALOW,EXPMAX,FRACT,UMAX,EXTRA1,EXTRA2,EXTRA3
      COMMON JMAX,L,NTYPE,JPOS,JNEG,KMAX,MMAX,NEXTR1,NEXTR2,NEXTR3
      COMMON NEXTR4,NEXTR5,NEXTR6,NEXTR7
      DIMENSION CA(400,2),DA(400,2),EX(400),CHAR(5,3)
      DO 10 J=1,JMAX
      HOLD=SQRT(CHAR(1,J)/CHAR(4,J))
      CONST(1,J)=CHAR(3,J)*HOLD/CHAR(1,J)
      CONST(2,J)=CHAR(4,J)/CHAR(5,J)
      CONST(3,J)=HOLD
   10 CONST(4,J)=CHAR(2,J)*(CHAR(3,J)**2)/CHAR(4,J)
      ITGRAD=1
```

```
      IF(NTYPE.GT.3)ITGRAD=2
      DO 20 J=1,JMAX
      X=0.5*((CAPK(1)/CHAR(3,J))**2)*CHAR(5,J)*CHAR(1,J)
      M=NMAX
      CALL CDCOMP(X,L(J),M,CA,DA,ALOW,ITGRAD)
      DO 20 I=1,ITGRAD
      DO 20 K=1,NMAX
      C(I,K,J)=CA(K,I)
   20 D(I,K,J)=DA(K,I)
      IF(NTYPE-2*(NTYPE/2).EQ.0)GO TO 40
      DO 30 J=1,JMAX
      X=CAPK(1)*GRAD(4,J)
      K=NMAX
      CALL BESSEL(X,K,EX,-1.0,ALOW)
      DO 30 I=1,NMAX
   30 GRAV(I,J)=EX(I)
   40 RETURN
      END



      SUBROUTINE CDCOMP(X,L,N,C,D,ALOW,ITGRAD)
C
C  SUBPROGRAM CDCOMP FOR TIME-SHARING SYSTEM
C
C  THIS SUBROUTINE COMPUTES THE CONSTANTS C(N,L,J) AND D(N,L,J) WHICH
C    ARISE IN A CYLINDRICALLY CUT-OUT V 'PERP' DISTRIBUTION FUNCTION.
C  'L' = 0,1,2,3 ARE TREATED NORMALLY
C  'L' GREATER THAN 3 IS CONSIDERED TO BE INFINITE AND THUS THE V 'PERP'
C    DISTRIBUTION FUNCTION IS A DELTA FUNCTION.
C  'N' IS TO BE GIVEN AS THE DIMENSION OF THE FIRST SUBSCRIPT OF C AND D
C    AND IS RETURNED AS THE HIGHEST POSITION WHICH CONTAINS A NON-ZERO
C    RESULT.
C  'ITGRAD' = 1, ONLY THE C AND D FUNCTIONS FOR L ARE COMPUTED
C  'ITGRAD' = 2, THE C AND D FUNCTIONS FOR BOTH L AND L+1 ARE COMPUTED
C    (FOR 'ITGRAD' = 2, 'L' = 3 IS CONSIDERED TO BE INFINITE).
C
      DIMENSION C(400,2),D(400,2),ARRAY(400),PQ(4,2)
      DO 10 M=1,N
      DO 10 J=1,ITGRAD
      C(M,J)=0.0
   10 D(M,J)=0.0
      IF(L.GT.3)GO TO 300
      IF(L.GT.2.AND.ITGRAD.GT.1)GO TO 300
C
C  NORMAL CALCULATION FOR L = 0,1,2,3
C
      CALL BESSEL(X,N,ARRAY,1.,ALOW)
      J=L+1
      GO TO (100,120,140,160),J
  100 PQ(1,1)=1.0
      PQ(2,1)=0.0
      PQ(3,1)=1.0
      PQ(4,1)=0.0
      IF(ITGRAD.EQ.1)GO TO 200
      J=2
```

```
      GO TO 121
  120 J=1
  121 DO 122 M=1,4
  122 PQ(M,J)=-X
      PQ(1,J)=1.+PQ(1,J)
      IF(J.EQ.2)GO TO 200
      IF(ITGRAD.EQ.1)GO TO 200
      J=2
      GO TO 141
  140 J=1
  141 HOLD=X*(X-1.)
      PQ(1,J)=HOLD-X+1.0
      PQ(2,J)=HOLD-0.5*X
      PQ(3,J)=HOLD
      PQ(4,J)=HOLD+0.5*X
      IF(J.EQ.2)GO TO 200
      IF(ITGRAD.EQ.1)GO TO 200
      J=2
      GO TO 161
  160 J=1
  161 TWOTH=2./3.
      HOLD=-X*(X*(TWOTH*X-1./TWOTH)+0.5*TWOTH)
      PQ(4,J)=HOLD
      PQ(3,J)=HOLD+X*(X/3.-TWOTH)
      PQ(2,J)=HOLD+X*(X-1./TWOTH)
      PQ(1,J)=PQ(3,J)+X*(X-2.0)+1.0
  200 DO 240 M=1,N
      IF(M.NE.1)GO TO 210
      DO 201 J=1,ITGRAD
      C(1,J)=PQ(1,J)*ARRAY(1)-PQ(2,J)*ARRAY(2)
  201 D(1,J)=PQ(3,J)*ARRAY(1)-PQ(4,J)*ARRAY(2)
      GO TO 240
  210 IF(L.EQ.0)GO TO 220
      HOLD=FLOAT(M-1)-0.5
      GO TO (211,214,217),L
  211 IF(ITGRAD.EQ.1)GO TO 220
      J=2
      GO TO 215
  214 J=1
  215 PQ(1,J)=PQ(1,J)+HOLD
      PQ(3,J)=PQ(3,J)+HOLD
      IF(J.EQ.2)GO TO 220
      IF(ITGRAD.EQ.1)GO TO 220
      J=2
      GO TO 218
  217 J=1
  218 PQ(1,J)=PQ(1,J)-HOLD*(X-2.)
      PQ(2,J)=PQ(2,J)-X*HOLD/3.
      PQ(3,J)=PQ(3,J)-HOLD*(X-1.)
      PQ(4,J)=PQ(4,J)-X*HOLD/3.
  220 DO 221 J=1,ITGRAD
      C(M,J)=PQ(1,J)*ARRAY(M)-0.5*PQ(2,J)*(ARRAY(M-1)+ARRAY(M+1))
  221 D(M,J)=PQ(3,J)*ARRAY(M)-0.5*PQ(4,J)*(ARRAY(M-1)+ARRAY(M+1))
  240 CONTINUE
      RETURN
C
```

```
C  DELTA FUNCTION DISTRIBUTION FOR L GREATER THAN 3
C
  300 HOLD=SQRT(2.*X)
      CALL BESSEL(HOLD,N,ARRAY,-1.,ALOW)
      J=HOLD
      C(1,1)=ARRAY(1)**2
      D(1,1)=-HOLD*ARRAY(1)*ARRAY(2)
      IF(ITGRAD.EQ.1)GO TO 3010
      C(1,2)=C(1,1)
      D(1,2)=D(1,1)
 3010 M=2
      IF(X.EQ.0.0)GO TO 400
      CLOW=10.*SQRT(ALOW)/HOLD
  301 IF(ABS(ARRAY(M)).GT.CLOW)GO TO 302
      TWOTH=0.0
      IF(M.GT.J)GO TO 400
      GO TO 303
  302 TWOTH=ARRAY(M)**2
  303 C(M,1)=TWOTH
      D(M,1)=0.5*HOLD*ARRAY(M)*(ARRAY(M-1)-ARRAY(M+1))
      IF(ITGRAD.EQ.1)GO TO 304
      C(M,2)=TWOTH
      D(M,2)=D(M,1)
  304 M=M+1
      GO TO 301
  400 N=M-1
      RETURN
      END



      SUBROUTINE BESSEL(X,N,ARRAY,SIGNA,ALOW)
C
C  SUBPROGRAM BESSEL FOR TIME-SHARING SYSTEM
C
C  THIS SUBROUTINE COMPUTES ALL ORDERS OF THE BESSEL FUNCTIONS J(M,X)
C    OR I(M,X) FOR A GIVEN ARGUMENT X.
C  USE 'SIGNA' = + 1. FOR I(M,X) AND
C      'SIGNA' = - 1. FOR J(M,X).
C  'ARRAY' IS THE VECTOR OF LENGTH 'N' IN WHICH THE RESULTS ARE TO BE
C    PLACED.  'N' MUST BE GIVEN AND SHOULD BE THE MAXIMUM DIMENSION
C    OF 'ARRAY'.
C  AFTER EXECUTION OF THIS SUBROUTINE, 'N' IS THE INDEX OF THE LAST
C    ELEMENT OF 'ARRAY' WHICH CONTAINS A NON-ZERO RESULT.  THE M-TH
C    ELEMENT OF 'ARRAY' CONTAINS J(M-1,X) OR I(M-1,X) DEPENDING ON THE
C    SIGN OF SIGNA.
C  ALOW IS TO BE GIVEN AS THE SMALLEST NUMBER POSSIBLE ON THE COMPUTER.
C
      DIMENSION ARRAY(400)
      NMAX=400
      BREAK=0.1
      SIGNT=1.0
      IF(X.LT.0.0) SIGNT=-SIGNT
      X=ABS(X)
      DO 99 I=1,N
   99 ARRAY(I)=0.0
```

```
   97 IF(X.GT.10.*EXP(0.5*ALOG(ALOW)))GO TO 101
      ARRAY(1)=1.0
      N=1
      RETURN
  101 IF(X.GE.BREAK) GO TO 200
C
C  SERIES METHOD - USED FOR X SMALLER THAN 0.1
C
      CLOW=10.*ALOW/X
       EXPX=1.0
      IF(SIGNA.LT.0.0)EXPX=EXP(X)
      I=1
      FMULT=X*X*SIGNA/4.0
      E=1.0
      GO TO 103
  102 E=E*(X/2.)/FLOAT(I-1)
  103 SUM=1.0
      ANPLUS=I
      AN=1.
      TERM=SUM
  104 SUME=SUM
      TERM=TERM*FMULT/(ANPLUS*AN)
      SUM=SUM+TERM
      ANPLUS=ANPLUS+1.0
      AN=AN+1.0
      IF(SUME-SUM.NE.0.0) GO TO 104
      ARRAY(I)=E*SUM/EXPX
      I=I+1
      IF(I.LE.N.AND.E.GT.CLOW)GO TO 102
      N=I-1
      GO TO 205
  150 WRITE(6,151)X
  151 FORMAT(50H ARGUMENT GIVEN TO BESSEL IS TOO LARGE, ARGUMENT =1PE15.
     17)
      CALL EXIT
C
C  RECURSION RELATION METHOD - USED FOR X LARGER THAN 0.1
C
  200 E=2.71828183
      CLOW=ALOG(1.E+08*ALOW)+X
      I=X
      IF(SIGNA.LT.0.0)I=2*I
  201 I=I+1
      AN=I
      IF((AN+0.5)*ALOG(E*X/(2.*AN)).GT.CLOW.AND.I.LT.N-1)GO TO 201
      IF(I.GT.NMAX)GO TO 150
      N=I
      ARRAY(I)=ALOW*1.E+08
      DO 202 I=2,N
      J=N-I+1
  202 ARRAY(J)=ARRAY(J+2)*SIGNA+2.0*FLOAT(J)*ARRAY(J+1)/X
      SUM=ARRAY(1)
      J=1
      IF(SIGNA.LT.0.0)J=2
      JLOW=J+1
      DO 203 I=JLOW,N,J
```

```
  203 SUM=SUM+2.0*ARRAY(I)
      DO 204 I=1,N
  204 ARRAY(I)=ARRAY(I)/SUM
  205 IF(SIGNT.GT.0.0)RETURN
      DO 206 I=2,N,2
  206 ARRAY(I)=-ARRAY(I)
      RETURN
      END


      FUNCTION P(U)
C
C   SUBPROGRAM P(U) FOR TIME-SHARING SYSTEM
C
      DIMENSION CONST(4,3),GRAD(5,3),L(3),CAPK(3),CCAPK(3)
      DIMENSION C(2,400,3),D(2,400,3),GRAV(400,3)
      DIMENSION ROOTP(100,2),HATRP(100,2),DHATRP(100,2)
      COMMON CCAPK,HATRP,DHATRP,CAPK,CONST,GRAD,C,D,GRAV,ROOTP
      COMMON ALOW,EXPMAX,FRACT,UMAX,EXTRA1,EXTRA2,EXTRA3
      COMMON JMAX,L,NTYPE,JPOS,JNEG,KMAX,MMAX,NEXTR1,NEXTR2,NEXTR3
      COMMON NEXTR4,NEXTR5,NEXTR6,NEXTR7
      NMAX=400
      NOGRAV=NTYPE-2*(NTYPE/2)
      P=0.0
      IF(U.NE.0.0.OR.NTYPE.NE.0)GO TO 80
      DO 70 J=1,JMAX
      IF(GRAD(5,J).NE.0.0)GO TO 80
   70 CONTINUE
      RETURN
   80 DO 400 J=1,JMAX
      HOLD=CAPK(1)*GRAD(4,J)+CONST(3,J)*(U-CAPK(2)*GRAD(5,J))/CONST(1,J)
      SIGNT=0.5
      IF(HOLD.LT.0.0)SIGNT=-SIGNT
      N=HOLD+SIGNT
      IF(CAPK(1).EQ.0.0)N=0
      NPOS=1
      NNEG=-1
      NMOD=0
      HOLD=HOLD*CONST(1,J)
   90 S=HOLD-FLOAT(N+NMOD)*CONST(1,J)
      IF(IABS(N+NMOD).GE.NMAX)GO TO 165
      SSQ=S*S
      IF(CAPK(2).NE.0.0)GO TO 97
      IF(SSQ.NE.0.0)GO TO 94
      FMULT=1.E-08/ALOW
      GO TO 95
   94 FMULT=1./SSQ
   95 SSQ=0.5
      GO TO 98
   97 SSQ=SSQ/(CAPK(2)*CAPK(2))
      IF(SSQ.GT.EXPMAX)GO TO 165
      FMULT=EXP(-SSQ)
   98 GMULT=1.0
      MMOD=0
      IF(NOGRAV.EQ.0)GO TO 110
```

```
      MPOS=1
      MNEG=-1
  100 K=IABS(MMOD)+1
      SIGNT=1.0
      IF(MMOD.GE.0)GO TO 105
      IF(MMOD-2*(MMOD/2).NE.0)SIGNT=-1.0
  105 GMULT=GRAV(K,J)*SIGNT
      IF(ABS(GMULT).LT.ALOW)GO TO 155
  110 K=N+NMOD-MMOD
      A=FLOAT(K)
      IF(CAPK(1).NE.0.0)A=A/CAPK(1)
      K=IABS(K)+1
      C1=S
      IF(CAPK(2).EQ.0.0)C1=0.0
      D1=CONST(1,J)*CONST(2,J)*(FLOAT(N+NMOD)-CAPK(1)*GRAD(4,J))
      TERM=0.0
      IF(NTYPE.LT.2)GO TO 130
      TEMP1=-GRAD(1,J)
      IF(NTYPE.LT.4)GO TO 120
      TEMP1=TEMP1+SSQ*GRAD(3,J)
      TERM=GRAD(2,J)*FLOAT(L(J)+1)*(C(2,K,J)*(A*C1-0.5*CAPK(1)/CONST(1,J
     1))+A*D1*D(2,K,J))-A*C1*GRAD(3,J)*C(1,K,J)
  120 C1=C1*(1.0+A*TEMP1)-0.5*CAPK(1)*TEMP1/CONST(1,J)
      D1=D1*(1.0+A*TEMP1)
  130 TERM=FMULT*GMULT*CONST(4,J)*(TERM+C1*C(1,K,J)+D1*D(1,K,J))
      IF((P+TERM)-P.EQ.0.0)GO TO 163
      P=P+TERM
      IF(NOGRAV.EQ.0.0)GO TO 180
  149 IF(MMOD)151,150,152
  150 MMOD=1
      GO TO 100
  151 IF(MPOS.EQ.0)GO TO 153
      MMOD=-MMOD+MPOS
      GO TO 100
  152 IF(MNEG.EQ.0)GO TO 154
      MMOD=-MMOD
      GO TO 100
  153 MMOD=MMOD+MNEG
      GO TO 100
  154 MMOD=MMOD+MPOS
      GO TO 100
  155 IF(MMOD)161,159,160
  159 IF(CAPK(2))165,149,165
  160 MPOS=0
      GO TO 162
  161 MNEG=0
  162 IF(MPOS.EQ.0.AND.MNEG.EQ.0)GO TO 180
      GO TO 149
  163 IF(NOGRAV.NE.0)GO TO 155
  165 IF(NMOD)170,300,169
  169 NPOS=0
      GO TO 171
  170 NNEG=0
  171 IF(NPOS.EQ.0.AND.NNEG.EQ.0)GO TO 400
  180 IF(NMOD)182,181,183
  181 NMOD=1
```

```
      GO TO 90
  182 IF(NPOS.EQ.0)GO TO 184
      NMOD=-NMOD+NPOS
      GO TO 90
  183 IF(NNEG.EQ.0)GO TO 185
      NMOD=-NMOD
      GO TO 90
  184 NMOD=NMOD+NNEG
      GO TO 90
  185 NMOD=NMOD+NPOS
      GO TO 90
  300 IF(CAPK(2).EQ.0.0)GO TO 180
  400 CONTINUE
      RETURN
      END



      FUNCTION ROOT(DUMMY,RFB,RFC,RFAE,RFRE)
C
C   SUBPROGRAM ROOT FOR TIME-SHARING SYSTEM
C
C      THIS SUBPROGRAM COMPUTES A ROOT OF A GIVEN FUNCTION.
C        DUMMY IS THE NAME OF THE SUBPROGRAM WHICH REPRESENTS THE FUNC.
C        RFB IS THE LOWER LIMIT OF THE RANGE IN WHICH THE ROOT IS TO BE
C          FOUND.
C        RFC IS THE UPPER LIMIT OF THE SAME RANGE.
C        RFAE IS THE ABSOLUTE ACCURACY TO BE ITERATED TO.
C        RFRE IS THE RELATIVE ACCURACY TO BE ITERATED TO.
C
      JRFS=1
      RFFB=DUMMY(RFB)
      SIGNB=SIGN(1.0,RFFB)
      IF(RFFB.EQ.0.0)SIGNB=0.0
      RFFC=DUMMY(RFC)
      SIGNC=SIGN(1.0,RFFC)
      IF(RFFC.EQ.0.0)SIGNC=0.0
      IF(SIGNB*SIGNC.LE.0.0)GO TO 9122
 9102 WRITE(6,200)RFB,RFC
  200 FORMAT(1X76HLIMITS GIVEN TO ROOT FUNCTION GENERATE FUNCTIONAL VALU
     1ES WITH THE SAME SIGNS,11H,LIMITS ARE,1PE18.7,4X3HAND,E18.7)
      ROOT=0.0
      RETURN
 9122 RFA=RFC
      RFFA=RFFC
      SIGNA=SIGNC
 9123 IF(ABS(RFFB)-ABS(RFFA))9131,9131,9130
 9130 RFC=RFB
      RFB=RFA
      RFA=RFC
      RFFC=RFFB
      SIGNC=SIGNB
      RFFB=RFFA
      SIGNB=SIGNA
      RFFA=RFFC
      SIGNA=SIGNC
```

```
 9131 RFD=0.5*(RFB-RFA)
      RFT=RFAE+RFRE*ABS(RFB)
      IF(RFFB)9156,9135,9156
 9135 ROOT=RFB
      RETURN
 9156 IF(IRFK)9137,9157,9137
 9157 IRFK=3
 9138 RFV=RFD
      GO TO 9140
 9137 IF(RFFB-RFFC)9139,9138,9139
 9139 RFV=(RFB-RFC)*RFFB/(RFFB-RFFC)
 9140 IF(ABS(RFD)-RFT)9143,9143,9144
 9143 JRFS=2
      GO TO 9147
 9144 IF(ABS(RFV)-RFT)9149,9147,9147
 9147 IF((RFD-RFV)*RFV)9148,9152,9152
 9148 RFX=RFB-RFD
      GO TO 9153
 9149 IF(RFD)9151,9150,9150
 9150 RFV=RFT
      GO TO 9152
 9151 RFV=-RFT
 9152 RFX=RFB-RFV
 9153 GO TO (9101,9100),JRFS
 9100 ROOT=RFX
      RETURN
 9101 RFC=RFB
      RFB=RFX
      RFFC=RFFB
      SIGNC=SIGNB
      RFFB=DUMMY(RFX)
      SIGNB=SIGN(1.0,RFFB)
      IF(RFFB.EQ.0.0)SIGNB=0.0
      IF(SIGNA*SIGNB)9158,9131,9159
 9158 IRFK=IRFK-1
      GO TO 9123
 9159 IRFK=2
      GO TO 9122
      END



      SUBROUTINE DISP(W,HR,HI,DERROR)
C
C  SUBPROGRAM DISP (AND DISPF) FOR TIME-SHARING SYSTEM
C
      DIMENSION CONST(4,3),GRAD(5,3),L(3),CAPK(3),CCAPK(3)
      DIMENSION C(2,400,3),D(2,400,3),GRAV(400,3)
      DIMENSION ROOTP(100,2),HATRP(100,2),DHATRP(100,2)
      COMMON CCAPK,HATRP,DHATRP,CAPK,CONST,GRAD,C,D,GRAV,ROOTP
      COMMON ALOW,EXPMAX,FRACT,UMAX,EXTRA1,EXTRA2,EXTRA3
      COMMON JMAX,L,NTYPE,JPOS,JNEG,KMAX,MMAX,NEXTR1,NEXTR2,NEXTR3
      COMMON NEXTR4,NEXTR5,NEXTR6,NEXTR7
      DIMENSION ZMOM(4,5)
      COMMON ALAMB,ZMOM
      DIMENSION HF(5),HFHOLD(5)
```

```
      NMAX=400
      NOGRAV=NTYPE-2*(NTYPE/2)
      ITYPE=NTYPE-2
      INDEX=2
      DO 10 I=1,INDEX
   10 HF(I)=0.0
      CKHOLD=CCAPK(2)
      KZERO=1
      IF(CKHOLD.EQ.0.0)KZERO=0
      DO 400 J=1,JMAX
      ITIME=1
      IZERO=0
      DO 20 I=1,INDEX
   20 HFHOLD(I)=HF(I)
      C1=D(1,1,J)
      IF(L(J).EQ.0)C1=C1-1.0
      IF(NOGRAV.EQ.0)GO TO 72
      C1=C1*GRAV(1,J)
      N=1
   71 N=N+2
      A=2.0*GRAV(N,J)*D(1,N,J)
      C1=C1+A
      IF(ABS(A).GT.DERROR*ABS(C1))GO TO 71
   72 HF(1)=HF(1)+C1*CONST(2,J)*CONST(4,J)
      HOLD=CAPK(1)*GRAD(4,J)+CONST(3,J)*(W-CKHOLD*GRAD(5,J))/CONST(1,J)
      C1=HOLD
      SIGNT=0.5
      IF(C1.LT.0.0)SIGNT=-SIGNT
      N=C1+SIGNT
      IF(CAPK(1).EQ.0.0)N=0
      HOLD=HOLD*CONST(1,J)
   80 IF(ITIME.GT.1)GO TO 81
      CCAPK(2)=0.0
      GO TO 82
   81 CCAPK(2)=CKHOLD
   82 NPOS=1
      NNEG=-1
      NMOD=0
   90 Z=HOLD-FLOAT(N+NMOD)*CONST(1,J)
      IF(IABS(N+NMOD).GE.NMAX)GO TO 165
      IF(ITIME.GT.1.OR.ABS(Z).GT.0.25*ABS(CKHOLD).OR.KZERO.EQ.0)GO TO 99
      IZERO=1
      DO 91 I=1,INDEX
   91 HF(I)=HFHOLD(I)
      GO TO 300
   99 CALL MOMENT(ITYPE,Z,J,ITIME,INDEX,IZERO)
      GMULT=1.0
      MMOD=0
      IF(NOGRAV.EQ.0)GO TO 110
      MPOS=1
      MNEG=-1
  100 K=IABS(MMOD)+1
      SIGNT=1.0
      IF(MMOD.GE.0)GO TO 105
      IF(MMOD-2*(MMOD/2).NE.0)SIGNT=-SIGNT
  105 GMULT=SIGNT*GRAV(K,J)
```

```
      IF(ABS(GMULT).LT.ALOW)GO TO 155
  110 K=N+NMOD-MMOD
      A=FLOAT(K)
      IF(CAPK(1).NE.0.0)A=A/CAPK(1)
      K=IABS(K)+1
      THOLD=0.5*CAPK(1)/CONST(1,J)
      IERROR=0
      DO 145 I=1,INDEX
      TERM=FLOAT(N+NMOD)
      IF(ITIME.EQ.2)GO TO 115
      IF(I.NE.1.AND.I.NE.4.AND.GRAD(5,J).EQ.0.0)GO TO 145
      IF(TERM.EQ.0.0)GO TO 115
      IF(I.EQ.1)TERM=HOLD/CONST(1,J)
  115 D1=CONST(1,J)*CONST(2,J)*(TERM-CAPK(1)*GRAD(4,J))
      TERM=0.0
      TEMP=1.0
      IF(NTYPE.LT.2)GO TO 130
      IF(NTYPE.LT.4)GO TO 120
      TERM=GRAD(2,J)*FLOAT(L(J)+1)*ZMOM(1,I)*(A*D1*D(2,K,J)-THOLD*C(2,K,
     1J))+GRAD(3,J)*ZMOM(3,I)*(A*D1*D(1,K,J)-THOLD*C(1,K,J))
      IF(ITIME.NE.1)TERM=TERM+GRAD(2,J)*FLOAT(L(J)+1)*C(2,K,J)*A*ZMOM(2,
     1I)+GRAD(3,J)*C(1,K,J)*A*(ZMOM(4,I)-ZMOM(2,I))
  120 TEMP=1.0-A*GRAD(1,J)
      TERM=TERM+GRAD(1,J)*THOLD*C(1,K,J)*ZMOM(1,I)
  130 IF(ITIME.NE.1)TERM=TERM+C(1,K,J)*ZMOM(2,I)*TEMP
      TERM=GMULT*CONST(4,J)*(TERM+D(1,K,J)*D1*TEMP*ZMOM(1,I))
  140 HF(I)=HF(I)-TERM
      IF(ABS(TERM).LE.DERROR*ABS(HF(I)))GO TO 145
      IERROR=1
  145 CONTINUE
      IF(IERROR.EQ.0)GO TO 163
      IF(NOGRAV.EQ.0)GO TO 180
  149 IF(MMOD)151,150,152
  150 MMOD=1
      GO TO 100
  151 IF(MPOS.EQ.0)GO TO 153
      MMOD=-MMOD+MPOS
      GO TO 100
  152 IF(MNEG.EQ.0)GO TO 154
      MMOD=-MMOD
      GO TO 100
  153 MMOD=MMOD+MNEG
      GO TO 100
  154 MMOD=MMOD+MPOS
      GO TO 100
  155 IF(MMOD)161,165,160
  160 MPOS=0
      GO TO 162
  161 MNEG=0
  162 IF(MPOS.EQ.0.AND.MNEG.EQ.0)GO TO 180
      GO TO 149
  163 IF(NOGRAV.NE.0)GO TO 155
  165 IF(NMOD)170,166,169
  166 IF(N)300,180,300
  169 NPOS=0
      GO TO 171
```

```
  170 NNEG=0
  171 IF(NPOS.EQ.0.AND.NNEG.EQ.0)GO TO 300
  180 IF(NMOD)182,181,183
  181 NMOD=1
      GO TO 90
  182 IF(NPOS.EQ.0)GO TO 184
      NMOD=-NMOD+NPOS
      GO TO 90
  183 IF(NNEG.EQ.0)GO TO 185
      NMOD=-NMOD
      GO TO 90
  184 NMOD=NMOD+NNEG
      GO TO 90
  185 NMOD=NMOD+NPOS
      GO TO 90
  300 ITIME=ITIME+1
      IF(ITIME.GT.2)GO TO 400
      IF(KZERO.NE.0)GO TO 80
  400 CONTINUE
      DO 410 I=1,INDEX
  410 HF(I)=2.0*HF(I)
      HOLD=1.0/(CCAPK(3)*CCAPK(3))
      HR=HOLD*HF(1)
      HI=HOLD*HF(2)
      RETURN
      END



      SUBROUTINE MOMENT(ITYPE,Z,J,ITIME,INDEX,IZERO)
C
C  SUBPROGRAM MOMENT FOR TIME-SHARING SYSTEM
C
      DIMENSION CONST(4,3),GRAD(5,3),L(3),CAPK(3),CCAPK(3)
      DIMENSION C(2,400,3),D(2,400,3),GRAV(400,3)
      DIMENSION ROOTP(100,2),HATRP(100,2),DHATRP(100,2)
      COMMON CCAPK,HATRP,DHATRP,CAPK,CONST,GRAD,C,D,GRAV,ROOTP
      COMMON ALOW,EXPMAX,FRACT,UMAX,EXTRA1,EXTRA2,EXTRA3
      COMMON JMAX,L,NTYPE,JPOS,JNEG,KMAX,MMAX,NEXTR1,NEXTR2,NEXTR3
      COMMON NEXTR4,NEXTR5,NEXTR6,NEXTR7
      DIMENSION ZMOM(4,5)
      COMMON ALAMB,ZMOM
      IF(ITIME.GT.1)GO TO 200
      IF(Z.NE.0.0)GO TO 110
      TEMP=1.E-08/ALOW
      DO 100 I=1,INDEX
  100 ZMOM(1,I)=TEMP
      GO TO 124
  110 ZMOM(1,1)=-1.0/Z
      ZMOM(1,2)=0.0
  124 IF(ITYPE.LE.1)RETURN
      DO 130 I=1,INDEX
  130 ZMOM(3,1)=0.5*ZMOM(1,1)
      RETURN
  200 ZHOLD=Z
      Z=Z/CCAPK(2)
```

```
      CALL ZETA(Z,0.0,ZR,ZI,DZR,DZI)
      IF(IZERO.NE.0)GO TO 300
      ZMOM(2,1)=-0.5*DZR
      ZMOM(2,2)=-0.5*DZI
      ZMOM(1,1)=ZMOM(2,1)/ZHOLD
      ZMOM(1,2)=ZMOM(2,2)/ZHOLD
      IF(ITYPE.LE.1)RETURN
      ZMOM(4,1)=0.5*(1.0-Z*Z*DZR)
      ZMOM(4,2)=-0.5*Z*Z*DZI
      ZMOM(3,1)=ZMOM(4,1)/ZHOLD
      ZMOM(3,2)=ZMOM(4,2)/ZHOLD
      RETURN
  300 ZMOM(1,1)=ZR/CCAPK(2)
      ZMOM(1,2)=ZI/CCAPK(2)
      ZMOM(2,1)=-0.5*DZR
      ZMOM(2,2)=-0.5*DZI
      IF(ITYPE.LE.1)RETURN
      ZMOM(3,1)=Z*ZMOM(2,1)/CCAPK(2)
      ZMOM(3,2)=Z*ZMOM(2,2)/CCAPK(2)
      ZMOM(4,1)=0.5*(1.0-Z*Z*DZR)
      ZMOM(4,2)=-0.5*Z*Z*DZI
      RETURN
      END
```